CHAPTER ONE

1.0 INTRODUCTION

1.1 Background to the study

Man has constantly been infected with various diseases which produce specific symptoms or affect specific location in the body since time immemorial. Most of these diseases get into human body system either through physical injury, abnormal cell growth/functioning or an exposure to some agents of transmission (pathogens). The presence and growth of these pathogenic biological agents (microorganisms) cause damage and disorders in their host organisms, hence resulting to infectious diseases (Brooke *et al*., 2014) and these pathogens have the ability to grow, multiply and combat or resist any opposing action against their debilitating activities.

Common infectious diseases are tuberculosis, malaria, HIV/AIDS, helminthiasis, hepatitis, meningitis, measles, pneumonia, typhoid to mention a few. Generally, they can be prevented, cured or curtailed by the use of natural or synthetic agents (drugs). According to Dr. Lee Jong-wook, a former Director-General of World Health Organization (WHO), water and sanitation is one of the primary drivers of public health. Once there can be a secured access to clean water, adequate sanitation facilities, regardless of the difference in their living status or conditions, a huge battle against all kinds of diseases will be won and probably, infections could notably be reduced or eradicated (WHO, 2004). Moreover, Brooke *et al*., 2014 reported that about 40% (2.5 billion people) of the world population lack adequate sanitation practices and facilities; a statistics which could be higher, in places where ignorance of hygiene and sanitary practices is being neglected.

1.2 Helminth infections: Prevalence and burden

Helminthiasis (a parasitic worm infection) is caused by a group of pathogenic macro-organisms reported to infect more than two billion of the world's population, with the most significant morbidity attributable to human soil-transmitted helminth (STH) infections (WHO, 2012a; Hotez *et al*., 2008; Holden-Dye and Walker, 2007). It is one of

the Neglected Tropical Diseases (NTDs) that infests poorest nations of the world and grows vigorously under poor sanitation (Kealey and Smith, 2010; Luong, 2003) and unsafe water supply (WHO, 2012a). General symptoms associated with this infection include stomach ache, fever, vomiting, loss of appetite, loss of blood, diarrhea, and dysentery. Helminthiasis is also an important infection of domestic pets, and a major disease in livestock production which often results to significant economic loss and threatening of the global food security (Williams *et al.*, 2014; Charlier *et al.*, 2014; Holden-Dye and Walker, 2007).

The four major species of nematodes commonly referred to as soil-transmitted helminth – *Ascaris lumbricoides* (roundworm), *Necator americanus* and *Ancylostoma duodenale* (hookworms), and *Trichuris trichiura* (whipworm) – have the greatest burden on human health, the highest number of infections occurring in the Americas, China, East Asia, and Sub-Saharan Africa (WHO, 2012a; WHO, 2012b; Hotez *et al.*, 2006). By estimation, Vercruysse *et al*., 2011 reported that approximately 135,000 deaths occur yearly, mainly due to hookworm, round worm and whipworm infections either through anaemia, intestinal or biliary obstruction or chronic dysentery. Although, they are not microscopic, their eggs which start the complex life cycle of infestation in humans and animals are, causing infections and health disorders either by tissue or organ damage (Jimenez-Cisneros and Maya-Rendon, 2007).

Problems such as vitamin deficiencies, anaemia, malnutrition, stunted growth, poor cognitive ability, less intellectual and mental development are associated with helminthiasis (Kealey and Smith, 2010; Bethony *et al*., 2006). Infected pregnant women, women of reproductive age and children, suffer from poor iron status and anaemia. Iron deficiency anaemia often contributes to maternal-foetal consequences such as premature birth and impaired lactation in pregnant women (Hotez *et al.*, 2003; WHO, 2002). For children living in endemic communities with poor nutritional status, the concurrent infection with multiple parasite species (polyparasitisms) is associated with malnutrition (Hall *et al.*, 2008; Ezeamama *et al.*, 2005). In some localities, however, the true effect of these worm infections in childhood health may be obscured when there is an overlap of malnutrition with poverty and STH endemicity (Sanchez *et al.*, 2013). In the tropical and sub-regions of the world, helminth infections often increase the susceptibility of host to malaria, HIV/AIDS and tuberculosis directly and indirectly (Hotez *et al.*, 2008; Brooker *et al*., 2006; Bethony *et al*., 2006).

For many years now, routine efforts have been relied upon to control these pathogenic parasites, predominantly by periodic mass administration of anthelmintic medications as preventive chemotherapy, mainly to school-age children and other groups at risk (Taylor-Robinson *et al*., 2015; Vercruysse *et al*., 2011; Albonico *et al*., 2008; WHO, 2006). Thus, the vision and effort according to WHO is to reduce the prevalence of STH infections to ≤ 1% by the year 2020 (Sanchez *et al*., 2013; WHO, 2012a).

1.3 Basis for research

Helminthiasis is ranked among the most important neglected tropical diseases (NTDs) of the world. There has been much attention and priority given to the so called big three infectious diseases (Simon, 2016) viz a viz; HIV/AIDS, tuberculosis and malaria because of their rate of mortality, compared to the NTDs as well as the enormous and frequently underestimated socioeconomic burden of the billion people living with one or more of the NTDs, and this has resulted in less attention to the funding of research and development in these areas (Mkhize *et al.,* 2017; Kealey and Smith, 2010; Engels and Savioli, 2006; Hotez *et al.,* 2007). The aggregated distribution of STHs and the predisposition of individuals to heavy infections are striking epidemiological features of human helminth infections and a major concern among poverty-stricken regions of the developing nations with poor hygiene and sanitation practices. Although infection may appear asymptomatic (Rosso *et al*., 1996) and rarely cause death, the burden of infection on the host's nutritional status and the overall health or well-being in relation to morbidity or mortality (Omitola *et al.,* 2016; Hotez *et al.*, 2006; Hotez *et al.*, 2007) can't be overemphasized.

Most control programs rely mainly on mass deworming (i.e the use of drugs) to reduce morbidity by decreasing worm burden. Nevertheless, rapid re-infection after treatment is on the increase. The rate of re-infection depends on the life expectancy of many helminths species (short-lived helminths re-infect more rapidly), the intensity of transmission, hygiene education as well as the treatment efficacy and coverage (Yap *et al.,* 2014; Norris *et al.,* 2012; Jia *et al.,* 2012; Hotez *et al.*, 2006). The low efficacy of single-dose treatment with drugs currently in use (Sanchez *et al.*, 2013), high rate of post treatment due to re-infection in high endemic areas and the diminished efficacy due to frequent, repeated and indiscriminate administration of drugs (Molefe *et al.,* 2013; Albonico *et al*., 2003) has reduced the effectiveness of periodic deworming, resulting in

emergence, re-emergence (Zerdo *et al.,* 2016; Speich *et al.,* 2016) and the gradual wide spread of anthelmintic resistance. This is evident among species of veterinary importance (Sutherland and Leathwick, 2011; Gilleard and Beech, 2007) with the development of nematode populations resistant to virtually all anthelmintic classes (Camurça-Vasconcelos *et al*., 2007), as well as the emergence of treatment failures in humans (Sanchez *et al.,* 2013; Grant *et al.,* 2010).

Also, cases of helminth co-infection with tuberculosis, HIV/AIDS and malaria are on the rise (Mkhize *et al.,* 2017; Simon, 2016; Alemayehu *et al.*, 2014; Dada-Adegbola *et al*., 2013; Getachew *et al*., 2013; Tchinda *et al.*, 2012; Tian *et al.,* 2012), which could alter their clinical presentation (Mhimbira *et al.,* 2017). Helminths act to affect the modulation of host immune system by inducing hypersensitivity, leading to acute allergy reaction, prolonging/complicating treatment as well as reducing treatment efficacy, and eventually increase the host's vulnerability to other pathogens and antigens. Thus, the transmission, susceptibility and the severity of these associated diseases often increases (Mulu *et al.,* 2014; Mulu *et al.*, 2013; Norris *et al.,* 2012; Mkhize-Kwitshana and Mabaso, 2012; van Riet *et al.,* 2007; Bethony *et al.*, 2006; Brooker *et al.*, 2006). Therefore, there is an urgent need to continually develop new potent anthelmintics and most importantly vaccines (Norris *et al.,* 2012; Williams *et al.,* 2014; Grant *et al.,* 2010), in addition to the fewer array of the drugs in existence, that would possess better pharmacological activity either by individual potency or in combination with others.

Benzimidazole (BZ) is a heterocyclic aromatic organic compound dubbed as a privileged structure and an important pharmacophore in medicinal chemistry (Khokra and Choudhary 2011; Jaya *et al.,* 2015; Maruthamuthu *et al.,* 2016). For many years of active research, BZs are known to possess a wide range of biological activities and besides these activities, they have high affinity for enzyme and protein receptors. The BZ nucleus has structural similarities with some purine based biological compounds such as the deoxyribonucleic acid (DNA). It is also a versatile structural motif in vitamin B_{12}, forming an integral part of its structure (Ramanpreet *et al.*, 2011; Panda *et al.*, 2012; Bansal and Silakari, 2012). Apart from the illustrious pharmacological importance of these class of compounds, they are also important intermediates in many organic reactions (Panda *et al.*, 2012).

There are eminent setbacks in the usage of the fewer rage of anthelmintics employed in both human and veterinary medicine. Triclabendazole for example is known to be safe and effective against both human and veterinary forms of facioliasis, however, it has a record of resistance in veterinary medicine, as well as non-availability for human treatment due to non-registration for use in some parts of the world (Panic *et al.*, 2014). Through various research findings from the biological profiles of BZ analogs, modifications by introducing a variety of substituents have proved that the broad spectrum of many biological activities could suitably be further modified and enhanced (Khan *et al.*, 2012). An example is a novel benzimidazole, BTP-Iso which is classed in the same family as Triclabendazole, investigated to possess antischistosomal activity. Thus, by way of drug repurposing/repositioning strategy, this indicates an increase in anthelmintic spectrum of activity through slight modification of a drug molecule (Panic *et al.*, 2014).

Moreover, the commonly explore broad-spectrum anthelmintic drugs of human and veterinary medicine stem from benzimidazole pharmacophore and most biologically active analogs have been observed to bear one or more substituent(s) or functional group(s) at 1, 2 and 5(or 6) positions (Bansal and Silakari, 2012). However, the benzimidazole drugs currently in use as anthelmintics both in human and veterinary medicine are not 2-furanyl and 2-phenyl/benzyl based structures.

1.4 Research aim

This work is designed to synthesise, characterise and investigate the anthelmintic activity of benzimidazole derivatives.

1.5 Research objectives

1. To synthesise a series of 2-furanyl and 2-phenyl/benzyl benzimidazoles (from commercially available reagents) and further characterise them using various spectroscopic techniques.
2. To determine the anthelmintic activities of synthesisd benzimidazoles, *in vitro.*

CHAPTER TWO

2.0 LITERATURE REVIEW

2.1 Benzimidazole – a versatile heterocyclic compound

Heterocycles are organic compounds containing one or more elements other than carbon, usually oxygen, nitrogen and sulphur, in a carbon-ring structure (Maruthamuthu *et al*., 2016; Eicher and Hauptmann, 2003). They are natural/synthetic aromatic entities which hold a high degree of diversity in modern drug discovery, such that the additions of a variety of substituents as modifications on the ring(s) often result in new products of compounds with better biological information/activity. Examples are the azoles (such as pyrrole, pyrazole, thiazole, imidazole, benzoxazole, benzimidazole, tetrazole), quinazolinones, quinazolines and thiocyanates (Maruthamuthu *et al*., 2016).

Benzimidazole, a bicyclic heterocycle, is made up of a benzene ring and an imidazole ring fused together. It is a fusion of a benzene to positions 4- and 5- of an imidazole, which is aromatic in nature. Tautomerism could be established between positions 1 and 3 on the imidazole ring due to a rapid exchange of proton on one of the nitrogen atoms carrying the proton and the other without a proton as illustrated in structures I, II, III and IV, figure **2.1**. As a result, positions 5- and 6- become chemically equivalent. However, isomerism occurs when it is a N-substituted compound and non-equivalent molecules are obtained as illustrated in structures V and VI, figure **2.1** (Bansal and Silakari, 2012; Townsend and Wise, 1990).

This fused nucleus is often regarded as ‘a master key’, ‘a multifunctional nucleus’ (Bansal and Silakari, 2012) and ‘a privileged structure’ (Maruthamuthu *et al*., 2016; Ajani *et al*., 2013; Santosh *et al*., 2011; Ramanpreet *et al*., 2011) because it has become an important central pharmacophore in many compounds that have a wide range of bioactivities. 5,6-dimethyl-N-(α-D-ribofuranosyl)benzimidazole **[2.1]** is an axial ligand for cobalt known to be an integral part of the structure of vitamin B_{12}, the most prominent benzimidazole compound in nature (Ajani *et al*., 2013; Ramanpreet *et al*., 2011; Townsend and Wise, 1990).

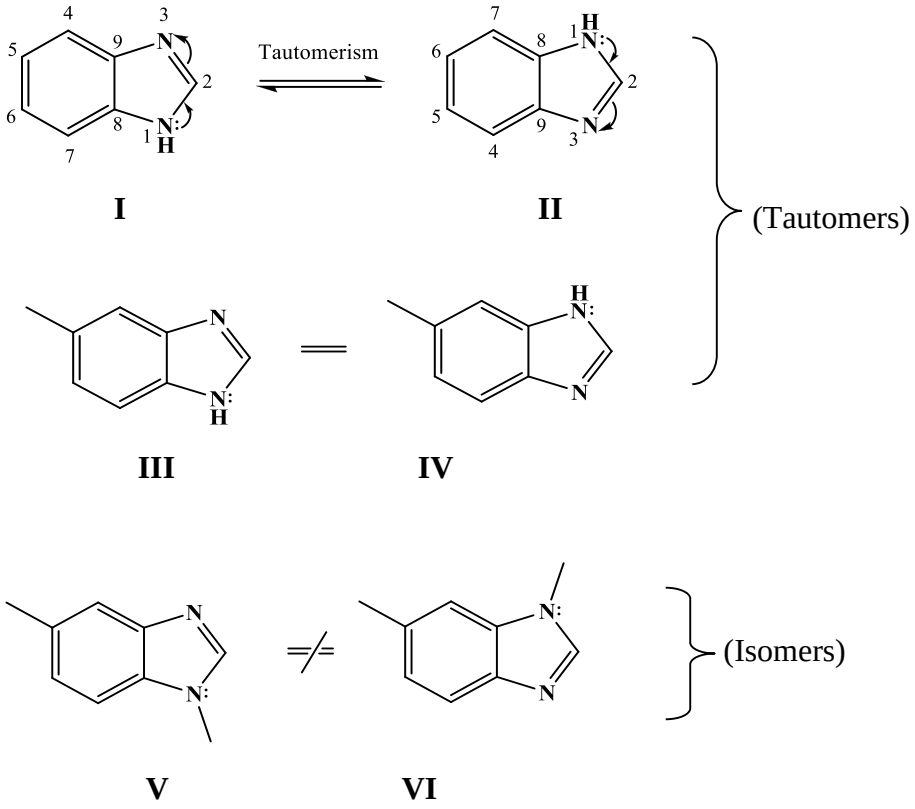

Figure 2.1. Tautomerism and isomerism in benzimidazole (Townsend and Wise, 1990)

With this however, came up the basis for further interest and extensive studies on benzimidazole nucleus, in order to continually develop potential chemotherapeutic agents, from which the discovery of thiabendazole for the treatment of parasitic diseases started (Jaeger and Carvalho-Costa, 2017; Townsend and Wise, 1990).

Moreover, benzimidazoles are known to act at different points of targets, bringing about varied pharmacological properties such as antibacterial, antifungal, antiviral, antiulcer, antitumor/anti-angiogenic, anthelmintic, anticonvulsant, analgesic, antidepressant, anti-diabetic, anti-inflammatory, anti-malarial, antioxidant, antiproliferative, proton pump inhibitors, antihistaminic, anticoagulants, antihypertensive, as well as anti-tubercular properties (Maruthamuthu *et al*., 2016; Alasmary *et al*., 2015; Temirak *et al*., 2014a and 2014b; Ajani *et al*., 2013; Gurvinda *et al*., 2013; Bansal and Silakari, 2012; Ramanpreet *et al*., 2011, Yar *et al*., 2009). Further potential pharmacological activities are against HIV, herpes (HSV-1), RNA, influenza and human cytomegalovirus (HCMV) (Panda *et al*., 2012). Some of these activities exhibited by widely used benzimidazole drugs were achievable due to the many benefits they possess, such as their selectivity and relatively low toxicity, broad-spectrum of activity, high efficacy, ease of administration and low cost (Jaeger and Carvalho-Costa, 2017).

Most of the biologically active benzimidazoles bear a functional group or combination of functional groups at either of the positions 1, 2, 5 or 6 (Bansal and Silakari, 2012; Santosh *et al*., 2011; Kalidhar and Kaur, 2011), most of which are 2-substituted products of ortho anilines (such as *o*-phenylenediamine and 2-nitroaniline), and many drugs came into existence when the substituents attached at different position on the benzimidazole nucleus were optimized (Bansal and Silakari, 2012). Examples of some of such drugs are:

- Albendazole **[2.2]**, Mebendazole **[2.3]**, Thiabendazole **[2.4]**, Fenbendazole **[2.5]**, Triclabendazole **[2.6]** as antihelmintics (Bansal and Silakari, 2012; Santosh *et al*., 2011).
- Omeprazole **[2.7]**, Lansoprazole **[2.8]**, Pantoprazole **[2.9]** as proton pump inhibitors/antiulcer (Bansal and Silakari, 2012; Santosh *et al*., 2011).
- Astemizole **[2.10]** as antihistaminic (Bansal and Silakari, 2012).
- Enviradine **[2.11]**, Enviroxime **[2.12]** as antiviral (Bansal and Silakari, 2012; Heinz and Vance, 1995).

- Candesarten cilexitil **[2.13]**, Telmisartan **[2.14]** as antihypertensive (Bansal and Silakari, 2012; Verdecchia *et al*., 2011).
- Bendamustine, **[2.15]**, Mebendazole **[2.3]** as antitumoral or anti-cancer (Pantziarka *et al*., 2014; Bansal and Silakari, 2012; Cheson and Leoni, 2011).
- Benoxaprofen analog **[2.16]** as anti-inflamatory (Bansal and Silakari, 2012).

Apart from these established drugs listed above, a vast number of benzimidazoles have been reported to exhibit promising pharmacological activities including many analogs such as the quinazoline, thiazole, phenothiazine, quinoxalinone, benzamide, naphthol, phenylamine, hydrazide, phenylthio-acetamide and Mannich-base derived analogs, thus making it a very important intermediate and building block to other products in several organic reactions (Zhou *et al*., 2013; ur Rehman *et al*., 2013; Panda *et al*., 2012; Chou *et al*., 2011; Al-Rashood and Abdel-Aziz, 2010; Patel and Singh, 2009; Ayhan-Kilcigil and Altanlar, 2003).

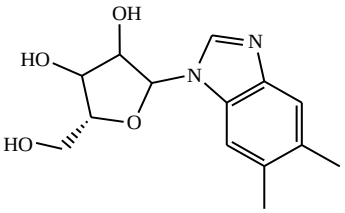

2.1

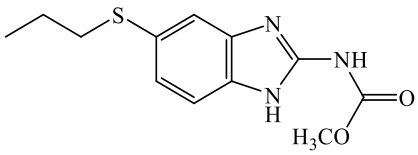

2.2

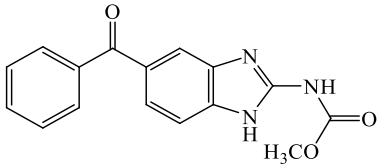

2.3

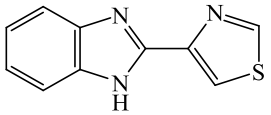

2.4

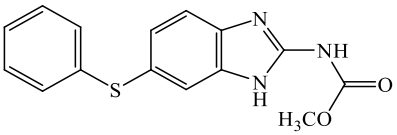

2.5

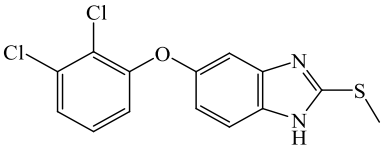

2.6

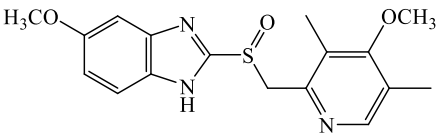

2.7

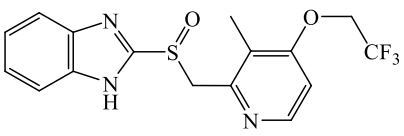

2.8

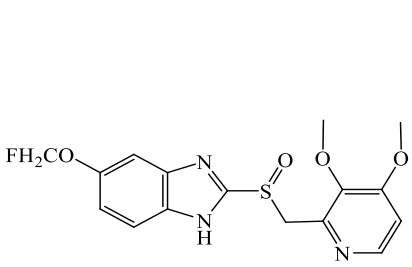

2.9

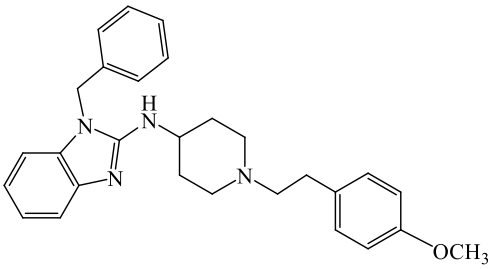

2.10

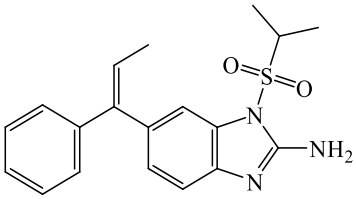

2.11

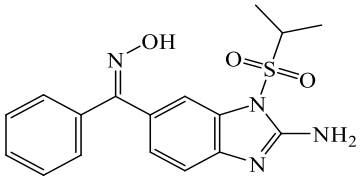

2.12

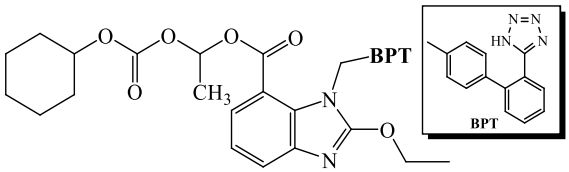

2.13

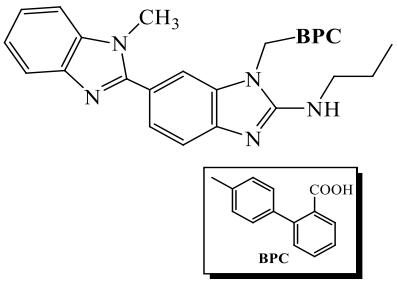

2.14

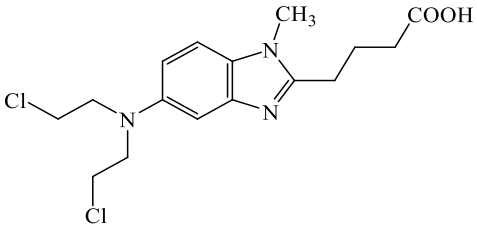

2.15

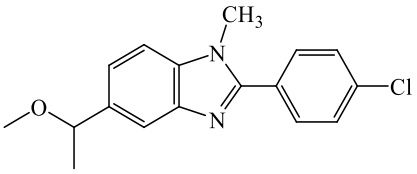

2.16

2.2 Methods of benzimidazoles synthesis

Quite a number of methods have been derived and applied to synthesise libraries of benzimidazoles that showed varied bioactivities. For products of high yield, purity and desired quality, continuous modification of methods of synthesis have spanned over years (Bansal and Silakari, 2012). Panda *et al*., 2012, reviewed comprehensive methods employed in the synthesis of numerous analogs of 2-arylbenzimidazoles with moderate to excellent yields using different solvents, reagents/catalysts and varied conditions of reaction such as temperature ranges and atmospheric condition.

Generally, the synthesis of benzimidazoles commonly involves two methods, both of which employs the use of *o*-phenylenediamine or its derivatives and could either be achieved conventionally under reflux condition or microwave irradiation for different combinations of reactants (Panda *et al*., 2012; Chou *et al*., 2011; Chawla *et al*., 2011). Solvents often employed are water, ethanol, acetonitrile, dimethyl formamide (DMF), toluene, tetrahydrofuran (THF), dioxane, glacia acetic acid (Panda *et al*., 2012; Secci *et al*., 2012; Panda and Jain, 2011), glycerol (Radatz *et al*., 2011) and xylene (Tagawa *et al*., 2008; Hegedus *et al*., 2006) to mention a few.

1. Reaction of *o*-phenylenediamines with organic acids and their derivatives: In the presence of several reagents such as strong acids (polyphosphoric acid or mineral acids), polymer-supported PPh_3, PCl_3, alumina, zeolite and K_2CO_3, *o*-phenylenediamines react with carboxylic acids and their derivatives according to the reaction below to afford 2-substututed benzimidazoles. However, under conventional methods (heating/refluxing), a high temperature range and/or longer time of reaction is often experienced to afford the desired products (Panda *et al*., 2012).

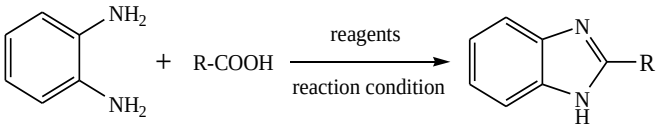

R = H, Alkyl group, Aromatic group

According to Chou *et al*., 2011, an acid catalysed synthesis of a series of benzimidazole linked quinoxalines and quinoxalinones on a polymer support according to the reaction steps below were achieved in shorter times using microwave condition.

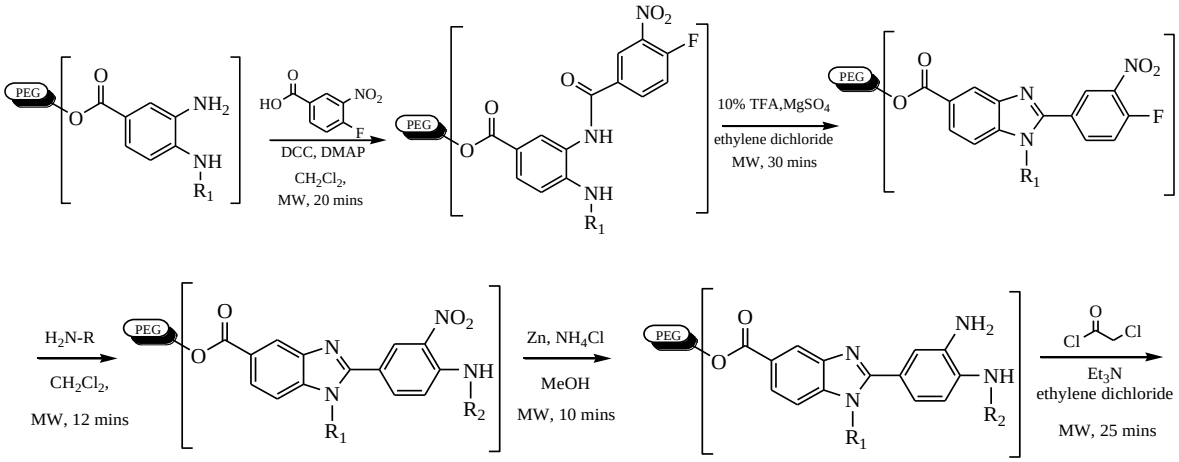

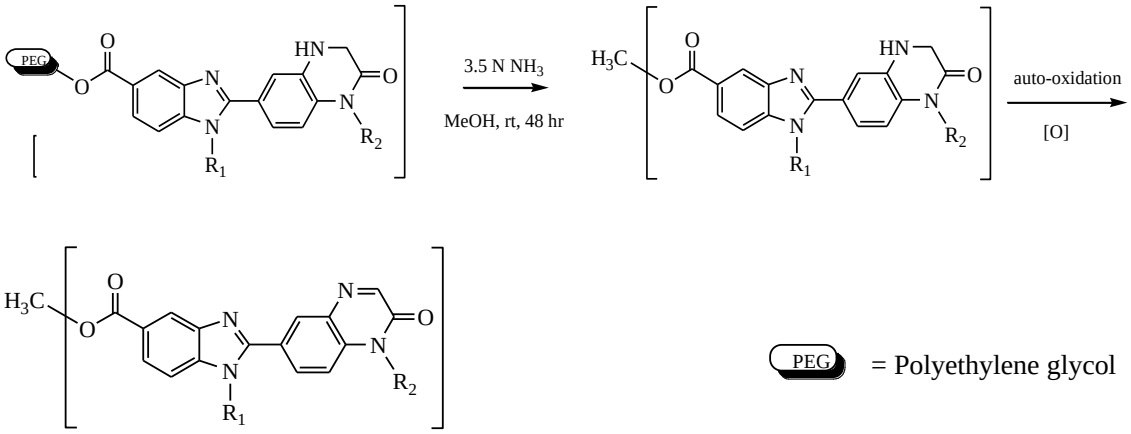

The synthesis of *N*-[4-(1*H*benzimidazol-2-yl)phenyl]-10*H*-phenothiazines in pyridine and under relux condition was achieved by reacting *o*-phenylenediamine and 4-[(10*H*-phenothiazin-10-yl-(substituted)-methyl)amino]benzoic acid within 6 hours (Panda *et al*., 2012) according to the reaction below.

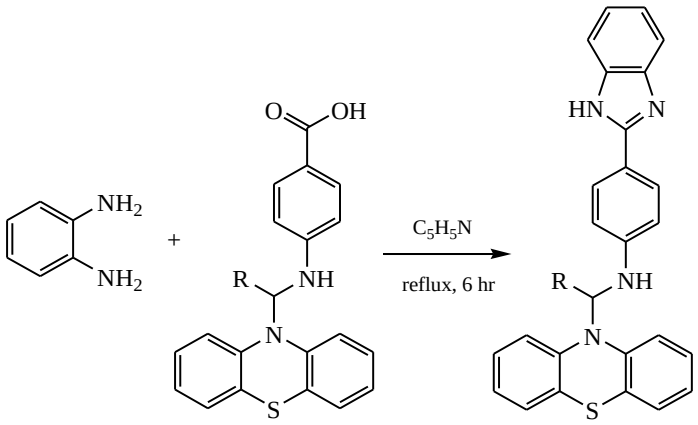

2. Reaction *o*-phenylenediamines with aldehydes and their derivatives: Utilising oxidative reagents such as $NaHSO_3$, $KHSO_4$, $Na_2S_2O_5$, $Na_2S_2O_4$, $In(OTf)_3$, $Yb(OTf)_3$, $Sc(OTf)_3$, $Cu(OTf)_2$, H_2O_2/HCl, MnO_2, benzofuroxane, nitrobenzene, oxone, 1,4-benzoquinone, Zn-proline, polymer supported hypervalent iodine, 2,3-dichloro-5,6-dicyanobenzoquinone (DDQ), and molecular oxygen, *o*-phenylenediamines undergo cyclocondensation reaction with aldehydes (Chari *et al*., 2013; López *et al*., 2009). This is a one-pot, two-step procedure which includes an oxidative cyclodehydrogenation of aniline Schiff base, often generated *in situ*. It is considered the most acceptable route (Panda *et al*., 2012).

2-Aryl substituted benzimidazoles were prepared by the microwave promoted reaction between *o*-phenylenediamine and derivatives of benzaldehyde using sodium hydrogen sulfite in dimethylacetamide (López *et al*., 2009) according to the reaction equation

below. Optimization of the reaction conditions was by varying irradiation time and the potency level of the microwave irradiation.

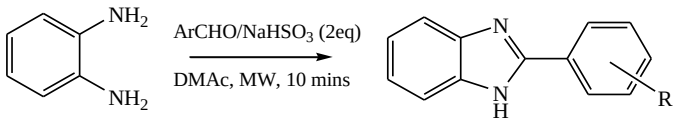

Performing control experiments under atmospheric N_2 (absence of air) using $Cu(OH)_2$ catalyst, Chari *et al.*, 2013 reported that the products of reactions in methanol between *o*-phenylenediamine and benzaldehydes had low yields. However, improved yields were observed at varied amount of catalyst (2 mol%, 5 mol%, 10 mol% and 15 mol% of $Cu(OH)_2$) and solvents (dichloromethane, methanol, acetonitrile and ethanol) but the best yield was obtained from a 10 mol% of catalyst at room temperature in methanol condition, isolating 2-phenyl-1*H*-benzimidazole in high yield within a short time. Earlier on, this reaction was carried out in methanol at room temperature and atmospheric oxygen in the absence of $Cu(OH)_2$ catalyst to afford a mixture of products, 2-phenylbenzimidazole and 1-benzyl-2-phenyl-1*H*-benzimidazole (as the side product), according to the equation of reaction below (Chari *et al.*, 2013).

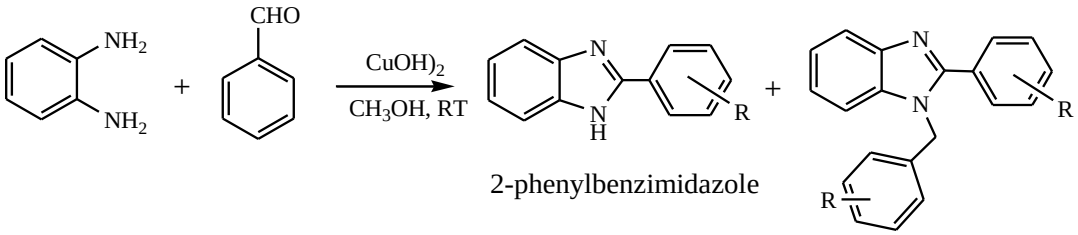

2-phenylbenzimidazole

1-benzyl-2-phenyl-1*H*-benzimidazole

Furthermore, benzimidazole synthesis can be achieved by reacting a couple of reagents such 2-nitroanilines with aryl aldehydes (Surpur *et al*., 2007; Yang *et al*., 2005), reacting *o*-aminoazo compounds with aldehydes as well as by the reduction of 2-nitro-4-methylacetanilide and reduction of acetylated *o*-nitroanilines, (Kalidhar and Kaur, 2011).

2.3 Spectroscopic techniques of organic compounds

Before the discovery of methods often applied to structural elucidation by the use of instruments (spectroscopic techniques), the structure of newly discovered compounds (often natural products) were usually confirmed by different chemical tests in order to identify the functional groups present. This approach of confirmation includes the

determination of unsaturation (either by catalytic hydrogenation, halogenation or ozonolysis), determining the nature of functional group (either by acetylation or using reagents such as sodium bisulphite, hydroxylamine, hydrazine and phenyl hydrazine), among many methods/approaches. Nuclear Magnetic Resonance (NMR) spectroscopy, Ultraviolet-Visible (UV-Vis) spectroscopy, Infrared (IR) spectroscopy and Mass spectrometry (MS) are the major techniques employed nowadays, and from these techniques, structural evidences deduced are based on energy absorption (from electromagnetic radiation) except for mass spectrometry which involves bombardment by a stream of charged particles such as electrons. Of great importance prior to analysis are the solvents used in dissolving metabolites isolated or compounds synthesised.

2.3.1 Infrared spectroscopy

The Infrared (IR) region is the region in the electromagnetic spectrum which spans between 4000 – 400 cm^{-1}. It gives information on the structural pattern of compounds that have covalent bonds. Only bonds (mainly of functional groups) having a dipole moment which can change as a function of time (i.e. the bond must present an electric dipole that is changing at the same frequency as the incoming radiation in order for energy to be transferred) are capable of absorbing energy in this region. Molecules absorb selected frequencies (energies) that match their natural frequencies. Fundamental absorptions, often referred to as modes of vibrational motion in IR active molecules are scissoring, rocking, wagging, twisting, bending and stretching vibrations: the latter two are the simplest types observed in molecules. When two vibrational frequencies couple to give a vibration of a new frequency within a molecule and is IR active, such is called a combination band. The infrared spectrum of a compound can either be determined in the neat, concentrated or diluted form. Factors that could influence the relative absorption of organic functional groups include mass effect, field effect, hydrogen bonding, ring strain, electronic effect, inductive and mesomeric effect (Kalsi, 2004; Silverstein *et al*., 2005; Pavia *et al*., 2001).

2.3.2 Ultraviolet-Visible (UV-Vis) spectroscopy

Organic compounds, most especially those with a high degree of conjugation (i.e. those with multiple bonds or aromatic conjugation within molecules), absorb light in the Ultraviolet (UV) or visible regions of the electromagnetic spectrum (the visible region corresponds to 800 – 400 nm, while the UV region to 400 – 200 nm). A molecule, on

absorption of energy in these regions, produces changes in electronic energy due to transitions of valence electrons from an occupied molecular orbital (a non-bonding p-orbital or a bonding π-orbital) to the next unoccupied-higher energy orbital (an anti-bonding π*-orbital or σ*-orbital) (Kalsi, 2004). The most probable observed transition is from the highest occupied molecular orbital (HOMO) to the lowest unoccupied molecular orbital (LUMO) (Pavia *et al*., 2001).

What is recorded in a UV spectrum is the wavelength of maximum absorption (λ_{max}) and the absorption strength or molar absorptivity (ε_{max}) as defined by the combined Beer-Lambart law as expressed below (Kalsi, 2004):

$$\log (I_o/I) = \varepsilon l c, \text{ or}$$

$$\varepsilon = A/cl$$

where: I_o = the intensity of incident light

I = the light transmitted through the sample solution

$\log (I_o/I)$ = the absorbance or optical density of the solution

ε = the molar absorptivity (extinction coefficient)

c = the concentration of solute ($moldm^{-3}$)

l = the path length of sample (cm)

Not all solvents are suitable for use in UV analysis. The solvent must be transparent within the wavelength range being examined, i.e it should not absorb UV radiation in the same region as the substance whose spectrum is being determined. Often times, water is used for water-soluble compounds and ethanol (which absorbs very weakly at most wavelengths) for organic-soluble compounds. Also, solvent polarity and pH can affect the absorption spectrum of an organic metabolite either by shifting its absorption maximum (λ_{max}) or change the energy and intensity of absorption (ε_{max}) (Kalsi, 2004; Pavia *et al*., 2001). The information obtained in the UV spectrum of an organic compound under investigation can help deduce the presence of a chromophore (functional groups such as the isolated and conjugated ethylenic system, acetylenic unsaturations, nitro, nitrile and carbonyls including acids and esters) (Brahmachari, 2009). The UV-Vis spectrum is generally recorded as a plot of absorbance against wavelength.

2.3.3 Mass spectrometry (MS)

Mass spectrometry does not involve electromagnetic energy absorption. Its concept is basically about ionisation of compounds, whereby molecules are bombarded by a stream of high-energy electrons and converting some of them to ions. The resulting ions get separated based on their mass-to-charge ratio (*m/z*) in a magnetic or electric field, and the number of ions representing each *m/z* unit are detected and recorded on a spectrum (a graph of the number of charged particles detected). In gas chromatography-mass spectrometry technique, the mass spectrometer acts in the role of a detector when coupled to a gas chromatograph (Silverstein *et al*., 2005; Pavia *et al*., 2001). This technique is principally used to measure the exact molecular weights, and from this the exact molecular formulae can be determined. Also, the presence of certain structural units can be recognised from the pattern within which the molecule prefers to fragment (Kalsi, 2004). According to Pavia *et al*., 2001, the molecular weight is determined from the molecular ion [M^+] peak owing to certain facts such as:

1. the [M^+] peak must correspond to the highest mass in the spectrum, excluding isotopic peaks that occur at even higher masses.

2. the [M^+] must have an odd number of electrons, this is as a result of an electron loss when the molecule becomes ionized to a radical-cation.

3. the [M^+] must have the capability to form the important fragment ions/radical cation (particularly the fragments of relatively high masses) in the spectrum by loss of logical neutral fragments.

4. if the corresponding [M^+] peak has nitrogen present in its molecule, the peak is often verified by "Nitrogen rule" which states that "if a compound has an even number of or no nitrogen atoms, its [M^+] will appear at an even mass value, and on the other hand if it's an odd number of nitrogen atoms will form a [M^+] with an odd mass.

High-resolution mass spectrometers are applied in the determination of a very precise molecular weight of substances. It differentiates compounds of the same nominal mass depending on the atoms contained in individual compound as illustrated in the example below (Pavia *et al*., 2001).

Compound	Precise molecular weight
C_3H_8O	60.05754
$C_2H_8N_2$	60.06884
$C_2H_4O_2$	60.02112
CH_4N_2O	60.03242

2.3.4 Nuclear magnetic resonance (NMR) spectroscopy

The characteristic property of atomic nuclei of many elemental isotopes, called spin, can be studied by Nuclear Magnetic Resonance (NMR) techniques. For every nucleus with a spin, the number of allowed spin states is determined by its nuclear spin quantum number, *I*. The more common nuclei, which possess *I* either as integral spins (i.e $I = 1, 2, 3....$) or fractional spins (i.e $I = 1/2, 3/2, 5/2$ ....), include ^{1}H, ^{13}C, ^{14}N, ^{17}O, ^{19}F and ^{31}P. However, those often useful to organic chemists and are of particular interest are ^{1}H, ^{13}C, ^{19}F and ^{31}P, all with $I = 1/2$. The phenomenon of NMR is said to occur once a charged nucleus spins to acquire a magnetic moment (μ). Under the influence of an applied external magnetic field (B_o), it generates a magnetic field of its own and energy is absorbed. The orientation of spin changes (i.e. precess) with respect to the applied field, either to be aligned (low energy) with the external field or opposed (high energy) to it. The stronger the applied field, the higher the rate of precession, which implies that the frequency of precession is directly proportional to the strength of the applied magnetic field (Pavia *et al*., 2001; Kalsi, 2004).

Also, the stronger the applied magnetic field, the greater the energy difference between the possible spin states. Many of the instruments required to observe transitions in nuclei of elements are being operated at varying frequencies. It is noteworthy to know that not all protons in a molecule have resonance at the same frequency (it varies), due to the fact that, they are always surrounded by electrons and exist in slightly different electronic environments. These differences in resonance frequency are very small, making it difficult to measure exactly and to locate NMR signals for any proton. However, this problem was solved by locating any signal in a spectrum relative to a reference signal from a standard compound added to the sample. Such a reference standard should be chemically unreactive, easily removed from the sample after measurement and should give a single sharp uninterfering NMR signal. By meeting all these characteristics, tetramethylsilane $(CH_3)_4Si$ also called TMS has become the reference compound of

choice for ^{1}H and ^{13}C NMR. The shift of a given proton from TMS, independent of the magnetic field strength, is a parameter known as the chemical shift, measured in δ units. Chemical shift expresses the amount by which a proton resonance is shifted from TMS in parts per million (ppm). Also, a phenomenon known as spin-spin, or *J* coupling explains the fact that resonance frequencies are perturbed by existing neighbouring NMR active nuclei in a manner dependent on the bonding electrons that connect the nuclei (Pavia *et al*., 2001; Kalsi, 2004).

Nuclear Magnetic Resonance (NMR) spectroscopy involves one dimensional (1-D) NMR technique and two dimensional (2-D) NMR technique. Examples of 1-D NMR are Attached Proton Transfer (APT) and Distortionless Enhancement by Polarisation Transfer (DEPT) which is of three types (DEPT 45, 90 and 135) (Mahato *et al*., 1992). Two dimensional NMR techniques generally provide information about nuclei-bonds connectivity and they include homonuclear Correlated Spectroscopy (COSY), Nuclear Overhauser Effect Spectroscopy (NOESY) and Heteronuclear Correlated Spectroscopy (HETCOR), Heteronuclear Multiple Quantum Correlation (HMQC), Heteronuclear Single Quantum Correlation (HSQC) and Heteronuclear Multiple Bond Correlation (HMBC) (Williams and King, 1990).

2.3.4.1 Proton nuclear magnetic resonance (^{1}H NMR) spectroscopy

Proton Nuclear Magnetic Resonance spectroscopy (^{1}H NMR) measures the magnetic moments of hydrogen atoms present in an organic compound. These hydrogen atoms (protons) are said to be positioned in different chemical environments within a molecule. Protons that are present in chemically identical environments are chemically equivalent and often exhibit the same chemical shift. Proton chemical shift values are usually influenced by factors such as solvent effect, magnetic anisotropy, hybridization effect, local diamagnetic shielding (electronegativity effect) and hydrogen bonding due to acidic and exchangeable protons (Pavia *et al*., 2001).

2.3.4.2 Carbon-13 nuclear magnetic resonance (^{13}C NMR) spectroscopy

The most abundant isotope of carbon, ^{12}C (spin, $I = 0$), is NMR inactive while ^{13}C (spin, $I = 1/2$), is NMR active. However, resonances of ^{13}C are more difficult to observe than those of ^{1}H. They are about 6000 time weaker due to the very low natural abundance (1.08%) of ^{13}C in nature and a smaller magnetogyric ratio. Thus, a greater number of individual scans of spectrum must be accumulated (Pavia *et al*., 2001). Proton-decoupled

carbon-13 NMR spectra are much simpler to interpret than ^{1}H NMR spectra because the technique eliminates all interactions between proton(s) and carbon nuclei. The DEPT experiment is useful in determining the presence of primary, secondary and tertiary carbon atoms by differentiating between the methyl (CH_3), methylene (CH_2) and methine (CH) groups. However, quaternary carbon signals are missing. DEPT 135 experiment produces spectra with CH and CH_3 signals in opposite phase to CH_2 signals, DEPT 90 experiment shows spectra with only CH signals, others been suppressed, while DEPT 45 provides spectra of all protonated carbons (CH, CH_2 and CH_3) signals in the same phase (Caytan *et al*., 2007).

2.3.4.3 Two dimensional nuclear magnetic resonance (2-D NMR) spectroscopy

These are experiments carried out in order to show in a molecule all coupling relationships in a two coordinate, three dimensional plot (either contour plot or stacked plot). These correlations, classified as homonuclear and heteronuclear, could either be through bond or through space coupling interractions. **Correlated spectroscopy (COSY)** is a homonuclear correlation experiment from which the spectrum obtained is two-dimensional. COSY experiment shows *diagonal peaks* (corresponding to those in a 1-D NMR experiment) that have the same frequency coordinate and appear along the diagonal of the plot, as well as *cross peaks* (located off the diagonal) which have different values for each frequency coordinate. COSY indicate through-bond couplings between pairs of nuclei, usually protons. **Nuclear overhausern enhancement spectroscopy (NOESY)** is a homonuclear correlation experiment similar to COSY, except that the cross peaks are coupling interactions between pair of protons close to each other through-space. It is often applicable to communicate information from connections made between different spin systems of larger molecules. This experiment is usually carried out in the phase sensitive mode so as to distinguish cross peaks due to positive NOE's (Williams and Fleming, 1987).

In addition, **heteronuclear correlated spectroscopy (HETCOR)** is a heteronuclear correlation experiment which reveals a coherence transfer of signals between non-identical spins typically of those from ^{13}C, ^{15}N and ^{1}H nuclei. The generated spectrum present a through-bond coupling interraction between ^{1}H and any other nucleus to which they are attached (often ^{13}C and ^{15}N). This is usually achieved by way of coherence transfer from ^{1}H to the unidentical nucleus and a further direct detection of such

unidentical nucleus. HETCOR experiments suffer poor sensitivity. Thus, modern practical skills such as **heteronuclear multiple quantum coherence (HMQC)** and **heteronuclear multiple bond correlation (HMBC)** experiments employ inverse (indirect chemical shift correlation) technique to provide the same correlation information and have improved sensitivities (Bruch, 1996).

2.4 Helminths and helminth infections

Helminths are invertebrates described as elongated, flat (platyhelminths) or cylindrical (round worms). They are classified based on the external and internal morphology of their egg, larval and adult stages. The groups which are clinically relevant are placed according to their general external shape and the host organ they inhabit. They are either naturally hermaphroditic or anatomically bisexual. The three major groups are the nematodes (roundworms), cestodes (tapeworms) and trematodes (flukes). To understand the epidemiology and pathogenesis of helminth diseases, as well as diagnose and treat hosts harbouring these parasites, the different stages in relation to their growth and development must be well understood (Castro, 1996).

Helminthiasis (helminth infection or worm infection) is one of the major diseases of veterinary animals and humans, with poor socioeconomic status, in many developing countries. It is caused mainly by parasitic worms which often live in the gastrointestinal tract of the host, and may also burrow into some other organs, inducing physiological damages. Helminth infection is grouped among the neglected tropical diseases (NTDs) of humans. Over 1.4 billion people are infected with one or more of seventeen NTDs, among which are schistosomiasis, lymphatic filariasis, onchocerciasis, trachoma and three soil-transmitted helminth infections (hookworm, ascariasis and trichuriasis), and are avowed the most common afflictions of the world's poorest people. The NTDs have a terrible impact on health, impede child growth and development, harm pregnant women (risk of giving birth to low birth-weight babies, poor milk production and high susceptibility to death during childbirth), causes disabilities and disfiguration and often long-term debilitating or even deadly illnesses (Norris *et al.*, 2012). Many infected individuals are frequently avoided/neglected by both their families and the community, and subsequently are often unable to work productively. This gradually leads to enormous economic losses for them, their families and their nations.

Gastrointestinal worm infections are generally associated with abdominal pains, loss of appetite, malnutrition, diarrhea, and anemia. Infections by roundworm (ascariasis), whipworm (trichuriasis), hookworm, lymphatic filariasis (elephantiasis), blinding trachoma, schistosomiasis and onchocerciasis (river blindness) affect more than 807, 604, 576, 200, 120, 80 and 40 million people worldwide respectively. They are the most common and important, owing to the large number of people affected (Skolnik and Ahmed, 2010). For effective clear out of clinical symptoms, reduction of morbidity and mortality rates or cure of the diseases, chemotherapy by the use of anthelmintics (drugs) is often employed. These anthelmintics are commercially available and are classified based on the similarity in their chemical structures and mode of actions. Examples include levamisole, piperazine, benzimidazoles (such as albendazole, mebendazole and thiabendazole), pyrantel, morantel, cyclodepsipeptides (Emodepside), macrocylic lactones (Ivermectin) and the oxindole alkaloids (Marcfortine A and Paraherquamide A) which are often employed singly or in combination (Keiser e*t al.,* 2012; Holden-Dye and Walker, 2007). Also, some promising bioactive plant extracts with anthelmintic properties have been reported (Ferreira *et al.,* 2013; Camurça-Vasconcelos *et al.,* 2008).

However, the therapeutic effect of these commercial drugs has been compromised due to regular use (coupled with inadequate flock management in ruminant animals) and repeated or indiscriminate administration (Ferreira *et al.,* 2013; Molefe *et al.,* 2012; Almeida *et al.,* 2010) which has resulted in the development of resistance to the drugs by the helminth parasites. As a result, expression of genes which are associated with resistance are on the rise, and are already within the population before anthelmintic treatment is carried out (Álvarez-Sánchez *et al.,* 2002). The increasing development of resisitance to the available drugs has necessitated the search for alternatives that are effective. However, there are written procedures and established protocols (anthelmintic assays) for determining the effectiveness of agents, such as plant extracts and synthetic compounds, against helminths. Some of these procedures are egg recovery assay, egg hatch assay (EHA), larval development assay (LDA), larval motility or mortality assay, larval feeding inhibition assay (LFIA), larval exsheathment assay (LEA) and adult worm motility test (Molefe *et al.,* 2013; Katiki *et al.,* 2011).

CHAPTER THREE

3.0 MATERIALS AND METHODS

3.1 Experimental reagents, apparatus and instruments

The commercial reagents employed in synthesis were purchased majorly from Sigma-Aldrich®, while few others were from Alfa Aesar, Tokyo Chemical Industry (TCI), ACROS organics™, Merck, Wako pure chemicals, Santa Cruz Biotechnology or Oakwood chemicals and were used without any further purification. They include *ortho*-phenylenediamine, 4-nitro-*o*-phenylene-diamine, 4-chloro-*o*-phenylenediamine, 4-fluoro-*o*-phenylenediamine, 4,5-dimethyl-*o*-phenylenediamine, furaldehyde, 5-methyl-furancarbaldehyde, benzaldehyde derivatives and sodium metabisulfite (also known as sodium pyrosulfite or sodium disulfite ($Na_2S_2O_5$)).

All solvents, including *n*-hexane, ethyl acetate, N,N-dimethyl formamide (DMF) and dichloromethane (DCM) were analytical grades. Distilled water was also used. Glass wares utilized are 100 mL round bottom flasks, beakers, conical flasks, reflux condensers, glass funnels, thin layer chromatography (TLC) developing tank and separating funnels. Heidolph MR 30001K and Heidolph MR Hei-standard magnetic stirrer/heater, electric oven, a Black and Decker electric gun heater, TLC (Kieselgel 60, 254, E. Merck, Germany) pre-coated aluminum plates and an ultraviolet light (uvitec UV-254/365 nm) apparatus were also employed. Other materials/apparatuses utilized are chiller, spatula, retort stand, magnetic beads, drysyn, magnetic rod, glass stirring rod and cotton wool. Centrifuge machine, electron microscope, glass slides, cover slips, test tubes, micro-pipette, graduated seives and syringes were utilised during the biological analysis together with Albendazole as the standard drug.

Proton nuclear magnetic resonance (^{1}H NMR) spectra of the synthesised compounds, in dueterated dimethyl sulphoxide (DMSO-d_6), were obtained on Avance (AV-400 and AV-500 MHz) spectrometers, while carbon-13 nuclear magnetic resonance (^{13}C NMR) spectra were recorded on Avance (AV-300, AV-400 and AV-500 MHz) instruments also in DMSO-d_6 (both ^{1}H NMR and ^{13}C NMR instruments were manufactured by Bruker). Chemical shift (δ) values were recorded in parts per million (ppm) to 2 decimal places

unrounded off and were referenced using DMSO-d_6 solvent signals at 2.50 and 40.00 ppm for ^{1}H and ^{13}C NMR respectively. Coupling constants, *J* were measured in Hertz (Hz) to 1 decimal place. Electron ionization-mass spectrometry (EI-MS) was carried out on Jeol MS 600H-1 and MAT 312/MAT 113D double focusing mass spectrometers to record the mass-to-charge ratios (*m/z*) of ions produced, while high resolution electron ionization-mass spectrometry (HREI-MS) was performed on a Jeol HX110 mass spectrometer. The IR spectra were recorded on Bruker Vector-22 and Shimadzu FTIR-8900 spectrometers using the potassium bromide (KBr) disc method to determine the absorption frequencies, $\bar{\upsilon}$ (cm^{-1}) of IR active functional groups. The UV spectroscopy analysis utilized a Thermoscientific Evolution 300UV-Visible spectrophotometer to determine the wavelenghts of maximum absorptions (λ_{max}) in methanol. Melting points were obtained on a Buchi M-560 apparatus and were uncorrected.

The following abbreviations were used in the assignment of peaks from ^{1}H NMR spectra: br (broad), s (singlet), d (doublet), dd (doublet of doublets), t (triplet), dt (doublets of triple) and m (multiplets). ^{13}C NMR chemical shift values were listed and assigned to specific carbon atoms. Abbreviations such as *str* (stretching vibration), *asy str* (asymmetric stretching vibration), *sym str* (symmetric stretching vibration) and *b* (bending vibration) were used in the IR spectra band assignments.

3.2 Synthesis of benzimidazoles

Various substituted benzimidazoles (BZs) were synthesised by reacting commercially available *o*-phenylenediamine and its derivatives (4-fluoro-*o*-phenylene-diamine, 4-chloro-*o*-phenylenediamine, 4-nitro-*o*-phenylenediamine and 4,5-dimethyl -*o*-phenyl-enediamine) with varieties of aromatic aldehydes in dimethylformamide (DMF), utilizing sodium metabisulfite ($Na_2S_2O_5$) as an oxidative/catalytic reagent (Khan *et al.*, 2012; Secci *et al*., 2012). They were obtained in moderate to high yields by a one-pot condensation reaction pathway which encompasses a two-step process, presumed to proceed through;

- the formation of sodium metasulfite adducts of the aldehydes, and
- oxidative cyclodehydrogenation of aniline Schiff's bases generated *in situ* (López *et al.,* 2009).

A general synthetic reaction route is represented in schemes **3.1(a** and **b)**, while a proposed reaction mechanism is presented in figures **3.1(a** and **b)**. Chemical shift values, δ (ppm) for both ^{1}H NMR and ^{13}C NMR were obtained in dimethylsulfoxide (DMSO-d_6) and tetramethyl-silane $(CH_3)_4Si$, (TMS) was used as internal standard. Ions produced in mass spectrometry (MS) analysis were separated according to their mass-to-charge ratios, (*m/z* values). While embeded in a solid disc-like potassium bromide (KBr), the compounds were analysed by infra-red (IR) spectroscopy for the various characteristic vibrational frequencies, $\bar{\upsilon}$ (cm^{-1}) of the functional groups present. Ultraviolet (UV) spectroscopic analysis was carried out after dissolving the compounds in methanol, to obtain wavelenghts of maximum absorptions, (λ_{max}). Other parameters such as the melting points and physical appearances of each synthesised compound were recorded. The experimental and percentage yields were also determined.

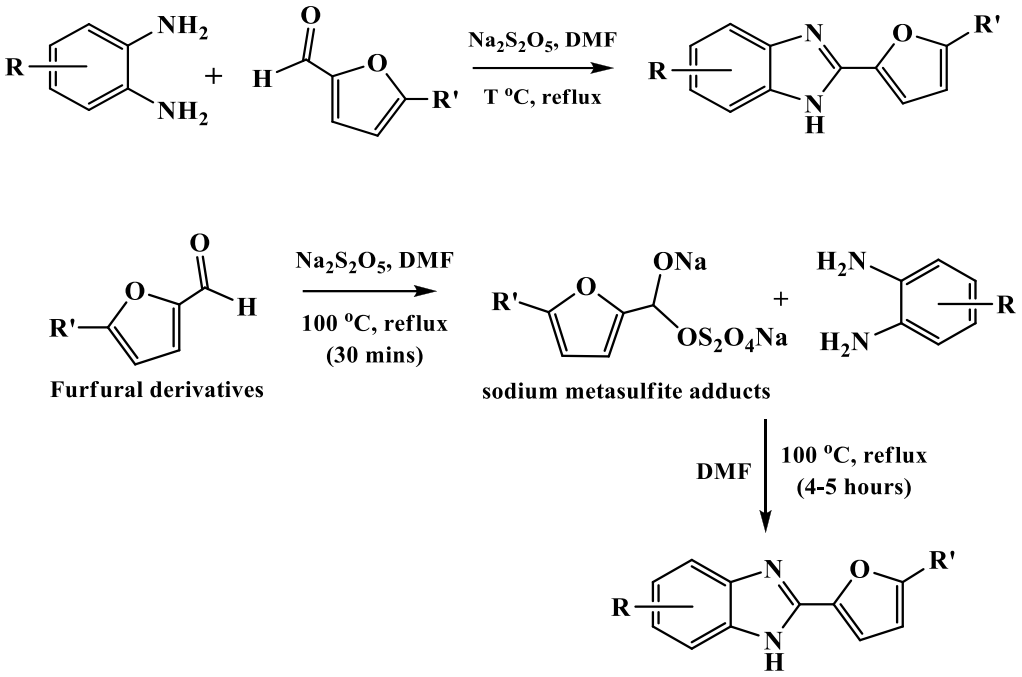

Scheme 3.1a. Synthesis of 2-substituted furan based benzimidazoles via sodium metasulfite adducts.

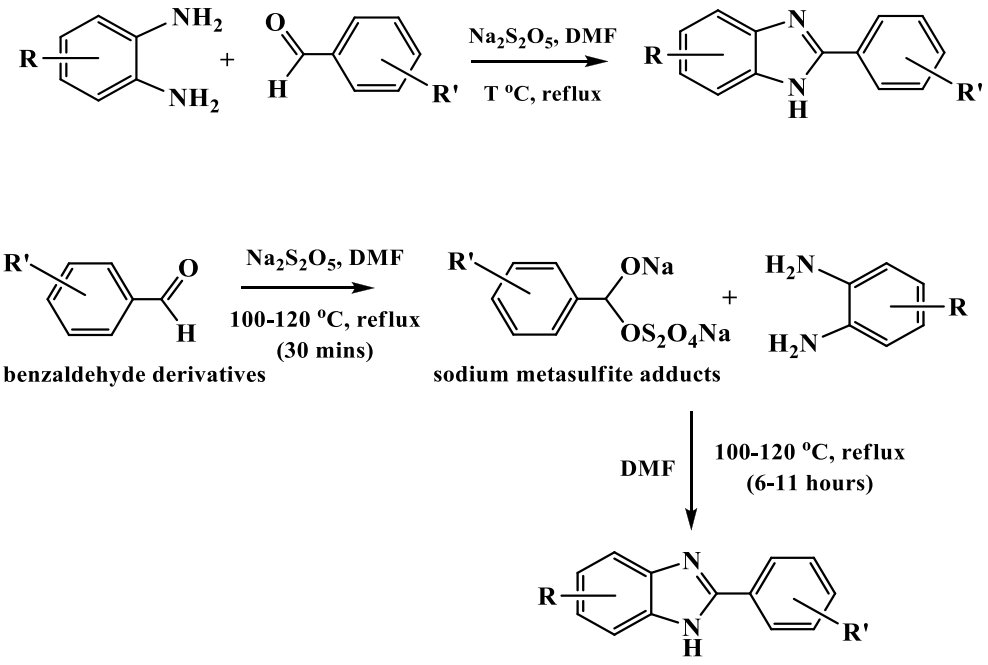

Scheme 3.1b. Synthesis of 2-substituted benzene based benzimidazoles (benzyl and phenyl products) via sodium metasulfite adducts.

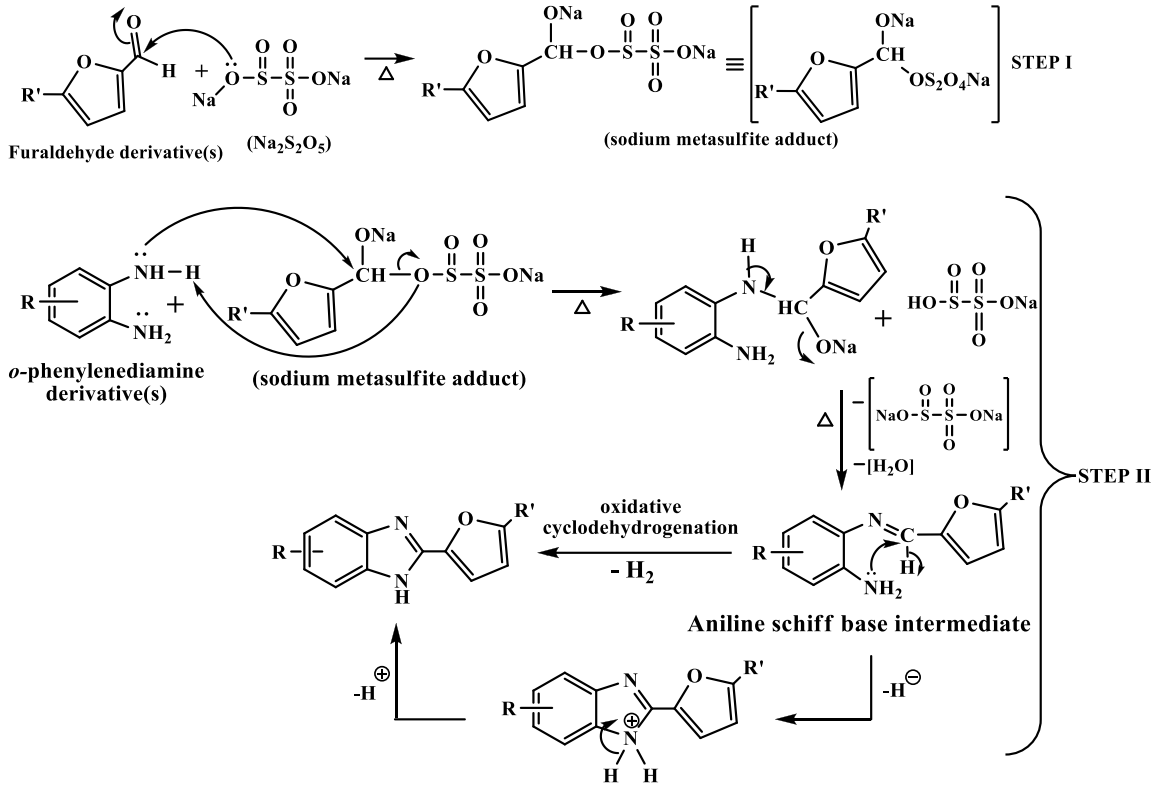

Figure 3.1a. Proposed mechanism of reaction involving a five-membered ring (furan based BZs)

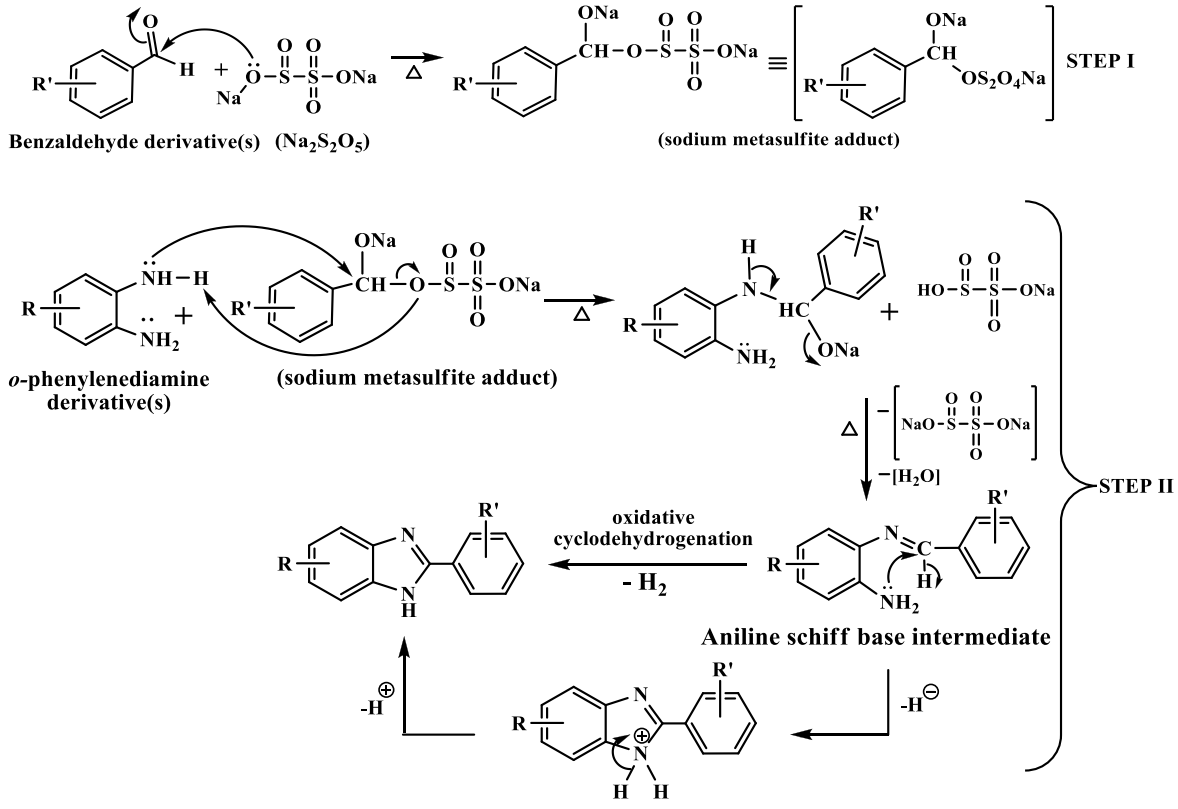

Figure 3.1b. Proposed mechanism of reaction involving a six-membered ring (benzene based BZs)

3.2.1 Synthesis of 2-(furan-2′-yl)-1*H*-benzo[*d*]imidazole (AKS-I-6)

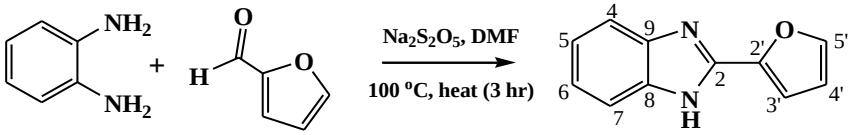

3.1 **3.2** **3.3**

In a round bottom flask (100 mL) fitted with a condenser and a magnetic stirrer, 2-furaldehyde **[3.2]** (0.083 mL, 1 mmol), sodium metabisulfite ($Na_2S_2O_5$) (0.19 g, 1 mmol) and N,N-dimethylformamide (DMF) (15 mL), were heated at 100 ^oC for 30 minutes. Into the reaction mixture after 30 minutes, *o*-phenylenediamine **[3.1]** (0.11 g, 1 mmol) was added and heated further for 2.5 hours. As the reaction progresses, it was monitored by TLC until completion. The resulting mixture after cooling to room temperature was added to cold water and the organic product extracted with dichloromethane (3 x 50 mL) from water. The separated organic layer was dried with sodium sulphate and the solvent evaporated to obtain a brown solid, with the code AKS-I-6 **[3.3]**, 54.8% yield (0.101 g), m.pt. 283-285 ^oC, R_f: 0.43 (hexane/ethyl acetate, 1:1). The followind chemical schift, $\boldsymbol{\delta_{H(ppm)}}$ (400 MHz, DMSO-d_6) values were obtained: 6.72 (1H, dd, $J_{4',3'}$ = 3.2 Hz, $J_{4',5'}$ = 1.6), 7.18 (1H, d, $J_{3',4'}$ = 3.2 Hz), 7.18 (2H, br s), 7.47 (1H, br s), 7.60 (1H, br s), 7.93 (1H, d, $J_{5',4'}$ = 1.2 Hz), 12.88 (1H, s); $\boldsymbol{\delta_{C(ppm)}}$ (100 MHz, DMSO-d_6): 112.25, 110.39, 121.86, 122.45, 143.57, 144.56, 145.53; **EI-MS** (*m/z* (relative abundance in %)): 52 (3), 64 (4), 92 (8), 102 (5), 129 (9), 156 (21), 184 [M^+] (100), 185 [M^++1] (12); **HREI-MS**: *m/z* calculated for $C_{11}H_8N_2O$ [M^+] is 184.0637, found 184.0639; **IR** ($\bar{\upsilon}$/cm^{-1}; KBr disc): ≈3400, 3069, 1621, 1521, 1490, 1227, 1012; **UV** (λ_{max}/nm; MeOH): 321, 306, 298, 250, 208.

3.2.2 Synthesis of 2-(5′-methylfuran-2′-yl)-1*H*-benzo[*d*]imidazole (AKS-I-7)

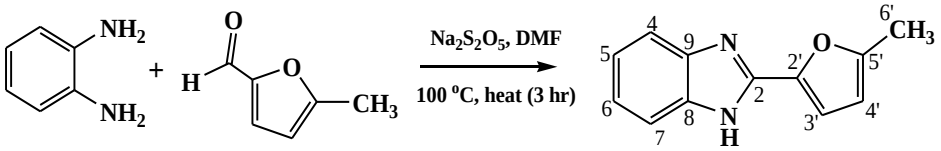

3.1 **3.4** **3.5**

A mixture of 5-methyl-furancarbaldehyde **[3.4]** (0.099 mL, 1 mmol), sodium metabisulfite (0.19 g, 1 mmol) and N,N-dimethylformamide (15 mL) was heated at 100 ^oC for 30 minutes in a round bottom flask (100 mL). Into the reaction mixture after 30 minutes, *o*-phenylenediamine **[3.1]** (0.11 g, 1 mmol) was added and heated further for

2.5 hours. Progress of reaction was monitored by TLC until completion. The resulting mixture after cooling to room temperature was added to cold water and freeze-dried. The brown solid product, AKS-I-7 **[3.5]**, obtained was worked-up with water and hot hexane in a 65.6% (0.130 g) yield, a m.pt. range of 274-276 ^{o}C and a 0.46 (hexane/ethyl acetate, 1:1) R_f value. $\boldsymbol{\delta_{H(ppm)}}$ (400 MHz, DMSO-d_6): 2.40 (3H, s), 6.34 (1H, s, $J_{4',3'}$ = 2.4 Hz), 7.08 (1H, d, $J_{3',4'}$ = 3.2 Hz), 7.16-7.18 (2H, m), 7.50-7.53 (2H, m); $\boldsymbol{\delta_{C(ppm)}}$ (75 MHz, DMSO-d_6): 13.41, 108.52, 111.68, 122.04, 143.63, 143.74, 153.77; **EI-MS** (*m/z* (relative abundance in %)): 63 (32), 90 (22), 155 (21), 169 (41), 183 (34), 198 [M^+] (100), 199 [M^++1] (14); **HREI-MS**: *m/z* calculated for $C_{12}H_{10}N_2O$ [M^+] is 198.0793, found 198.0800; **IR** ($\bar{\upsilon}$/cm^{-1}; KBr disc): 3447, 3054, 2953, 2805, 1632, 1570, 1423, 1275, 1020; **UV** (λ_{max}/nm; MeOH): 326, 311, 253, 248, 210.

3.2.3 Synthesis of 5-fluoro-2-(furan-2′-yl)-1*H*-benzo[*d*]imidazole (AKS-I-8)

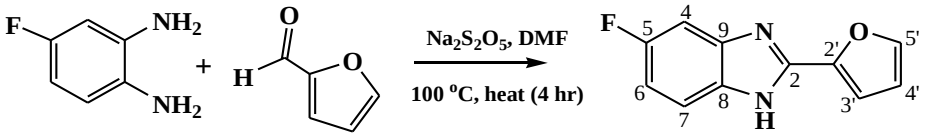

3.6 **3.2** **3.7**

In a round bottom flask (100 mL), a mixture of 2-furaldehyde **[3.2]** (0.083 mL, 1 mmol), N,N-dimethylformamide (15 mL) and sodium metabisulfite (0.19 g, 1 mmol) was heated at 100 ^{o}C for 30 minutes. Into the reaction mixture after 30 minutes, 4-fluoro-*o*-phenylenediamine **[3.6]** (0.13 g, 1 mmol) was also added and heated further for 3.5 hours. Progress of reaction was monitored by TLC until completion. The resulting mixture after cooling to room temperature was added to cold water and freeze-dried. The solid product obtained was worked-up with water and hot hexane to afford the compound coded AKS-I-8 **[3.7]** (a brown solid), 50.9% (0.103 g) yield, with a m.pt. of 194-197 ^{o}C and R_f: 0.47 (hexane/ethyl acetate, 1:1). $\boldsymbol{\delta_{H(ppm)}}$ (400 MHz, DMSO-d_6): 6.75 (1H, dd, $J_{4',3'}$ = 3.2 Hz, $J_{4',5'}$ = 1.6 Hz), 7.11 (1H, dt, $J_{6,7}$ = 10.0 Hz, $J_{6,4}$ = 2.4 Hz), 7.24 (1H, d, $J_{3',4'}$ = 3.2 Hz), 7.38 (1H, dd, $J_{7,6}$ = 9.6 Hz, $J_{7,F\text{-}5}$ = 2.0 Hz), 7.54-7.57 (1H, m), 7.97 (1H, s); $\boldsymbol{\delta_{C(ppm)}}$ (100 MHz, DMSO-d_6): 110.68, 112.28, 144.71, 145.20, 157.50, 159.84; **EI-MS** (*m/z* (relative abundance in %)): 81 (18), 108 (39), 121 (30), 147 (62), 174 (71), 202 [M^+] (100), 203 [M^++1] (38); **HREI-MS**: *m/z* calculated for $C_{11}H_7FN_2O$ [M^+] is 202.0542, found 202.0539. **IR** ($\bar{\upsilon}$/cm^{-1}; KBr disc): ≈3400, 3120, 1639, 1523, 1449, 1230, 1142; **UV** (λ_{max}/nm; MeOH): 323, 309, 248, 208.

3.2.4 Synthesis of 5-fluoro-2-(5′-methylfuran-2′-yl)-1*H*-benzo[*d*]imidazole (AKS-I-9)

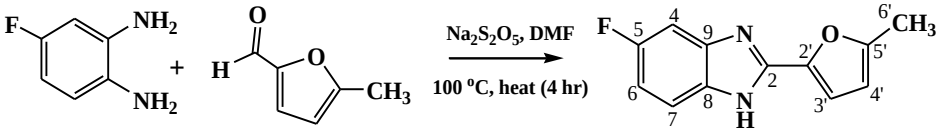

3.6 **3.4** **3.8**

In the solvent N,N-dimethylformamide (15 mL), 5-methyl-furancarbaldehyde **[3.4]** (0.099 mL, 1 mmol) and sodium metabisulfite (0.19 g, 1 mmol) were heated at 100 °C for 30 minutes in a round bottom flask (100 mL). After 30 minutes of reaction, 4-fluoro-*o*-phenylenediamine **[3.6]** (0.13 g, 1 mmol) was added into the mixture and heated further for 3.5 hours. Progress of reaction was monitored by TLC until completion. The resulting mixture after cooling to room temperature was added to cold water and freeze-dried. The brown precipitate obtained was worked-up with water and hot hexane to afford the solid compound, AKS-I-9 **[3.8]**, with a yield of 69.4% (0.150 g), m.pt. 148-151 °C and a 0.50 (hexane/ethyl acetate, 1:1) R_f value. $\boldsymbol{\delta_{H(ppm)}}$ (400 MHz, DMSO-d_6): 2.41 (3H, s), 6.37 (1H, d, $J_{4',3'}$ = 2.4 Hz), 7.10 (1H, dt, $J_{6,7}$ = 10.0 Hz, $J_{6,4}$ = 2.4 Hz), 7.15 (1H, d, $J_{3',4'}$ = 3.2 Hz), 7.36 (1H, dd, $J_{7,6}$ = 9.2 Hz, $J_{7,F\text{-}5}$ = 2.0 Hz), 7.52-7.55 (1H, m); $\boldsymbol{\delta_{C(ppm)}}$ (125 MHz, DMSO-d_6): 13.49, 108.87, 110.45, 110.65, 112.84, 144.58, 154.56, 157.86, 159.74; **EI-MS** (*m/z* (relative abundance in %)): 69 (37), 91 (8), 108 (18), 147 (16), 173 (24), 187 (50), 201 (32), 216 [M^+] (100), 217 [M^++1] (11); **HREI-MS**: *m/z* calculated for $C_{12}H_9FN_2O$ [M^+] is 216.0699, found 216.0704; **IR** ($\bar{\upsilon}$/cm^{-1}; KBr disc): ≈3400, 3120, 1639, 1523, 1449, 1230, 1142; **UV** (λ_{max}/nm; MeOH): 309, 301, 255, 213.

3.2.5 Synthesis of 5-chloro-2-(furan-2′-yl)-1*H*-benzo[*d*]imidazole (AKS-I-10)

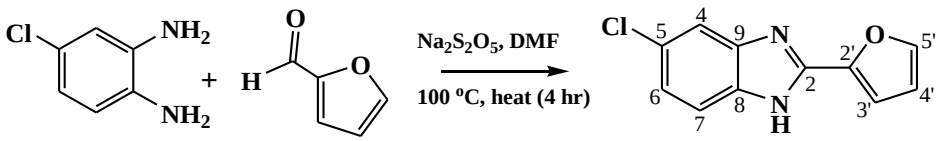

3.9 **3.2** **3.10**

In a round bottom flask (100 mL) supplied with a reflux set-up, 2-furaldehyde **[3.2]** (0.083 mL, 1 mmol), N,N-dimethylformamide (15 mL) and sodium metabisulfite (0.19 g, 1 mmol) were heated at 100 °C for 30 minutes. After 30 minutes of reaction, 4-chloro-*o*-phenylenediamine **[3.9]** (0.14 g, 1 mmol) was added and heated further for 3.5 hours. Progress of reaction was monitored by TLC until completion. The resulting mixture after cooling to room temperature was added to cold water and freeze-dried. The dark-

brown solid product obtained was worked-up with water and hot hexane to give the compound AKS-I-10 **[3.10]**, 0.198 g (90.6% yield), a m.pt. range of 109-111 ^{o}C and a R_f: 0.49 (hexane/ethyl acetate, 1:1). $\boldsymbol{\delta_{H(ppm)}}$ (400 MHz, DMSO-d_6): 6.75 (1H, dd, $J_{4',3'}$ = 3.2 Hz, $J_{4',5'}$ = 1.6 Hz), 7.21-7.24 (2H, m), 7.57 (1H, d $J_{7,6}$ = 8.4 Hz), 7.60 (1H, s), 7.97 (1H, d, $J_{5',4'}$ = 1.2 Hz); **EI-MS** (*m/z* (relative abundance in %)): 63 (27), 109 (8), 124 (18), 155 (65), 190 (26), 218 [M^+] (100), 220 [M^++2] (33); **HREI-MS**: *m/z* calculated for $C_{11}H_7ClN_2O$ [M^+] is 218.0247, found 218.0241; **IR** ($\bar{\upsilon}$/cm^{-1}; KBr disc): ≈3400, 3118, 1636, 1519, 1408, 1231, 1018, 1063; **UV** (λ_{max}/nm; MeOH): 326, 311, 253, 249, 207.

3.2.6 Synthesis of 5-chloro-2-(5′-methylfuran-2′-yl)-1*H*-benzo[*d*]imidazole (AKS-I-11)

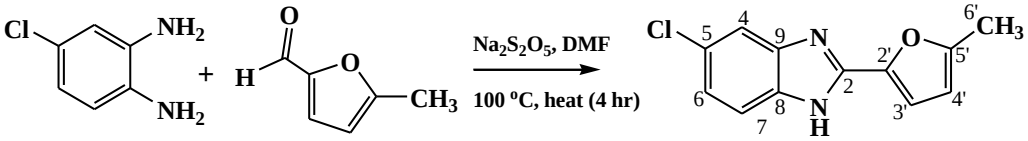

3.9 **3.4** **3.11**

5-Methyl-furancarbaldehyde **[3.4]** (0.099 mL, 1 mmol) and sodium metabisulfite (0.19 g, 1 mmol) were heated at 100 ^{o}C for 30 minutes in N,N-dimethylformamide (15 mL) solvent. Into the reaction mixture after 30 minutes, 4-chloro-*o*-phenylenediamine **[3.9]** (0.14 g, 1 mmol) was added and heated further for 3.5 hours. Progress of reaction was monitored by TLC until completion. The resulting mixture after cooling to room temperature was added to cold water and freeze-dried. The dark-brown solid product obtained was worked-up with water and hot hexane to afford the compound AKS-I-11 **[3.11]**, with a yield of 78.2% (0.182 g), m.pt. 163-165 ^{o}C and R_f: 0.51 (hexane/ethyl acetate, 1:1). $\boldsymbol{\delta_{H(ppm)}}$ (400 MHz, DMSO-d_6): 6.35 (1H, d, $J_{4',3'}$ = 2.4 Hz), 7.11 (1H, d, $J_{3',4'}$ = 3.6 Hz), 7.20 (1H, dd, $J_{6,7}$ = 8.8 Hz, $J_{6,4}$ = 2.0 Hz), 7.52 (1H, d, $J_{7,6}$ = 8.4 Hz), 7.55 (1H, s); **EI-MS** (*m/z* (relative abundance in %)): 95 (11), 116 (8), 189 (17), 203 (23), 217 (25), 232 [M^+] (100), 234 [M^++2] (48); **HREI-MS**: *m/z* calculated for $C_{12}H_9ClN_2O$ [M^+] is 232.0403, found 232.0383. **IR** ($\bar{\upsilon}$/cm^{-1}; KBr disc): ≈3400, 3007, 2918, 2834, 1630, 1569, 1418, 1212, 1019, 1059; **UV** (λ_{max}/nm; MeOH): 311, 277, 257, 214.

3.2.7 Synthesis of 2-(furan-2′-yl)-5,6-dimethyl-1*H*-benzo[*d*]imidazole (AKS-I-12)

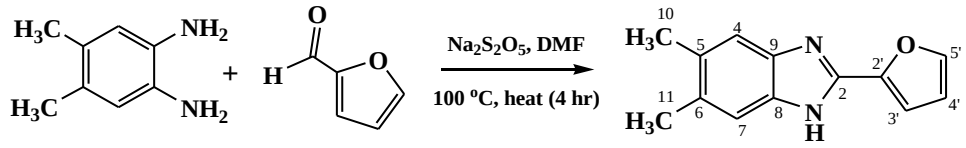

3.12 **3.2** **3.13**

Within a 100 mL round bottom flask, 2-furaldehyde **[3.2]** (0.083 mL, 1 mmol), N,N-dimethylformamide (15 mL) and sodium metabisulfite (0.19 g, 1 mmol) were heated at 100 °C for 30 minutes. After 30 minutes of reaction, 4,5-dimethyl-1,2-phenylenediamine **[3.12]** (0.14 g, 1 mmol) was added and heated further for 3.5 hours. Progress of reaction was monitored by TLC until completion. The resulting mixture after cooling to room temperature was added to cold water and freeze-dried. The product obtained was worked-up with water and hot hexane to afford the brown solid, AKS-I-12 **[3.13]**, 0.131 g (61.7% yield), m.pt. 166-168 °C and a 0.41 (hexane/ethyl acetate, 1:1) R_f value. $\boldsymbol{\delta_{H(ppm)}}$ (400 MHz, DMSO-d_6): 2.28 (3H, s), 2.30 (3H, s), 6.69 (1H, dd, $J_{4',3'}$ = 3.2 Hz, $J_{4',5'}$ = 2.0 Hz), 7.10 (1H, d, $J_{3',4'}$ = 3.2 Hz), 7.23 (1H, s), 7.36 (1H, s), 7.88 (1H, s, $J_{5',3'}$ = 0.8 Hz), 12.60 (1H, s); **EI-MS** (*m/z* (relative abundance in %)): 65 (38), 81 (54), 91 (50), 106 (15), 169 (26), 183 (38), 197 (73), 212 [M^+] (100), 213 [M^++1] (47); **HREI-MS**: *m/z* calculated for $C_{13}H_{12}N_2O$ [M^+] is 212.0950, found 212.0948. **IR** ($\bar{\upsilon}$/cm^{-1}; KBr disc): ≈3400, 3120, 2926, 2856, 1643, 1524, 1448, 1233, 1013; **UV** (λ_{max}/nm; MeOH): 312, 250, 213.

3.2.8 Synthesis of 5,6-dimethyl-2-(5′-methylfuran-2′-yl)-1*H*-benzo[*d*]imidazole (AKS-I-13)

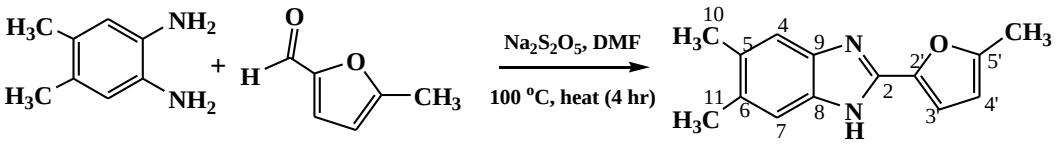

3.12 **3.4** **3.14**

A mixture of 5-methyl-furancarbaldehyde **[3.4]** (0.099 mL, 1 mmol) and sodium metabisulfite (0.19 g, 1 mmol) in N,N-dimethylformamide (15 mL) was heated at 100 °C in a round bottom flask (100 mL) for 30 minutes. Into the reaction mixture after 30 minutes, 4,5-dimethyl-1,2-phenylenediamine **[3.12]** (0.14 g, 1 mmol) was added and heated further for 3.5 hours. Progress of reaction was monitored by TLC until completion. The resulting mixture after cooling to room temperature was added to cold water and freeze-dried. The solid dark-brown product obtained was worked-up with

water and hot hexane to afford the compound, AKS-I-13 **[3.14]**, 0.141 g (62.3% yield), m.pt. 225-227 ^{o}C and a R_f value of 0.43 (hexane/ethyl acetate, 1:1). The following are the $\boldsymbol{\delta_{H(ppm)}}$ (400 MHz, DMSO-d_6) values: 2.30 (6H, s), 2.40 (3H, s), 6.35 (1H, d, $J_{4',3'}$ = 2.4 Hz), 7.09 (1H, d, $J_{3',4'}$ = 2.8 Hz), 7.31 (2H, s); **EI-MS** (*m/z* (relative abundance in %)): 69 (49), 91 (38), 105 (16), 113 (27), 169 (18), 183 (34), 197 (20), 211 (64), 226 [M^+] (100), 227 [M^++1] (42); **HREI-MS**: *m/z* calculated for $C_{14}H_{14}N_2O$ [M^+] is 226.1106, found 226.1091. **IR** ($\bar{\upsilon}$/cm^{-1}; KBr disc): 3407, 3028, 2917, 2851, 1644, 1570, 1439, 1207, 1018; **UV** (λ_{max}/nm; MeOH): 325, 312, 258, 214.

3.2.9 Synthesis of 2-(furan-2′-yl)-5-nitro-1*H*-benzo[*d*]imidazole (AKS-I-14)

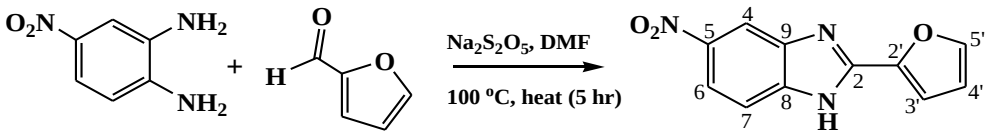

3.15 **3.2** **3.16**

In a 100 mL round bottom flask, 2-furaldehyde **[3.2]** (0.083 mL, 1 mmol), N,N-dimethylformamide (15 mL) and sodium metabisulfite (0.19 g, 1 mmol) were heated at 100 ^{o}C. Into this reaction mixture after 30 minutes, 4-nitro-*o*-phenylenediamine **[3.15]** (0.15 g, 1 mmol) was added and heated further for 4.5 hours. Reaction progress was monitored by TLC until completion. The product obtained after cooling to room temperature resulted in a precipitate on addition to cold water, which was then filtered, dried and further worked-up with hot hexane to afford the compound, AKS-I-14 **[3.16]** (a brown solid) with a yield of 69.4% (0.159 g), m.pt. 219-220 ^{o}C and a R_f of 0.37 (hexane/ethyl acetate, 1:1). $\boldsymbol{\delta_{H(ppm)}}$ (400 MHz, DMSO-d_6): 6.79 (1H, dd, $J_{4',3'}$ = 3.2 Hz, $J_{4',5'}$ = 1.6 Hz), 7.35 (1H, d, $J_{3',4'}$ = 3.2 Hz), 7.73 (1H, d, $J_{7,6}$ = 8.8 Hz), 8.04 (1-H, s), 8.13 (1H, dd, $J_{6,4}$ = 2.0 Hz, $J_{6,7}$ = 8.8 Hz), 8.42 (1H, s); **EI-MS** (*m/z* (relative abundance in %)): 63 (57), 78 (66), 81 (54), 90 (29), 101 (26), 128 (28), 156 (60), 183 (62), 199 (46), 229 [M^+] (100), 230 [M^++1] (31); **HREI-MS**: *m/z* calculated for $C_{11}H_7N_3O_3$ [M^+] is 229.0487, found 229.0484. **IR** ($\bar{\upsilon}$/cm^{-1}; KBr disc): 3374, 3121, 1633, 1515, 1471, 1340, 1235, 1067; **UV** (λ_{max}/nm; MeOH): 338, 278, 208.

3.2.10 Synthesis of 2-(3′-(benzyloxy)-4′-methoxyphenyl)-1*H*-benzo[*d*]imidazole (AKS-I-34)

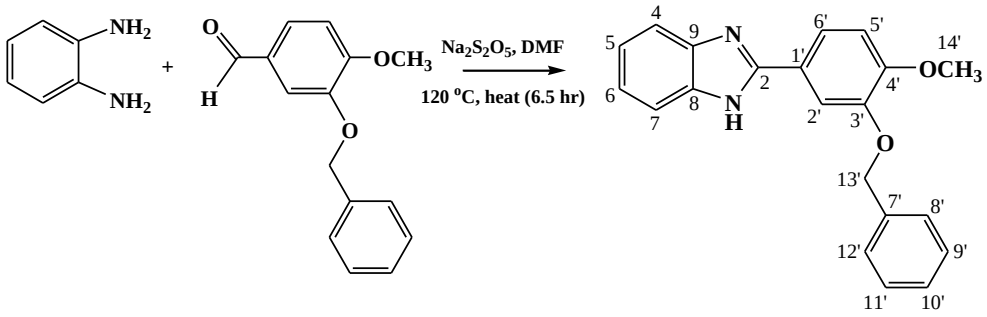

3.1 **3.17** **3.18**

A mixture of 3-benzyloxy-4-methoxy-benzaldehyde **[3.17]** (0.24 g, 1 mmol), sodium metabisulfite, $Na_2S_2O_5$ (0.19 g, 1 mmol) and 15 mL of N,N-dimethylformamide (DMF) at 100 °C were heated in a round bottom flask (100 mL) for 30 minutes. After 30 minutes of reaction, *o*-phenylenediamine **[3.1]** (0.11 g, 1 mmol) was added to the resulting reaction mixture and heated further for 6.5 hours. Reaction progress was monitored by TLC until it was completed. The precipitate formed after pouring into iced-water was filtered, dried and further worked-up with hot hexane to afford a white solid compound, AKS-I-34 **[3.18]** with 89.0% (0.294 g) yield, m.pt. 116-119 °C and a 0.44 (hexane/ethyl acetate, 1:1) R_f value. The following $\boldsymbol{\delta_{H(ppm)}}$ (400 MHz, DMSO-d_6) were obtained: 3.85 (3H, s), 5.19 (2H, s), 7.20 (1H, d $J_{5',6'}$ = 8.4 Hz), 7.21-7.23 (2H, m), 7.36 (1H, t, $J_{10',11'}$ = $J_{10',9'}$ = 7.6 Hz), 7.43 (2H, t, $J_{11',10'}$ = $J_{9',10'}$ = 7. 6 Hz), 7.51 (2H, d, $J_{12',11'}$ = $J_{8',9'}$ = 7.2 Hz), 7.58-7.60 (2H, m), 7.78 (1H, dd, $J_{6',5'}$ = 8.4 Hz), 7.89 (1H, d, $J_{2',6'}$ = 1.6 Hz); $\boldsymbol{\delta_{C(ppm)}}$ (75 MHz, DMSO-d_6): 55.76, 70.09, 111.58, 112.24, 114.57, 120.11, 121.43, 122.43, 127.92, 127.96, 128.44, 136.77, 148.00, 150.98, 151.08; **EI-MS** (*m/z* (relative abundance in %)): 18 (28), 28 (54), 65 (8), 91 (100), 211 (12), 239 (87), 301 (6), 330 [M^+] (52), 331 [M^++1] (12); **HREI-MS**: *m/z* calculated for $C_{21}H_{18}N_2O_2$ [M^+] is 330.148, found 330.1350. **IR** ($\bar{\upsilon}$/cm^{-1}; KBr disc): 3419, 3063, 2927, 1601, 1505, 1450, 1265, 1018; **UV** (λ_{max}/nm; MeOH): 311, 222, 214.

3.2.11 Synthesis of 2-(3′-(benzyloxy)-4′-methoxyphenyl)-5-fluoro-1*H*-benzo[*d*] imidazole (AKS-I-35)

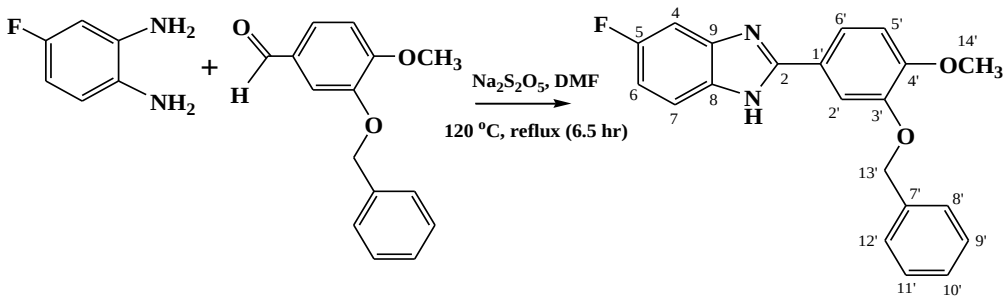

3.6 **3.17** **3.19**

In a 100 mL round bottom flask, a mixture of 3-benzyloxy-4-methoxybenzaldehyde **[3.17]** (0.24 g, 1 mmol), N,N-dimethylformamide (15 mL) and sodium metabisulfite (0.19 g, 1 mmol) were heated at 100 °C for 30 minutes. 4-Fluoro-*o*-phenylenediamine **[3.6]** (0.13 g, 1 mmol) was added to the resulting reaction mixture after 30 minutes and heated further for 6 hours. Reaction progress was monitored by TLC until it was completed. The precipitate formed after pouring into iced-water was filtered, dried and further worked-up with hot hexane to afford the brown solid, AKS-I-35 **[3.19]**, 91.0% (0.317 g) yield, m.pt. 176-178 °C and a R_f of 0.51 (hexane/ethyl acetate, 1:1). The following are the $\boldsymbol{\delta_{H(ppm)}}$ (400 MHz, DMSO-d_6) values obtained: 3.85 (3H, s), 5.18 (2H, s), 7.10 (1H, dt, $J_{6,4}$ = 2.0 Hz, $J_{6,F-5}$ = 8.4 Hz), 7.20 (1H, d, $J_{5',6'}$ = 8.8 Hz), 7.36 (1H, t, $J_{10',11'} = J_{10',9'}$ = 7.2 Hz), 7.41 (1H, d, $J_{7,6}$ = 7.6 Hz), 7.43 (2H, t, $J_{11',10'} = J_{9',10'}$ = 7.2 Hz), 7.51 (2H, d, $J_{12',11'} = J_{8',9'}$ = 7.2 Hz), 7.56-7.60 (1H, m), 7.77 (1H, dd, $J_{6',5'}$ = 8.4 Hz), 7.87 (1H, d, $J_{2',6'}$ = 1.6 Hz); $\boldsymbol{\delta_{C(ppm)}}$ (75 MHz, DMSO-d_6): 55.7, 70.14, 100.68, 101.06, 110.27, 110.61, 111.72, 112.30, 115.12, 120.21, 121.02, 127.83, 127.90, 128.38, 136.71, 148.00, 151.29, 152.29, 157.17, 160.30; **EI-MS** (*m/z* (relative abundance in %)): 18 (13), 65 (6), 91 (100), 186 (6), 227 (9), 257 (77), 348 [M^+] (46), 349 [M^++1] (11),; **HREI-MS**: *m/z* calculated for $C_{21}H_{17}FN_2O_2$ [M^+] is 348.1274, found 348.1286; **IR** ($\bar{\upsilon}$/cm^{-1}; KBr disc): 3418, ≈3050, 2924, 2853, 1631, 1600, 1508, 1447, 1267, 1025, 1145; **UV** (λ_{max}/nm; MeOH): 311, 250, 222.

3.2.12 Synthesis of 2-(3′-(benzyloxy)-4′-methoxyphenyl)-5-chloro-1*H*-benzo[*d*] imidazole (AKS-I-36)

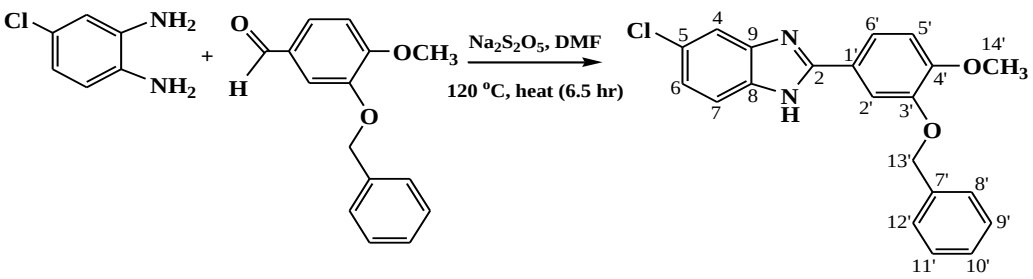

3.9 **3.17** **3.20**

At 100 °C, a mixture of 3-benzyloxy-4-methoxybenzaldehyde **[3.17]** (0.24 g, 1 mmol), N,N-dimethylformamide (15 mL) and sodium metabisulfite (0.19 g, 1 mmol) were heated for 30 minutes in a 100 mL round bottom flask. 4-Chloro-*o*-phenylenediamine **[3.9]** (0.14 g, 1 mmol) was added to the resulting reaction mixture after 30 minutes and heated further for 6 hours. Reaction progress was monitored by TLC until it was completed. The precipitate formed after pouring into iced-water was filtered, dried and further worked-up with hot hexane to afford a brown compound with the code AKS-I-36 **[3.20]**, 94.0% (0.343 g) yield, m.pt. 112-114 °C and a 0.55 (hexane/ethyl acetate, 1:1) R_f value. Obtained are the following $\boldsymbol{\delta_{H(ppm)}}$ (400 MHz, DMSO-d_6) values: 3.85 (3H, s), 5.18 (2H, s), 7.19 (1H, d, $J_{5',6'}$ = 8.4 Hz), 7.24 (1H, dd, $J_{6,4}$ = 1.6 Hz, $J_{6,7}$ = 8.4 Hz), 7.36 (1H, t, $J_{10',11'} = J_{10',9'}$ = 7.2 Hz), 7.43 (2H, t, $J_{11',12'} = J_{9',8'}$ = 7.2 Hz), 7.51 (2H, d, $J_{12',11'} = J_{8',9'}$ = 7.2 Hz), 7.59 (1H, d, $J_{7,6}$ = 8.4 Hz), 7.62 (1H, s), 7.77 (1H, dd, $J_{6',2'}$ = 1.6 Hz, $J_{6',5'}$ = 8.4 Hz), 7.87 (1H, d, $J_{2',6'}$ = 1.6 Hz); $\boldsymbol{\delta_{C(ppm)}}$ (75 MHz, DMSO-d_6): 55.75, 70.08, 111.60, 112.22, 120.24, 121.29, 122.46, 126.52, 127.92, 127.96, 128.43, 136.75, 148.00, 151.23, 152.50; **EI-MS** (*m/z* (relative abundance in %)): 18 (7), 65 (18), 91 (100), 245 (24), 259 (11), 273 (91), 335 (11), 364 [M^+] (81), 366 [M^++2] (48); **HREI-MS**: *m/z* calculated for $C_{21}H_{17}ClN_2O_2$ [M^+] is 364.0979, found 364.0983; **IR** ($\bar{\upsilon}$/cm^{-1}; KBr disc): 3418, 3067, 2929, 1603, 1502, 1452, 1267, 1019, 1058; **UV** (λ_{max}/nm; MeOH): 316, 226.

3.2.13 Synthesis of 2-(3′-(benzyloxy)-4′-methoxyphenyl)-5-nitro-1*H*-benzo[*d*] imidazole (AKS-I-37)

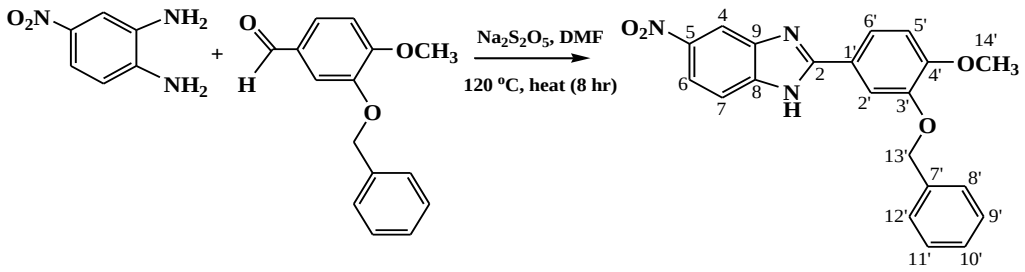

3.15 **3.17** **3.21**

In a 100 mL round bottom flask, a mixture of 3-benzyloxy-4-methoxybenzaldehyde **[3.17]** (0.24 g, 1 mmol), N,N-dimethylformamide (15 mL) and sodium metabisulfite (0.19 g, 1 mmol) were heated at 100 °C for 30 minutes. To the resulting reaction mixture after 30 minutes, 4-nitro-*o*-phenylenediamine **[3.15]** (0.15 g, 1 mmol) was added and heated for another 6 hours. Monitoring the reaction progress by TLC, product was eventually achieved after 8 hours. The solid precipitate formed after pouring the mixture into iced-water was filtered, dried and further worked-up with hot hexane to afford an orange compound, AKS-I-37 **[3.21]** with a yield of 90.6% (0.340 g), m.pt. 110-113 °C and R_f: 0.45 (hexane/ethyl acetate, 1:1). The following $\boldsymbol{\delta_{H(ppm)}}$ (400 MHz, DMSO-d_6) were obtained: 3.86 (3H, s), 5.20 (2H, s), 7.22 (1H, d, $J_{5',6'}$ = 8.4 Hz), 7.36 (1H, t, $J_{10',11'} = J_{10',9'}$ = 7.2 Hz), 7.43 (2H, t, $J_{11',12'} = J_{9',8'}$ = 7.2 Hz), 7.51 (2H, d, $J_{12',11'} = J_{8',9'}$ = 7.2 Hz), 7.74 (1H, d, $J_{7,6}$ = 8.8 Hz), 7.83 (1H, dd, $J_{6',5'}$ = 8.4 Hz, $J_{6',2'}$ = 2.0 Hz), 7.92 (1H, d, $J_{2',6'}$ = 1.6 Hz), 8.12 (1H, dd, $J_{6,4}$ = 2.0 Hz, $J_{6,7}$ = 8.8 Hz), 8.42 (1H, s); $\boldsymbol{\delta_{C(ppm)}}$ (75 MHz, DMSO-d_6): 55.76, 70.14, 111.90, 112.27, 117.77, 120.63, 121.28, 127.83, 127.91, 128.37, 136.71, 142.52, 148.03, 151.62, 155.86; **EI-MS** (*m/z* (relative abundance in %)): 18 (18), 28 (30), 65 (10), 91 (100), 210 (8) 227 (9), 254 (9), 284 (87), 345 (13), 375 [M^+] (61), 376 [M^++1] (14); **HREI-MS**: *m/z* calculated for $C_{21}H_{17}N_3O_4$ [M^+] is 375.1219, found 375.1233; **IR** ($\bar{\upsilon}$/cm^{-1}; KBr disc): 3325, 3072, 2931, 1600, 1504, 1338, 1449, 1268, 1019; **UV** (λ_{max}/nm; MeOH): 218, 230, 282, 344.

3.2.14 Synthesis of 2-(3′-(benzyloxy)-4′-methoxyphenyl)-5,6-dimethyl-1*H*-benzo [*d*]imidazole (AKS-I-38)

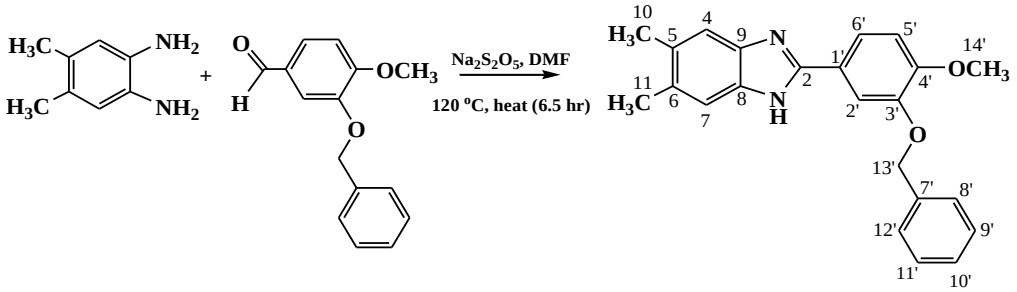

3.12 **3.17** **3.22**

In a 100 mL round bottom flask, a mixture of 3-benzyloxy-4-methoxybenzaldehyde **[3.17]** (0.24 g, 1 mmol), N,N-dimethylformamide (15 mL) and sodium metabisulfite (0.19 g, 1 mmol) was heated at 100 °C. Into the resulting reaction mixture after 30 minutes, 4,5-dimethyl-*o*-phenylenediamine **[3.12]** (0.14 g, 1 mmol) was added and heated within another 6 hours. Reaction progress was monitored by TLC until it was completed. The precipitate formed after adding the product from the reaction mixture into iced-water was filtered, dried and further worked-up with hot hexane to afford a white solid compound, AKS-I-38 **[3.22]**, with a yield of 97.6% (0.350 g), a m.pt. 106-109 °C and R_f value of 0.45 (hexane/ethyl acetate, 1:1). $\boldsymbol{\delta_{H(ppm)}}$ (400 MHz, DMSO-d_6): 2.31 (6H, s), 3.84 (3H, s), 5.18 (2H, s), 7.33 (2H, s), 7.16 (1H, d, $J_{5',6'}$ = 8.8 Hz), 7.36 (1H, t, $J_{10',11'} = J_{10',9'}$ = 7.6 Hz), 7.43 (2H, t, $J_{11',12'} = J_{9',8'}$ = 7.2 Hz, $J_{11',10'} = J_{9',10'}$ = 7.6 Hz), 7.51 (2H, d, $J_{12',11'} = J_{8',9'}$ = 7.2 Hz), 7.73 (1H, dd, $J_{6',2'}$ = 1.2 Hz, $J_{6',5'}$ = 8.4 Hz), 7.85 (1H, d, $J_{2',6'}$ = 1.6 Hz); **EI-MS** (*m/z* (relative abundance in %)): 18 (43), 91 (58), 239 (28), 253 (14), 267 (100), 329 (8), 358 [M^+] (77), 359 [M^++1] (24); **HREI-MS**: *m/z* calculated for $C_{23}H_{22}N_2O_2$ [M^+] is 358.1681, found 358.1690; **IR** ($\bar{\upsilon}$/cm^{-1}; KBr disc): 3416, 3160, 2925, 1606, 1504, 1455, 1263, 1019; **UV** (λ_{max}/nm; MeOH): 316, 253, 228, 222.

3.2.15 Synthesis of 2-(2′-(benzyloxy)phenyl)-5-fluoro-1*H*-benzo[*d*]imidazole (AKS - I-39)

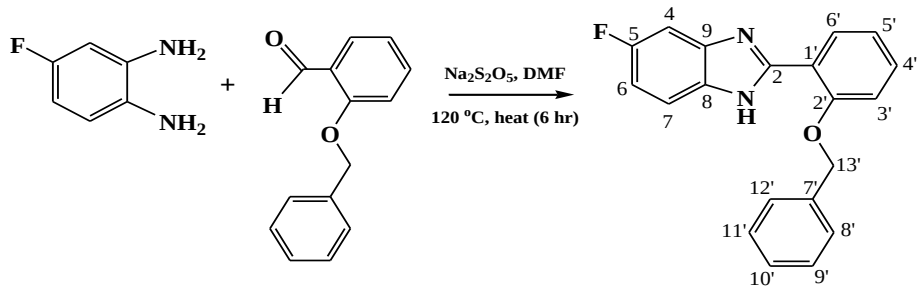

3.6 **3.23** **3.24**

2-Benzyloxybenzaldehyde **[3.23]** (0.21 g, 1 mmol), N,N-dimethylformamide (15 mL) and sodium metabisulfite (0.19 g, 1 mmol) were heated in a round bottom flask (100 mL) at 120 °C for 30 minutes. Into the reaction mixture after 30 minutes, 4-fluoro-*o*-phenylenediamine **[3.6]** (0.13 g, 1 mmol) was added and heated further for 5.5 hours. Progress of reaction was monitored by TLC until completion. The resulting mixture after cooling to room temperature was added to cold water and the precipitate formed was filtered, dried and worked-up with hot hexane to afford the compound coded AKS-I-39 **[3.24]** (brown solid), 54.3% (0.173 g) yield, with a m.pt. of 125-127 °C and R_f of 0.68 (hexane/ethyl acetate, 1:1). Obtained were the following chemical shift, $\boldsymbol{\delta_{H(ppm)}}$ (400 MHz, DMSO-d_6) values: 5.51 (2H, s), 7.09 (2H, t, $J_{6,7}$ = 7.2 Hz, $J_{5',6'}$ = 8.0 Hz), 7.20 (1H, d, $J_{3',4'}$ = 8.4 Hz), 7.28 (1H, t, $J_{10',9'}$ = 7.2 Hz), 7.32-7.38 (3H, m), 7.41 (1H, d, $J_{7,6}$ = 7.2 Hz), 7.48 (2H, d, $J_{12',11'} = J_{8',9'}$ = 7.6 Hz), 7.61-7.64 (1H, m), 8.24 (1H, dd, $J_{6',5'}$ = 8.0 Hz), ≈12.50 (1H, br s); **EI-MS** (*m/z* (relative abundance in %)): 65 (13), 77 (5),90 (100), 199 (16), 212 (28), 227 (11), 301 (35), 318 [M^+] (78), 319 [M^++1] (22); **HREI-MS**: *m/z* calculated for $C_{20}H_{15}FN_2O$ [M^+] is 318.1168, found 318.1158; **IR** ($\bar{\upsilon}$/cm^{-1}; KBr disc): 3413, 3062, 2925, 2876, 1629, 1593, 1528, 1463, 1234, 1007, 1131; **UV** (λ_{max}/nm; MeOH): 313, 295, 214.

3.2.16 Synthesis of 2-(2′-(benzyloxy)phenyl)-5-chloro-1*H*-benzo[*d*]imidazole (AKS -I-40)

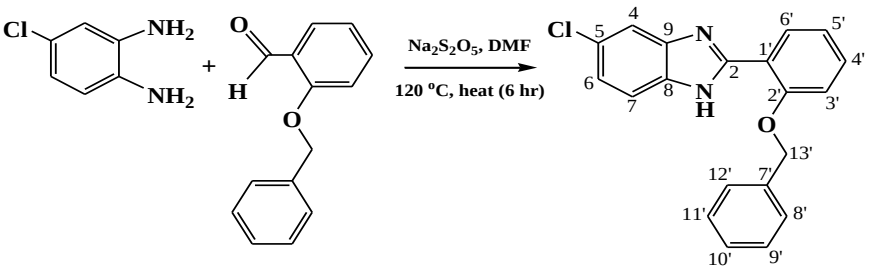

3.9 **3.23** **3.25**

2-Benzyloxybenzaldehyde **[3.23]** (0.21 g, 1 mmol), sodium metabisulfite (0.19 g, 1 mmol) and N,N-dimethylformamide (15 mL) were heated in a round bottom flask (100 mL) at 120 °C for 30 minutes. Into the reaction mixture after 30 minutes, 4-chloro-*o*-phenylenediamine [**3.9**] (0.14 g, 1 mmol) was added and heated further for 5.5 hours. Progress of reaction was monitored by TLC until completion. The resulting mixture after cooling to room temperature was added to cold water and the solid precipitate formed was filtered, dried and worked-up with hot hexane to afford a dark-brown solid, AKS-I-40 **[3.25]** with a 60.9% (0.204 g) yield, m.pt. 127-129 °C and R_f: 0.69 (hexane/ethyl acetate, 1:1). $\delta_{H(ppm)}$ (400 MHz, DMSO-d_6): 5.51 (2H, s), 7.09 (1H, t, $J_{5',6'}$ = 7.6 Hz), 7.21 (1H, d, $J_{3',4'}$ = 8.4 Hz), 7.24 (1H, dd, $J_{6,7}$ = 8.8 Hz, $J_{6,4}$ = 2.0 Hz), 7.28 (1H, t, $J_{10',9'}$ = 7.2 Hz), 7.36 (2H, t, $J_{11',12'}$ = $J_{9',8'}$ = 7.2 Hz), 7.41 (1H, dt, $J_{4',3'}$ = 8.8 Hz, $J_{4',6'}$ = 1.6 Hz), 7.48 (2H, d, $J_{12',11'}$ = $J_{8',9'}$ = 7.2 Hz), 7.65 (1H, d, $J_{7,6}$ = 8.4 Hz), 7.67 (1H, d, $J_{4,6}$ = 1.6 Hz), 8.25 (1H, dd, $J_{6',4'}$ = 1.6 Hz, $J_{6',5'}$ = 8.0 Hz); **EI-MS** (*m/z* (relative abundance in %)): 44 (7), 65 (7), 91 (100), 197 (7), 228 (9), 317 (13), 333 [M^+] (46), 335 [M^++2] (23); **HREI-MS**: *m/z* calculated for $C_{20}H_{15}ClN_2O$ [M^+] is 334.0873, found 334.0872. **IR** ($\bar{\upsilon}$/cm^{-1}; KBr disc): 3409, 3032, 2923, 2868, 1594, 1463, 1237, 1048; **UV** (λ_{max}/nm; MeOH): 316, 214.

3.2.17 Synthesis of 2-(2′-(benzyloxy)phenyl)-5,6-dimethyl-1*H*-benzo[*d*]imidazole (AKS-I-42)

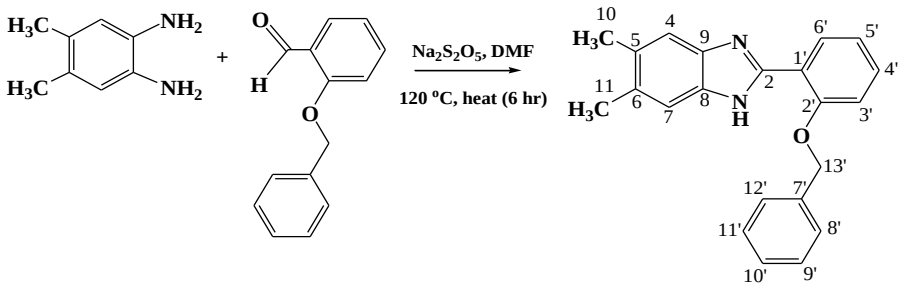

3.12 **3.23** **3.26**

A mixture of 2-benzyloxybenzaldehyde **[3.23]** (0.21 g, 1 mmol), sodium metabisulfite (0.19 g, 1 mmol) and N,N-dimethylformamide (15 mL) were heated at 120 °C in a round bottom flask (100 mL) for 30 minutes. Into the reaction mixture after 30 minutes, 4,5-dimethyl-*o*-phenylenediamine **[3.12]** (0.14 g, 1 mmol) was added and heated further for 5.5 hours. Progress of reaction was monitored by TLC until completion. The resulting mixture after cooling to room temperature was added to cold water and the precipitate formed was filtered, dried and worked-up with hot hexane to afford a brown solid, AKS-I-42 **[3.26]** with a 74.6% yield (0.245 g), m.pt. 130-132 °C and a R_f of 0.63 (hexane/ethyl acetate, 1:1). The following are the $\boldsymbol{\delta_{H(ppm)}}$ (400 MHz, DMSO-d_6): 2.32 (6H, s), 5.48 (2H, s), 7.08 (1H, t, $J_{5',6'}$ = 7.6 Hz), 7.19 (1H, d, $J_{3',4'}$ = 8.4 Hz), 7.29 (1H, t, $J_{10',11'}$ = 7.2 Hz), 7.36 (3H, t, $J_{11',12'} = J_{9',8'} = J_{4',5'}$ = 7.2 Hz), 7.39 (2H, s), 7.48 (2H, d, $J_{12',11'} = J_{8',9'}$ = 7.2 Hz), 8.21 (1H, dd, $J_{6',4'}$ = 1.2 Hz, $J_{6',5'}$ = 7.6 Hz), 12.23 (1H, br s); **EI-MS** (*m/z* (relative abundance in %)): 44 (16), 65 (14), 91 (93), 209 (29), 222 (54), 237 (72), 251 (22), 311 (42), 328 [M^+] (100), 329 [M^++1] (25); **HREI-MS**: *m/z* calculated for $C_{22}H_{20}N_2O$ [M^+] is 328.1576, found 328.1579; **IR** ($\bar{\upsilon}$/cm^{-1}; KBr disc): 3306, 3029, 2923, 2860, 1581, 1528, 1451, 1217, 1014; **UV** (λ_{max}/nm; MeOH): 316, 312, 229, 222.

3.2.18 Synthesis of 2-(3′-(benzyloxy)phenyl)-5-fluoro-1*H*-benzo[*d*]imidazole (AKS -I-43)

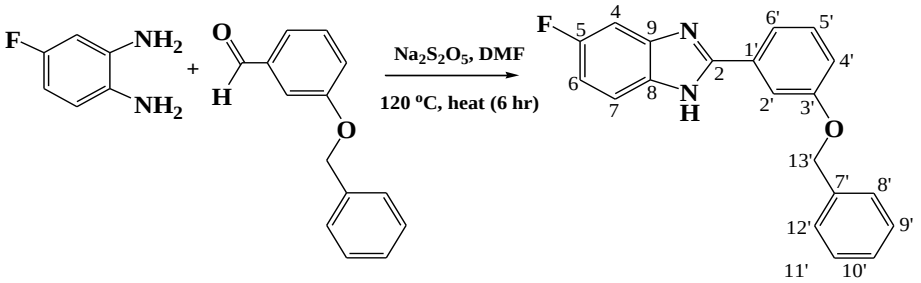

3.6 **3.27** **3.28**

A mixture of 3-benzyloxybenzaldehyde **[3.27]** (0.21 g, 1 mmol), sodium metabisulfite (0.19 g, 1 mmol) and N,N-dimethylformamide (15 mL) was heated at 120 °C in a 100 mL round bottom flask for 30 minutes. 4-Fluoro-*o*-phenylenediamine **[3.6]** (0.13 g, 1 mmol) was added to the resulting reaction mixture and futher heated for 5.5 hours. Reaction progress was monitored by TLC until completion. The resulting product, on cooling to room temperature, was transferred into iced-water to obtain a precipitate which was filtered, dried and worked-up with hot hexane to afford a brown solid, AKS-I-43 **[3.28]**, 88.0% (0.280 g) yield, with a m.pt. 201-204 °C and R_f of 0.65 (hexane/ethyl acetate, 1:1). $\boldsymbol{\delta_{H(ppm)}}$ (500 MHz, DMSO-d_6): 5.20 (2H, s), 7.08 (1H, dt, $J_{6,4}$ = 2.5 Hz, $J_{6,7}$ = 8.5 Hz), 7.15 (1H, dd, $J_{4'6'}$ = 2.0 Hz, $J_{4'5'}$ = 8.0 Hz), 7.35 (1H, t, $J_{10',9'}$ = 7.5 Hz), 7.42 (3H, m), 7.48 (1H, t, $J_{5',4'}$ = 8.0 Hz), 7.50 (2H, d, $J_{12',11'} = J_{8',9'}$ = 7.5 Hz), 7.58 (1H, br s), 7.75 (1H, d, $J_{6',5'}$ = 7.5 Hz), 7.82 (1H, s), 13.05 (1H, br d); **EI-MS** (*m/z* (relative abundance in %)): 18 (37), 28 (4), 65 (6), 91 (100), 228 (4), 318 [M^+] (70), 319 [M^++1] (17); **HREI-MS**: *m/z* calculated for $C_{20}H_{15}FN_2O$ [M^+] is 318.1168, found 318.1185; 307; **IR** ($\bar{\upsilon}$/cm^{-1}; KBr disc): 3449, 3061, 2922, 1597, 1537, 1451, 1229, 1139; **UV** (λ_{max}/nm; MeOH): 304, 299, 222.

3.2.19 Synthesis of 2-(3′-(benzyloxy)phenyl)-5-chloro-1*H*-benzo[*d*]imidazole (AKS -I-44)

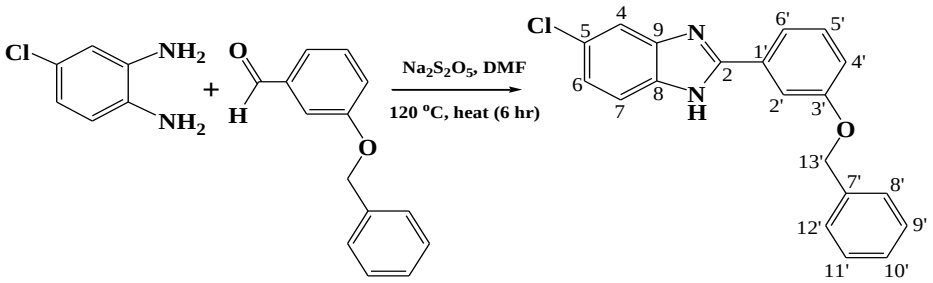

3.9 **3.27** **3.29**

A mixture of 3-benzyloxybenzaldehyde **[3.27]** (0.21 g, 1 mmol), sodium metabisulfite (0.19 g, 1 mmol) and N,N-dimethylformamide (15 mL) was heated at 120 °C in a 100 mL round bottom flask for 30 minutes. Into the resulting reaction mixture, 0.14 g (1 mmol) of 4-chloro-*o*-phenylenediamine **[3.27]** was added and heated for another 5.5 hours. Reaction progress was monitored by TLC until completion. The crude product was added to iced-water on cooling to room temperature. The precipitate obtained was filtered, dried and worked-up with hot hexane to afford a dark-brown solid compound, AKS-I-44 **[3.29]** with 87.2% (0.292 g) yield, a m.pt. of 102-104 °C and a 0.66 (hexane/ethyl acetate, 1:1) R_f value. The following are the $\boldsymbol{\delta_{H(ppm)}}$ (400 MHz, DMSO-d_6) values obtained: 5.21 (2H, s), 7.18 (1H, dd, $J_{4',2'}$ = 1.6 Hz, $J_{4',5'}$ = 8.0 Hz), 7.26 (1H, dd, $J_{6,4}$ = 1.6 Hz, $J_{6,7}$ = 8.4 Hz), 7.36 (1H, t, $J_{10',11'} = J_{10',9'}$ = 7.6 Hz), 7.42 (2H, t, $J_{11',10'} = J_{9',10'}$ = 7.6 Hz), 7.50 (2H, d, $J_{12',11'} = J_{8',9'}$ = 7.6 Hz), 7.50 (1H, t, $J_{5',6'}$ = 7.6 Hz), 7.62 (1H, d, $J_{7,6}$ = 8.4 Hz), 7.66 (1H, s), 7.76 (1H, d, $J_{6',5'}$ = 7.6 Hz), 7.83 (1H, s); **EI-MS** (*m/z* (relative abundance in %)): 18 (17), 65 (12), 91 (100), 215 (6), 244 (3), 334 [M^+] (67), 336 [M^++1] (26); **HREI-MS**: *m/z* calculated for $C_{20}H_{15}ClN_2O$ [M^+] is 334.0873, found 334.0895; **IR** ($\bar{\upsilon}$/cm^{-1}; KBr disc): 3418, 3063, 2921, 2866, 1658, 1591, 1484, 1453, 1224, 1024; **UV** (λ_{max}/nm; MeOH): 310, 222.

3.2.20 Synthesis of 2-(4′-(benzyloxy)phenyl)-5-fluoro-1*H*-benzo[*d*]imidazole (AKS -I-45)

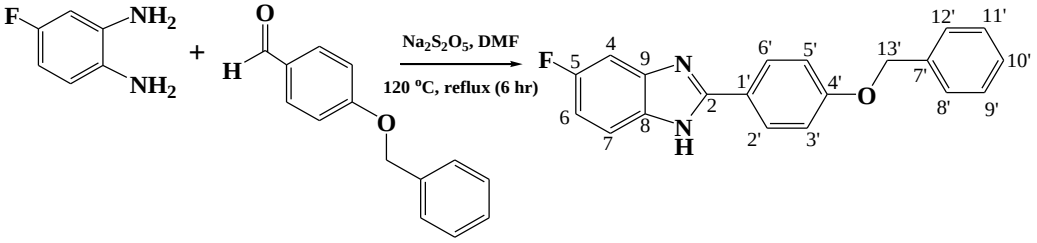

3.6 **3.30** **3.31**

4-Benzyloxybenzaldehyde **[3.30]** (0.21 g, 1 mmol), N,N-dimethylformamide (15 mL) and sodium metabisulfite (0.19 g, 1 mmol) were heated at 120 °C in a round bottom flask (100 mL) for 30 minutes. Into the reaction mixture after 30 minutes, 4-fluoro-*o*-phenylenediamine **[3.6]** (0.13 g, 1 mmol) was added and heated further for 5.5 hours. Progress of reaction was monitored by TLC until completion. The resulting mixture after cooling to room temperature was added to cold water and the brown precipitate obtained was filtered, dried and worked-up with hot hexane to afford the compound coded AKS-I-45 **[3.31]**, having a yield of 93.9% (0.299 g), with a m.pt. 223-226 °C and R_f of 0.60 (hexane/ethyl acetate, 1:1). The $\boldsymbol{\delta_{H(ppm)}}$ (400 MHz, DMSO-d_6) are as follows: 5.19 (2H, s), 7.08 (1H, dt $J_{6,7}$ = 9.6 Hz, $J_{6,4}$ = 2.0 Hz), 7.21 (2H, d, $J_{5',6'} = J_{3',2'}$ = 8.8 Hz), 7.38 (2H, m), 7.42 (2H, t, $J_{11',12'} = J_{9',8'}$ = 7.2 Hz), 7.48 (2H, d, $J_{12',11'} = J_{8',9'}$ = 7.2 Hz), 7.54-7.57 (1H, m), 8.09 (2H, d, $J_{6',5'} = J_{2',3'}$ = 8.8 Hz); **EI-MS** (*m/z* (relative abundance in %)): 44 (5), 65 (6), 91 (100), 197 (9), 227 (8), 318 [M^+] (30), 319 [M^++1] (7); **HREI-MS**: *m/z* calculated for $C_{20}H_{15}FN_2O$ [M^+] is 318.1168, found 318.1161; **IR** ($\bar{\upsilon}$/cm^{-1}; KBr disc): 3419, 3063, 2928, 2877, 1609, 1500, 1442, 1251, 1141; **UV** (λ_{max}/nm; MeOH): 310, 299, 249, 214.

3.2.21 Synthesis of 2-(4′-(benzyloxy)phenyl)-5,6-dimethyl-1*H*-benzo[*d*]imidazole (AKS-I-46)

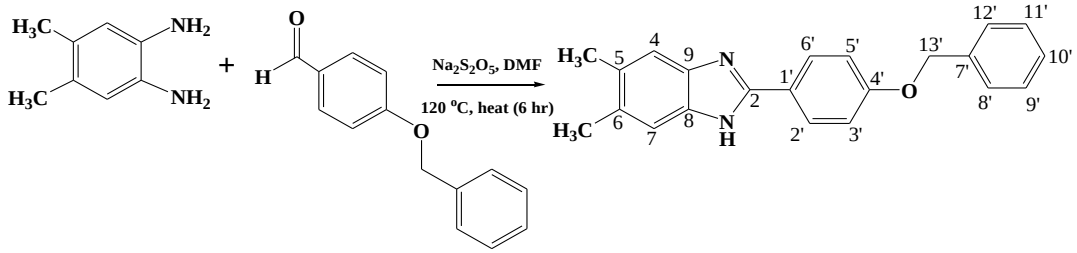

3.12 **3.30** **3.32**

A mixture of N,N-dimethylformamide (15 mL), 4-benzyloxybenzaldehyde **[3.30]** (0.21 g, 1 mmol) and sodium metabisulfite (0.19 g, 1 mmol) were heated in a 100 mL round bottom flask at 120 °C for 30 minutes. Into the reaction mixture after 30 minutes, 4,5-

dimethyl-*o*-phenylenediamine **[3.12]** (0.14 g, 1 mmol) was added and heated further for 5.5 hours. Progress of reaction was monitored by TLC until completion. The resulting mixture after cooling to room temperature was added to cold water and the precipitate obtained was filtered, dried and worked-up with hot hexane to afford a white solid, AKS-I-46 **[3.32]**, 94.7% yield (0.311 g), m.pt. 251-253 ^{o}C and a 0.46 (hexane/ethyl acetate, 1:1) R_f value. The following are the $\boldsymbol{\delta_{H(ppm)}}$ (400 MHz, DMSO-d_6) values: 2.32 (s, 6H), 5.20 (s, 2H), 7.22 (d, 2H, $J_{5',6'} = J_{3',2'} = 8.8$ Hz), 7.37 (m, 3H), 7.42 (t, 2H, $J_{11',12'} = J_{9',8'} = 7.2$ Hz), 7.48 (d, 2H, $J_{12',11'} = J_{8',9'} = 7.2$ Hz), 8.08 (d, 2H, $J_{6',5'} = J_{2',3'} = 8.8$ Hz); **EI-MS** (*m/z* (relative abundance in %)): 44 (3), 65 (5), 91 (62), 197 (9), 209 (15), 237 (100), 328 [M^+] (66), 329 [M^++1] (15); **HREI-MS**: *m/z* calculated for $C_{22}H_{20}N_2O$ [M^+] is 328.1576, found 328.1563; **IR** ($\bar{\upsilon}$/cm^{-1}; KBr disc): 3424, 3036, 2923, 2859, 1610, 1502, 1456, 1257; **UV** (λ_{max}/nm; MeOH): 311, 253, 214.

3.2.22 Synthesis of 2-(5′-bromo-2′-fluorophenyl)-5-nitro-1*H*-benzo[*d*]imidazole (AKS-I-48)

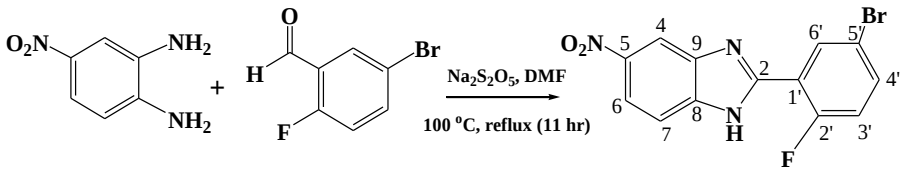

3.15 **3.33** **3.34**

A mixture of 5-bromo-2-fluorobenzaldehyde **[3.33]** (0.20 g, 1 mmol), N,N-dimethylformamide (15 mL) and sodium metabisulfite (0.19 g, 1 mmol) was heated at 100 ^{o}C in a 100 mL round bottom flask for 30 minutes. Into the resulting reaction mixture after 30 minutes, 4-nitro-*o*-phenylenediamine **[3.15]** (0.153 g, 1 mmol) was added and heated further for 10.5 hours. Progress of reaction was monitored by TLC until completion. The resulting mixture after cooling to room temperature was added to cold water and the precipitate obtained was filtered, dried and worked-up with hot hexane to afford a brown solid compound with the code AKS-I-48 **[3.34]**, 0.14 g (42.5% yield), m.pt. 228-230 ^{o}C and a R_f of 0.55 (hexane/ethyl acetate, 1:1). The $\boldsymbol{\delta_{H(ppm)}}$ (400 MHz, DMSO-d_6) values obtained are: 7.52 (1H, t, $J_{3',4'} = 8.8$ Hz), 7.81-7.83 (2H, m), 8.18 (1H, dd, $J_{4',6'} = 2.0$ Hz, $J_{4',3'} = 8.8$ Hz), 8.39 (1H, dd, $J_{6,4} = 2.4$ Hz, $J_{6,7} = 6.4$ Hz), 8.54 (1H, s), 13.33 (1H, br s); $\boldsymbol{\delta_{C(ppm)}}$ (100 MHz, DMSO-d_6): 118.31, 119.09, 119.32, 132.36, 135.36, 135.45, 116.83, 119.19, 143.06, 149.54, 157.52, 160.03; **EI-MS** (*m/z* (relative abundance in %)): 63 (18), 90 (15), 105 (6), 210 (23), 289 (25), 305 (24), 335 [M^+] (100), 337 [M^++2] (98); **HREI-MS**: *m/z* calculated for $C_{13}H_7BrFN_3O_2$ [M^+] is 334.9706,

found 334.9703. **IR** ($\bar{\upsilon}$/cm^{-1}; KBr disc): 3615, 3106, 1629, 1591, 1474, 1523, 1343, 885; **UV** (λ_{max}/nm; MeOH): 324, 261, 213.

3.2.23 Synthesis of 5,6-dimethyl-2-(2′,3′,4′-trimethoxyphenyl)-1*H*-benzo[*d*] imidazole (AKS-I-49)

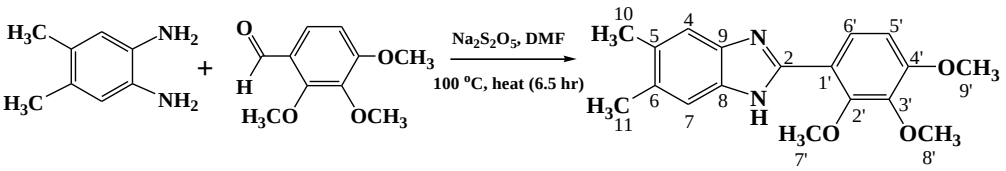

3.12 **3.35** **3.36**

A mixture of the reagents 2,3,4-trimethoxybenzaldehyde [**3.35**] (0.20 g, 1 mmol) and sodium metabisulfite (0.19 g, 1 mmol) in the solvent N,N-dimethylformamide (15 mL), was heated at 100 °C for 30 minutes in a round bottom flask (100 mL). Into the resulting reaction mixture after 30 minutes, 4,5-dimethyl-*o*-phenylenediamine [**3.12**] (0.14 g, 1 mmol) was added and heated further for 6.5 hours. Progress of reaction was monitored by TLC until completion. The resulting mixture after cooling to room temperature was added to cold water and the precipitate obtained was filtered, dried and worked-up with hot hexane to afford a white solid product, AKS-I-49 [**3.36**], with a yield of 49.0% (0.153 g), m.pt. 188-190 °C and R_f value of 0.30 (hexane/ethyl acetate, 1:1). The following are the $\boldsymbol{\delta_{H(ppm)}}$ (400 MHz, DMSO-d_6) values deduced: 2.30 (6H, s), 3.82 (3H, s), 3.86 (3H, s), 3.88 (3H, s), 6.98 (1H, d, $J_{5',6'}$ = 9.2 Hz), 7.35 (2H, s), 7.92 (1H, d, $J_{6',5'}$ = 8.8 Hz), 11.93 (1H, br s, -NH); $\boldsymbol{\delta_{C(ppm)}}$ (75 MHz, DMSO-d_6): 19.98, 55.98, 60.50, 61.26, 108.47, 115.06, 116.19, 124.31, 130.04, 141.71, 147.69, 151.28, 154.60; **EI-MS** (*m/z* (relative abundance in %)): 64 (9), 91 (7), 156 (11), 183 (14), 254 (26), 266 (23), 281 (19), 297 (100), 312 [M$^+$] (94), 313 [M$^+$+1] (21); **HREI-MS**: *m/z* calculated for $C_{18}H_{20}N_2O_3$ [M$^+$] is 312.1474, found 312.1470; **IR** ($\bar{\upsilon}$/cm^{-1}; KBr disc): 3314, 3102, 2943, 1597, 1479, 1457, 1288, 1083; **UV** (λ_{max}/nm; MeOH): 311, 252, 2128.

3.2.24 Synthesis of 2′-(1*H*-benzo[*d*]imidazol-2-yl)-3′-bromo-6′-methoxyphenol (AKS-I-50)

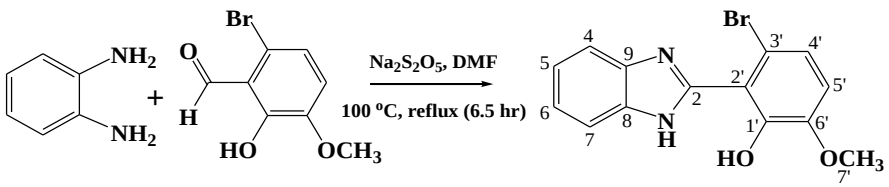

3.1 **3.37** **3.38**

In a 100 mL round bottom flask, a mixture of the reagents 6-bromo-2-hydroxy-3-methoxybenzaldehyde **[3.37]** (0.23 g, 1 mmol) and sodium metabisulfite (0.19 g, 1 mmol) in N,N-dimethylformamide (15 mL) as the solvent was heated at 100 ^{o}C for 30 minutes. *o*-Phenylenediamine **[3.1]** (0.14 g, 1 mmol) was added to the resulting reaction mixture after 30 minutes and heated further for 6.5 hours. Reaction progress was monitored by TLC until it was completed. The precipitate formed after adding the crude product into iced-water was filtered, dried and further worked-up with hot hexane to afford a yellow solid, AKS-I-50 **[3.38]**, a yield of 41.8% (0.133 g), m.pt. 178-181 ^{o}C and R_f value of 0.55 (hexane/ethyl acetate, 1:1). $\boldsymbol{\delta_{H(ppm)}}$ (400 MHz, DMSO-d_6): 3.84 (3H, s), 7.07 (1H, d, $J_{5',4'}$ = 8.8 Hz), 7.18 (1H, d, $J_{4',5'}$ = 8.8 Hz), 7.22-7.24 (2H, m), 7.60-7.62 (2H, m), 11.77 (1H, br d); **EI-MS** (*m/z* (relative abundance in %)): 44 (3), 167 (22), 195 (9), 209 (7), 240 (14), 275 (28), 291 (31), 303 (14), 318 [M^+] (89), 320 [M^++2] (100); **HREI-MS**: *m/z* calculated for $C_{14}H_{11}BrN_2O_2$ [M^+] is 318.0004, found 318.0015; **IR** ($\bar{\upsilon}$/cm^{-1}; KBr disc): 3336, ≈3100, 2925, 1585, 1450, 1245, 989; **UV** (λ_{max}/nm; MeOH): 282, 229, 214.

3.2.25 Synthesis of 3′-bromo-2′-(5-fluoro-1*H*-benzo[*d*]imidazol-2-yl)-6′-methoxy-phenol (AKS-I-51)

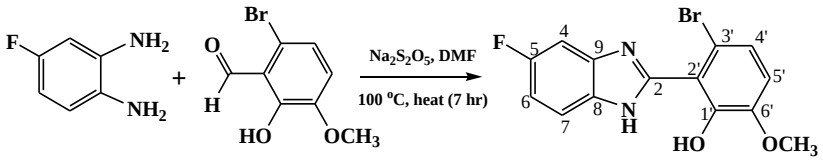

3.6 **3.37** **3.39**

In a round bottom flask (100 mL), a mixture of 6-bromo-2-hydroxy-3-methoxy-benzaldehyde **[3.37]** (0.23 g, 1 mmol), sodium metabisulfite (0.19 g, 1 mmol) and 15 mL of the solvent N,N-dimethylformamide was heated at 100 ^{o}C for 30 minutes. 4-Fluoro-*o*-phenylenediamine **[3.6]** (0.13 g, 1 mmol) was added to the resulting reaction mixture and heated further for about 6.5 hours. Reaction progress was monitored by TLC until it was completed. The yellow precipitate formed after pouring the crude product into iced-water was filtered, dried and further worked-up with hot hexane to afford the compound with the code AKS-I-51 **[3.39]**, a yield of 65.0% (0.219 g), m.pt. of 210-213 ^{o}C and a 0.50 (hexane/ethyl acetate, 1:1) R_f value. The chemical shift signals, $\boldsymbol{\delta_{H(ppm)}}$ (400 MHz, DMSO-d_6) are as follows: 3.84 (3H, s), 7.05-7.10 (2H, m), 7.17 (1H, d, $J_{4',5'}$ = 8.8 Hz), 7.40 (1H, dd, $J_{7,6}$ = 7.6 Hz), 7.57-7.61 (1H, m), 11.56 (1H, br s); $\boldsymbol{\delta_{C(ppm)}}$ (75 MHz, DMSO-d_6): 56.10, 109.95, 110.29, 114.07, 114.33, 117.65, 118.77, 122.50,

112.58, 118.72, 147.56, 147.85, 149.62, 156.95, 160.07; **EI-MS** (*m/z* (relative abundance in %)): 110 (6), 227 (7), 240 (15), 258 (25), 293 (42), 307 (40), 318 (20), 320 (22), 336 [M^+] (99), 338 [M^++2] (100), 185 (38),; **HREI-MS**: *m/z* calculated for $C_{14}H_{10}BrFN_2O_2$ [M^+] is 335.9910, found 335.9904; **IR** ($\bar{\upsilon}$/cm^{-1}; KBr disc): 3336, ≈3100, 2931, 1591, 1450, 1247, 1136; **UV** (λ_{max}/nm; MeOH): 287, 228, 212.

3.2.26 Synthesis of 3′-bromo-2′-(5-chloro-1*H*-benzo[*d*]imidazol-2-yl)-6′-methoxy-phenol (AKS-I-52)

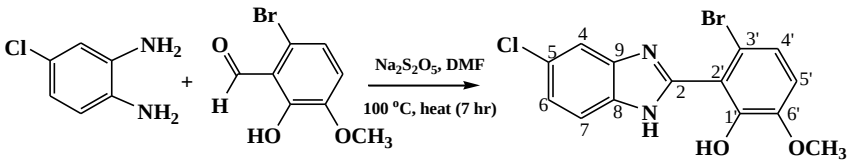

3.9 **3.37** **3.40**

In a round bottom flask (100 mL), a mixture of N,N-dimethylformamide (15 mL), 6-bromo-2-hydroxy-3-methoxybenzaldehyde **[3.37]** (0.23 g, 1 mmol) and sodium metabisulfite (0.19 g, 1 mmol) was heated at 100 °C for 30 minutes. 4-Chloro-*o*-phenylenediamine **[3.9]** (0.14 g, 1 mmol) was added to the resulting reaction mixture and heated for another 6.5 hours. Reaction progress was monitored by TLC until it was completed. The brown precipitate formed after pouring the crude product into iced-water was filtered, dried and further worked-up with hot hexane to afford the compound AKS-I-52 **[3.40]**, with a yield of 83.7% (0.296 g), m.pt. 214-216 °C and a 0.52 (hexane/ethyl acetate, 1:1) R_f value. The chemical shift, $\boldsymbol{\delta_{H(ppm)}}$ (400 MHz, DMSO-d_6) values obtained from are as follows: 3.85 (3H, s), 7.08 (1H, d, $J_{5',4'}$ = 8.8 Hz), 7.17 (1H, d, $J_{4',5'}$ = 8.8 Hz), 7.25 (1H, dd, $J_{6,7}$ = 8.4 Hz, $J_{6,4}$ = 2.0 Hz), 7.61 (1H, d, $J_{7,6}$ = 8.4 Hz), 7.65 (1H, s), 10.00-12.50 (2H, br s); $\boldsymbol{\delta_{C(ppm)}}$ (75 MHz, DMSO-d_6): 56.16, 112.67, 114.38, 118.85, 122.17, 122.48, 126.27, 147.52, 147.76, 149.69; **EI-MS** (*m/z* (relative abundance in %)): 126 (4), 201 (36), 215 (11), 229 (14), 274 (9), 334 (19), 336 (25), 352 [M^+] (80), 354 [M^++2] (100), 356 [M^++4] (28); **HREI-MS**: *m/z* calculated for $C_{14}H_{10}BrClN_2O_2$ [M^+] is 351.9614, found 351.9602; **IR** ($\bar{\upsilon}$/cm^{-1}; KBr disc): 3336, ≈3100, 2837, 1587, 1458, 1247, 1053, 875; **UV** (λ_{max}/nm; MeOH): 291, 213.

3.2.27 Synthesis of 3′-bromo-2′-(5,6-dimethyl-1*H*-benzo[*d*]imidazol-2-yl)-6′-methoxyphenol (AKS-I-54)

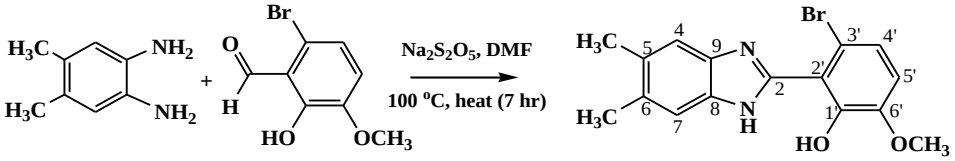

3.12 **3.37** **3.41**

In a round bottom flask (100 mL) equipped with a magnetic stirrer, the mixture of N,N-dimethylformamide (15 mL), 6-bromo-2-hydroxy-3-methoxybenzaldehyde **[3.37]** (0.23 g, 1 mmol) and sodium metabisulfite (0.19 g, 1 mmol) was heated at 100 °C for 30 minutes. 4,5-dimethyl-*o*-phenylenediamine **[3.12]** (0.14 g, 1 mmol) was added to the resulting reaction mixture and heated for another 6.5 hours. Reaction progress was monitored by TLC until it was completed. The precipitate formed after pouring the crude product into iced-water was filtered, dried and further worked-up with hot hexane to afford a brown solid, AKS-I-54 **[3.41]**, 75.7% (0.263 g) yield, m.pt. 236-239 °C and a R_f value of 0.52 (hexane/ethyl acetate, 1:1). The values obtained from spectroscopic analysis are as follows; $\boldsymbol{\delta_{H(ppm)}}$ (400 MHz, DMSO-d_6): 2.32 (6H, s), 3.83 (3H, s), 7.04 (1H, d, $J_{5',4'}$ = 8.8 Hz), 7.16 (1H, d, $J_{4',5'}$ = 8.8 Hz), 7.39 (2H, s), 11.88 (1H, br s); **EI-MS** (*m/z* (relative abundance in %)): 90 (13), 195 (46), 225 (9), 250 (15), 268 (21), 305 (43), 317 (38), 328 (28), 346 [M^+] (100), 348 [M^++2] (95); **HREI-MS**: *m/z* calculated for $C_{16}H_{15}BrN_2O_2$ [M^+] is 346.0317, found 346.0295; **IR** ($\bar{\upsilon}$/cm^{-1}; KBr disc): 3359, ≈3010, 2931, 2846, 1583, 1461, 1251, 1056; **UV** (λ_{max}/nm; MeOH): 291, 229, 222, 213.

3.2.28 Synthesis of 4′-(5-fluoro-1*H*-benzo[*d*]imidazol-2-yl)-2′,6′-dimethoxyphenol (AKS-I-55)

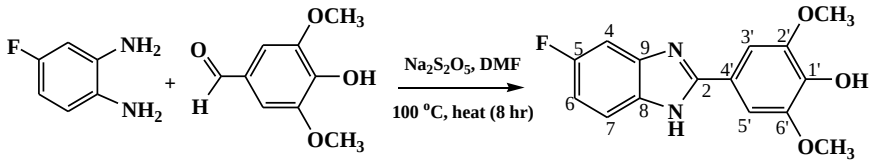

3.6 **3.42** **3.43**

A mixture of 3,5-dimethoxy-4-hydroxybenzaldehyde (Syringaldehyde) **[3.42]** (0.18 g, 1 mmol), the organic solvent N,N-dimethylformamide (15 mL) and sodium metabisulfite (0.19 g, 1 mmol) was heated in a round bottom flask (100 mL) at 100 °C for 30 minutes. 4-Fluoro-*o*-phenylenediamine **[3.6]** (0.13 g, 1 mmol) was introduced into the reaction mixture and heated further for 7.5 hours. Reaction progress was monitored by TLC until completion. The crude product at room temperature was added

to iced-water. The precipitate obtain was filtered, dried and worked-up with hot hexane to afford a brown solid compound, AKS-I-55 **[3.43]**, 55.9% (0.161 g) yield, m.pt. 311-313 ^{o}C and R_f value of 0.36 (hexane/ethyl acetate, 7:3). $\boldsymbol{\delta_{H(ppm)}}$ (400 MHz, DMSO-d_6): 3.88 (6H, s), 7.21 (1H, dt, $J_{6,7}$ = 8.8 Hz, $J_{6,4}$ = 2.4 Hz), 7.49-7.51 (3H, m), 7.64-7.68 (1H, m), 9.29 (1H, br s); $\boldsymbol{\delta_{C(ppm)}}$ (100 MHz, DMSO-d_6): 56.23, 100.54, 100.81, 104.89, 111.54, 111.80, 115.00, 116.02, 139.29, 148.27, 152.06, 158.01, 160.37; **EI-MS** (*m/z* (relative abundance in %)): 83 (7), 108 (3), 213 (7), 245 (18), 257 (16), 273 (10), 288 [M^+] (100), 289 [M^++1] (19); **HREI-MS**: *m/z* calculated for $C_{15}H_{13}FN_2O_3$ [M^+] is 288.0910, found 288.0908. **IR** ($\bar{\upsilon}$/cm^{-1}; KBr disc): 3516, 3375, ≈3050, 2937, 1612, 1510, 1477, 1232, 1112, 1145; **UV** (λ_{max}/nm; MeOH): 316, 217.

3.2.29 Synthesis of 4′-(5-chloro-1*H*-benzo[*d*]imidazol-2-yl)-2′,6′-dimethoxyphenol (AKS-I-56)

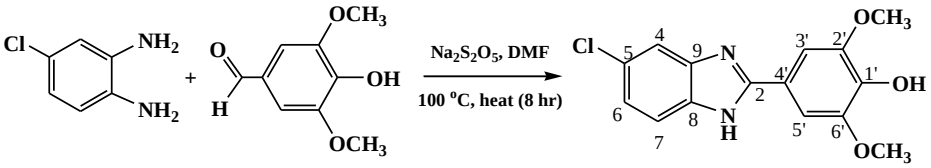

3.9 **3.42** **3.44**

A mixture of 3,5-dimethoxy-4-hydroxybenzaldehyde (Syringaldehyde) **[3.42]** (0.18 g, 1 mmol) and sodium metabisulfite (0.19 g, 1 mmol) as well as the solvent N,N-dimethylformamide (15 mL) was heated at 100 ^{o}C in a 100 mL round bottom flask for 30 minutes. Into the resulting reaction mixture, 4-chloro-*o*-phenylenediamine **[3.9]** (0.14 g, 1 mmol) was added and heated further for 7.5 hours. Reaction progress was monitored by TLC until completion. The resulting mixture after cooling to room temperature was added to cold water and the dark-brown precipitate obtained was filtered, dried and worked-up with hot hexane to afford the compound AKS-I-56 **[3.44]**, with 83.0% yield (0.253 g), m.pt. 284-286 ^{o}C and R_f of 0.45 (hexane/ethyl acetate, 7:3). The $\boldsymbol{\delta_{H(ppm)}}$ (400 MHz, DMSO-d_6) values obtained are as follows: 3.88 (6H, s), 7.32 (1H, dd, $J_{6,4}$ = 2.0 Hz, $J_{6,7}$ = 8.4 Hz), 7.49 (2H, s), 7.64 (1H, d, $J_{7,6}$ = 8.4 Hz), 7.68 (1H, s), 9.24 (1H, br s); **EI-MS** (*m/z* (relative abundance in %)): 44 (13), 177 (4), 218 (10), 246 (8), 258 (14), 273 (14), 289 (10), 304 [M^+] (100), 306 [M^++2] (34); **HREI-MS**: *m/z* calculated for $C_{15}H_{13}ClN_2O_3$ [M^+] is 304.0615, found 304.0616. **IR** ($\bar{\upsilon}$/cm^{-1}; KBr disc): ≈3500, ≈3200, 3114, 2941, 2844, 1627, 1504, 1467, 1234, 1118; **UV** (λ_{max}/nm; MeOH): 319, 259, 222.

3.2.30 Synthesis of 4′-(5-fluoro-1*H*-benzo[*d*]imidazol-2-yl)benzene-1′,2′,3′-triol (AKS-I-57)

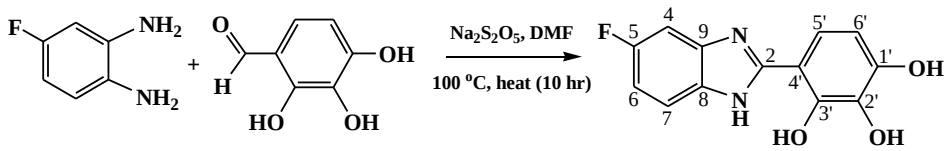

3.6 **3.45** **3.46**

A mixture of 2,3,4-trihydroxybenzaldehyde **[3.45]** (0.15 g, 1 mmol), sodium metabisulfite (0.19 g, 1 mmol) and N,N-dimethylformamide (15 mL) in a round bottom flask (100 mL) was heated at 100 °C for 30 minutes. 4-Chloro-*o*-phenylenediamine **[3.6]** (0.14 g, 1 mmol) was added into the reaction mixture after 30 minutes and heated further for 9.5 hours. Progress of reaction was monitored by TLC until completion. On cooling the resulting mixture to room temperature, a precipitate was obtained from iced-cold water which was filtered, dried and worked-up with hot hexane to afford a brown solid compound, AKS-I-57 **[3.46]**, 91.0% (0.237 g) yield, m.pt. 287-288 °C, R_f: 0.64 (hexane/ethyl acetate, 7:3). $\boldsymbol{\delta_{H(ppm)}}$ (400 MHz, DMSO-d_6): 6.49 (1H, d, $J_{6',5'}$ = 8.4 Hz), 7.14 (1H, dt, $J_{6,4}$ = 2.0 Hz, $J_{6,F\text{-}5}$ = 8.8 Hz), 7.35 (1H, d, $J_{5',6'}$ = 8.8 Hz), 7.43 (1H, d, $J_{7,6}$ = 8.0 Hz), 7.58-7.62 (1H, m, H-4), 8.58 (1H, br s), 9.61 (1H, br d), 13.00 (2H, br s); **EI-MS** (*m/z* (relative abundance in %)): 44 (53), 161 (24), 186 (12), 203 (4), 231 (24), 260 [M^+] (100), 261 [M^++1] (29); **HREI-MS**: *m/z* calculated for $C_{15}H_9FN_2O_3$ [M^+] is 260.0597, found 260.0599; **IR** ($\bar{\upsilon}$/cm^{-1}; KBr disc): ≈3400, 3240, 3066, 1624, 1494, 1461, 1143, 1110; **UV** (λ_{max}/nm; MeOH): 327, 315, 267, 222.

3.2.31 Synthesis of 4′-(5-fluoro-1*H*-benzo[*d*]imidazol-2-yl)-2′-methoxyphenyl acetate (AKS-I-59)

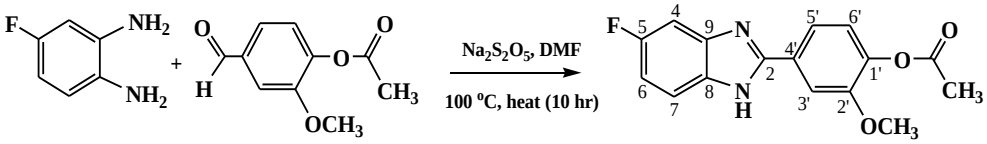

3.6 **3.47** **3.48**

Vanillin acetate (4-Acetoxy-3-methoxybenzaldehyde) **[3.47]** (0.19 g, 1 mmol), sodium metabisulfite (0.19 g, 1 mmol) and N,N-dimethylformamide (15 mL) were heated at 100 °C in a 100 mL round bottom flask for 30 minutes. Into the reaction mixture after 30 minutes, 4-fluoro-*o*-phenylenediamine **[3.6]** (0.13 g, 1 mmol) was added and heated further for 9.5 hours. Reaction progress was monitored by TLC until completion. The product obtained was added to cold water after cooling to room temperature and the

brown precipitate obtained was filtered, dried and worked-up with hot hexane to afford the solid compound, AKS-I-59 **[3.48]**, in a 55.0% yield (0.164 g), m.pt. 124-127 ^{o}C and with a 0.36 (hexane/ethyl acetate, 1:1) R_f value. The $\boldsymbol{\delta_{H(ppm)}}$ (400 MHz, DMSO-d_6) is given as follows: 2.29 (3H, s), 3.89 (3H, s), 7.12 (1H, dt, $J_{6,4}$ = 2.4 Hz, $J_{6,7}$ = 9.2 Hz), 7.29 (1H, d, $J_{6',5'}$ = 8.0 Hz), 7.44 (1H, dd, $J_{7,6}$ = 9.2 Hz, $J_{7,F\text{-}5}$ = 2.0 Hz), 7.60-7.63 (1H, m), 7.75 (1H, dd, $J_{5',3'}$ = 1.6 Hz, $J_{5',6'}$ = 8.4 Hz), 7.89 (1H, d, $J_{3',5'}$ = 1.6 Hz); **EI-MS** (*m/z* (relative abundance in %)): 43 (7), 187 (9), 200 (11), 215 (18), 228 (12), 243 (13), 258 (100), 300 [M^+] (10); **HREI-MS**: *m/z* calculated for $C_{16}H_{13}FN_2O_3$ [M^+] is 300.0910, found 300.0903. **IR** ($\bar{\upsilon}$/cm^{-1}; KBr disc): 3415, 3079, 2932, 2854, 1761, 1633, 1603, 1504, 1475, 1207, 1139; **UV** (λ_{max}/nm; MeOH): 310, 214.

3.2.32 Synthesis of 4′-(5-chloro-1*H*-benzo[*d*]imidazol-2-yl)-2′-methoxyphenyl acetate (AKS-I-60)

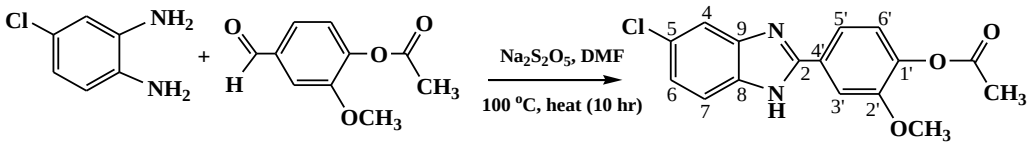

3.9 **3.47** **3.49**

The reagents 4-acetoxy-3-methoxybenzaldehyde (Vanillin acetate) **[3.47]** (0.19 g, 1 mmol) and sodium metabisulfite (0.19 g, 1 mmol) in an organic solvent, N,N-dimethylformamide (15 mL) were heated at 100 ^{o}C in a round bottom flask (100 mL) for 30 minutes. After 30 minutes, 4-chloro-*o*-phenylenediamine **[3.9]** (0.142 g, 1 mmol) was added into the reaction mixture and heated further for 9.5 hours. Progress of reaction was monitored by TLC until completion. After cooling to room temperature, the resulting mixture was poured into iced-cold water and the precipitate obtained filtered, dried and worked-up with hot hexane to afford a dark-brown solid compound, AKS-I-60 **[3.49]**, with a m.pt. range of 128-129 ^{o}C, a 61.9% (0.196 g) yield and a 0.38 (hexane/ethyl acetate, 1:1) R_f value. The chemical shifts, $\boldsymbol{\delta_{H(ppm)}}$ (400 MHz, DMSO-d_6) obtained are as follows: 2.29 (3H, s), 3.90 (3H, s), 7.26 (1H, dd, $J_{6,7}$ = 8.8 Hz, $J_{6,4}$ = 2.0 Hz), 7.29 (1H, d, $J_{6',5'}$ = 8.4 Hz), 7.63 (1H, d, $J_{7,6}$ = 8.8 Hz), 7.66 (1H, s), 7.76 (1H, dd, $J_{5',3'}$ = 1.6 Hz, $J_{5',6'}$ = 8.4 Hz), 7.89 (1H, d, $J_{3',5'}$ = 1.6 Hz); **EI-MS** (*m/z* (relative abundance in %)): 63 (21), 90 (11), 137 (12), 168 (16), 203 (15), 231 (27), 245 (23), 259 (15), 276 (54), 274 (100), 316 [M^+] (36), 318 [M^++2] (13); **HREI-MS**: *m/z* calculated for $C_{16}H_{13}ClN_2O_3$ [M^+] is 316.0615, found 316.0621. **IR** ($\bar{\upsilon}$/cm^{-1}; KBr disc): 3076, 2935, 1758, 1656, 1600, 1500, 1431, 1204, 1060; **UV** (λ_{max}/nm; MeOH): 312, 247, 222.

3.2.33 Synthesis of 2′-methoxy-4′-(5-nitro-1H-benzo[d]imidazol-2-yl)phenyl acetate (AKS-I-61)

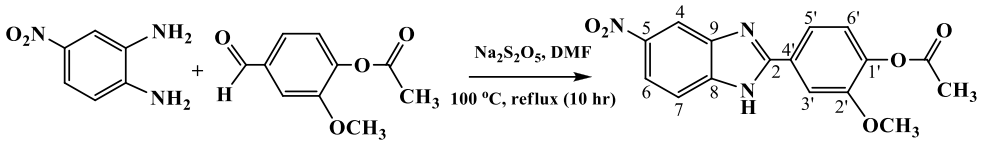

3.15 **3.47** **3.50**

A mixture of 4-acetoxy-3-methoxybenzaldehyde (Vanillin acetate) **[3.47]** (0.19 g, 1 mmol), 15 mL N,N-dimethylformamide and sodium metabisulfite (0.19 g, 1 mmol) was heated in a round bottom flask (100 mL) at 100 °C for 30 minutes. Into the reaction mixture after 30 minutes, 4-chloro-*o*-phenylenediamine **[3.15]** (0.142 g, 1 mmol) was added and heated further for 9.5 hours. Reaction progress was monitored by TLC until it was completed. After cooling to room temperature, the resulting mixture was added to cold water and the yellow solid precipitate obtained was filtered, dried and worked-up with hot hexane to afford the compound, AKS-I-61 **[3.50]**, 70.6% (0.231 g) yield, m.pt. 203-207 °C and R_f value of 0.31 in a hexane/ethyl acetate (1:1) solvent ratio. The following $\boldsymbol{\delta_{H(ppm)}}$ (400 MHz, DMSO-d_6) values were obtained: 2.29 (3H, s), 3.91 (3H, s), 7.34 (1H, d, $J_{6',5'}$ = 8.4 Hz), 7.83 (1H, d, $J_{5',6'}$ = 8.4 Hz), 7.77 (1H, br s), 7.94 (1H, s), 8.15 (1H, d, $J_{7,6}$ = 8.4 Hz), 8.50 (1H, br s), 13.61 (1H, br s); **EI-MS** (*m/z* (relative abundance in %)): 51 (5), 69 (14), 90 (11), 212 (10), 239 (20), 255 (25), 327 [M^+] (8), 285 (100), 297 (3); **HREI-MS**: *m/z* calculated for $C_{16}H_{13}N_3O_5$ [M^+] is 327.0855, found 327.0856. **IR** ($\bar{\upsilon}$/cm^{-1}; KBr disc): 3315, 3101, 2959, 1760, 1501, 1338, 1214; **UV** (λ_{max}/nm; MeOH): 330, 269, 213.

3.2.34 Synthesis of 2-(2′-bromo-4′,5′-dimethoxyphenyl)-1*H*-benzo[*d*]imidazole (AKS-I-63)

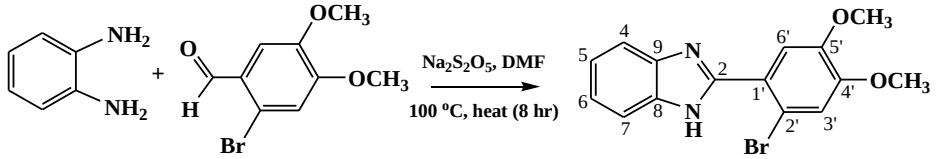

3.1 **3.51** **3.52**

2-Bromo-4,5-dimethoxybenzaldehyde **[3.51]** (0.25 g, 1 mmol), sodium metabisulfite (0.19 g, 1 mmol) as well as N,N-dimethylformamide (15 mL) and were heated in a round bottom flask (100 mL) equipped with a magnetic stirrer at 100 °C for 30 minutes. *o*-Phenylenediamine **[3.1]** (0.11 g, 1 mmol) was added into the resulting reaction mixture after 30 minutes and heated further for 7.5 hours. Progress of reaction was monitored

by TLC. The resulting reaction mixture was cooled to room temperature and then added to cold water to obtain a precipitate which was filtered, dried and worked-up with hot hexane to afford a pale-brown solid compound, AKS-I-63 **[3.52]**, 61.6% (0.205 g) yield, m.pt. 186-188 ^{o}C and a 0.34 (hexane/ethyl acetate, 1:1) R_f value. The following $\boldsymbol{\delta_{H(ppm)}}$ (400 MHz, DMSO-d_6) were obtained: 3.85 (3H, s), 7.20 (1H, t, $J_{5,6}$ = 7.2 Hz), 7.24 (1H, t, $J_{6,5}$ = 7.2 Hz), 7.30 (1H, s), 7.33 (1H, s), 7.53 (1H, d, $J_{7,6}$ = 7.2 Hz), 7.67 (1H, d, $J_{4,5}$ = 7.6 Hz), 12.55 (1H, s); **EI-MS** (*m/z* (relative abundance in %)): 43 (5), 105 (5), 167 (15), 195 (22), 210 (6), 254 (4), 288 (14), 303 (26), 319 (21), 332 [M^+] (100), 334 [M^++2] (99); **HREI-MS**: *m/z* calculated for $C_{15}H_{13}N_2O_2Br$ [M^+] is 332.0160, found 332.0144. **IR** ($\bar{\upsilon}$/cm^{-1}; KBr disc): ≈3300, 3053, 2959, 2840, 1598, 1501, 1441, 1210, 866; **UV** (λ_{max}/nm; MeOH): 291, 222.

3.2.35 Synthesis of 2-(2′-bromo-4′,5′-dimethoxyphenyl)-5-fluoro-1*H*-benzo[*d*] imidazole (AKS-I-64)

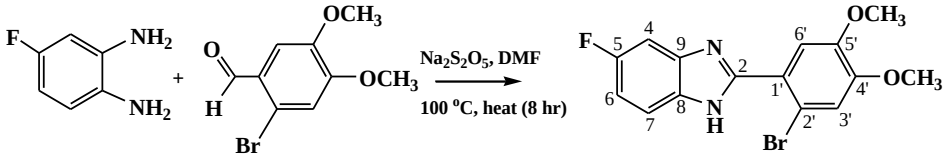

3.6 **3.51** **3.53**

2-Bromo-4,5-dimethoxybenzaldehyde **[3.51]** (0.25 g, 1 mmol), 15 mL N,N-dimethyl-formamide and sodium metabisulfite (0.19 g, 1 mmol) were heated at 100 ^{o}C in a round bottom flask (100 mL) for 30 minutes. 4-fluoro-*o*-Phenylenediamine **[3.6]** (0.13 g, 1 mmol) was added into the resulting reaction mixture after 30 minutes and heated further for 7.5 hours. Reaction progress was monitored by TLC until completion. The resulting mixture was cooled to room temperature and then added to cold water to obtain a precipitate which was filtered, dried and worked-up with hot hexane to afford a brown precipitate (AKS-I-64 **[3.53]**),with a 69.8% (0.245 g) yield, m.pt. 115-118 ^{o}C and a R_f value of 0.44 (hexane/ethyl acetate, 1:1). The chemical shifts, $\boldsymbol{\delta_{H(ppm)}}$ (500 MHz, DMSO-d_6) obtained are as follows: 3.81 (3H, s), 3.85 (3H, s), 7.09 (1H, dt, $J_{6,4}$ = 2.0 Hz, $J_{6,7}$ = 9.0 Hz), 7.33 (1H, s), 7.30 (1H, s), 7.40 (1H, br d, $J_{7,6}$ = 8.5 Hz), 7.59 (1H, br s), 12.73 (1H, br d); **EI-MS** (*m/z* (relative abundance in %)): 43 (6), 57 (10), 110 (4), 185 (11), 198 (7), 213 (23), 228 (8), 307 (14), 321 (23), 335 (19), 350 [M^+] (99), 352 [M^++2] (100); **HREI-MS**: *m/z* calculated for $C_{15}H_{12}N_2O_2BrF$ [M^+] is 350.0066, found 350.0063. **IR** ($\bar{\upsilon}$/cm^{-1}; KBr disc): 3568, 3004, 2953, 2836, 1633, 1602, 1504, 1443, 1267, 1035, 1136, 900; **UV** (λ_{max}/nm; MeOH): 296, 222, 214.

3.2.36 Synthesis of 2-(2′-bromo-4′,5′-dimethoxyphenyl)-5-chloro-1*H*-benzo[*d*] imidazole (AKS-I-65)

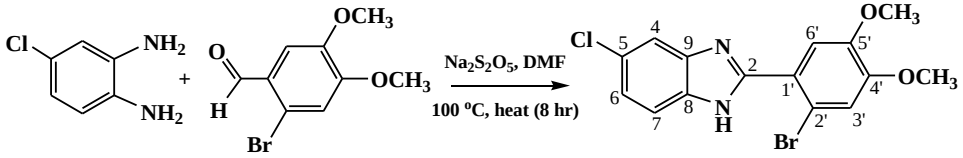

3.9 **3.51** **3.54**

In a round bottom flask (100 mL) equipped with a condenser and a magnetic stirrer, N,N-dimethylformamide (15 mL), 2-bromo-4,5-dimethoxybenzaldehyde **[3.51]** (0.25 g, 1 mmol) and sodium metabisulfite (0.19 g, 1 mmol) were heated at 100 °C for 30 minutes. 4-chloro-*o*-Phenylenediamine **[3.9]** (0.142 g, 1 mmol) was added into the resulting reaction mixture after 30 minutes and heated further for 7.5 hours. Progress of reaction was monitored by TLC until the starting materials were consumed. The resulting mixture was cooled to room temperature and then added to cold water to obtain a brown precipitate which was filtered, dried and worked-up with hot hexane to afford the compound, AKS-I-65 **[3.54]** with a yield of 58.8% (0.216 g), m.pt. 113-115 °C and R_f of 0.46 (hexane/ethyl acetate, 1:1). The ^{1}H NMR chemical shifts, $\boldsymbol{\delta_{H(ppm)}}$ (400 MHz, DMSO-d_6) obtained are as follows: 3.81 (3H, s), 3.86 (3H, s), 7.26 (1H, dd, $J_{6,4}$ = 1.6 Hz, $J_{6,7}$ = 8.4 Hz), 7.31 (1H, s), 7.34 (1H, s), 7.62 (1H, d, $J_{7,6}$ = 8.4 Hz), 7.66 (1H, s); **EI-MS** (*m/z* (relative abundance in %)): 43 (3), 166 (5), 184 (4), 201 (11), 215 (7), 229 (29), 272 (5), 322 (16), 337 (31), 353 (21), 366 [M^+] (81), 368 [M^++2] (100), 370 [M^++4] (26); **HREI-MS**: *m/z* calculated for $C_{15}H_{12}N_2O_2BrCl$ [M^+] is 365.9771, found 365.9804. **IR** ($\bar{\upsilon}$/cm^{-1}; KBr disc): ≈3350, 3092, 2939, 2840, 1602, 1497, 1435, 1257, 1213, 1028, 989; **UV** (λ_{max}/nm; MeOH): 298, 222.

3.2.37 Synthesis of 2-(2′-chloro-3′,4′-dimethoxyphenyl)-5-fluoro-1*H*-benzo[*d*] imidazole (AKS-I-73)

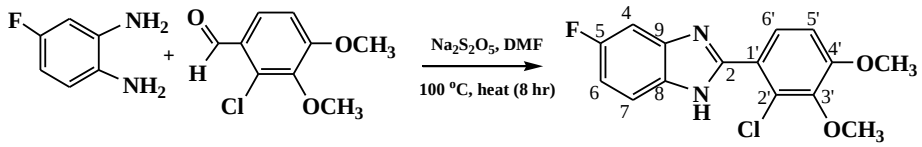

3.6 **3.55** **3.56**

In a round bottom (100 mL) flask equipped with a magnetic stirrer, a mixure of N,N-dimethylformamide (15 mL), 2-chloro-3,4-dimethoxybenzaldehyde **[3.55]** (0.20 g, 1 mmol) and sodium metabisulfite (0.19 g, 1 mmol) was heated at 100 °C for 30 minutes. 4-fluoro-*o*-phenylenediamine **[3.6]** (0.13 g, 1 mmol) was added after 30 minutes into the reaction mixture and heated further for 7.5 hours. Reaction progress was monitored

by TLC until it was completed. After cooling to room temperature, the resulting mixture was added to cold water and the precipitate obtained was filtered, dried and worked-up with hot hexane to afford the brown solid, AKS-I-73 **[3.56]** with a yield of 62.3% (0.191 g), m.pt. 142-145 ^{o}C and 0.38 (hexane/ethyl acetate, 1:1) R_f value. The following chemical shifts, $\boldsymbol{\delta_{H(ppm)}}$ (500 MHz, DMSO-d_6) were obtained: 3.80 (3H, s), 3.91 (3H, s), 7.08 (1H, dt, $J_{6,4}$ = 2.5 Hz, $J_{6,7}$ = 9.0 Hz), 7.23 (1H, d, $J_{5',6'}$ = 8.5 Hz), 7.39 (1H, d, $J_{7,6}$ = 8.5 Hz), 7.57-7.60 (1H, m), 7.63 (1H, d, $J_{6',5'}$ = 9.0 Hz), 12.72 (1H, br s); **EI-MS** (*m/z* (relative abundance in %)): 44 (15), 83 (100), 185 (39), 228 (7), 248 (13), 263 (30), 291 (11), 306 [M^+] (66), 308 [M^++2] (25); **HREI-MS**: *m/z* calculated for $C_{15}H_{12}ClFN_2O_2$ [M^+] is 306.0566, found 306.0571. **IR** ($\bar{\upsilon}$/cm^{-1}; KBr disc): 3151, 2945, 2845, 1630, 1596, 1460, 1284, 1041, 1136; **UV** (λ_{max}/nm; MeOH): 298, 248, 213.

3.2.38 Synthesis of 2′,4′-dichloro-6′-(5,6-dimethyl-1*H*-benzo[*d*]imidazol-2-yl) phenol (AKS-I-98)

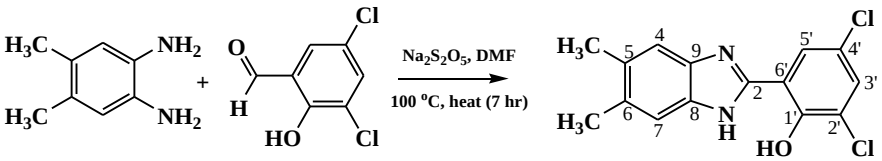

3.12 **3.57** **3.58**

In a round bottom flask (100 mL) equipped with a condenser and a magnetic stirrer, N,N-dimethylformamide (15 mL), 3,5-dichlorosalicylaldehyde **[3.57]** (0.191 g, 1 mmol) and sodium metabisulfite (0.19 g, 1 mmol) were heated at 100 ^{o}C for 30 minutes. 4,5-Dimethyl-*o*-phenylenediamine **[3.12]** (0.14 g, 1 mmol) was added into the reaction mixture afterwards and heated further for 6.5 hours. Reaction progress was monitored by TLC until completion. The resulting mixture, after cooling to room temperature, was added to cold water and the precipitate obtained was filtered, dried and worked-up with hot hexane to afford yellow solid compound coded AKS-I-98 **[3.58]**, having a 98.0% (0.301 g) yield, m.pt. 305-308 ^{o}C and R_f of 0.69 (hexane/ethyl acetate, 1:1). $\boldsymbol{\delta_{H(ppm)}}$ (400 MHz, DMSO-d_6): 7.46 (2H, s), 2.34 (6H, s), 7.65 (1H, d, $J_{3',5'}$ = 2.4 Hz), 8.11 (1H, d, $J_{5',3'}$ = 2.0 Hz), 13.71 (1H, br s); **EI-MS** (*m/z* (relative abundance in %)): 91 (3), 118 (2), 153 (3), 243 (6), 271 (4), 291 (14), 306 [M^+] (100), 308 [M^++2] (66), 310 [M^++4] (8); **HREI-MS**: *m/z* calculated for $C_{15}H_{12}N_2OCl_2$ [M^+] is 306.0327, found 306.0334; **IR** ($\bar{\upsilon}$/cm^{-1}; KBr disc): 3071, 2970, 1618, 1485, 1416, 1260, 1148; **UV** (λ_{max}/nm; MeOH): 346, 334, 307, 230.

3.2.39 Synthesis of 4′-(5-fluoro-1*H*-benzo[*d*]imidazol-2-yl)benzene-1′,3′-diol (AKS-I-99)

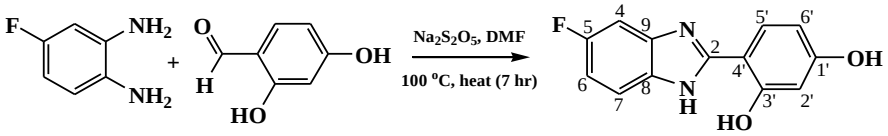

3.6 **3.59** **3.60**

A mixture of N,N-dimethylformamide (15 mL), 2,4-dihydroxybenzaldehyde **[3.59]** (0.14 g, 1 mmol) and sodium metabisulfite (0.19 g, 1 mmol) in a round bottom flask (100 mL) was heated at 100 °C. 4-Fluoro-*o*-phenylenediamine **[3.6]** (0.13 g, 1 mmol) was added into the reaction mixture after 30 minutes and heated further for 6.5 hours. Reaction progress was monitored by TLC until completion. After cooling to room temperature, the resulting mixture was added to iced-cold water and the brown precipitate obtained was filtered, dried and worked-up with hot hexane to afford a solid compound, AKS-I-99 **[3.60]**, with a yield of 65.6% (0.160 g), m.pt. 260-263 °C and R_f of 0.70 (hexane/ethyl acetate, 1:1). The following are the $\delta_{H(ppm)}$ (400 MHz, DMSO-d_6) values obtained: 6.43 (1H, s), 6.47 (1H, dd, $J_{6',2'}$ = 1.6 Hz, $J_{6',5'}$ = 8.8 Hz), 7.15 (1H, dt, $J_{6,4}$ = 2.0 Hz, $J_{6,7}$ = 8.8 Hz), 7.44 (1H, dd, $J_{7,F\text{-}5}$ = 1.2 Hz, $J_{7,6}$ = 8.8 Hz), 7.59-7.62 (1H, m), 7.84 (1H, d $J_{5',6'}$ = 8.4 Hz), 10.14 (1H, s), 13.06 (1H, br s); **EI-MS** (*m/z* (relative abundance in %)): 83 (3), 108 (6), 136 (2), 161 (4), 174 (4), 187 (44), 215 (9), 244 [M^+] (100), 245 [M^++1] (20); **HREI-MS**: *m/z* calculated for $C_{13}H_9N_2O_2F$ [M^+] is 244.0648, found 244.0651. **IR** ($\bar{\upsilon}$/cm^{-1}; KBr disc): 3347, 1617, 1492, 1145, 1110; **UV** (λ_{max}/nm; MeOH): 316, 293, 245, 215.

3.2.40 Synthesis of 2′-(5,6-dimethyl-1*H*-benzo[*d*]imidazol-2-yl)benzene-1′,4′-diol (AKS-I-100)

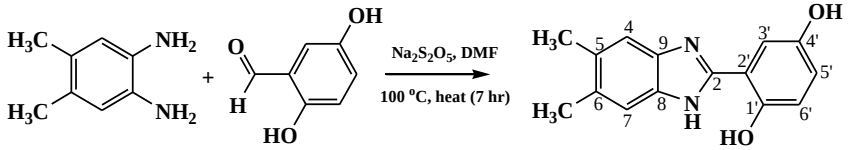

3.12 **3.61** **3.62**

In a 100 mL round bottom flask, a mixture of N,N-dimethylformamide (15 mL), 2,5-dihydroxybenzaldehyde **[3.61]** (0.14 g, 1 mmol) and sodium metabisulfite (0.19 g, 1 mmol) was heated at 100 °C for 30 minutes. 4,5-dimethyl-*o*-phenylenediamine **[3.12]** (0.14 g, 1 mmol) was added into the resulting reaction mixture and heated further for 6.5 hours. Reaction progress was monitored by TLC until completion. After cooling to room temperature, the mixture was added to iced-water and a brown precipitate was obtain which was filtered, dried and worked-up with hot hexane to afford the compound,

AKS-I-100 **[3.62]**, 84.2% (0.214 g) yield, m.pt. 315-317 ºC and a 0.67 (hexane/ethyl acetate, 1:1) R_f value. The following $\boldsymbol{\delta_{H(ppm)}}$ (400 MHz, DMSO-d_6) was obtained: 2.33 (6H, s), 6.85 (2H, s), 7.38 (1H, s), 7.42 (2H, s), 9.11 (1H, s), ≈12.80 (1H, br s); **EI-MS** (*m/z* (relative abundance in %)): 91 (4), 120 (3), 197 (16), 239 (9), 254 [M^+] (100), 255 [M^++1] (15); **HREI-MS**: *m/z* calculated for $C_{15}H_{14}N_2O_2$ [M^+] is 254.1055, found 254.1065; **IR** ($\bar{\upsilon}/cm^{-1}$; KBr disc): 3481, 3260, 2920, 2856, 1626, 1561, 1503, 1098; **UV** (λ_{max}/nm; MeOH): 339, 307, 298, 228, 222.

3.3 Anthelmintic assay

3.3.1 Sample collection

Fresh faecal samples from cattle at Akinyele Local Government Abattoir, Moniya Ibadan were collected directly from the rectum with disposable gloves. These samples were labelled and taken to the diagnostic parasitology laboratory of the Department of Veterinary Parasitology and Entomology, University of Ibadan, Ibadan for processing to determine which is(are) positive, having nematode eggs.

3.3.2 Egg diagnostic method

The principle of egg floatation technique was used to determine the presence of nematode eggs in the faecal samples obtained from naturally infected cattle according to a modified method by Roepstorff and Nansen, 1998. Approximately 3 g of the samples were weighed into a container, homogenised in about 50 mL of saturated salt solution (floatation fluid) and the feacal suspension filtered through 1 mm and 150 μm sieves. The filtrate collected was transferred into centrifuge tubes and faecal debris discarded. The centrifuge tubes were topped up with the filtrate, such that a convex meniscus is observed at the top. Microscope coverslips were placed over the tubes and left to stand for 10 minutes, such that nematode eggs which has lower specific gravity floats to the surface. The coverslips, were carefully lifted with the drop of floatation solution attached and placed on microscope slides and viewed at X100 and X400 magnifications to examine for the presence of nematode eggs.

3.3.3 Egg recovery method

The protocol used in egg recovery was performed following the methods by Molefe *et al.,* 2013 and Katiki *et al.,* 2011 with modifications. About 5 g of fresh faecal samples from cattle was weighed into a container and homogenised with distilled water to obtain a suspension (slurry). This suspension was then filtered through sieves with graduated apertures 1000, 150, 75 μm respectively into another container. The filtrate was

transferred into 15 mL centrifuge tubes and centrifuged at 1500 rpm for 5 minutes. The supernatant was decanted and the sediments suspended in saturated NaCl solution. The sediment suspension was centrifuged. Following the principle of floatation, nematode eggs were collected by decanting the supernatant into a 25 μm sieve. The eggs retained within the sieve were washed severally with distilled water to remove the traces of salt, and finally carefully back washed into a 50 mL beaker. By counting the number of eggs in two aliquots of 0.2 mL of the suspension on a microscope slide repeatedly, the concentration of the eggs was estimated and the mean number of eggs per 0.1 mL was calculated to be approximately 73 eggs.

3.3.4 Egg hatch inhibitory assay

The egg hatch inhibition (EHI) of the test compounds was carried out using a modification of the method described by Molefe *et al.,* 2013 and Katiki *et al.,* 2011. The test was carried out using 0.2 mL of the egg suspension pipetted into test tubes. The synthesised compounds were dissolved in 10% DMSO (DMSO + distilled water). Different concentrations of the test compound, 100, 50, 25 and 12.5 μg/μL, were prepared and used. Into the egg suspensions were added 0.2 mL of the dissolved compounds, each tube receiving concentrations equivalent to the label on it. The experiment was set up in triplicates of four test tubes for each test compound concentration. Albendazole, a commercial anthelmintic drug, prepared in equivalent concentrations in 10% DMSO was employed as the standard serving as positive control. Distilled water was used as negative control. After 48 hours of incubation at room temperature, aliquots of the mixture from each tube were viewed under an inverted light microscope to count the eggs and first-stage larvae (L_1). The percentage egg hatch inhibition (%EHI) was calculated using the formula by Cala *et al.,* 2012 as written below and the effective concentration required to induce 50% inhibition of egg from hatching (IC_{50}) was evaluated.

$$\boldsymbol{EHI = \frac{[Eggs + L_1] - L_1}{Eggs + L_1} \times 100}$$

3.4 Statistical analysis

The mean percent egg hatch inhibition and the dose response curve were obtained using Microsoft Excel package, while the IC_{50} was determined using Finney probit analysis.

CHAPTER FOUR

4.0 RESULTS AND DISCUSSION

4.1 Characterisation of the synthesised benzimidazoles

This study entails the synthesis of benzimidazoles possessing either the furanyl, substituted furanyl or substituted phenyl/benzyl groups attached to carbon at position -2, and groups having different electron donating or withdrawing substituents attached to any of carbons at positions -5 or -6 or both in order to afford derivatives with enhanced anthelmintic activity. The synthetic routes employed were summarized in schemes **3.1a** and **3.1b** as outlined in chapter three. The spectroscopic characterisations of these synthesised benzimidazoles are hereby reported.

4.1.1 Characterisation of 2-(furan-2′-yl)-1*H*-benzo[*d*]imidazole (AKS-I-6)

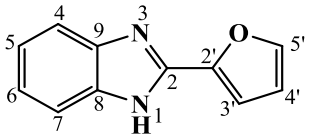

2-(Furan-2′-yl)-1*H*-benzo[*d*]imidazole (AKS-I-6) was obtained as a brown solid, 0.101 g (54.80% yield); m.pt. 283-285 ^{o}C [literature: 285-287 ^{o}C (Mohan *et al*., 2015; Temirak *et al*., 2014b)]; R_f: 0.43 (hexane/ethyl acetate, 1:1).

The proton nuclear magnetic resonance, ^{1}H NMR spectrum (400 MHz, DMSO-d_6) (figures **4.1** and **4.2**) show a total of five signals in δ (ppm) units and are assigned as 12.88 (s, 1H, -NH) to the secondary amine proton, seen to be the most deshielded, while each of the signals at 7.93 (d, 1H, $J_{5',4'}$ = 1.2 Hz, H-5′), three broad peaks 7.60, 7.47, 7.18 corresponding to (1H, br s, H-4), 7.47 (1H, br s, H-7) and (br s, 2H, H-6, H-5) respectively, as well as 7.18 (d, 1H, $J_{3',4'}$ = 3.2 Hz, H-3′), 6.72 (dd, $J_{4',3'}$ = 3.2 Hz, $J_{4',5'}$ = 1.6 Hz H-4′) were assigned to the aromatic methine protons. There is the rapid exchange of proton between nitrogens at positions 1 and 3 on the imidazole ring and tautomerism is established. As a result of this, positions 5- and 6- become chemically equivalent, thus, the broad singlet at δ (ppm) 7.18. On the furan ring, protons at positions 3′and 4′ couples with a coupling constant, *J* of 3.2. The broad-band decoupled carbon-13 nuclear magnetic

resonance, ^{13}C NMR (100 MHz, DMSO-d_6) spectrum (figure **4.3**) shows resonance peaks in δ (ppm) units assigned as 145.53 (C-2), 143.57 (C-9, C-8, C-2′) to four quartenary carbons, and 144.56 (C-5′), 122.45 (C-6), 121.86 (C-5), 112.25 (C-7, C-4), 110.39 (C-4′, C-3′) to seven methine carbons. The spectrum obtained from the Distortionless Enhancement by Polarization Transfer, DEPTH-135 (100 MHz, DMSO-d_6) experiment (figure **4.4**) further confirms the respective methine carbons.

The spectrum (figure **4.5**) representing the electron impact-mass spectrometry (EI-MS) analysis shows the molecular ion, M^+ as the most intense/base peak corresponding to a mass-to-charge ratio, *m/z* 184 $[C_{11}H_8N_2O]^+$ alongside a $[M^+{+}1]$ peak at *m/z* 185. Cleavage of the M^+ at the furan ring produced the fragment with *m/z* of 156 by a loss of $CHO^{\bullet}$ radical corresponding to M^+-29. An α-cleavage that led to opening of the furan ring (i.e. breakage of the bond between C-2′ and O), followed by loss of $C_3H_3O^{\bullet}$ radical is suggestive of the peak with *m/z* of 129. Fragmentation at the imidazole ring led to the *m/z* at 92, corresponding to $[M\text{-}C_6H_6N]^+$ and a further loss of acetylene resulted to the fragment with *m/z* of 65 corresponding to $[C_4H_3N]^{\bullet+}$. The *m/z* of 184.0639 (calculated, 184.0637) obtained from high resolution electron impact-mass spectrometry (HREI-MS) analysis corresponds to the formula $C_{11}H_8N_2O$, further confirming the compound.

The Infrared (IR) absorption spectrum (figure **4.6)** shows vibrational bands with characteristic vibrational frequencies, $\bar{\upsilon}$ (cm^{-1}) for some functional groups assigned to the secondary (2º) amine N–H_{str}, aromatic C–H_{str}, C=N_{str}, two aromatic C=C_{str}, asymmetric and symmetric C–O–C_{str} of ether, correspond to ≈3400, 3069, 1621, 1521, 1490, 1227 and 1012 cm^{-1} respectively. The Ultra-violet (UV) analysis (figure **4.7**) showed maximum absorptions (λ_{max}) at 321, 306, 250 and 208 nm, indicative of n→π* and π→π* transitions. Comparisons of the ^{1}H NMR spectroscopic data with those from literature were consistent (Mohan *et al*., 2015; Temirak *et al*., 2014b). Summary of the ^{1}H NMR and ^{13}C NMR spectra is represented in table **4.1**.

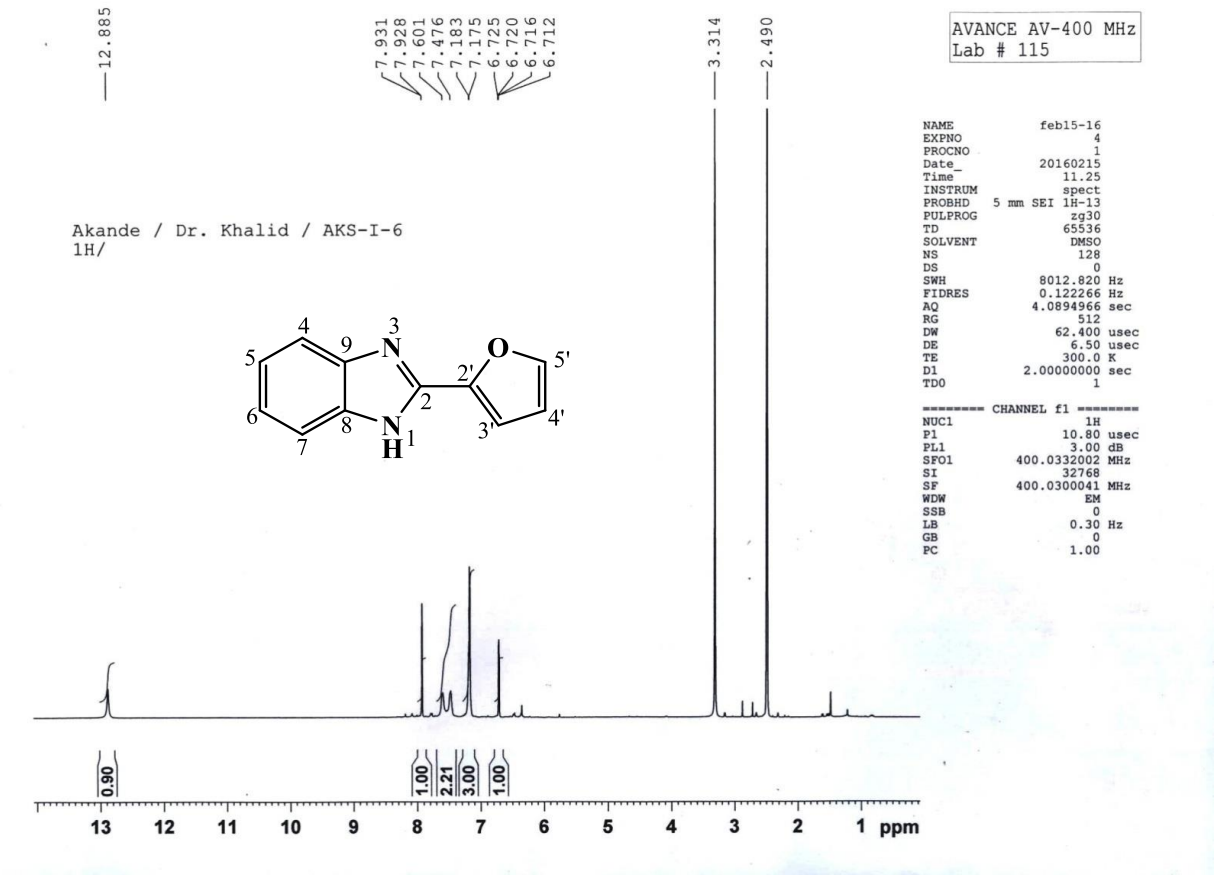

Figure 4.1. ^{1}H NMR (400 MHz, DMSO-d_6) spectrum of AKS-I-6

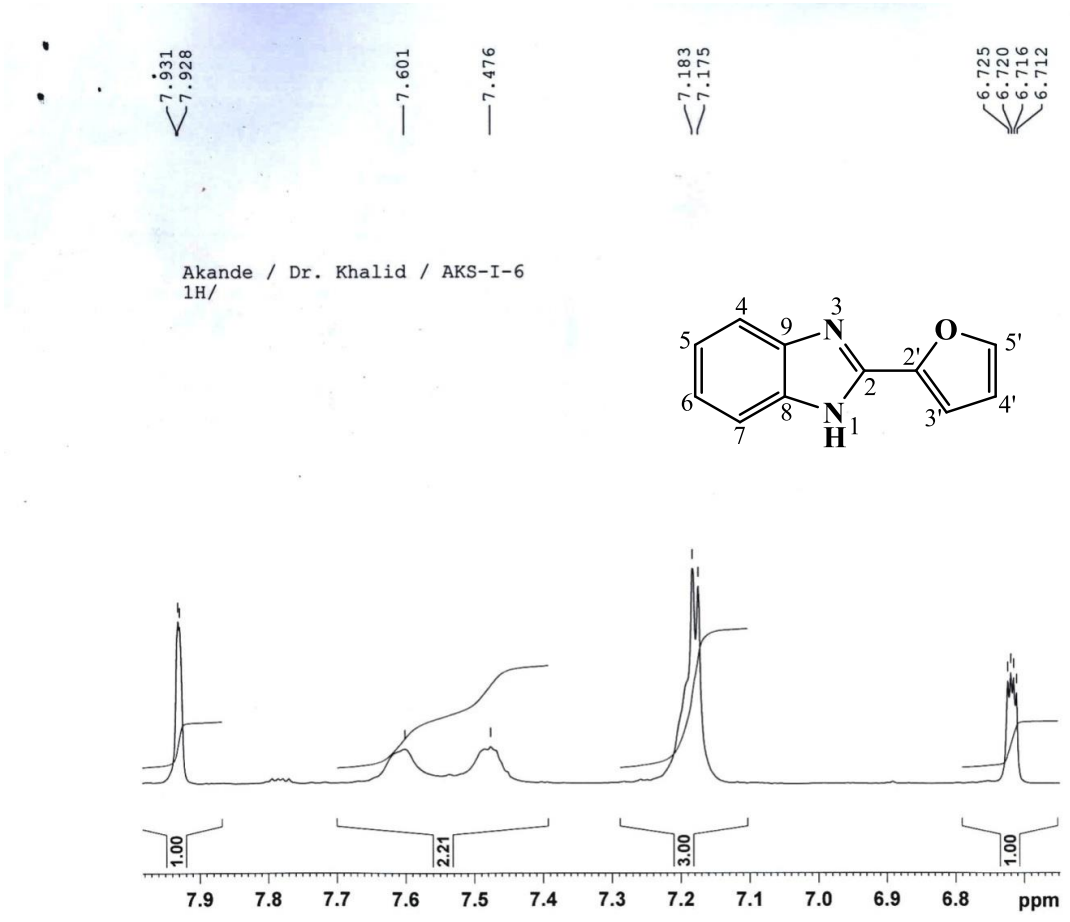

Figure 4.2. ^{1}H NMR (400 MHz, DMSO-d_6) spectrum of AKS-I-6 aromatic region (Expanded)

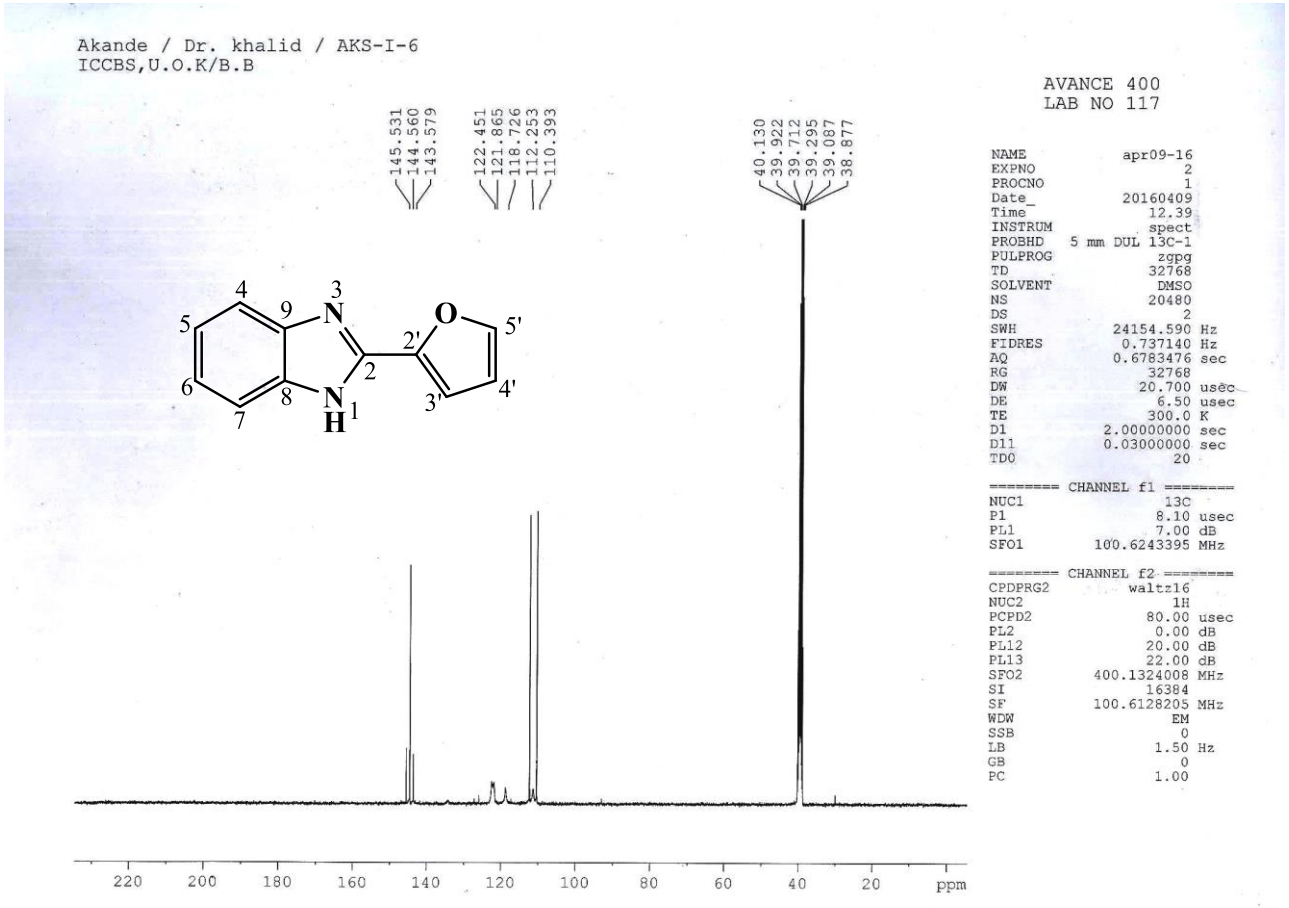

Figure 4.3. ^{13}C NMR (100 MHz, DMSO-d_6) spectrum of AKS-I-6

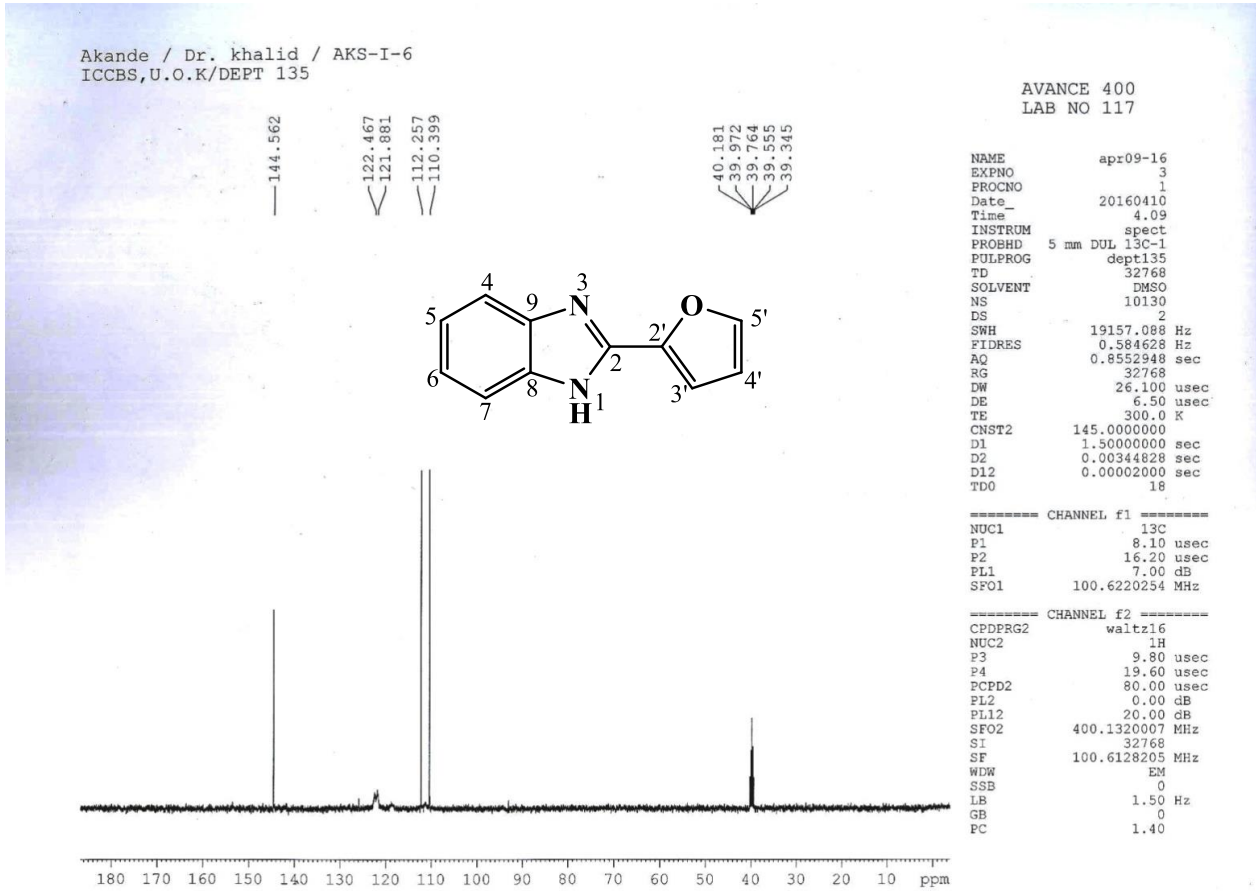

Figure 4.4. DEPTH-135 (100 MHz, DMSO-d_6) spectrum of AKS-I-6

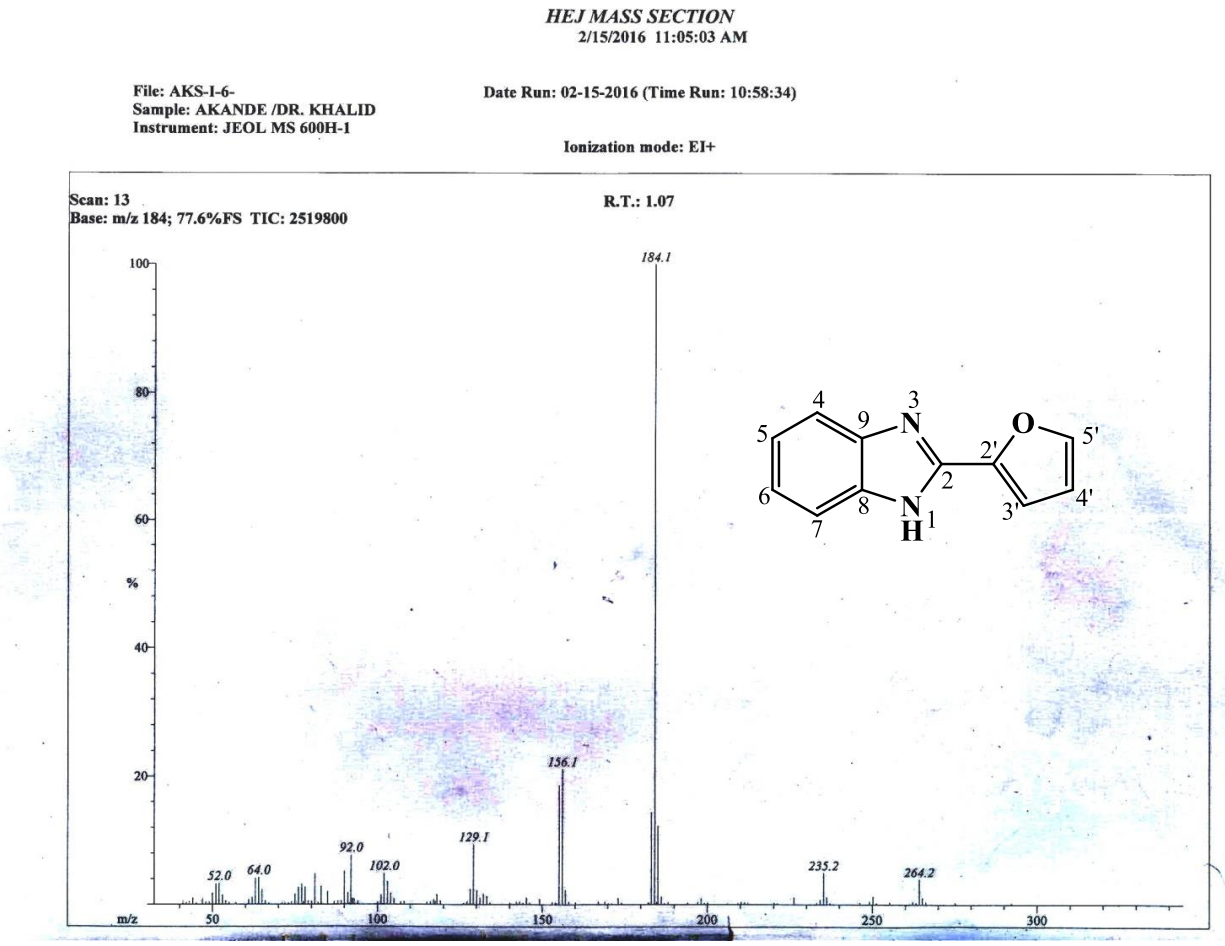

Figure 4.5. EI-MS spectrum of AKS-I-6

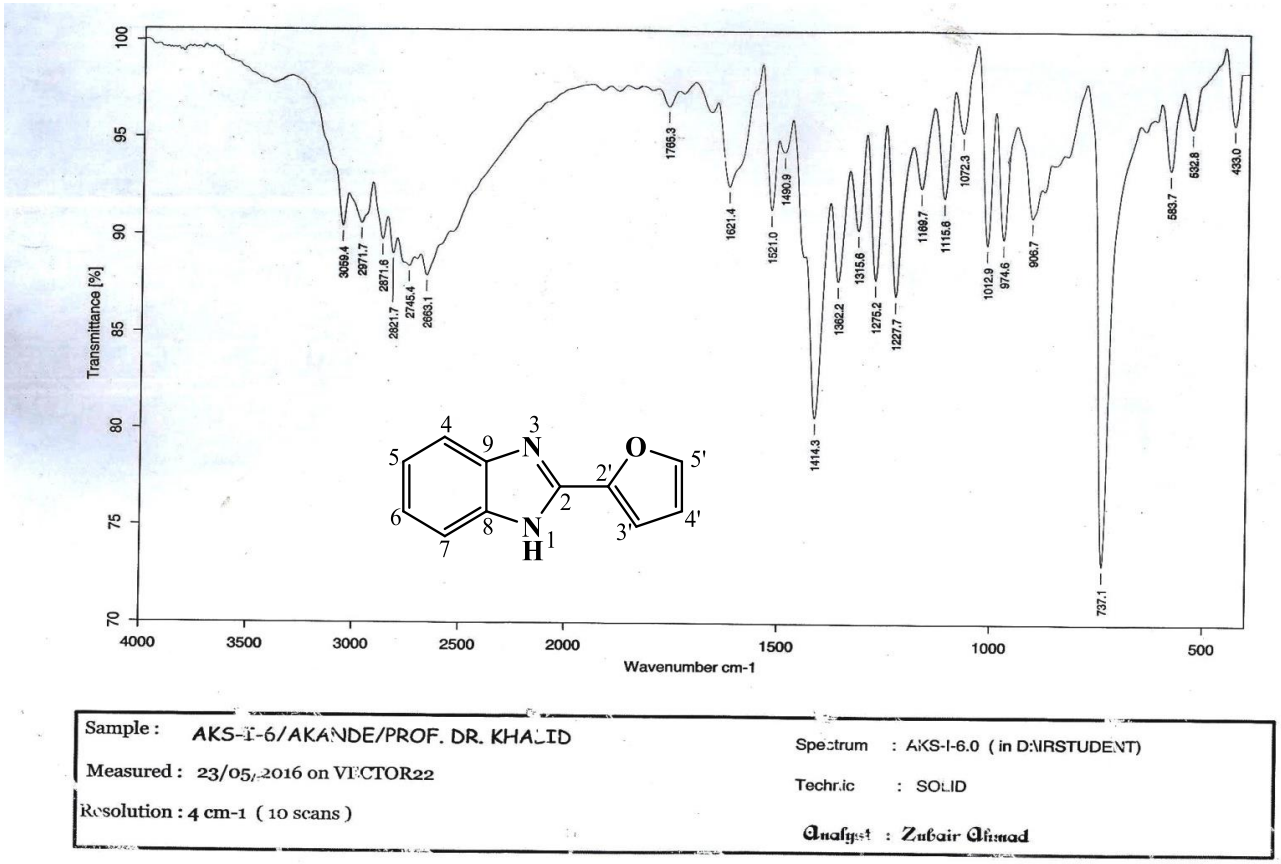

Figusre 4.6. IR spectrum of AKS-I-6

THERMO ELECTRON ~ VISIONpro SOFTWARE V4.10

Operator Name	ARSHAD ALAM	Date of Report	5/24/2016
Department	Analytical laboratory#004 TWC	Time of Report	9:21:05AM
Organization	ICCBS.Karachi University.		
Information	Prof Dr.Khalid ./ Akande.		

Scan Graph

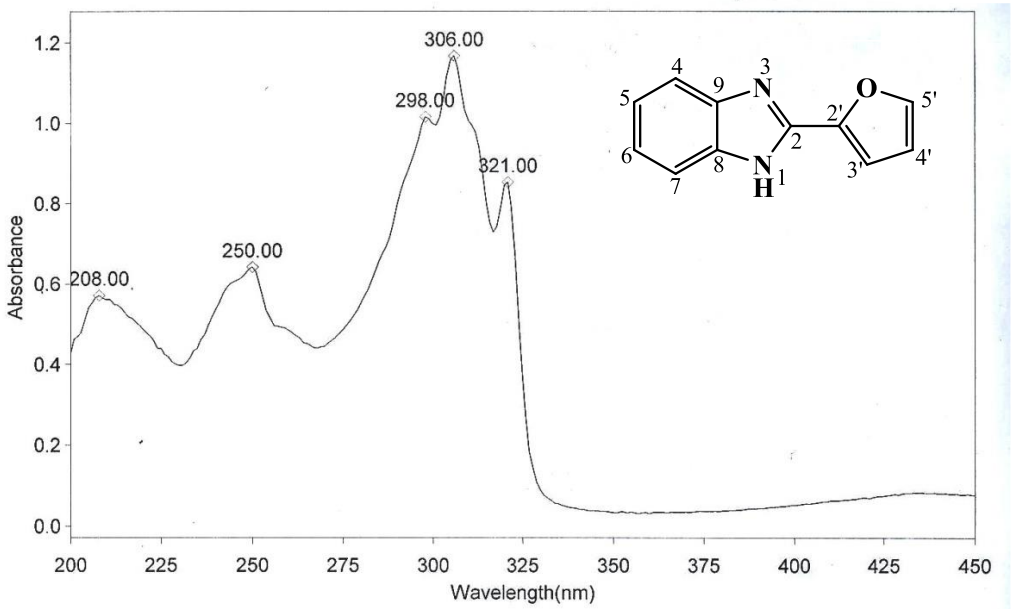

Results Table - AKS- I- 6.sre,AKS- I- 6,Cycle01

nm	A	**Peak Pick Method**
208.00	0.572	Find 8 Peaks Above -3.0000 A
250.00	0.642	Start Wavelength 200.00 nm
298.00	1.016	Stop Wavelength 450.00 nm
306.00	1.168	Sort By Wavelength
321.00	0.854	Sensitivity Manual
Rising Points	3	
Falling Points	3	
Min. Change	0.0000	

Page 1, Scan Graph

Figure 4.7. UV spectrum of AKS-I-6

Table 4.1. Summary of the ^{1}H NMR and ^{13}C NMR spectra of AKS-I-6

Position	δ ^{1}H [mult., J_{HH} (Hz)] (ppm)	Mohan *et al*., 2015	Temirak *et al*., 2014b	δ ^{13}C (ppm)	DEPT-135
1	12.88 [s]	12.91 [s]	13.00 [s]	-	-
2	-	-	-	145.53	-
3	-	-	-	-	-
4	7.47 [s]	7.54 [s]	7.49 [m]	112.25	CH
5	7.18 [br s]	7.20 [m]	7.16 [m]	121.86	CH
6	7.18 [br s]	7.20 [m]	7.16 [m]	122.45	CH
7	7.60 [s]	7.54 [s]	7.49 [m]	112.25	CH
8	-	-	-	143.57	-
9	-	-	-	143.57	-
1′	-	-	-	-	-
2′	-	-	-	143.57	-
3′	7.18 [d, $J_{3',4'}$ = 3.2]	7.20 [m]	7.15 [dd, *J* = 3.0]	110.39	CH
4′	6.72 [dd, $J_{4',3'}$ = 3.2, $J_{4',5'}$ = 1.6]	6.71 [dd, *J* = 3.3, 1.6]	6.69 [dd, *J* = 3.0]	110.39	CH
5′	7.93 [d, $J_{5',4'}$ = 1.2]	7.96 [dd, *J* = 1.6, 0.9]	7.90 [dd, *J* = 3.0]	144.56	CH

4.1.2 Characterisation of 2-(5′-methylfuran-2′-yl)-1*H*-benzo[*d*]imidazole (AKS-I-7)

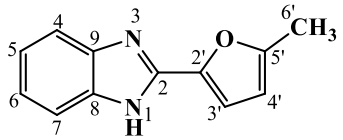

2-(5′-Methylfuran-2′-yl)-1*H*-benzo[*d*]imidazole (AKS-I-7) is a brown solid compound obtained in with a yield of 65.6% (0.130 g), m.pt. range of 274-276 ^{o}C [lit. 275-277 ^{o}C (Temirak *et al*., 2014b)] and a R_f of 0.46 (hexane/ethyl acetate, 1:1). Figures **4.8** and **4.9** are the spectra obtained from ^{1}H NMR analysis (400 MHz, DMSO-d_6) in δ (ppm) units. Five peaks representing the aromatic methine protons are assigned as 7.50-7.53 (2H, m, H-4, H-7), multiplet peaks at 7.16-7.18 (2H, m, H-5, H-6) for protons on positions 5 and 6, 7.08 (1H, d, $J_{3',4'}$ = 3.2 Hz, H-3′) and 6.34 (d, 1H, $J_{4',3'}$ = 2.4 Hz, H-4′). The upfield signal at 2.40 (s, 3H, 6′-CH_3) represents the methyl protons. The multiplets observed for peaks of protons at positions 4, 5, 6 and 7 (chemical equivalence) are due to rapid exchange of the proton between positions 1 and 3 and therefore an overlap of peaks. The 2^{o} amine proton peak expected to resonate further downfield was not captured on the spectrum.

The ^{13}C NMR (100 MHz, DMSO-d_6) spectrum in figure **4.10** reveals a total of chemical shifts, δ (ppm) as 143.63 (C-8, C-9), 143.74 (C-2′) and 153.77 (C-2, C-5′), representing four quartenary carbons, 122.04 (C-6, C-5), 111.68 (C-7, C-4) and 108.52 (C-4′, C-3′) representing six methine carbons, while 13.41 (C-6′) represents the methyl carbon. DEPTH-135 (100 MHz, DMSO-d_6) spectrum in figure **4.11** further confirms the respective methine and methyl carbons.

The *m/z* of 198 and 199 obtained from EI-MS analysis (figure **4.12**) corresponds to the molecular ion, M^+ peak (the base peak) and a [M^++1] peak respectively. The *m/z* 183 corresponds to [M-CH_3 (side chain)]$^+$. The *m/z* at 169 is suggestive of an α-cleavage between C-5′ and O of the M^+, followed by the loss of $C_2H_5^{\bullet}$ radical. The [M-CH_2CO]$^+$ fragment corresponds to *m/z* 155 peak. Fragmentation at the imidazole ring resulted in a *m/z* 90 $[C_6H_4N]^{\bullet+}$ ion and a subsequent *m/z* of 63 due to a loss of C_2H_2 which corresponds to $[C_5H_3]^{\bullet+}$. The *m/z* 198.0800 (calculated, 198.0793) obtained from HREI-MS analysis corresponding to the molecular formula $C_{12}H_{10}N_2O$, further confirmed the compound. The IR absorption spectrum (figure **4.13**) shows diagnostic absorption bands with vibrational frequencies, $\bar{\upsilon}$ (cm^{-1}) at 3447, 3054, 2953, 2805, 1632, 1570, 1423, 1275 and

1020 indicative of an amine N–H_{str}, aromatic C–H_{str}, aliphatic C–$H_{asy\ str}$ and C–$H_{sym\ str}$, C=N_{str}, aromatic C=C_{str}, C–H_b of methyl side chain, C–O–C_{asy} and C–O–$C_{sym\ str}$ of ether respectively. The maximum absorptions from UV spectrum (figure **4.14**) shows wavelenghts, (λ_{max}) at 326, 311, 253 and 210 nm that are indicative of n→π* and π→π* transitions. All corresponding ^{1}H NMR data was found to be consistent with previously published values (Temirak *et al*., 2014b). Table **4.2** shows the summary of ^{1}H NMR and ^{13}C NMR spectra.

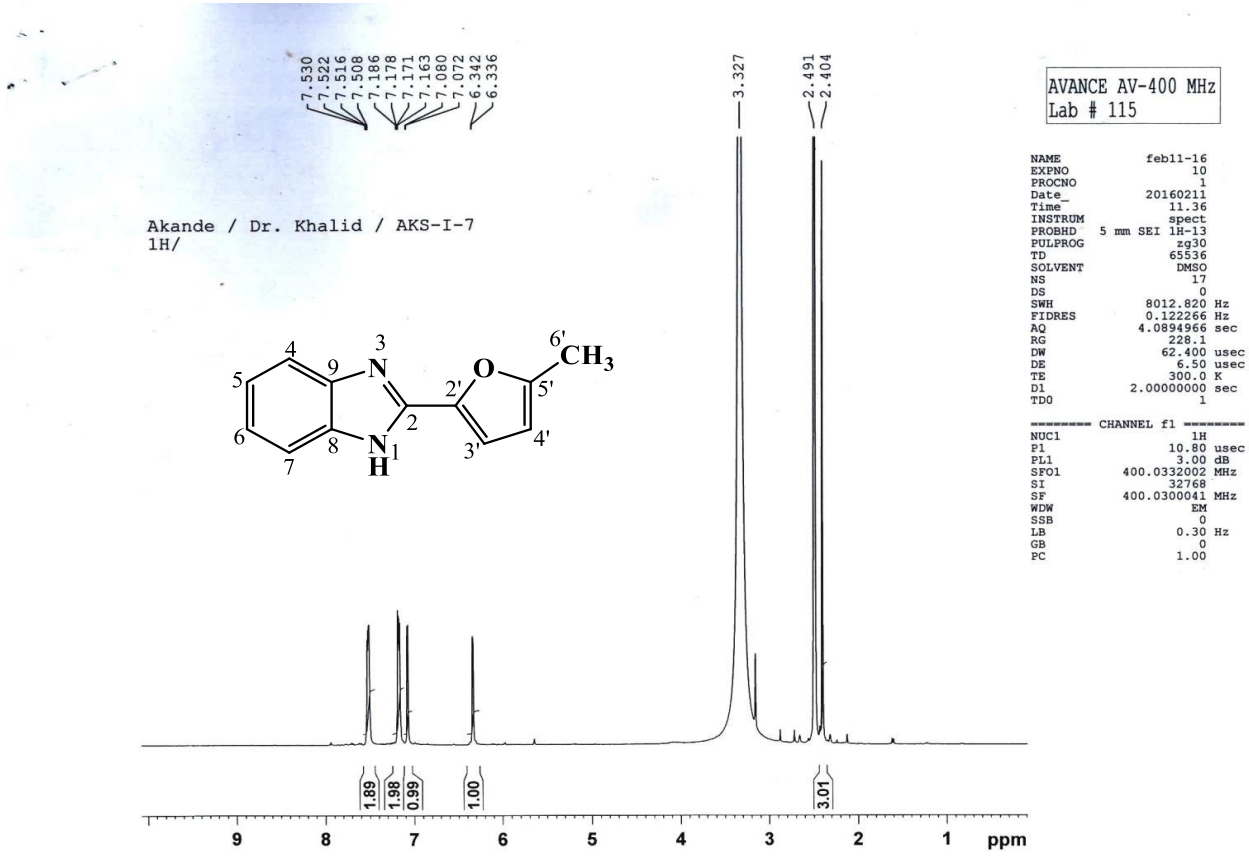

Figure 4.8. ^{1}H NMR (400 MHz, DMSO-d_6) spectrum of AKS-I-7

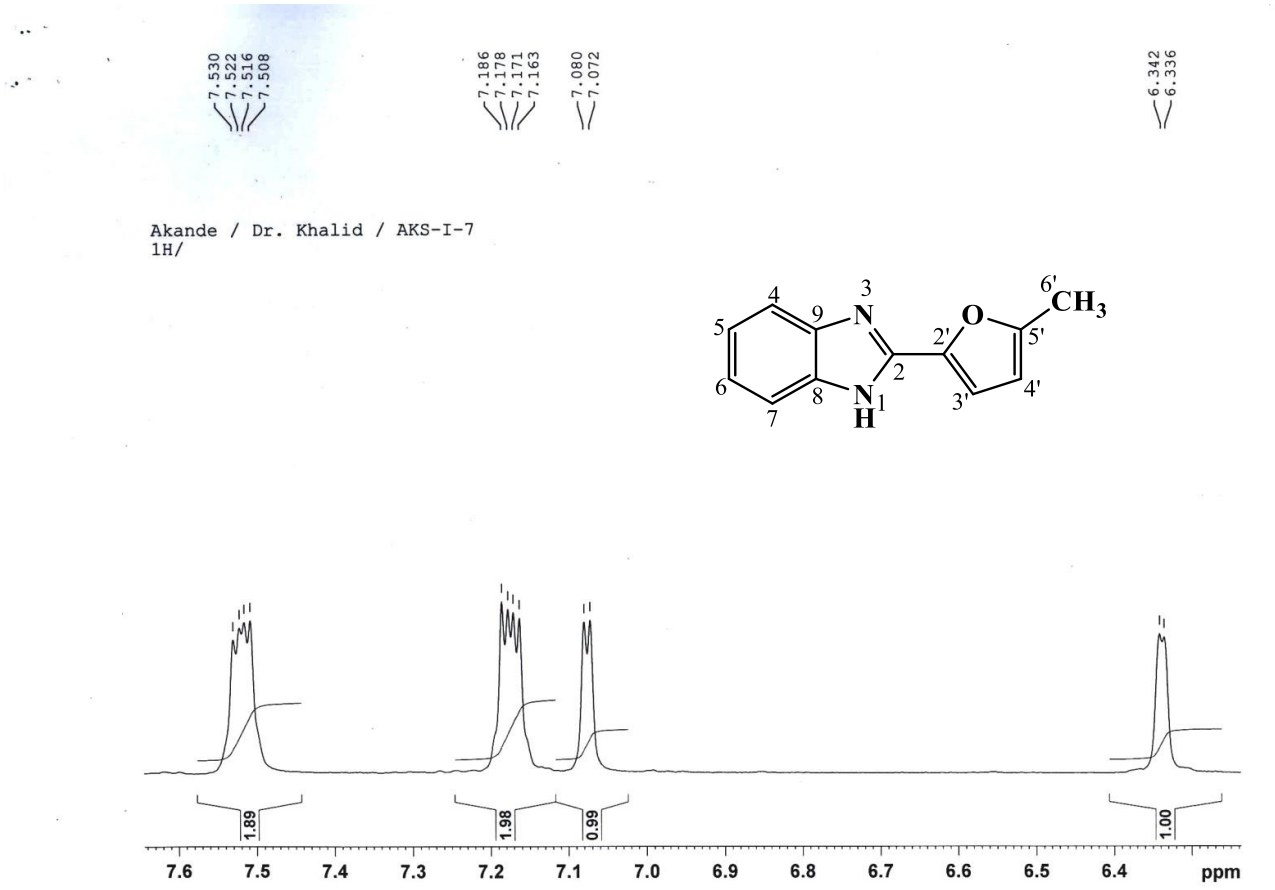

Figure 4.9. ^{1}H NMR (400 MHz, DMSO-d_6) spectrum of AKS-I-7 aromatic region (Expanded)

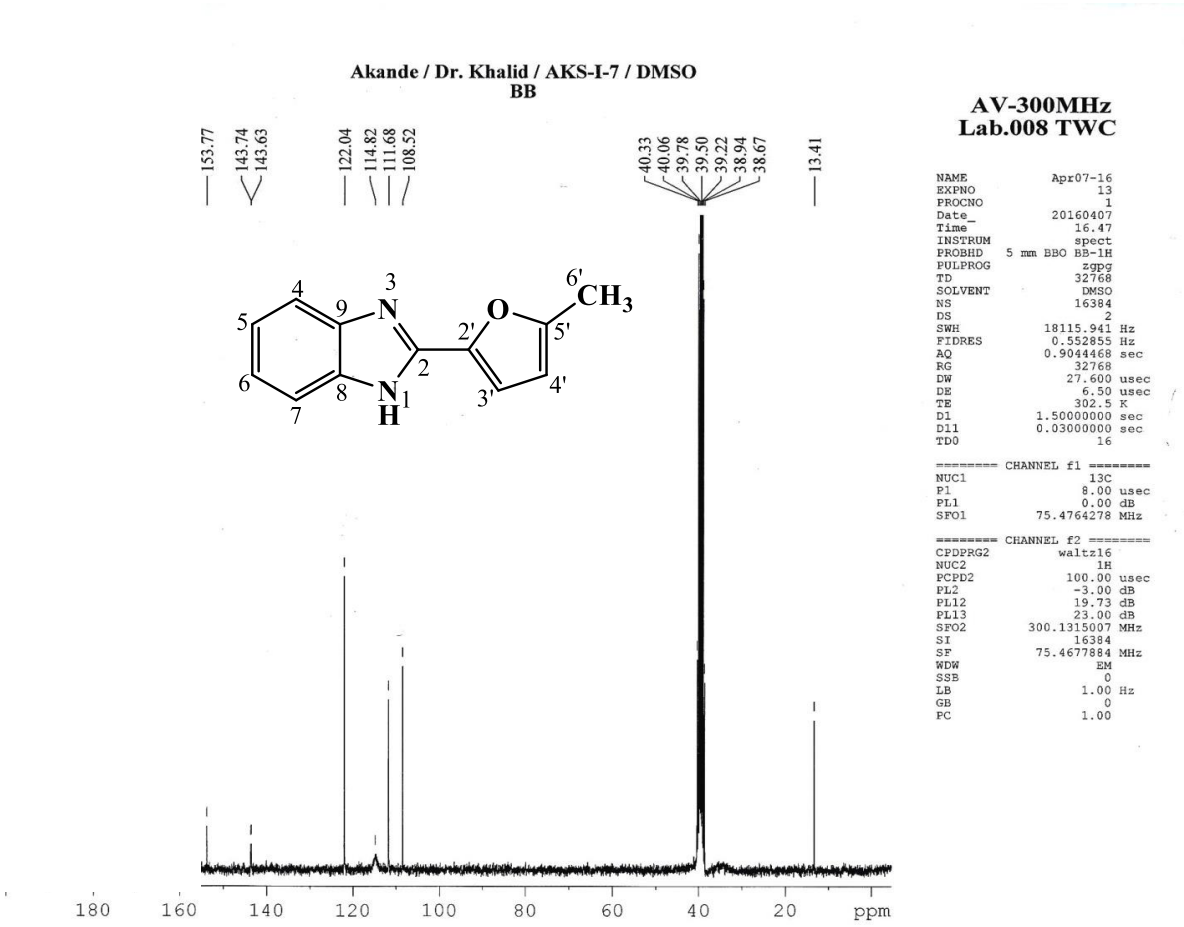

Figure 4.10. ^{13}C NMR (75 MHz, DMSO-d_6) spectrum of AKS-I-7

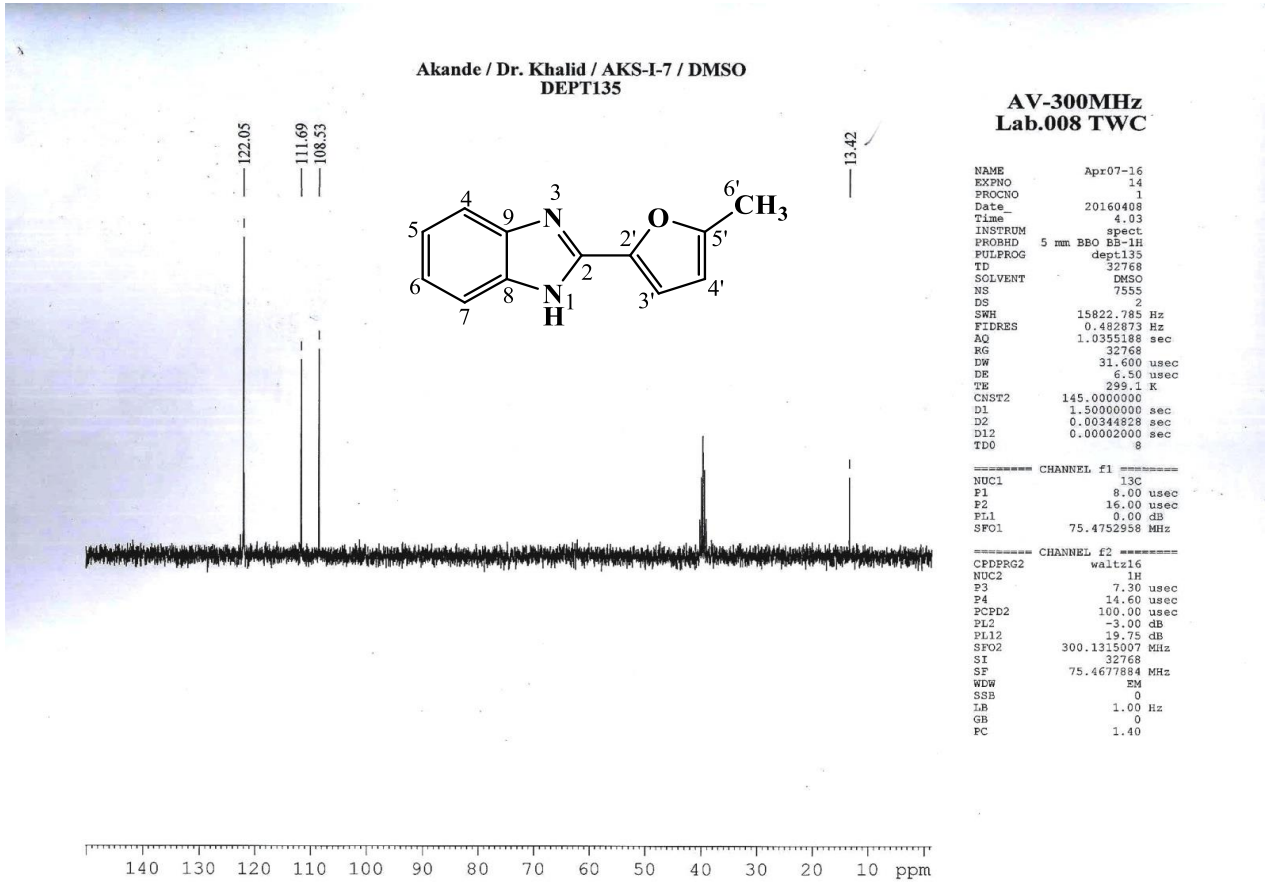

Figure 4.11. DEPTH-135 (75 MHz, DMSO-d_6) spectrum of AKS-I-7

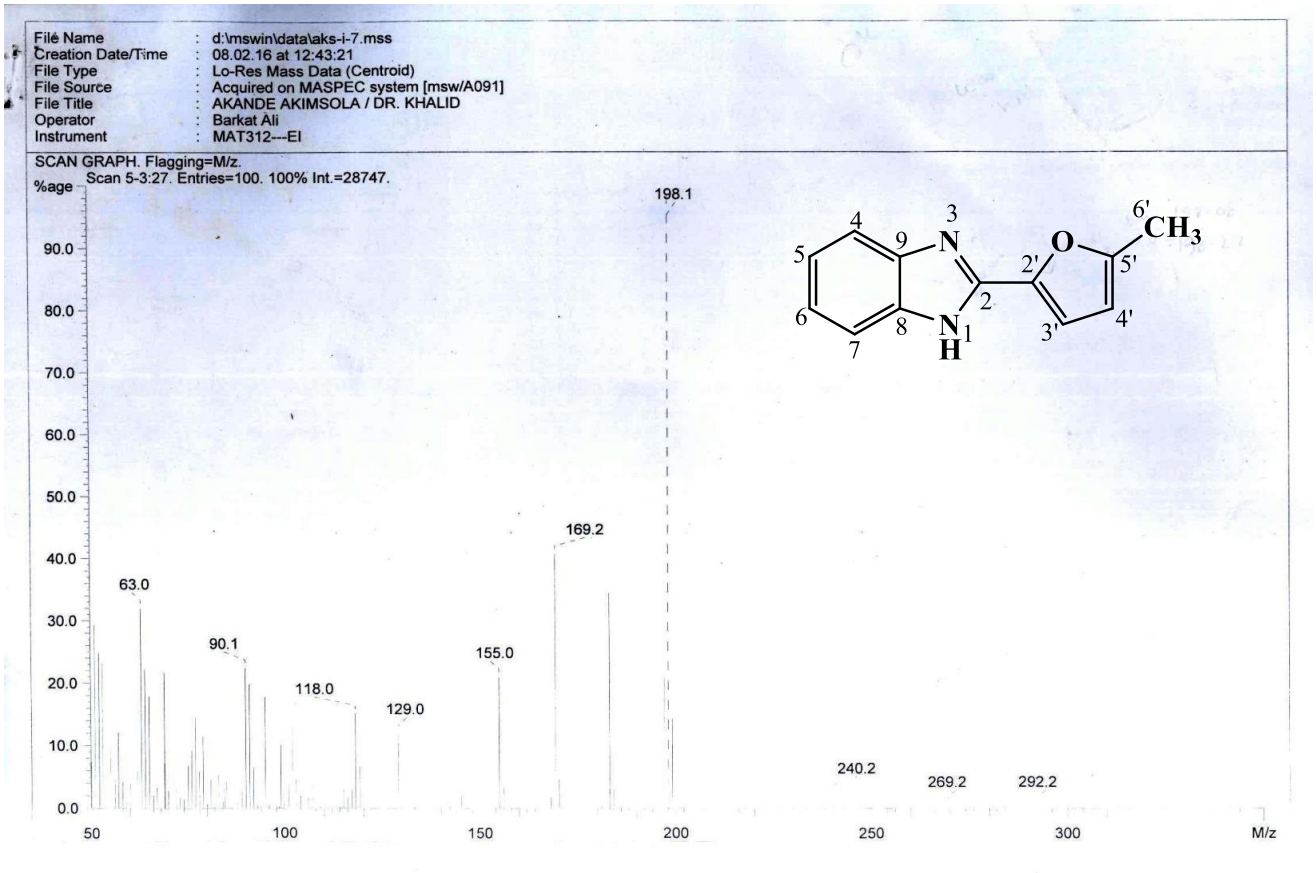

Figure 4.12. EI-MS spectrum of AKS-I-7

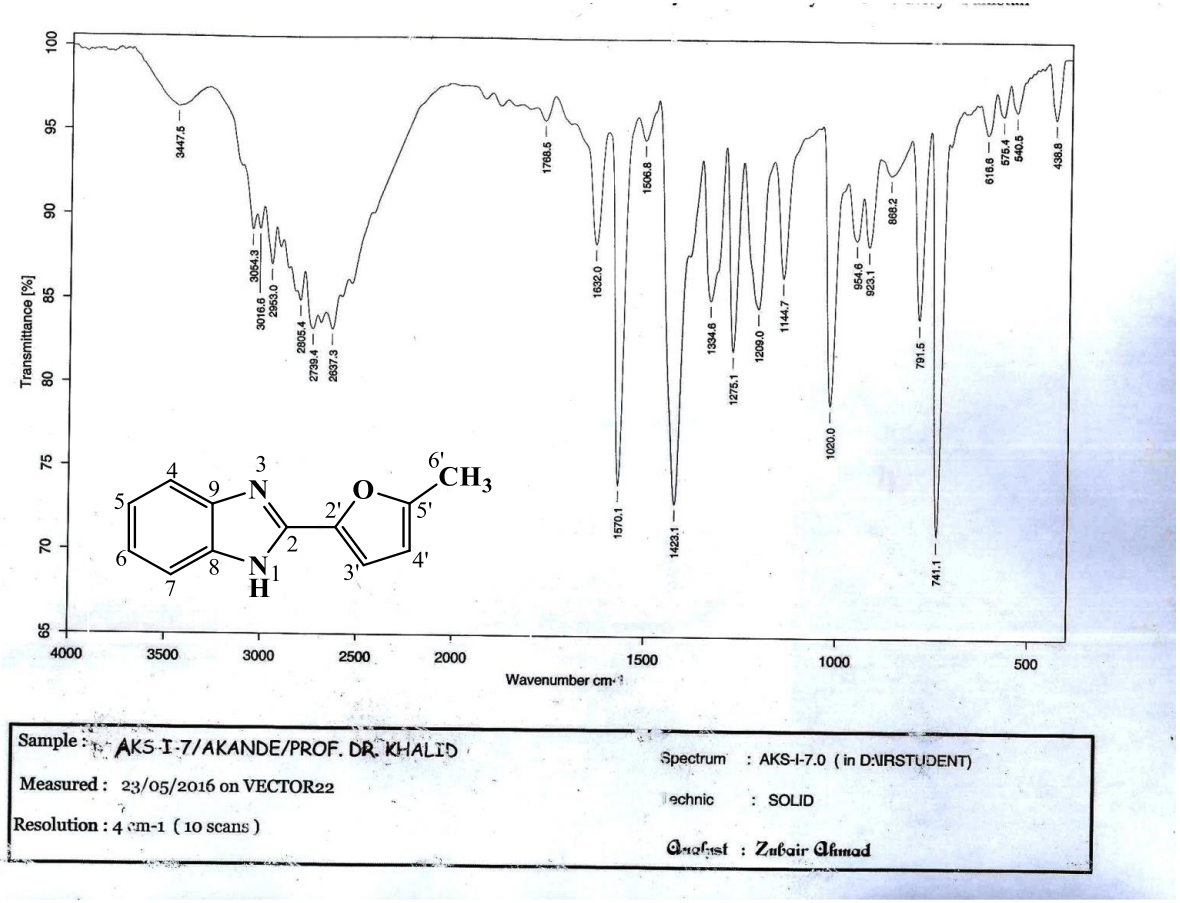

Figure 4.13. IR spectrum of AKS-I-7

THERMO ELECTRON ~ VISIONpro SOFTWARE V4.10

Operator Name	ARSHAD ALAM	Date of Report	5/24/2016
Department	Analytical laboratory#004 TWC	Time of Report	9:28:35AM
Organization	ICCBS.Karachi University.		
Information	Prof Dr.Khalid ./ Akande.		

Scan Graph

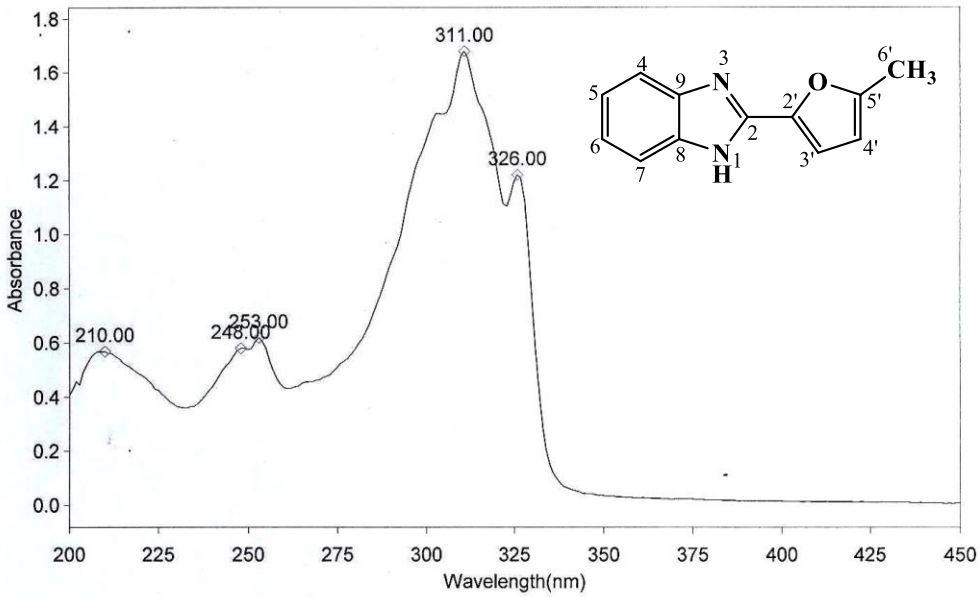

Results Table - AKS- I- 7.sre,AKS - I- 7,Cycle01

nm	A	**Peak Pick Method**
210.00	0.568	Find 8 Peaks Above -3.0000 A
248.00	0.580	Start Wavelength 200.00 nm
253.00	0.618	Stop Wavelength 450.00 nm
311.00	1.680	Sort By Wavelength
326.00	1.220	Sensitivity Medium

Page 1, Scan Graph

Figure 4.14. UV spectrum of AKS-I-7

Table 4.2. Summary of the ^{1}H NMR and ^{13}C NMR spectra of AKS-I-7

Position	δ ^{1}H [mult., J_{HH} (Hz)] (ppm)	Temirak *et al.*, 2014b	δ ^{13}C (ppm)	DEPT-135
1	-	12.00 [s]	-	-
2	-	-	153.77	-
3	-	-	-	-
4	7.53-7.50 [m]	7.49 [m]	111.68	CH
5	7.18-7.16 [m]	7.13 [m]	122.04	CH
6	7.18-7.16 [m]	7.13 [m]	122.04	CH
7	7.53-7.50 [m]	7.49 [m]	111.68	CH
8	-	-	143.63	-
9	-	-	143.63	-
1′	-	-	-	-
2′	-	-	143.74	-
3′	7.08 [d, $J_{3',4'}$ = 3.2]	7.05 [d, J = 3.0]	108.52	CH
4′	6.34 [d, $J_{4',3'}$ = 2.4]	6.31 [dd, J = 3.0]	108.52	CH
5′	-	-	153.77	-
6′	2.40 [s]	2.36 [s]	13.41	CH_3

4.1.3 Characterisation of 5-fluoro-2-(furan-2′-yl)-1*H*-benzo[*d*]imidazole (AKS-I-8)

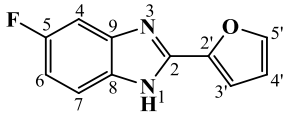

The compound, AKS-I-8 was obtained as a brown solid, 0.103 g (50.9% yield), a m.pt. of 194-197 ^{o}C and a R_f of 0.47 (hexane/ethyl acetate, 1:1). Six signals shown on the ^{1}H NMR spectra (400 MHz, DMSO-d_6) (figures **4.15** and **4.16**) obtained in δ (ppm) values are assigned to six protons as 7.97 (1H, s, H-5′), 7.54-7.57 (1H, m, H-4), 7.38 (1H, $J_{7,6}$ = 9.6 Hz, $J_{7,F-5}$ = 2.0 Hz, H-7), 7.24 (1H, d, $J_{3',4'}$ = 3.2 Hz, H-3′), 7.11 (1H, dt, $J_{6,7}$ = 10.0 Hz, $J_{6,4}$ = 2.4 Hz, H-6) and 6.75 (1H, dd, $J_{4',3'}$ = 3.2 Hz, $J_{4',5'}$ = 1.6 Hz, H-4′) representing the aromatic methine protons. The multiplet peak observed for proton on position 4 and the further splitting of the doublet and triplet peaks for protons on positions 6 and 7 were due to the influence of fluorine in ortho and para positions with respect to H-4 and H-7. The amine proton (expected to resonate further in the low field region) was not captured.

The signals from ^{13}C NMR (100 MHz, DMSO-d_6) broad band spectrum in figure **4.17** shows six resonance peaks in δ (ppm) units due to overlapps, representing five tertiary carbons as 159.84 (C-5, C-2), 157.50 (C-9, C-8, C-2′) and six methine carbons as 144.71 (C-5′), 112.28 (C-6, C-4, C-4′), 110.68 (C-7, C-3′). The DEPTH-135 (100 MHz, DMSO-d_6) experiment (figure **4.18**) further corroborates the respective methine carbons. The NMR spectra data were consistent with the one from literature (Diao *et al.*, 2009).

The EI-MS analysis (spectrum in figure **4.19**) established a *m/z* of 202 and 203, representing the most intense molecular ion, M^+ peak and a M^++1 peak respectively. The *m/z* at 174 is suggestive of the fragment ion $[M\text{-}CHO]^+$ which resulted from an α cleavage of the furan ring followed by a loss of CHO$^{\bullet}$ radical. The *m/z* at 147 corresponds to the fragment $[C_8H_7N_2O]^{\bullet+}$ and a further loss of ethylene resulted to *m/z* of 121 $[C_6H_5N_2O]^{\bullet+}$. A cleavage of M^+ at the imidazole ring produced the fragment ion with *m/z* of 106 corresponding to $[C_6H_4NO]^{\bullet+}$. The *m/z* 81 corresponding to $[C_5H_5O]^+$ is due to the entire furan moity fragment. The *m/z* 69 is suggestive of the residual imidazole fragment ion $[C_3H_5N_2]^{\bullet+}$. From HREI-MS analysis, the *m/z* of 202.0539 (calculated, 202.0542) further confirms the compound with a corresponding molecular formula, $C_{11}H_7FN_2O$.

The absorption bands from the IR spectrum in figure **4.20** displays the vibrational frequencies, $\bar{\upsilon}$ (cm^{-1}) of functional groups assigned as ≈3400 (N–H_{str} of 2^{o} amine), 3120

(aromatic C–H_{str}), 1639 (C=N_{str}), 1523, 1449 (aromatic C=C_{str}), 1230 (C–O–C_{str} of ether) and 1142 (C–F_{str}). The UV spectrum in figure **4.21** shows wavelenghts of maximum absorptions, (λ_{max}) at 323, 309, 248 and 208 nm indicative of n→π* and π→π* transitions. Summary of the ^{1}H NMR and ^{13}C NMR spectra is represented in table **4.3**.

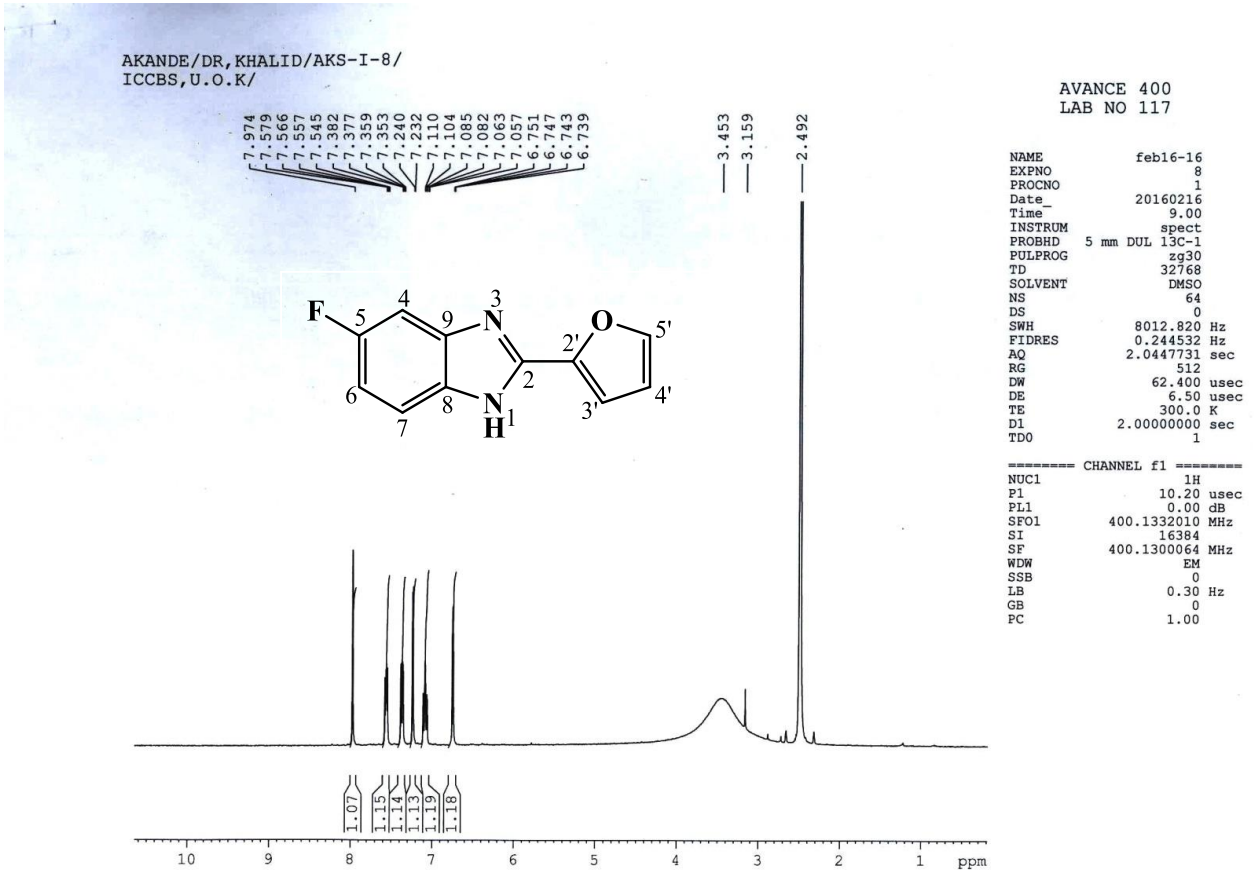

Figure 4.15. ^{1}H NMR (400 MHz, DMSO-d_6) spectrum of AKS-I-8

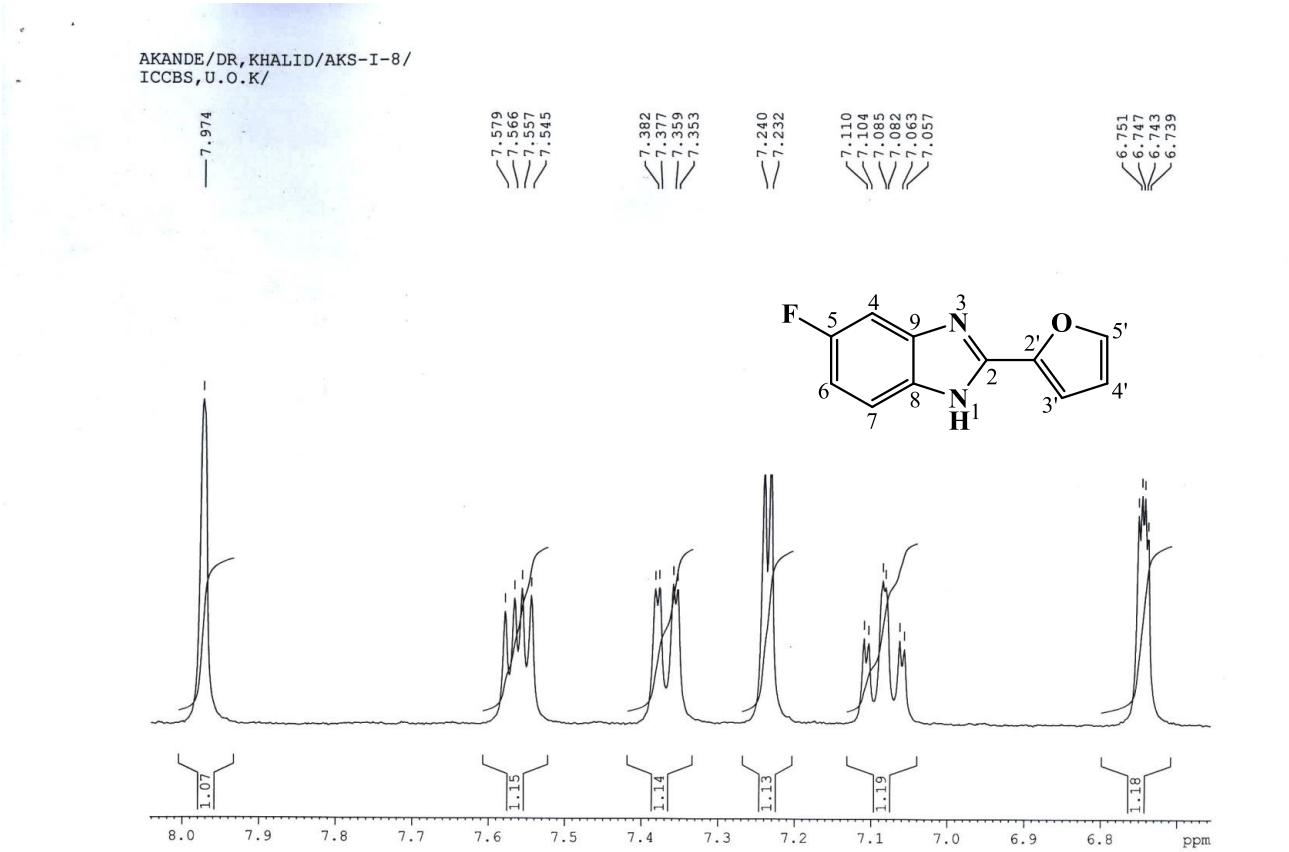

Figure 4.16. ^{1}H NMR (400 MHz, DMSO-d_6) spectrum of AKS-I-8 aromatic region (Expanded)

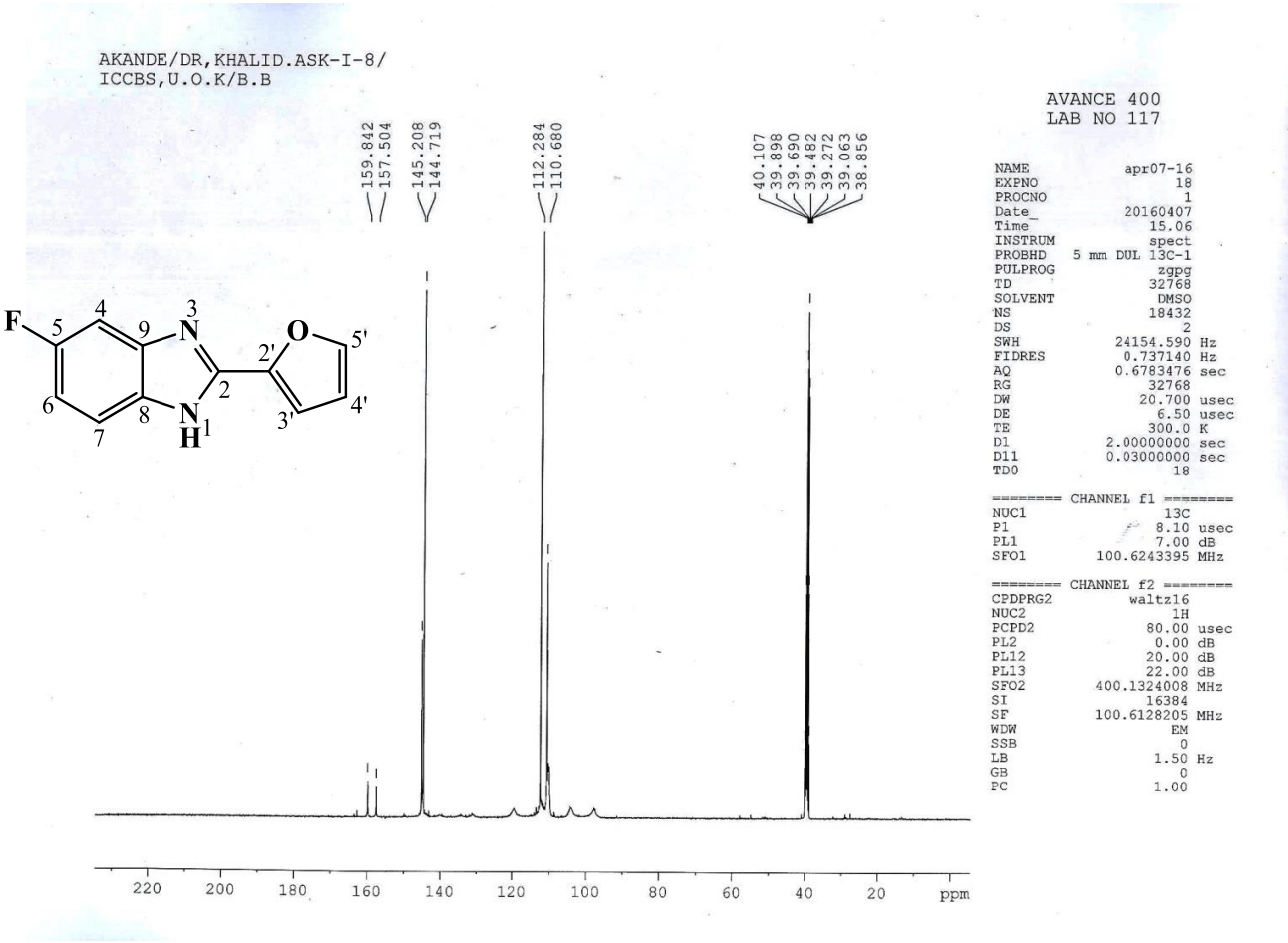

Figure 4.17. ^{13}C NMR (100 MHz, DMSO-d_6) spectrum of AKS-I-8

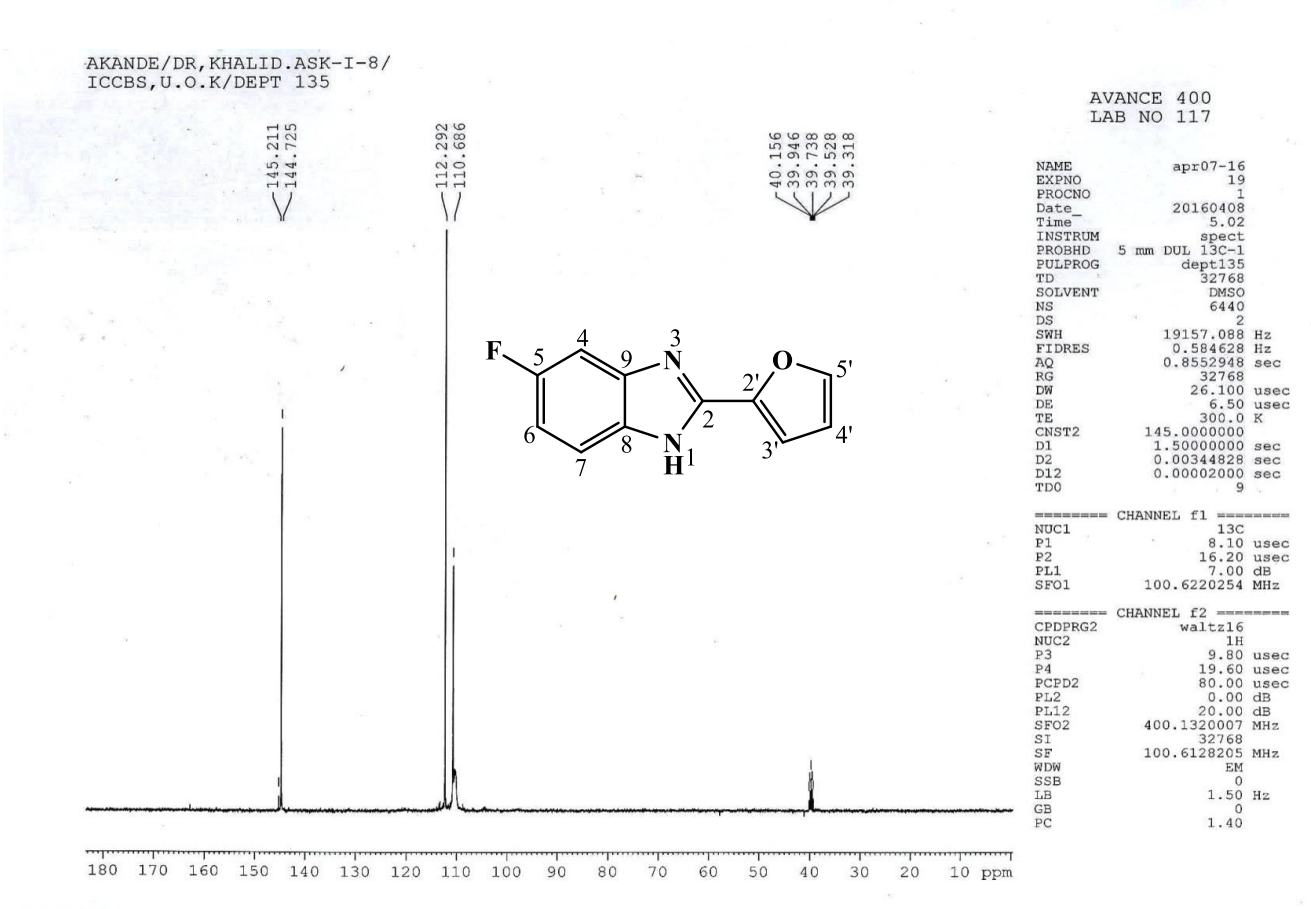

Figure 4.18. DEPTH-135 (100 MHz, DMSO-d_6) spectrum of AKS-I-8

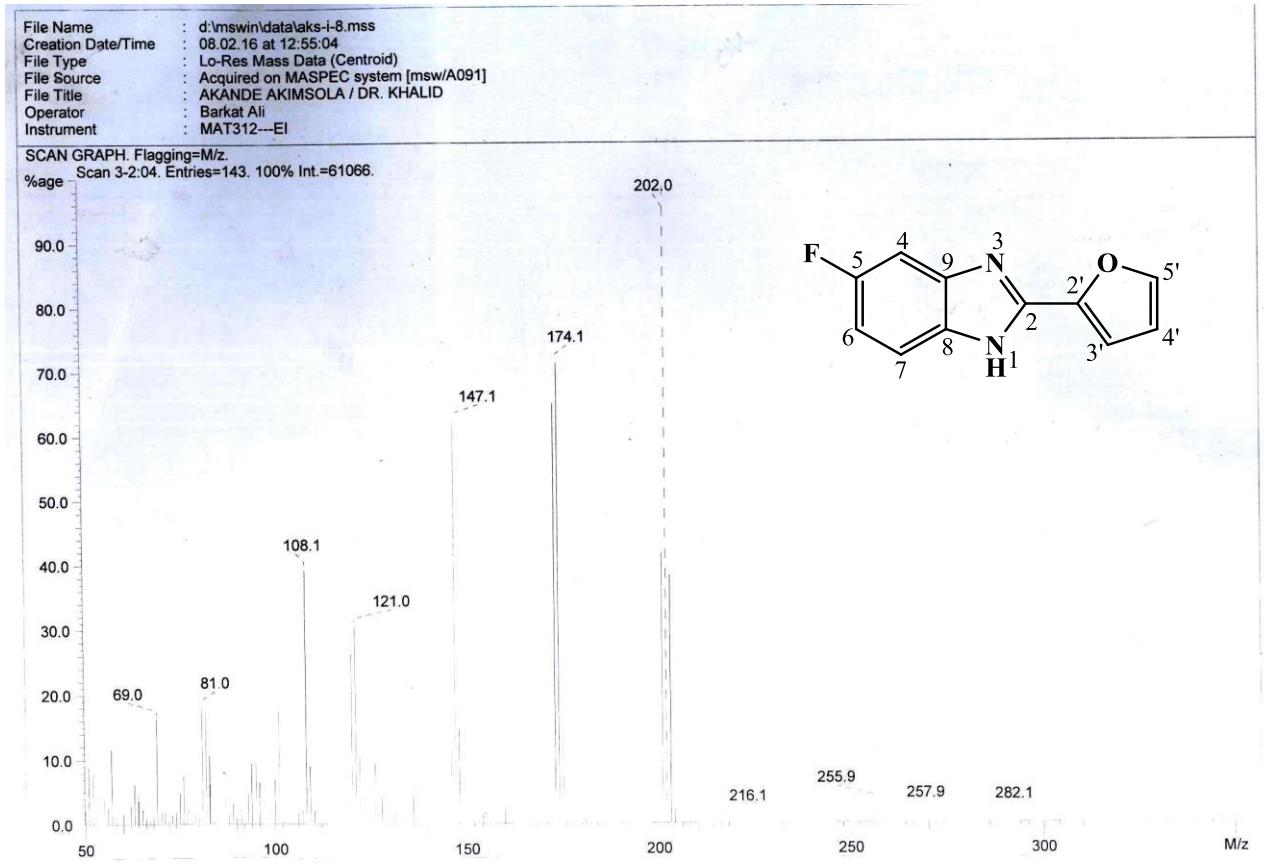

Figure 4.19. EI-MS spectrum of AKS-I-8

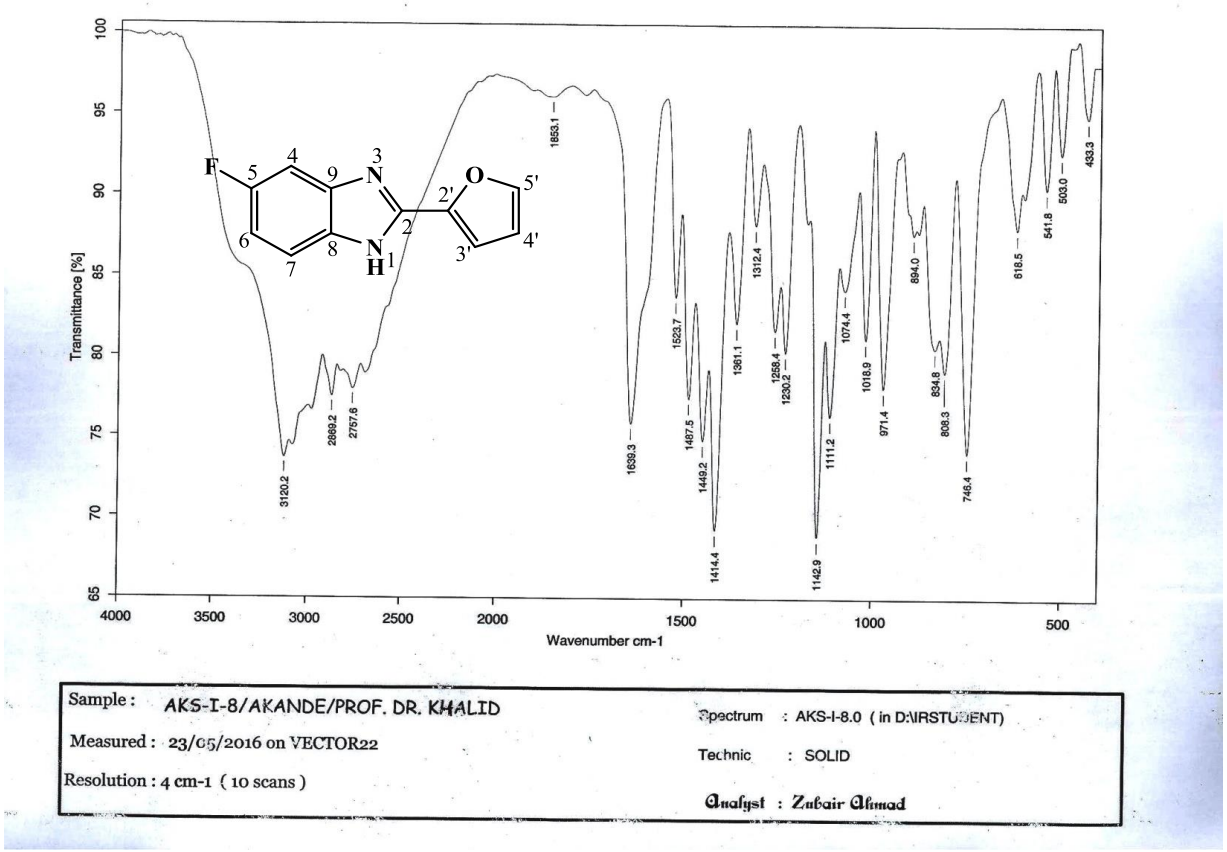

Figure 4.20. IR spectrum of AKS-I-8

THERMO ELECTRON ~ VISIONpro SOFTWARE V4.10

Operator Name	ARSHAD ALAM	Date of Report	5/24/2016
Department	Analytical laboratory#004 TWC	Time of Report	9:33:09AM
Organization	ICCBS.Karachi University.		
Information	Prof Dr.Khalid ./ Akande.		

Scan Graph

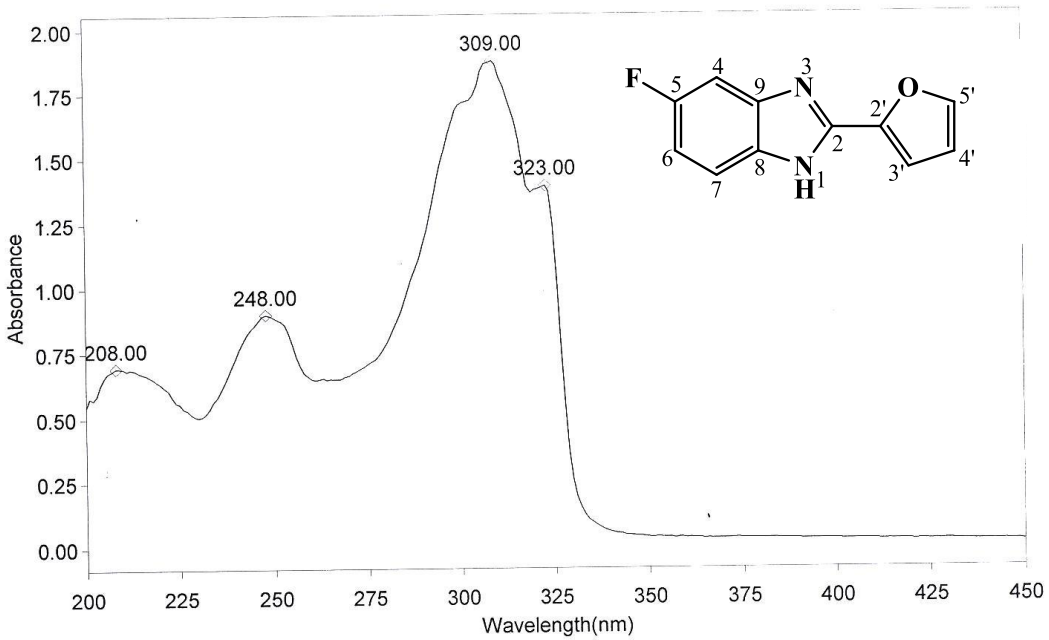

Results Table - AKS- I- 8.sre,AKS- I- 8,Cycle01

nm	A	**Peak Pick Method**
208.00	0.694	Find 8 Peaks Above -3.0000 A
248.00	0.897	Start Wavelength 200.00 nm
309.00	1.876	Stop Wavelength 450.00 nm
323.00	1.390	Sort By Wavelength
Sensitivity	Medium	

Page 1, Scan Graph

Figure 4.21. UV spectrum of AKS-I-8

Table 4.3. Summary of the ^{1}H NMR and ^{13}C NMR spectra of AKS-I-8

Position	δ ^{1}H [mult., J_{HH} (Hz)] (ppm)	Diao *et al*., 2009	δ ^{13}C (ppm)	DEPT-135
1	-	-	-	-
2	-	-	159.84	-
3	-	-	-	-
4	7.57-7.54 [m]	7.58 [dd, J = 9.0, 5.0]	112.28	CH
5	-	-	159.84	-
6	7.11 [dt, $J_{6,7}$ = 10.0, $J_{6,4}$ = 2.4]	7.09 [dt, J = 9.5, 2.0]	112.28	CH
7	7.38 [dd, $J_{7,6}$ = 9.6, $J_{7,F\text{-}5}$ = 2.0]	7.38 [dd, J = 9.5, 2.0]	110.68	CH
8	-	-	157.50	-
9	-	-	157.50	-
1′	-	-	-	-
2′	-	-	157.50	-
3′	7.24 [d, $J_{3',4'}$ = 3.2]	7.22 [d, J = 3.5]	110.68	CH
4′	6.75 [dd, $J_{4',3'}$ = 3.2, $J_{4',5'}$ = 1.6]	6.75 [dd, J = 3.5, 2.0]	112.28	CH
5′	7.97 [s]	7.96 [s]	144.71	CH

4.1.4 Characterisation of 5-fluoro-2-(5′-methylfuran-2′-yl)-1*H*-benzo[*d*] imidazole (AKS-I-9)

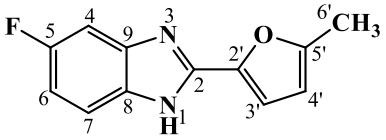

The brown solid compound, AKS-I-9 was obtained in a yield of 69.4% (0.150 g) with a m.pt. of 148-151 ^{o}C and a 0.50 (hexane/ethyl acetate, 1:1) R_f value.

The resonances, δ (ppm) from ^{1}H NMR spectra (400 MHz, DMSO-d_6) (figures **4.22** and **4.23**) display a total of six peaks assigned as 7.52-7.55 (1H, m, H-4), 7.36 (1H, dd, $J_{7,6}$ = 9.2 Hz, $J_{7,F\text{-}5}$ = 2.0 Hz, H-7), 7.15 (1H, d, $J_{3',4'}$ = 3.2 Hz, H-3′), 7.10 (1H, dt, $J_{6,4}$ = 2.4 Hz, $J_{6,7}$ = 10.0 Hz, H-6) and 6.37 (1H, d, $J_{4',3'}$ = 2.4 Hz, H-4′) each representing the aromatic methine protons and 2.41 (3H, s, 6′-CH_3) representing the methyl protons. Also the effect of an ortho/para positioning of fluorine atom to H-4 and H-7 respectively on the six-membered ring resulted in a multiplet peak for proton at position 4, and a further splitting of the triplet and doublet peaks arising from protons on positions 6 and 7 respectively. The amine proton was not captured.

Proton decoupled ^{13}C NMR (125 MHz, DMSO-d_6) spectrum (figure **4.24**) shows resonance peaks in δ (ppm) units, representing 12 carbon atoms assigned as 159.74 (C-5), 157.86 (C-5′), 154.56 (C-2), 144.58 (C-9, C-8, C-2′) to six tertiary carbons, 112.84 (C-7), 110.65 (C-6), 110.45 (C-4), 108.87 (C-4′, C-3′) to five methine carbons and 13.49 (C-6′) to the methyl carbon. The DEPTH-135 (125 MHz, DMSO-d_6) spectrum (figure **4.25**) reaffirms the positions of the respective methine carbons.

The EI-MS spectrum (figure **4.26**) shows the molecular ion (also the base peak), M^+ at a *m/z* 216 together with a $[M^+{+}1]$ peak at *m/z* 217. Fragment ion *m/z* 201 is indicative of the methyl side chain cleavage from the M^+. The *m/z* 187 is due to a loss of C_2H_4 molecule which corresponds to $[C_{10}H_4FN_2O]^{\bullet+}$. A α cleavage followed by the loss of $[CH_2{=}CH{-}O^{\bullet}]$ radical on the M^+ led to the fragment ion at *m/z* 173. Cleavage of the M^+ at the imidazole ring gave a *m/z* 108 fragment corresponding to $[C_6H_3FN]^{\bullet+}$ which on further loss of a $F^{\bullet}$ radical gave the stable ion with a *m/z* 91. Cleavage of the entire furan moity affords the *m/z* 81 corresponding to $[C_5H_5O]^+$. The residual imidazole fragment ion $[C_3H_5N_2]^{\bullet+}$ is equivalent to *m/z* 69. From HREI-MS analysis, the *m/z* of 216.0704

(calculated, 216.0699) was obtained corresponding to the molecular formula $C_{12}H_9FN_2O$ [M^+] and further confirms the the compound.

Absorption bands from IR spectrum (figure **4.27**) indicated characteristic vibrational frequencies, $\bar{\upsilon}$ (cm^{-1}) such as 3380, 3111, 2924, 2850, 1639, 1570, 1424, 1215 and 1022 and 1145 for N–H_{str} of amine, aromatic C–H_{str}, aliphatic C–$H_{asy\ str}$ and C–$H_{sym\ str}$, C=N_{str}, aromatic C=C_{str}, C–H_b of the methyl side chain, asymmetric and symmetric C–O–C_{str} of ether, and C–F_{str} respectively. The maximum wavelenghts of absorptions (λ_{max}) obtained from UV analysis (figure **4.28**) at 301, 255 and 213 nm, conote $n\rightarrow\pi^*$ and $\pi\rightarrow\pi^*$ transitions. Table **4.4** summarily highlights the ^1H NMR and ^{13}C NMR spectra peak values. Although no reference for this compound was found from literature, but it was confirmed on SciFinder© to have been synthesised.

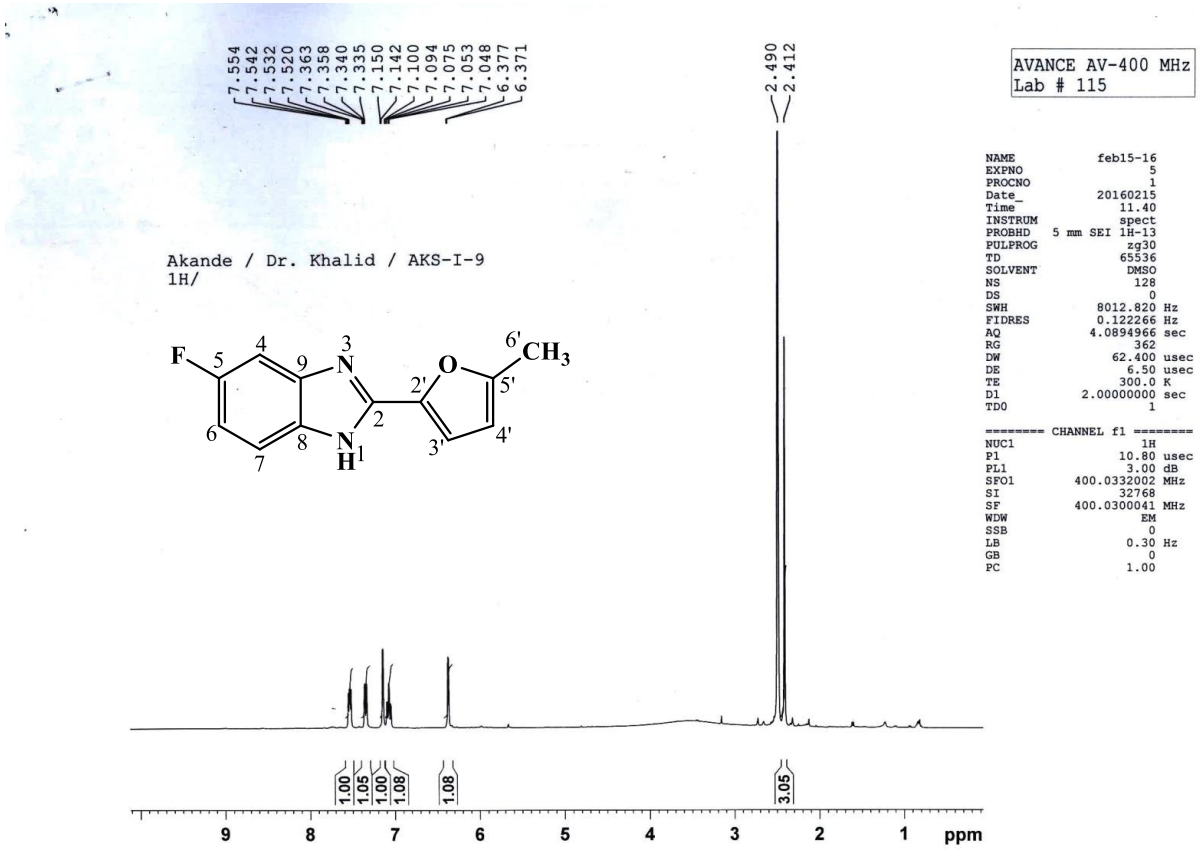

Figure 4.22. ^{1}H NMR (400 MHz, DMSO-d_6) spectrum of AKS-I-9

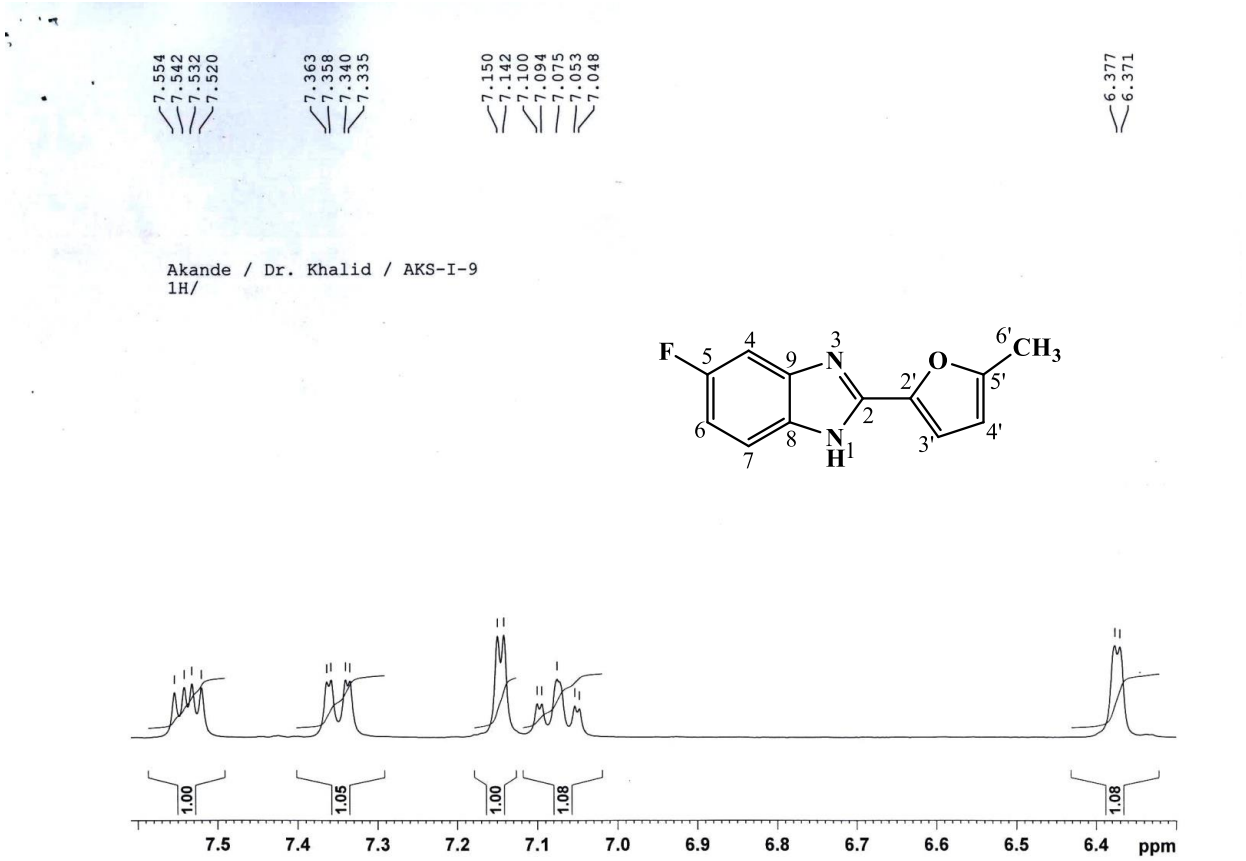

Figure 4.23. ^{1}H NMR (400 MHz, DMSO-d_6) spectrum of AKS-I-9 aromatic region (Expanded)

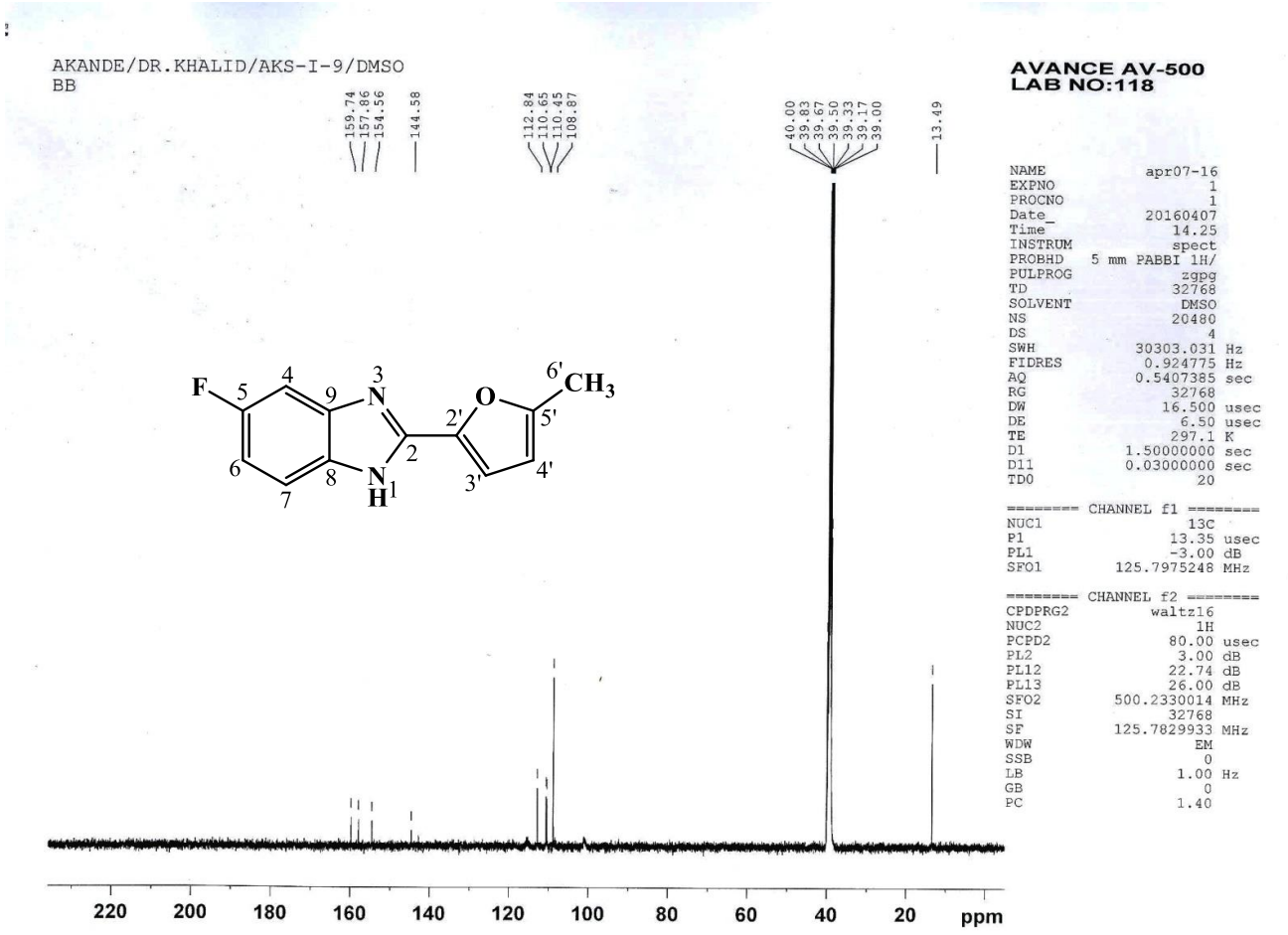

Figure 4.24. ^{13}C NMR (125 MHz, DMSO-d_6) spectrum of AKS-I-9

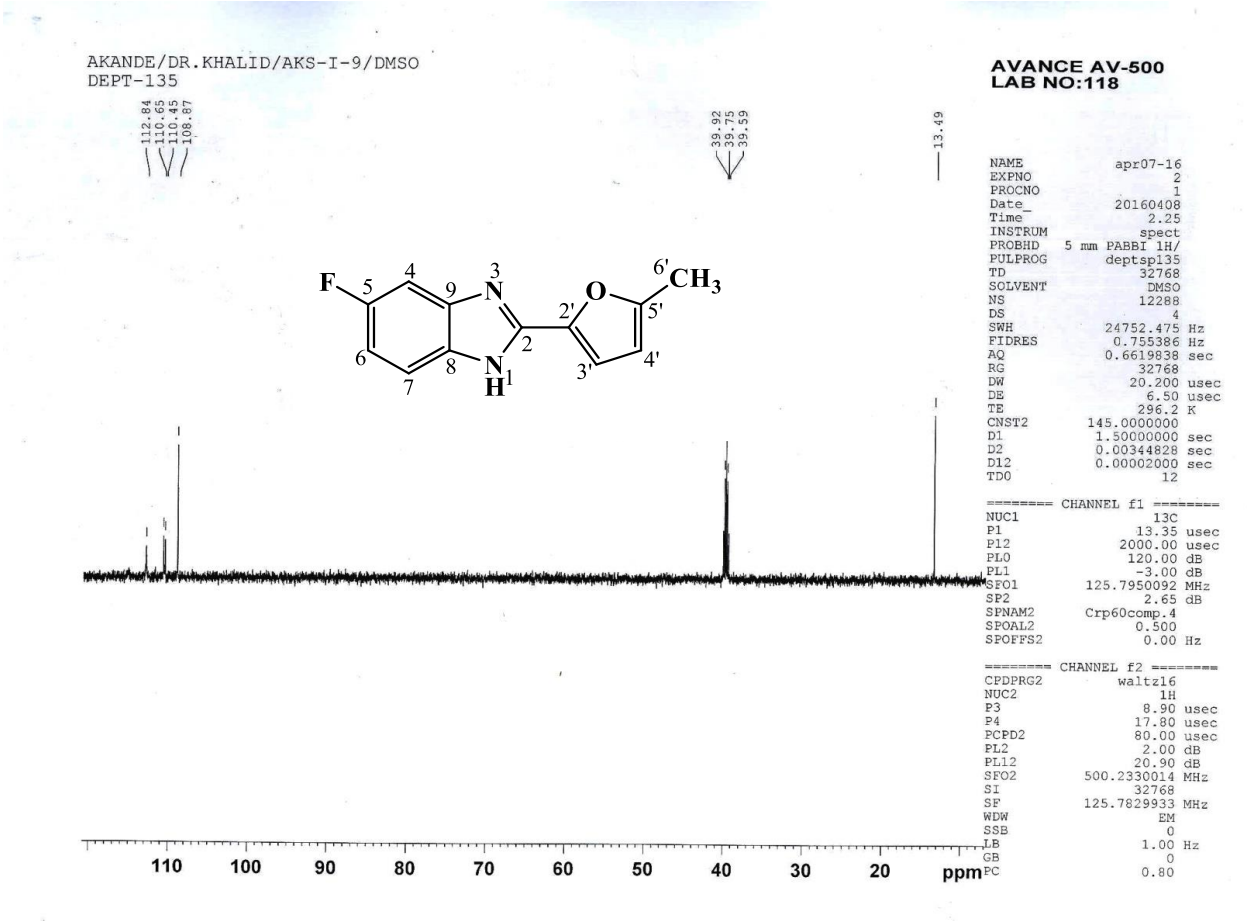

Figure 4.25. DEPTH-135 (125 MHz, DMSO-d_6) spectrum AKS-I-9

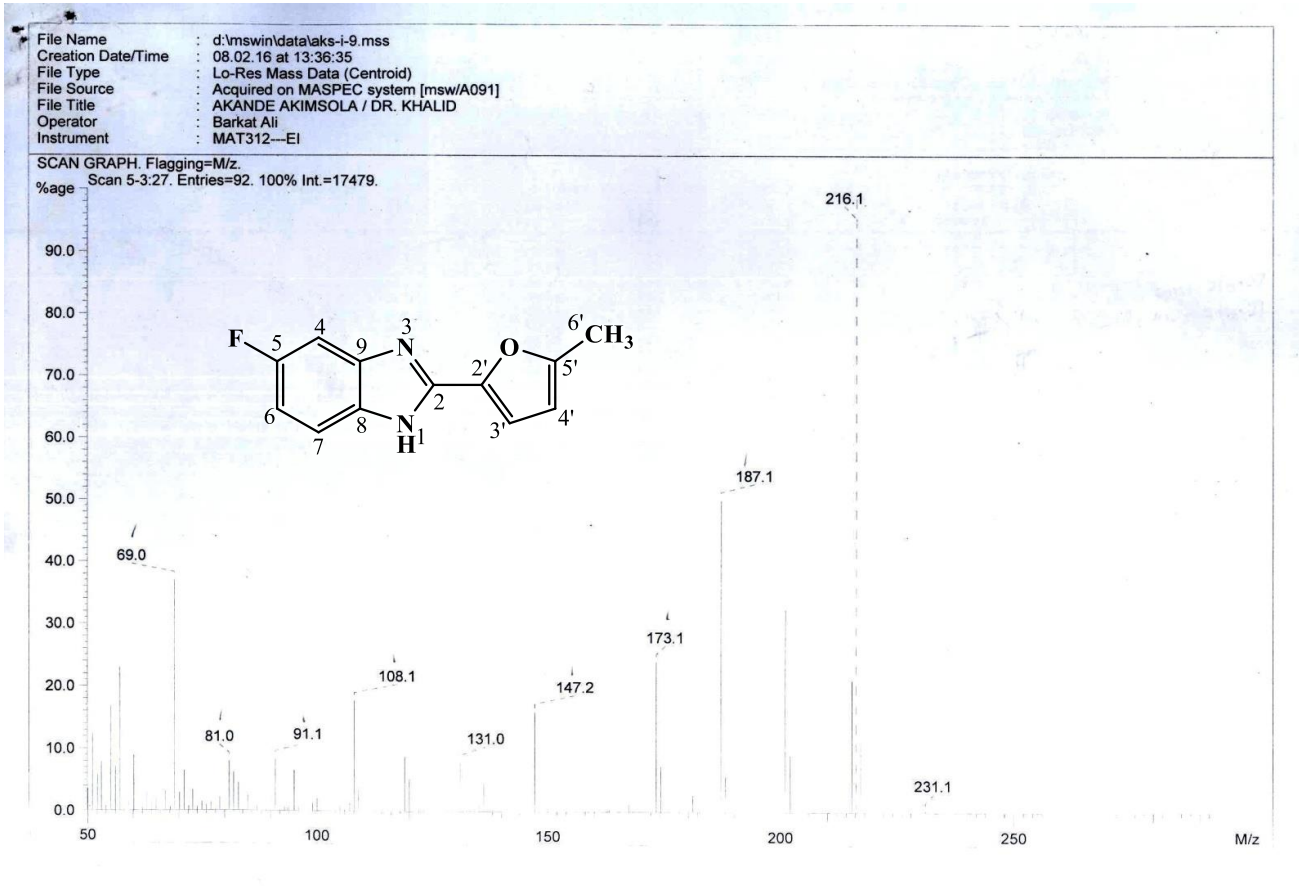

Figure 4.26. EI-MS spectrum of AKS-I-9

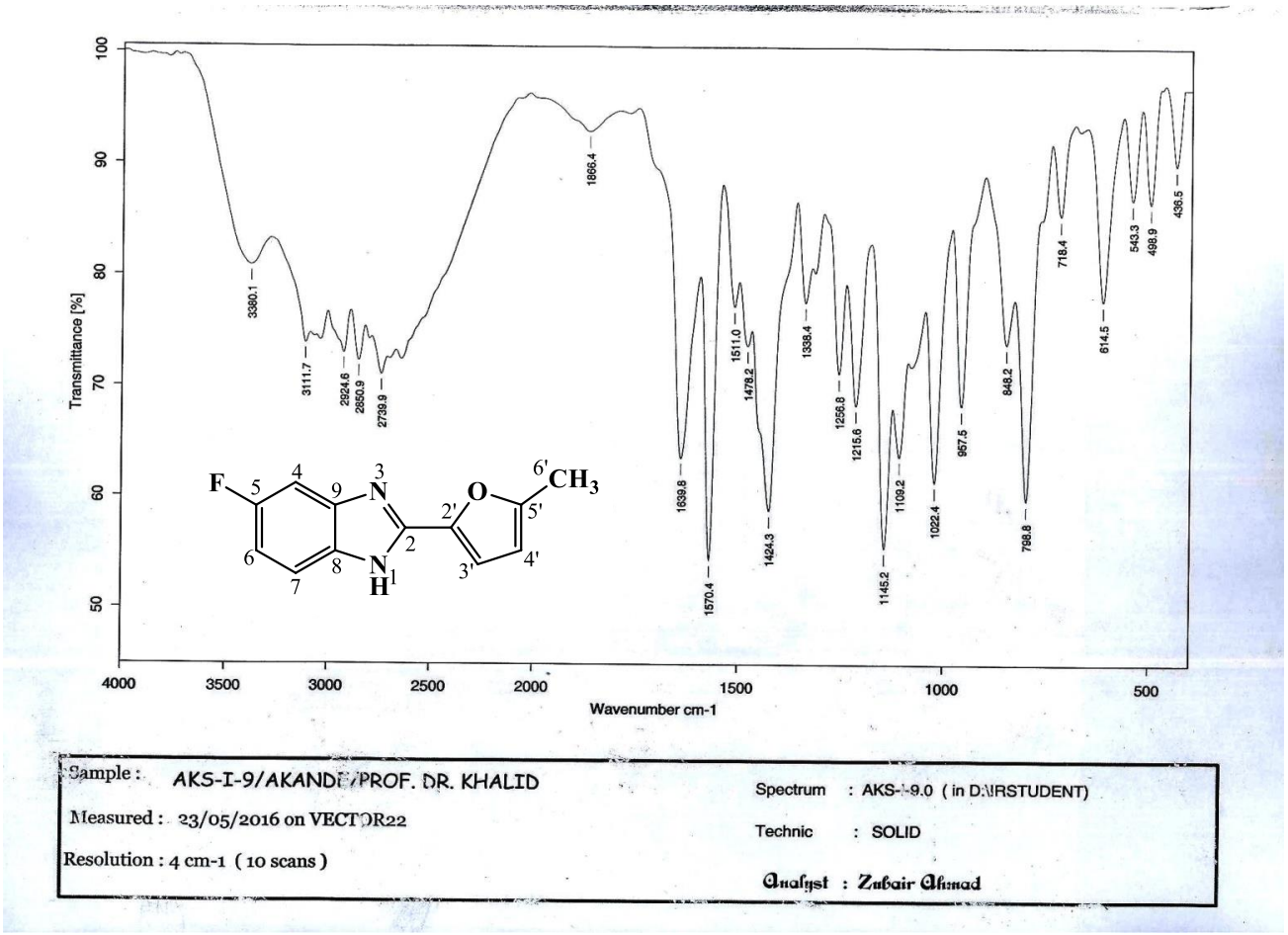

Figure 4.27. IR spectrum of AKS-I-9

THERMO ELECTRON ~ VISIONpro SOFTWARE V4.10

Operator Name	ARSHAD ALAM	Date of Report	5/24/2016
Department	Analytical laboratory#004 TWC	Time of Report	9:37:29AM
Organization	ICCBS.Karachi University.		
Information	Prof Dr.Khalid ./ Akande.		

Scan Graph

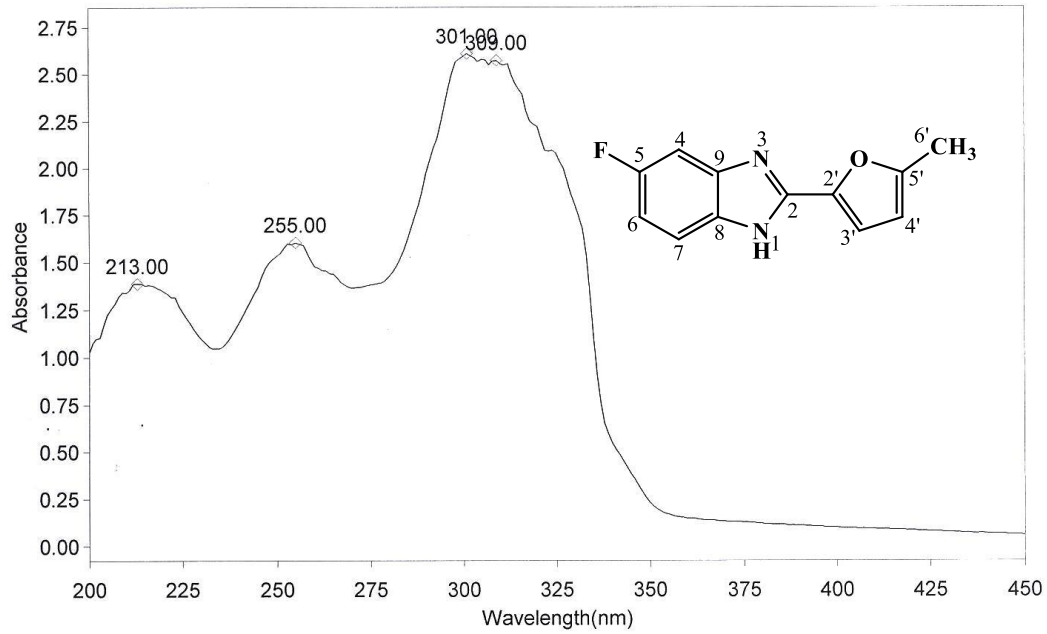

Results Table - AKS- I- 9.sre,AKS- I- 9,Cycle01

nm	A	**Peak Pick Method**
213.00	1.390	Find 8 Peaks Above -3.0000 A
255.00	1.605	Start Wavelength 200.00 nm
301.00	2.609	Stop Wavelength 450.00 nm
309.00	2.573	Sort By Wavelength
Sensitivity	Medium	

Page 1, Scan Graph

Figure 4.28. UV spectrum of AKS-I-9

Table 4.4. Summary of the ^{1}H NMR and ^{13}C NMR spectra of AKS-I-9

Position	δ ^{1}H [mult., J_{HH} (Hz)] (ppm)	δ ^{13}C (ppm)	DEPT-135
1	-	-	-
2	-	154.56	-
3	-	-	-
4	7.55-7.52 [m]	110.45	CH
5	-	159.74	-
6	7.10 [dt, $J_{6,7}$ = 10.0, $J_{6,4}$ = 2.4]	110.65	CH
7	7.36 [dd, $J_{7,6}$ = 9.2, $J_{7,F\text{-}5}$ = 2.0]	112.84	CH
8	-	144.58	-
9	-	144.58	-
1′	-	-	-
2′	-	144.58	-
3′	7.15 [d, $J_{3',4'}$ = 3.2]	108.87	CH
4′	6.37 [d, $J_{4',3'}$ = 2.4]	108.87	CH
5′	-	157.86	-
6′-CH_3	2.41 [s]	13.49	CH_3

4.1.5 Characterisation of 5-chloro-2-(furan-2′-yl)-1*H*-benzo[*d*]imidazole (AKS-I-10)

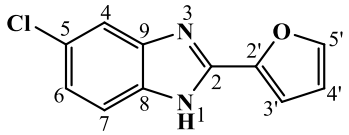

5-Chloro-2-(furan-2′-yl)-1*H*-benzo[*d*]imidazole (AKS-I-10) is a black solid, 90.6% (0.198 g) yield, a m.pt. of 109-111 ^{o}C and a 0.49 (hexane/ethyl acetate, 1:1) R_f value. The ^{1}H NMR analysis (400 MHz, DMSO-d_6) is represented in figures **4.29** and **4.30**. All chemical shifts, δ (ppm) obtained are due to resonances of the six methine protons, assigned as 7.97 (1H, d, $J_{5',4'}$ = 1.2 Hz, H-5′), 7.60 (1H, s, H-4; a broad peak), 7.57 (1H, d, $J_{7,6}$ = 8.4 Hz, H-7), 7.24 (2H, m, H-6, H-3′ and 6.75 (1H, dd, $J_{4',3'}$ = 3.2 Hz, $J_{4',5'}$ = 1.6 Hz, H-4′). However, the amine proton peak expected to resonate further downfield was not captured.

The EI-MS spectrum (figure **4.31**) is characterised by peak patterns spaced two mass units apart due to the presence of a chlorine atom. The *m/z* of the molecular ion (also the base peak), M^+ peak is at 218 while the isotope peak [M^++2] is at 220. The fragment ion with *m/z* 190 $[M\text{-}CHO]^+$ resulted from furan ring opening (α cleavage) followed by a loss of CHO$^{\bullet}$ radical, and a further loss of HCl corresponds to *m/z* 155 fragment ion. Cleavage at the imidazole ring affords a *m/z* of 124 which corresponds to $[C_6H_3ClN]^+$. The fragment $[C_6H_3ClN]^+$, on losing a N$^{\bullet}$ radical resulted to the peak at *m/z* 109. If however, the fragment $[C_6H_3ClN]^+$ loses $C_2H_2Cl^{\bullet}$ radical, would give a stable fragment ion at *m/z* 63. The HREI-MS analysis afforded a *m/z* of 218.0241 (calculated 218.0247) which corresponds to the molecular formula $C_{11}H_7ClN_2O$, thus confirming the compound.

The IR spectrum (figure **4.32**) shows characteristic absorption bands with vibrational frequencies, $\bar{\upsilon}$ (cm^{-1}) assigned to functional groups such as N–H$_{str}$ of 2^{o} amine, aromatic C–H$_{str}$, C=N$_{str}$, two aromatic C=C$_{str}$, asymmetric and symmetric C–O–C$_{str}$ of ether, and C–Cl$_{str}$ corresponding to ≈3400, 3118, 1636, 1519, 1408, 1231, 1018 and 1063 cm^{-1} respectively. The UV spectrum (figure **4.33**) shows λ_{max} at 326, 311, 249 and 207 nm indictive of n→π* and π→π* transitions. Table **4.5** represents the summary of ^{1}H NMR spectra. Likewise, SciFinder© confirmed the existence of this compound, but no reference citation was found from literature.

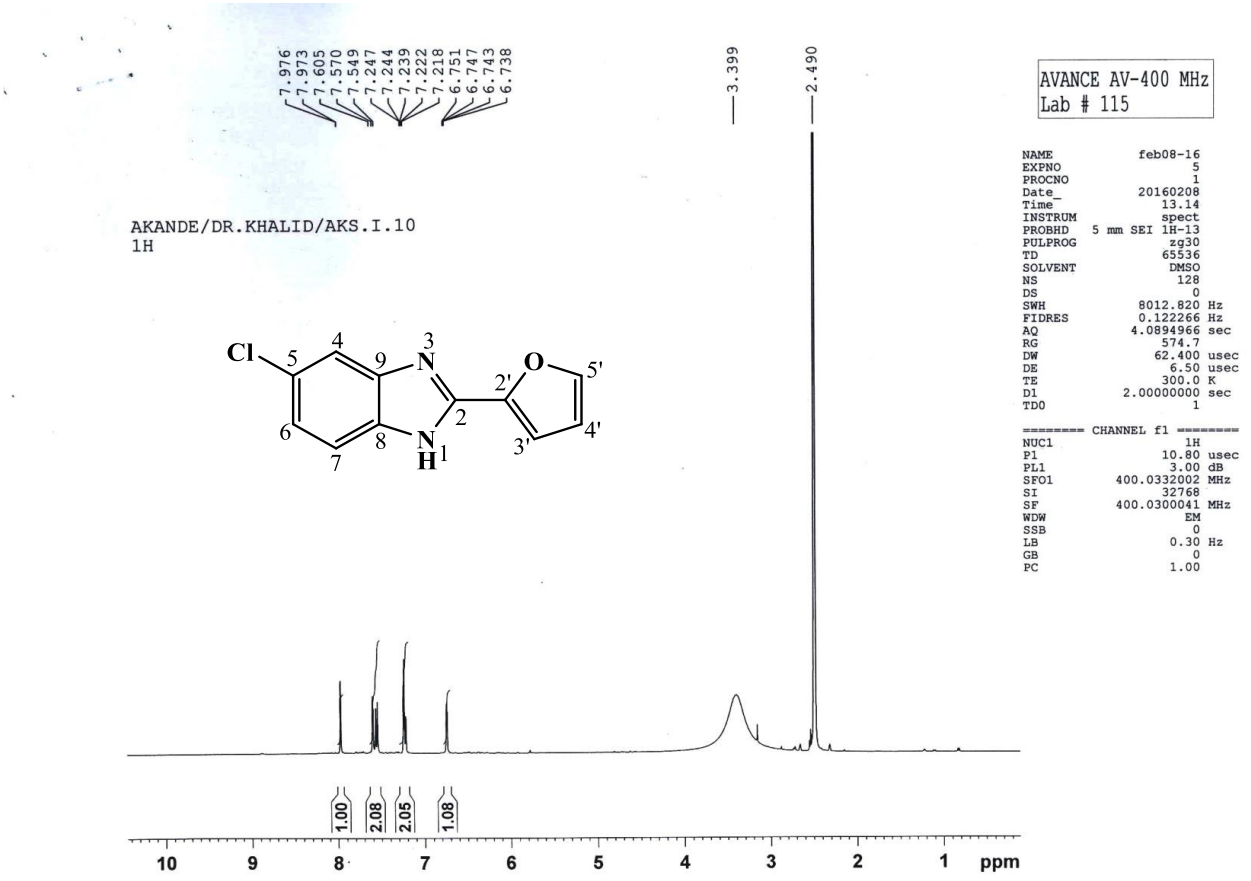

Figure 4.29. ^{1}H NMR (400 MHz, DMSO-d_6) spectrum of AKS-I-10

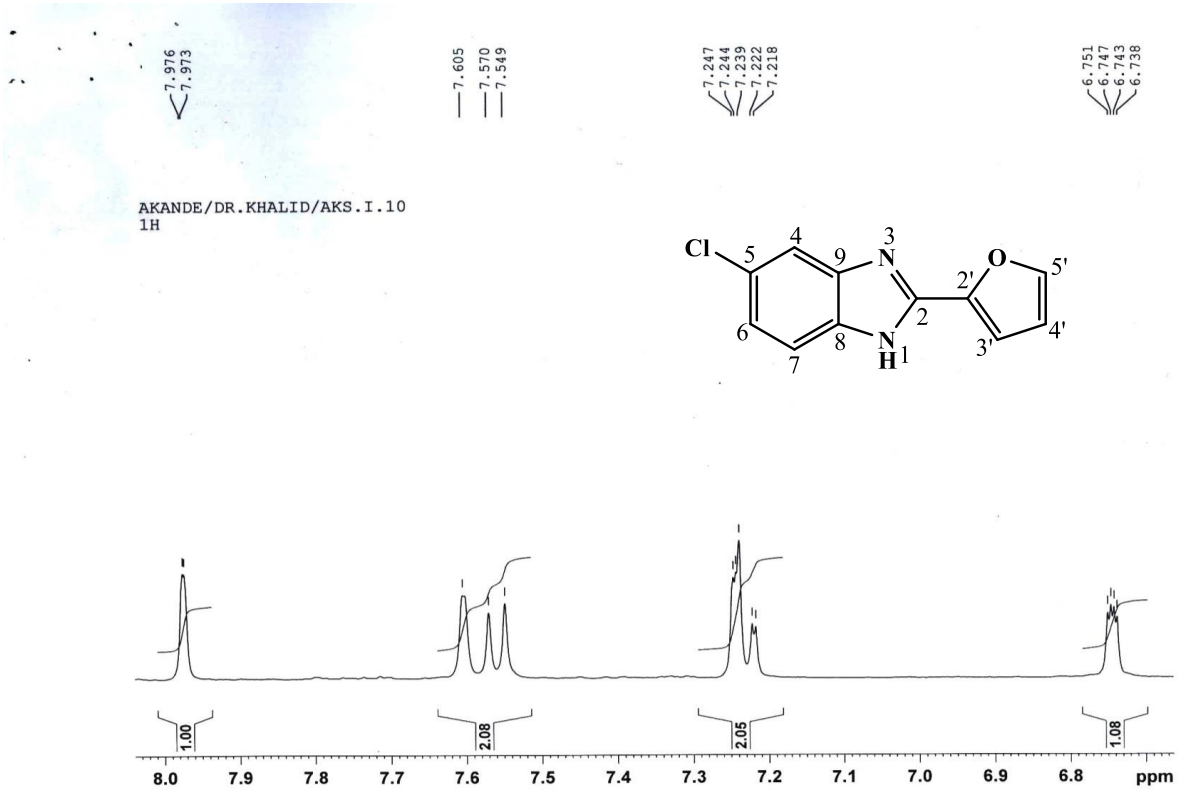

Figure 4.30. ^{1}H NMR (400 MHz, DMSO-d_6) spectrum of AKS-I-10 aromatic region (Expanded)

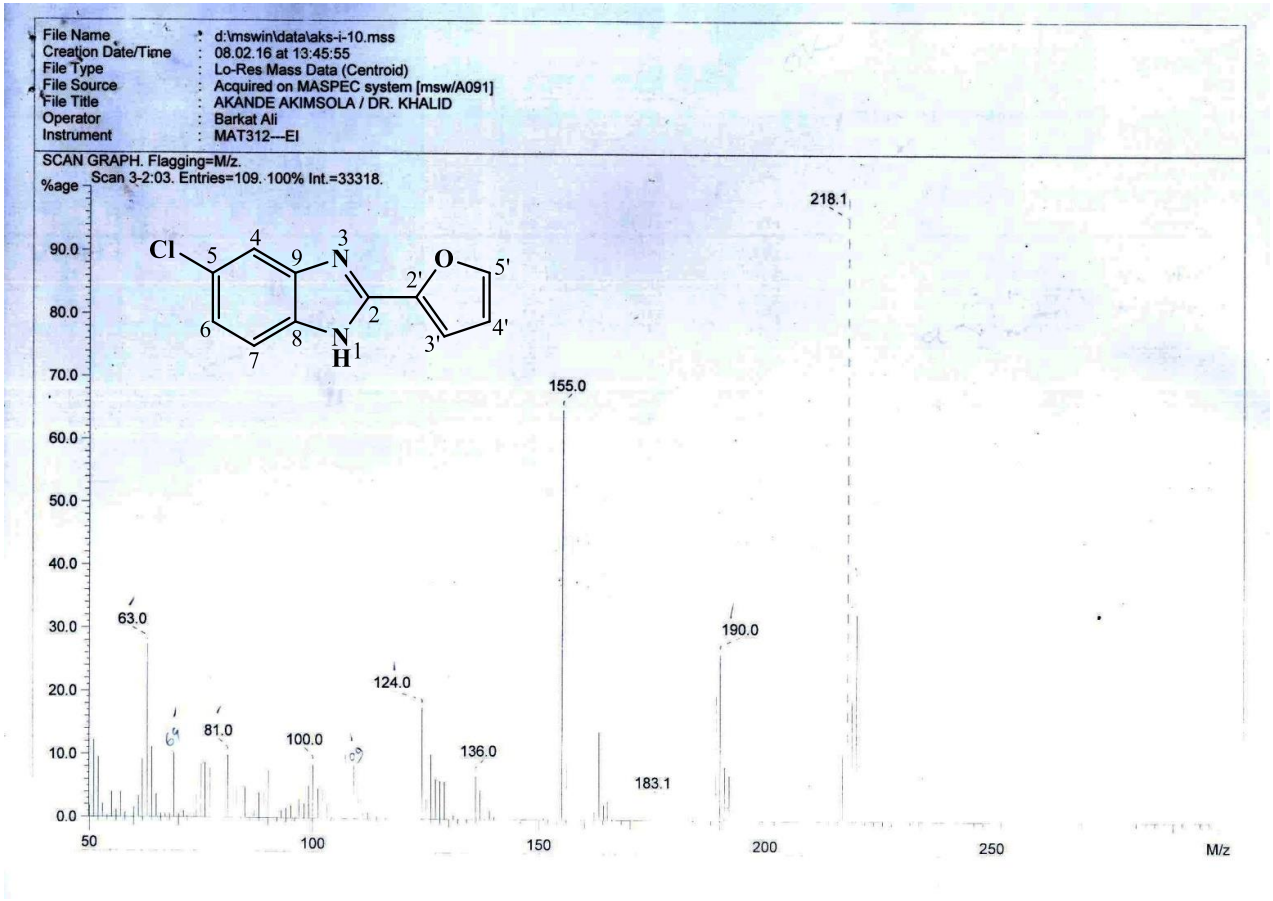

Figure 4.31. EI-MS spectrum of AKS-I-10

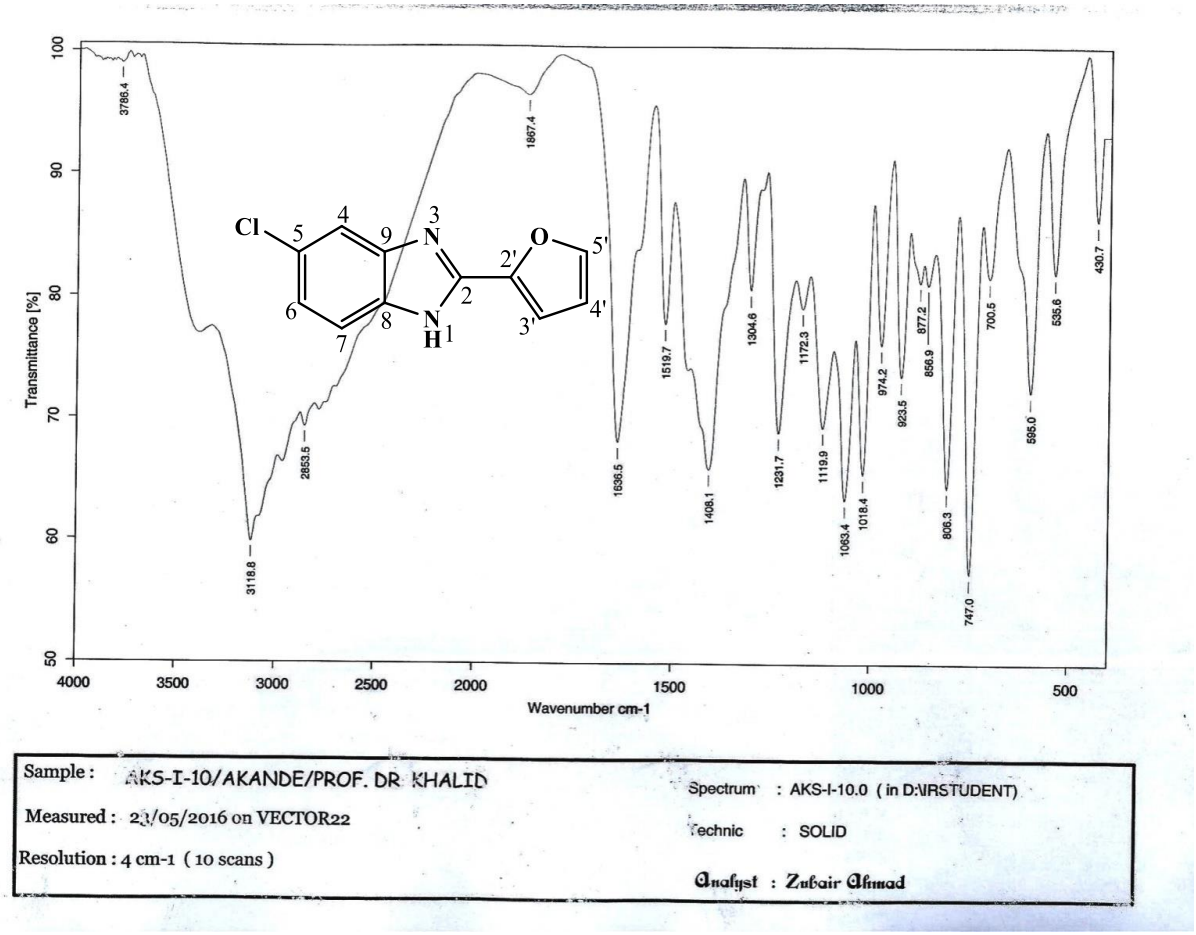

Figure 4.32. IR spectrum of AKS-I-10

THERMO ELECTRON ~ VISIONpro SOFTWARE V4.10

Operator Name	ARSHAD ALAM	Date of Report	5/24/2016
Department	Analytical laboratory#004 TWC	Time of Report	9:46:13AM
Organization	ICCBS.Karachi University.		
Information	Prof Dr.Khalid ./ Akande.		

Scan Graph

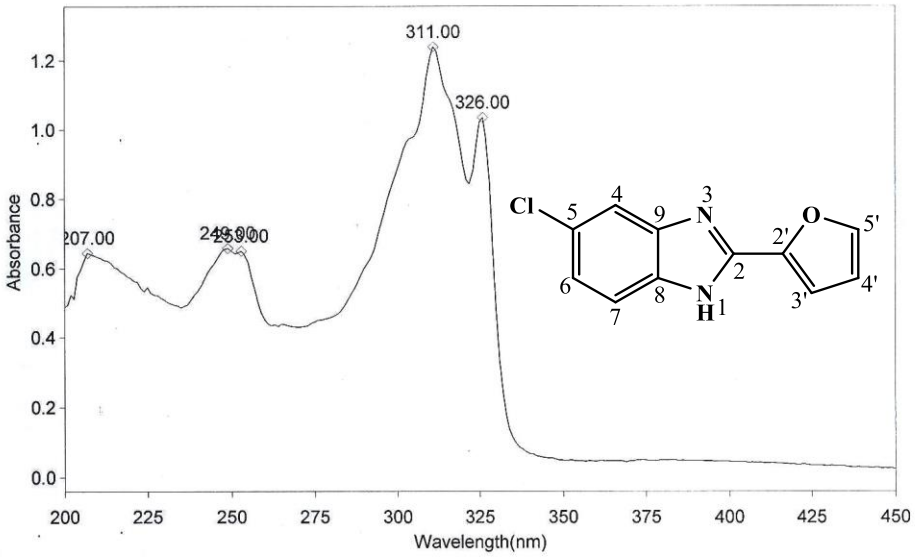

Results Table - AKS- I- 10.sre,AKS- I- 10,Cycle01

nm	A	Peak Pick Method
207.00	0.644	Find 8 Peaks Above -3.0000 A
249.00	0.657	Start Wavelength 200.00 nm
253.00	0.649	Stop Wavelength 450.00 nm
311.00	1.239	Sort By Wavelength
326.00	1.034	Sensitivity Medium

Page 1, Scan Graph

Figure 4.33. UV spectrum of AKS-I-10

Table 4.5. Summary of the ^{1}H NMR spectra of AKS-I-10

Position	δ ^{1}H [mult., J_{HH} (Hz)] (ppm)
1	-
2	-
3	-
4	7.60 [s]
5	-
6	7.24 [dd, $J_{6,7}$ = 8.4, $J_{6,4}$ = 2.0]
7	7.57 [d, $J_{7,6}$ = 8.4]
8	-
9	-
1′	-
2′	-
3′	7.24 [d, $J_{3',4'}$ = 3.2]
4′	6.75 [dd, $J_{4',3'}$ = 3.2, $J_{4',5'}$ = 1.6]
5′	7.97 [d, $J_{5',4'}$ = 1.2]

4.1.6 Characterisation of 5-chloro-2-(5′-methylfuran-2′-yl)-1*H*-benzo[*d*]imidazole (AKS-I-11)

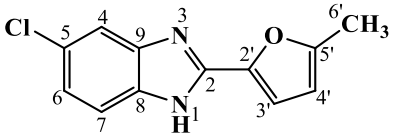

The black compound, AKS-I-11 was obtained as a solid in a 78.2% yield (0.182 g), m.pt. 163-165 ^{o}C and a R_f of 0.51 (hexane/ethyl acetate, 1:1). Figures **4.34** and **4.35** represent the ^{1}H NMR spectra (400 MHz, DMSO-d_6). The following five chemical shift, δ (ppm) values were deduced for eight protons, and are assigned as 7.55 (1H, s, H-4), 7.52 (1H, d, $J_{7,6}$ = 8.4 Hz, H-7), 7.20 (1H, dd, $J_{6,7}$ = 8.8 Hz, $J_{6,4}$ = 2.0 Hz, H-6), 7.11 (1H, d, $J_{3',4'}$ = 3.6 Hz, H-3′) and 6.35 (1H, d, $J_{4',3'}$ = 2.4 Hz, H-4′) to the aromatic methine protons, while the intense peak with δ (ppm) 2.40 (3H, s, 6′-CH_3) is assigned to the methyl protons on the furan ring. The peak for the amine proton, expected to be seen further downfield, was not captured.

Fragmentation patterns on the EI-MS spectrum (figure **4.36**) is characterised by some peak spaced two mass units apart due to the presence of a chlorine atom. The molecular ion, M^+ peak (base peak) and a [M^++2] peak (isotope peak) have *m/z* values at 232 and 234 respectively. De-methylation of the molecular ion [M^+-CH_3] side chain generated the fragment with *m/z* of 217. The loss of $C_2H_5^{\bullet}$ radical is indicative of the fragment with *m/z* of 203. M^+ - $C_3H_7^{\bullet}$ sugests the fragment ion with *m/z* 189. Cleavage of the entire furan moity and a simultaneous loss of $Cl^{\bullet}$ radical hints at the fragment with *m/z* 116 $[C_7H_4N_2]^{\bullet+}$. A spling away of the methyl side chain followed by another cleavage at the imidazole ring resulted in the stable radical ions corresponding to $[C_6H_3ClN]^{\bullet+}$ and $[C_5H_5NO]^{\bullet+}$ with *m/z* 124 and 95 respectively. HREI-MS analysis yielded the *m/z* at 232.0383 (calculated 232.0403) corresponding to the molecular formula $C_{12}H_9ClN_2O$, which further confirms the compound.

The IR spectrum (figure **4.37**) shows vibrational absorption frequencies $\bar{\upsilon}$ (cm^{-1}) at ≈3400, 3007, 2918, 2834, 1630, 1569, 1418, 1212, 1019 and 1059 correlating with the amine N–H_{str}, aromatic C–H_{str}, methyl C–$H_{asy\ str}$ and C–$H_{sym\ str}$, C=N_{str}, aromatic C=C_{str}, methyl C–H_b, C–O–C_{asy} and $_{sym\ str}$ of ether, and C–Cl_{str}. Figure **4.38** represents the UV spectrum, presenting absorption maxima, (λ_{max}) at 311, 277, 257 and 214 nm attributed to n→π* and π→π* transitions. Table **4.6** represents a summary of the ^{1}H NMR spectra. This is also a compound with no citation from literature, but its existence was confirmed on SciFinder©.

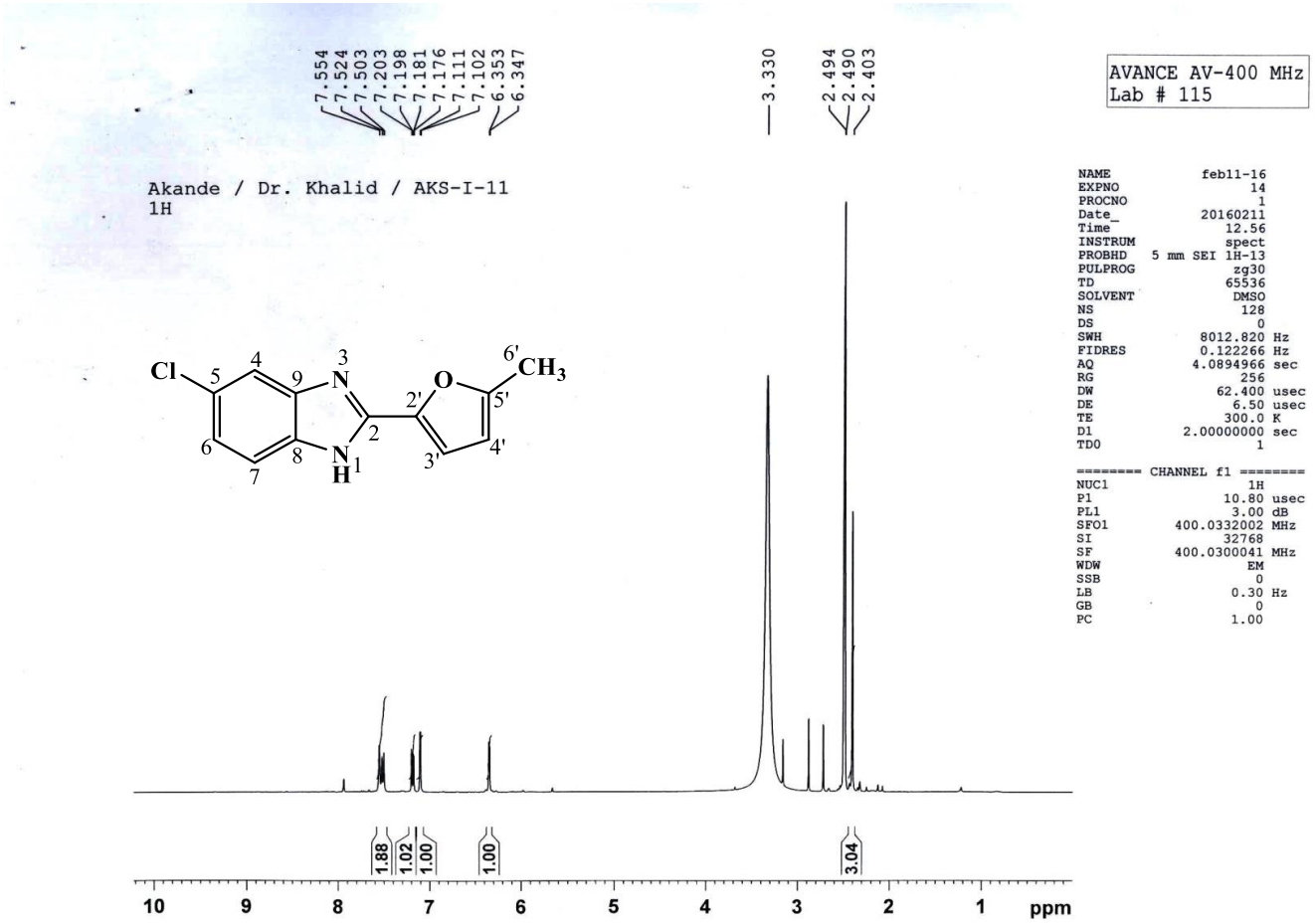

Figure 4.34. ^{1}H NMR (400 MHz, DMSO-d_6) spectrum of AKS-I-11

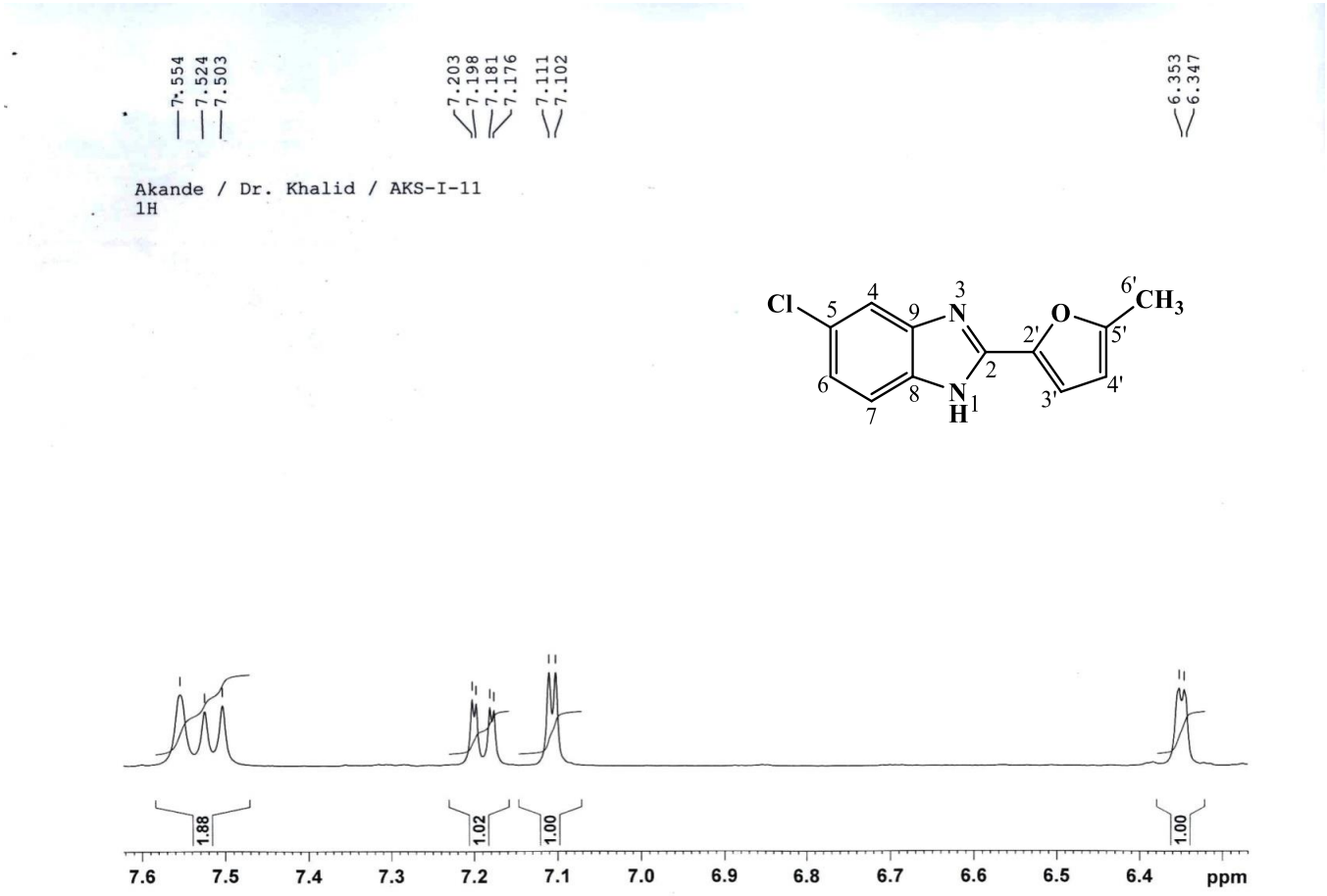

Figure 4.35. ^{1}H NMR (400 MHz, DMSO-d_6) spectrum of AKS-I-11 aromatic region (Expanded)

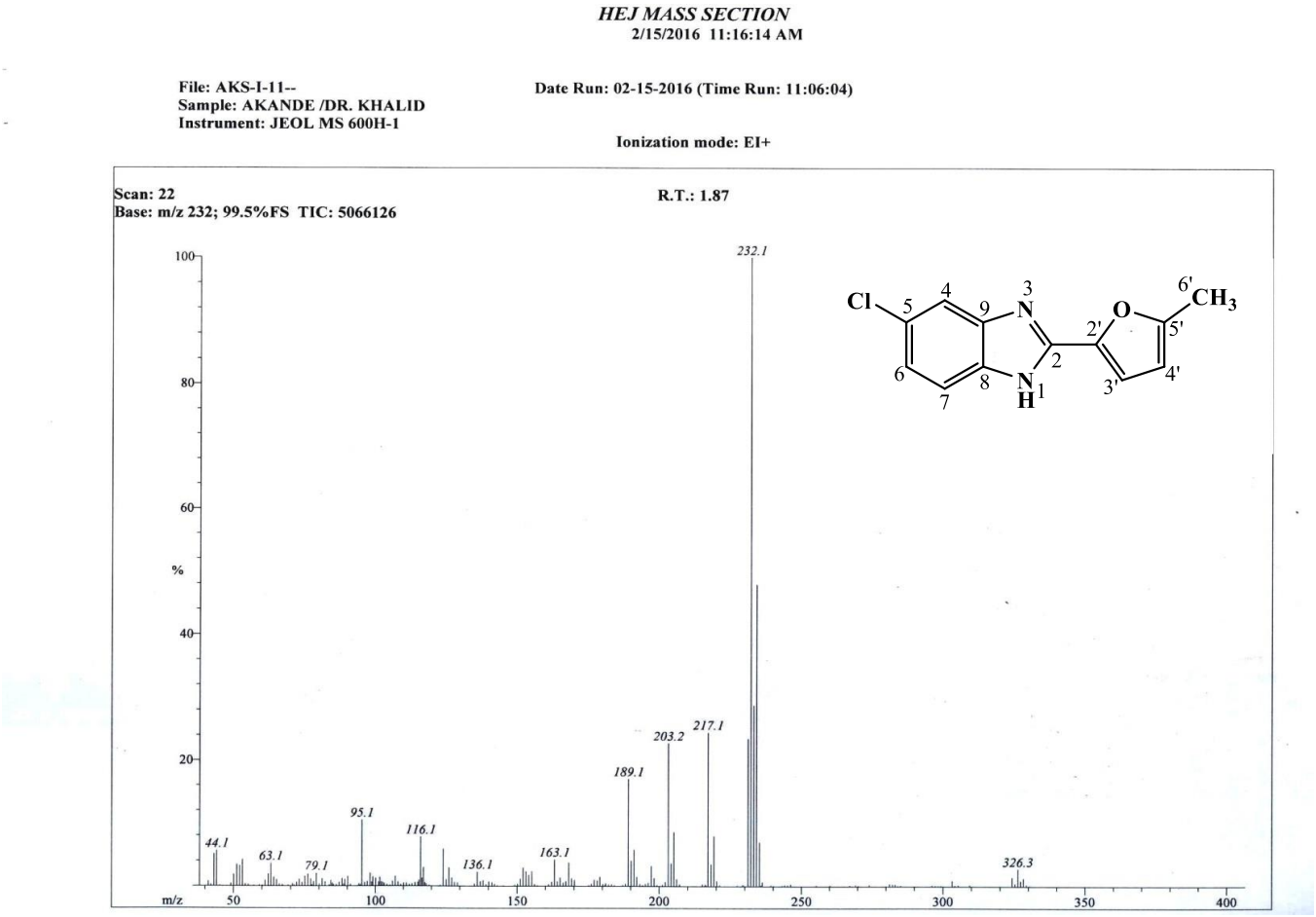

Figure 4.36. EI-MS spectrum of AKS-I-11

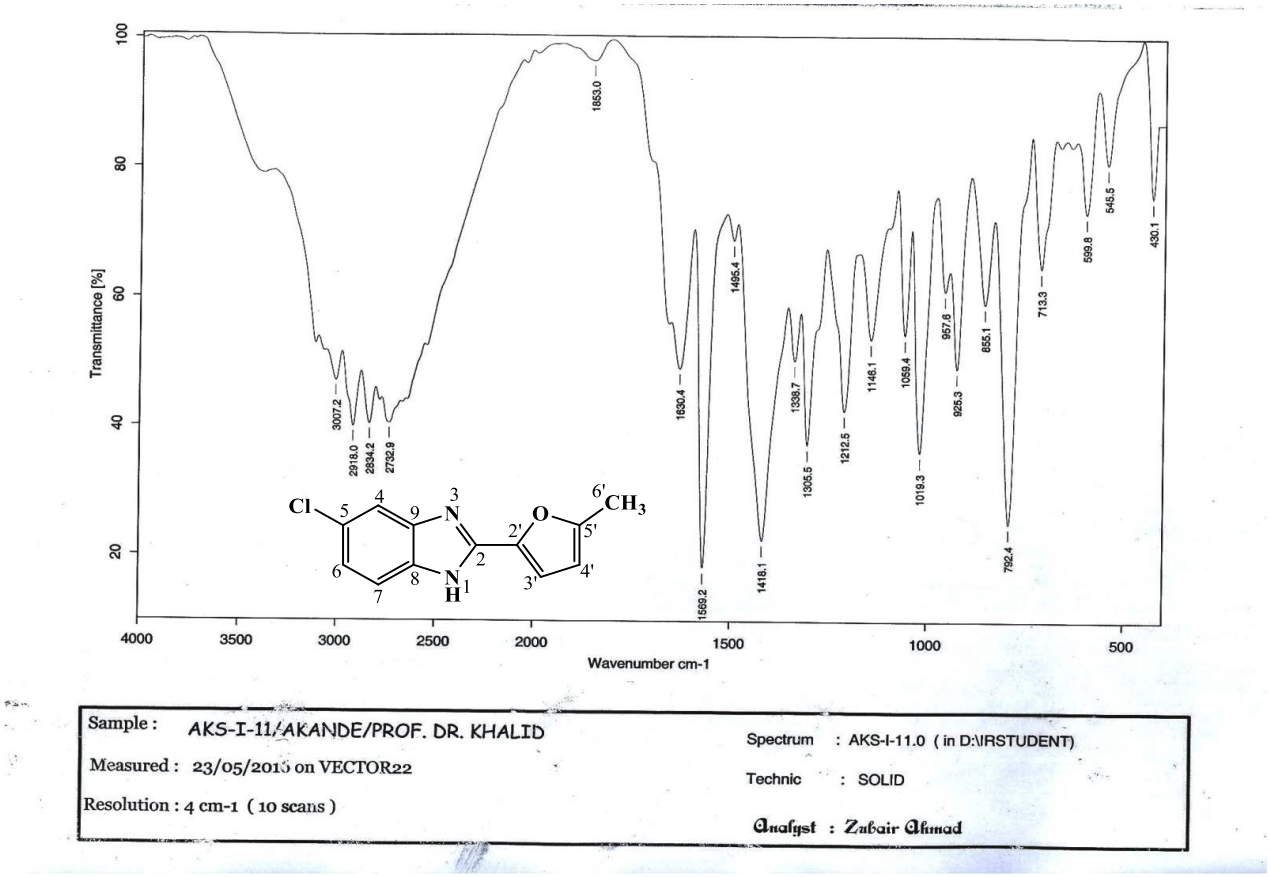

Figure 4.37. IR spectrum of AKS-I-11

THERMO ELECTRON ~ VISIONpro SOFTWARE V4.10

Operator Name	ARSHAD ALAM	Date of Report	5/24/2016
Department	Analytical laboratory#004 TWC	Time of Report	9:52:06AM
Organization	ICCBS.Karachi University.		
Information	Prof Dr.Khalid ./ Akande.		

Scan Graph

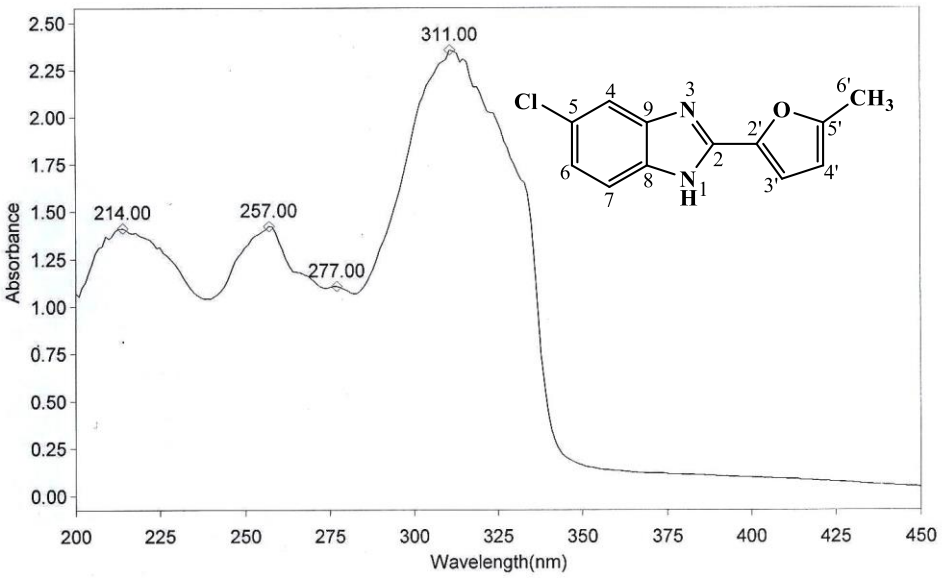

Results Table - AKS- I- 11.sre,AKS - I - 11,Cycle01

nm	A	**Peak Pick Method**
214.00	1.412	Find 8 Peaks Above -3.0000 A
257.00	1.421	Start Wavelength 200.00 nm
277.00	1.108	Stop Wavelength 450.00 nm
311.00	2.357	Sort By Wavelength
Sensitivity	Medium	

Page 1, Scan Graph

Figure 4.38. UV spectrum of AKS-I-11

Table 4.6. Summary of the ^{1}H NMR spectra of AKS-I-11

Position	δ ^{1}H [mult., J_{HH} (Hz)] (ppm)
1	-
2	-
3	-
4	7.55 [s]
5	-
6	7.20 [dd, $J_{6,7}$ = 8.8, $J_{6,4}$ = 2.0]
7	7.52 [d, $J_{7,6}$ = 8.4]
8	-
9	-
1′	-
2′	-
3′	7.11 [d, $J_{3',4'}$ = 3.6]
4′	6.35 [d, $J_{4',3'}$ = 2.4]
5′	-
6′-CH_3	2.40 [s]

4.1.7 Characterisation of 2-(furan-2′-yl)-5,6-dimethyl-1*H*-benzo[*d*]imidazole (AKS-I-12)

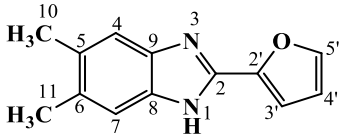

The brown solid compound, AKS-I-12 has a yield of 61.7% (0.131 g), a m.pt. of 166-168 ^{o}C and R_f of 0.41 (hexane/ethyl acetate, 1:1). Figures **4.39** and **4.40** show the ^{1}H NMR spectra (400 MHz, DMSO-d_6) and the chemical shifts, δ (ppm) acquired for twelve protons which are assigned as 12.60 (1H, s, -NH) to the most deshielded of the protons, a 2^{o} amine proton, 7.88 (1H, d, $J_{5',3'}$ = 0.8 Hz, H-5′), 7.36 (1H, s, H-4), 7.23 (1H, s, H-7), 7.10 (1H, d, $J_{3',4'}$ = 3.2 Hz, H-3′), 6.69 (1H, dd, $J_{4',3'}$ = 3.2 Hz, $J_{4',5'}$ = 2.0 Hz, H-4′) to aromatic methine protons. The δ (ppm) 2.30 (3H, s, 10-CH_3) and 2.28 (3H, s, 11-CH_3) were however assigned to six most shielded of the protons, the dimethyl protons. Each methyl has its protons resonating in the same chemical environment. Protons at positions 3′ and 4′ show ortho coupling with a *J* value of 3.2. The ^{1}H NMR spectra data obtained agrees with that of Lam *et al*., 2014.

The molecular ion, M^+ has its peak with *m/z* 212 (base peak), while [M^++1] peak is at *m/z* 213 as represented in the EI-MS spectrum (figure **4.41**). The fragment ions, [M-CH_3]$^+$ and [M-$CH_3^{\bullet}$-$CH_3^{\bullet}$ or (M-$CHO^{\bullet}$)]$^+$ are indicative of the *m/z* 197 and 183 respectively. The peak at *m/z* 169 is suggestive of a successive elimination of $CH_3^{\bullet}$ and $CHO^{\bullet}$ radicals [M-$CH_3^{\bullet}$-$CHO^{\bullet}$]$^+$, corresponding to $[C_{11}H_9N_2]^{\bullet+}$. Further cleavage of the ion $[C_{11}H_6N_2O]^{\bullet+}$ with *m/z* of 183 at the imidazole ring generated the fragment *m/z* 91 $[C_6H_5N]^{\bullet+}$ which inturn cleaved to produce the ion with *m/z* 65 $[C_5H_5]^+$ by a further loss of acetylene. However, the radical fragment obtained the imidazole ring cleaves, resulted to the ion at *m/z* of 81 $[C_5H_5O]^+$ on further loss of $N^{\bullet}$ radical. The *m/z* found corresponding to the molecular formula $C_{13}H_{12}N_2O$ from HREI-MS analysis is 212.0948 (calculated 212.0950), which further comfirms the compound.

The IR absorption spectrum (figure **4.42**) shows diagnostic vibrational frequencies, $\bar{\upsilon}$ (cm^{-1}) of bonds assignable to the amine N–H$_{str}$, aromatic C–H$_{str}$, aliphatic C–H$_{asy\ str}$ and C–H$_{sym\ str}$, C=N$_{str}$, aromatic C=C$_{str}$, C–H$_b$ of aliphatic side chain, and the asymmetric and symmetric C–O–C$_{str}$ of ether akin to ≈3400, 3120, 2926, 2856, 1643, 1524, 1448, 1233 and 1013 cm^{-1} respectively. The UV spectrum (figure **4.43**) showed wavelenghts of maximum absorptions (λ_{max}) at 312, 250 and 213 nm indicative of n→π* and π→π*transitions. The summary of ^{1}H NMR spectra is represented in table **4.7**.

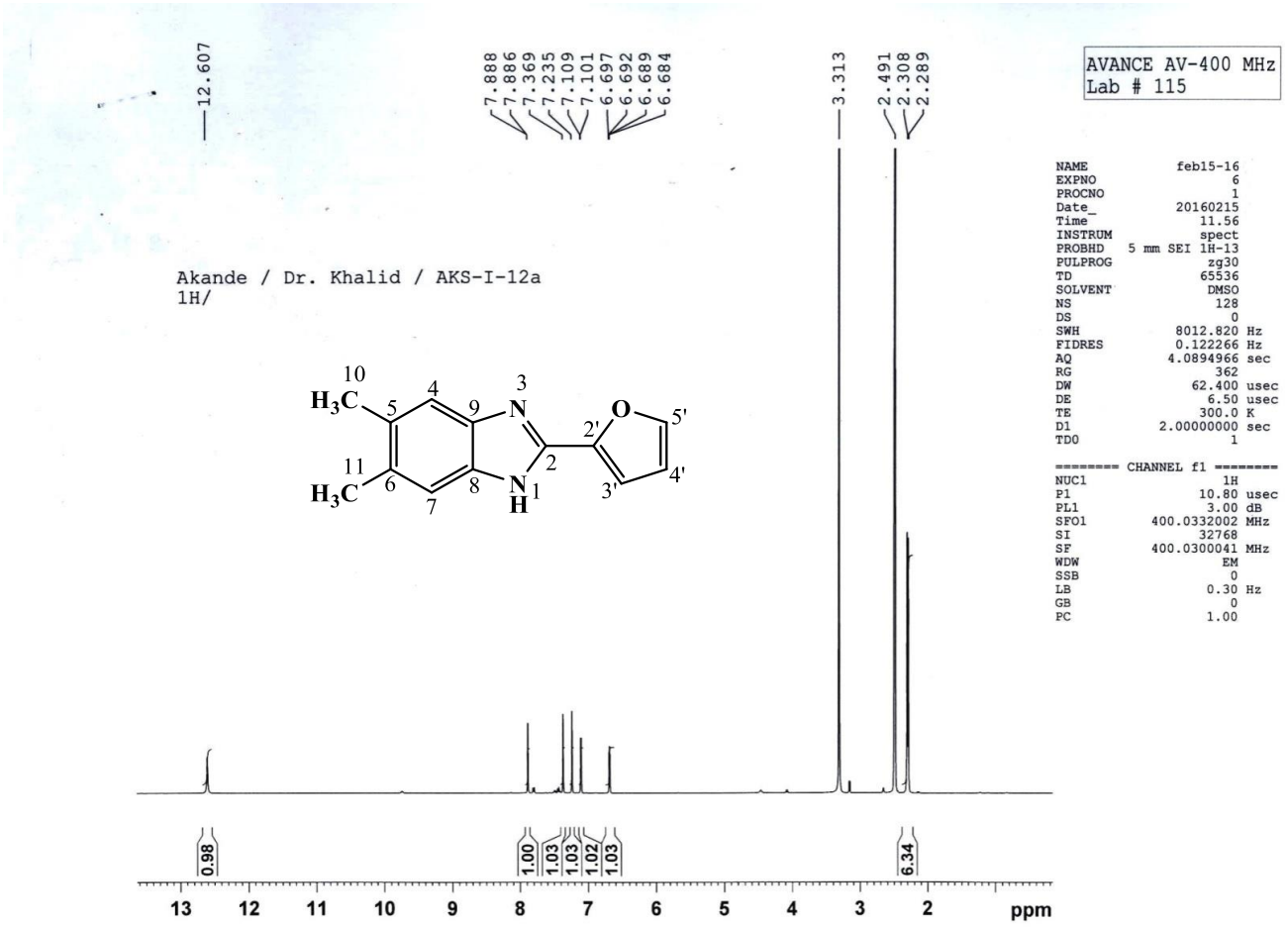

Figure 4.39. ^{1}H NMR (400 MHz, DMSO-d_6) spectrum of AKS-I-12

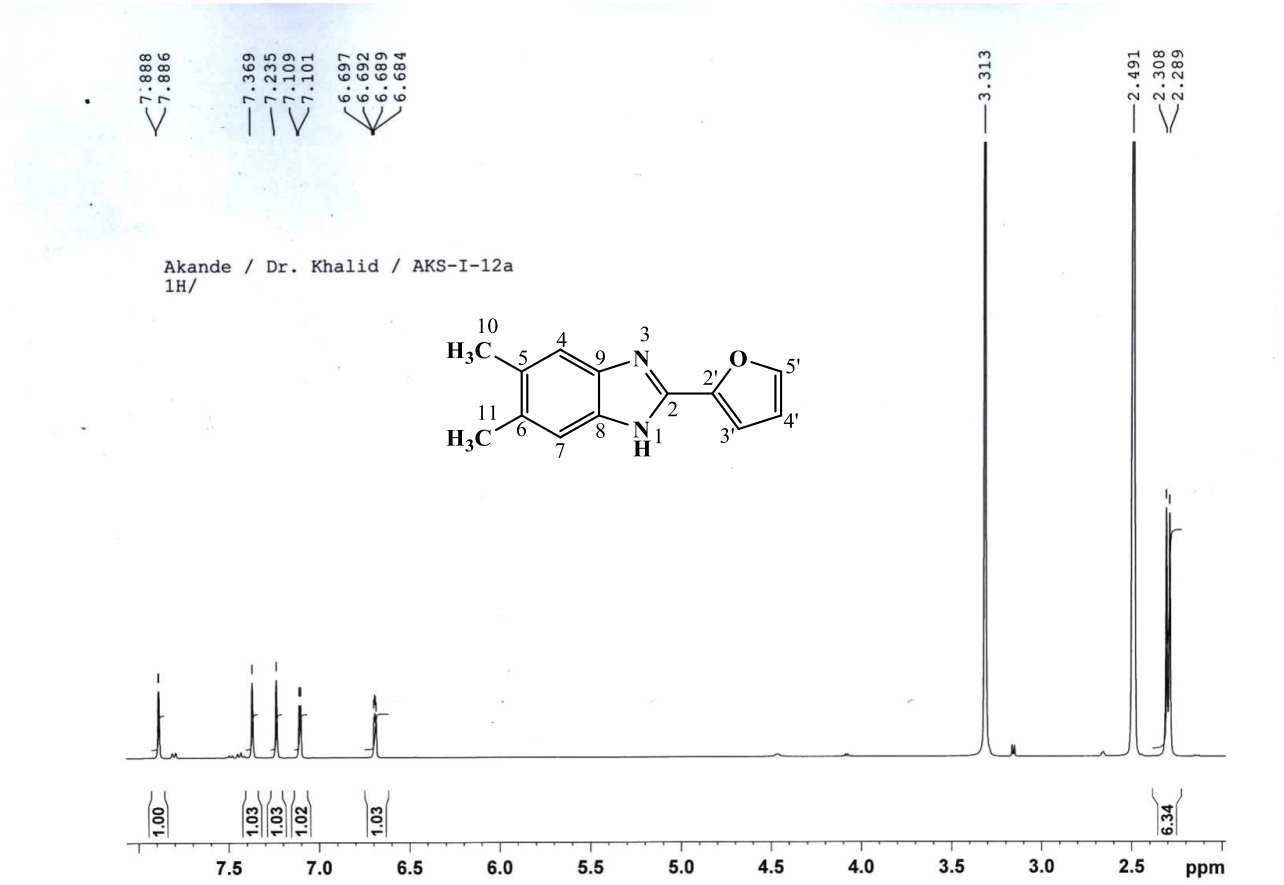

Figure 4.40. ^{1}H NMR (400 MHz, DMSO-d_6) spectrum of AKS-I-12 (Expanded)

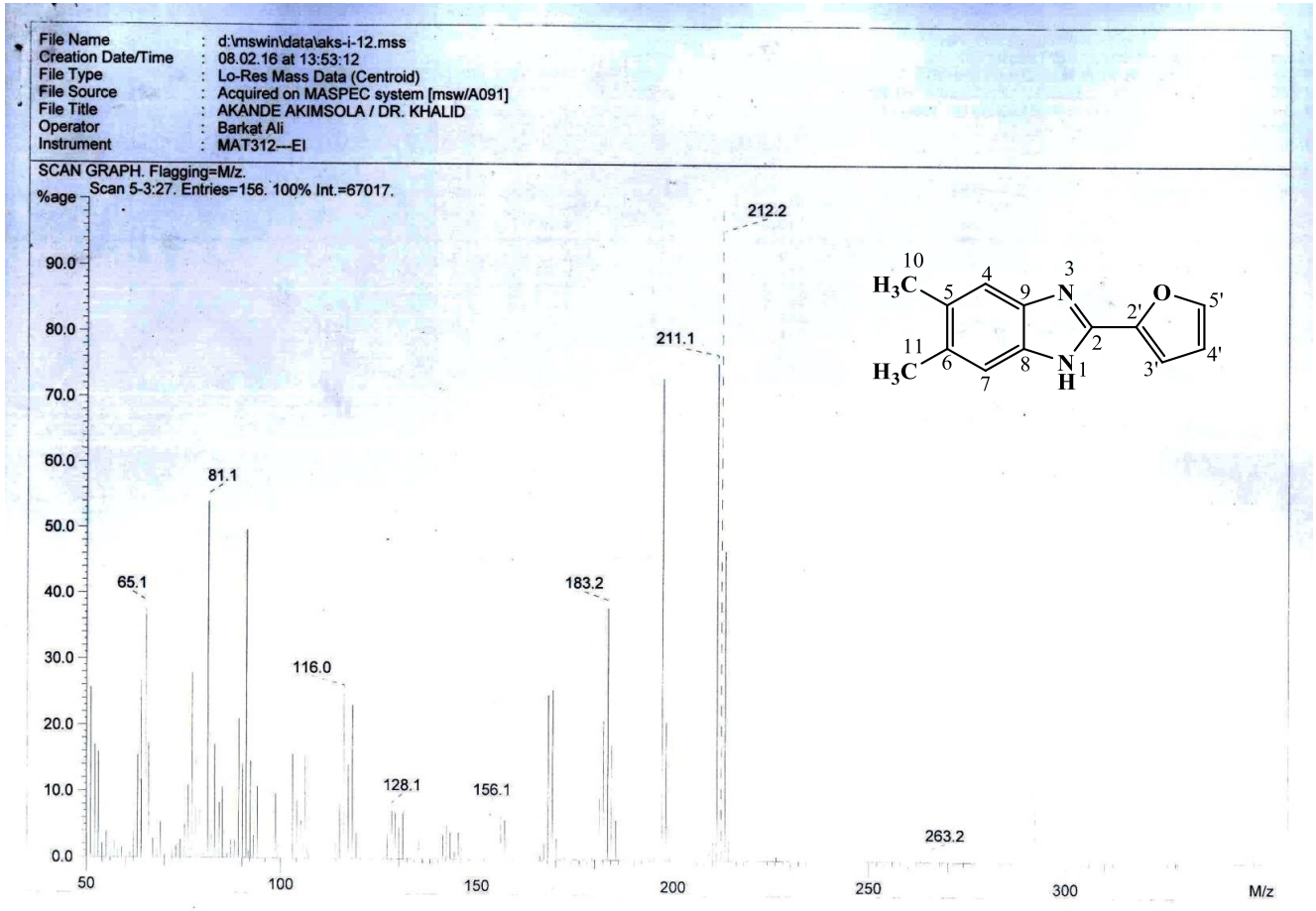

Figure 4.41. EI-MS spectrum of AKS-I-12

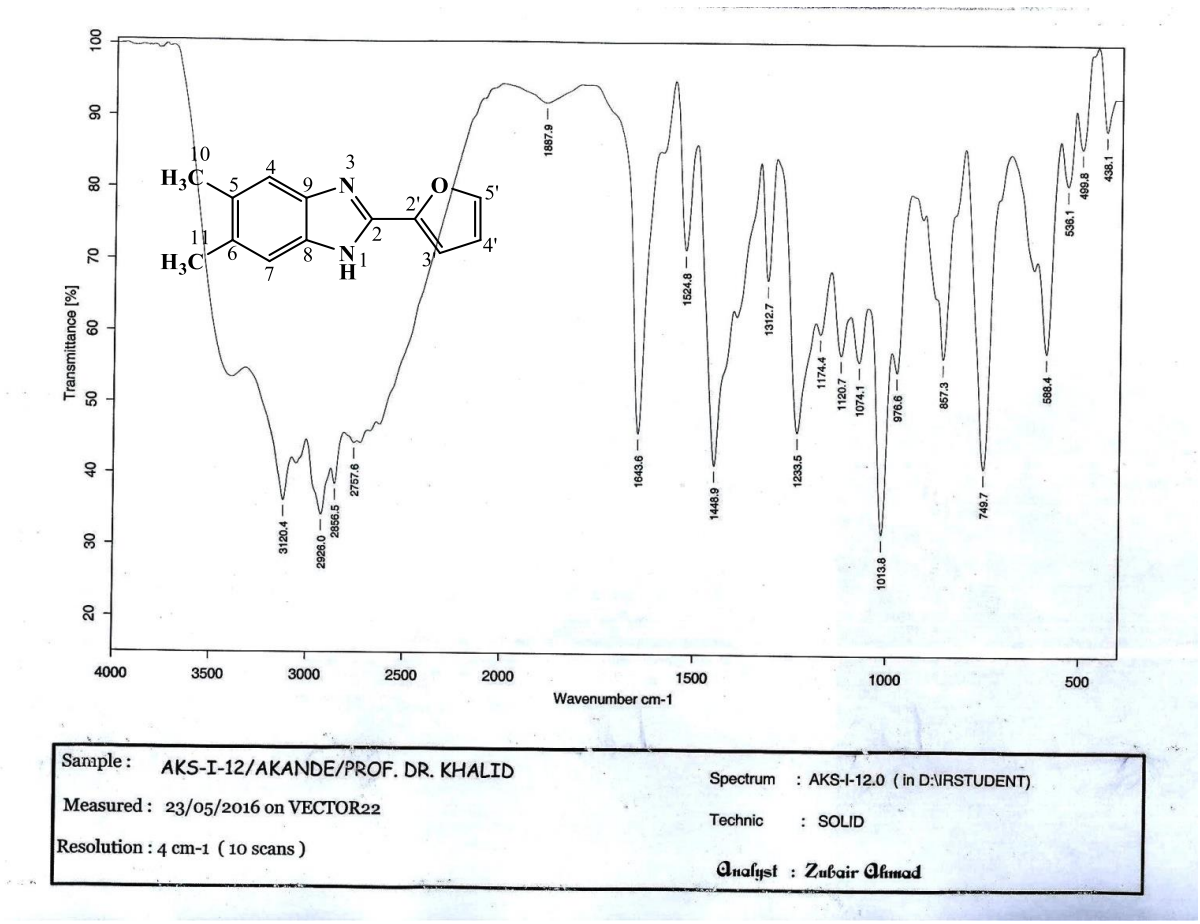

Figure 4.42. IR spectrum of AKS-I-12

THERMO ELECTRON ~ VISIONpro SOFTWARE V4.10

Operator Name	ARSHAD ALAM	Date of Report	5/24/2016
Department	Analytical laboratory#004 TWC	Time of Report	9:55:47AM
Organization	ICCBS.Karachi University.		
Information	Prof Dr.Khalid ./ Akande.		

Scan Graph

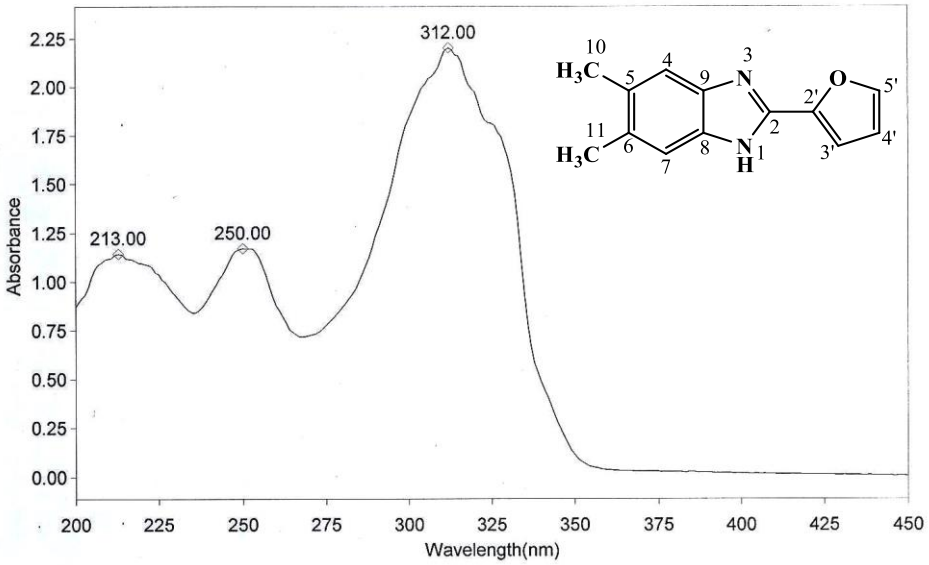

Results Table - AKS- I- 12.sre,AKS- I- 12,Cycle01

nm	A	**Peak Pick Method**
213.00	1.143	Find 8 Peaks Above -3.0000 A
250.00	1.169	Start Wavelength 200.00 nm
312.00	2.202	Stop Wavelength 450.00 nm
		Sort By Wavelength
Sensitivity	Auto	

Page 1, Scan Graph

Figure 4.43. UV spectrum of AKS-I-12

Table 4.7. Summary of the ^{1}H NMR spectra AKS-I-12

Position	δ ^{1}H [mult., J_{HH} (Hz)] (ppm)	Lam *et al*., 2014
1	12.60 [s]	12.43 [br]
2	-	-
3	-	-
4	7.36 [s]	7.46 [s]
5	-	-
6	-	-
7	7.23 [s]	7.46 [s]
8	-	-
9	-	-
1′	-	-
2′	-	-
3′	7.10 [d, $J_{3',4'}$ = 3.2]	7.59 [d, J = 3.6]
4′	6.69 [dd, $J_{4',3'}$ = 3.2, $J_{4',5'}$ = 2.0]	6.90 [dd, J = 3.6, 1.7]
5′	7.88 [d, $J_{5',3'}$ = 0.8]	8.18 [m]
10-CH_3	2.30 [s]	2.33 [s]
11-CH_3	2.28 [s]	2.33 [s]

4.1.8 Characterisation of 5,6-dimethyl-2-(5′-methylfuran-2′-yl)-1*H*-benzo[*d*] imidazole (AKS-I-13)

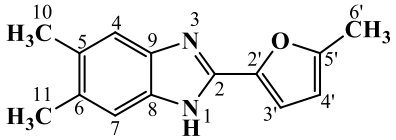

5,6-dimethyl-2-(5′-methylfuran-2′-yl)-1*H*-benzo[*d*]imidazole (AKS-I-13) was obtained as a dark-brown solid, 0.141 g (62.3% yield), m.pt. of 225-227 ^{o}C and 0.43 (hexane/ethyl acetate, 1:1) R_f value.

The ^{1}H NMR spectra (400 MHz, DMSO-d_6) (figures **4.44** and **4.45)** show resonance peaks in δ (ppm) units at 7.31 (2H, s, H-7, H-4; chemically equivalent), 7.09 (1H, d, $J_{3',4'}$ = 2.8 Hz, H-3′) and 6.35 (1H, d, $J_{4',3'}$ = 2.4 Hz, H-4′) for the aromatic methine protons, while at 2.40 (3H, s, 6′-CH_3) is a singlet for the three methyl protons on the furan ring and 2.30 (6H, s, 10-CH_3, 11-CH_3) also is a singlet for 6 chemically equivalent methyl protons on the benzimidazole ring. The amine proton peak was not captured. The ^{1}H NMR data were found consistent with those from literature (Schwob and Kempe, 2016; Weires *et al*., 2012).

The EI-MS spectrum (figure **4.46**) showed *m/z* 226 for the molecular ion, M^+ (also the base peak) and a *m/z* 227 corresponding to [M^++1] peak. Fragment ions at *m/z* 211, 197 and 183 are due to loss of one, two and three $CH_3^{\bullet}$ radical(s) successively corresponding to [M-CH_3]$^+$, [M-CH_3-CH_3]$^+$ and [M-CH_3-CH_3-CH_3]$^+$ respectively. Further cleavage at imidazole ring of *m/z* 183 produced a radical cation with *m/z* 91 $[C_6H_5N]^{\bullet+}$ and the radical generated alongside cleaves to give *m/z* of 69 $[C_4H_5O]^+$. The fragment with *m/z* 169 is indicative of $OH^{\bullet}$ radical loss from *m/z* 183 fragment. HREI-MS analysis gave a *m/z* at 226.1091 (calculated 226.1106), corresponding to the molecular formula, $C_{14}H_{14}N_2O$ of the compound [M^+].

The IR absorption bands (figure **4.47**) shows characteristic stretching vibrational frequencies, $\bar{\upsilon}$ (cm^{-1}) of bonds assigned as 3407 (amine N–H_{str}), 3028 (aromatic C–H_{str}), 2917, 2851 (aliphatic C–$H_{asy\ str}$ and C–$H_{sym\ str}$), 1644 (C=N_{str}), 1570 (aromatic C=C_{str}), 1439 (C–H_b of methyl side chains), 1207, 1018 (C–O–C_{asy} and C–O–$C_{sym\ str}$ of ether respectively). The λ_{max} obtained from UV analysis (figure **4.48**) at 325, 312, 258 and 214 nm are characteristic n→π* and π→π* transitions. Summary of the ^{1}H NMR spectra is represented in table **4.8**.

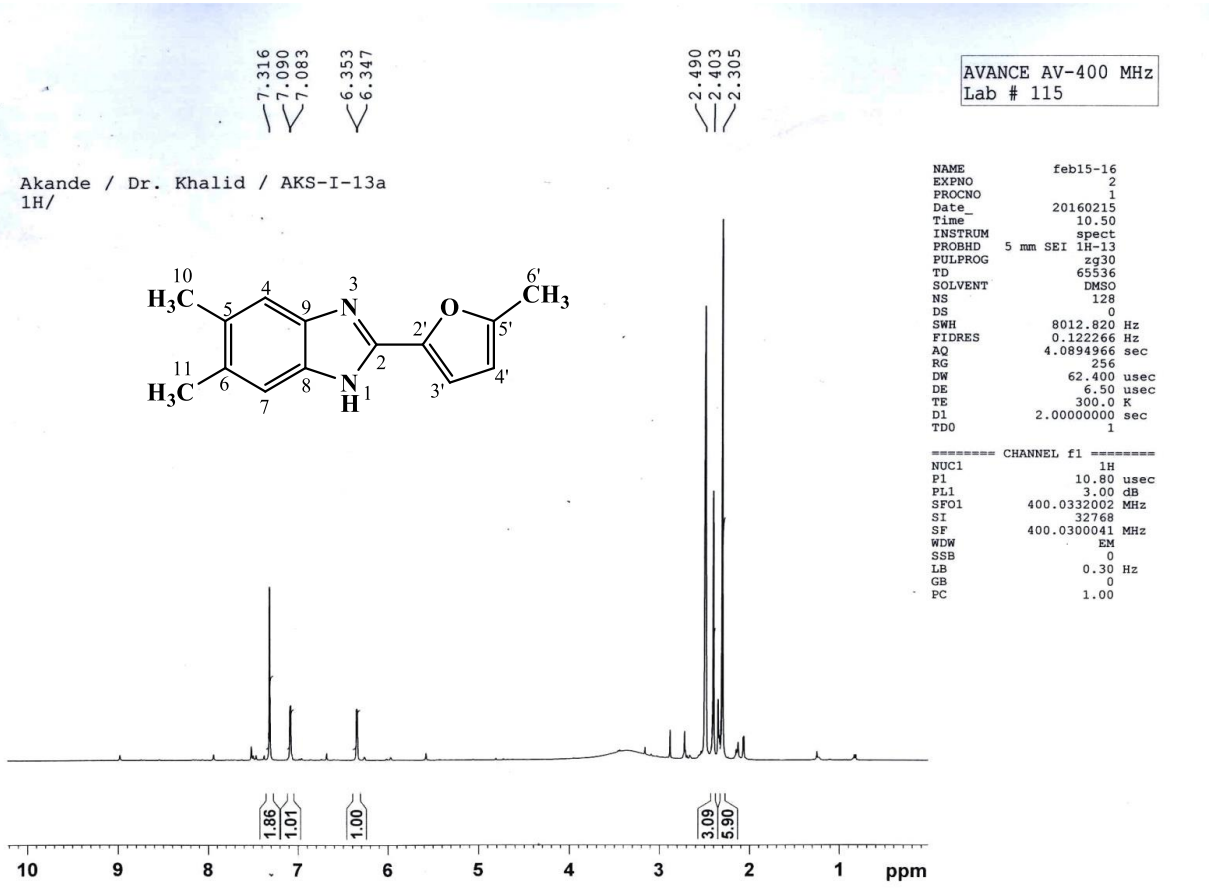

Figure 4.44. ^{1}H NMR (400 MHz, DMSO-d_6) spectrum of AKS-I-13

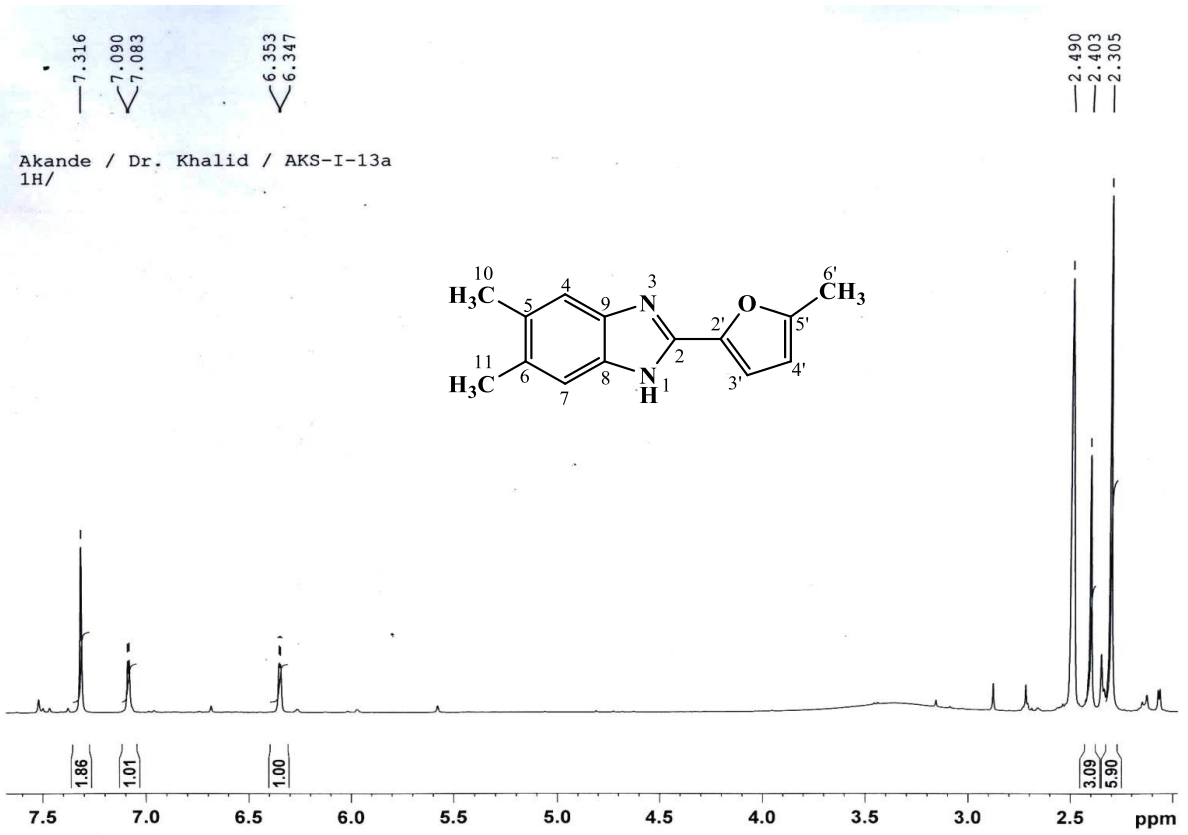

Figure 4.45. ^{1}H NMR (400 MHz, DMSO-d_6) spectrum of AKS-I-13 (Expanded)

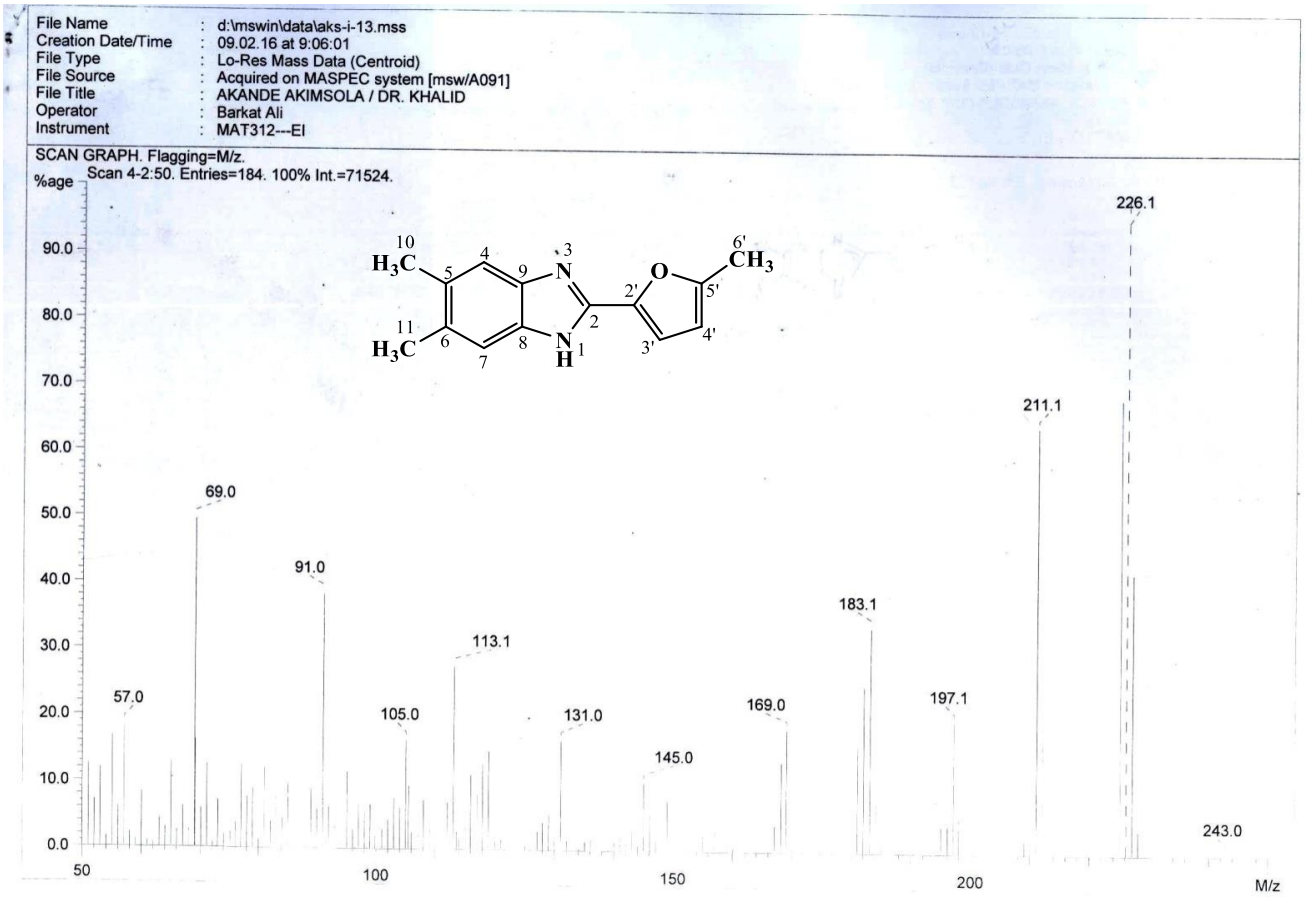

Figure 4.46. EI-MS spectrum of AKS-I-13

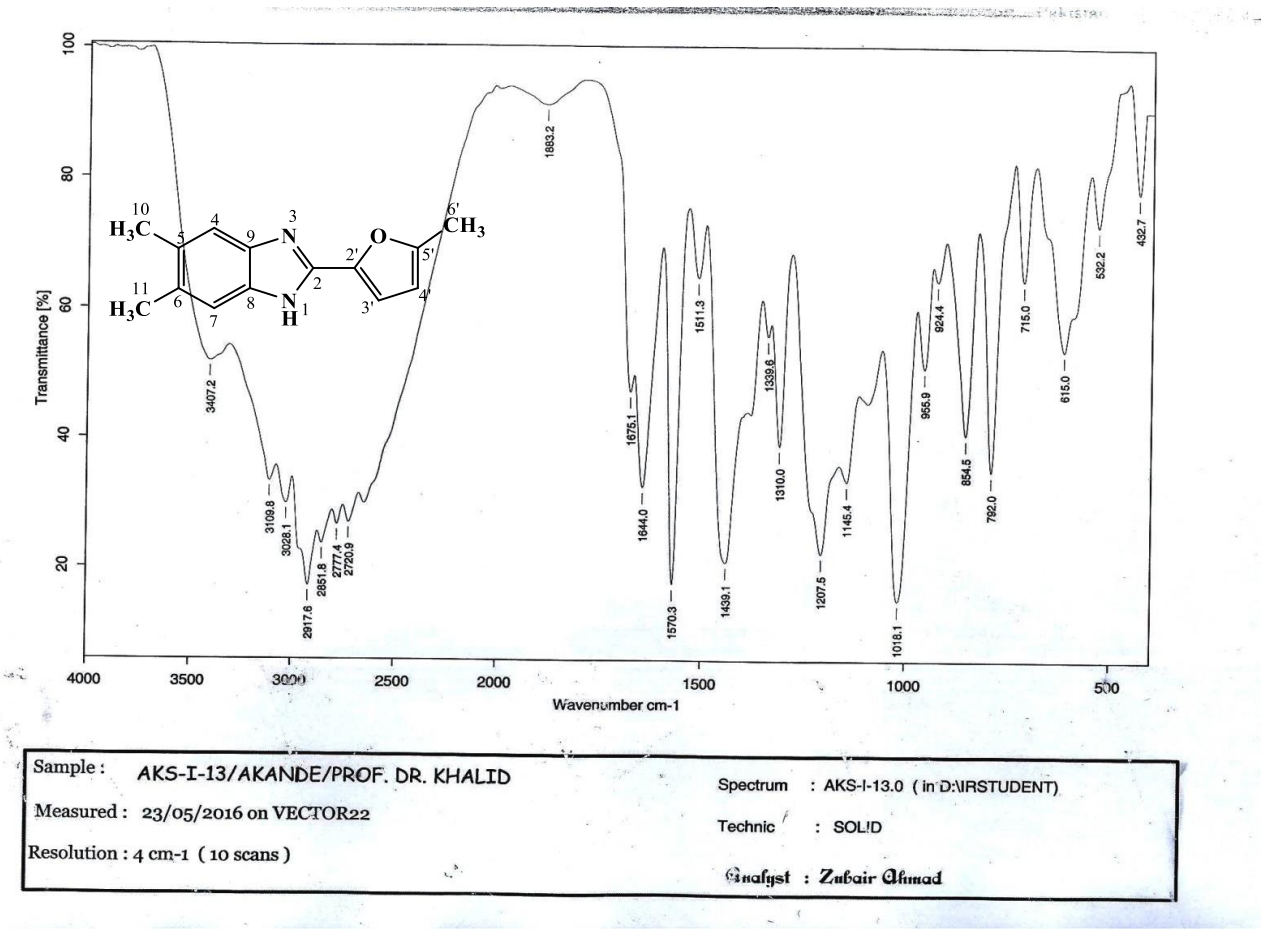

Figure 4.47. IR spectrum of AKS-I-13

THERMO ELECTRON ~ VISIONpro SOFTWARE V4.10

Operator Name	ARSHAD ALAM	Date of Report	5/24/2016
Department	Analytical laboratory#004 TWC	Time of Report	10:02:09AM
Organization	ICCBS.Karachi University.		
Information	Prof Dr.Khalid ./ Akande.		

Scan Graph

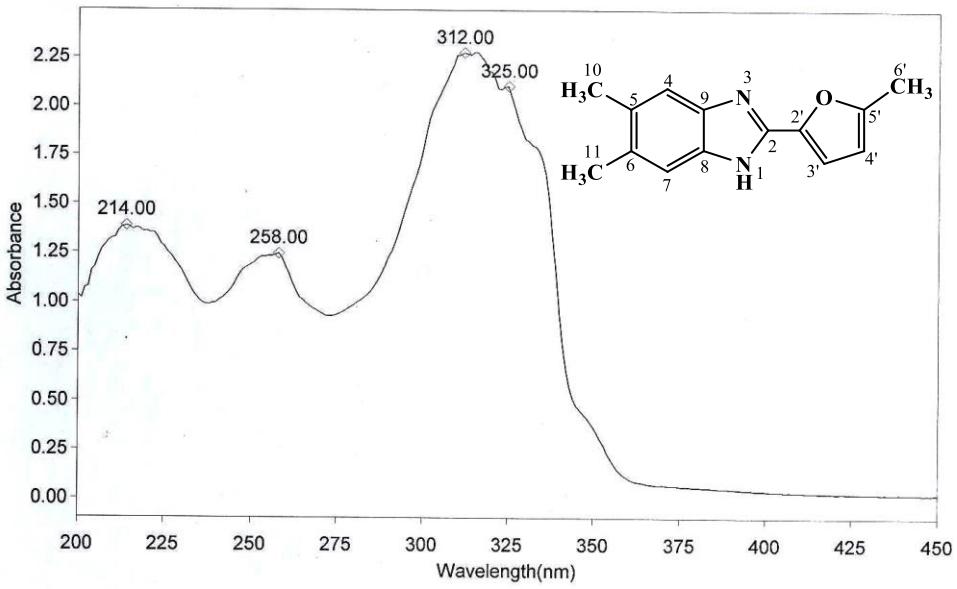

Results Table - AKS- I- 13.sre,AKS- I- 13,Cycle01

nm	A	Peak Pick Method
214.00	1.387	Find 8 Peaks Above -3.0000 A
258.00	1.244	Start Wavelength 200.00 nm
312.00	2.276	Stop Wavelength 450.00 nm
325.00	2.102	Sort By Wavelength
Sensitivity	Medium	

Page 1, Scan Graph

Figure 4.48. UV spectrum of AKS-I-13

Table 4.8. Summary of the ^{1}H NMR spectra of AKS-I-13

Position	δ ^{1}H [mult., J_{HH} (Hz)] (ppm)	Weires *et al.*, 2012	Schwob and Kempe, 2016
1	-	12.47 [br s]	12.54 [s]
2	-	-	-
3	-	-	-
4	7.31 [s]	7.35 [s]	7.34-7.24 [m]
5	-	-	-
6	-	-	-
7	7.31 [s]	7.22 [s]	7.34-7.24 [m]
8	-	-	-
9	-	-	-
1′	-	-	-
2′	-	-	-
3′	7.09 [d, $J_{3',4'}$ = 2.8]	6.99 [d, J = 3.5]	7.01 [d]
4′	6.35 [d, $J_{4',3'}$ = 2.4]	6.30 [dd, J = 3.5]	6.31 [d]
6′-CH_3	2.40 [s]	2.40 [s]	2.39 [s]
10-CH_3	2.30 [s]	2.31 [s]	2.30 [s]
11-CH_3	2.30 [s]	2.29 [s]	2.30 [s]

4.1.9 Characterisation of 2-(furan-2′-yl)-5-nitro-1*H*-benzo[*d*]imidazole (AKS-I-14)

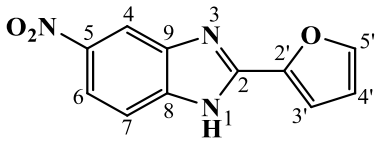

The brown compound, AKS-I-14 is a solid, obtained with a yield of 69.4% (0.159 g), m.pt. 219-220 ^{o}C [literature: 222-223 ^{o}C (Kumar *et al.*, 2013)] and a R_f of 0.37 in a hexane/ethyl acetate (1:1) solvent system. All six resonance peaks in the ^{1}H NMR (400 MHz, DMSO-d_6) spectra (figures **4.49** and **4.50**) with chemical shift δ (ppm) values assigned as 8.42 (1H, s H-4), 8.13 (1H, dd, $J_{6,4}$ = 2.0 Hz, $J_{6,7}$ = 8.8 Hz, H-6), 8.04 (1H, s, H-5′), 7.73 (1H, d, $J_{7,6}$ = 8.8 Hz, H-7), 7.35 (1H, d, $J_{3',4'}$ = 3.2 Hz, H-3′) and 6.79 (1H, dd, $J_{4',3'}$ = 3.2 Hz, $J_{4',5'}$ = 1.6 Hz, H-4′) represents the aromatic methine protons.. Proton at position 6, showed ortho coupling with that at position 7 (J = 8.8 Hz), and it further shows a meta coupling with the proton at position 7 (J = 2.0 Hz). However, a splitting was not observed for the peak of proton at position 5′ possibly due to the proton fast relaxing under the influence of an external magnetic field. The amine proton, expected to resonate further downfield, was not captured. Comparison of the ^{1}H NMR data with those obtained by Kumar *et al.*, 2013 were in agreement.

The EI-MS spectrum (figure **4.51**) shows molecular ion, M^+ and M^++1 peaks at *m/z* 229 (base peak) and 230 respectively. Characteristic peaks at *m/z* 199 and 183 are due to loss of NO$^{\bullet}$ and $NO_2^{\bullet}$ radicals respectively corresponding to $[M\text{-}NO]^+$ and $[M\text{-}NO_2]^+$ fragment ions. When the ion with *m/z* 199 further loses a CH_2=CH-O$^{\bullet}$ radical, a fragment with *m/z* of 156 was generated. The *m/z* of 81 is suggestive of $[C_5H_5O]^+$ fragment from the furan moity. Cleavage of the ion with *m/z* 183 on the imidazole ring could generate both a bicyclic ion with *m/z* 90 $[C_6H_4N]^+$ and a fragment with *m/z* 78 $[C_6H_6]^+$. Further cleavage of the bicyclic fragment (*m/z* 90) by losing CN is suggestive of the fragment with *m/z* 63 $[C_5H_4]^+$. From HREI-MS analysis, an ion which matches the molecular formula $C_{11}H_7N_3O_3$ $[M^+]$ was found with *m/z* of 229.0484 (calculated, 229.0487).

The IR spectrum (figure **4.52**) shows absorption frequencies, $\bar{\upsilon}$ (cm^{-1}) at 3374 (amine N–H$_{str}$), 3121 (aromatic C–H$_{str}$), 1633 (C=N$_{str}$), 1515, 1340 (N=O$_{asy\ str}$ and N=O$_{sym\ str}$ of nitro group), 1471 (aromatics C=C$_{str}$), 1235, 1067 (C–O$_{asy\ str}$ and C–O$_{sym\ str}$ of ether). Transitions obtainable from the UV spectrum (figure **4.53**) show corresponding λ_{max} at 338, 278 and 208 nm mainly due to n→π* transitions, the latter two typical of NO_2. Summary of the ^{1}H NMR spectra is represented in table **4.9**.

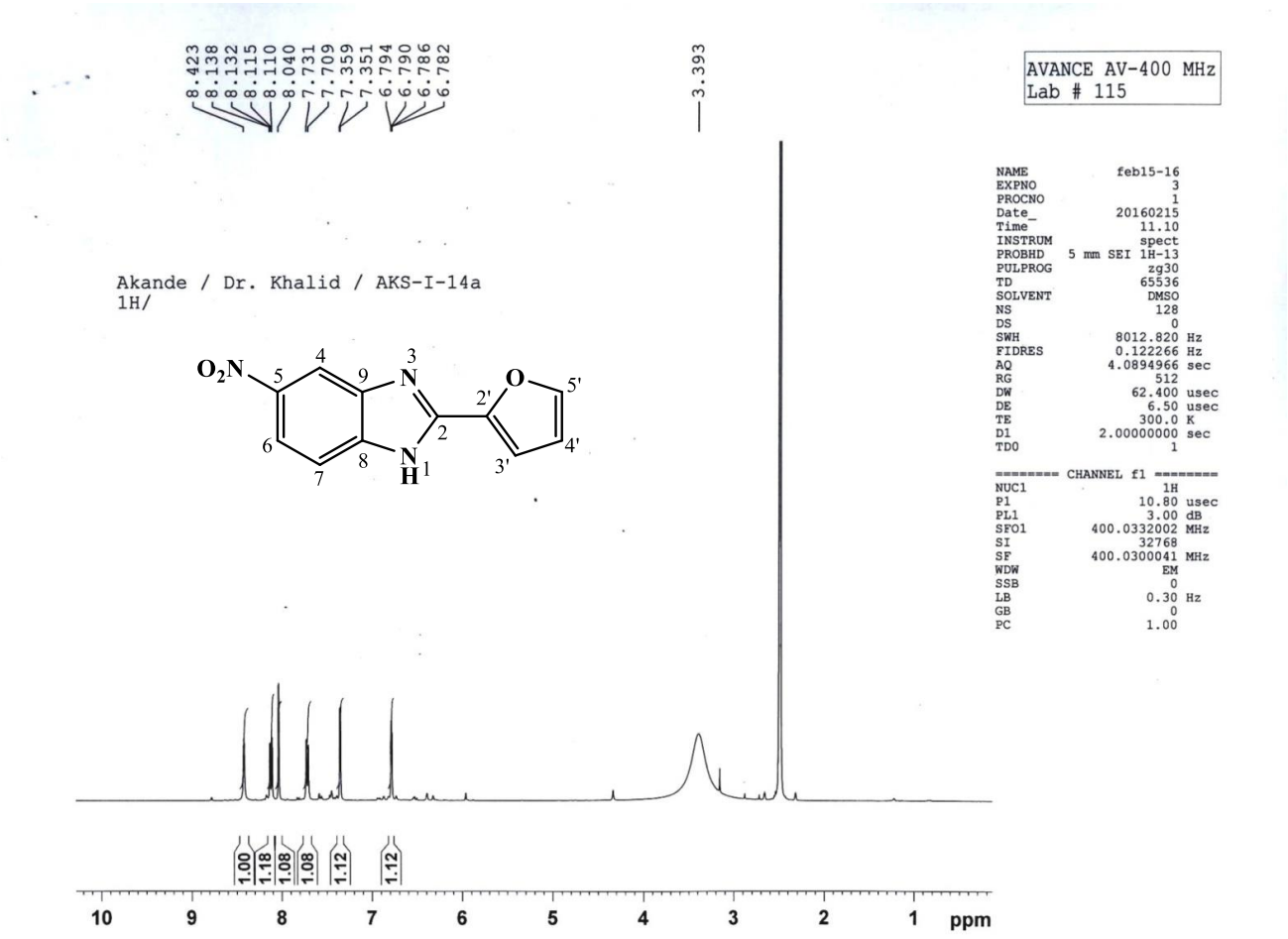

Figure 4.49. ^{1}H NMR (400 MHz, DMSO-d_6) spectrum of AKS-I-14

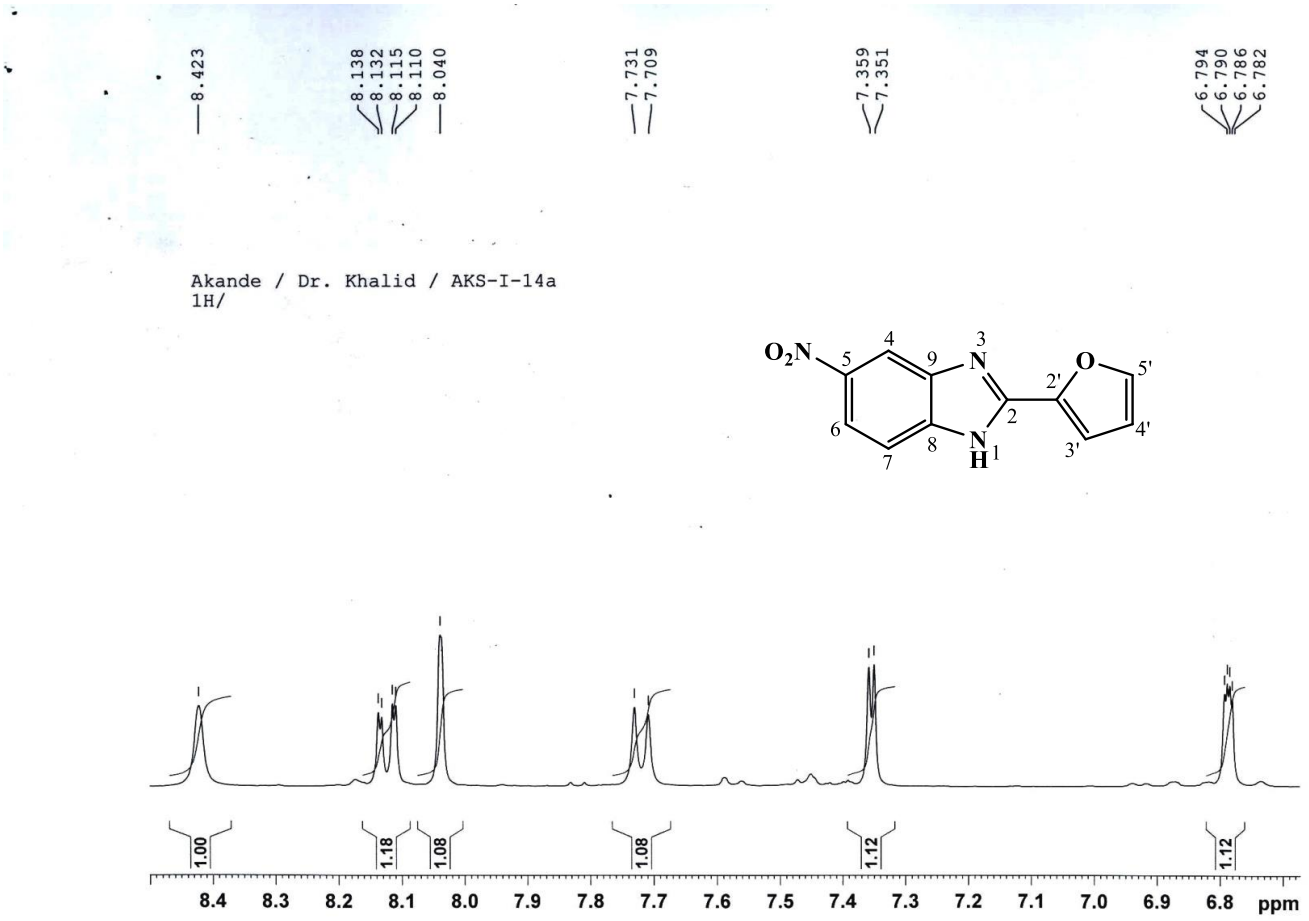

Figure 4.50. ^{1}H NMR (400 MHz, DMSO-d_6) spectrum of AKS-I-14 aromatic region (Expanded)

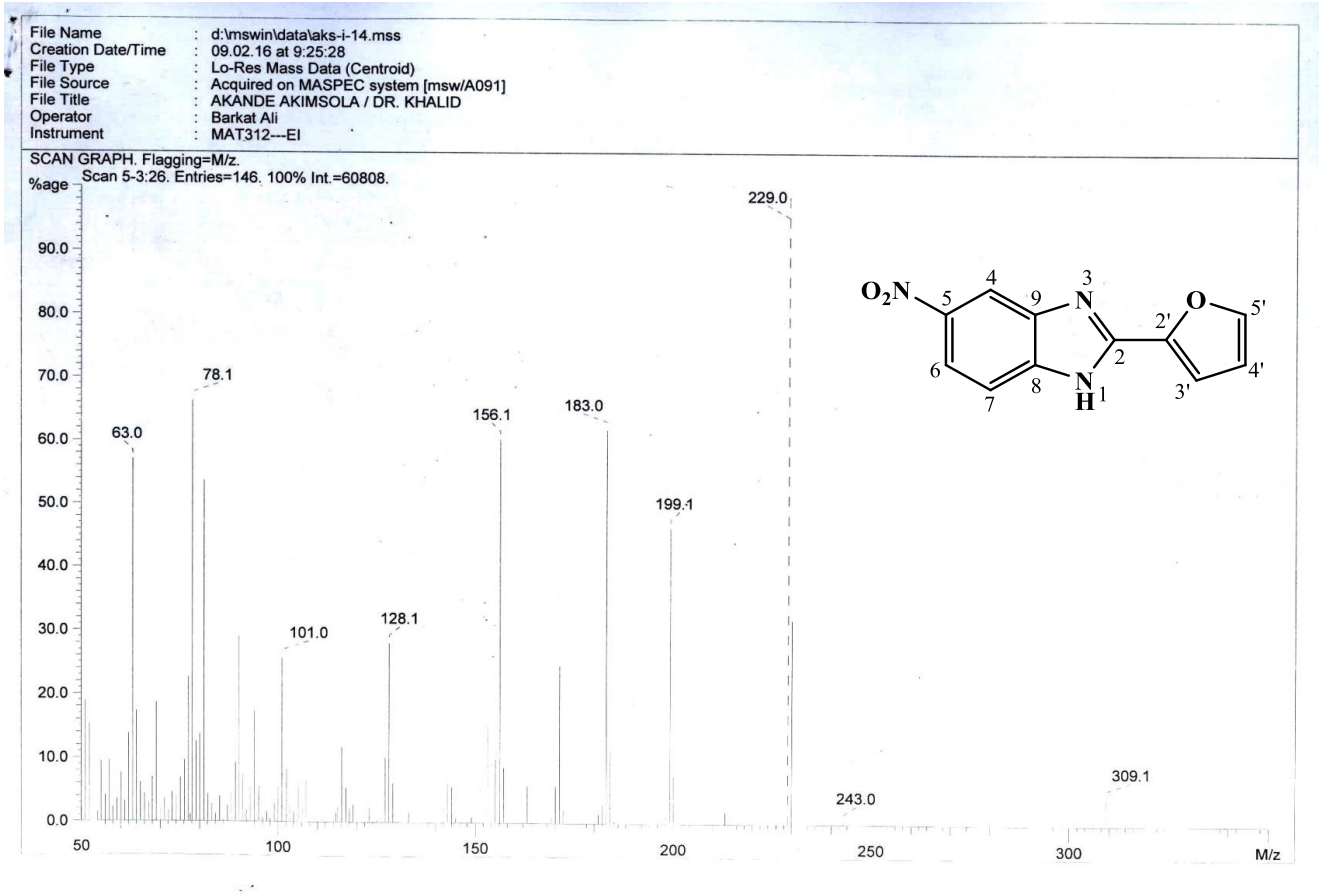

Figure 4.51. EI-MS spectrum of AKS-I-14

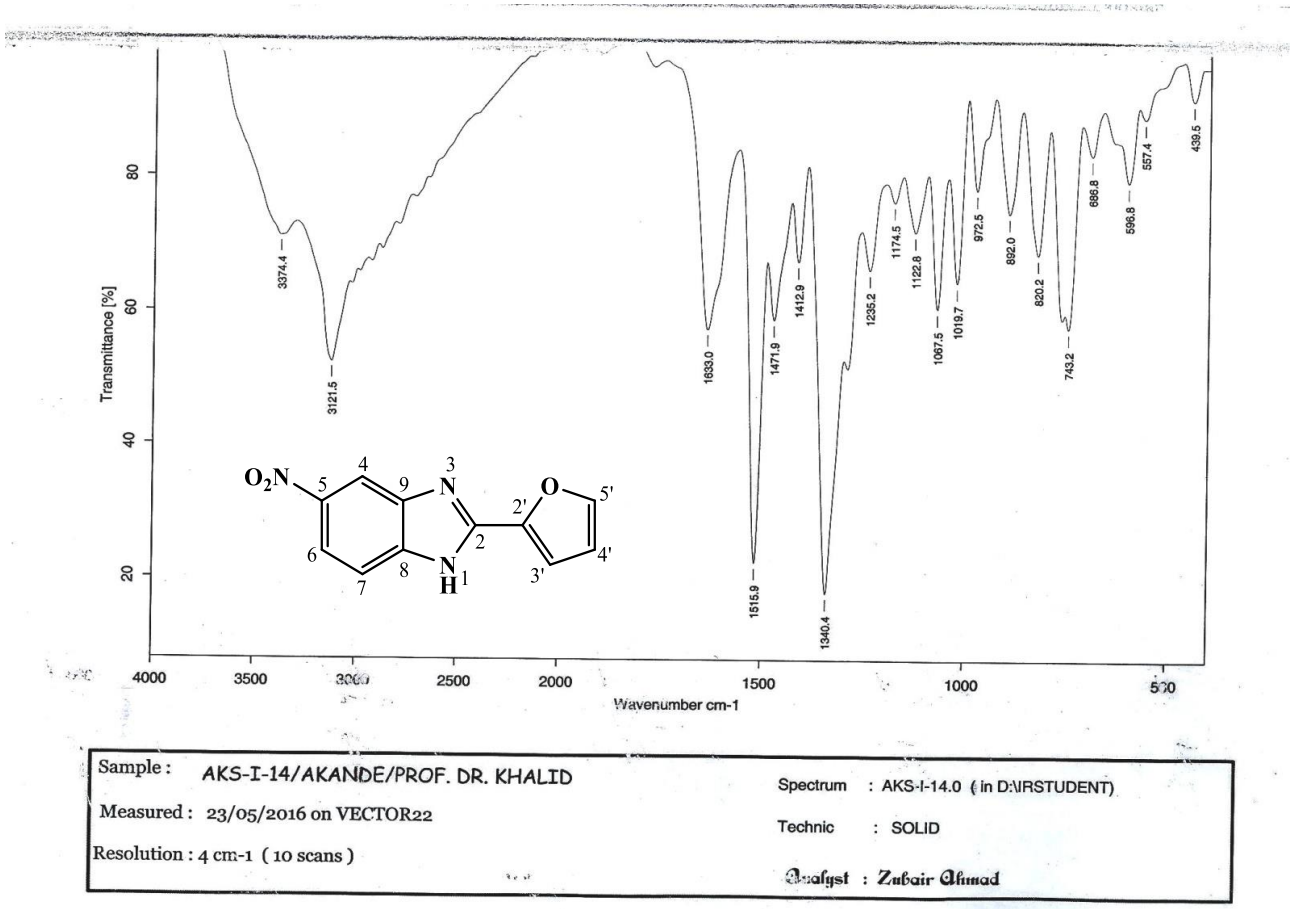

Figure 4.52. IR spectrum of AKS-I-14

THERMO ELECTRON ~ VISIONpro SOFTWARE V4.10

Operator Name	ARSHAD ALAM	Date of Report	5/24/2016
Department	Analytical laboratory#004 TWC	Time of Report	10:10:07AM
Organization	ICCBS.Karachi University.		
Information	Prof Dr.Khalid ./ Akande.		

Scan Graph

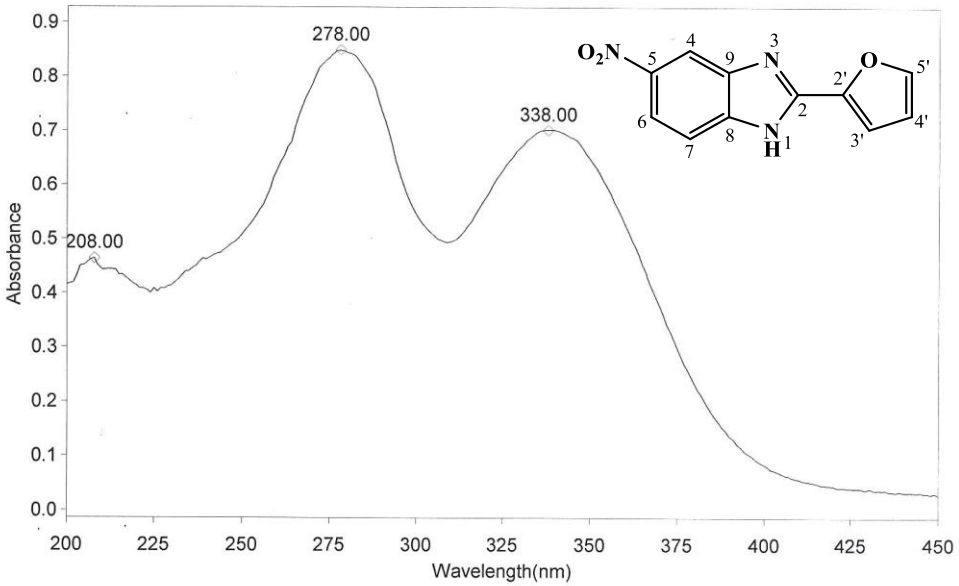

Results Table - AKS- I- 14.sre,AKS- I- 14,Cycle01

nm	A	**Peak Pick Method**
208.00	0.463	Find 8 Peaks Above -3.0000 A
278.00	0.850	Start Wavelength 200.00 nm
338.00	0.701	Stop Wavelength 450.00 nm
		Sort By Wavelength
Sensitivity	Medium	

Page 1, Scan Graph

Figure 4.53. UV spectrum of AKS-I-14

Table 4.9. Summary of the ^{1}H NMR spectra of AKS-I-14

Position	δ ^{1}H [mult., J_{HH} (Hz)] (ppm)	Kumar *et al*., 2013
1	-	-
2	-	-
3	-	-
4	8.42 [s]	8.00 [s]
5	-	-
6	8.13 [dd, $J_{6,7}$ = 8.8, $J_{6,4}$ = 2.0]	8.07 [dd, J = 8.9, J = 2.1]
7	7.73 [d, $J_{7,6}$ = 8.8]	7.67 [d, J = 8.9]
8	-	
9	-	
1′	-	
2′	-	
3′	7.35 [d, $J_{3',4'}$ = 3.2]	7.31 [d, J = 3.4]
4′	6.79 [dd, $J_{4',3'}$ = 3.2, $J_{4',5'}$ = 1.6]	6.75 [dd, J = 3.4, J = 1.5]
5′	8.04 [s]	8.38 [s]

4.1.10 Characterisation of 2-(3′-(benzyloxy)-4′-methoxyphenyl)-1*H*-benzo[*d*] imidazole (AKS-I-34)

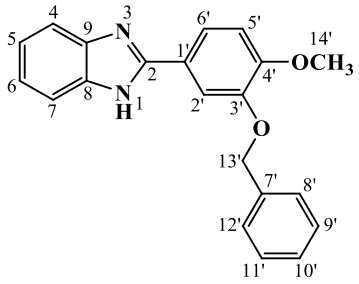

The white compound, AKS-I-34 is a solid obtained with a yield of 89.0% (0.294 g), a m.pt. 116-119 ^{o}C and R_f value of 0.44 (hexane/ethyl acetate, 1:1).

The chemical shift values, δ (ppm) representing 10 resonances obtained from ^{1}H NMR spectra (400 MHz, DMSO-d_6) (figures **4.54** and **4.55**) and were assigned to 12 aromatic methine protons as 7.89 (1H, d, $J_{2',6'}$ = 1.6 Hz, H-2′; most deshielded of the methine protons), 7.78 (1H, d, $J_{6',5'}$ = 8.4 Hz, H-6′), a multiplet at 7.58-7.60 (2H, m, H-7, H-4), 7.51 (2H, d, $J_{8',9'} = J_{12',11'}$ = 7.2 Hz, H-8′, H-12′), 7.43 (2H, t, $J_{9',10'} = J_{11',10'}$ = 7.6 Hz, H-9′, H-11′), 7.36 (1H, t, $J_{10',11'} = J_{10',9'}$ = 7.6 Hz, H-10′), 7.21-7.23 (2H, m, H-5, H-6; another multiplet) and 7.20 (1H, d, $J_{5',6'}$ = 8.4 Hz, H-5′), two methylene protons as 5.19 (2H, s, 13′-OCH_2-) and to three methoxy protons as 3.85 (3H, s, 14′-OCH_3). Multiple splitting observed for H-7, H-6, H-5 and H-4 is indicative of protons resonating in the same chemical environment and thus, peak overlaps. The doublet signals at δ 7.78 and 7.20 are as a result of H-6′ and H-5′ coupling to each other while the signals at δ 5.19 and 3.85 appear as singlets corresponding to two chemically equivalent methylene protons and three chemically equivalent methoxy protons respectively. The spectrum was not extended to capture the deshielded 2^{o} amine proton which is expected to resonate further downfield.

The ^{13}C NMR spectra (75 MHz, DMSO-d_6) (figures **4.56** and **4.57**) show signals in δ (ppm) values, assigned as 151.08 (C-2), 150.98 (C-4′, C-3′), 148.00 (C-9, C-8), 136.77 (C-7′), 121.43 (C-1′) to seven quarternary carbons, 128.44 (C-11′, C-9′′), 127.96 (C-10′), 127.92 (C-12′, C-8′), 122.43 (C-6, C-5), 120.11 (C-6′), 114.57 (C-7, C-4), 112.24 (C-2′), 111.58 (C-5′), to twelve aromatic methine carbons, 70.09 (C-13′) to methylene carbon, and 55.76 (C-14′) to methoxy carbon. These were further resolved in the DEPTH experiments with DEPTH-135 (75 MHz, DMSO-d_6) spectrum (figures **4.58**) affirming the respective methine and methoxy carbons recorded on the positive mode of the

spectrum and the methylene carbon on the negative mode while DEPTH-90 (75 MHz, DMSO-d_6) spectrum (figures **4.59**) corroborates the DEPTH-135 experiment for the methine carbon peaks.

The molecular ion, M^+ and $[M^+ + 1]$ peaks at *m/z* 330 and 331 respectively can be deduced from the EI-MS spectrum (figure **4.60**). Ion peaks with *m/z* 239 and 91(base peak), match up with the fragmentions, M^+-91 and M^+-239 corresponding to $[C_{14}H_{11}N_2O_2]^{\bullet +}$ and $[C_7H_7]^+$ (tropylium ion) respectively. The *m/z* of 28 and 18 obtained are typical of $^+C{\equiv}O^-$ /N≡N (air) and H_2O/NH_4^+ peaks. From HREI-MS analysis, the *m/z* of 330.1350 (calculated 330.1368) further confirmed the compound, corresponding to molecular formula, $C_{21}H_{18}N_2O_2$.

Absorption bands of IR active bonds are represented in figure **4.61**. Vibrational frequencies, $\bar{\upsilon}$ (cm^{-1}) assignable to some typical bonds are represented as 3419 ($N–H_{str}$) of 2º amine, 3063 (aromatic $C–H_{str}$), 2927 (aliphatic $C–H_{asy\ str}$), 1601, 1505 (aromatic $C{=}C_{str}$), 1450 (aliphatic $C–H_b$), 1265, 1018 ($C–O–C_{asy\ str}$ and $C–O–C_{sym\ str}$) of ether respectively. Figure **4.62** represents the UV spectrum showing wavelenght of maximum absorptions (λ_{max}) at 311, 222 and 214 nm, corresponding to $n\rightarrow\pi^*$ and $\pi\rightarrow\pi^*$ transitions. The summary of ^1H NMR and ^{13}C NMR spectra is represented in table **4.10**.

Furthermore, AKS-I-34 is a new compound and is an additions to the library of organic chemistry. In the same view, compounds AKS-I-35 to AKS-I-65 as well as AKS-I-73, AKS-I-98, AKS-I-99 and AKS-I-100 discussed subsequently are also new.

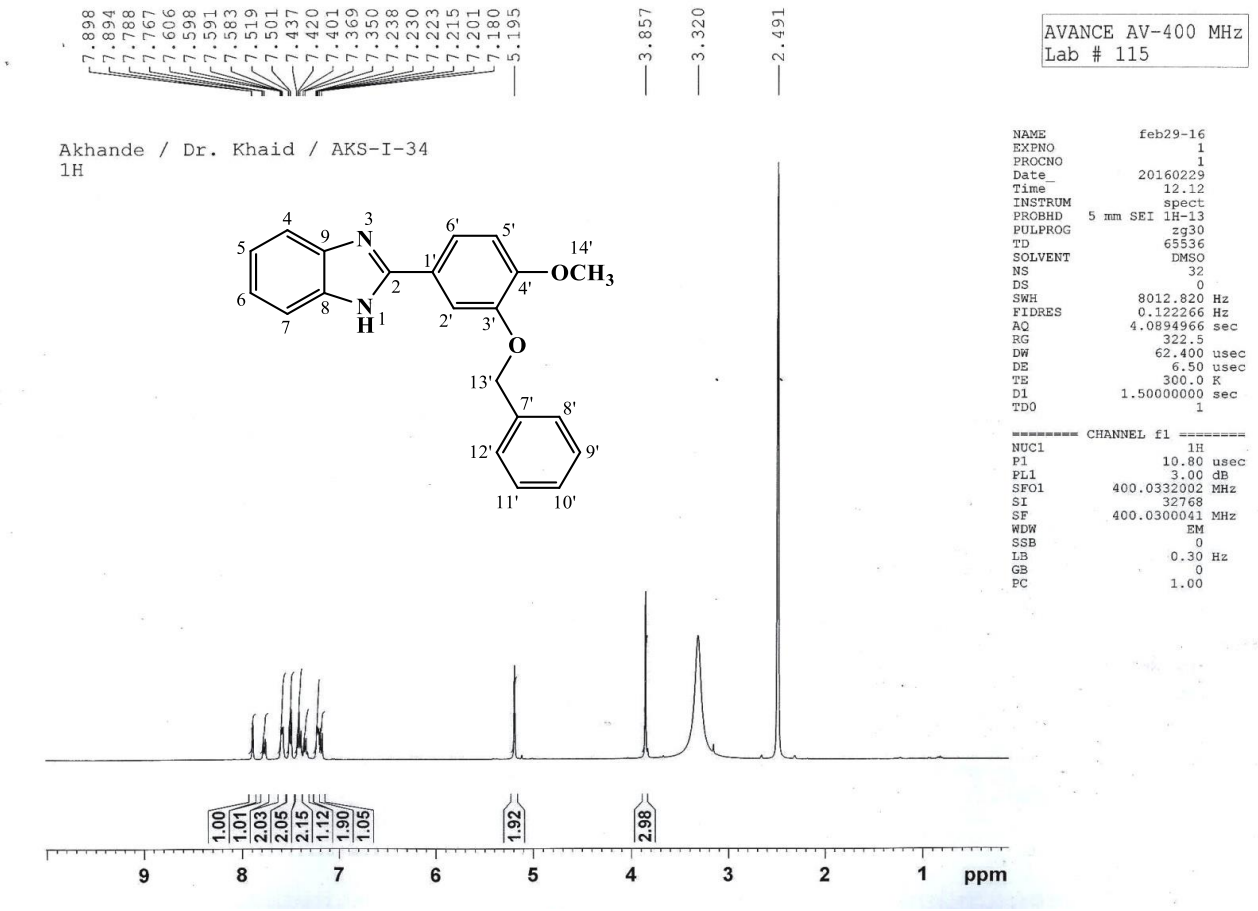

Figure 4.54. ^{1}H NMR (400 MHz, DMSO-d_6) spectrum of AKS-I-34

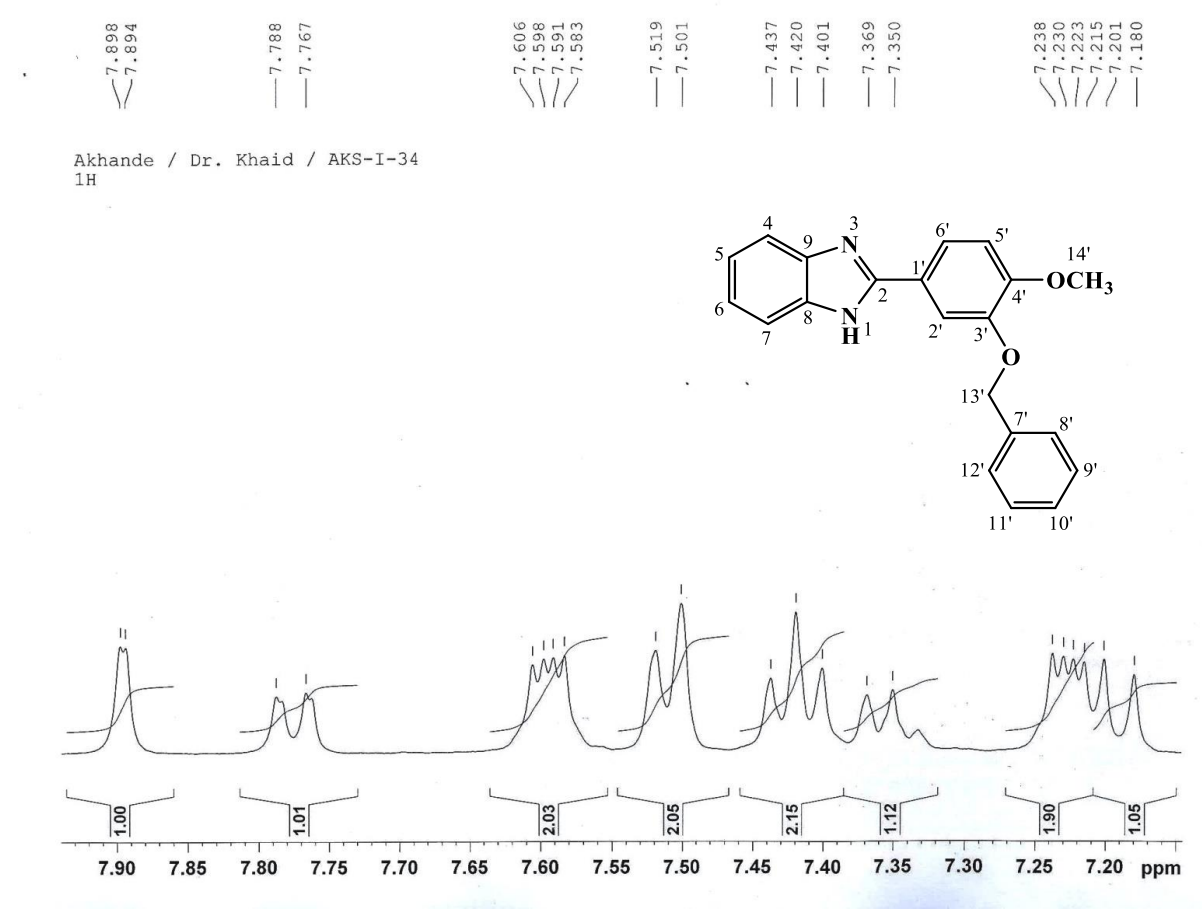

Figure 4.55. ^{1}H NMR (400 MHz, DMSO-d_6) spectrum of AKS-I-34 aromatic region (Expanded)

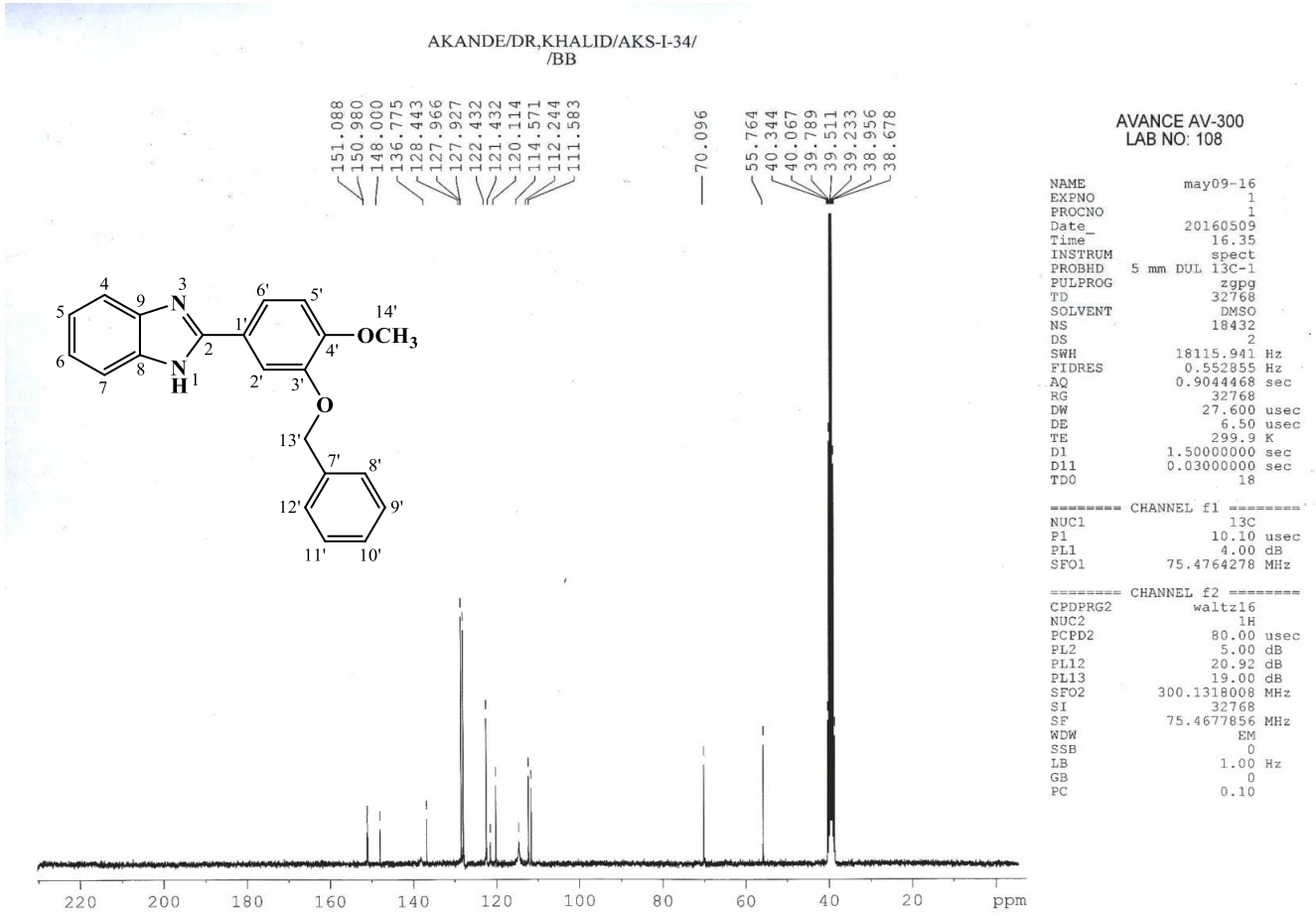

Figure 4.56. ^{13}C NMR (75 MHz, DMSO-d_6) spectrum of AKS-I-34

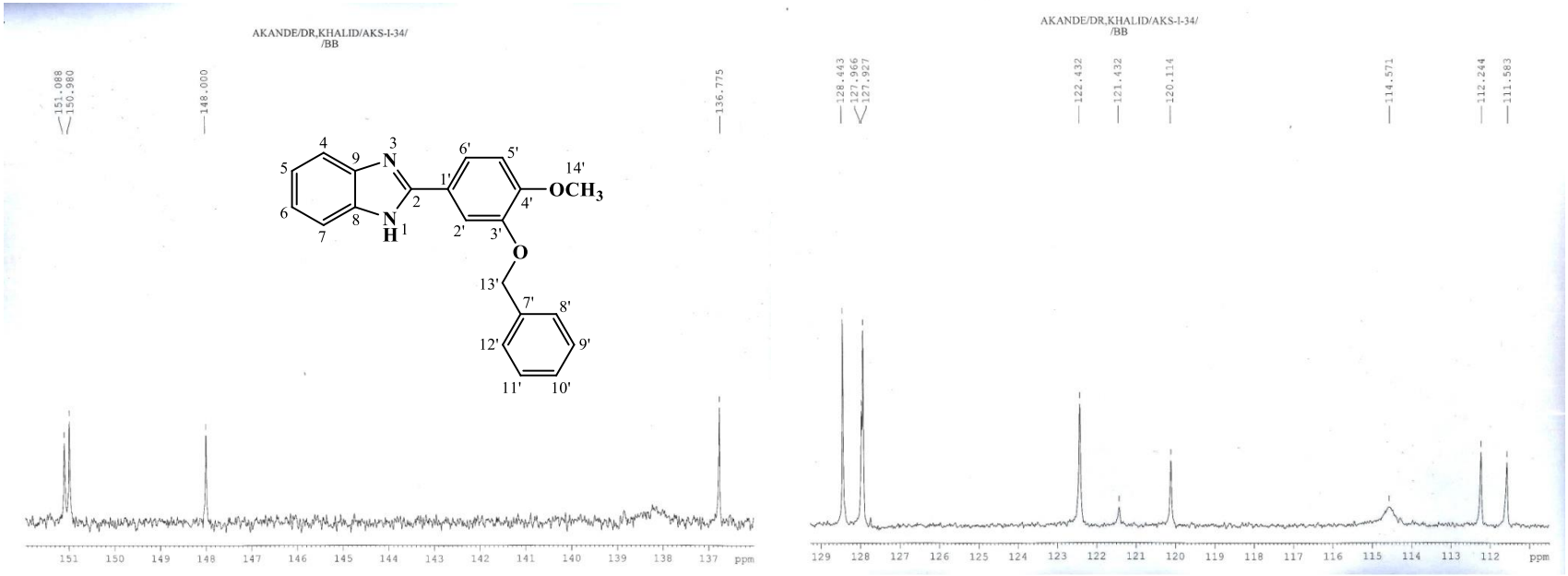

Figure 4.57. ^{13}C NMR (75 MHz, DMSO-d_6) spectra of AKS-I-34 (Expanded)

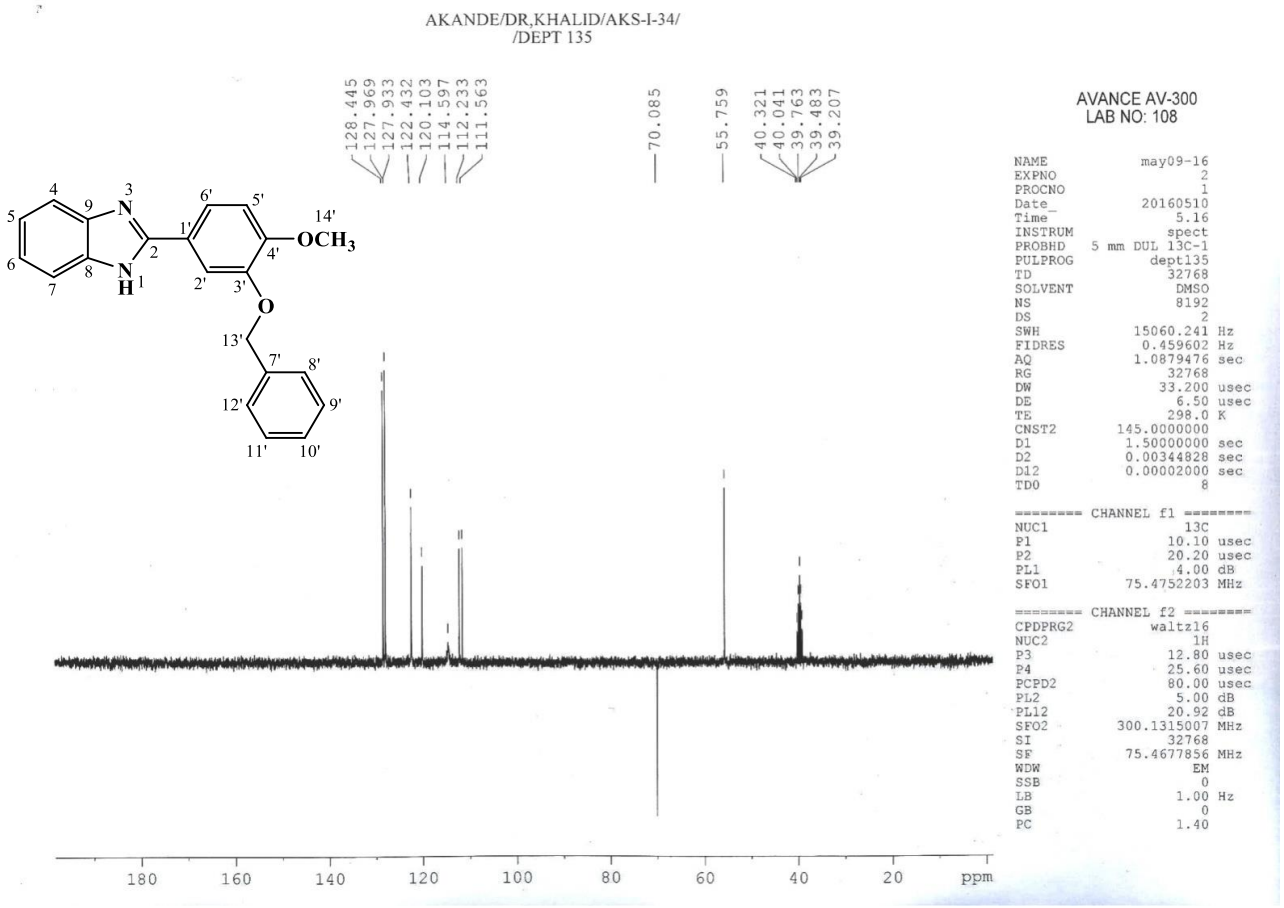

Figure 4.58. DEPTH-135 (75 MHz, DMSO-d_6) spectrum of AKS-I-34

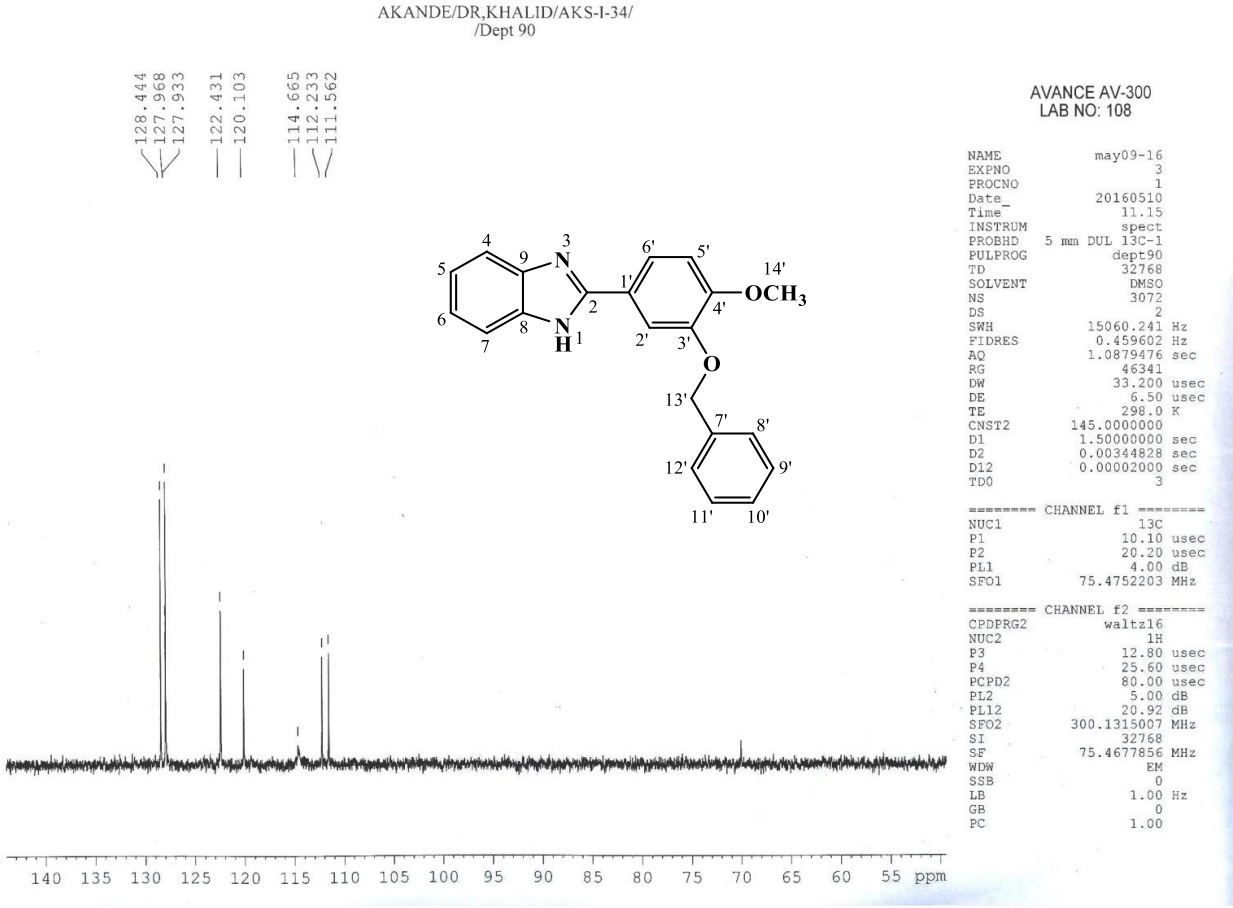

Figure 4.59. DEPTH-90 (75 MHz, DMSO-d_6) spectrum of AKS-I-34

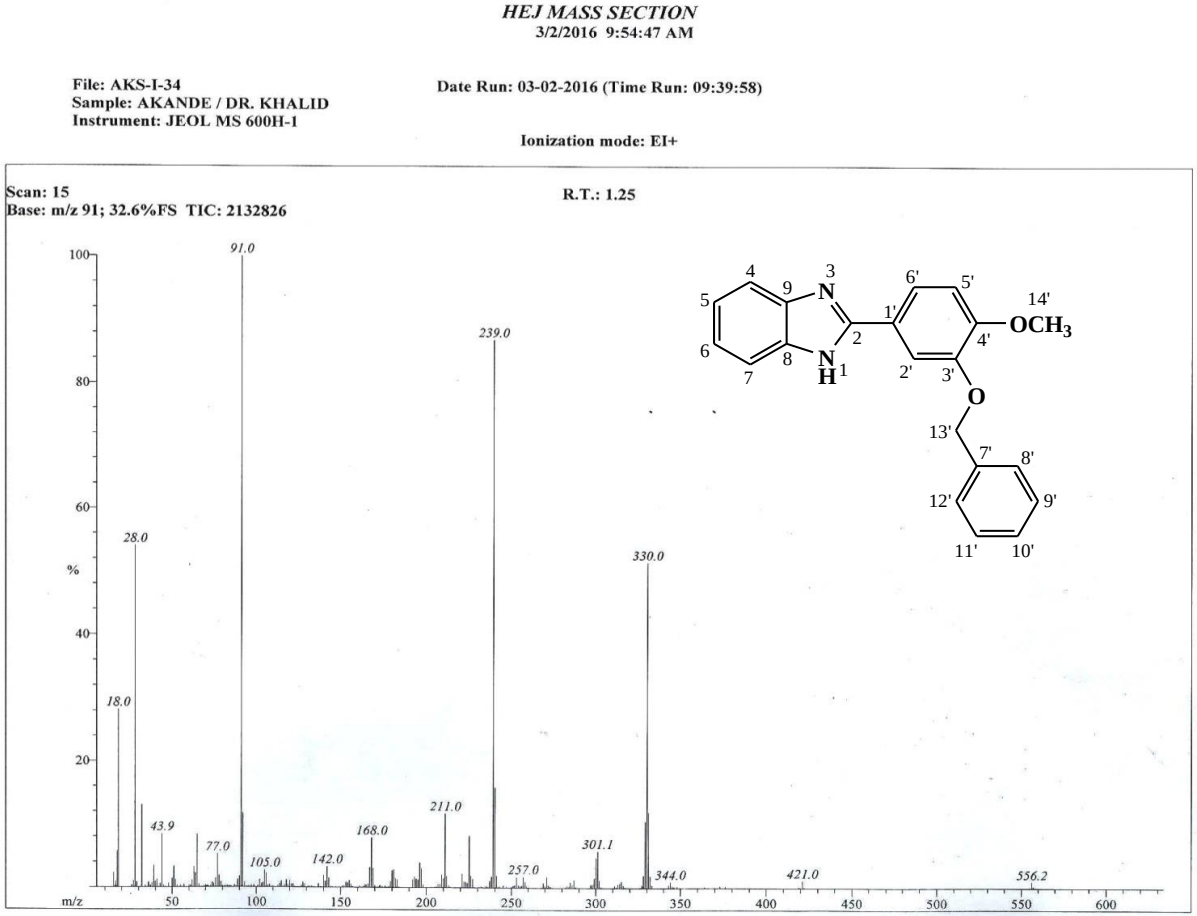

Figure 4.60. EI-MS spectrum of AKS-I-34

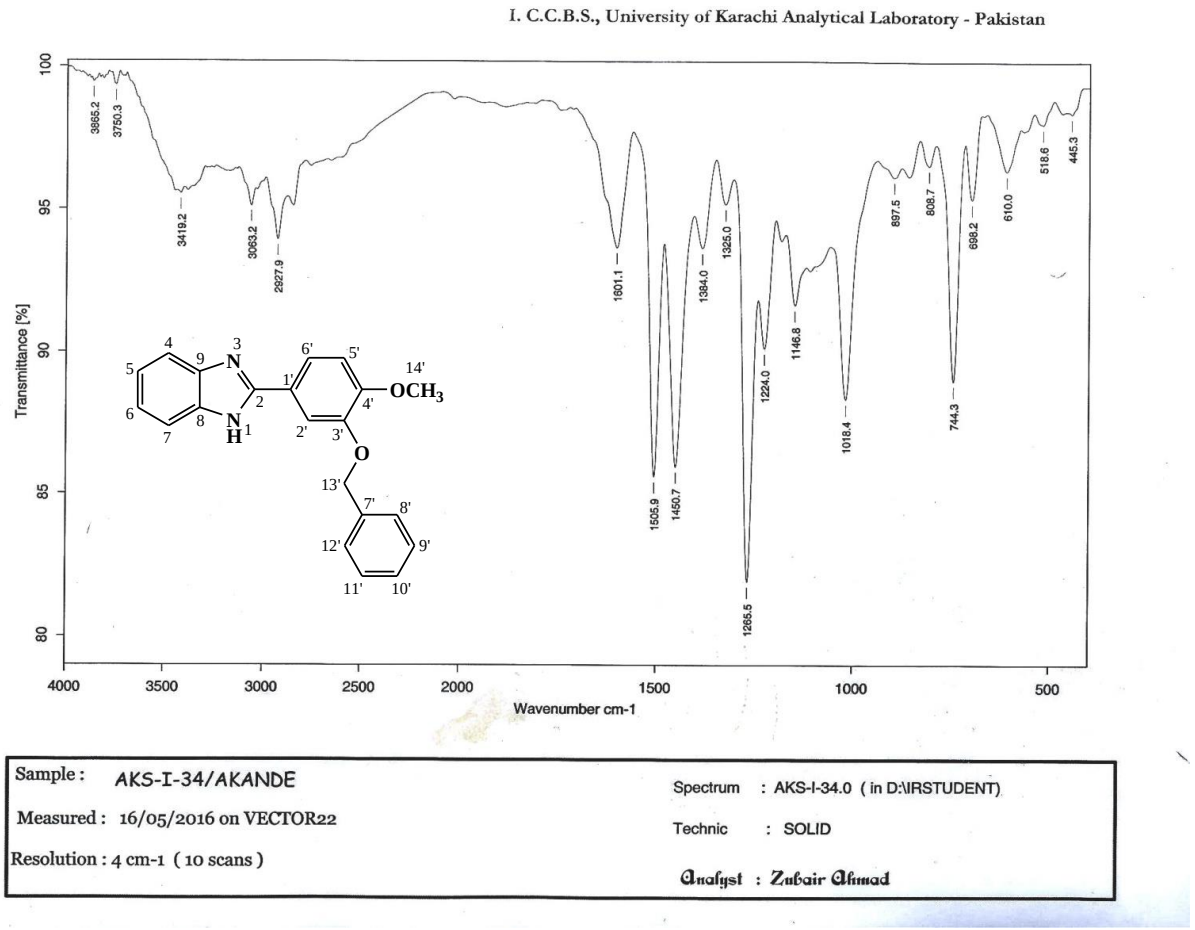

Figure 4.61. IR spectrum of AKS-I-34

THERMO ELECTRON ~ VISIONpro SOFTWARE V4.10

Operator Name	ARSHAD ALAM	Date of Report	5/20/2016
Department	Analytical laboratory#004 TWC	Time of Report	10:13:28AM
Organization	ICCBS.Karachi University.		
Information	Prof Dr. Khalid / Akande.		

Scan Graph

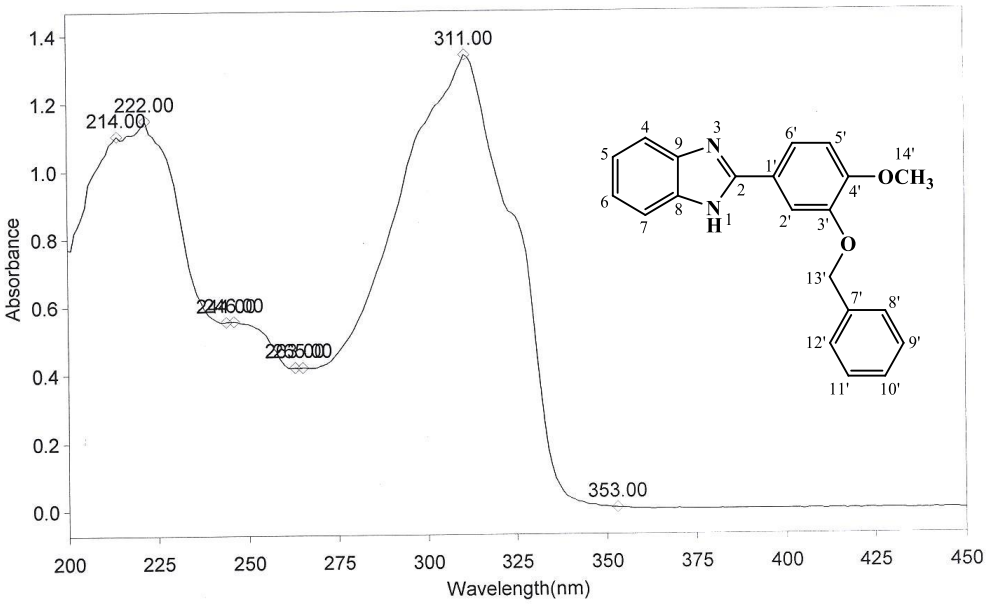

Results Table - AKS- I- 34.sre, AKS- I- 34,Cycle01

nm	A
214.00	1.105
222.00	1.151
244.00	0.554
246.00	0.556
263.00	0.419
265.00	0.420
311.00	1.339
353.00	0.005

Peak Pick Method

Find 8 Peaks Above -3.0000 A
Start Wavelength 200.00 nm
Stop Wavelength 450.00 nm
Sort By Wavelength
Sensitivity Very High

Page 1, Scan Graph

Figure 4.62. UV spectrum of AKS-I-34

Table 4.10. Summary of the ^{1}H NMR and ^{13}C NMR spectra of AKS-I-34

Position	δ ^{1}H [mult., J_{HH} (Hz)] (ppm)	δ ^{13}C (ppm)	DEPT-135	DEPT-90
1	-	-	-	-
2	-	151.08	-	-
3	-	-	-	-
4	7.60-7.58 [m]	114.57	CH	CH
5	7.23-7.21 [m]	122.43	CH	CH
6	7.23-7.21 [m]	122.43	CH	CH
7	7.60-7.58 [m]	114.57	CH	CH
8	-	148.00	-	-
9	-	148.00	-	-
1′	-	121.43	-	-
2′	7.89 [d, $J_{2',6'}$ = 1.6]	112.24	CH	CH
3′	-	150.98	-	-
4′	-	150.98	-	-
5′	7.20 [d, $J_{5',6'}$ = 8.4]	111.58	CH	CH
6′	7.78 [d, $J_{6',5'}$ = 8.4]	120.11	CH	CH
7′	-	136.77	-	-
8′	7.51 [d, $J_{8',9'}$ = 7.2]	127.92	CH	CH
9′	7.43 [t, $J_{9',10'}$ = 7. 6]	128.44	CH	CH
10′	7.36 [t, $J_{10',11'} = J_{10',9'}$ = 7.6]	127.96	CH	CH
11′	7.43 [t, $J_{11',10'}$ = 7. 6]	128.44	CH	CH
12′	7.51 [d, $J_{12',11'}$ = 7.2]	127.92	CH	CH
13′-OCH_2-	5.19 [s]	70.09	CH_2	-
14′-OCH_3	3.85 [s]	55.76	OCH_3	-

4.1.11 Characterisation of 2-(3′-(benzyloxy)-4′-methoxyphenyl)-5-fluoro-1*H*benzo[*d*]imidazole (AKS-I-35)

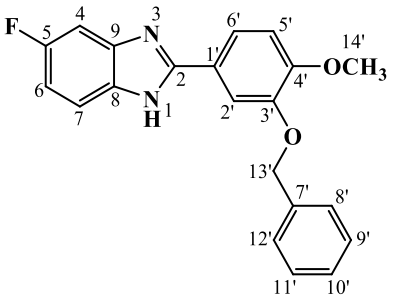

2-(3′-(Benzyloxy)-4′-methoxyphenyl)-5-fluoro-1*H*-benzo[*d*]imidazole (AKS-I-35) was obtained as a brown solid, 0.317 g (91.0% yield), m.pt. 176-178 ^{o}C and a R_f of 0.51 (hexane/ethyl acetate, 1:1).

From the ^{1}H NMR analysis (400 MHz, DMSO-d_6) represented in figures **4.63** and **4.64**, 10 proton resonances, δ (ppm) were assigned to the methine protons as 7.87 (1H, d, $J_{2',6'}$ = 1.6 Hz, H-2′), 7.77 (1H, dd, $J_{6',5'}$ = 8.4 Hz, H-6′), a multiplet peak at 7.56-7.60 (1H, m, H-4), resulting from the influence of a fluorine atom, 7.51 (2H, d, $J_{8',9'} = J_{12',11'}$ = 7.2 Hz, H-8′, H-12′), 7.43 (2H, t, $J_{11',10'} = J_{9',10'}$ = 7.2 Hz, H-11′, H-9′), 7.41 (1H, d, $J_{7,6}$ = 7.6 Hz, H-7), 7.36 (1H, t, $J_{10',9'} = J_{10',11'}$ = 7.2 Hz, H-10′), 7.20 (1H, d, $J_{5',6'}$ = 8.8 Hz, H-5′) and a doublet of tripplet peak also due to a proton coupling with a fluorine atom at 7.10 (1H, dt, $J_{6,F\text{-}5}$ = 8.4 Hz, $J_{6,4}$ = 2.0 Hz, H-6). The methylene and the methoxy protons appear as singlets at δ 5.18 (s, 2H, 13′-OCH_2-) and δ 3.85 (s, 3H, 14′-OCH_3) respectively. The amine proton peak, expected further downfield, was not captured.

Chemical shift, δ (ppm) values from ^{13}C NMR spectra (75 MHz, DMSO-d_6) (figures **4.65** and **4.66**) show 20 resonances assigned to carbon atoms as 160.30 (C-5), 157.17 (C-2), 152.29 (C-3′), 151.29 (C-4′), 148.00 (C-9, C-8), 136.71 (C-7′), 121.02 (C-1′) representing eight quarternary carbons, 128.38 (C-11′, C-9′′), 127.90 (C-10′), 127.83 (C-12′, C-8′), 120.21 (C-6′, C-7), 115.12 (C-7), 112.30 (C-2′), 111.72 (C-5′), 110.61, 101.06 (C-6), 110.27, 100.68 (C-4) representing eleven methine carbons, 70.14 (C-13′) representing the methylene carbon and 55.76 (C-14′) representing the methoxy carbon. From DEPTH-135 (75 MHz, DMSO-d_6) experiment, the spectrum (figures **4.67**) confirms the respective methine and methoxy carbons in the positive phase as well as the methylene carbon in the negative phase, while DEPTH-90 (75 MHz, DMSO-d_6) spectrum (figures **4.68**) harmonizes the respective methine carbon peaks.

The EI-MS spectrum (figure **4.69**) shows the molecular ion, M^+ and $[M^+{+}1]$ peaks with *m/z* of 348 and 349 respectively. The observed prominent base peak at *m/z* 91 $[C_7H_7]^+$ is a tropylium ion generated by a α-cleavage of the ether (O–CH_2) functional group corresponding to $[M\text{-}257]^+$. Elimination of HC≡CH molecule from the base peak gave the *m/z* 65 fragment. Peak at *m/z* 257 is due to $[M\text{-}C_7H_7]^+$. The *m/z* of 227 was generated by the fragmentation, $[M\text{-}257\text{-}30]^+$ corresponding to $[C_{14}H_{10}FN_2O_2]^+$ while that at *m/z* 186 corresponds to the fragment, $[C_{11}H_7FN_2]^+$. The *m/z* 18 is a characteristic water peak. The *m/z* obtained from HREI-MS analysis which coincides with the molecular formular $C_{21}H_{17}FN_2O_2$, was at 348.1286 (calculated 348.1274), further confirming the compound.

The IR absorption spectrum in figure **4.70** shows vibrational bands from which some are assignable to bonds such as N–H_{str} of secondary amine, aromatic C–H_{str}, aliphatic C–$H_{asy\ str}$ and C–$H_{sym\ str}$, C=N_{str}, two aromatic C=C_{str}, aliphatic C–H_b, C–O–$C_{asy\ str}$ and C–O–$C_{sym\ str}$ of ether, and C–F_{str} corresponding to vibrational frequencies, $\bar{\upsilon}$ (cm^{-1}) 3418, ≈3050, 2924, 2853, 1631, 1600, 1508, 1447, 1267, 1025 and 1145 respectively.

The wavelenght of maximum absorptions (λ_{max}) from UV spectrum (figure **4.71**) are at 311, 250 and 222 nm indicative of n→π* and π→π* transitions. Table **4.11** shows the summary of ^{1}H NMR and ^{13}C NMR spectra.

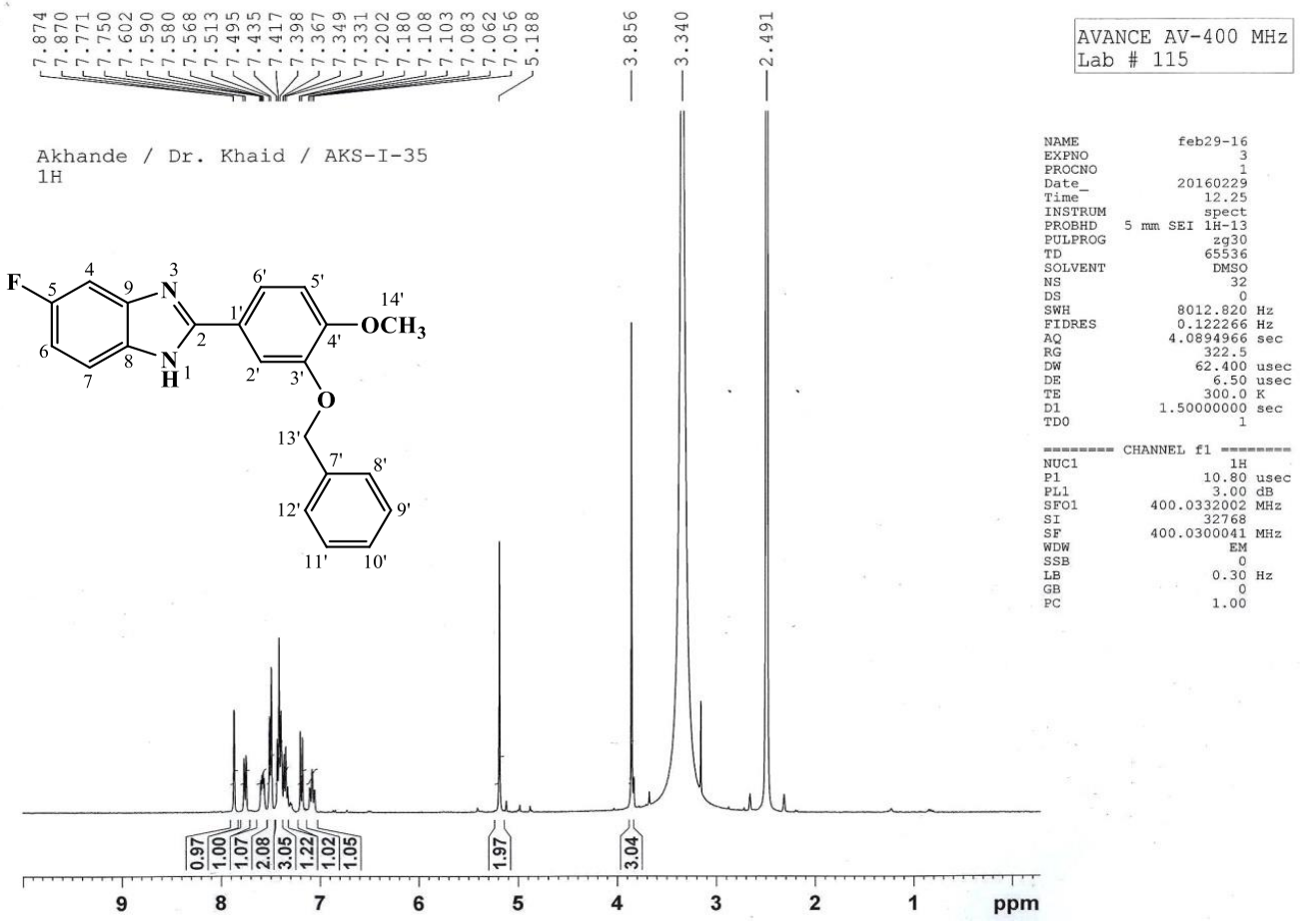

Figure 4.63. ^{1}H NMR (400 MHz, DMSO-d_6) spectrum of AKS-I-35

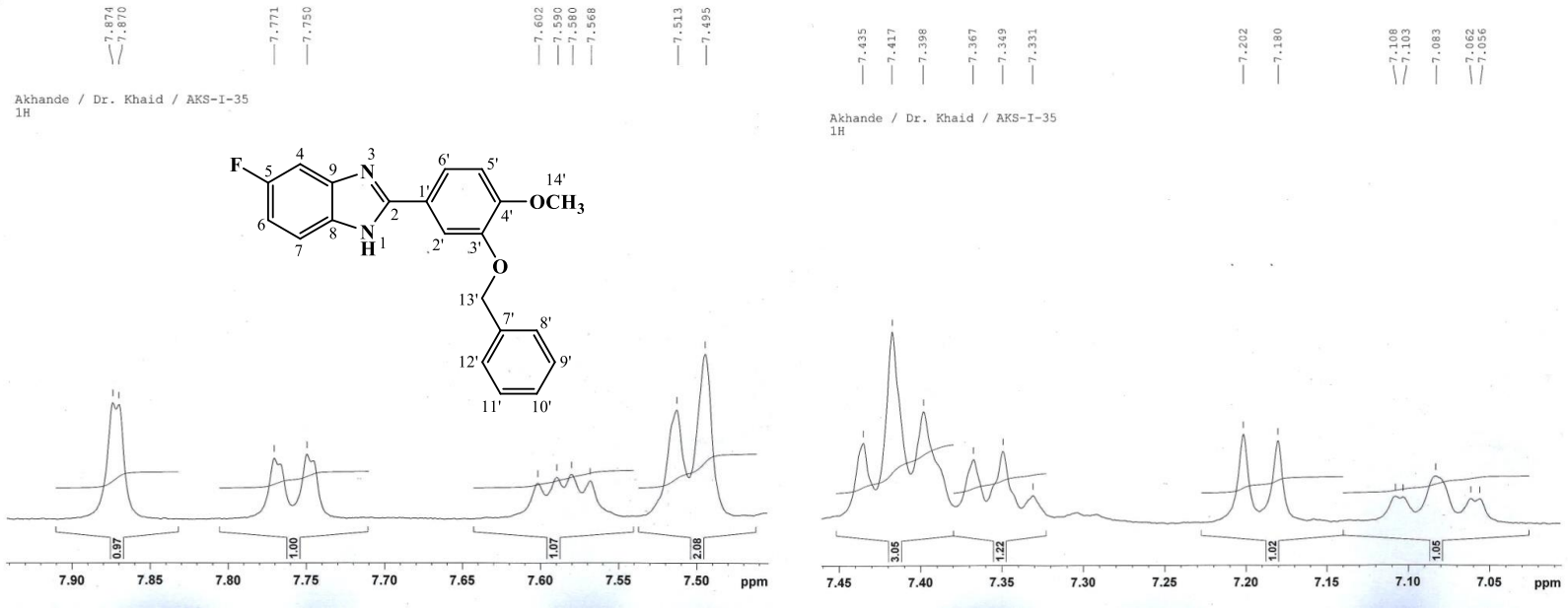

Figure 4.64. ^{1}H NMR (400 MHz, DMSO-d_6) spectra of AKS-I-35 aromatic region (Expanded)

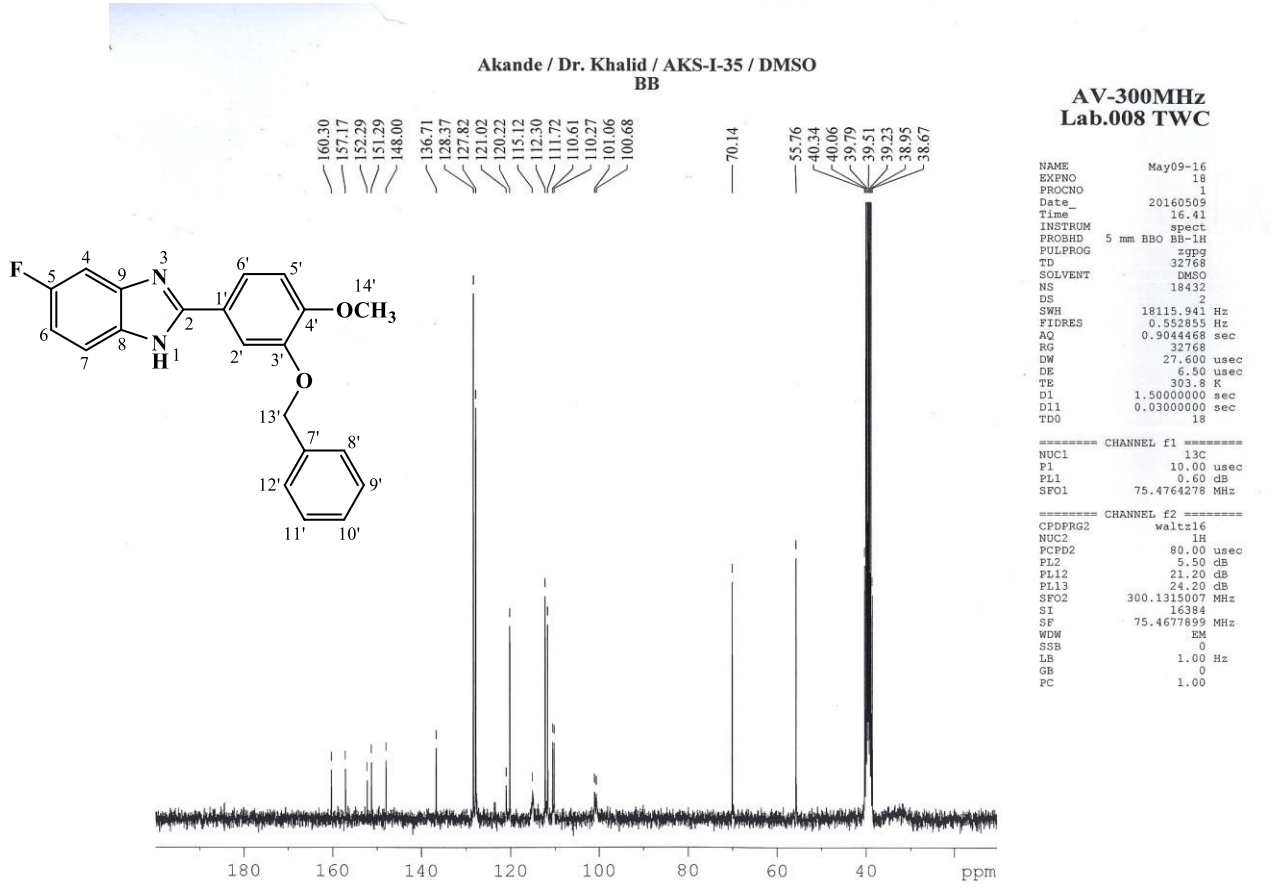

Figure 4.65. ^{13}C NMR (75 MHz, DMSO-d_6) spectrum of AKS-I-35

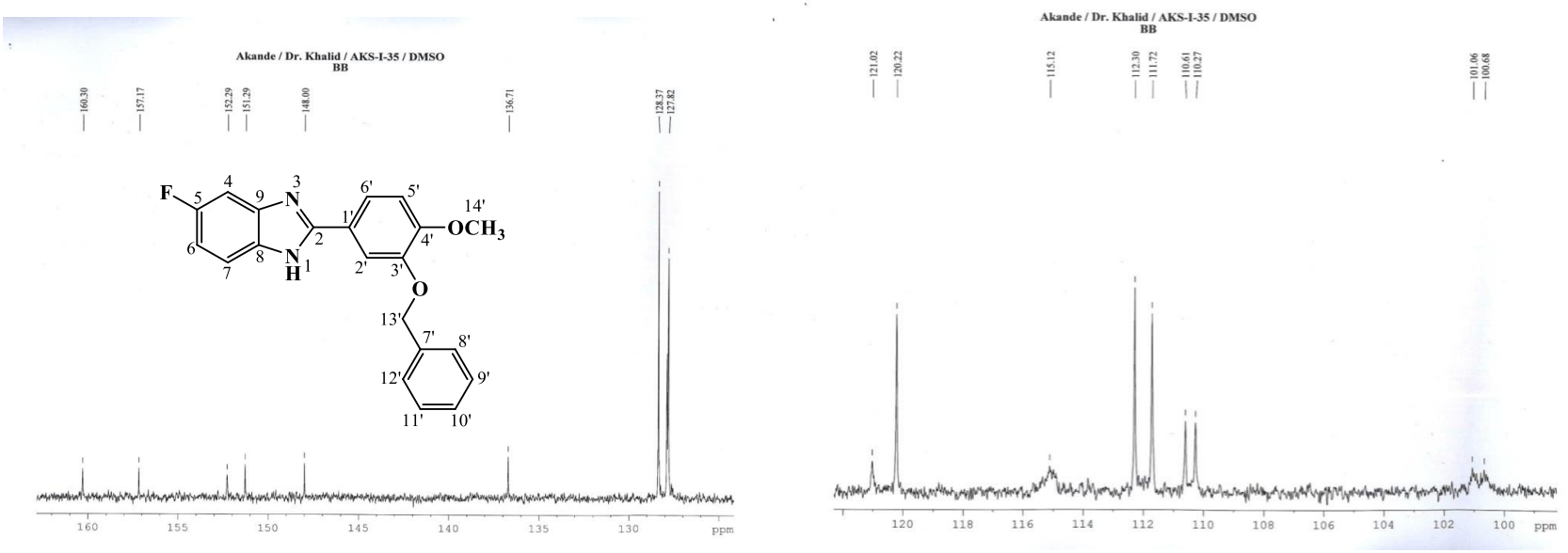

Figure 4.66. ^{13}C NMR (75 MHz, DMSO-d_6) spectra of AKS-I-35 (Expanded)

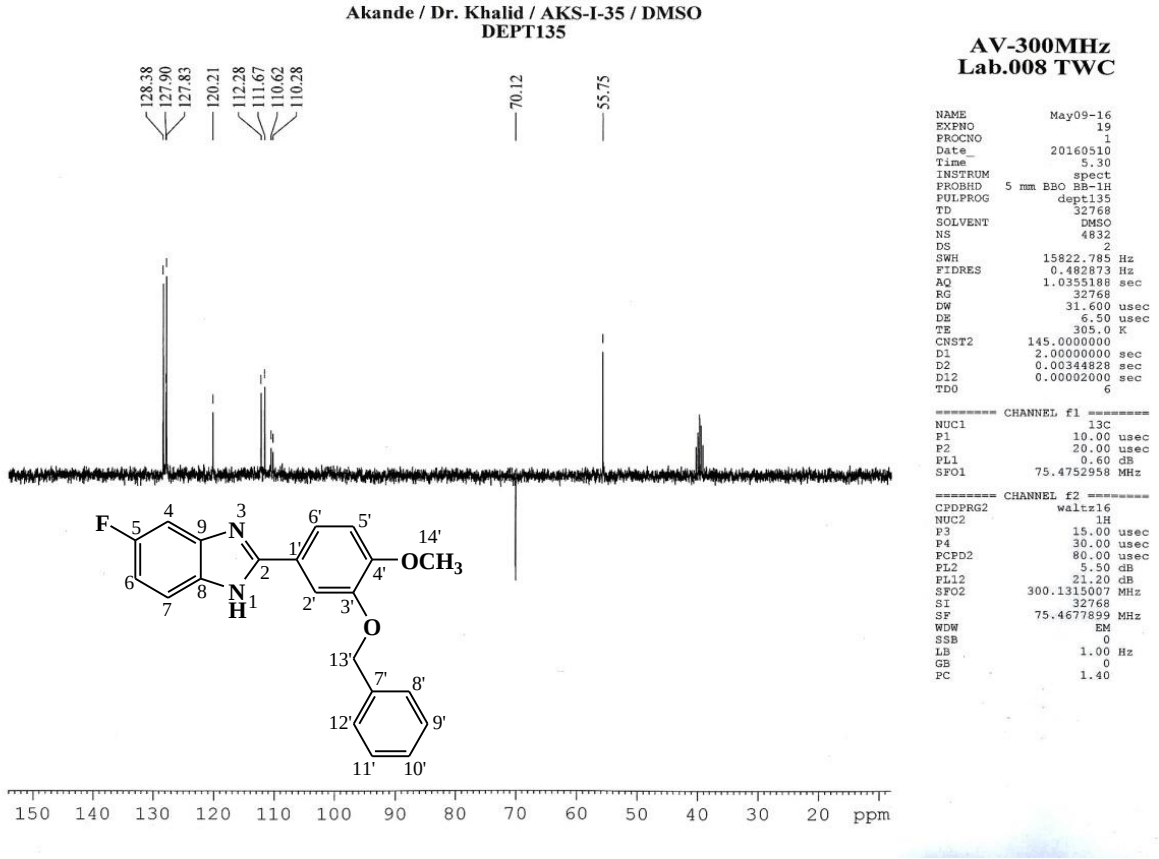

Figure 4.67. DEPTH-135 (75 MHz, DMSO-d_6) spectrum of AKS-I-35

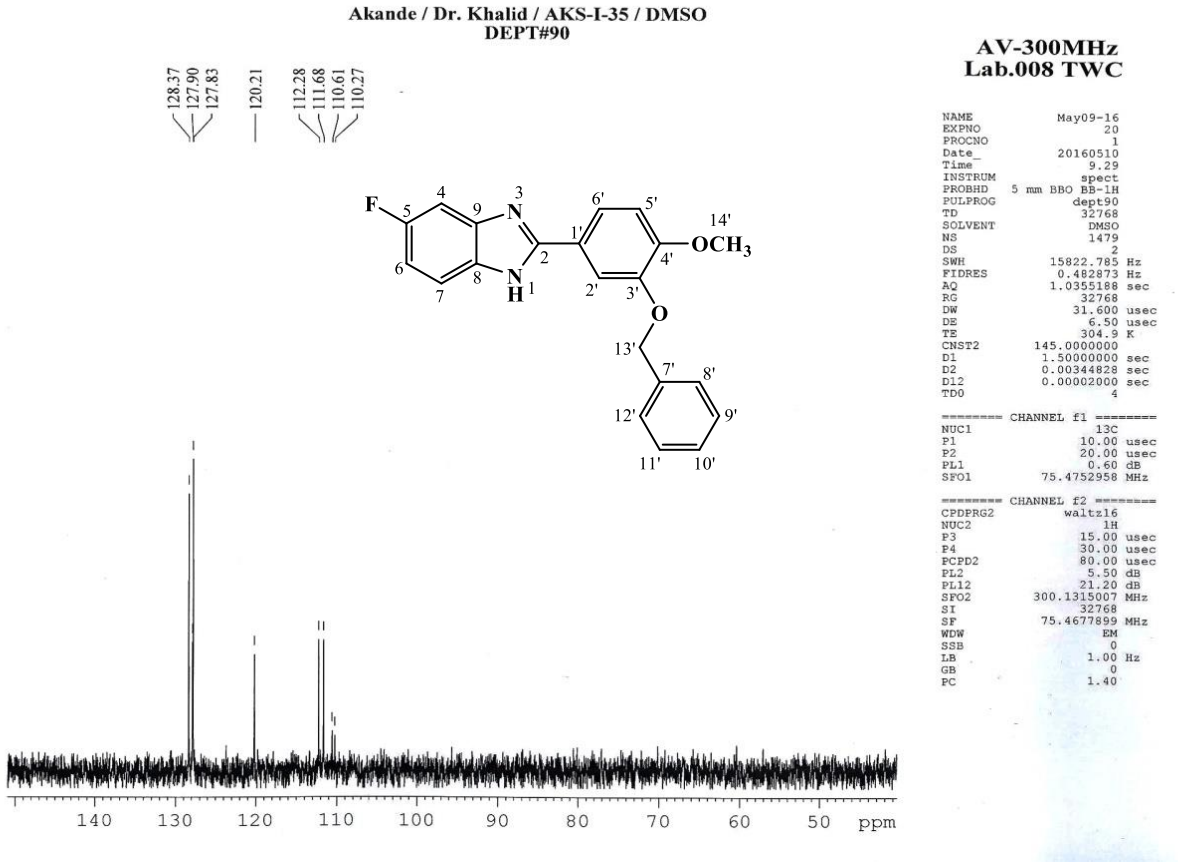

Figure 4.68. DEPTH-90 (75 MHz, DMSO-d_6) spectrum of AKS-I-35

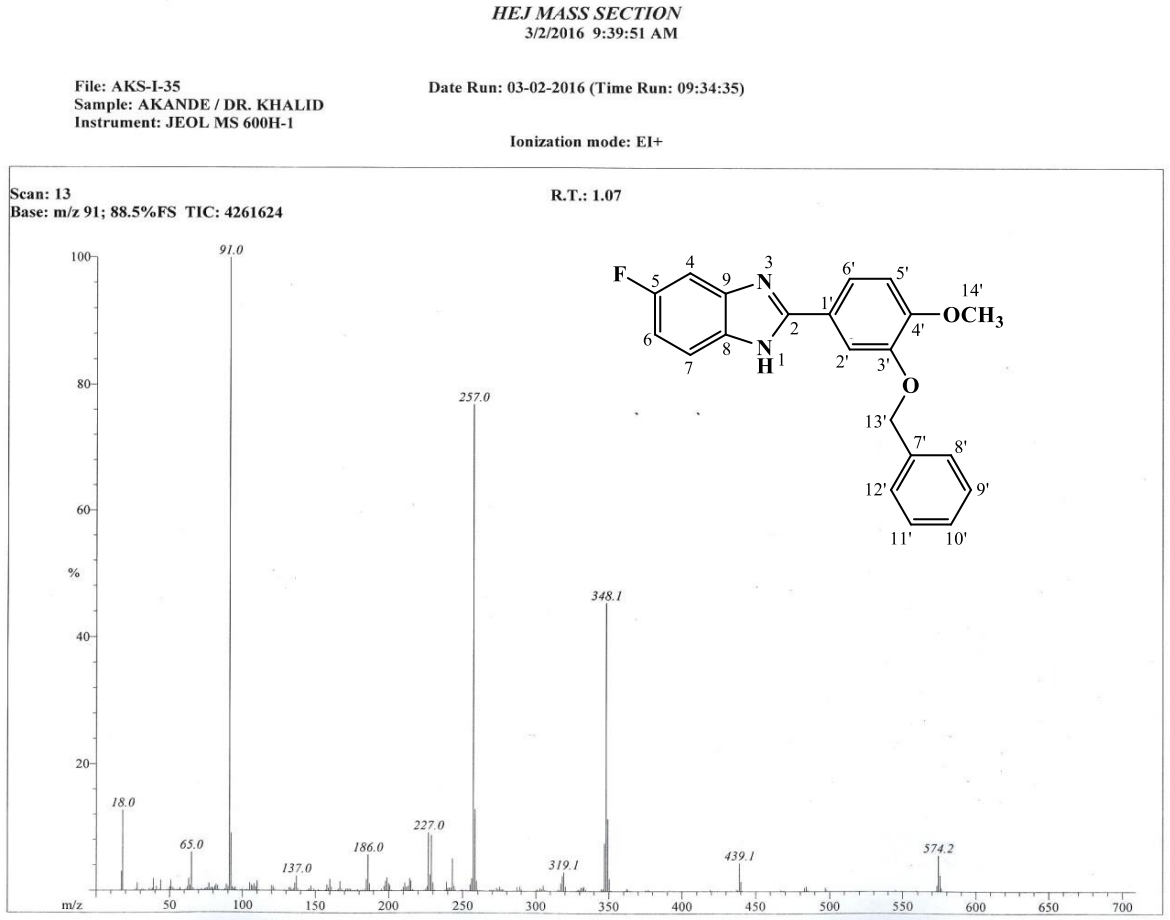

Figure 4.69. EI-MS spectrum of AKS-I-35

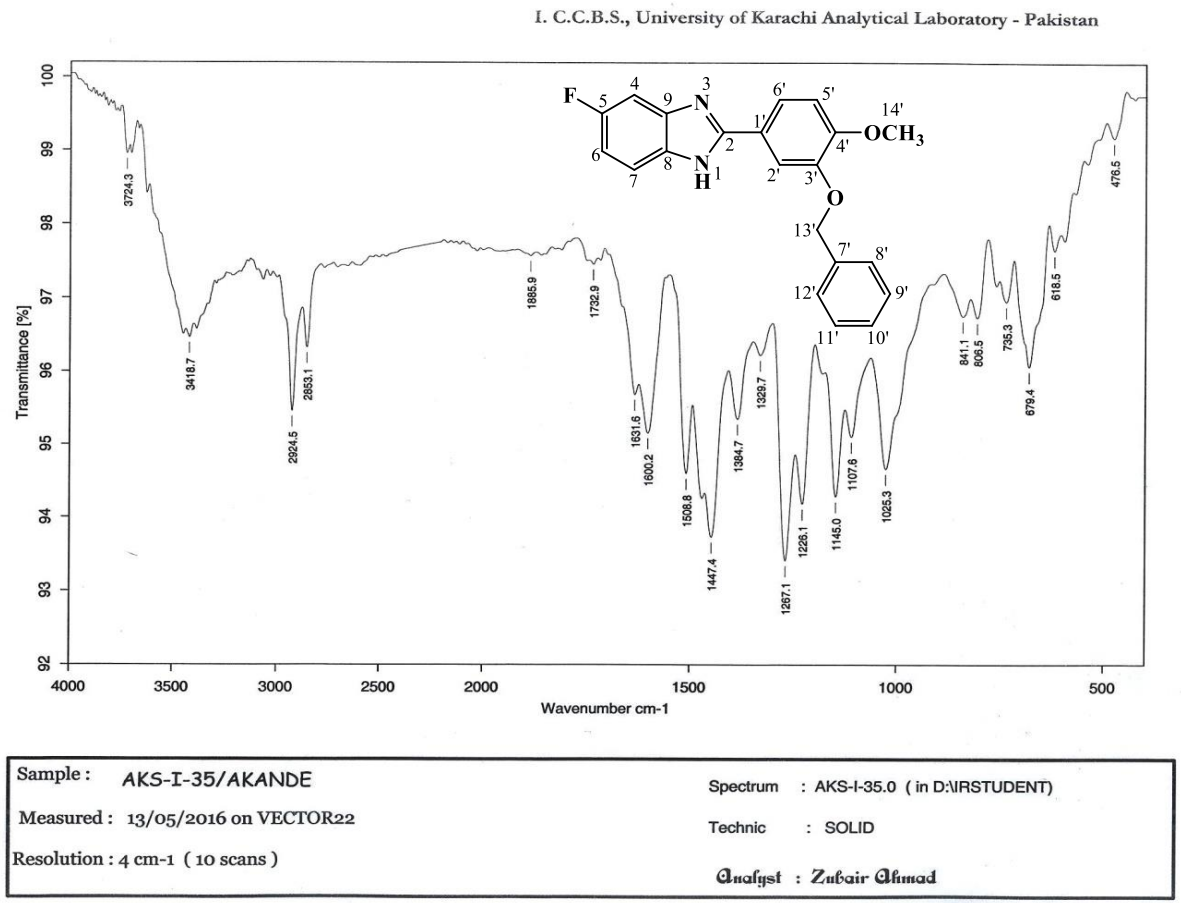

Figure 4.70. IR spectrum of AKS-I-35

THERMO ELECTRON ~ VISIONpro SOFTWARE V4.10

Operator Name	ARSHAD ALAM	Date of Report	5/16/2016
Department	Analytical laboratory#004 TWC	Time of Report	10:05:36AM
Organization	ICCBS.Karachi University.		
Information	Prof Dr. Khalid / Akande.		

Scan Graph

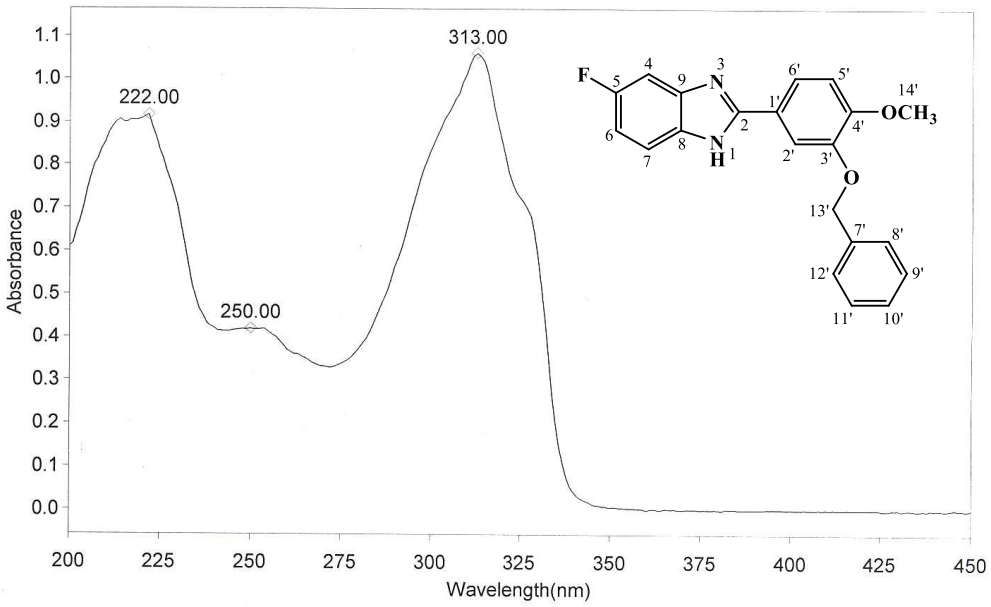

Results Table - AKS- I- 35.sre, AKS- I- 35,Cycle01

nm	A	**Peak Pick Method**
222.00	0.917	Find 8 Peaks Above -3.0000 A
250.00	0.419	Start Wavelength 200.00 nm
313.00	1.061	Stop Wavelength 450.00 nm
		Sort By Wavelength
Sensitivity	Medium	

Page 1, Scan Graph

Figure 4.71. UV spectrum of AKS-I-35

Table 4.11. Summary of the ^{1}H NMR and ^{13}C NMR spectra of AKS-I-35

Position	δ ^{1}H [mult., J_{HH} (Hz)] (ppm)	δ ^{13}C (ppm)	DEPT-135	DEPT-90
1	-	-	-	-
2	-	157.17	-	-
3	-	-	-	-
4	7.60-7.56 [m]	110.27, 100.68	CH	CH
5	-	160.30	-	-
6	7.10 [dt, $J_{6,F-5}$ = 8.4, $J_{6,4}$ = 2.0]	110.61, 101.06	CH	CH
7	7.41 [d, $J_{7,6}$ = 7.6]	120.22, 115.12	CH	CH
8	-	148.00	-	-
9	-	148.00	-	-
1′	-	121.02	-	-
2′	7.87 [d, $J_{2',6'}$ = 1.6]	112.30	CH	CH
3′	-	152.29	-	-
4′	-	151.29	-	-
5′	7.20 [d, $J_{5',6'}$ = 8.8]	111.72	CH	CH
6′	7.77 [dd, $J_{6',5'}$ = 8.4]	120.22	CH	CH
7′	-	136.71	-	-
8′	7.51 [d, $J_{8',9'}$ = 7.2]	127.83	CH	CH
9′	7.43 [t, $J_{9',8'}$ = 7.2]	128.38	CH	CH
10′	7.36 [t, $J_{10',11'}$ = $J_{10',9'}$ = 7.2]	127.90	CH	CH
11′	7.43 [t, $J_{11',12'}$ = 7.2]	128.38	CH	CH
12′	7.51 [d, $J_{12',11'}$ = 7.2]	127.83	CH	CH
13′-OCH_2-	5.18 [s]	70.12	CH_2	-
14′-OCH_3	3.85 [s]	55.75	OCH_3	-

4.1.12 Characterisation of 2-(3′-(benzyloxy)-4′-methoxyphenyl)-5-chloro-1*H*-benzo[*d*]imidazole (AKS-I-36)

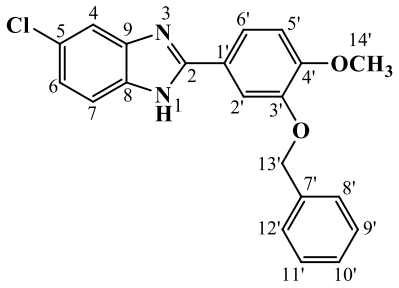

The compound AKS-I-36 is a brown solid with a yield of 94.0% (0.343 g), m.pt. 112-114 ^{o}C and a R_f of 0.55 (hexane/ethyl acetate, 1:1).

Eleven resonance peaks were obtained on the ^{1}H NMR spectra (400 MHz, DMSO-d_6) (figure **4.72** and **4.73**) with δ (ppm) values assigned as 7.87 (1H, d, $J_{2',6'}$ = 1.6 Hz, H-2′), 7.77 (1H, dd, $J_{6',5'}$ = 8.4 Hz, $J_{6',2'}$ = 1.6 Hz, H-6′), 7.62 (1H, s, H-4), 7.59 (1H, d, $J_{7,6}$ = 8.4 Hz, H-7), 7.51 (2H, d, $J_{12',11'} = J_{8',9'}$ = 7.2 Hz, H-12′, H-8′), 7.43 (2H, t, $J_{9',8'} = J_{11',12'}$ = 7.2 Hz, H-9′, H-11′), 7.36 (1H, t, $J_{10',11'} = J_{10',9'}$ = 7.2 Hz, H-10′), 7.24 (1H, dd, $J_{6,4}$ = 1.6 Hz, $J_{6,7}$ = 8.4 Hz, H-6), 7.19 (1H, d, $J_{5',6'}$ = 8.4 Hz, H-5′) to the aromatic methine protons, 5.18 (2H, s, 13′-OCH_2-) to the methylene protons and 3.85 (3H, s, 14′-OCH_3) to the methoxy protons. Protons at positions 6 and 7 (J = 8.4 Hz) as well as protons at positions8′, 9′, 10′, 11′ and 12′ (J = 7.2 Hz) all shows ortho couplings. The amine proton was not captured.

Broad band ^{13}C NMR (75 MHz, DMSO-d_6) spectrum (figure **4.74**) and its expansion (figure **4.75**) established fifteen resonance peaks, δ (ppm), assigned as 152.50 (C-2), 151.23 (C-4′, C-3′), 148.00 (C-9, C-8), 136.75 (C-7′), 126.52 (C-5), 121.29 (C-1′) to eight quarternary carbons, 128.43 (C-11′, C-9′′), 127.96 (C-10′), 127.92 (C-12′, C-8′), 122.46 (C-6), 120.24 (C-6′), 112.22 (C-7, C-4), 111.60 (C-5′, C-2′) to eleven methine carbons, 70.08 (C-13′) to one methylene carbon, and 55.75 (C-14′) to one methoxy carbon. DEPTH-135 (75 MHz, DMSO-d_6) and DEPTH-90 (75 MHz, DMSO-d_6) experiments (figures **4.76** and **4.77** respectively) further harmonize the methine and methoxy carbon peaks expressed on the positive quadrant, and the methylene carbon peaks expressed on the negative quadrant.

The EI-MS spectrum in figure **4.78** shows the molecular ion, [M^+] peak with a *m/z* of 364, an isotope peak, [M^++2] due to the presence chlorine atom with *m/z* 366, and many prominent fragment ion peaks which include the peaks at *m/z* 273, 245 and 91. A α-

leavage on the M^+ at O–CH_2 (ether) bond resulted in *m/z* of 273 $[C_{14}H_{10}ClN_2O_2]^+$ and *m/z* 91 $[C_7H_7]^+$ corresponding to M^+-91 and M^+-273 respectively. A resulting $[M^+ + 2]$-$CH_3O^{\cdot}$ cleavage is suggestive of the fragment ion at *m/z* 335 which on further disintegration gave a peak with *m/z* of 245 by losing $[C_7H_7]^{\cdot}$ radical. A further loss of $CH_2{=}C{=}O^{\cdot}$ radical from the fragment with *m/z* 245 led to the peak with *m/z* of 202 $[C_{11}H_7ClN_2]^+$. The *m/z* of 65 is a frequently observed peak due to $[C_5H_5]^+$ fragment. The observed *m/z* of 364.0983 (calculated 364.0979) obtained from HREI-MS, matches the molecular formula, $C_{21}H_{17}ClN_2O_2$ $[M^+]$, thus further comfirming the compound.

The vibrational bands (figure **4.79**) of characteristic IR active bonds, absorb vibrational frequencies, $\bar{\upsilon}$ (cm^{-1}) assigned as 3418, 3067, 2929, 1603, 1502, 1452, 1267, 1019, 1058 cm^{-1} to N–H_{str} of 2º amine, aromatic C–H_{str}, aliphatic C–$H_{asy\ str}$, two aromatic C=C_{str}, C–H_b of CH_3/CH_2, C–O–$C_{asy\ str}$ and C–O–$C_{sym\ str}$ of ether, and C–Cl_{str} respectively. Figure **4.80** is the UV spectrum indicative of n→π* and π→π* transitions with absorption maxima (λ_{max}) at 316, 226 and 222 nm. Summary of the ^1H NMR and ^{13}C NMR spectra is shown in table **4.12**.

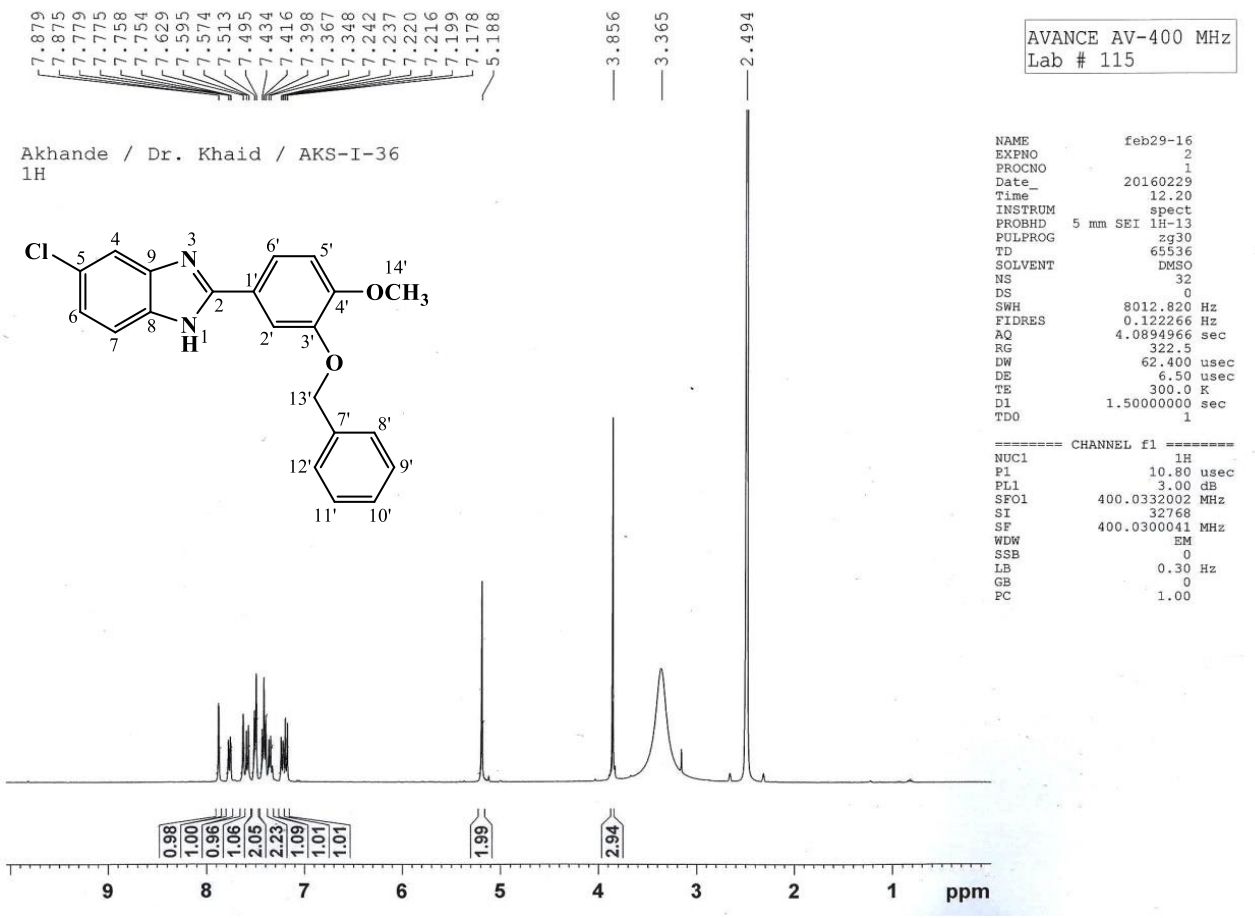

Figure 4.72. ^{1}H NMR (400 MHz, DMSO-d_6) spectrum of AKS-I-36

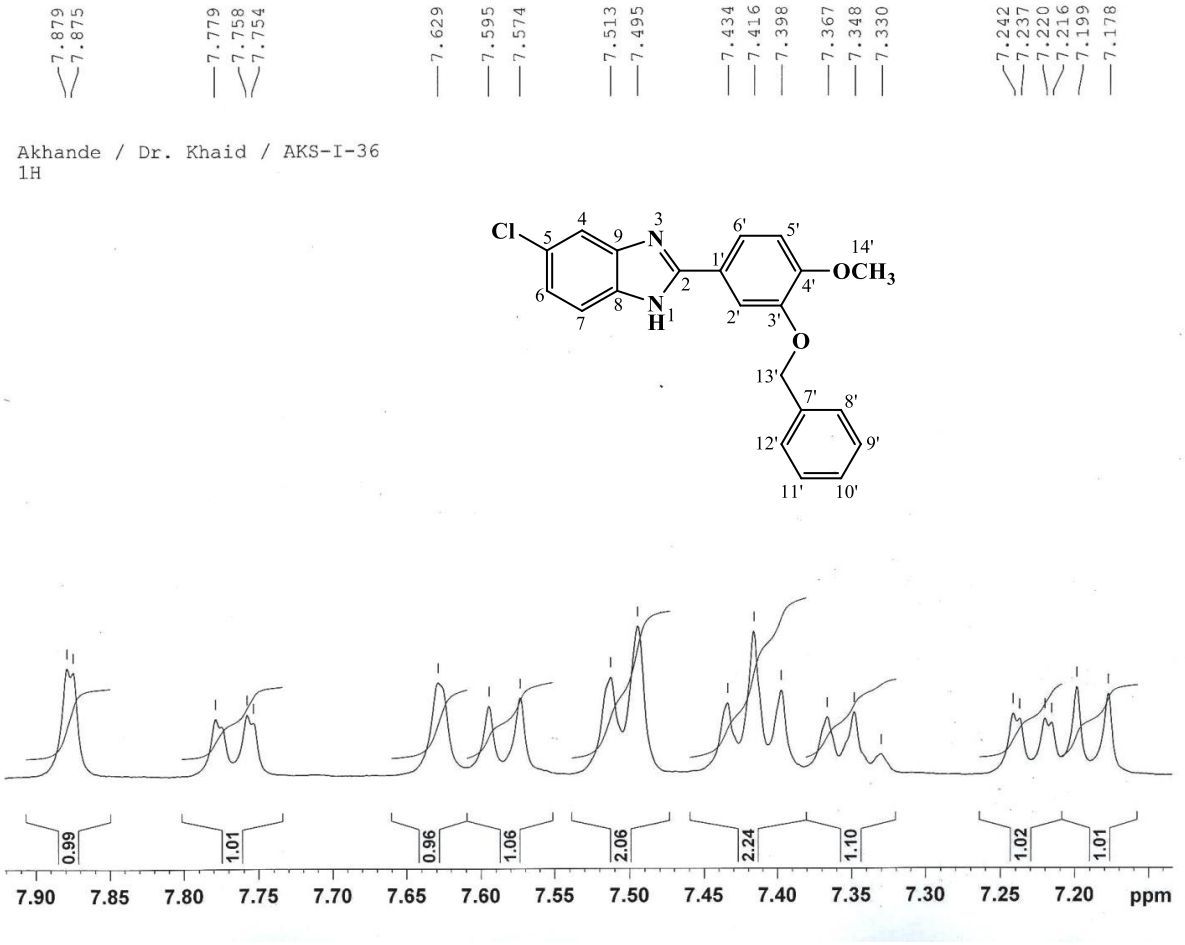

Figure 4.73. ^{1}H NMR (400 MHz, DMSO-d_6) spectrum of AKS-I-36 aromatic region (Expanded)

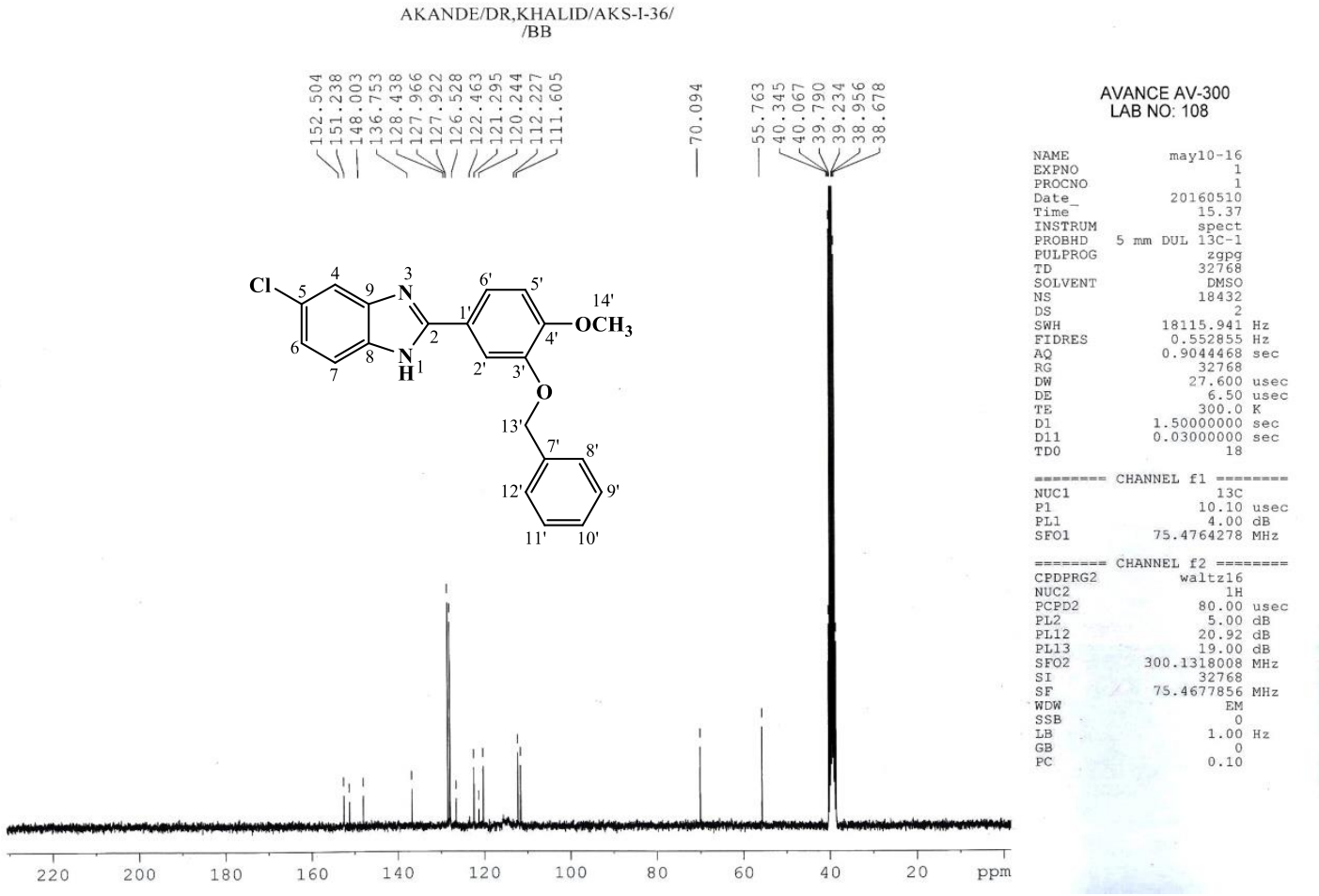

Figure 4.74. ^{13}C NMR (75 MHz, DMSO-d_6) spectrum of AKS-I-36

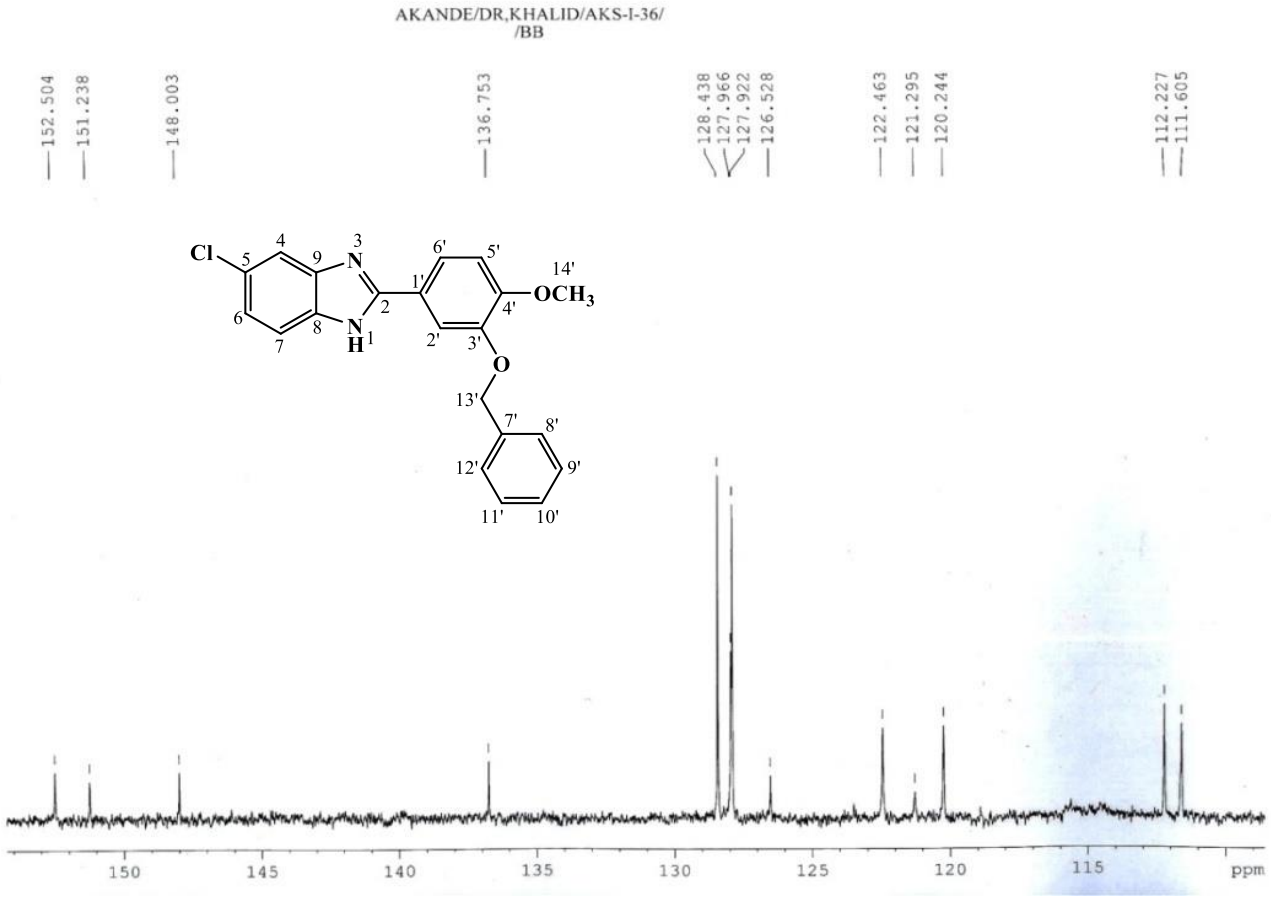

Figure 4.75. ^{13}C NMR (75 MHz, DMSO-d_6) spectrum of AKS-I-36 (Expanded)

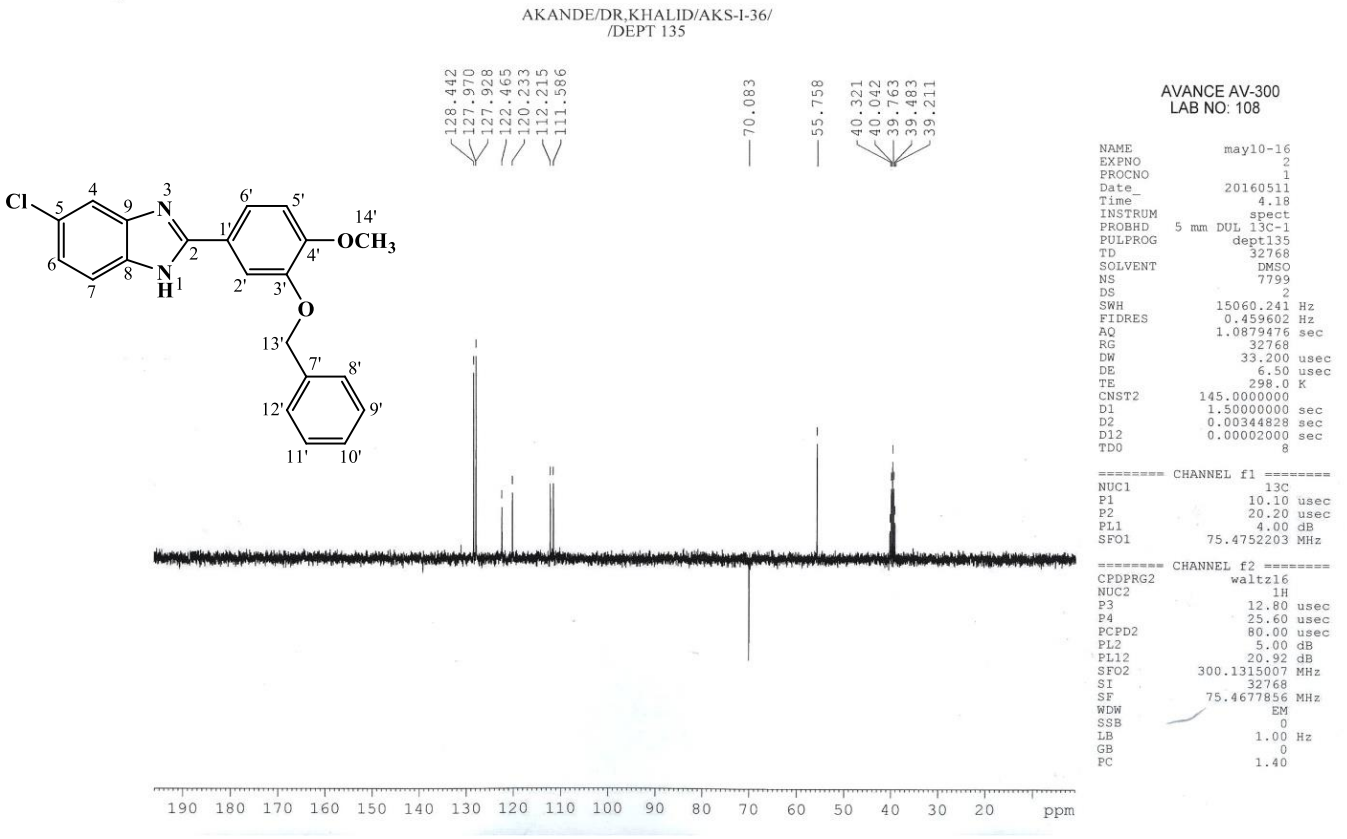

Figure 4.76. DEPTH-135 (75 MHz, DMSO-d_6) spectrum of AKS-I-36

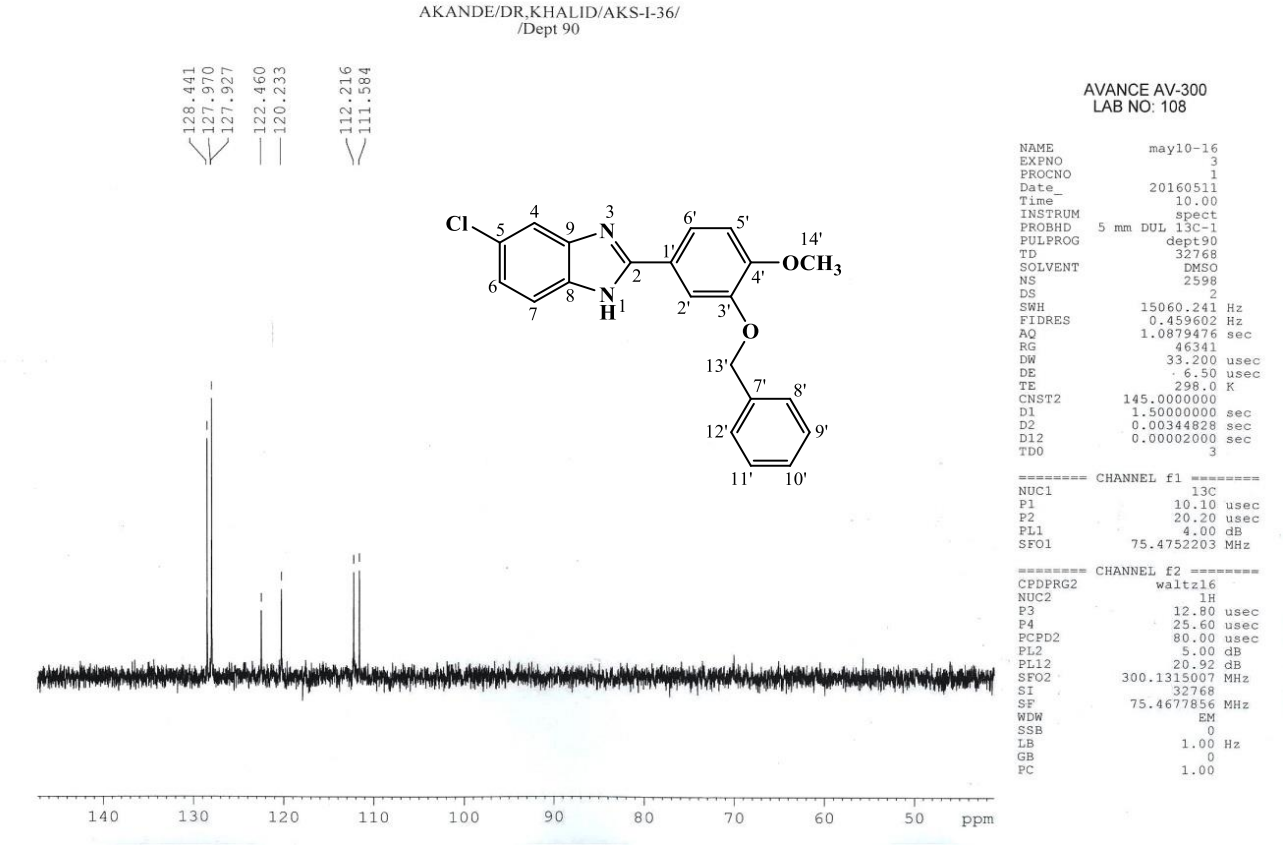

Figure 4.77. DEPTH-90 (75 MHz, DMSO-d_6) spectrum of AKS-I-36

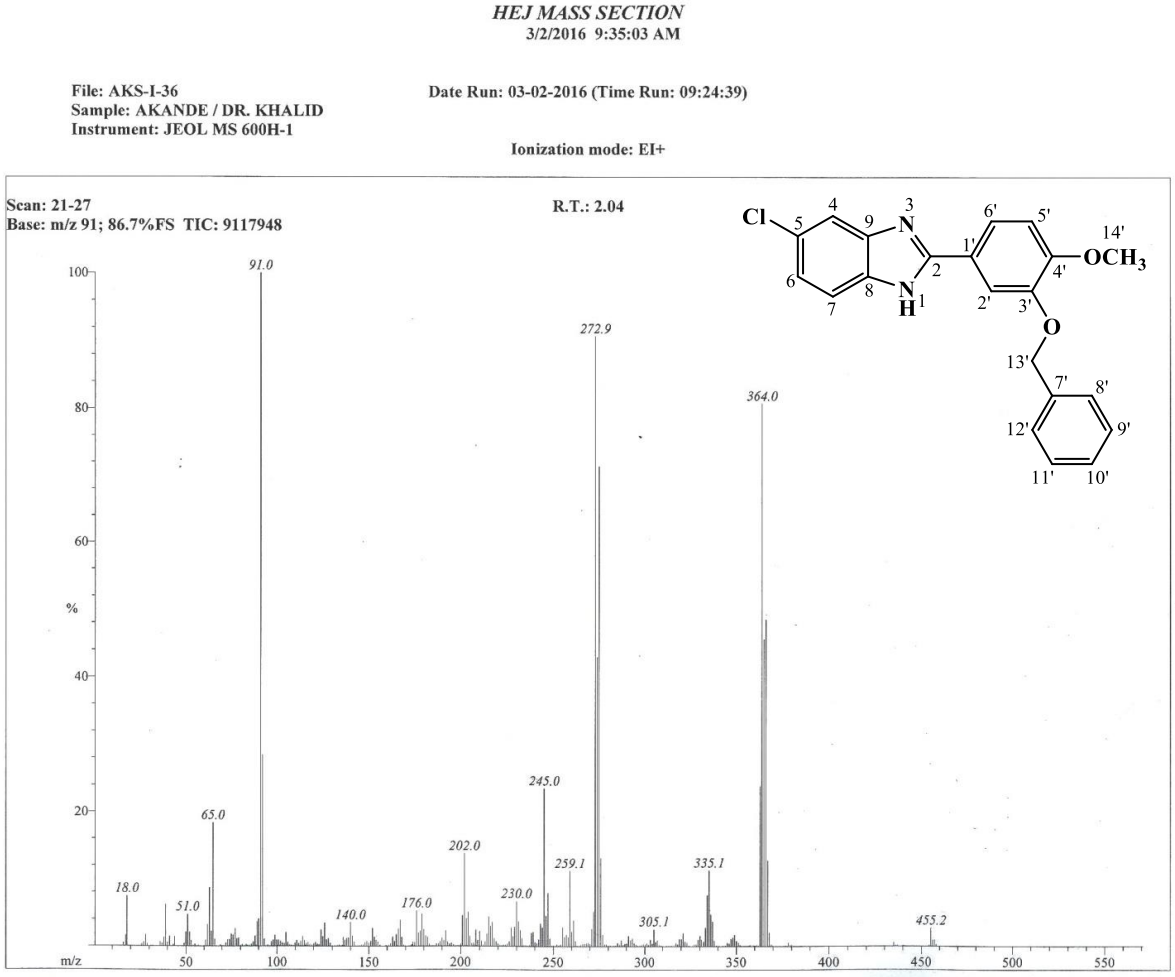

Figure 4.78. EI-MS spectrum of AKS-I-36

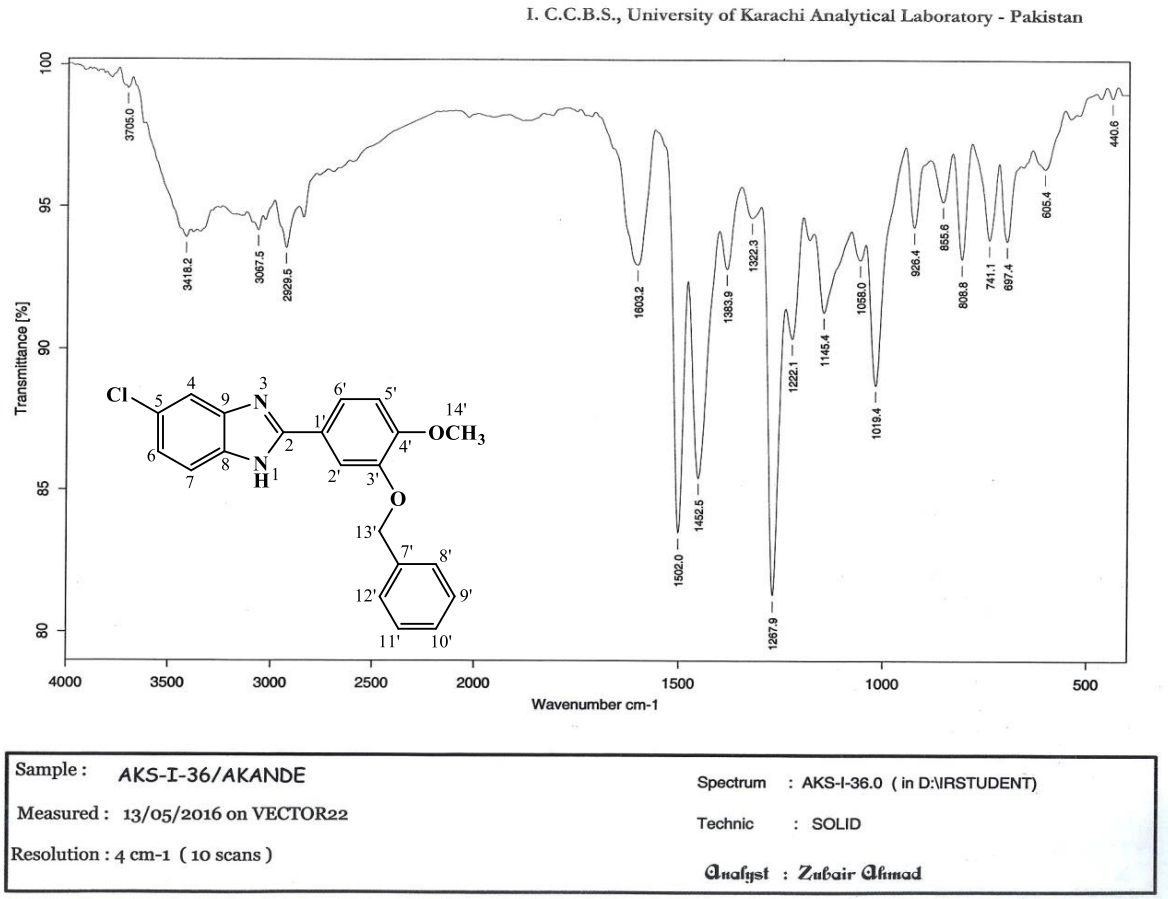

Figure 4.79. IR spectrum of AKS-I-36

THERMO ELECTRON ~ VISIONpro SOFTWARE V4.10

Operator Name	ARSHAD ALAM	Date of Report	5/20/2016
Department	Analytical laboratory#004 TWC	Time of Report	10:21:27AM
Organization	ICCBS.Karachi University.		
Information	Prof Dr. Khalid / Akande.		

Scan Graph

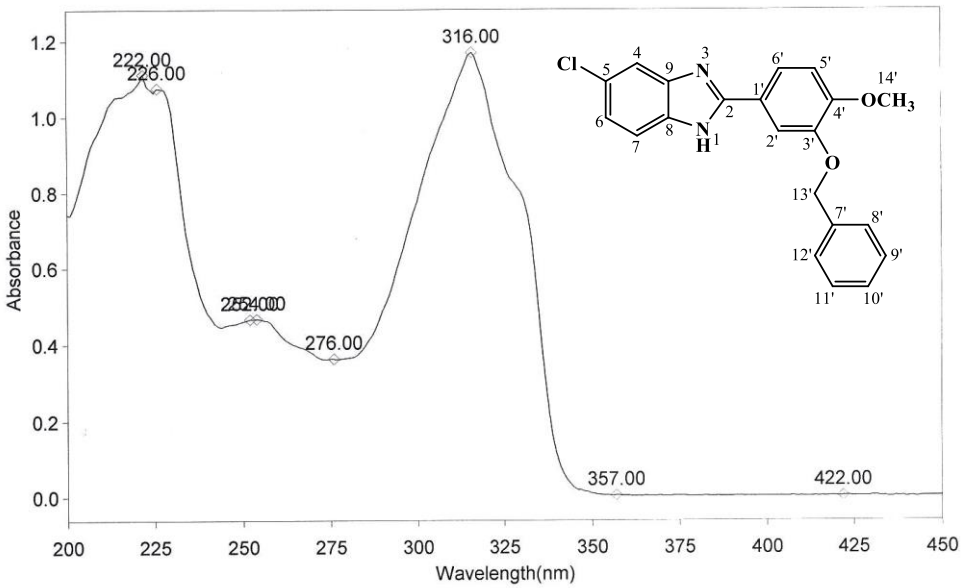

Results Table - AKS- I- 36.sre, AKS- I- 36,Cycle01

nm	A	Peak Pick Method
222.00	1.110	Find 8 Peaks Above -3.0000 A
226.00	1.074	Start Wavelength 200.00 nm
252.00	0.466	Stop Wavelength 450.00 nm
254.00	0.466	Sort By Wavelength
276.00	0.363	Sensitivity Very High
316.00	1.169	
357.00	0.005	
422.00	0.003	

Page 1, Scan Graph

Figure 4.80. UV spectrum of AKS-I-36

Table 4.12. Summary of the ^{1}H NMR and ^{13}C NMR spectra of AKS-I-36

Position	δ ^{1}H [mult., J_{HH} (Hz)] (ppm)	δ ^{13}C (ppm)	DEPT-135	DEPT-90
1	-	-	-	-
2	-	152.50	-	-
3	-	-	-	-
4	7.62 [s]	112.22	CH	CH
5	-	126½2	-	-
6	7.24 [dd, $J_{6,7}$ = 8.4, $J_{6,4}$ = 1.6]	122.46	CH	CH
7	7.59 [d, $J_{7,6}$ = 8.4]	112.22	CH	CH
8	-	148.00	-	-
9	-	148.00	-	-
1′	-	121.29	-	-
2′	7.87 [d, $J_{2',6'}$ = 1.6]	111.60	CH	CH
3′	-	151.23	-	-
4′	-	151.23	-	-
5′	7.19 [d, $J_{5',6'}$ = 8.4]	111.60	CH	CH
6′	7.77 [dd, $J_{6',5'}$ = 8.4, $J_{6',2'}$ = 1.6]	120.24	CH	CH
7′	-	136.75	-	-
8′	7.51 [d, $J_{8',9'}$ = 7.2]	127.92	CH	CH
9′	7.43 [t, $J_{9',8'}$ = 7.2]	128.43	CH	CH
10′	7.36 [t, $J_{10',11'}$ = $J_{10',9'}$ = 7.2]	127.96	CH	CH
11′	7.43 [t, $J_{11',12'}$ = 7.2]	128.43	CH	CH
12′	7.51 [d, $J_{12',11'}$ = 7.2]	127.92	CH	CH
13′-OCH_2-	5.18 [s]	70.09	CH_2	-
14′-OCH_3	3.85 [s]	55.76	OCH_3	-

4.1.13 Characterisation of 2-(3′-(benzyloxy)-4′-methoxyphenyl)-5-nitro-1*H*-benzo[*d*]imidazole (AKS-I-37)

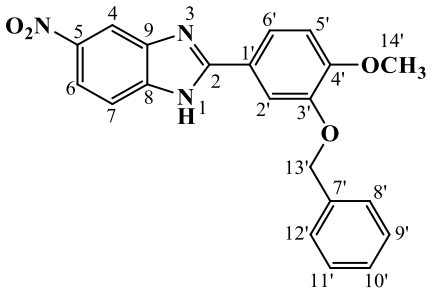

2-(3′-(Benzyloxy)-4′-methoxyphenyl)-5-nitro-1*H*-benzo[*d*]imidazole (AKS-I-37) is an orange solid with a yield of 90.6% (0.340 g), a m.pt. of 110-113 ^{o}C and a R_f of 0.45 (hexane/ethyl acetate, 1:1).

Represented in figures **4.81** and **4.82** are the ^{1}H NMR spectra (400 MHz, DMSO-d_6) with δ (ppm) values assigned to eleven aromatic methine protons as 8.42 (1H, s, H-4), 8.12 (1H, dd, $J_{6,7}$ = 8.8 Hz, $J_{6,4}$ = 2.0 Hz, H-6), 7.92 (1H, d, $J_{2',6'}$ = 1.6 Hz, H-2′), a doublet of doublet peak at 7.83 (1H, dd, $J_{6',5'}$ = 8.4 Hz, H-6′), 7.74 (1H, d, $J_{7,6}$ = 8.8 Hz, H-7), 7.51 (2H, d, $J_{8',9'} = J_{12',11'}$ = 7.2 Hz, H-8′, H-12′), 7.43 (2H, t, $J_{9',8'} = J_{11',12'}$ = 7.2 Hz, H-9′, H-11′), 7.36 (1H, t, $J_{10',11'} = J_{10',9'}$ = 7.2 Hz, H-10′), 7.22 (1H, d, $J_{5',6'}$ = 8.4 Hz, H-5′), to two methylene protons as 5.20 (s, 2H, -OCH_2-) and three methoxy protons as 3.86 (s, 3H, 4′-OCH_3). The deshielded amine proton was not captured.

Fourteen signals from ^{13}C NMR (75 MHz, DMSO-d_6) spectra, represented in figures **4.83** and **4.84**, show chemical shift, δ (ppm) values assigned as 155.86 (C-2), 151.62 (C-4′, C-3′), 148.03 (C-9, C-8), 142.52 (C-5), 136.71 (C-7′), 121.28 (C-1′), representing eight quarternary carbons, 128.37 (C-11′, C-9′′), 127.91 (C-10′), 127.83 (C-12′, C-8′), 120.63 (C-6′), 117.77 (C-7, C-6), 112.27 (C-5′, C-2′), 111.90 (C-4), representing eleven methine carbons, 70.14 (C-13′), representing methylene carbon and 55.76 (C-14′) representing the methoxy carbon. The DEPTH-135 (75 MHz, DMSO-d_6) spectrum (figure **4.85**) confirms the methine and methoxy peaks in positive phase, while the methylene carbon peak is in the negative phase. The DEPTH-90 (75 MHz, DMSO-d_6) spectrum (figures **4.86**) corroborates the peaks for the methine carbons.

The EI-MS spectrum (figure **4.87**) provides information on the fragment ion peaks produced according to their mass-to-charge ratio, *m/z*. The molecular ion peak, [M^+] is at *m/z* of 375. Characteristic M^+-$NO^{\cdot}$ and M^+-$NO_2^{\cdot}$ is indicative of fragment ions with peaks at *m/z* 345 and 328 respectively. Likewise, M^+-91 and M^+-284 cleavages gave ions

with prominent *m/z* of 284 and 91 (tropylium ion as the base peak) respectively corresponding to $[C_{14}H_{10}N_3O_4]^+$ and $[C_7H_7]^+$. The ion with *m/z* 284 further cleaves by loss of $CH_3O^{\cdot}$ generating a smaller fragment at *m/z* 254. The *m/z* of 65 is characteristic of $[C_5H_5]^+$ fragment while *m/z* at 28 and 18 are suggestive of CO (air) and H_2O/NH_4 peaks respectively. HREI-MS analysis further confirmed the compound's molecular formula, $C_{21}H_{17}N_3O_4$ at a *m/z* of 375.1233 (calculated 375.1219).

The spectrum (figure **4.88**) obtained from IR analysis gave rise to a series of absorption bands. Vibrational frequencies, $\bar{\upsilon}$ (cm^{-1}) of some characteristic bonds are assigned as 3325, 3072, 2931, 1600, 1504, 1338, 1449, 1268 and 1019 respectively for $N–H_{str}$ of 2º amine, $C–H_{str}$ aromatic, $C–H_{str}$ aliphatic, two aromatic $C=C_{str}$, $N=O_{sym\ str}$ of the nitro group, aliphatic $C–H_b$ of CH_2/CH_3, asymmetric $C–O_{str}$ and symmetric $C–O_{str}$ of ether.

Figure **4.89** represents the UV spectrum with wavelenghts of maximum absorptions, (λ_{max}) at 218, 230, 282 and 344 nm suggesting both $n\rightarrow\pi^*$ and $\pi\rightarrow\pi^*$ transitions. Table **4.13** presents the summary of the compound's ^1H NMR and ^{13}C NMR spectra.

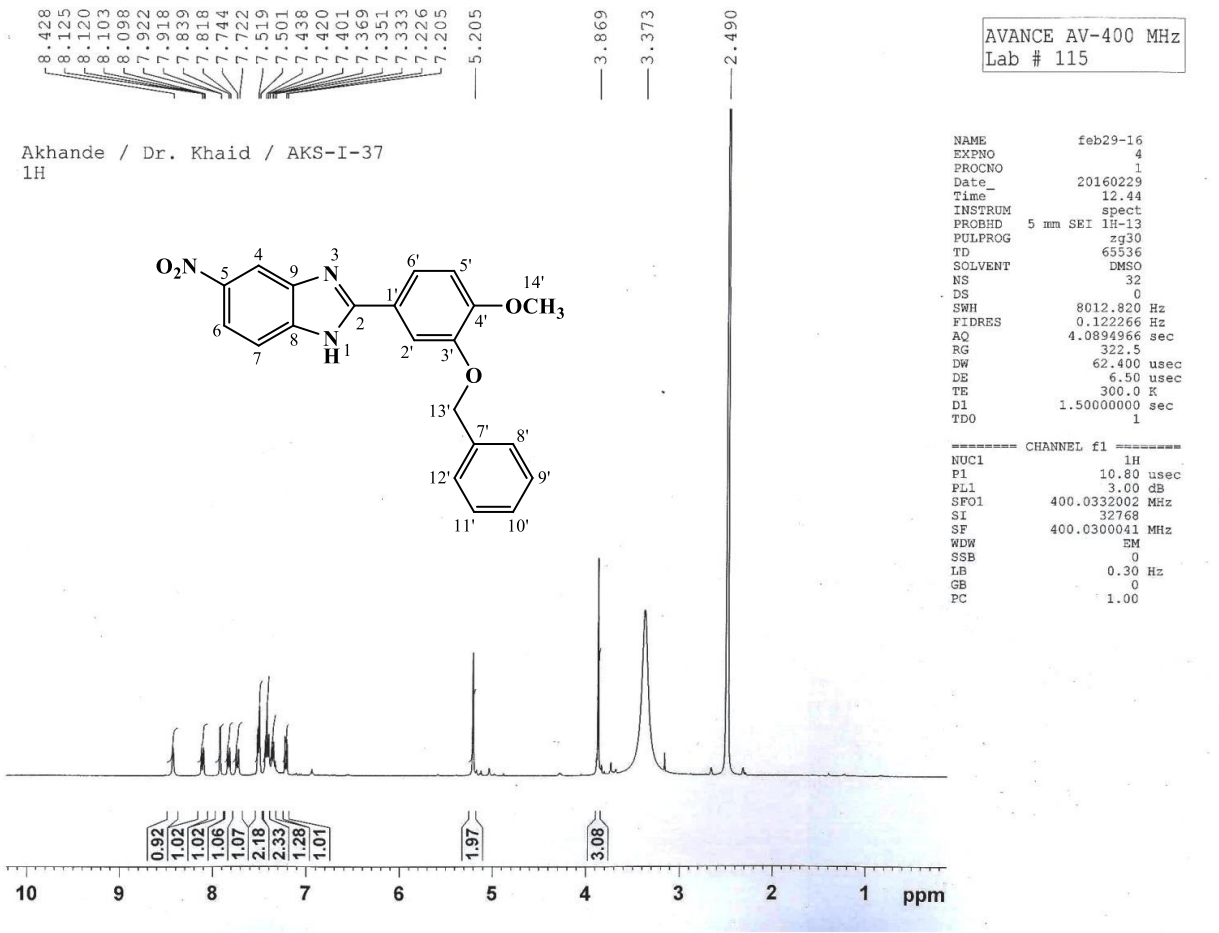

Figure 4.81. ^{1}H NMR (400 MHz, DMSO-d_6) spectrum of AKS-I-37

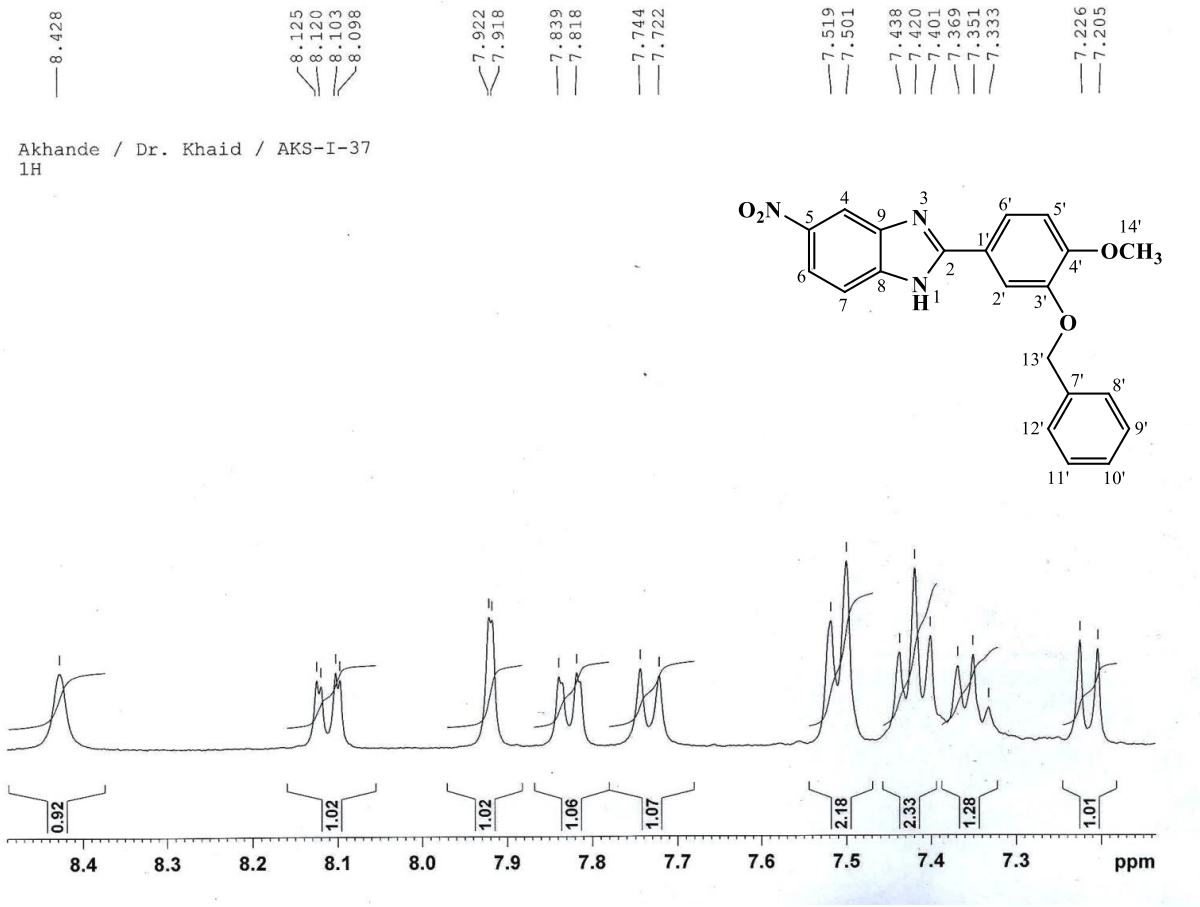

Figure 4.82. ^{1}H NMR (400 MHz, DMSO-d_6) spectrum of AKS-I-37 aromatic region (Expanded)

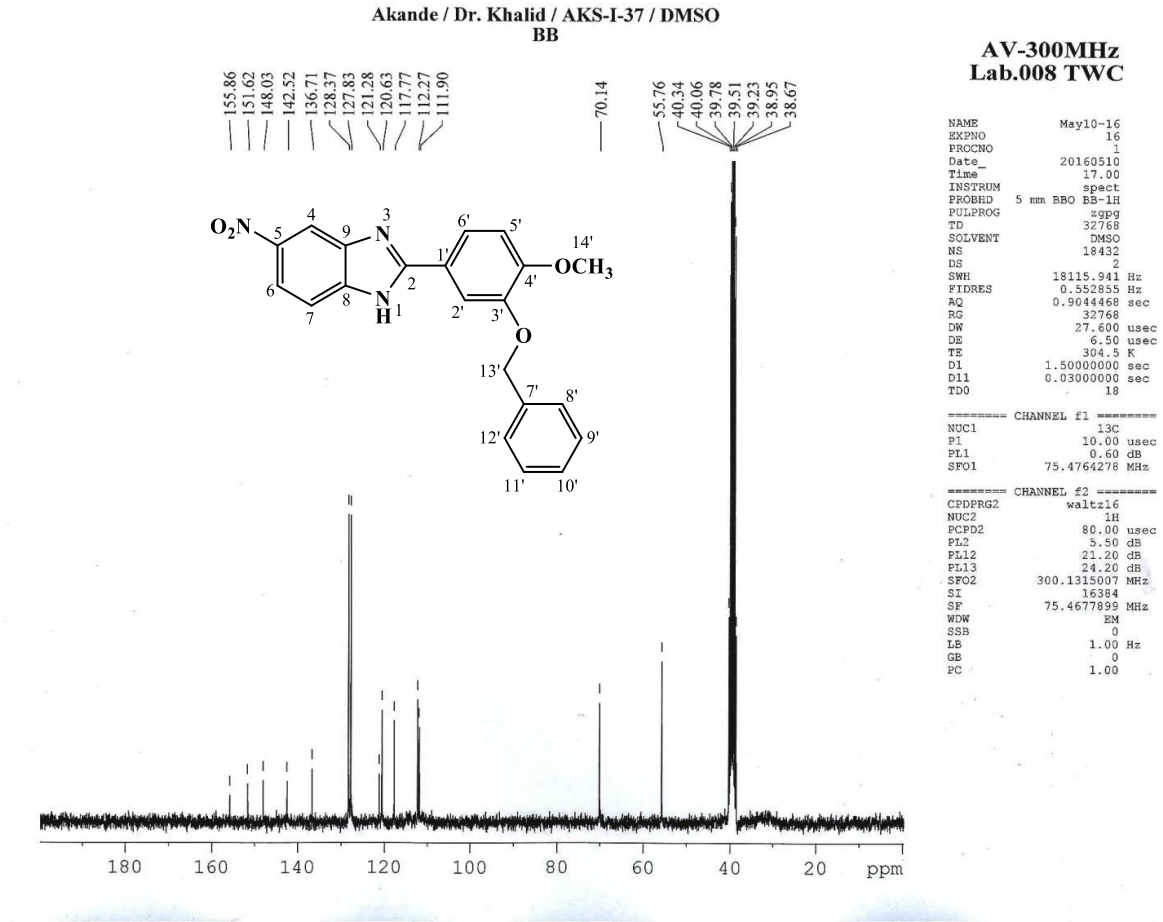

Figure 4.83. ^{13}C NMR (75 MHz, DMSO-d_6) spectrum of AKS-I-37

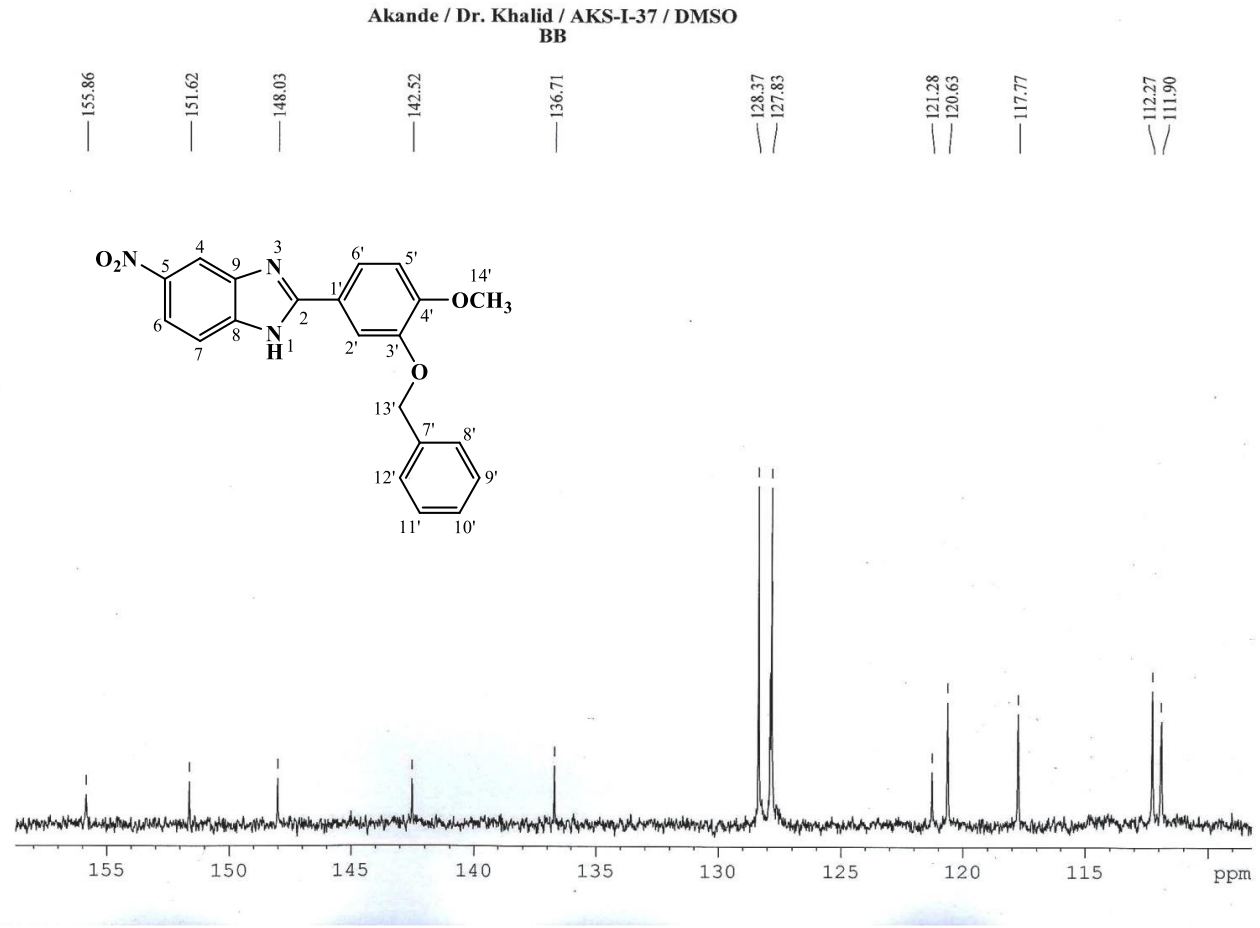

Figure 4.84. ^{13}C NMR (75 MHz, DMSO-d_6) spectrum of AKS-I-37 (Expanded)

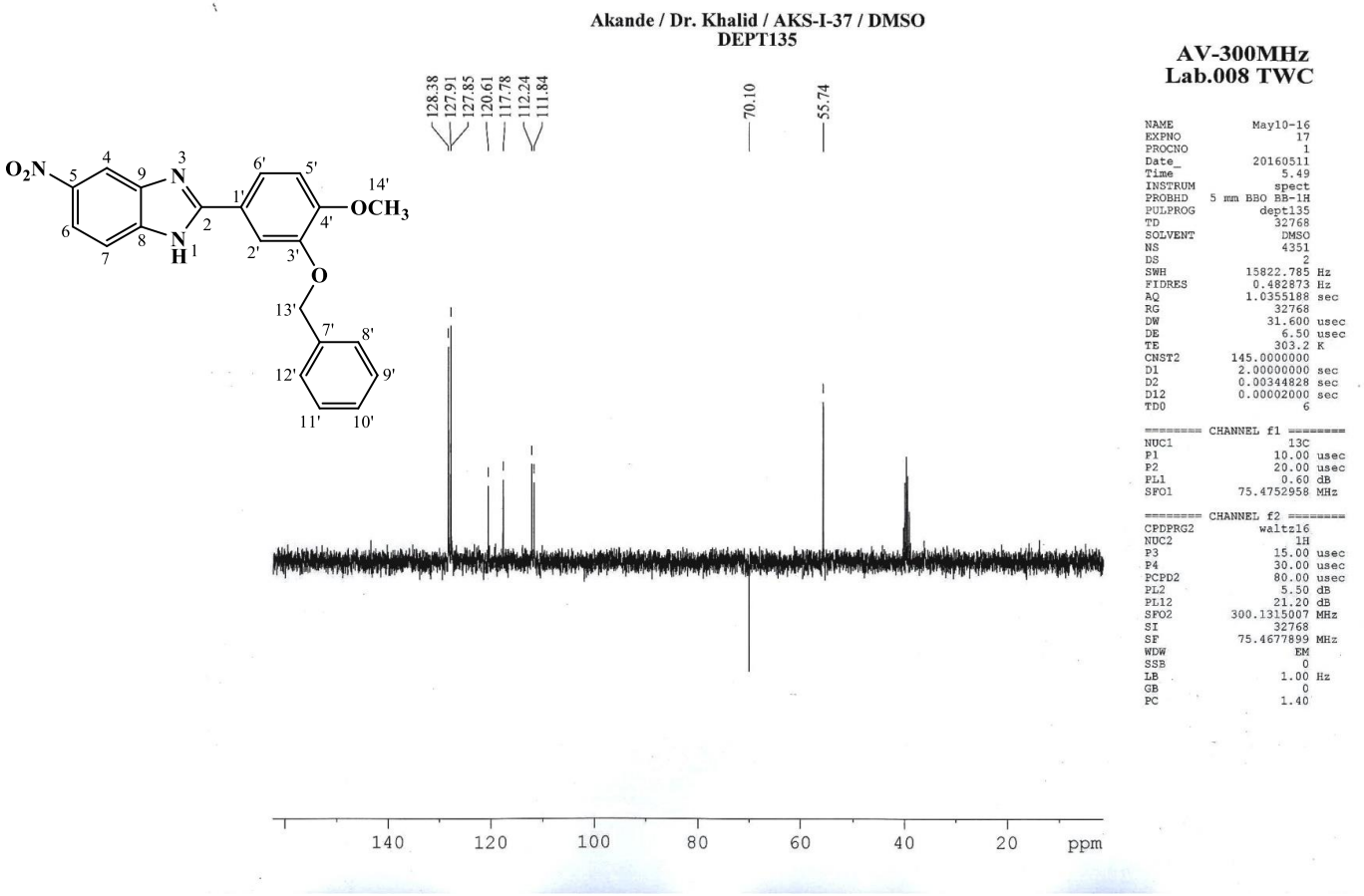

Figure 4.85. DEPTH-135 (75 MHz, DMSO-d_6) spectrum of AKS-I-37

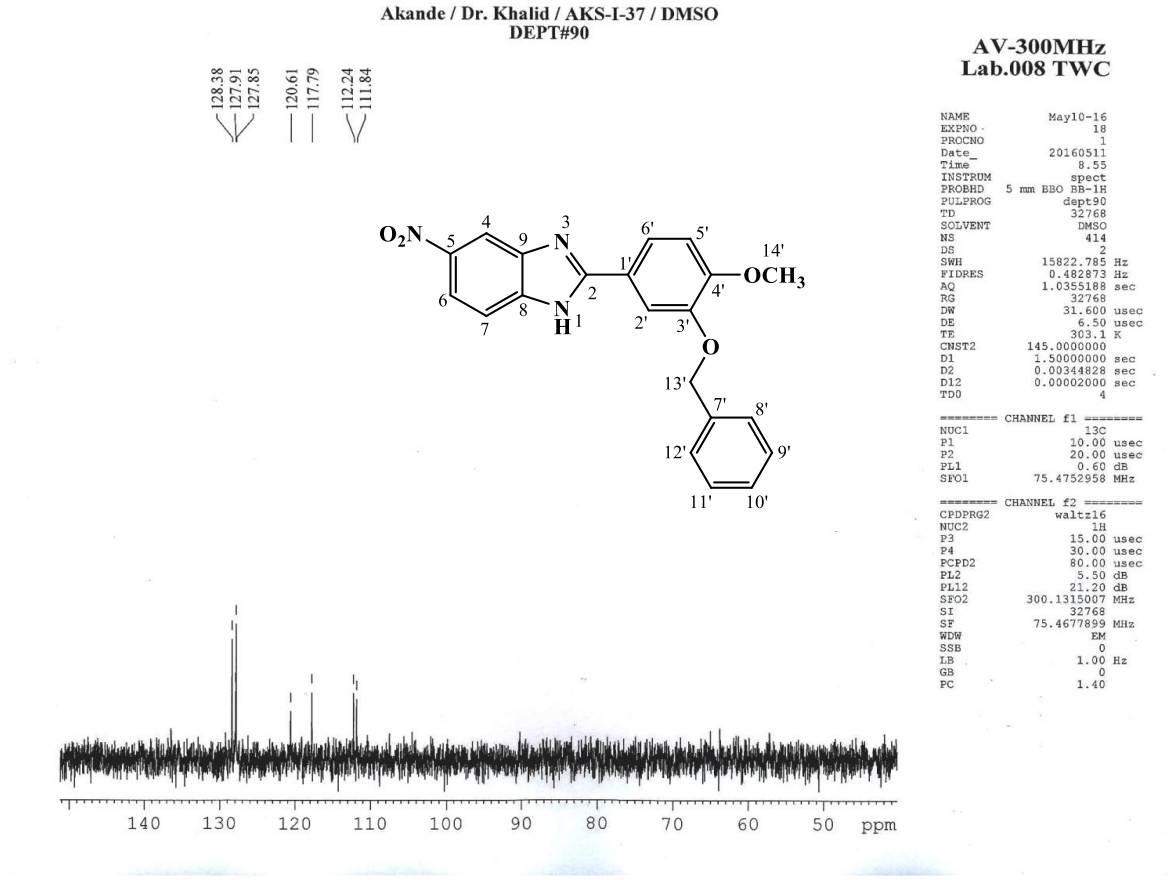

Figure 4.86. DEPTH-90 (75 MHz, DMSO-d_6) spectrum of AKS-I-37

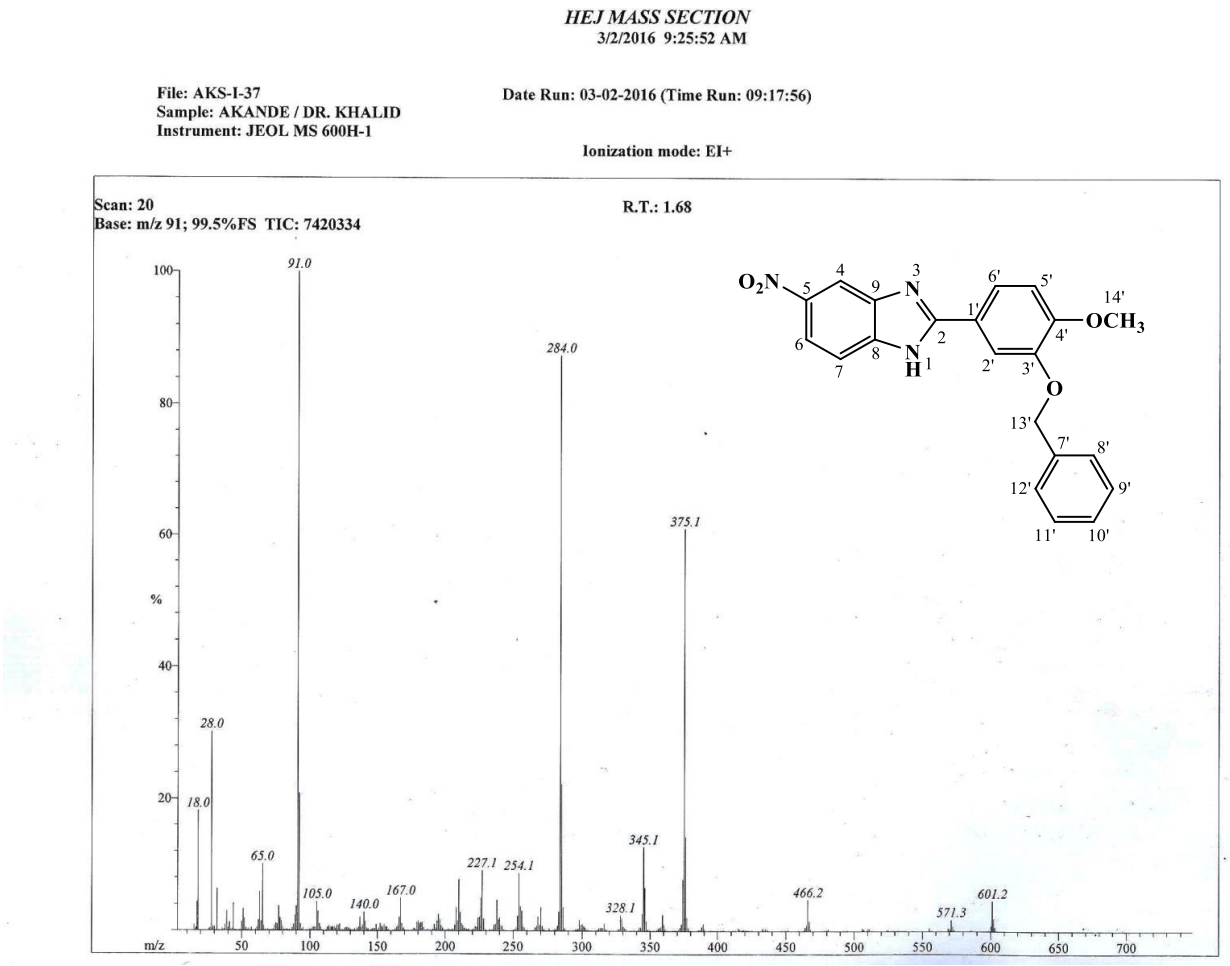

Figure 4.87. EI-MS spectrum of AKS-I-37

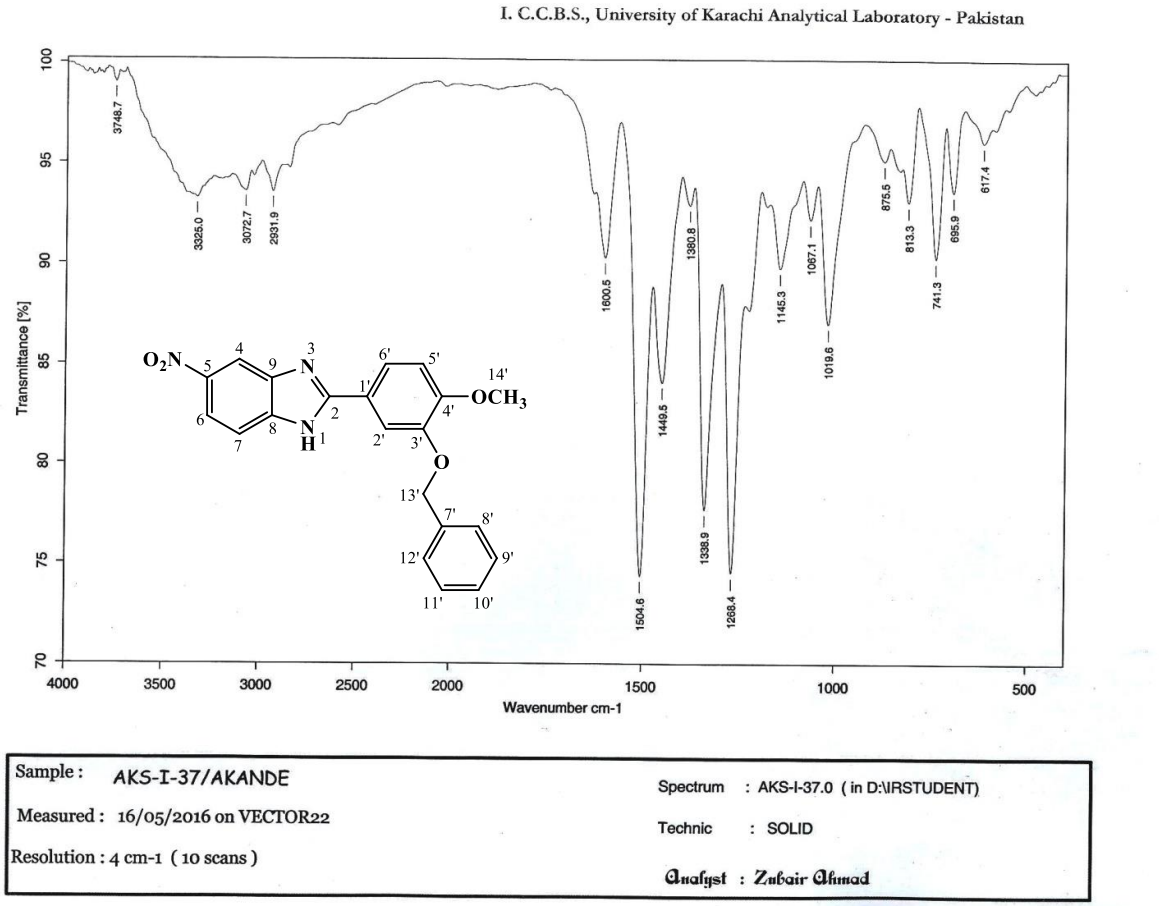

Figure 4.88. IR spectrum of AKS-I-37

THERMO ELECTRON ~ VISIONpro SOFTWARE V4.10

Operator Name	ARSHAD ALAM	Date of Report	5/20/2016
Department	Analytical laboratory#004 TWC	Time of Report	10:23:18AM
Organization	ICCBS.Karachi University.		
Information	Prof Dr. Khalid / Akande.		

Scan Graph

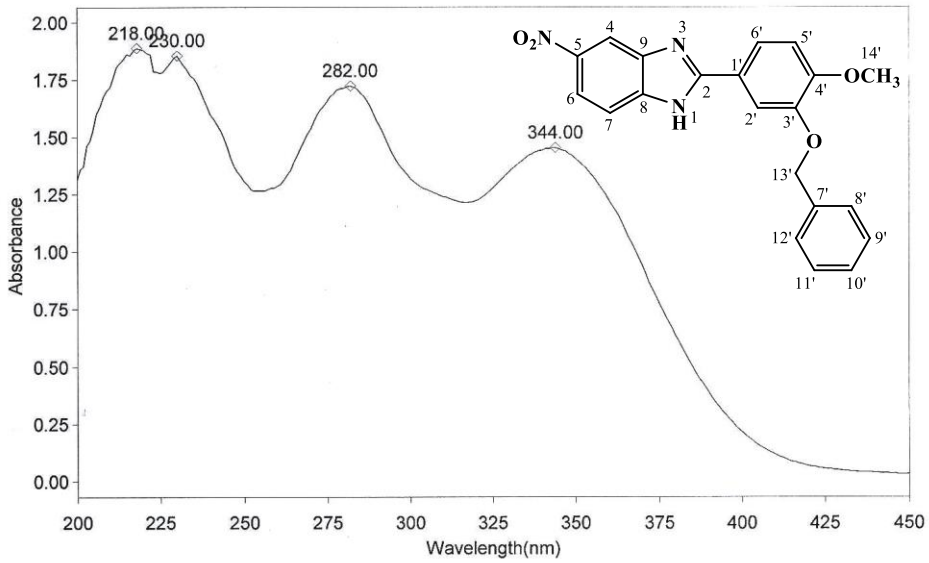

Results Table - AKS- I- 37.sre, AKS- I- 37,Cycle01

nm	A	**Peak Pick Method**
218.00	1.888	Find 8 Peaks Above -3.0000 A
230.00	1.855	Start Wavelength 200.00 nm
282.00	1.723	Stop Wavelength 450.00 nm
344.00	1.452	Sort By Wavelength
Sensitivity	Very Low	

Page 1, Scan Graph

Figure 4.89. UV spectrum of AKS-I-37

Table 4.13. Summary of the ^{1}H NMR and ^{13}C NMR spectra of AKS-I-37

Position	δ ^{1}H [mult., J_{HH} (Hz)] (ppm)	δ ^{13}C (ppm)	DEPT-135	DEPT-90
1	-	-	-	-
2	-	155.86	-	-
3	-	-	-	-
4	8.42 [s]	111.90	CH	CH
5	-	142.52	-	-
6	8.12 [dd, $J_{6,7}$ = 8.8, $J_{6,4}$ = 2.0]	117.77	CH	CH
7	7.74 [d, $J_{7,6}$ = 8.8]	117.77	CH	CH
8	-	148.03	-	-
9	-	148.03	-	-
1′	-	121.28	-	-
2′	7.92 [d, $J_{2',6'}$ = 1.6]	112.27	CH	CH
3′	-	151.62	-	-
4′	-	151.62	-	-
5′	7.22 [d, $J_{5',6'}$ = 8.4]	112.27	CH	CH
6′	7.83 [dd, $J_{6',5'}$ = 8.4]	120.63	CH	CH
7′	-	136.71	-	-
8′	7.51 [d, $J_{8',9'}$ = 7.2]	127.83	CH	CH
9′	7.43 [t, $J_{9',8'}$ = 7.2]	128.38	CH	CH
10′	7.36 [t, $J_{10',11'}$ = $J_{10',9'}$ = 7.2]	127.91	CH	CH
11′	7.43 [t, $J_{11',12'}$ = 7.2]	128.38	CH	CH
12′	7.51 [d, $J_{12',11'}$ = 7.2]	127.85	CH	CH
13′-OCH_2-	5.20 [s]	70.10	CH_2	-
14′-OCH_3	3.86 [s]	55.74	OCH_3	-

4.1.14 Characterisation of 2-(3′-(benzyloxy)-4′-methoxyphenyl)-5,6-dimethyl-1*H*-benzo[*d*]imidazole (AKS-I-38)

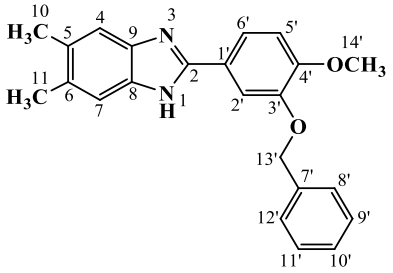

2-(3′-(Benzyloxy)-4′-methoxyphenyl)-5,6-dimethyl-1*H*-benzo[*d*]imidazole (AKS-I-38) was obtained as a white solid, 0.350 g (97.6% yield), m.pt. 106-109 ^{o}C and R_f of 0.45 (hexane/ethyl acetate, 1:1).

Ten resonance peaks were obtained from the ^{1}H NMR spectra (400 MHz, DMSO-d_6) as represented in figures **4.90** and **4.91** with chemical shift values, δ (ppm) assigned as 7.85 (1H, d, $J_{2',6'}$ = 1.6 Hz, H-2′), 7.73 (1H, dd, $J_{6',5'}$ = 8.4 Hz, $J_{6',2'}$ = 1.2 Hz, H-6′), 7.51 (2H, d, $J_{8',9'} = J_{12',11'}$ = 7.2 Hz, H-8′, H-11′), 7.43 (2H, t, $J_{11',12'} = J_{9',8'}$ = 7.2 Hz, $J_{11',10'} = J_{9',10'}$ = 7.6 Hz, H-11′, H-9′), 7.36 (1H, t, $J_{10',11'} = J_{10',9'}$ = 7.6 Hz, H-10′), 7.33 (2H, s, H-7, H-4; chemically equivalent), 7.16 (1H, d $J_{5',6'}$ = 8.8 Hz, H-5′) to ten methine protons, 5.18 (2H, s, 13′-OCH_2-) to two methylene protons, 3.84 (3H, s, 14′-OCH_3) to three methoxy protons and 2.31 (6H, s, 10-CH_3, 11-CH_3) to six equivalent methyl protons. The downfield amine proton was not captured on the spectrum.

The EI-MS spectrum (figure **4.92**) shows the molecular ion peak, [M^+] at *m/z* 358 and a [M^++1] peak at *m/z* 359. The M^+ further fragmentated, producing prominent peaks at *m/z* of 267 (the base peak) and *m/z* 91, corresponding to $[C_{16}H_{15}N_2O_2]^+$ and $[C_7H_7]^+$ ions respectively. The *m/z* of 329 is suggestive of a double loss of methyl radical [$2CH_3^{\bullet}$] from the M^+. Fragmentation by loss of $CH_3^{\bullet}$ and $C_7H_7^{\bullet}$ radicals consecutively corresponds to *m/z* 253 $[C_{15}H_{13}N_2O_2]^+$. Fragment ion with *m/z* 239 is indicative of fragmentation either by loss of $2CH_3^{\bullet}$ and $C_7H_7^{\bullet}$ radicals or by a cleavage of the imidazole ring, corresponding to $[C_{14}H_{11}N_2O_2]^+$ or $[C_{15}H_{13}NO_2]^+$ respectively. The HREI-MS analysis yielded a *m/z* of 358.1690 (calculated 358.1681), corresponding to the molecular formular, $C_{23}H_{22}N_2O_2$ [M^+]. This further confirms the compound.

The IR spectrum (figure **4.93**) shows absorption bands deduced from the compound. Some characteristic vibrational frequencies, $\bar{\upsilon}$ (cm^{-1}) are 3416, 3160, 2925, 1606, 1504, 1455, 1263 and 1019 corresponding to N–H_{str}, aromatic C–H_{str}, aliphatic C–H_{str}, two

aromatic C=C_{str}, C–H_b of CH_3/CH_2, C–$O_{asy\ str}$ and C–$O_{sym\ str}$ of ether respectively. Wavelenghts of maximum absorptions, (λ_{max}) from the UV spectrum (figure **4.94**) are 316, 253, 228 and 222 nm, corresponding to n→π* and π→π* transitions. Table **4.14** represents the summary of ^{1}H NMR spectra.

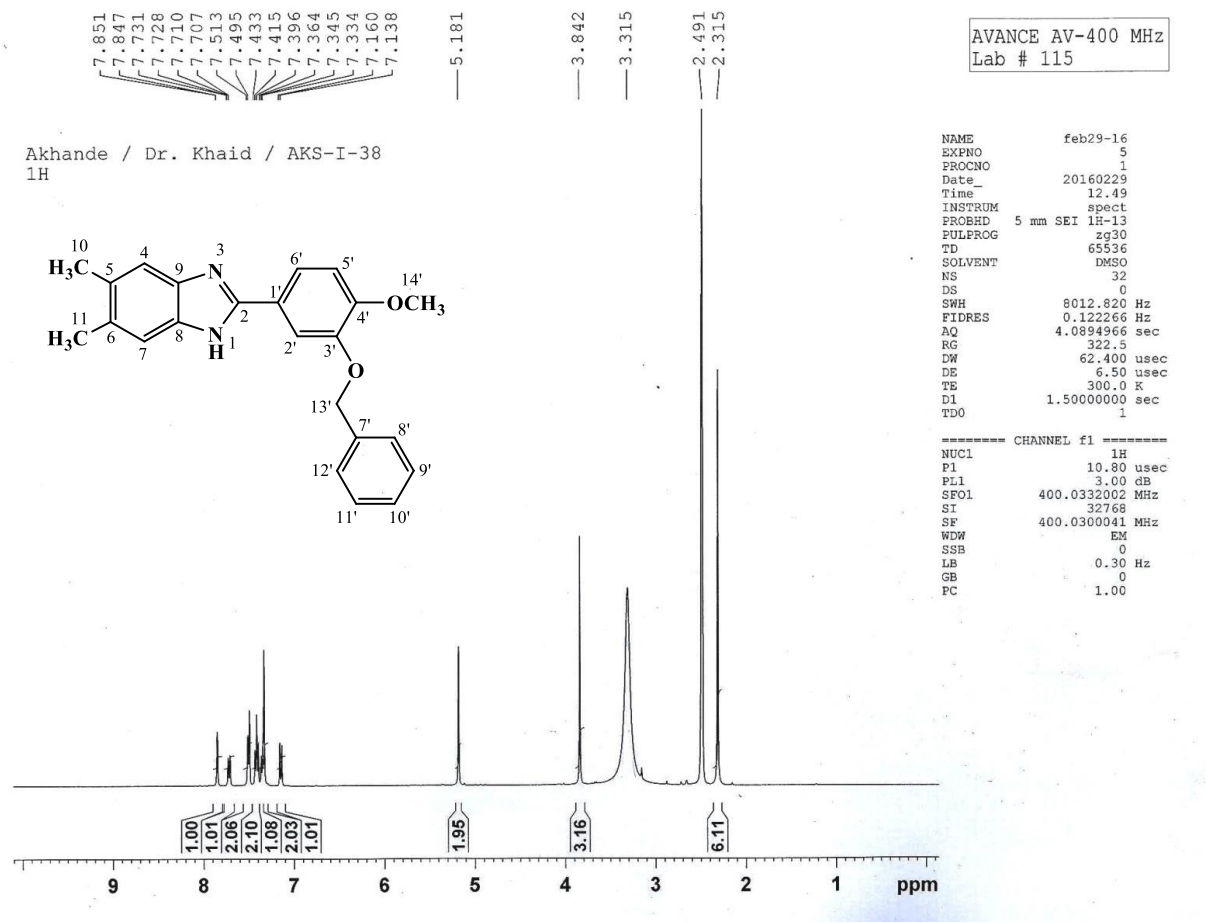

Figure 4.90. ^{1}H NMR (400 MHz, DMSO-d_6) spectrum of AKS-I-38

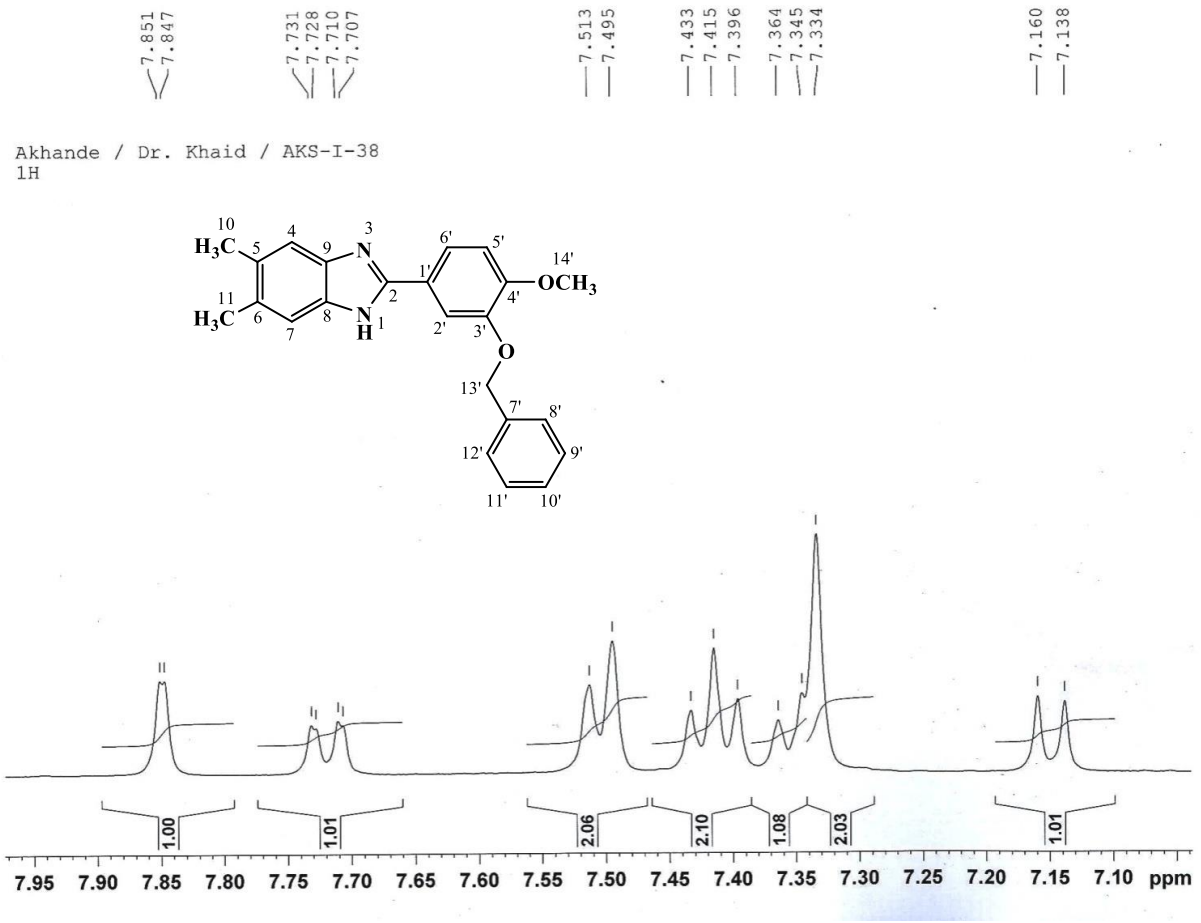

Figure 4.91. ^{1}H NMR (400 MHz, DMSO-d_6) spectrum of AKS-I-38 aromatic region (Expanded)

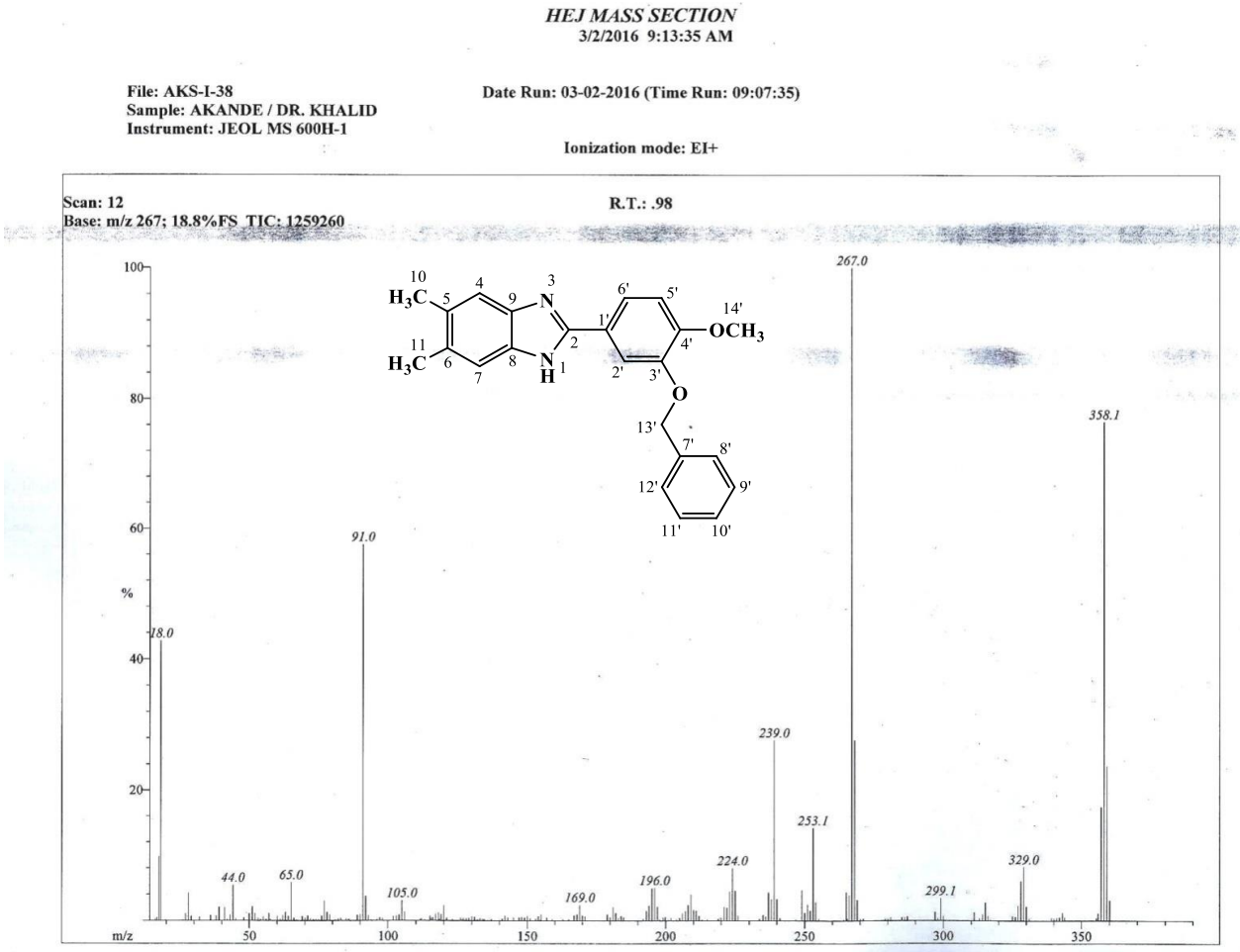

Figure 4.92. EI-MS spectrum of AKS-I-38

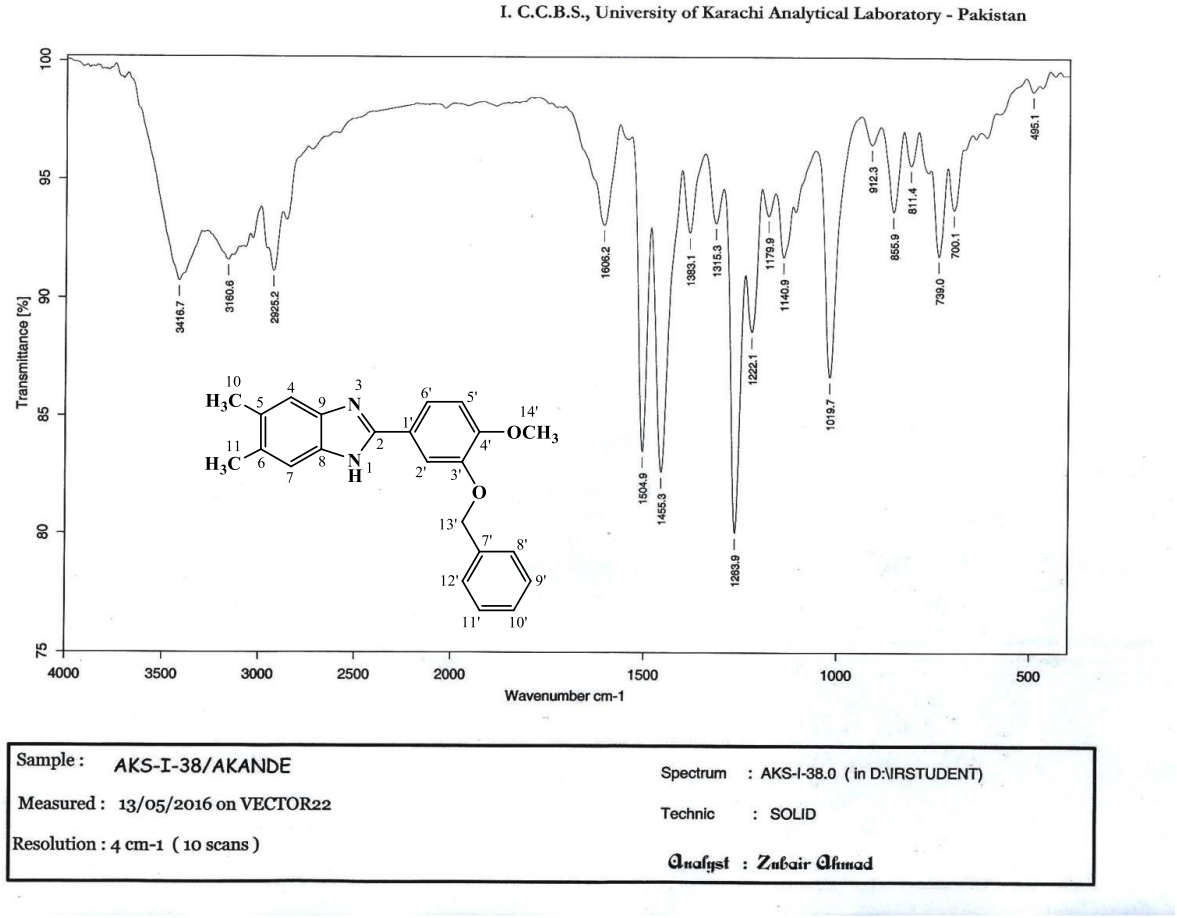

Figure 4.93. IR spectrum of AKS-I-38

THERMO ELECTRON ~ VISIONpro SOFTWARE V4.10

Operator Name	ARSHAD ALAM	Date of Report	5/20/2016
Department	Analytical laboratory#004 TWC	Time of Report	10:25:17AM
Organization	ICCBS.Karachi University.		
Information	Prof Dr. Khalid / Akande.		

Scan Graph

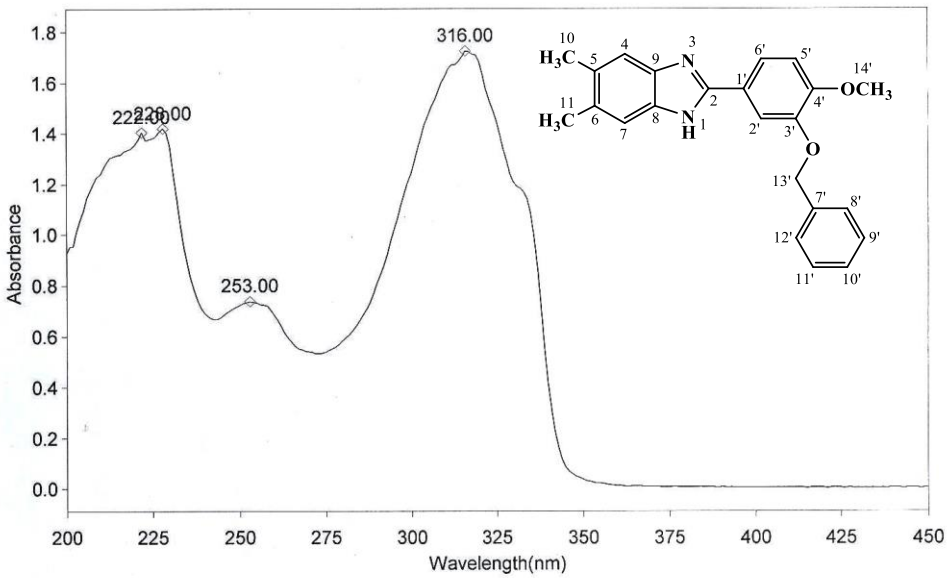

Results Table - AKS- I- 38.sre, AKS- I- 38,Cycle01

nm	A	**Peak Pick Method**
222.00	1.404	Find 8 Peaks Above -3.0000 A
228.00	1.420	Start Wavelength 200.00 nm
253.00	0.737	Stop Wavelength 350.00 nm
316.00	1.725	Sort By Wavelength
Sensitivity	Very High	

Page 1, Scan Graph

Figure 4.94. UV spectrum of AKS-I-38

Table 4.14. Summary of the ^{1}H NMR spectra of AKS-I-38

Position	δ ^{1}H [mult., J_{HH} (Hz)] (ppm)
1	-
2	-
3	-
4	7.33 [s]
5	-
6	-
7	7.33 [s]
8	-
9	-
1′	-
2′	7.85 [d, $J_{2',6'}$ = 1.6]
3′	-
4′	-
5′	7.16 [d, $J_{5',6'}$ = 8.8]
6′	7.73 [dd, $J_{6',5'}$ = 8.4, $J_{6',2'}$ = 1.2]
7′	-
8′	7.51 [d, $J_{8',9'}$ = 7.2]
9′	7.43 [t, $J_{9',8'}$ = 7.2; $J_{9',10'}$ = 7.6]
10′	7.36 [t, $J_{10',11'}$ = $J_{10',9'}$ = 7.6]
11′	7.43 [t, $J_{11',10'}$ = 7.6; $J_{11',12'}$ = 7.2]
12′	7.51 [d, $J_{12',11'}$ = 7.2]
13′-OCH_2-	5.18 [s]
14′-OCH_3	3.84[s]
10-CH_3	2.31
11-CH_3	2.31

4.1.15 Characterisation of 2-(2′-(benzyloxy)phenyl)-5-fluoro-1*H*-benzo[*d*] imidazole (AKS-I-39)

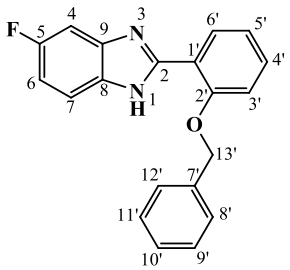

The brown compound, AKS-I-39 is a solid with a yield of 54.3% (0.173 g), a m.pt. 125-127 ^{o}C and a 0.68 (hexane/ethyl acetate, 1:1) R_f value.

Ten resonance peaks, δ (ppm) values were obtained from the ^{1}H NMR spectra (400 MHz, DMSO-d_6) (figures **4.95** and **4.96**) and were assigned as ≈12.50 (1H, br s, -NH) to the deshelded amine proton, 8.24 (1H, dd, $J_{6',5'}$ = 8.0 Hz, H-6′), 7.64-7.61 (1H, m, H-4) (the multiplet peak for proton at position 4 was due to the influence of a fluorine atom), 7.48 (2H, d, $J_{12',11'} = J_{8',9'}$ = 7.6 Hz, H-12′, H-8′), 7.41 (1H, d, $J_{7,6}$ = 7.2 Hz, H-7), another multiplet at 7.38-7.32 (3H, m, H-11′, H-9′, H-4′), 7.28 (1H, t, $J_{10',9'}$ = 7.2 Hz, H-10′), 7.20 (1H, d, $J_{3',4'}$ = 8.4 Hz, H-3′), 7.09 (2H, t, $J_{6,7}$ = 7.2 Hz, H-6, $J_{5',6'}$ = 8.0 Hz, H-5′) to the methine protons and 5.51 (2H, s, 13′-OCH_2-) to the methylene protons.

As presented in figure **4.97**, the EI-MS spectrum shows molecular ion, M^+ peak at *m/z* 318 and a [M^+-1] peak at *m/z* 317 indicating a loss of $H^{\bullet}$. The peak at *m/z* of 301 is suggestive of [M^+-NH_3] fragment. Cleavages of both bonds α to oxygen resulted in the prominent peaks at *m/z* 212 $[C_{13}H_8FN_2]^+$ and 91 $[C_7H_7]^+$ (base peak) respectively. The *m/z* of 65 is indicative of a $[C_5H_5]^+$ fragment. The observed *m/z* from HREI-MS analysis is 318.1158 (calculated, 318.1168), corresponding to the molecular formula $C_{20}H_{15}FN_2O$ which further confirms the compound.

Representative absorption bands from IR spectrum (figure **4.98**) have vibrational frequencies, $\bar{\upsilon}$ (cm^{-1}) reported as 3413 (N–H_{str} of 2º amine), 3062 (aromatic C–H_{str}), 2925, 2876 (aliphatic C–$H_{asy\ str}$ and C–$H_{sym\ str}$), 1629 (C=N_{str}), 1593, 1528 (aromatic C=C_{str}), 1463 (C–H_b), 1234, 1007 (asymmetric and symmetric C–O_{str}) and 1131 (C–F_{str}). Figure **4.99** represents the UV spectrum showing maximum absorptions, (λ_{max}) at 313, 295 and 214 nm corresponding to n→π* and π→π* transitions. Summary of the ^{1}H NMR spectra is represented in table **4.15**.

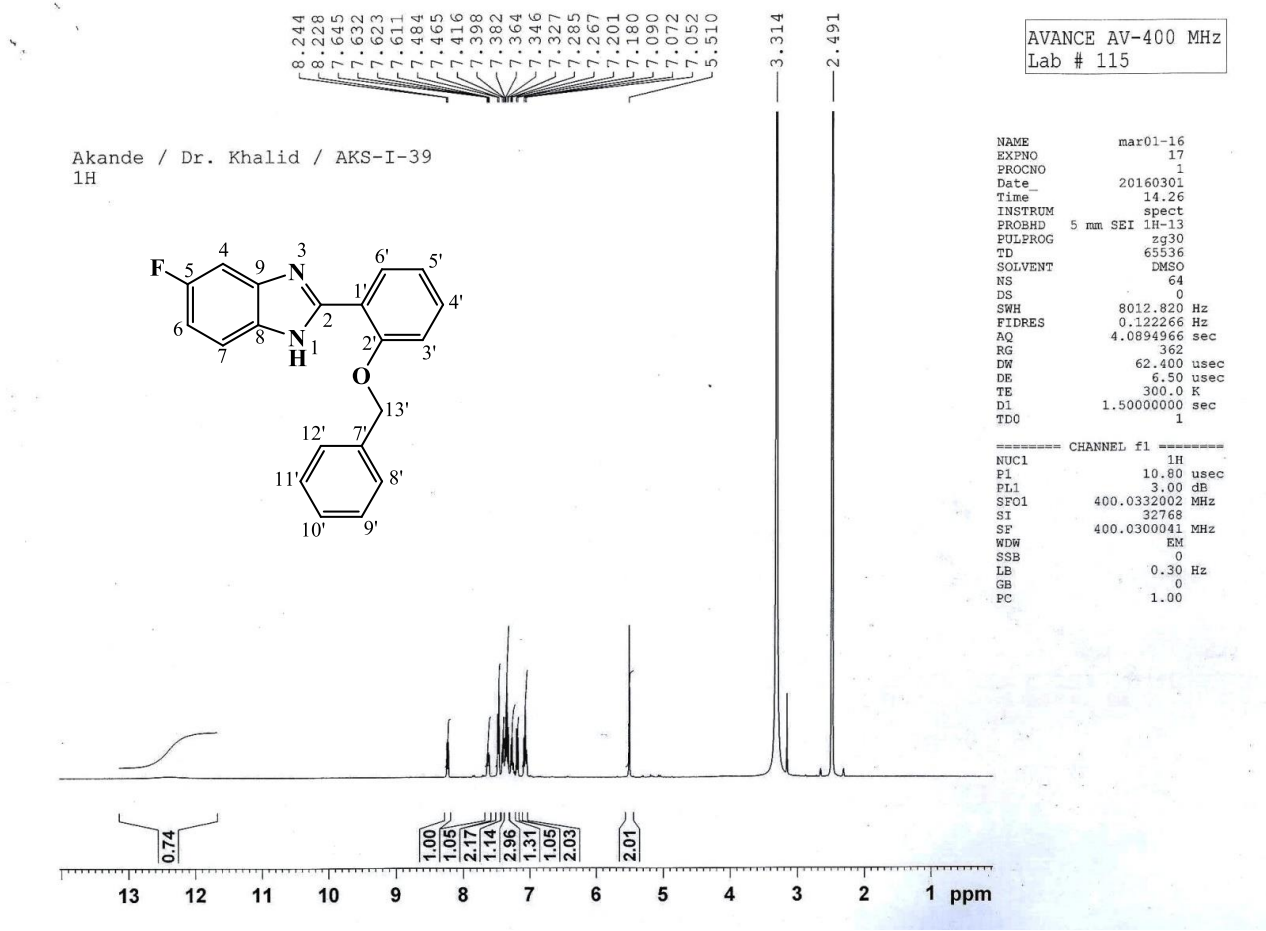

Figure 4.95. ^{1}H NMR (400 MHz, DMSO-d_6) spectrum of AKS-I-39

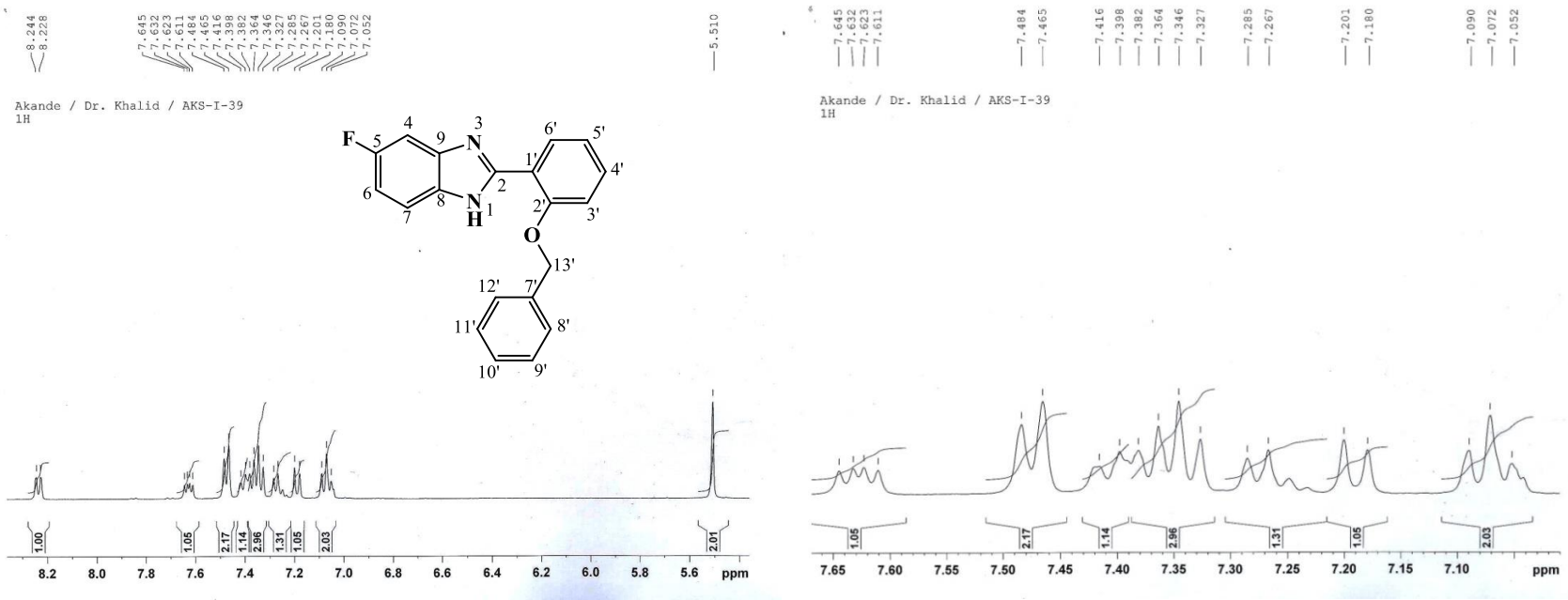

Figure 4.96. ^{1}H NMR (400 MHz, DMSO-d_6) spectra of AKS-I-39 (Expanded)

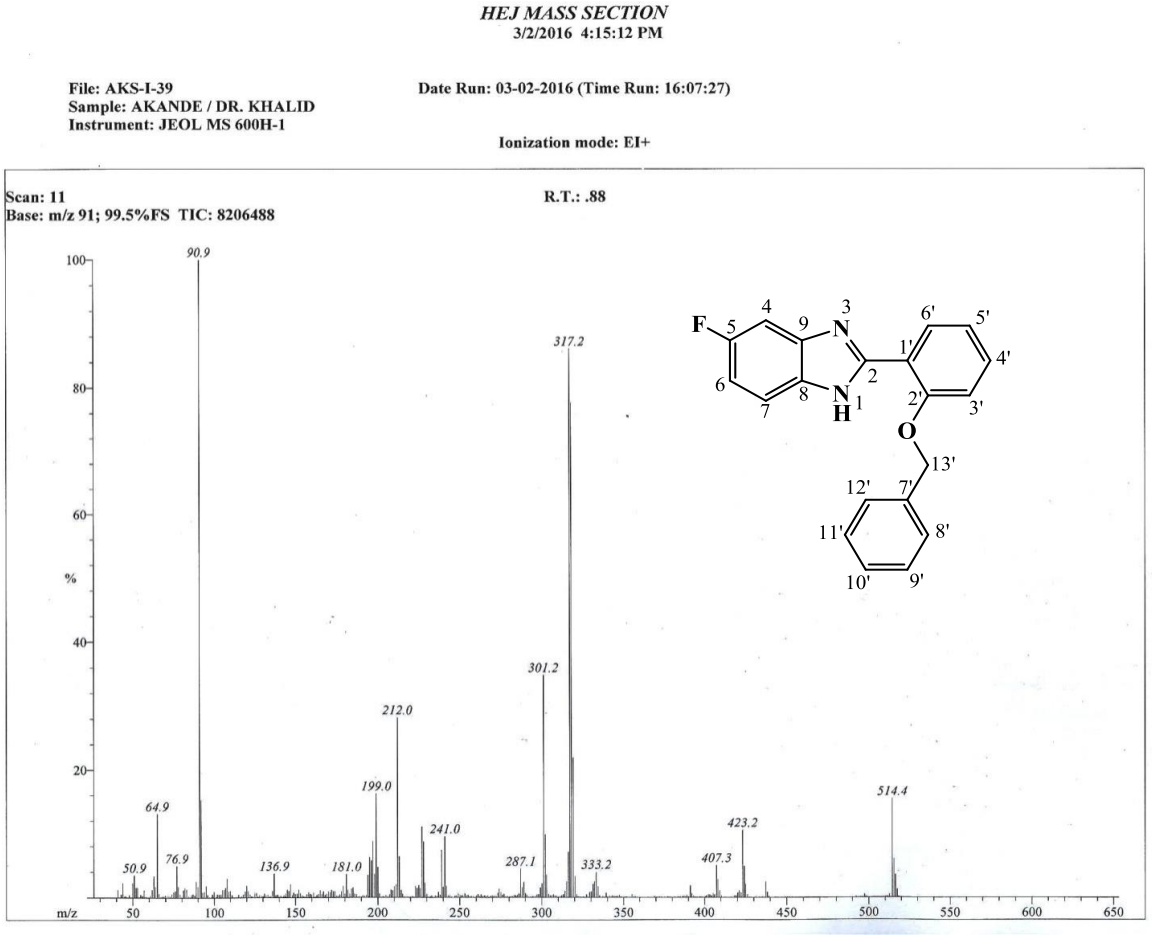

Figure 4.97. EI-MS spectrum of AKS-I-39

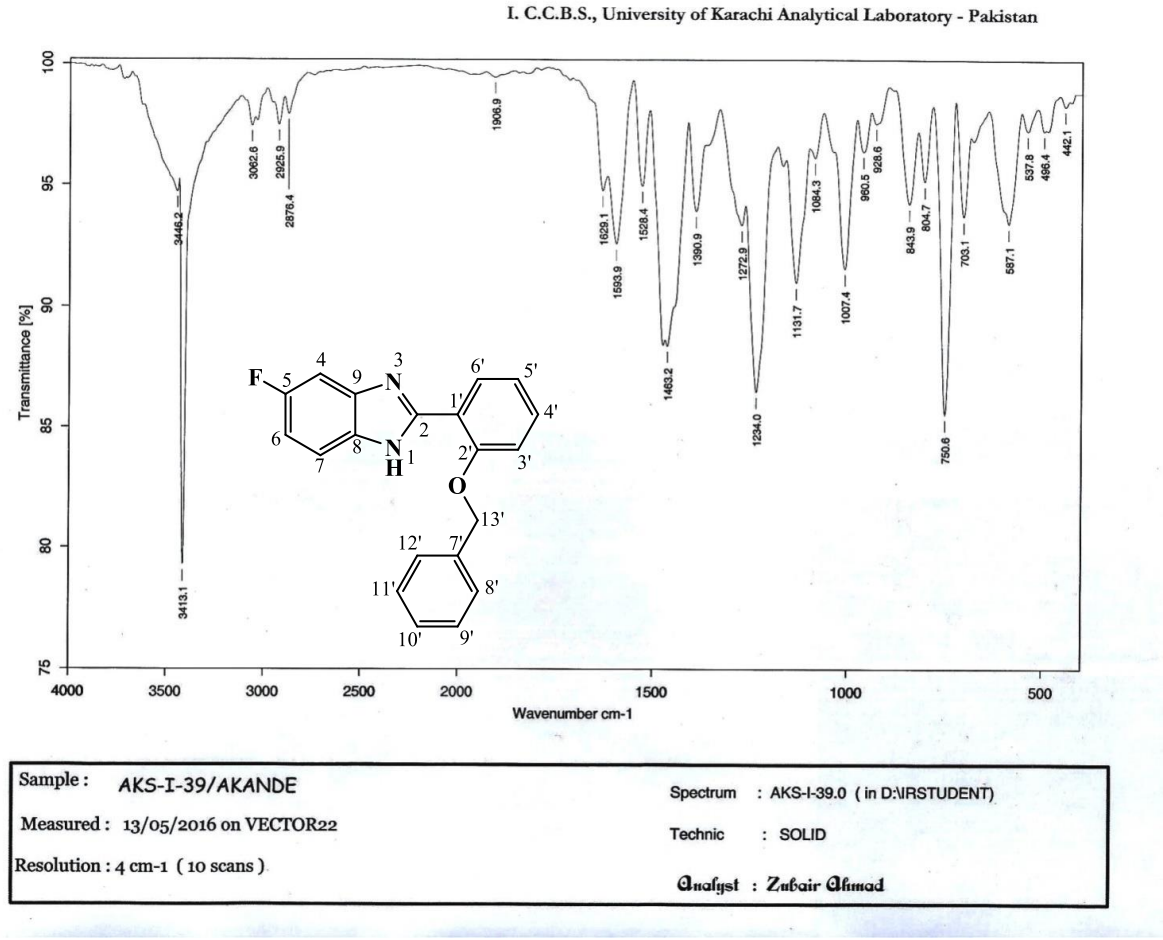

Figure 4.98. IR spectrum of AKS-I-39

THERMO ELECTRON ~ VISIONpro SOFTWARE V4.10

Operator Name	ARSHAD ALAM	Date of Report	5/20/2016
Department	Analytical laboratory#004 TWC	Time of Report	10:26:39AM
Organization	ICCBS.Karachi University.		
Information	Prof Dr. Khalid / Akande.		

Scan Graph

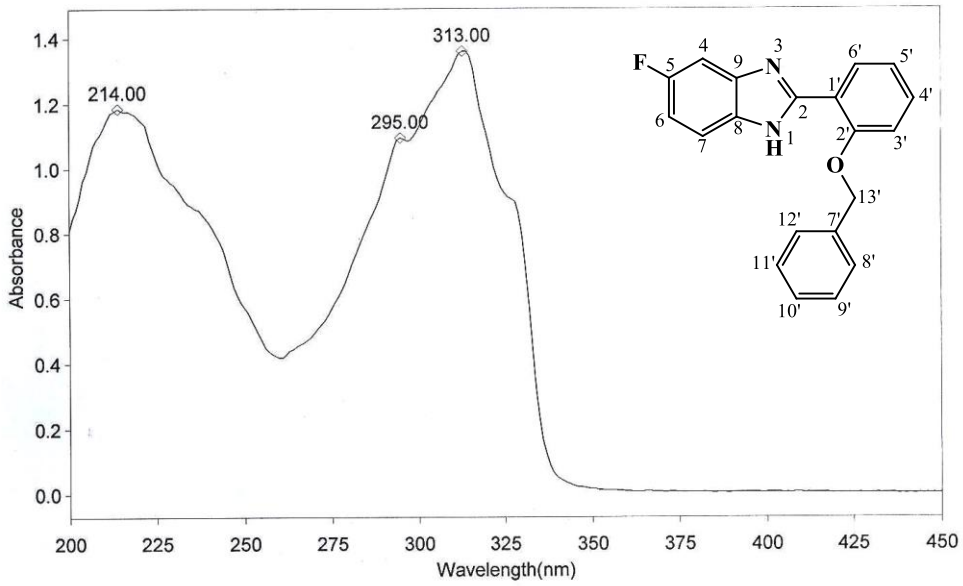

Results Table - AKS- I- 39.sre, AKS- I- 39,Cycle01

nm	A	Peak Pick Method
214.00	1.185	Find 8 Peaks Above -3.0000 A
295.00	1.094	Start Wavelength 200.00 nm
313.00	1.360	Stop Wavelength 450.00 nm
		Sort By Wavelength
Sensitivity	Medium	

Page 1, Scan Graph

Figure 4.99. UV spectrum of AKS-I-39

Table 4.15. Summary of the ^{1}H NMR spectra of AKS-I-39

Position	δ ^{1}H [mult., J_{HH} (Hz)] (ppm)
1	≈12.50 [br s]
2	-
3	-
4	7.64-7.61 [m]
5	-
6	7.09 [t, $J_{6,7}$ = 7.2]
7	7.41 [d, $J_{7,6}$ = 7.2]
8	-
9	-
1′	-
2′	-
3′	7.20 [d, $J_{3',4'}$ = 8.4]
4′	7.38-7.32 [m]
5′	7.09 [t, $J_{5',6'}$ = 8.0]
6′	8.24 [dd, $J_{6',5'}$ = 8.0]
7′	-
8′	7.48 [d, $J_{8',9'}$ = 7.6]
9′	7.38-7.32 [m]
10′	7.28 [t, $J_{10',9'}$ = 7.2]
11′	7.38-7.32 [m]
12′	7.48 [d, $J_{12',11'}$ = 7.6]
13′-OCH_2-	5.51 [s]

4.1.16 Characterisation of 2-(2′-(benzyloxy)phenyl)-5-chloro-1*H*-benzo[*d*] imidazole (AKS-I-40)

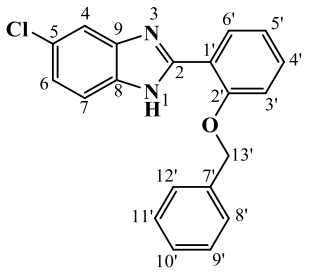

The dark-brown compound, AKS-I-40 was obtained as a solid compound, 60.9% (0.204 g) yield, a m.pt. 127-129 ^{o}C and a R_f of 0.69 in a hexane/ethyl acetate (1:1) solvent system.

The ^{1}H NMR spectra (400 MHz, DMSO-d_6) (figures **4.100** and **4.101**) show eleven resonances, δ (ppm) without capturing the deshielded amine proton expected to be seen further downfield. These were assigned as 8.25 (1H, dd, $J_{6',4'}$ = 1.6 Hz, $J_{6',5'}$ = 8.0 Hz, H-6′), 7.67 (d, 1H, $J_{4,6}$ = 1.6 Hz, H-4), 7.65 (1H, d, $J_{7,6}$ = 8.4 Hz, H-7), 7.48 (2H, d, $J_{12',11'}$ = $J_{8',9'}$ = 7.2 Hz, H-12′, H-8′), 7.41 (1H, dt, $J_{4',3'}$ = 8.8 Hz, $J_{4',6'}$ = 1.6 Hz, H-4′), 7.36 (2H, t, $J_{11',12'}$ = $J_{9',8'}$ = 7.2 Hz, H-11′, H-9′), 7.28 (1H, t, $J_{10',9'}$ = 7.2 Hz, H-10′) 7.24 (1H, t, $J_{6,4}$ = 2.0 Hz, $J_{6,7}$ = 8.8 Hz, H-6), 7.21 (1H, d, $J_{3',4'}$ = 8.4 Hz, H-3′), 7.09 (1H, t, $J_{5',6'}$ = 7.6 Hz, H-5′) to twelve methine protons and 5.51 (2H, s, 13′-OCH_2-) to two methylene protons.

Form EI-MS analysis, the presence of a chlorine atom gave rise to some peak patterns spaced two mass units apart (figure **4.102**). The *m/z* at 333 is indicative of [M^+-1] peak and a corresponding isotope peak of *m/z* 335 [M^++2]. Subsequent loss of NH_3 is suggestive of a *m/z* of 317. Bond cleavage α to oxygen resulted in the formation of the most intense peak at *m/z* of 91 (base peak). The common *m/z* of 65 is indicative of the fragment corresponding to $[C_5H_5]^+$. The *m/z* of 334.0872 (calculated 334.0873) found for the formula $C_{20}H_{15}ClN_2O$ from HREI-MS analysis further confirms the compound.

The IR spectrum (figure **4.103**) provides characteristic absorption frequencies, $\bar{\upsilon}$ (cm^{-1}) at 3409, 3032, 2923, 2868, 1594, 1463, 1237 and 1048 which connote amine N–H_{str}, aromatic C–H_{str}, aliphatic C–$H_{asy\ str}$ and C–$H_{sym\ str}$, aromatic C=C_{str}, C–H_b of CH_2, C–O_{str} of ether and C–Cl_{str} respectively. The UV spectrum (figure **4.104**) shows λ_{max} at 316 and 214 nm indicative of n→π* and π→π* transitions. The summary of the ^{1}H NMR spectra is presented in table **4.16**.

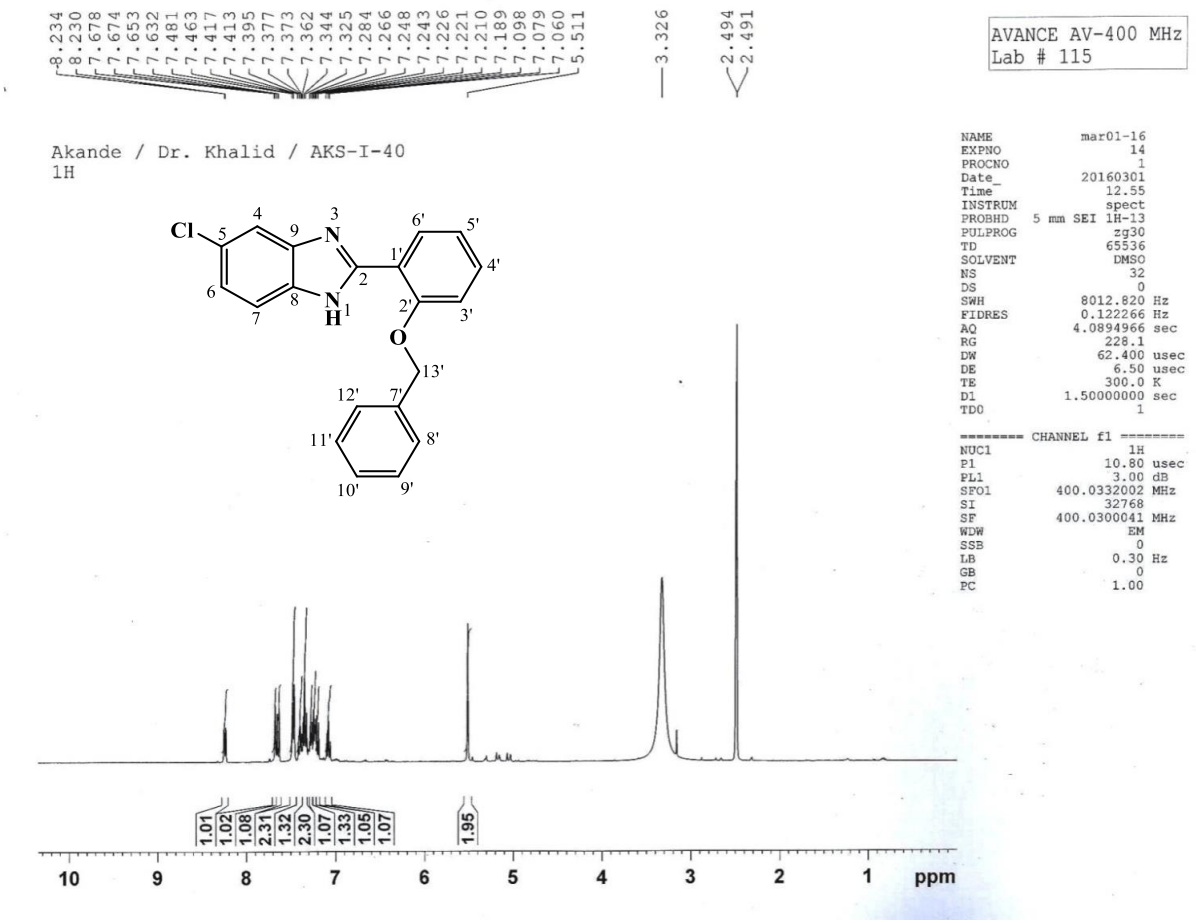

Figure 4.100. ^{1}H NMR (400 MHz, DMSO-d_6) spectrum of AKS-I-40

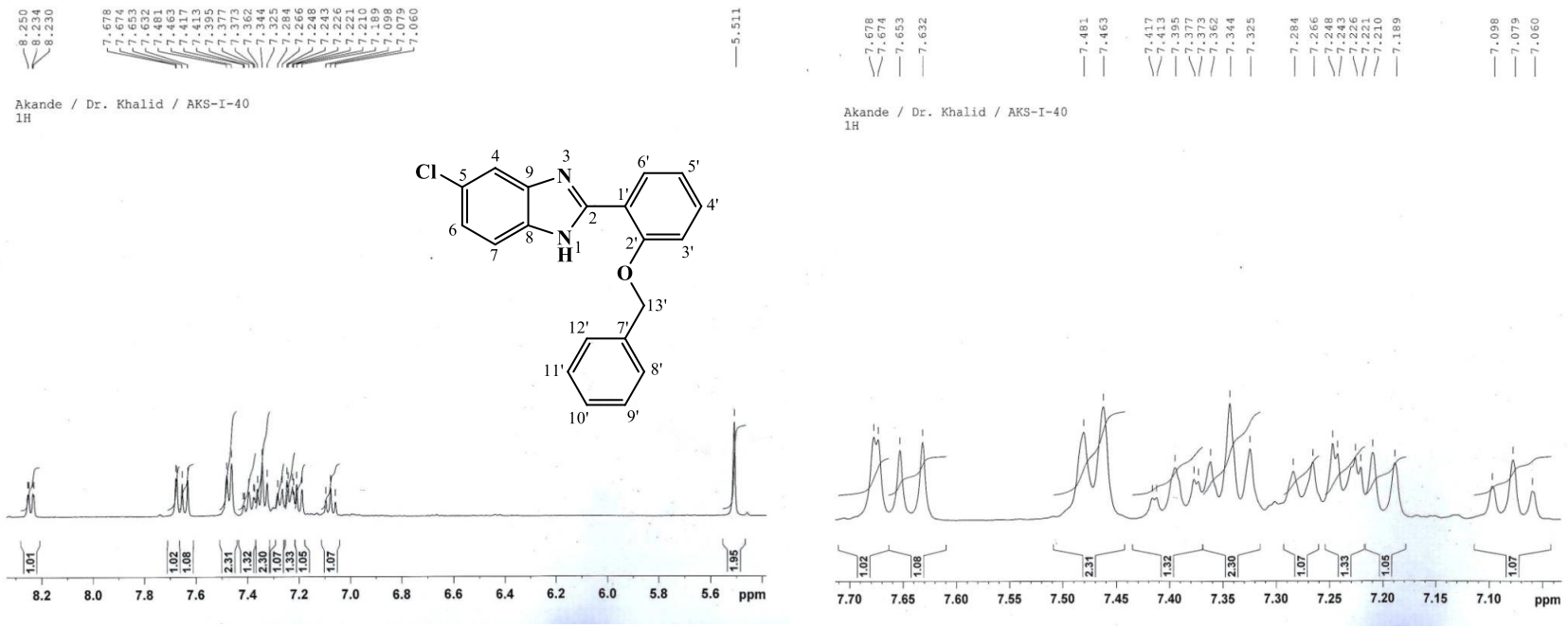

Figure 4.101. ^{1}H NMR (400 MHz, DMSO-d_6) spectra of AKS-I-40 (Expanded)

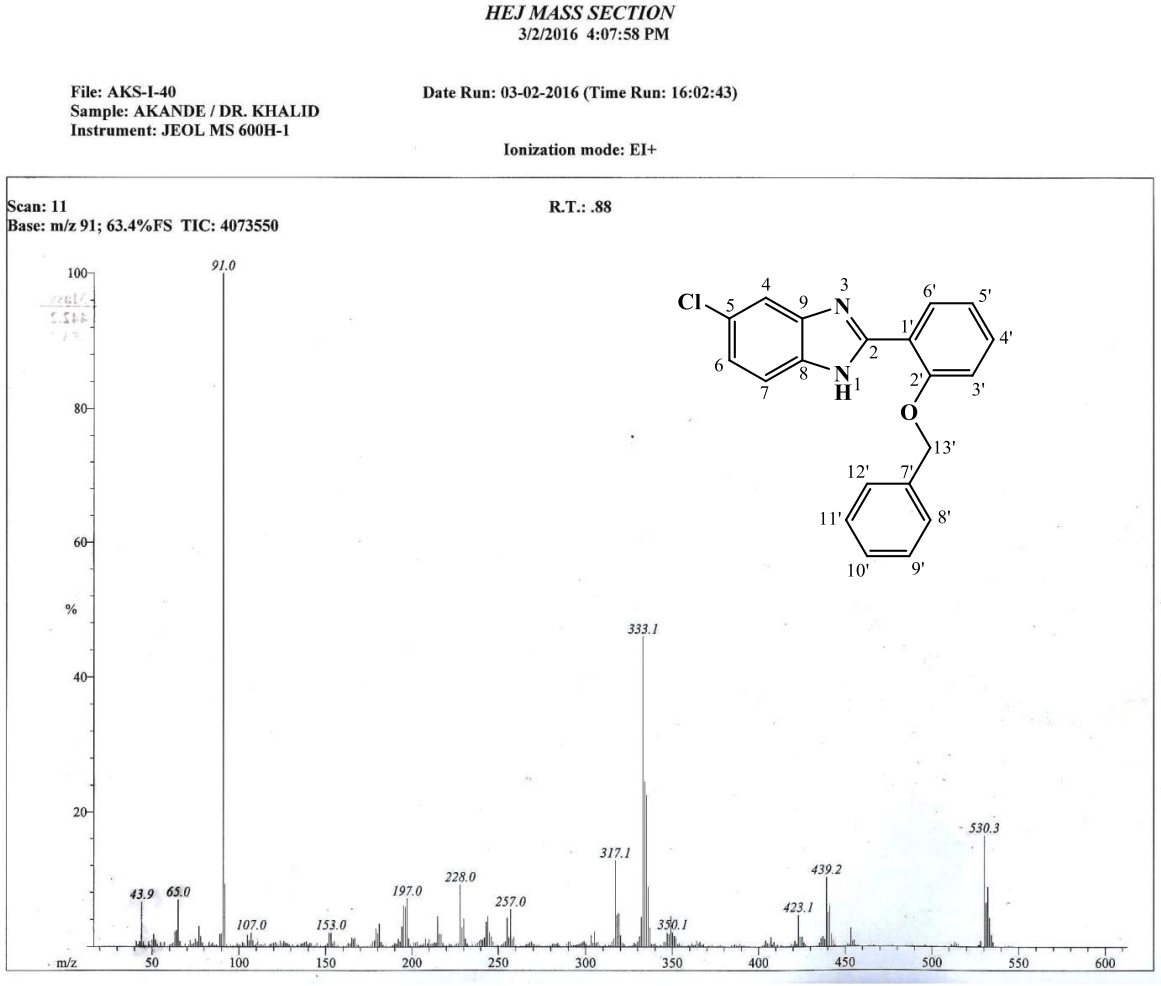

Figure 4.102. EI-MS spectrum of AKS-I-40

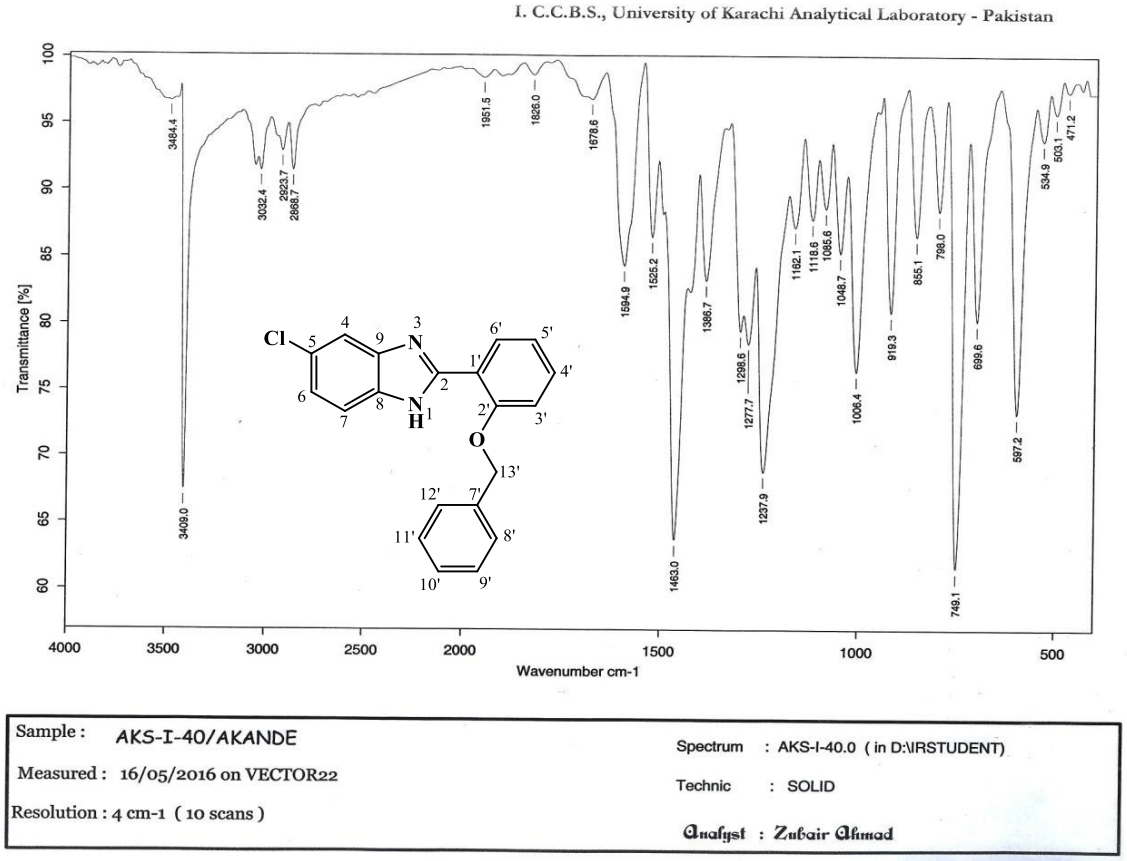

Figure 4.103. IR spectrum of AKS-I-40

THERMO ELECTRON ~ VISIONpro SOFTWARE V4.10

Operator Name	ARSHAD ALAM	Date of Report	5/20/2016
Department	Analytical laboratory#004 TWC	Time of Report	10:27:53AM
Organization	ICCBS.Karachi University.		
Information	Prof Dr. Khalid / Akande.		

Scan Graph

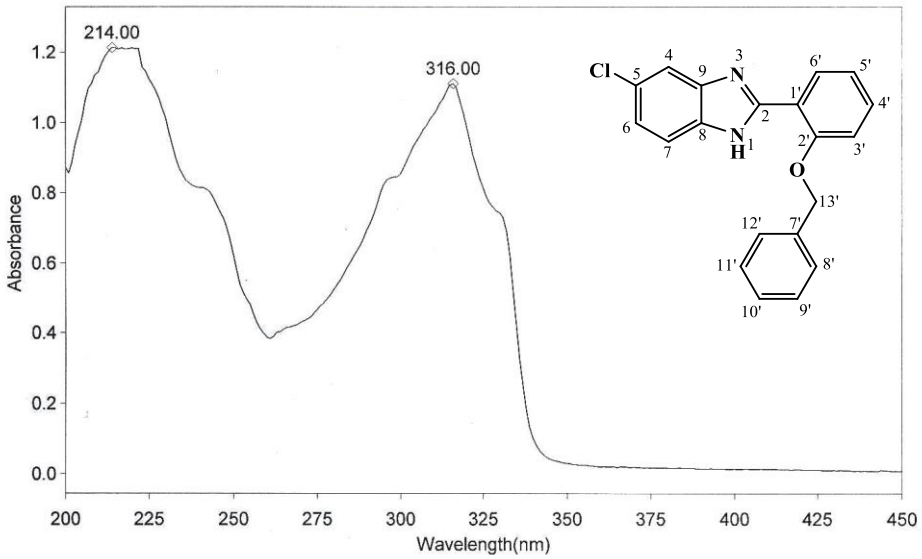

Results Table - AKS- I- 40.sre, AKS- I- 40,Cycle01

nm	A
214.00	1.214
316.00	1.110

Sensitivity	Medium

Peak Pick Method
Find 8 Peaks Above -3.0000 A
Start Wavelength 200.00 nm
Stop Wavelength 450.00 nm
Sort By Wavelength

Page 1, Scan Graph

Figure 4.104. UV spectrum of AKS-I-40

Table 4.16. Summary of the ^{1}H NMR spectra of AKS-I-40

Position	δ ^{1}H [mult., J_{HH} (Hz)] (ppm)
1	-
2	-
3	-
4	7.67 [d, $J_{4,6}$ = 1.6]
5	-
6	7.24 [dd, $J_{6,7}$ = 8.8, $J_{6,4}$ = 2.0]
7	7.65 [d, $J_{7,6}$ = 8.4]
8	-
9	-
1′	-
2′	-
3′	7.21 [d, $J_{3',4'}$ = 8.4]
4′	7.41 [dt, $J_{4',3'}$ = 8.8, $J_{4',6'}$ = 1.6]
5′	7.09 [t, $J_{5',6'}$ = 7.6]
6′	8.25 [dd, $J_{6',5'}$ = 8.0, $J_{6',4'}$ = 1.6]
7′	-
8′	7.48 [d, $J_{8',9'}$ = 7.2]
9′	7.36 [t, $J_{9',8'}$ = 7.2]
10′	7.28 [t, $J_{10',9'}$ = 7.2]
11′	7.36 [t, $J_{11',12'}$ = 7.2]
12′	7.48 [d, $J_{12',11'}$ = 7.2]
13′-OCH_2-	5.51 [s]

4.1.17 Characterisation of 2-(2′-(benzyloxy)phenyl)-5,6-dimethyl-1*H*-benzo[*d*] imidazole (AKS-I-42)

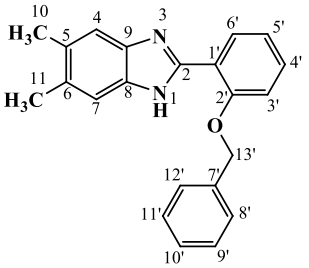

Compound 2-(2′-(benzyloxy)phenyl)-5,6-dimethyl-1*H*-benzo[*d*]imidazole (AKS-I-42) is a brown solid with a yield of 74.6% (0.245 g), a m.pt. of 130-132 ^{o}C and a R_f value of 0.63 (hexane/ethyl acetate, 1:1).

The ten resonances observed on the ^{1}H NMR spectra (400 MHz, DMSO-d_6) (figures **4.105** and **4.106**) provide chemical shift, δ (ppm) values assigned as 12.23 (1H, br s, -NH) to amine proton, 8.21 (1H, dd, $J_{6',4'}$ = 1.2 Hz, $J_{6',5'}$ = 7.6 Hz, H-6′), 7.48 (2H, d, $J_{12',11'}$ = $J_{8',9'}$ = 7.2 Hz, H-12′, H-8′), 7.39 (2H, s, H-7, H-4; chemically equivalent), 7.36 (3H, t, $J_{4',5'}$ = $J_{9',8'}$ = $J_{11',12'}$ = 7.2 Hz, H-4′, H-9′, H-11′), 7.29 (1H, t, $J_{10',11'}$ = 7.2 Hz, H-10′), 7.19 (1H, d, $J_{3',4'}$ = 8.4 Hz, H-3′), 7.08 (1H, t, $J_{5',6'}$ = 7.6 Hz, H-5′) to eleven methine protons, 5.48 (s, 2H, 13′-OCH_2-) to two methylene protons and 2.32 to six equivalent methyl protons (6H, s, 11-CH_3, 10-CH_3).

The EI-MS spectrum (figure **4.107**) reveals the most intense peak at *m/z* of 328 for the molecular ion and a [M^++1] peak at *m/z* of 329. Peak with *m/z* of 311 is suggestive of M^+-CH_3-H_2 fragment. Fragmentation at either side of C–O bond produced fragment ions with *m/z* of 237, 222 and 91. Cleavage of the imidazole ring resulted in a *m/z* of 209, corresponding to $[C_{14}H_{11}NO]^+$. Further confirming the compound, the *m/z* of 328.1579 (calculated 328.1576) was deduced from HREI-MS analysis, corresponding to the formula, $C_{22}H_{20}N_2O$.

The IR spectrum (figure **4.108**) indicated vibrational absorption frequencies $\bar{\upsilon}$ (cm^{-1}) at 3306, 3029, 2923, 2860, 1581, 1528, 1451, 1217 and 1014 assigned to N–H_{str} of amine, aromatic C–H_{str}, aliphatic C–$H_{asy\ str}$ and C–$H_{sym\ str}$, two aromatic C=C_{str}, C–H_b of CH_2, C–$O_{asy\ str}$ and C–$O_{sym\ str}$ of ether respectively. Figure **4.109** represents the UV spectrum showing wavelenghts of maximum absorptions (λ_{max}) at 316, 312, 229 and 222 nm corresponding to n→π* and π→π* transitions. Summary of the ^{1}H NMR spectra is represented in table **4.17**.

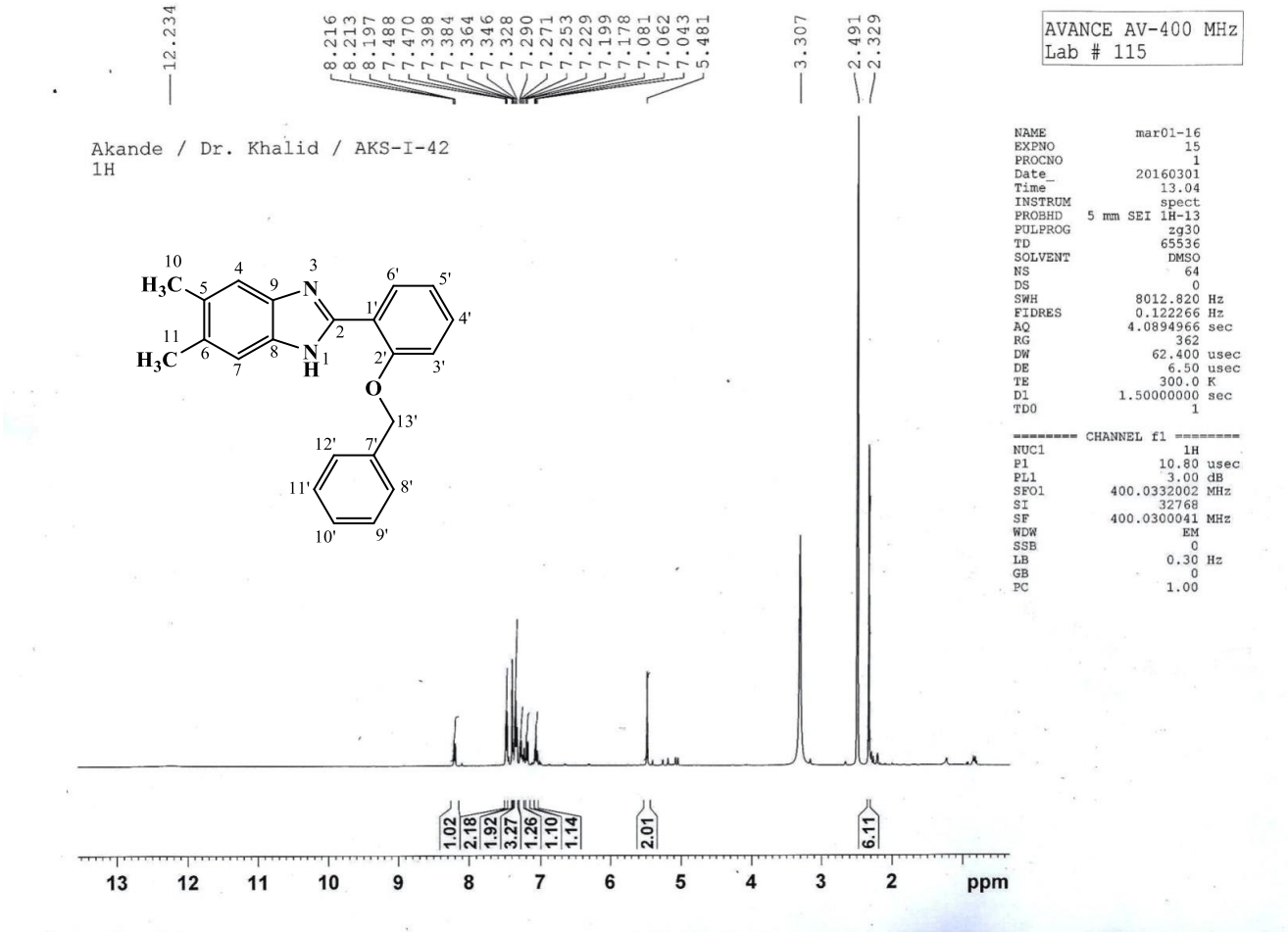

Figure 4.105. ^{1}H NMR (400 MHz, DMSO-d_6) spectrum of AKS-I-42

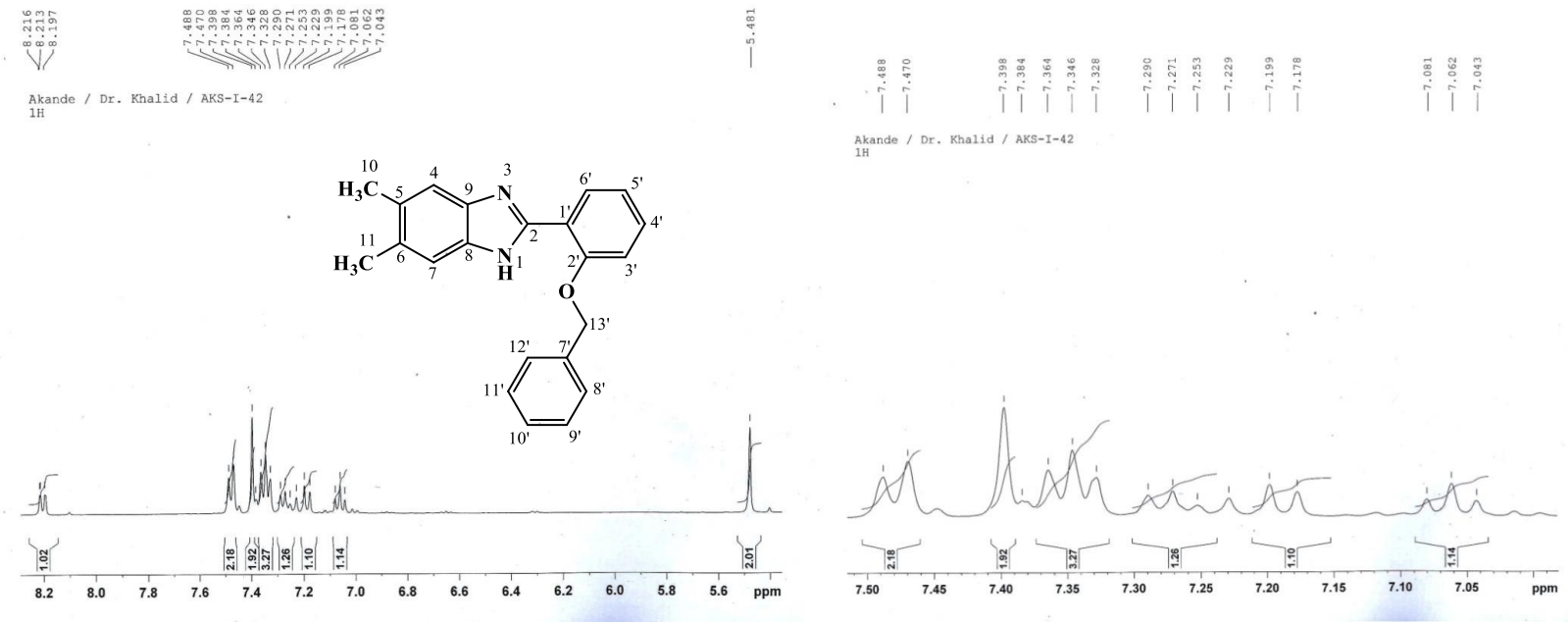

Figure 4.106. ^{1}H NMR (400 MHz, DMSO-d_6) spectra of AKS-I-42 (Expanded)

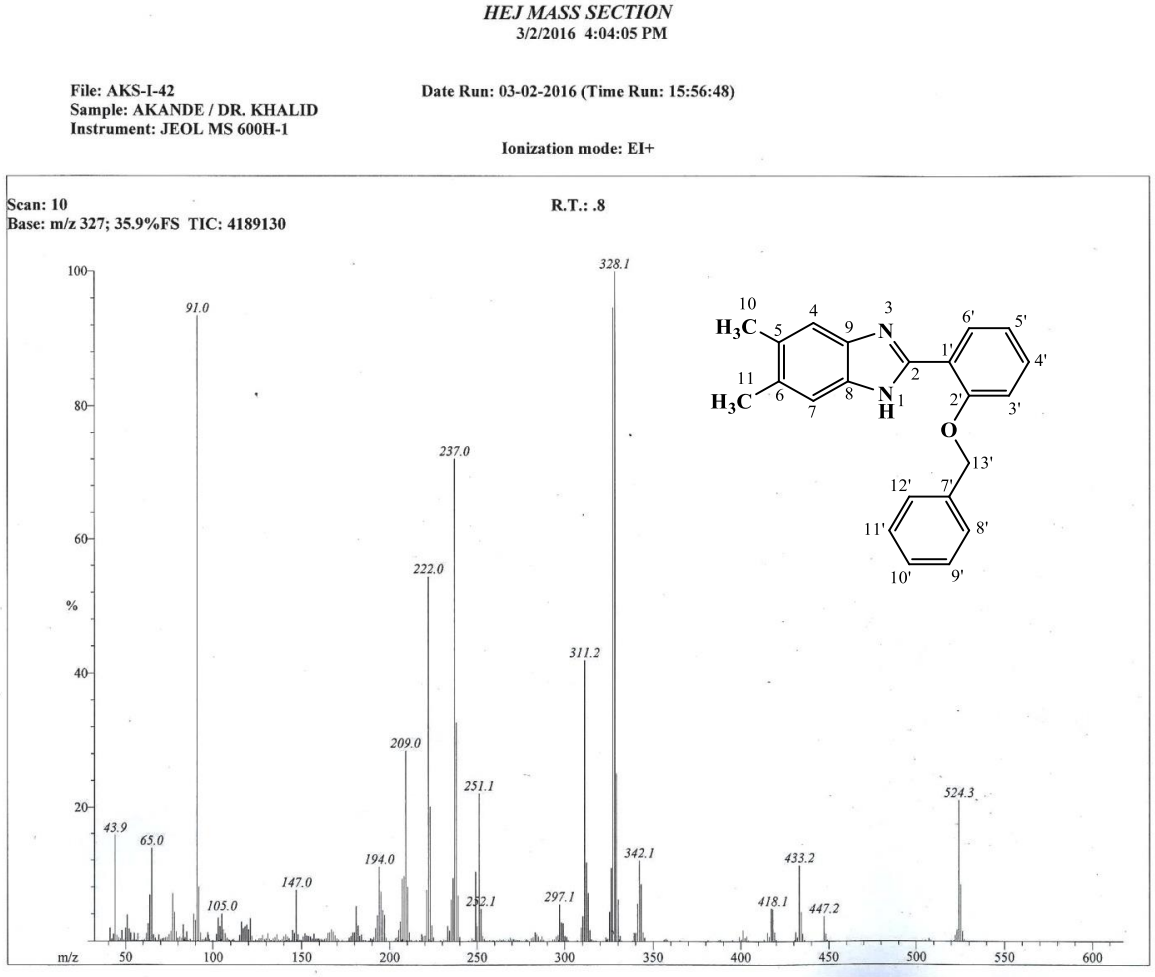

Figure 4.107. EI-MS spectrum of AKS-I-42

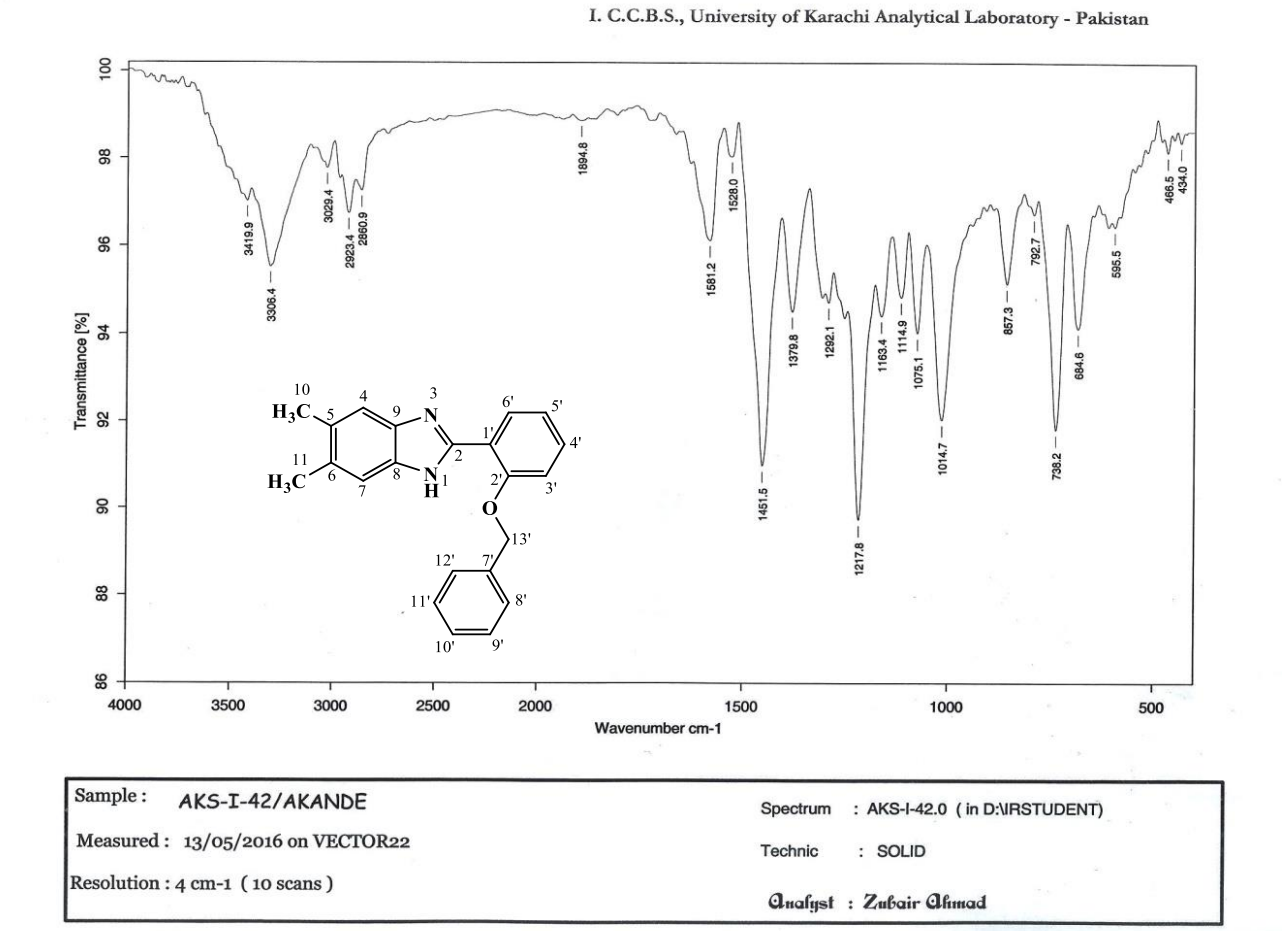

Figure 4.108. IR spectrum of AKS-I-42

THERMO ELECTRON ~ VISIONpro SOFTWARE V4.10

Operator Name	ARSHAD ALAM	Date of Report	5/20/2016
Department	Analytical laboratory#004 TWC	Time of Report	10:31:06AM
Organization	ICCBS.Karachi University.		
Information	Prof Dr. Khalid / Akande.		

Scan Graph

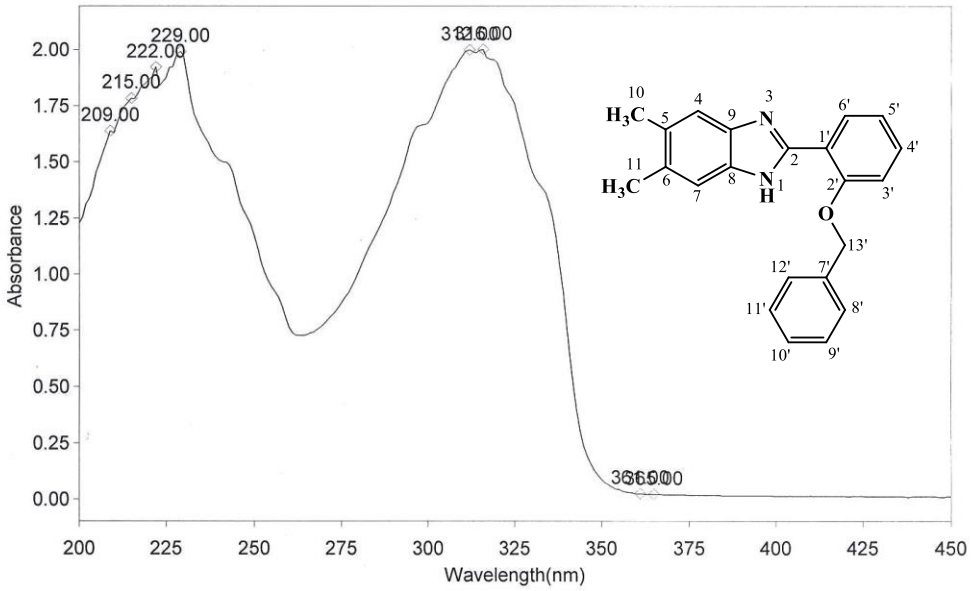

Results Table - AKS- I- 42.sre, .- I- 42,Cycle01

nm	A
209.00	1.636
215.00	1.783
222.00	1.919
229.00	1.990
312.00	1.998
316.00	2.001
361.00	0.025
365.00	0.022

Peak Pick Method

Find 8 Peaks Above -3.0000 A	
Start Wavelength 200.00 nm	
Stop Wavelength 450.00 nm	
Sort By Wavelength	
Sensitivity	Manual
Rising Points	1
Falling Points	1
Min. Change	0.0000

Page 1, Scan Graph

Figure 4.109. UV spectrum of AKS-I-42

Table 4.17. Summary of the ^{1}H NMR spectra of AKS-I-42

Position	δ ^{1}H [mult., J_{HH} (Hz)] (ppm)
1	12.23 [br s]
2	-
3	-
4	7.39 [s]
5	-
6	-
7	7.39 [s]
8	-
9	-
1′	-
2′	-
3′	7.19 [d, $J_{3',4'}$ = 8.4]
4′	7.36 [t, $J_{4',3'}$ = 7.2]
5′	7.08 [t, $J_{5',6'}$ = 7.6]
6′	8.21 [dd, $J_{6',5'}$ = 7.6, $J_{6',4'}$ = 1.2]
7′	-
8′	7.48 [d, $J_{8',9'}$ = 7.2]
9′	7.36 [t, $J_{9',8'}$ = $J_{9',10'}$ = 7.2]
10′	7.29 [t, $J_{10',11'}$ = 7.2]
11′	7.36 [t, $J_{11',10'}$ = $J_{11',12'}$ = 7.2]
12′	7.48 [d, $J_{12',11'}$ = 7.2]
13′-OCH_2-	5.48 [s]
10-CH_3	2.32 [s]
11-CH_3	2.32 [s]

4.1.18 Characterisation of 2-(3′-(benzyloxy)phenyl)-5-fluoro-1*H*-benzo[*d*] imidazole (AKS-I-43)

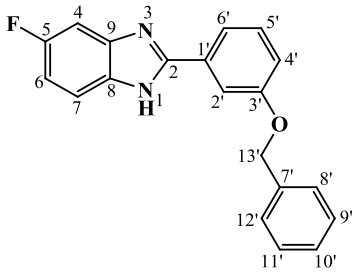

2-(3′-(Benzyloxy)phenyl)-5-fluoro-1*H*-benzo[*d*]imidazole (AKS-I-43) was obtained as a brown solid, 0.280 g (88.0% yield), a m.pt. of 201-204 ^{o}C and a R_f of 0.65 (hexane/ethyl acetate, 1:1).

Presented in figures **4.110** and **4.111** are the ^{1}H NMR (500 MHz, DMSO-d_6) spectra with eleven chemical shift, δ (ppm) values assigned to fifteen protons as follows: 13.05-13.02 (1H, br d, -NH) depicting the amine proton, 7.82 (1H, s, H-2′), 7.75 (1H, d, $J_{6',5'}$ = 7.5 Hz, H-6′), 7.58 (1H, br s, H-4), 7.50 (2H, d, = $J_{8',9'}$ = $J_{12',11'}$ 7.5 Hz, H-8′, H-12′), 7.48 (t, 1H, $J_{5',4'}$ = 8.0 Hz, H-5′), a multiplet at 7.42 (3H, m, H-11′, H-9′, H-7), 7.35 (1H, t, $J_{10',9'}$ = 7.5 Hz, H-10′), 7.15 (1H, dd, $J_{4'6'}$ = 2.0 Hz, $J_{4'5'}$ = 8.0 Hz, H-4′), 7.08 (1H, dt, $J_{6,4}$ = 2.5 Hz, $J_{6,7}$ = 8.5 Hz, H-6) depicting the twelve methine protons and 5.20 (2H, s, -OCH_2-) depicting the two methylene protons. The further splitting of the peak observed for proton at position 6 as well as broadning of peak for proton at position 4 is as a result of the ortho couplings. The doublet of doublet peak seen for proton at position 4′ is due to ortho and meta couplings with those at positions 5′ (J = 8.0 Hz) and 6′/2′ (J = 2.0 Hz) respectively.

The EI-MS spectrum (figure **4.112**) revealed the molecular ion, M^+ peak at *m/z* of 318 while the [M^++1] peak is at *m/z* 319. Cleavage of the α bond to oxygen produced *m/z* 228 and a prominent base peak at *m/z* 91, corresponding to $[C_{13}H_8FN_2O]^{\bullet+}$ and $[C_7H_7]^+$ ions respectively. The peak often observed at *m/z* of 65 is indicative of the fragment $[C_5H_5]^+$. The *m/z* 28 is suggestive of either a $[CO]^+$ or $[CH–NH]^+$ fragment ion. HREI-MS analysis further confirmed the compound by revealing a *m/z* of 318.1185 (calculated 318.1168), corresponding to a molecular formular $C_{20}H_{15}FN_2O$.

The IR spectrum (figure **4.113**) indicated vibrational absorption frequencies $\bar{\upsilon}$ (cm^{-1}) at 3449 (N–H_{str} of amine), 3061 (aromatic C–H_{str}), 2922 (aliphatic C–$H_{asy\ str}$), 1597, 1537 (aromatic C=C_{str}), 1451 (C–H_b), 1229 (C–O_{str} of ether) and 1139 (C–F_{str}). The UV

spectrum (figure **4.114**) shows maximum absorptions (λ_{max}) at 307, 304, 299 and 222 nm indicating n→π* and π→π* transitions. The summary of ^{1}H NMR spectra is as represented in table **4.18**.

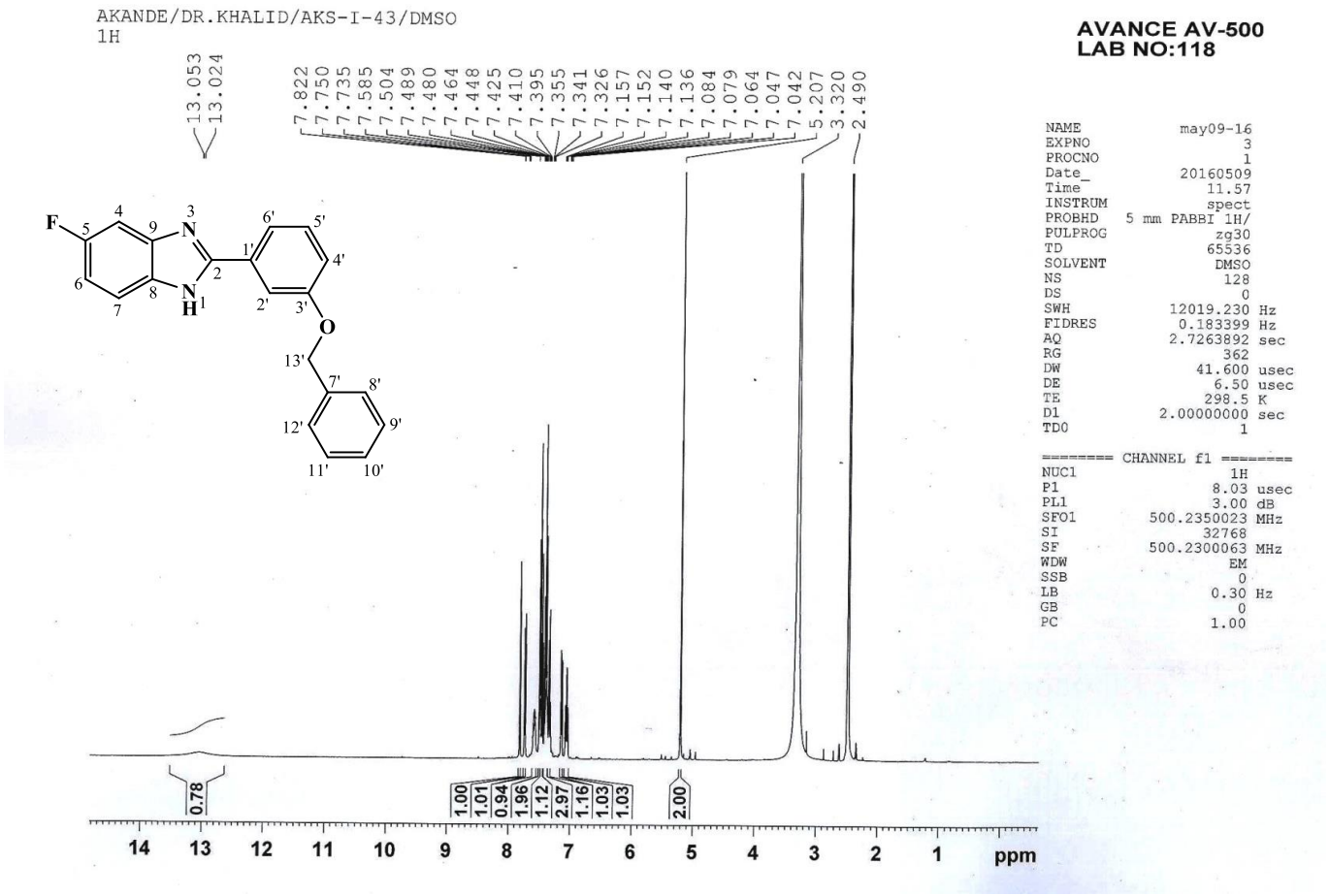

Figure 4.110. ^{1}H NMR (500 MHz, DMSO-d_6) spectrum of AKS-I-43

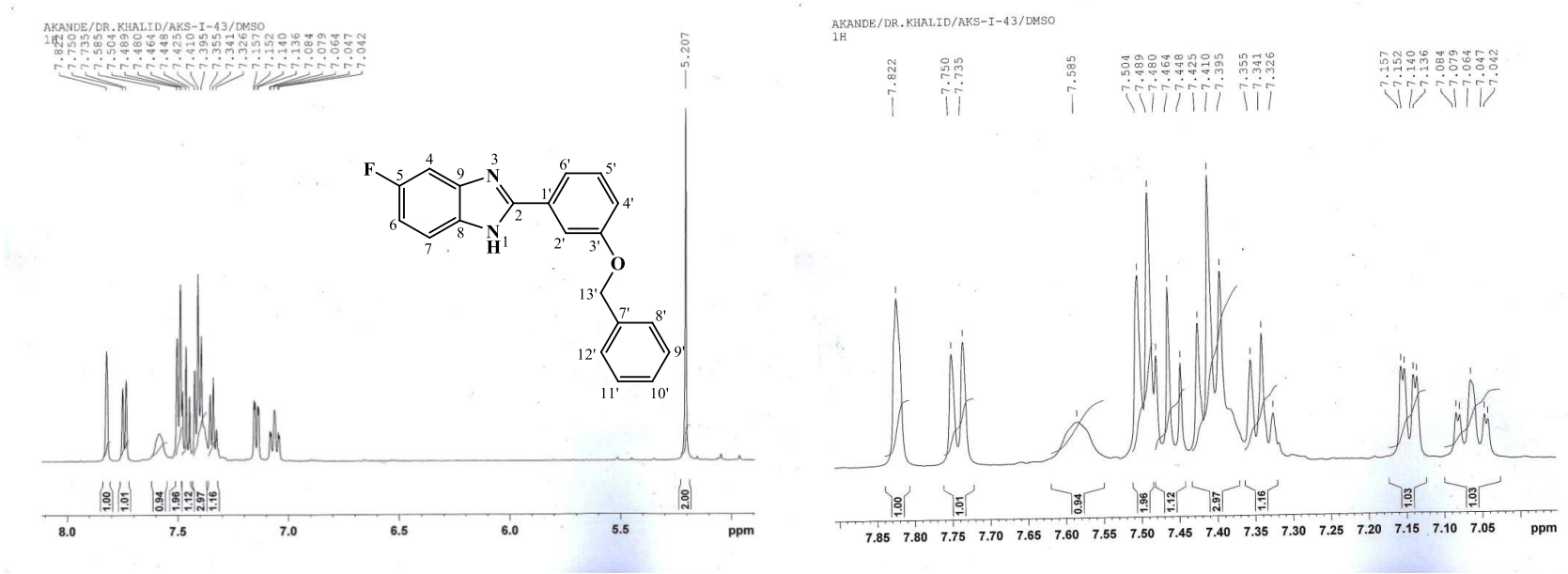

Figure 4.111. ^{1}H NMR (500 MHz, DMSO-d_6) spectra of AKS-I-43 (Expanded)

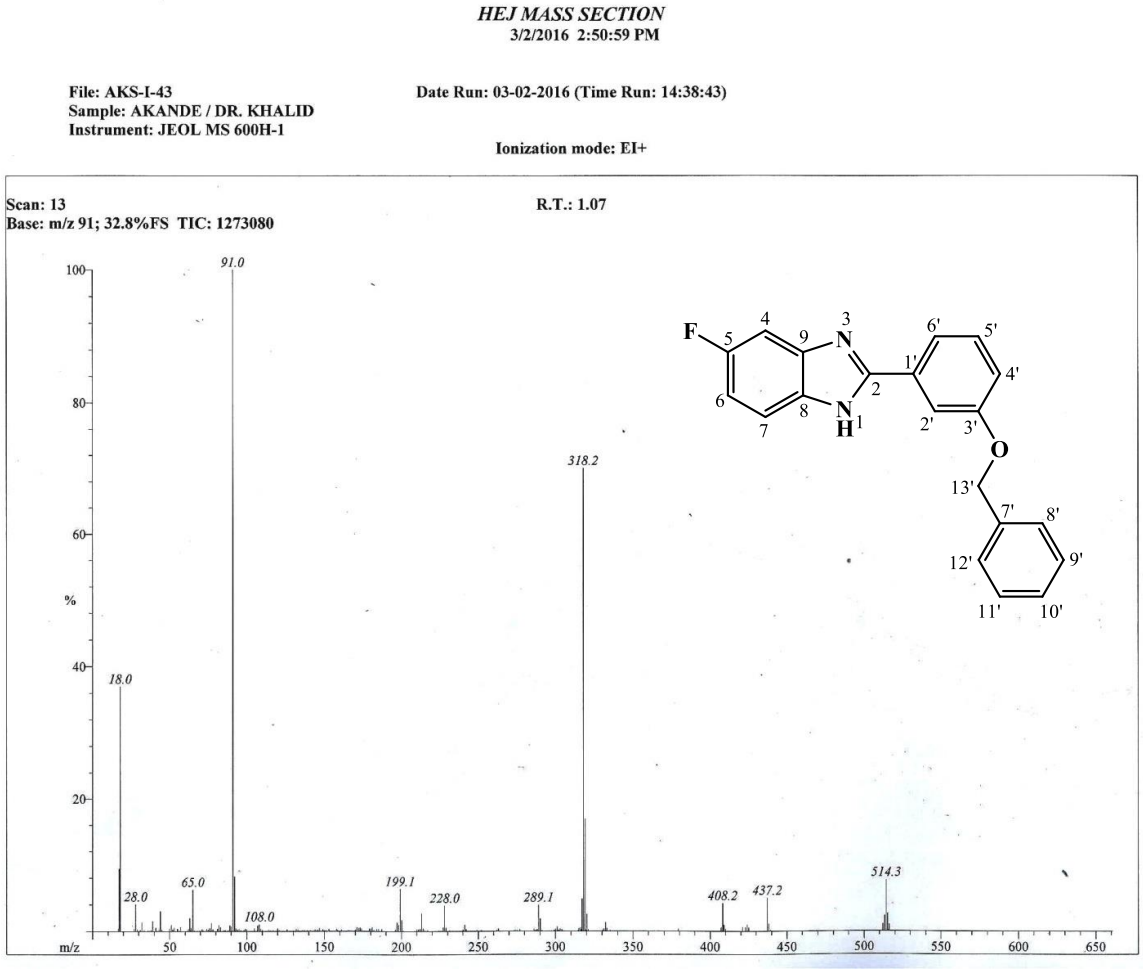

Figure 4.112. EI-MS spectrum of AKS-I-43

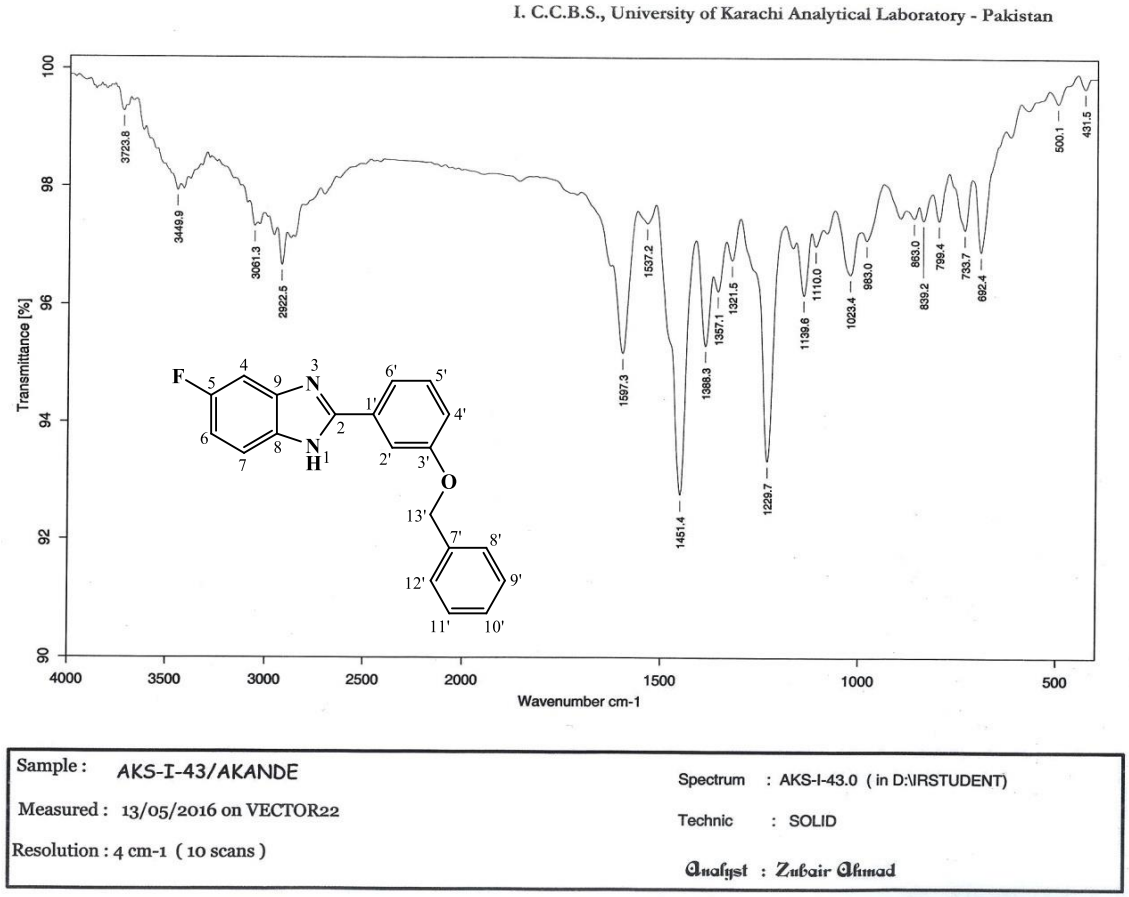

Figure 4.113. IR spectrum of AKS-I-43

THERMO ELECTRON ~ VISIONpro SOFTWARE V4.10

Operator Name	ARSHAD ALAM	Date of Report	5/20/2016
Department	Analytical laboratory#004 TWC	Time of Report	10:32:43AM
Organization	ICCBS.Karachi University.		
Information	Prof Dr. Khalid / Akande.		

Scan Graph

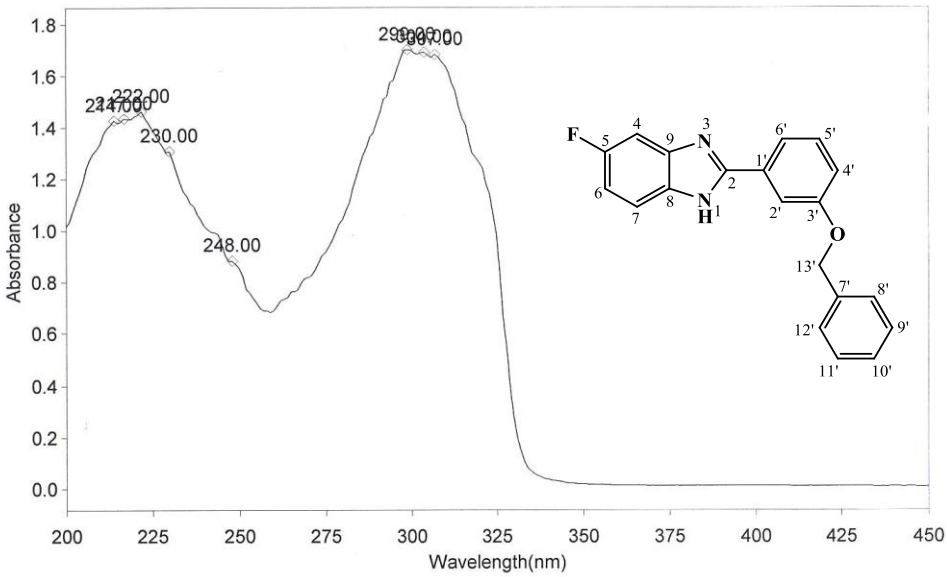

Results Table - AKS- I- 43.sre, - I- 43,Cycle01

nm	A
214.00	1.428
217.00	1.435
222.00	1.463
230.00	1.309
248.00	0.882
299.00	1.702
304.00	1.693
307.00	1.684

Peak Pick Method

Find 8 Peaks Above -3.0000 A
Start Wavelength 200.00 nm
Stop Wavelength 450.00 nm
Sort By Wavelength
Sensitivity Very High

Page 1, Scan Graph

Figure 4.114. UV spectrum of AKS-I-43

Table 4.18. Summary of the ^{1}H NMR spectra of AKS-I-43

Position	δ ^{1}H [mult., J_{HH} (Hz)] (ppm)
1	13.05 [d]
2	-
3	-
4	7.58 [br s]
5	-
6	7.08 [dt, $J_{6,7}$ = 8.5, $J_{6,4}$ = 2.5]
7	7.42-7.39 [m]
8	-
9	-
1′	-
2′	7.82 [s]
3′	-
4′	7.15 [dd, $J_{4'5'}$ = 8.0, $J_{4'6'}$ = 2.0]
5′	7.48 [t, $J_{5',4'}$ = 8.0]
6′	7.75 [d, $J_{6',5'}$ = 7.5]
7′	-
8′	7.50 [d, $J_{8',9'}$ = 7.5]
9′	7.42-7.39 [m]
10′	7.35 [t, $J_{10',9'}$ = 7.5]
11′	7.42-7.39 [m]
12′	7.50 [d, $J_{12',11'}$ = 7.5]
13′-OCH_2-	5.20 [s]

4.1.19 Characterisation of 2-(3′-(benzyloxy)phenyl)-5-chloro-1*H*-benzo[*d*] imidazole (AKS-I-44)

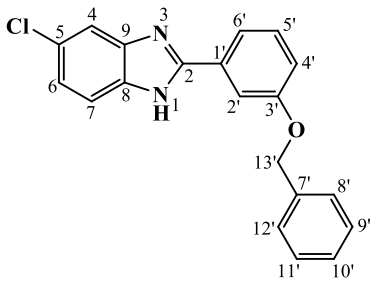

Compound 2-(3′-(benzyloxy)phenyl)-5-chloro-1*H*-benzo[*d*]imidazole (AKS-I-44) was obtained as a dark-brown solid, 0.292 g (87.2% yield), a m.pt. of 102-104 ^{o}C and R_f value of 0.66 in a hexane/ethyl acetate (1:1) solvent system.

Revealed on ^{1}H NMR spectra (400 MHz, DMSO-d_6) (Figures **4.115** and **4.116**) are ten chemical shifts, δ (ppm) of peaks from fifteen protons. They are assigned to twelve methine protons as 7.83 (1H, s, H-2′), 7.76 (1H, d, $J_{6',5'}$ = 7.6 Hz, H-6′), 7.50 (2H, d, $J_{12',11'} = J_{8',9'}$ = 7.6 Hz, H-12′, H-8′), 7.66 (1H, s, H-4), 7.62 (1H, d, $J_{7,6}$ = 8.4 Hz, H-7), 7.50 (1H, t, $J_{5',6'}$ = 7.6 Hz, H-5′), 7.42 (2H, t, $J_{11',10'} = J_{9',10'}$ = 7.6 Hz, H-11′, H-9′), 7.36 (1H, t, $J_{10',11'} = J_{10',9'}$ = 7.6 Hz, H-10′), 7.26 (1H, dd, $J_{6,7}$ = 8.4 Hz, $J_{6,4}$ = 1.6 Hz, H-6), 7.18 (1H, dd, $J_{4',5'}$ = 8.0 Hz, $J_{4',2'}$ = 1.6 Hz, H-4′), and two methylene protons as 5.21 (2H, s, -OCH_2-), while the amine proton (expected to resonate further downfield) was not captured. Protons at positions 6′ and 5′ ortho coupled with each other (J = 7.6 Hz) and in like manner, proton 4′ exhibited ortho coupling with proton 5′ (J = 8.0 Hz) and on the other hand coupled with proton 6′ (J = 1.6 Hz) on meta position. The signal at δ_H 7.50 are overlapping peaks of two protons that are doublets and a proton that is a triplet.

The EI-MS spectrum (figure **4.117**) produced a molecular ion, M^+ peak and a [M^++2] isotope peak are at *m/z* at 334 and 336 respectively. Peaks at *m/z* 244 and 91 (base peak) are due to α–bond cleavages of ether corresponding to $[C_{13}H_9ClN_2O]^{\bullet+}$ and $[C_7H_7]^+$ respectively,. The elimination of CHO$^{\bullet}$ from *m/z* of 244 is suggestive of the fragment at *m/z* 215 which corresponds to $[C_{12}H_8ClN_2]^+$. The *m/z* of 65 is indicative of $[C_5H_5]^+$ ion. The molecular formula, $C_{20}H_{15}ClN_2O$, matches the *m/z* of 334.0895 (calculated 334.0873) from HREI-MS analysis, further confirming the compound.

The IR spectrum (figure **4.118**) shows absorption frequencies, $\bar{\upsilon}$ (cm^{-1}) such as 3418, 3063, 2921, 2866, 1658, 1591, 1484, 1453, 1224 and 1024 corresponding to N–H_{str} of 2^{o} amine, aromatic C–H_{str}, aliphatic C–$H_{asy\ str}$ and C–$H_{sym\ str}$, C=N_{str}, aromatic C=C_{str}, C–

H_b of CH_2, asymmetric and symmetric C–O_{str} of ether respectively. Figure **4.119** presents the wavelenghts of maximum absorptions, (λ_{max}) from UV analysis at 310 and 222 nm corresponding to n→π* and π→π* transitions. The summary of ^{1}H NMR spectra is represented in table **4.19**.

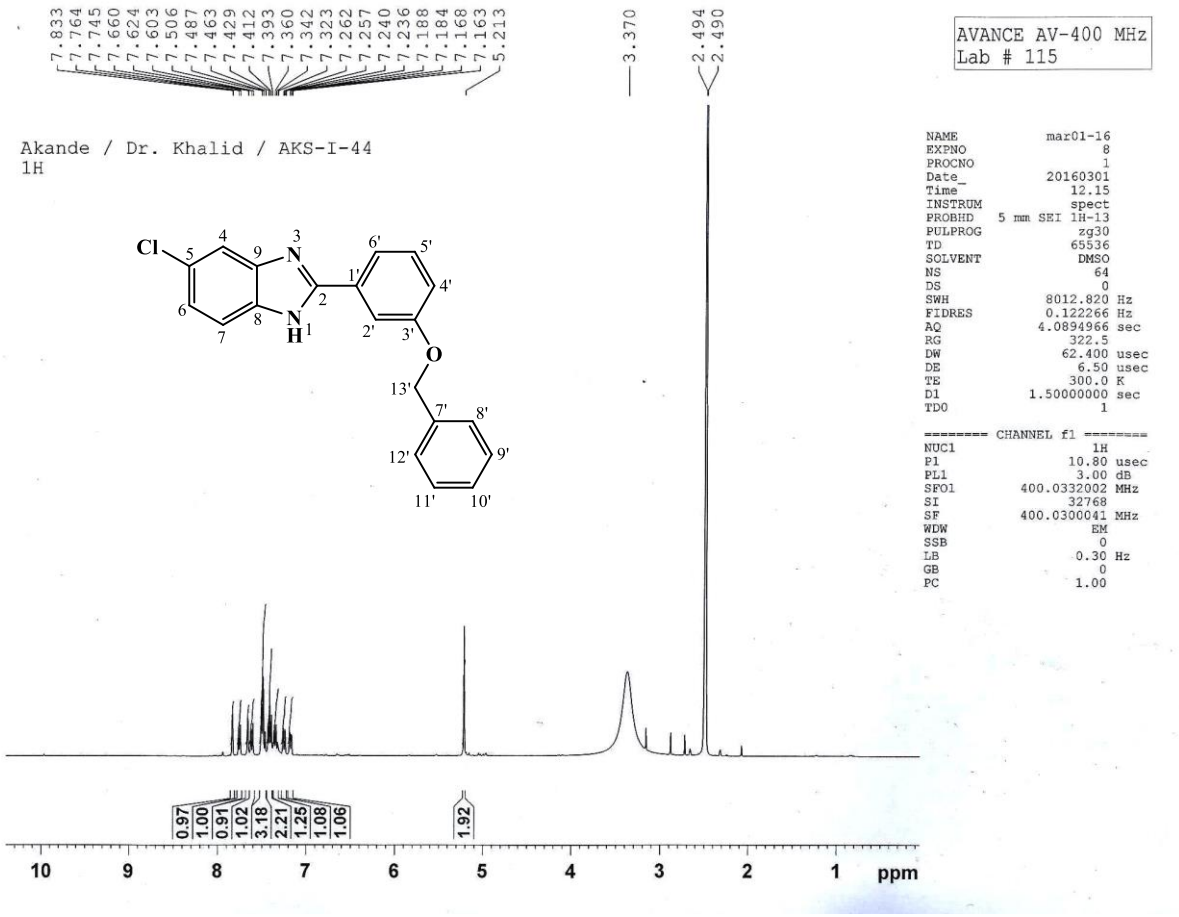

Figure 4.115. ^{1}H NMR (400 MHz, DMSO-d_6) spectrum of AKS-I-44

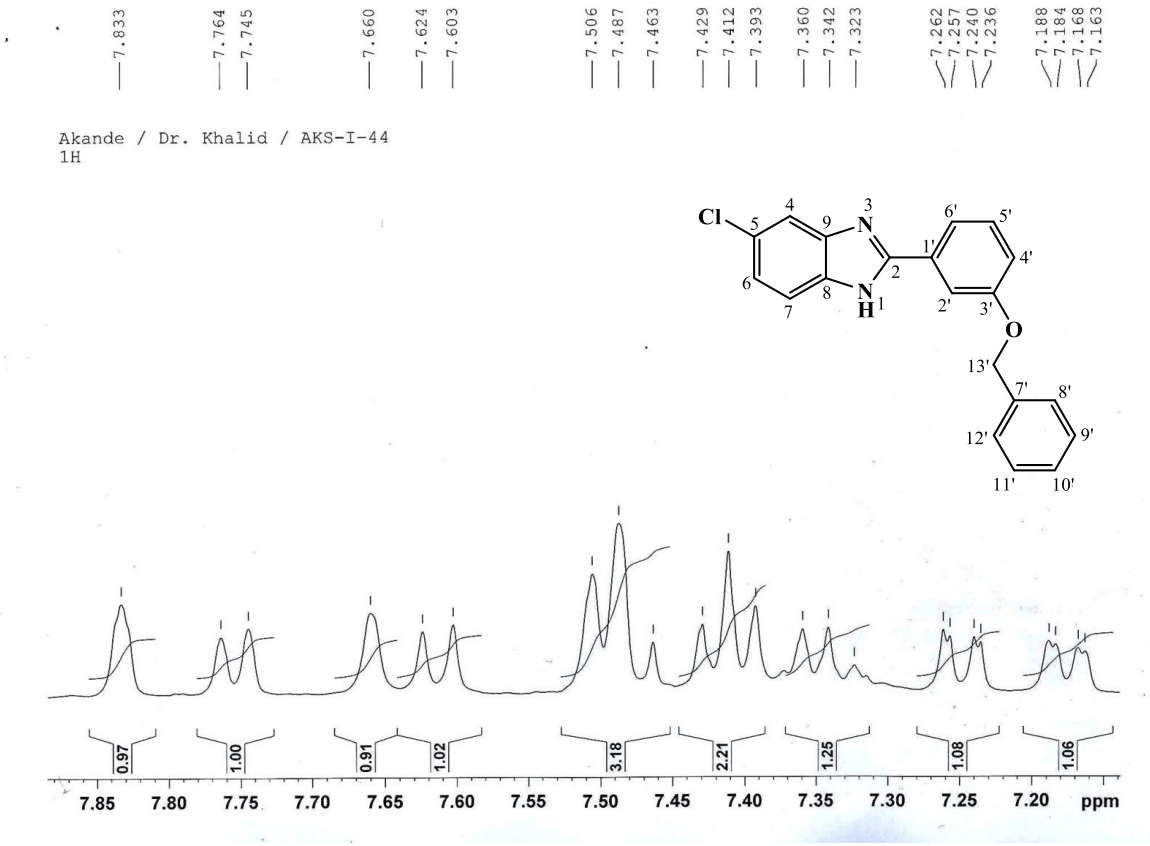

Figure 4.116. ^{1}H NMR (400 MHz, DMSO-d_6) spectrum of AKS-I-44 aromatic region (Expanded)

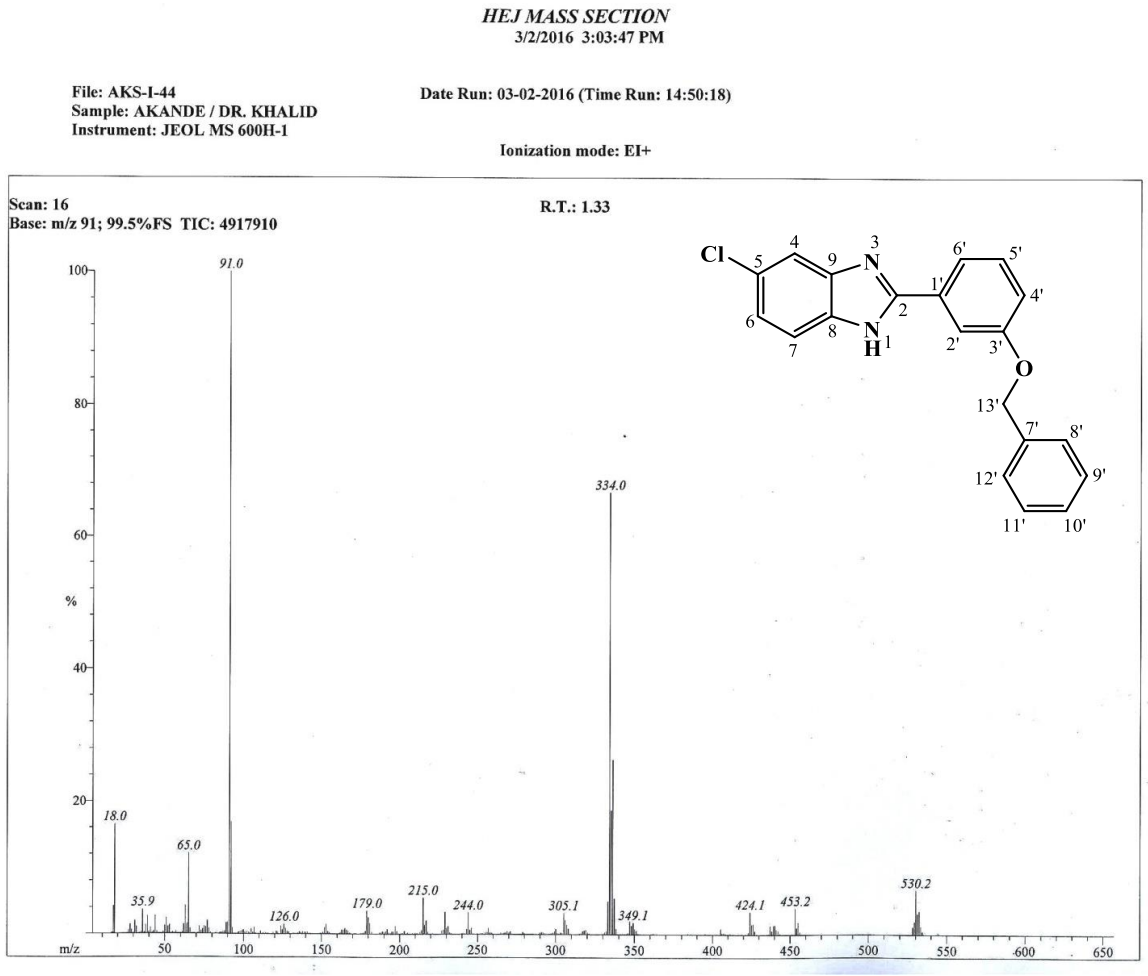

Figure 4.117. EI-MS spectrum of AKS-I-44

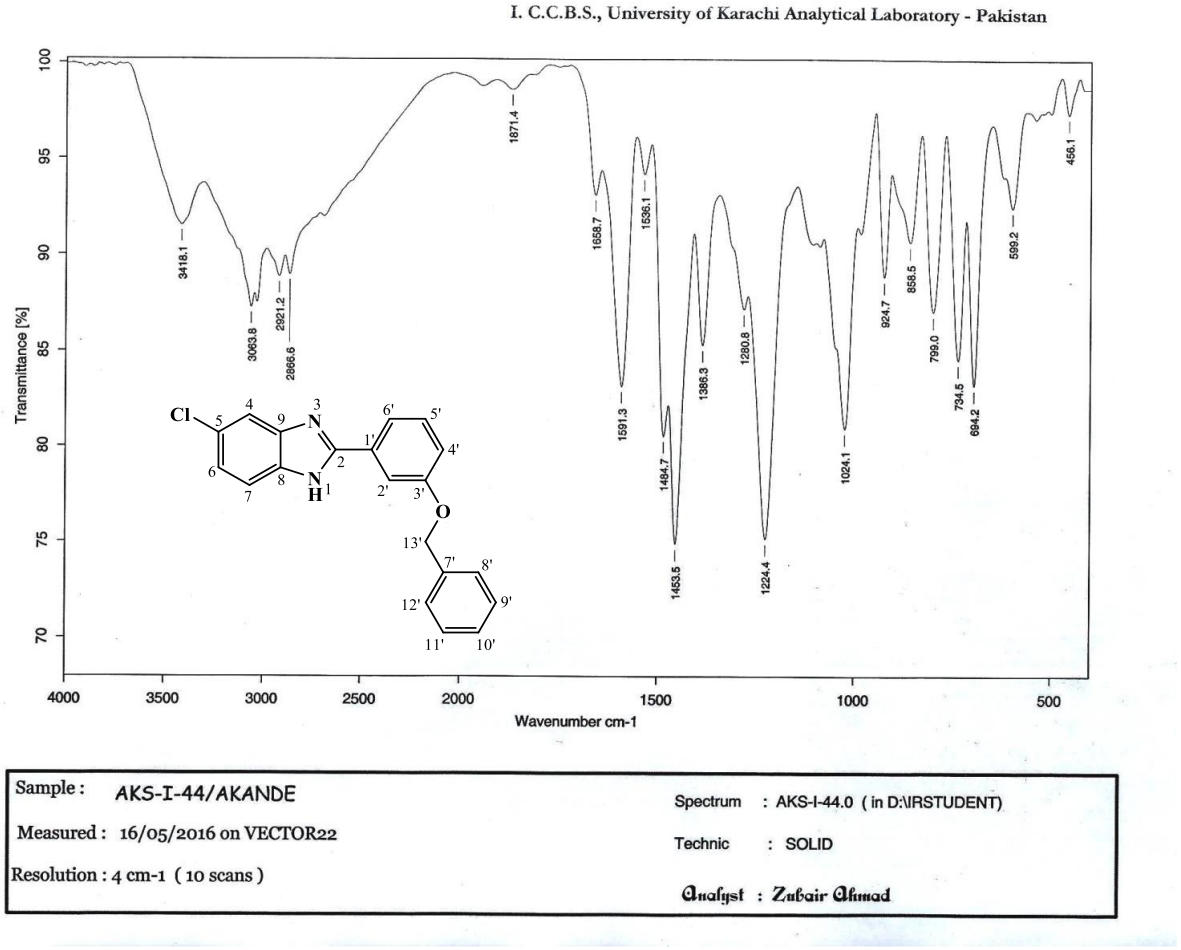

Figure 4.118. IR spectrum of AKS-I-44

THERMO ELECTRON ~ VISIONpro SOFTWARE V4.10

Operator Name	ARSHAD ALAM	Date of Report	5/20/2016
Department	Analytical laboratory#004 TWC	Time of Report	10:34:19AM
Organization	ICCBS.Karachi University.		
Information	Prof Dr. Khalid / Akande.		

Scan Graph

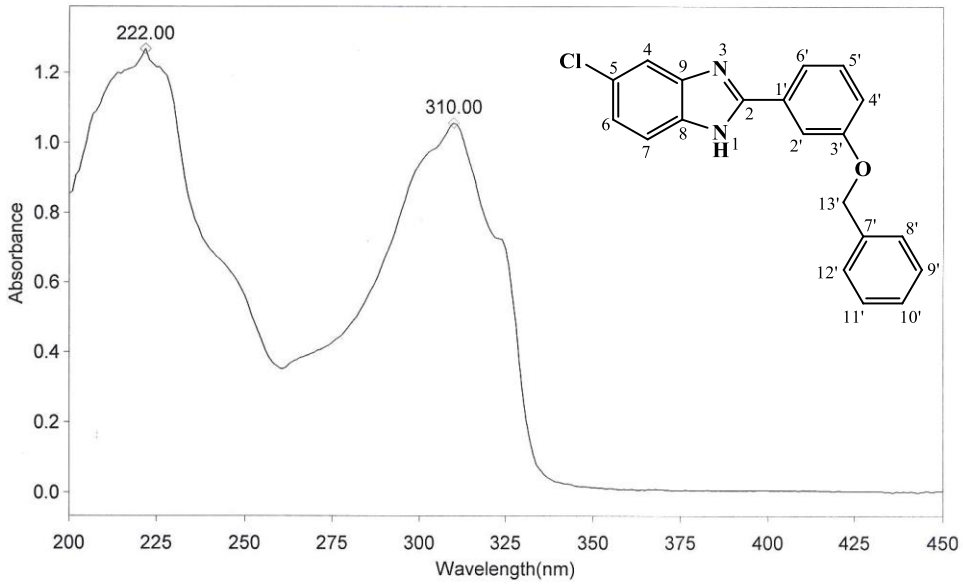

Results Table - AKS- I- 44.sre, AKS- I- 44,Cycle01

nm	A	**Peak Pick Method**
222.00	1.269	Find 8 Peaks Above -3.0000 A
310.00	1.056	Start Wavelength 200.00 nm
		Stop Wavelength 450.00 nm
		Sort By Wavelength
Sensitivity	Very Low	

Page 1, Scan Graph

Figure 4.119. UV spectrum of AKS-I-44

Table 4.19. Summary of the ^{1}H NMR spectra of AKS-I-44

Position	δ ^{1}H [mult., J_{HH} (Hz)] (ppm)
1	-
2	-
3	-
4	7.66 [s]
5	-
6	7.26 [dd, $J_{6,7}$ = 8.4, $J_{6,4}$ = 1.6]
7	7.62 [d, $J_{7,6}$ = 8.4]
8	-
9	-
1′	-
2′	7.83 [s]
3′	-
4′	7.18 [dd, $J_{4',5'}$ = 8.0, $J_{4',2'}$ = 1.6]
5′	7.50 [t, $J_{5',6'}$ = 7.6]
6′	7.76 [d, $J_{6',5'}$ = 7.6]
7′	-
8′	7.50 [d, $J_{8',9'}$ = 7.6]
9′	7.42 [t, $J_{9',8'}$ = $J_{9',10'}$ = 7.6]
10′	7.36 [t, $J_{10',9'}$ = $J_{10',11'}$ = 7.6]
11′	7.42 [t, $J_{11',10'}$ = $J_{11',12'}$ = 7.6]
12′	7.50 [d, 2H, $J_{12',11'}$ = 7.6]
13′-OCH_2-	5.21[s]

4.1.20 Characterisation of 2-(4′-(benzyloxy)phenyl)-5-fluoro-1*H*-benzo[*d*] imidazole (AKS-I-45)

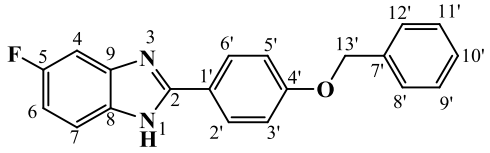

The brown compound, AKS-I-45 is a solid with a yield of 93.9% (0.299 g), a m.pt. 223-226 ^{o}C and a R_f of 0.60 (hexane/ethyl acetate, 1:1).

Eight proton signals were obtained in δ (ppm) units from ^{1}H NMR spectra (400 MHz, DMSO-d_6) (figures **4.120** and **4.121**) and assigned to fourteen protons as 8.09 (2H, d, $J_{6',5'} = J_{2',3'}$ = 8.8 Hz, H-6′, H-2′), 7.57-7.54 (1H, m, H-4), 7.48 (2H, d, $J_{12',11'} = J_{8',9'}$ = 7.2 Hz, H-12′, H-8′), 7.42 (2H, t, $J_{11',12'} = J_{9',8'}$ = 7.2 Hz, H-11′, H-9′), 7.38-7.32 (2H, m, H-10′, H-7), 7.21 (2H, d, $J_{3',2'} = J_{5',6'}$ = 8.8 Hz, H-3′, H-5′), 7.08 (1H, dt, $J_{6,7}$ = 9.6 Hz, $J_{6,4}$ = 2.0 Hz, H-6) representing the twelve methine protons, and 5.19 (2H, s, 13′-OCH_2-) representing the two methylene protons. The amine proton was not capture. The influence of fluorine was also characteristic of the splitting patterns exhibited by protons on positions 4 (multiplet) and 6 (doublet of triplet).

EI-MS spectrum (figure **4.122**) shows *m/z* of the molecular ion, M^+ peak and a $[M^+ + 1]$ peak at 318 and 319. The *m/z* 227 and 91 (base peak) resulted from an α–bond cleavage of ether corresponding to $[C_{13}H_8FN_2O]^+$ and $[C_7H_7]^+$ respectively. The *m/z* of 65 corresponds to $[C_5H_5]^+$ fragment ion. The fragment, *m/z* 227 $[C_{13}H_8FN_2O]^+$ further cleaves to give a *m/z* of 197 $[C_{13}H_6FN_2]^+$ by eliminating CH_2=O. Further confirming the compound from HREI-MS analysis, the *m/z* of 318.1161 (calculated 318.1168) was found corresponding to the molecular formula $C_{20}H_{15}FN_2O$.

From IR spectrum (figure **4.123**), the frequencies of vibration, $\bar{\upsilon}$ (cm^{-1}) of bonds assignable to some functional groups are 3419, 3063, 2928, 2877, 1609, 1500, 1442, 1251 and 1141 corresponding to N–H_{str} of amine, aromatic C–H_{str}, asymmetric and symmetric aliphatic C–H_{str}, aromatic C=C_{str}, aliphatic C–H_b of CH_2, C–$O_{asy\ str}$ of ether and C–F_{str} respectively. The UV spectrum (figure **4.124**) shows maximum absorptions (λ_{max}) at 310, 299, 249 and 214 nm resulting from n→π* and π→π* transitions. The ^{1}H NMR spectra data is summerised in table **4.20**.

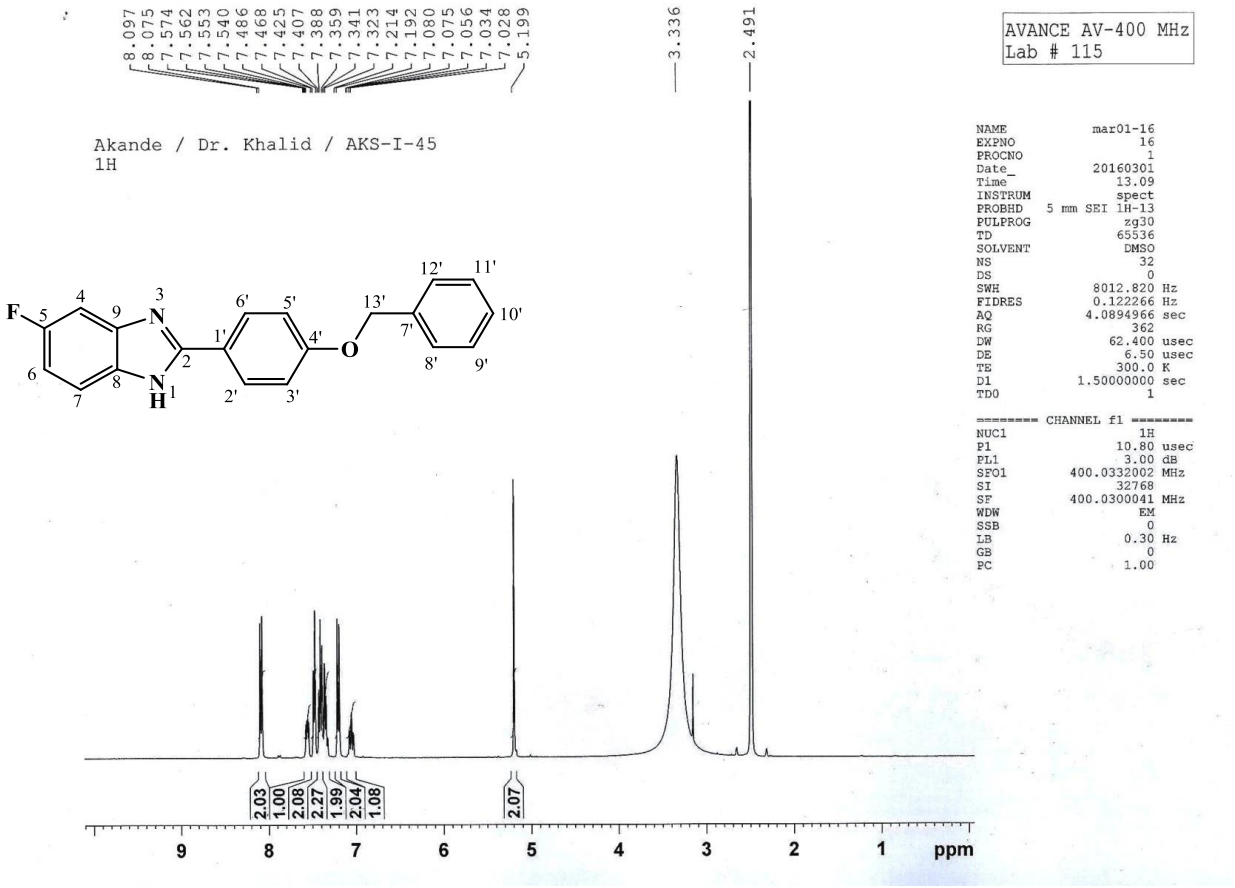

Figure 4.120. ^{1}H NMR (400 MHz, DMSO-d_6) spectrum of AKS-I-45

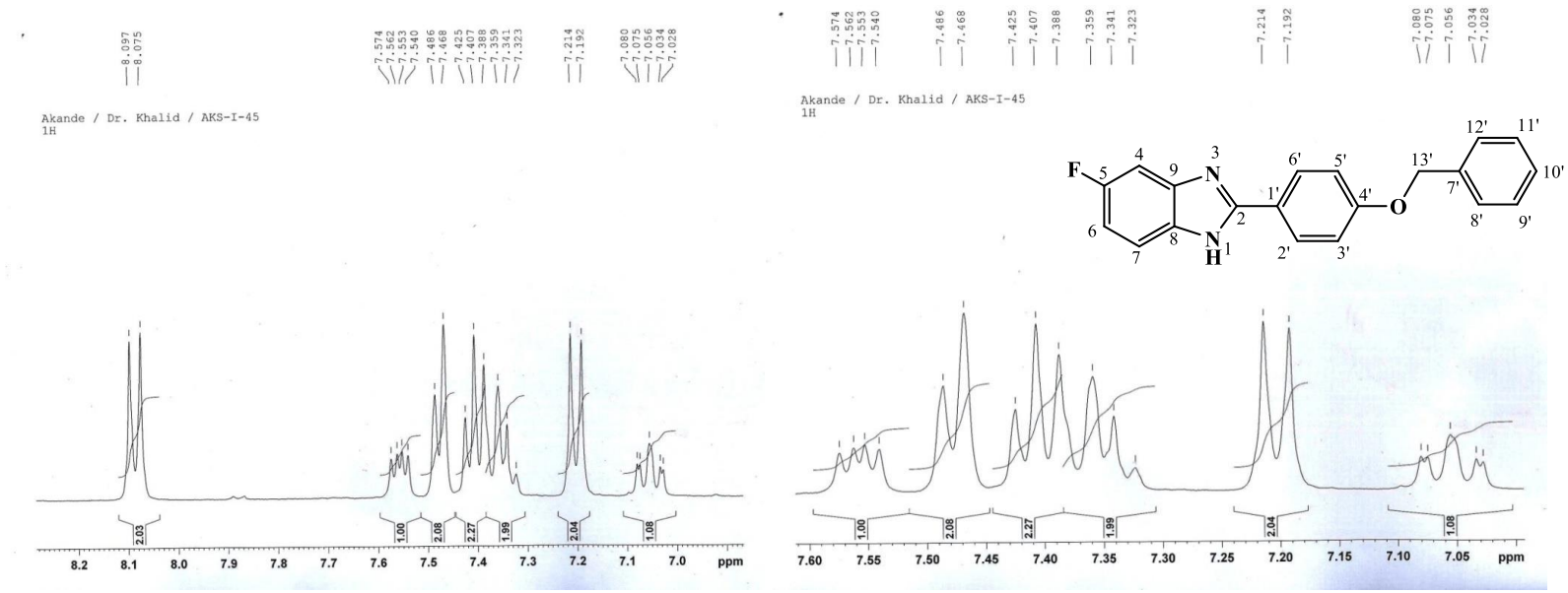

Figure 4.121. ^{1}H NMR (400 MHz, DMSO-d_6) spectra of AKS-I-45 aromatic region (Expanded)

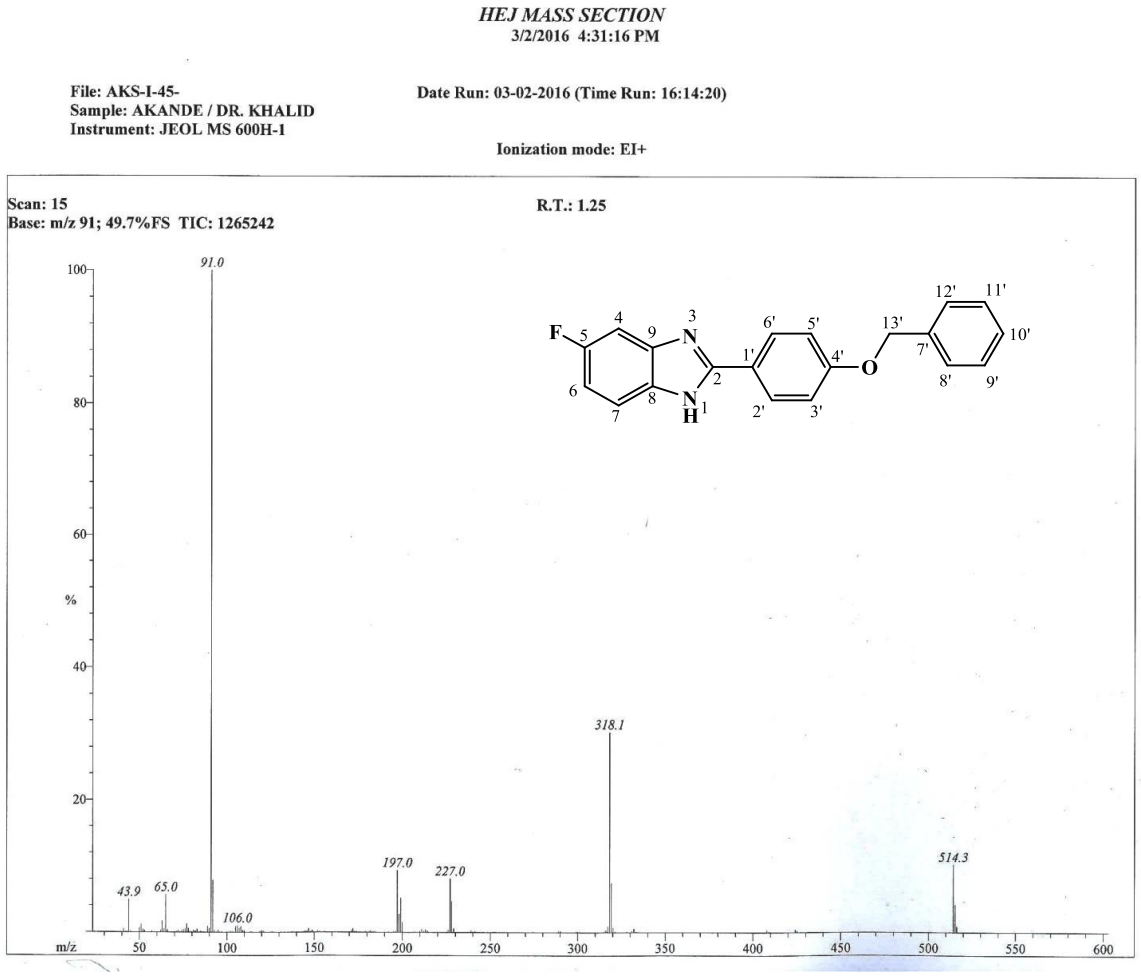

Figure 4.122. EI-MS spectrum of AKS-I-45

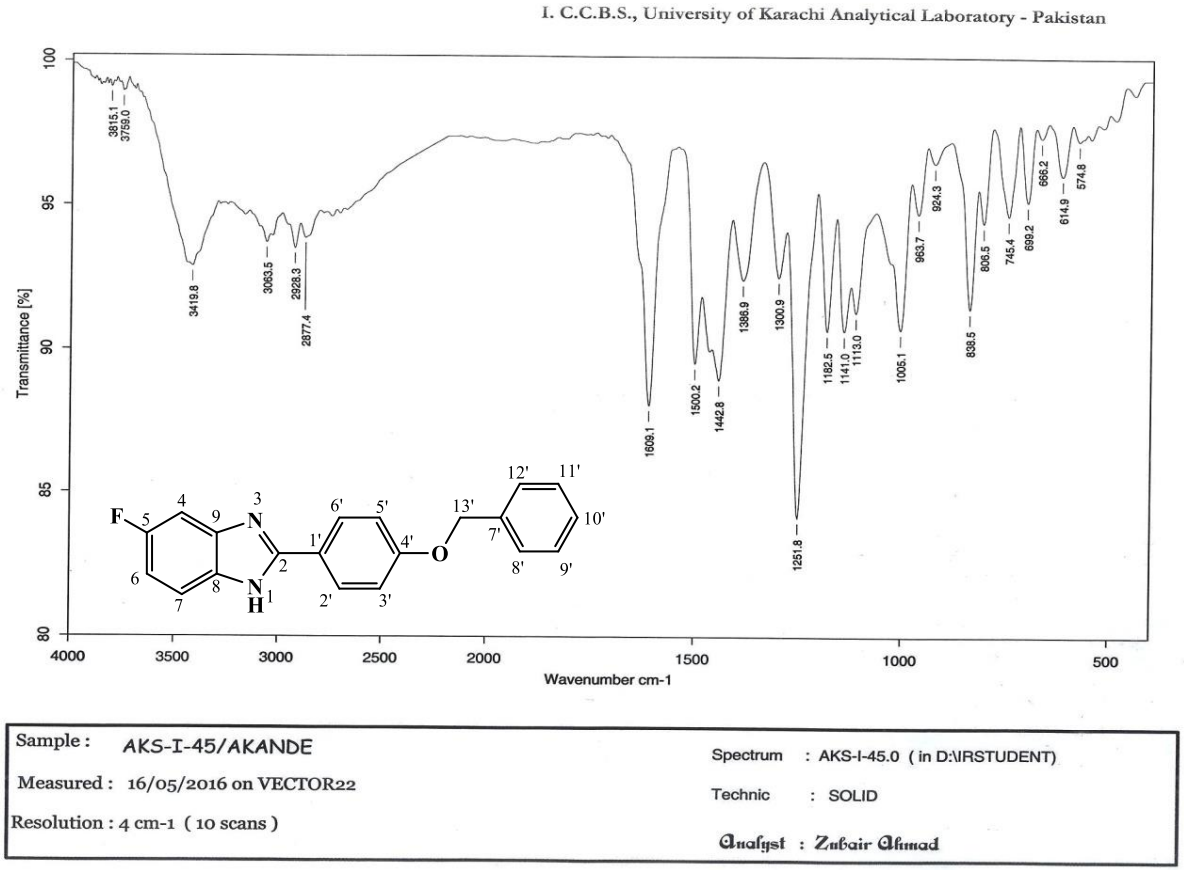

Figure 4.123. IR spectrum of AKS-I-45

THERMO ELECTRON ~ VISIONpro SOFTWARE V4.10

Operator Name	ARSHAD ALAM	Date of Report	5/20/2016
Department	Analytical laboratory#004 TWC	Time of Report	10:35:37AM
Organization	ICCBS.Karachi University.		
Information	Prof Dr. Khalid / Akande.		

Scan Graph

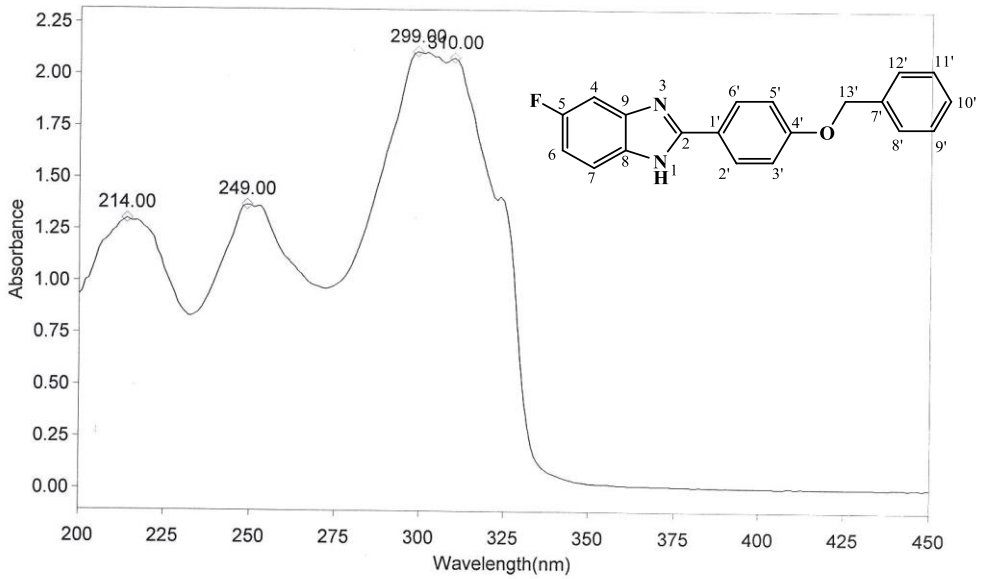

Results Table - ASK- I- 45.sre, - I- 45,Cycle01

nm	A	**Peak Pick Method**
214.00	1.304	Find 8 Peaks Above -3.0000 A
249.00	1.370	Start Wavelength 200.00 nm
299.00	2.114	Stop Wavelength 450.00 nm
310.00	2.084	Sort By Wavelength
Sensitivity	Low	

Page 1, Scan Graph

Figure 4.124. UV spectrum of AKS-I-45

Table 4.20. Summary of the ^{1}H NMR spectra of AKS-I-45

Position	δ ^{1}H [mult., J_{HH} (Hz)] (ppm)
1	-
2	-
3	-
4	7.57-7.54 [m]
5	-
6	7.08 [dt, $J_{6,7}$ = 9.6, $J_{6,4}$ = 2.0]
7	7.38-7.32 [m]
8	-
9	-
1′	-
2′	8.09 [d, $J_{2',3'}$ = 8.8]
3′	7.21 [d, $J_{3',2'}$ = 8.8]
4′	-
5′	7.21 [d, $J_{5',6'}$ = 8.8]
6′	8.09 [d, $J_{6',5'}$ =8.8]
7′	-
8′	7.48 [d, $J_{8',9'}$ = 7.2]
9′	7.42 [t, $J_{9',8'}$ = 7.2]
10′	7.38-7.32 [m]
11′	7.42 [t, $J_{11',12'}$ = 7.2]
12′	7.48 [d, $J_{12',11'}$ = 7.2]
13′-OCH_2-	5.19 [s]

4.1.21 Characterisation of 2-(4′-(benzyloxy)phenyl)-5,6-dimethyl-1*H*-benzo[*d*] imidazole (AKS-I-46)

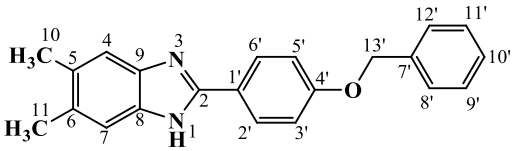

Compound 2-(4′-(benzyloxy)phenyl)-5,6-dimethyl-1*H*-benzo[*d*]imidazole (AKS-I-46) was obtained as a white solid, 0.311 g (94.7% yield), m.pt. 251-253 ^{o}C and R_f of 0.46 (hexane/ethyl acetate, 1:1).

Figures **4.125** and **4.126** show the proton signals obtained from ^{1}H NMR analysis (400 MHz, DMSO-d_6) in δ (ppm) units, and are assigned as 8.08 (2H, d, $J_{6',5'} = J_{2',3'} = 8.8$ Hz, H-6′, H-2′), 7.48 (2H, d, $J_{12',11'} = J_{8',9'} = 7.2$ Hz, H-12′, H-8′), 7.42 (2H, t, $J_{11',12'} = J_{9',8'} = 7.2$ Hz, H-11′, H-9′), 7.37-7.34 (3H, m, H-10′, H-7, H-4), 7.22 (2H, d $J_{5',6'} = J_{3',2'} = 8.8$ Hz, H-5′, H-3′) to methine protons, 5.20 (2H, s, 13′-OCH_2-) to methylene protons, and 2.32 (6H, s, 11-CH_3, 10-CH_3) to six equivalent dimethyl protons. The amine proton peak, expected to appear further downfield (low field), was not captured. The pairs of methane protons which resonated in the same chemical environment are at positions 7 and 4 (singlet), 6′ and 2′ (doublet), 5′ and 3′ (doublet), 12′ and 8′ (doublet) and 11′ and 9′, respectively. Also, the two methyl had their six protons resonating in the same environment as a singlet.

From EI-MS spectrum (figure **4.127**), the molecular ion, M^+ peak and the $[M^+ + 1]$ peak are at *m/z* of 328 and 329 respectively. The base peak at *m/z* of 237 $[C_{15}H_{13}N_2O]^{\bullet+}$ and tropylium ion $[C_7H_7]^+$ at *m/z* of 91, both resulted from α-bond cleavage of ether functional group. A further loss of CO or $2CH_3^{\bullet}$ from the base peak resulted in *m/z* of 209 $[C_{14}H_{13}N_2]^{\bullet+}$ and a characteristic *m/z* of 65 is indicative of $[C_5H_5]^+$ ion. Also, a loss of $CH_2C{=}N$ from the base peak is suggestive of *m/z* 197 which corresponds to $[C_{13}H_{11}NO]^+$. To further confirming the compound from HREI-MS analysis, the *m/z* corresponding to the formula, $C_{22}H_{20}N_2O$ was obtained at 328.1563 (calculated, 328.1576).

The IR spectrum (figure **4.128**) shows assignable vibrational frequencies, $\bar{\upsilon}$ (cm^{-1}) at 3424, 3036, 2923, 2859, 1610, 1502, 1456 and 1257 signifying the presence of an amine N–H*str*, aromatic C–H*str*, aliphatic C–H*asy str* and C–H*sym str*, aromatic C=C*str*, C–H*b* of CH_3/CH_2 and C–O*str* of ether espectively. Represented in figure **4.129** is the UV spectrum

showing the wavelenghts of maximum absorptions, (λ_{max}) at 311, , 253 and 214 nm indicative of n→π*and π→π* transitions. Table **4.21** represents the summary of ^{1}H NMR spectra.

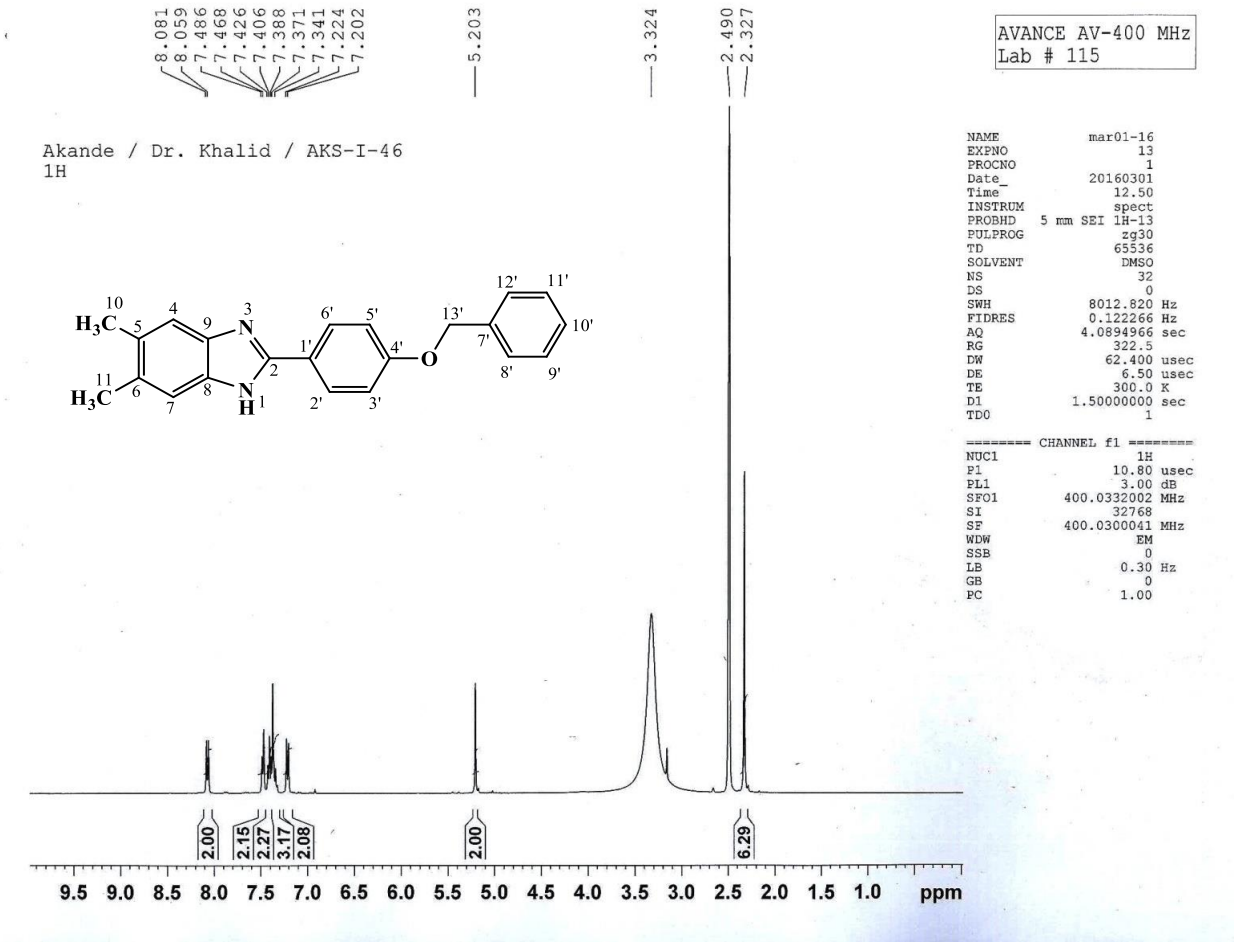

Figure 4.125. ^{1}H NMR (400 MHz, DMSO-d_6) spectrum of AKS-I-46

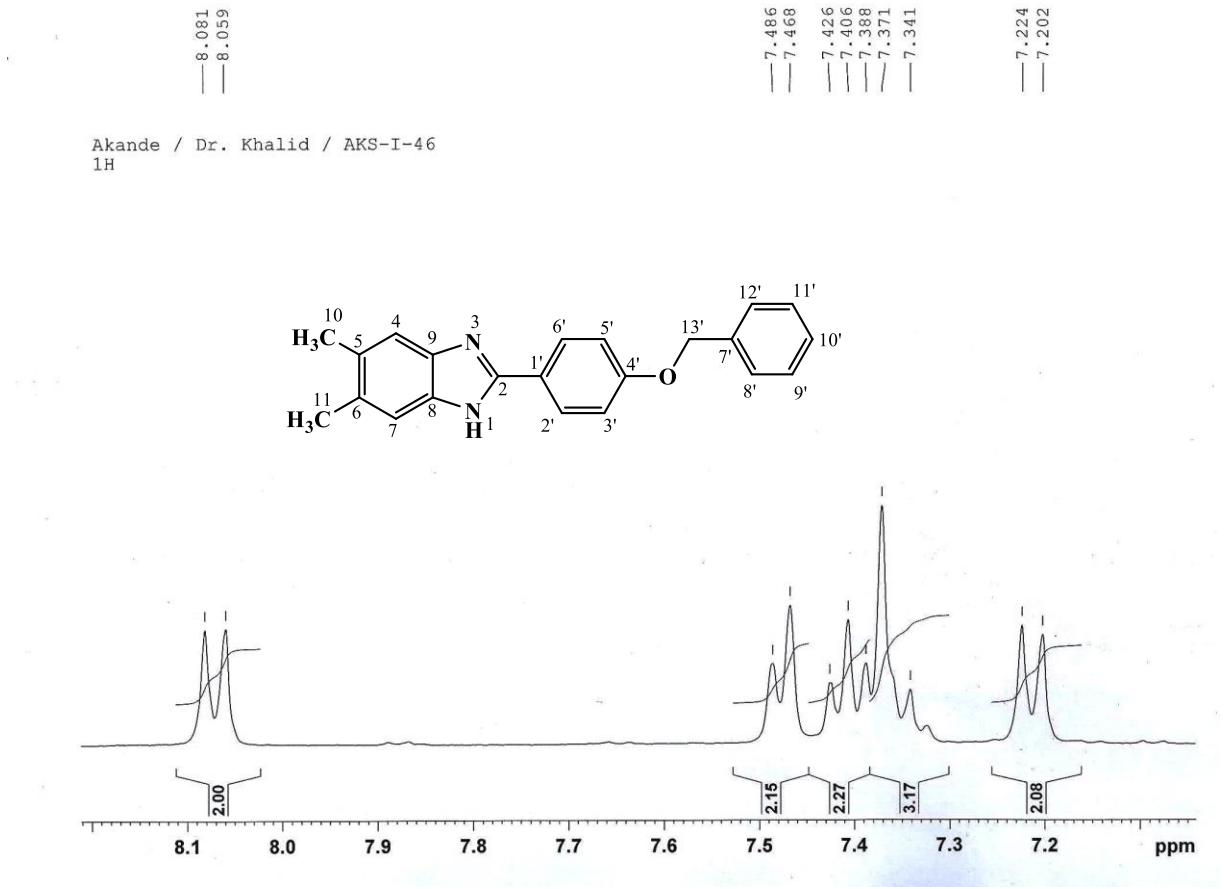

Figure 4.126. ^{1}H NMR (400 MHz, DMSO-d_6) spectrum of AKS-I-46 aromatic region (Expanded)

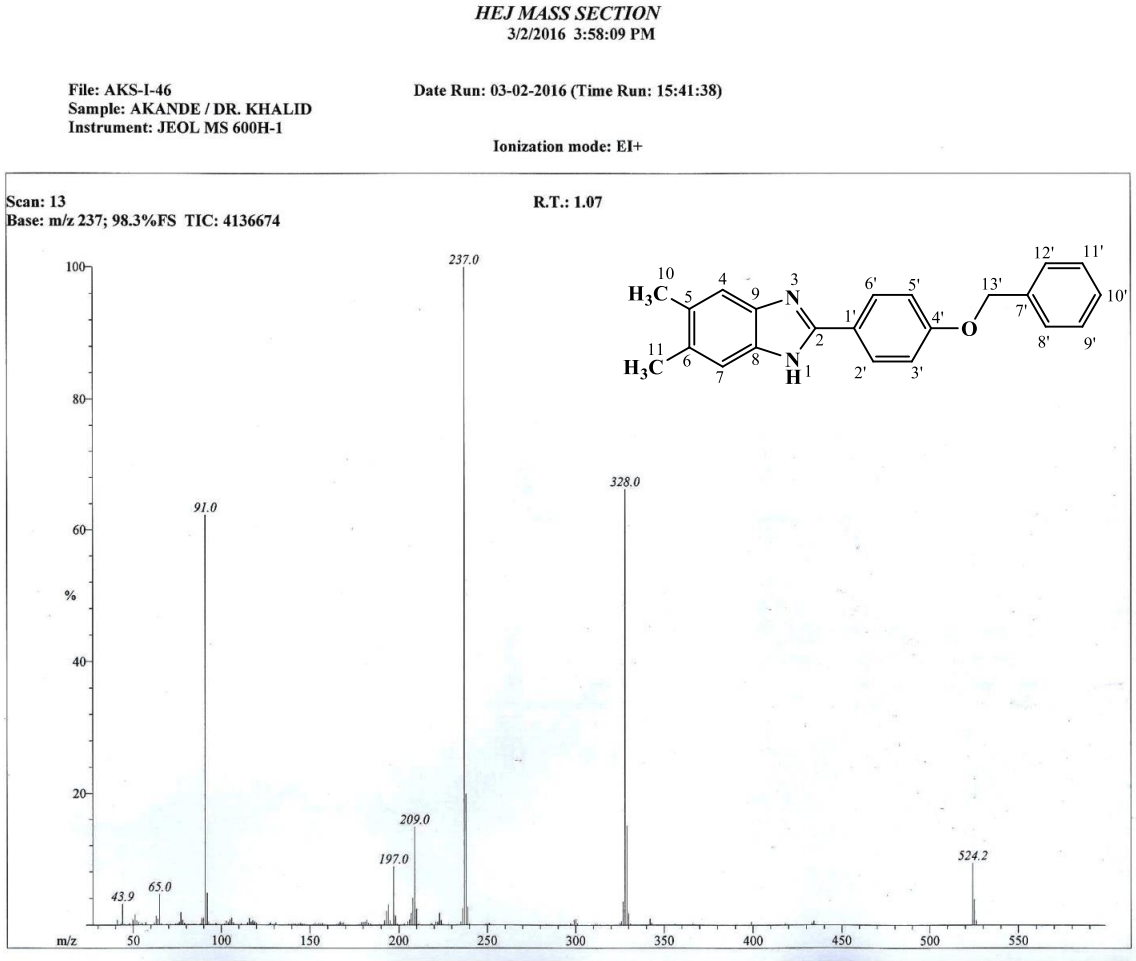

Figure 4.127. EI-MS spectrum of AKS-I-46

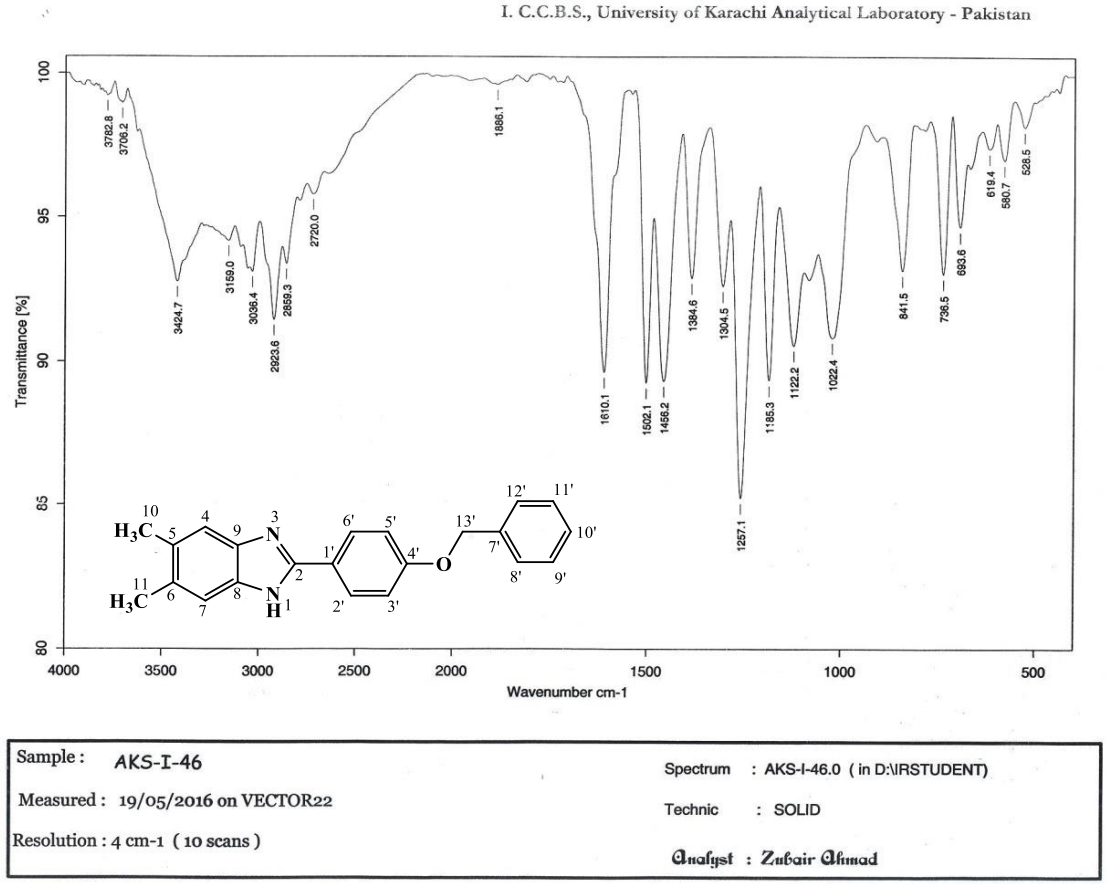

Figure 4.128. IR spectrum of AKS-I-46

THERMO ELECTRON ~ VISIONpro SOFTWARE V4.10

Operator Name	ARSHAD ALAM	Date of Report	5/20/2016
Department	Analytical laboratory#004 TWC	Time of Report	9:52:59AM
Organization	ICCBS.Karachi University.		
Information	Prof Dr. Khalid / Akande.		

Scan Graph

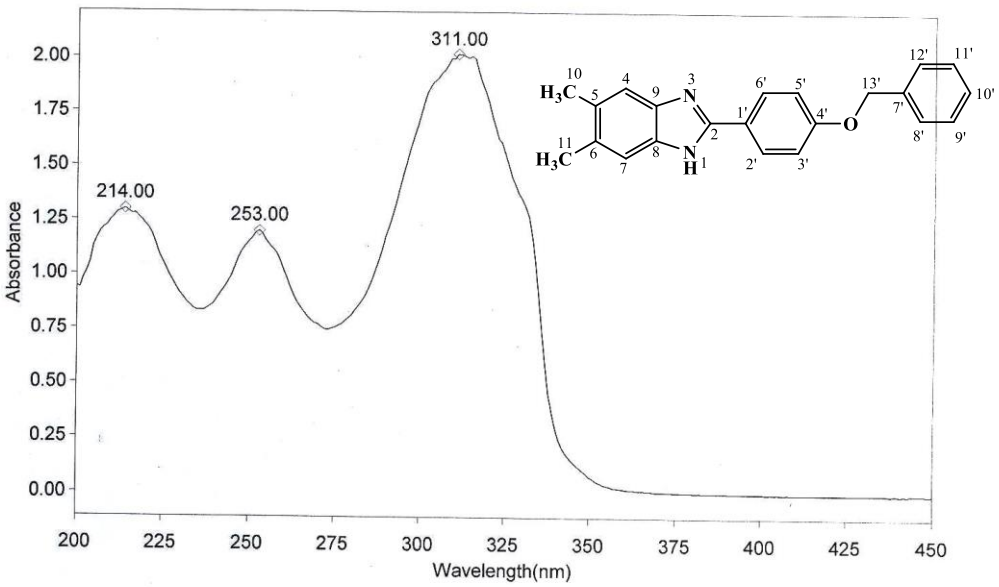

Results Table - AKS- I- 46.sre,AKS- I- 46,Cycle01

nm	A
214.00	1.299
253.00	1.201
311.00	2.021

Peak Pick Method
Find 8 Peaks Above -3.0000 A
Start Wavelength 200.00 nm
Stop Wavelength 450.00 nm
Sort By Wavelength

Sensitivity Very Low

Figure 4.129. UV spectrum of AKS-I-46

Table 4.21. Summary of the ^{1}H NMR spectra of AKS-I-46

Position	δ ^{1}H [mult., J_{HH} (Hz)] (ppm)
1	-
2	-
3	-
4	7.37-7.34 [m]
5	-
6	-
7	7.37-7.34 [m]
8	-
9	-
1′	-
2′	8.08 [d, $J_{2',3'}$ = 8.8]
3′	7.22 [d, $J_{3',2'}$ = 8.8]
4′	-
5′	7.22 [d, $J_{5',6'}$ = 8.8]
6′	8.08 [d, $J_{6',5'}$ =8.8]
7′	-
8′	7.48 [d, $J_{8',9'}$ = 7.2]
9′	7.42 [t, $J_{9',8'}$ = 7.2]
10′	7.37-7.34 [m]
11′	7.42 [t, $J_{11',12'}$ = 7.2]
12′	7.48 [d, $J_{12',11'}$ = 7.2]
13′-OCH_2-	5.20 [s]
10-CH_3	2.32 [s]
11-CH_3	2.32 [s]

4.1.22 Characterisation of 2-(5′-bromo-2′-fluorophenyl)-5-nitro-1*H*-benzo[*d*] imidazole (AKS-I-48)

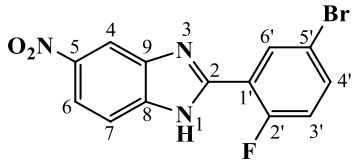

The brown compound, AKS-I-48 is a solid with a yield of 50.2% (0.168 g), a m.pt. of 228-230 ^{o}C and a R_f value of 0.55 in a hexane/ethyl acetate (1:1) solvent system.

The ^{1}H NMR spectra (400 MHz, DMSO-d_6) represented in figures **4.130** and **4.131** exhibit six resonance peaks, δ (ppm) representing the amine proton, assigned as 13.33 (1H, br s, -NH), six methine protons as 8.54 (1H, s, H-4), 8.18 (1H, dd, $J_{4',3'}$ = 8.8 Hz, $J_{4',6'}$ = 2.0 Hz, H-4′), 8.39 (1H, dd, $J_{6,7}$ = 6.4 Hz, $J_{6,4}$ = 2.4 Hz, H-6), a multiplet at 7.81-7.83 (2H, m, H-7, H-6′) and 7.52 (1H, t, $J_{3',4'}$ = 8.8 Hz, H-3′). Protons on positions 4′ and 3′ couple with each other (ortho coupling).

Thirteen chemical shift, δ (ppm) signals obtained from ^{13}C NMR spectra (75 MHz, DMSO-d_6) (figures **4.132** and **4.133**) reveal seven quartenary carbons assigned as 149.54 (C-8, C-9), 143.06 (C-5), 157.52 (C-2), 160.03 (C-2′), 119.19 (C-1′), 116.83, 116.81 (C-5′) and six methine carbons assigned as 119.32 (C-7), 132.36 (C-6), 119.09 (C-4), 135.45 (C-6′), 135.36 (C-4′), 118.31 (C-3′). Result from DEPTH-135 (100 MHz, DMSO-d_6) experiment (spetrum in figure **4.134**) also justifies the respective methine carbons.

The mass-to-charge ratios, *m/z* obtained from EI-MS analysis (figure **4.135**) for the molecular ion, M^+ and an isotope peak, $[M^+$+2] due to the presence of a bromine atom, were at 335 (base peak) and 337 respectively. Fragment ion at *m/z* of 305 resulted from M^+-NO, which corresponds to $[C_{13}H_7BrFN_2O]^+$ while the ion at *m/z* 289 was produced from M^+-NO_2, which corresponds to $[C_{13}H_7BrFN_2]^+$. The fragment ion originating from M^+-NO_2-Br corresponds to a *m/z* of 210 $[C_{13}H_7FN_2]^+$ which further cleaves at the imidazole ring to form a fragment at *m/z* of 90 $[C_6H_5N]^+$. The *m/z* of 90 further fragmented to an ion with *m/z* 63 $[C_5H_3]^+$. The *m/z* of 334.9703 (calculated, 334.9706), obtained from HREI-MS analysis, corresponds to the molecular formula $C_{13}H_7BrFN_3O_2$, further confirming the compound.

The spectrum in figure **4.136** shows absorption bands from IR analysis assignable to vibrational frequencies, $\bar{\upsilon}$ (cm^{-1}) typical of N–H_{str} of 2^{o} amine, aromatic C–H_{str}, C=N_{str}, aromatic C=C_{str}, N=$O_{asy\ str}$ and N=$O_{sym\ str}$ of NO_2 and C–Br_{str}, matching up to 3615, 3106,

1629, 1591, 1474, 1523, 1343 and 885 cm^{-1} respectively. The UV spectrum (figure **4.137**) shows wavelengths of maximum absorptions (λ_{max}) at 324, 261 and 213 nm corresponding to n→π*and π→π* transitions. Represented in table **4.22** is the summary of ^{1}H NMR and ^{13}C NMR spectra.

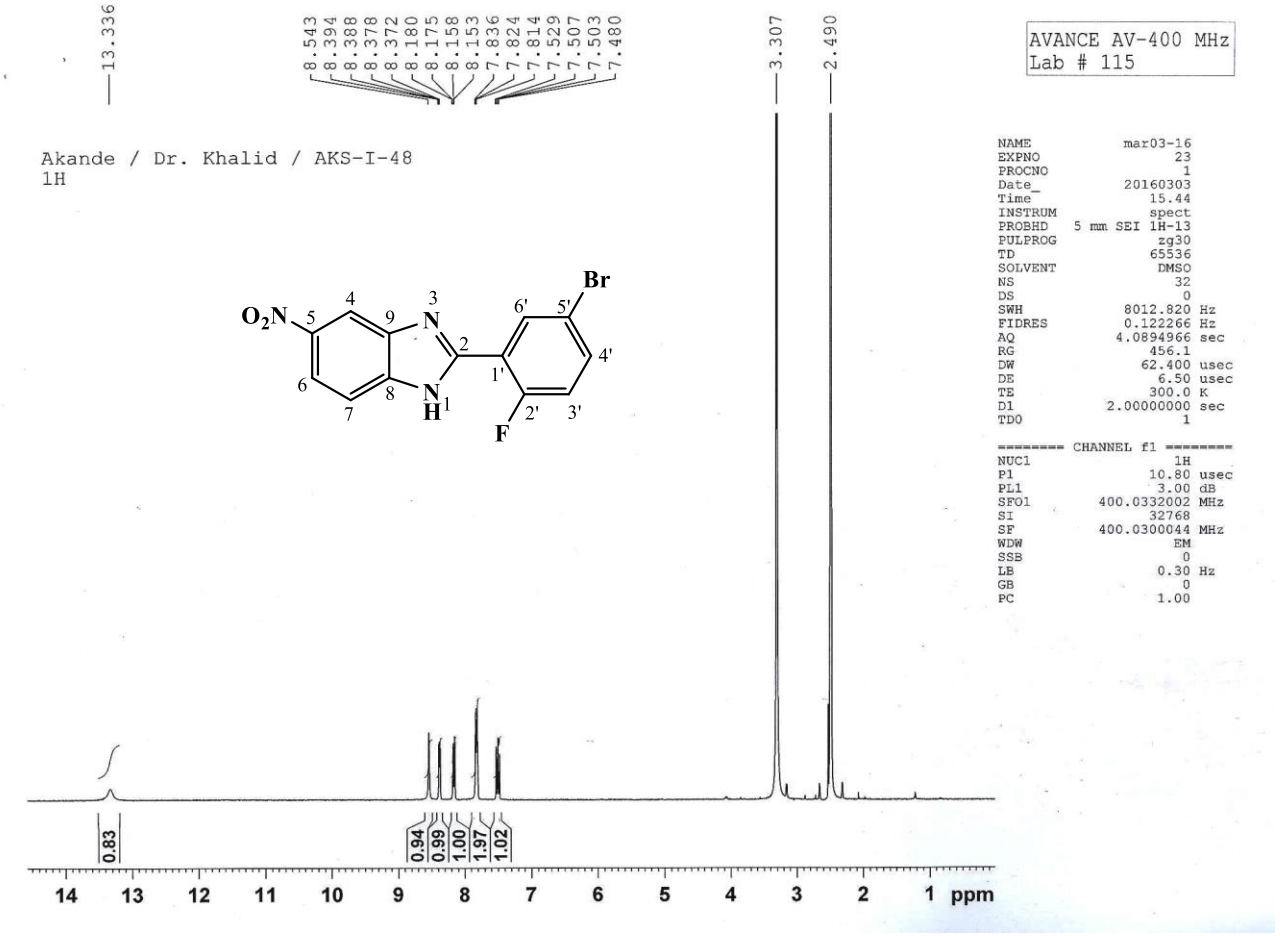

Figure 4.130. ^{1}H NMR (400 MHz, DMSO-d_6) spectrum of AKS-I-48

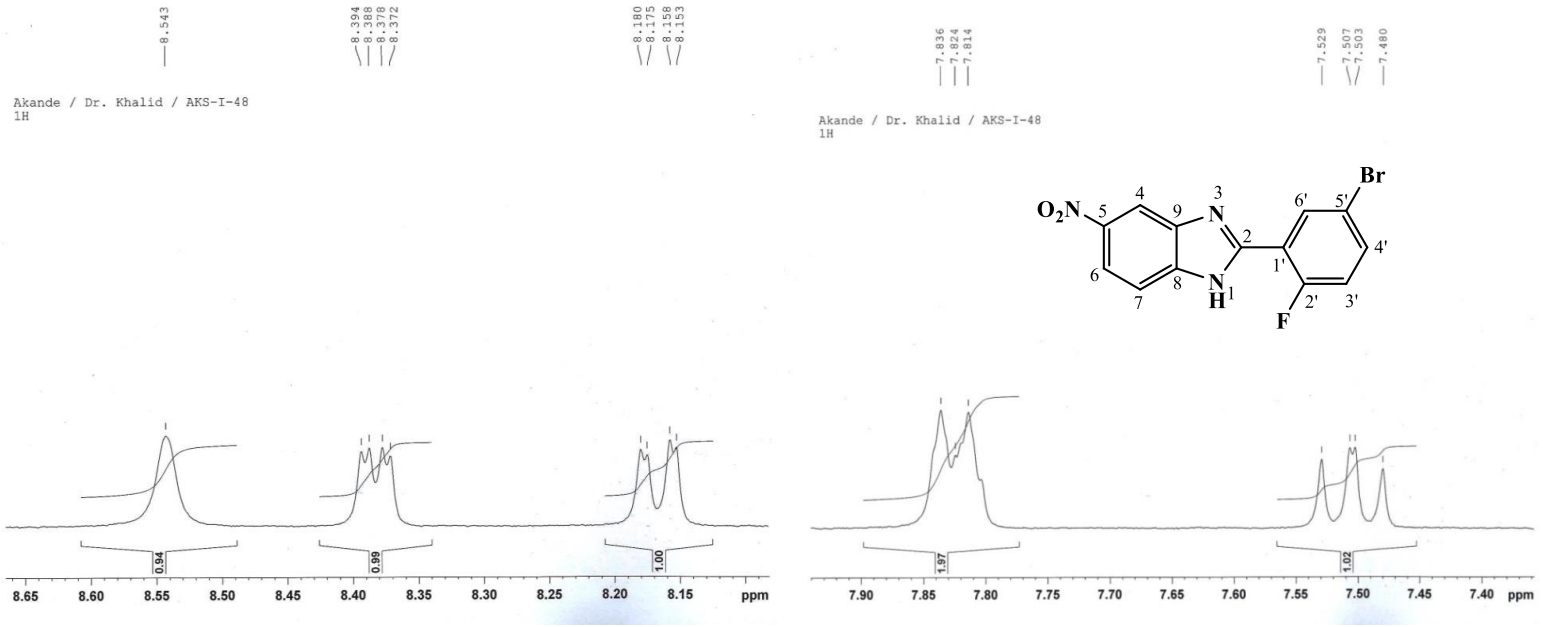

Figure 4.131. ^{1}H NMR (400 MHz, DMSO-d_6) spectra of AKS-I-48 (Expanded)

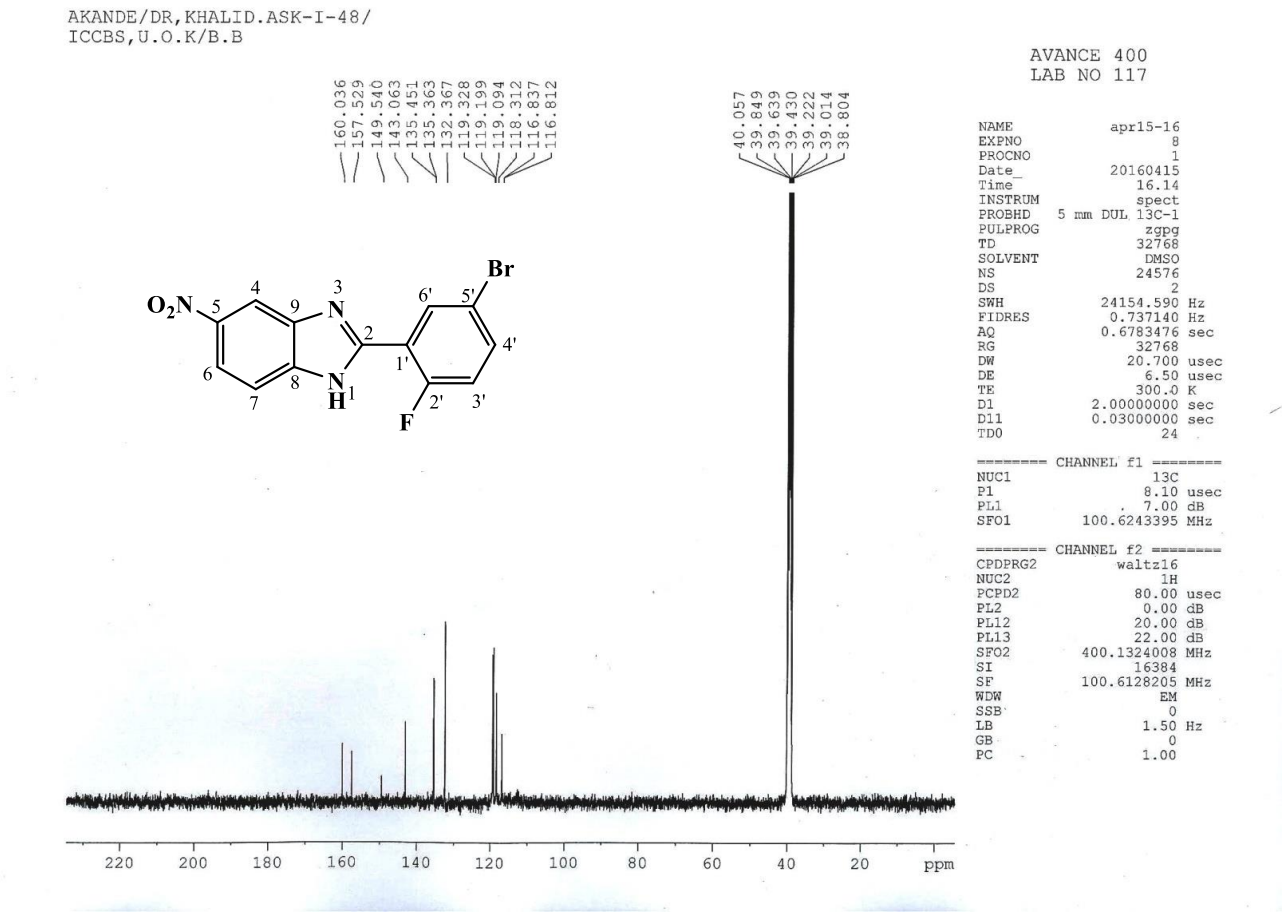

Figure 4.132. ^{13}C NMR (100 MHz, DMSO-d_6) spectrum of AKS-I-48

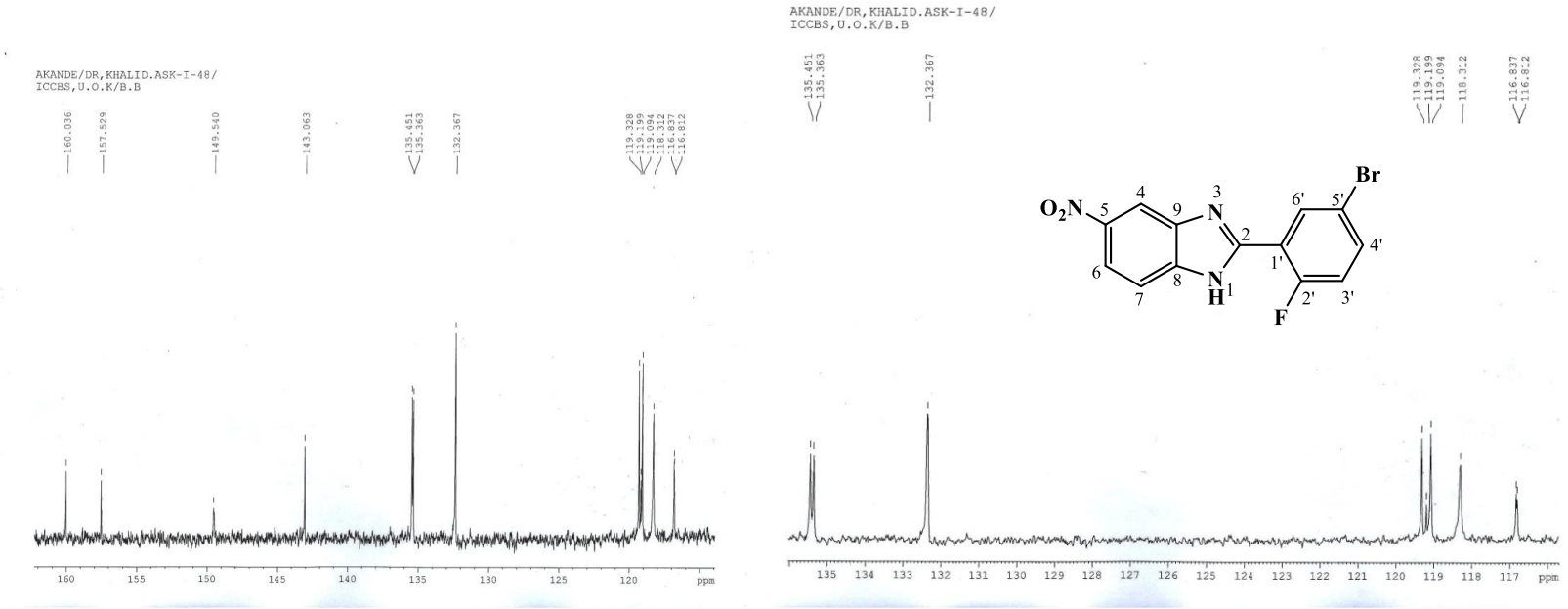

Figure 4.133. ^{13}C NMR (100 MHz, DMSO-d_6) spectrum of AKS-I-48 (Expanded)

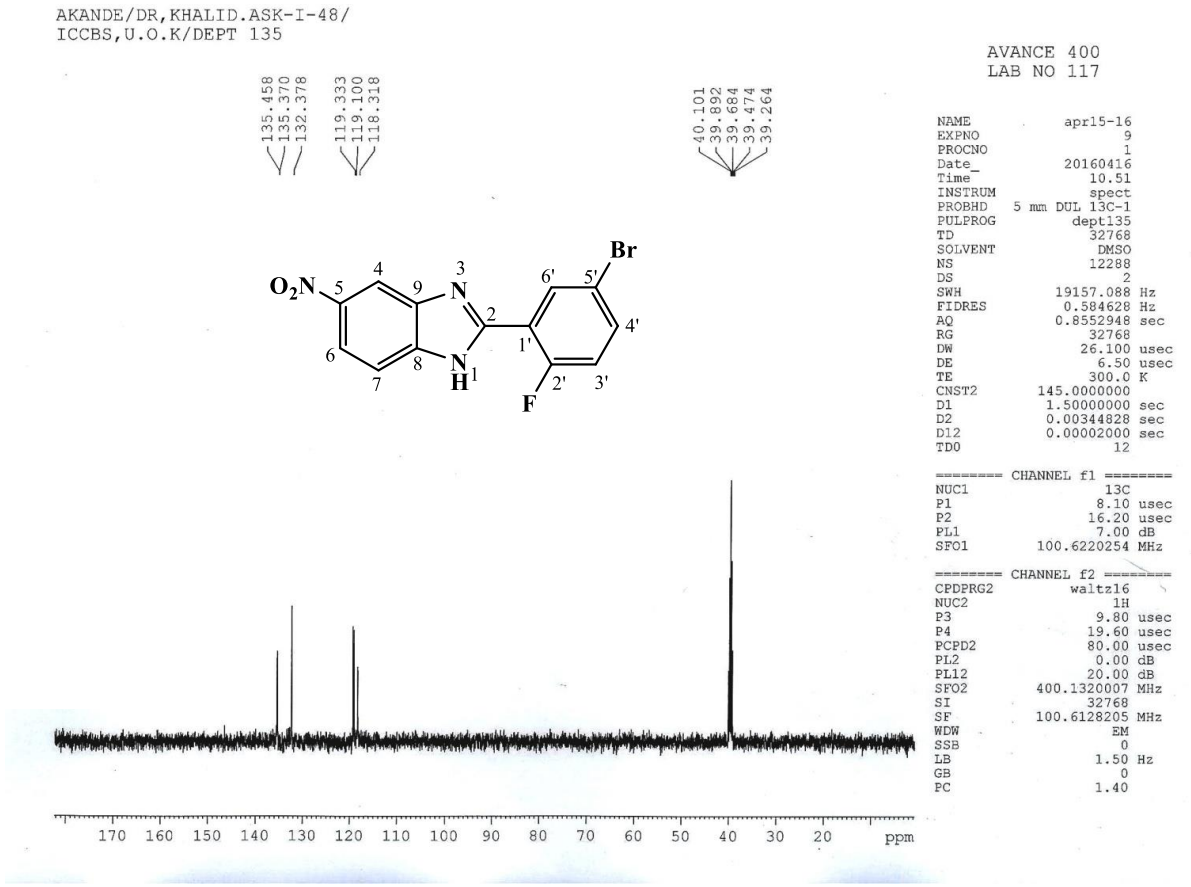

Figure 4.134. DEPTH-135 (100 MHz, DMSO-d_6) spectrum of AKS-I-48

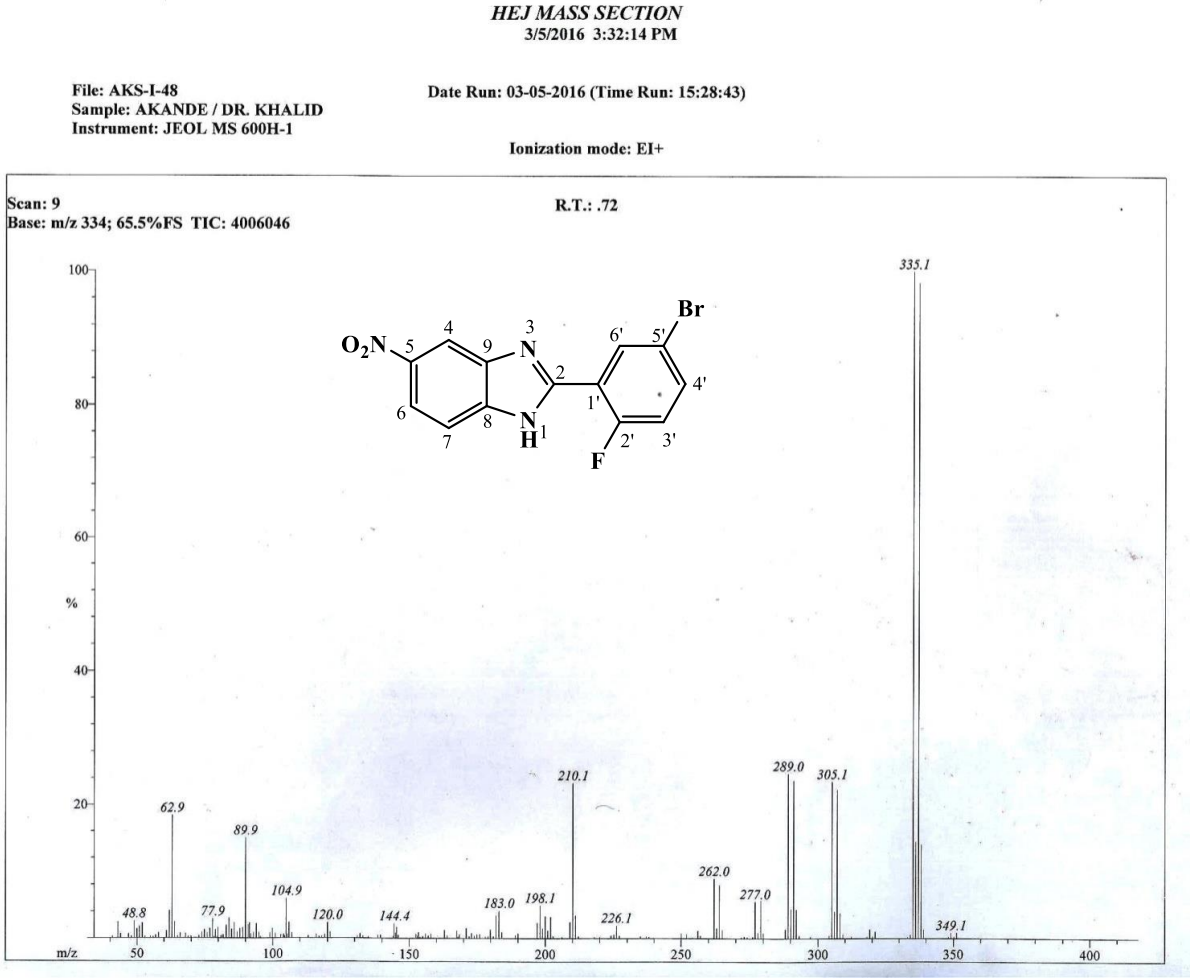

Figure 4.135. EI-MS spectrum of AKS-I-48

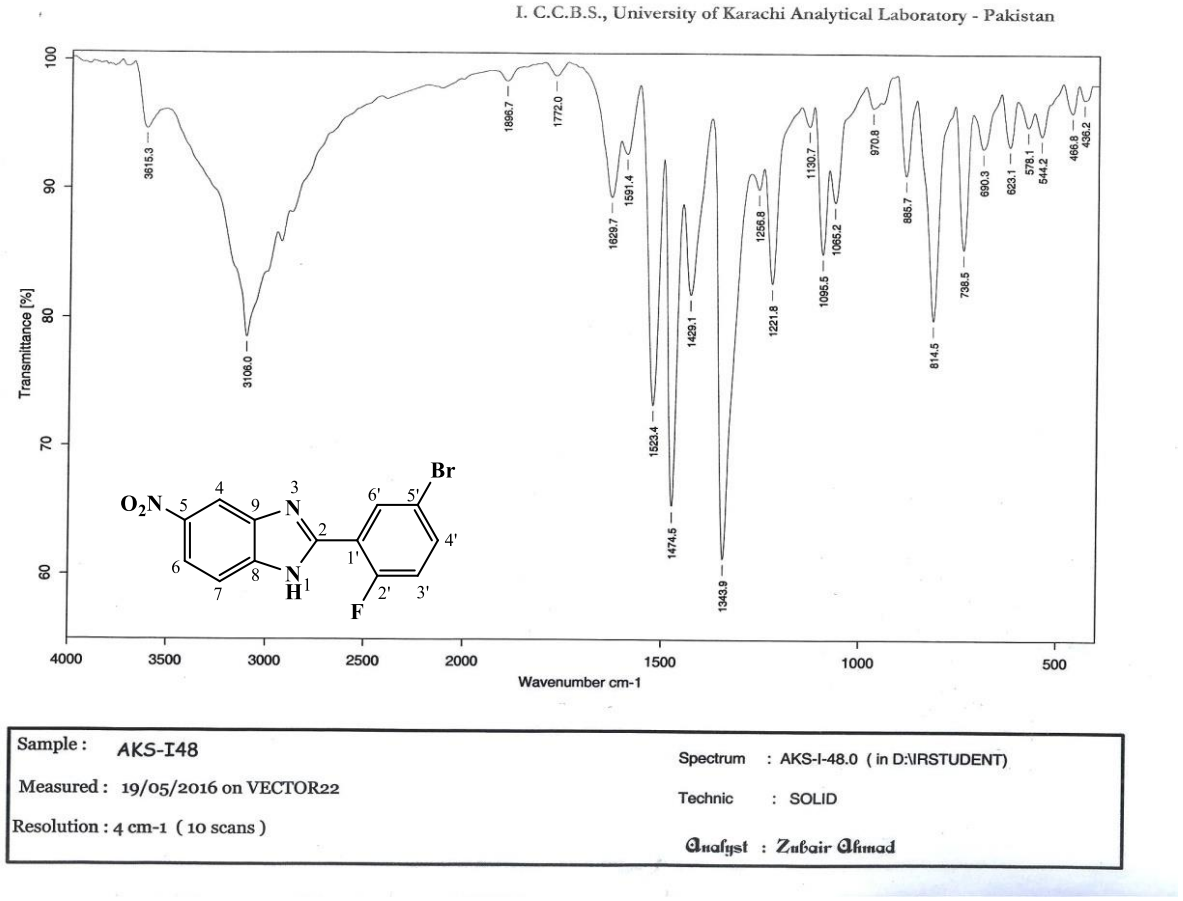

Figure 4.136. IR spectrum of AKS-I-48

THERMO ELECTRON ~ VISIONpro SOFTWARE V4.10

Operator Name	ARSHAD ALAM	Date of Report	5/20/2016
Department	Analytical laboratory#004 TWC	Time of Report	10:00:44AM
Organization	ICCBS.Karachi University.		
Information	Prof Dr. Khalid / Akande.		

Scan Graph

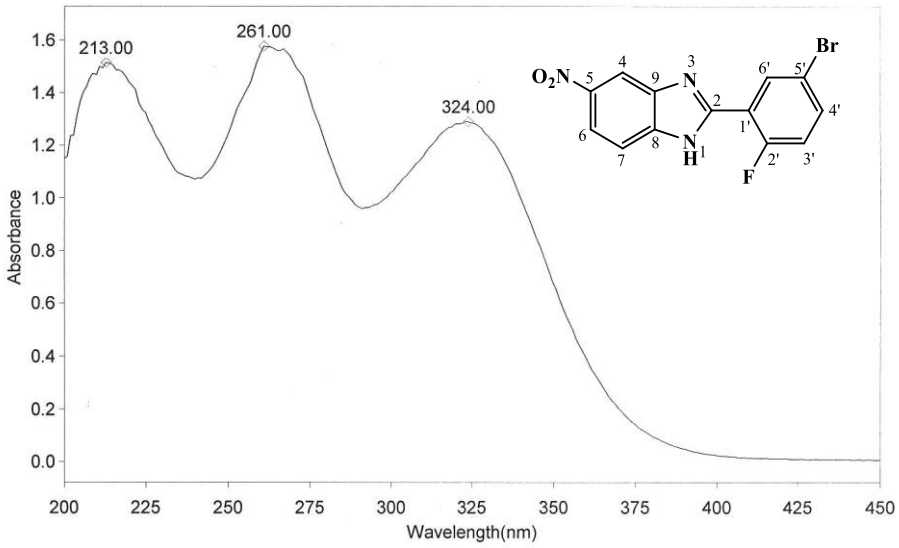

Results Table - AKS- I- 48.sre,AKS-I- 48,Cycle01

nm	A	**Peak Pick Method**
213.00	1.514	Find 8 Peaks Above -3.0000 A
261.00	1.578	Start Wavelength 200.00 nm
324.00	1.289	Stop Wavelength 450.00 nm
		Sort By Wavelength
Sensitivity	Auto	

Page 1, Scan Graph

Figure 4.137. UV spectrum of AKS-I-48

Table 4.22. Summary of the ^{1}H NMR and ^{13}C NMR spectra of AKS-I-48

Position	δ ^{1}H [mult., J_{HH} (Hz)] (ppm)	δ ^{13}C (ppm)	DEPT-135
1	13.33 [br s]	-	-
2	-	157.52	-
3	-	-	-
4	8.54 [s]	119.09	CH
5	-	143.06	-
6	8.39 [dd, $J_{6,7}$ = 6.4, $J_{6,4}$ = 2.4]	132.36	CH
7	7.83-7.81 [m]	119.32	CH
8	-	149.54	-
9	-	149.54	-
1′	-	119.19	-
2′	-	160.03	-
3′	7.52 [dt, $J_{3',4'}$ = 8.8]	118.31	CH
4′	8.18 [dd, $J_{4',3'}$ = 8.8]	135.36	CH
5′	-	116.83, 116.81	-
6′	7.83-7.81 [m]	135.45	CH

4.1.23 Characterisation of 5,6-dimethyl-2-(2′,3′,4′-trimethoxyphenyl)-1*H*-benzo [*d*]imidazole (AKS-I-49)

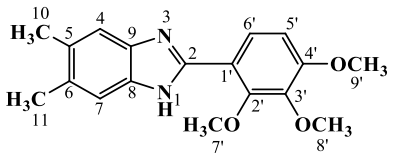

The compound, AKS-I-49 is a white solid, with a yield of 49.0% (0.153 g), a m.pt. range of 188-190 ^{o}C and a R_f value of 0.30 in a hexane/ethyl acetate (1:1) solvent system.

Presented in figures **4.138** and **4.139**, the ^{1}H NMR spectra (400 MHz, DMSO-d_6) show seven chemical shift values, δ (ppm) representing twenty protons. These values are assigned as follows: 11.93 (1H, br s, -NH) to the amine proton, 7.92 (d, 1H, $J_{6',5'}$ = 8.8 Hz, H-6′), a value at 7.35 (2H, s, H-4, H-7; chemically equivalent due to tautomerism between positions 1 and 3), 6.98 (d, 1H, $J_{5',6'}$ = 9.2 Hz, H-5′) to four aromatic methine protons, 3.88 (3H, s, 7′-OCH_3), 3.86 (3H, s, 9′-OCH_3), 3.82 (3H, s, 8′-OCH_3) to nine trimethoxy protons, and 2.30 (6H, s, 11-, 10-CH_3) to six equivalent dimethyl protons.

Figures **4.140** and **4.141** also present twelve resonances from ^{13}C NMR (75 MHz, DMSO-d_6) analysis with the chemical shift, δ (ppm) values assigned as 147.69 (C-9, C-8), 130.04 (C-6, C-5), 151.28 (C-2), 154.60 (C-4′), 116.19 (C-3′), 141.71 (C-2′), 115.06 (C-1′) to nine quarternary carbons, 124.31 (C-5′, C-6′), 108.47 (C-4, C-7) to four methine carbons, 61.26 (C-7′), 60.50 (C-8′), 55.98 (C-9′) to three methoxy carbons and 19.98 (C-11, C-10) to two methyl carbons. DEPTH-135 (75 MHz, DMSO-d_6) spectrum (figure **4.142**) also confirmed the respective methine, methoxy and methyl carbons, all peaks showing up in the positive mode.

The EI-MS spectrum (figure **4.143**) shows ion peaks produced according to their mass-to-charge ratios, *m/z*. Peaks at *m/z* 312 and 313 represent the molecular ion [M^+] and [M^++1] peaks. The base peak at *m/z* of 297 is due to loss of $CH_3^{\bullet}$ radical from the molecular ion. Fragment ion with *m/z* of 281 is suggestive of M^+-$CH_3O^{\bullet}$ or M^+-$2CH_3^{\bullet}$+$H^{\bullet}$ cleavage while the cleavage, M^+-CH_3O-CH_3 is indicative of the fragment ion at *m/z* 266 corresponding to [$C_{16}H_{14}N_2O_2$]. Loss of the dimethyl side chain along with a methoxy group from M^+ is indicative of the peak at *m/z* 254, which corresponds to $[C_{15}H_{14}N_2O_2]^+$ fragment. From HREI-MS analysis, the *m/z* corresponding to the molecular formula $C_{18}H_{20}N_2O_3$ was obtained at 312.1470 (calculated, 312.1474). This further confirms the compound.

The IR spectrum (figure **4.144**) indicated vibrational frequencies $\bar{\upsilon}$ (cm^{-1}) at 3314, 3102, 2943, 1597, 1479, 1457, 1288 and 1083 corresponding to N–H_{str} of amine, aromatic C–H_{str}, aliphatic C–H_{str}, two aromatic C=C_{str}, C–H_b of CH_3, and asymmetric and symmetric C–O_{str} of ether respectively. The UV spectrum shows wavelenght of maximum absorptions (λ_{max}), corresponding to $n\rightarrow\pi^*$ and $\pi\rightarrow\pi^*$ transitions at 311, 252 and 228 nm (figure **4.145**). Summary of the ^1H NMR and ^{13}C NMR spectra is represented in table **4.23**.

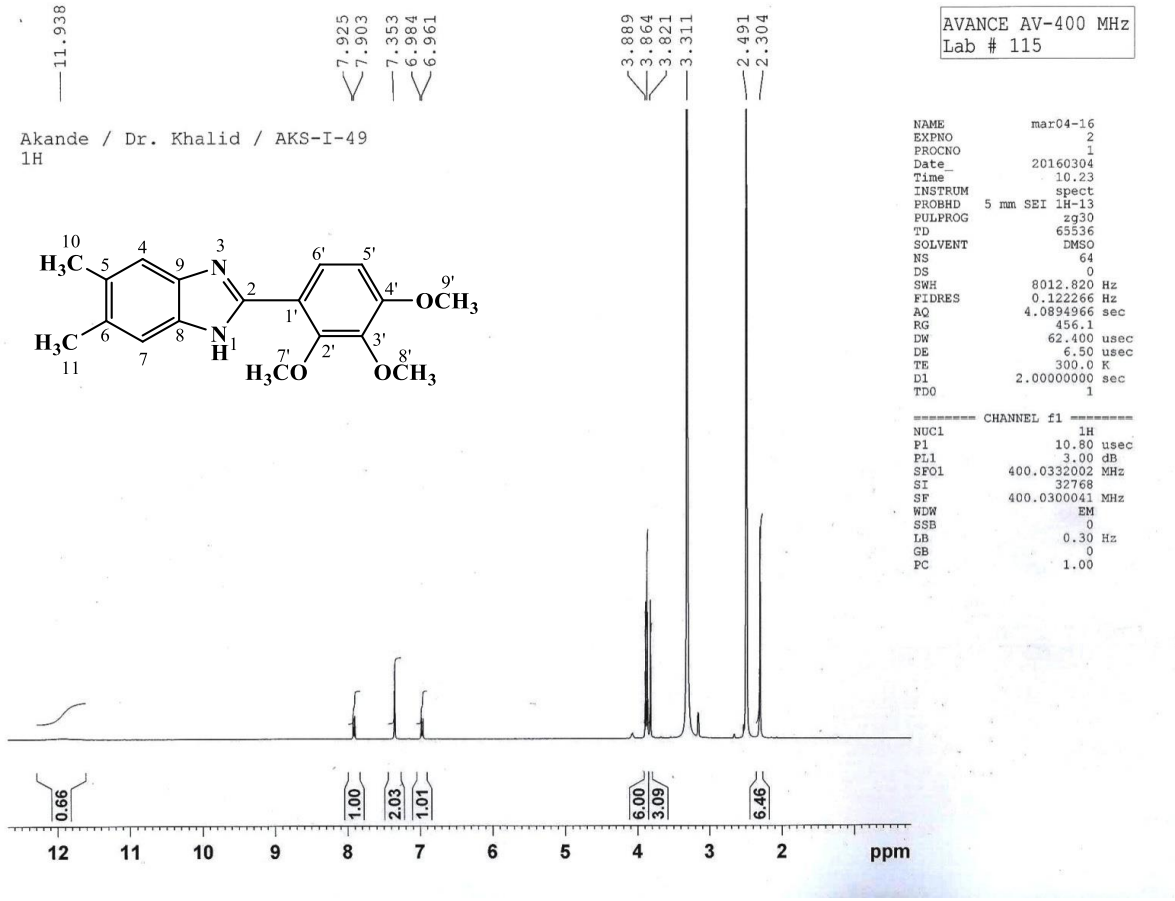

Figure 4.138. ^{1}H NMR (400 MHz, DMSO-d_6) spectrum of AKS-I-49

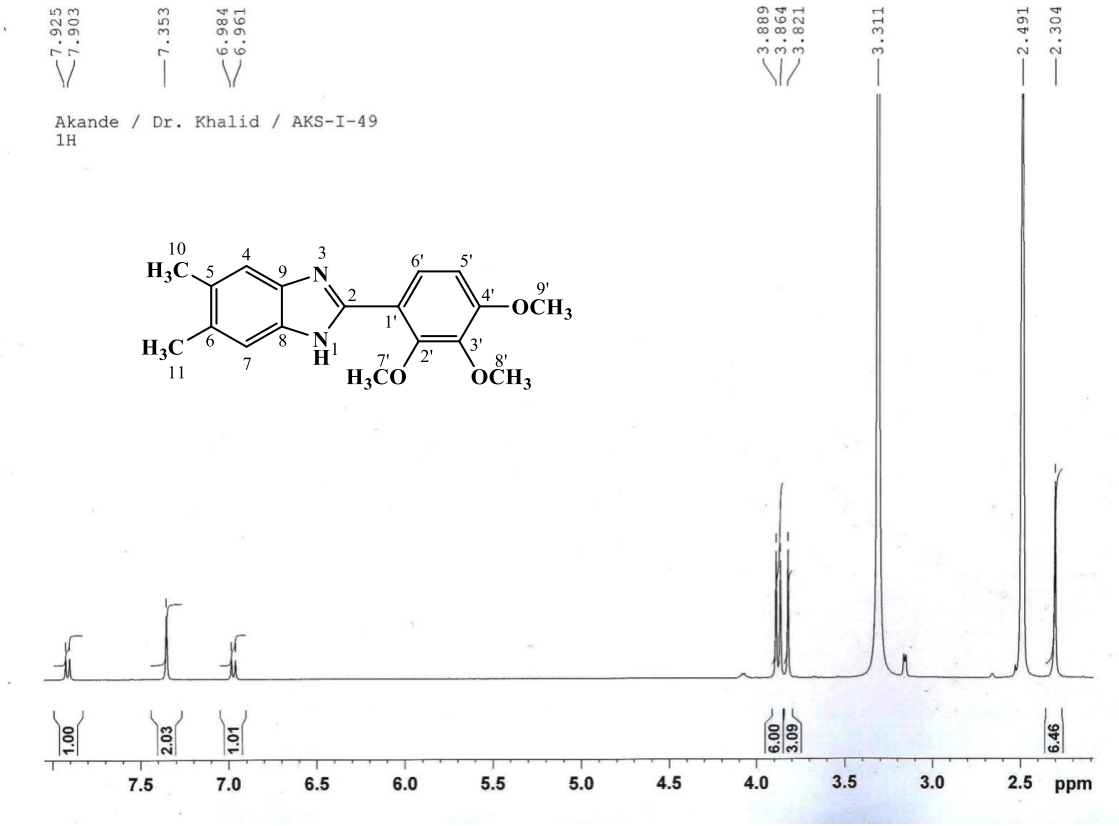

Figure 4.139. ^{1}H NMR (400 MHz, DMSO-d_6) spectrum of AKS-I-49 (Expanded)

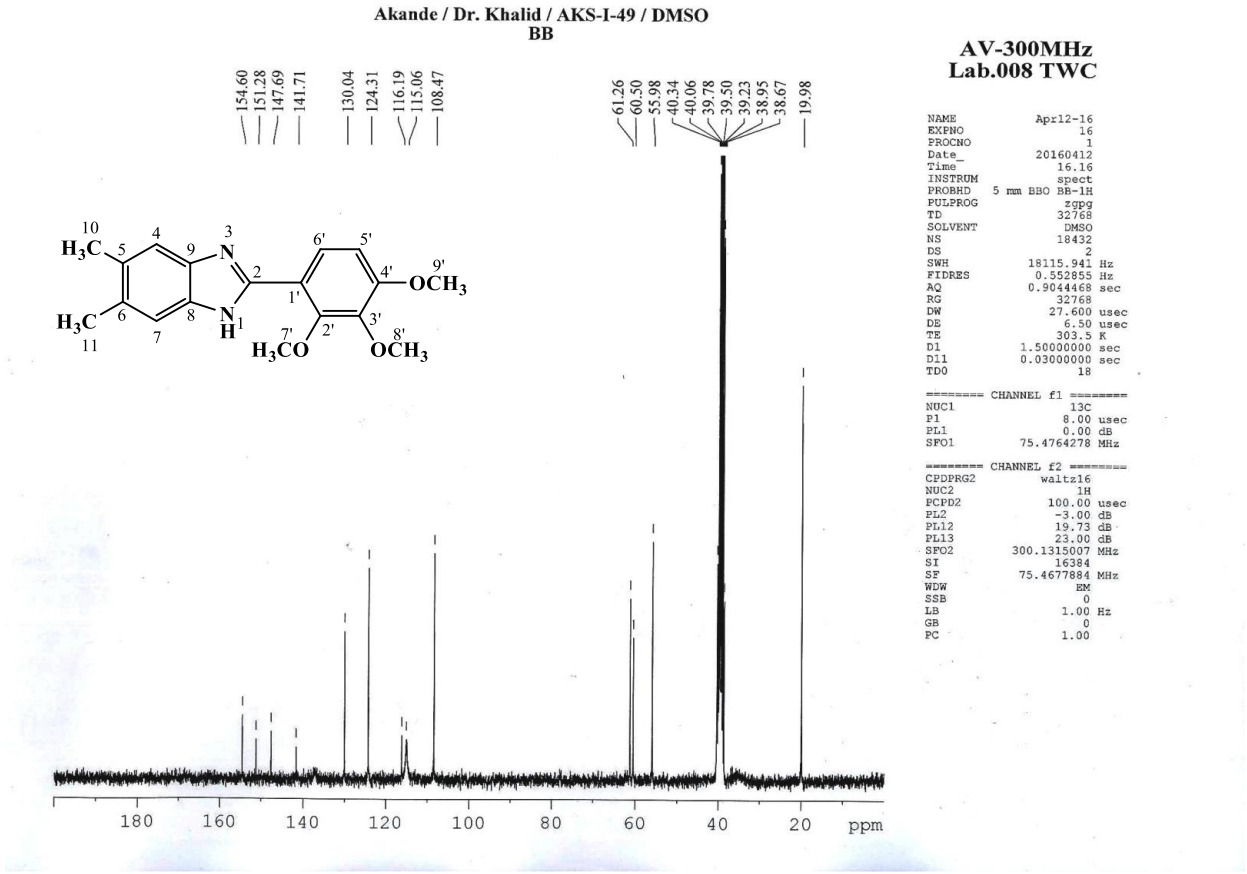

Figure 4.140. ^{13}C NMR (75 MHz, DMSO-d_6) spectrum of AKS-I-49

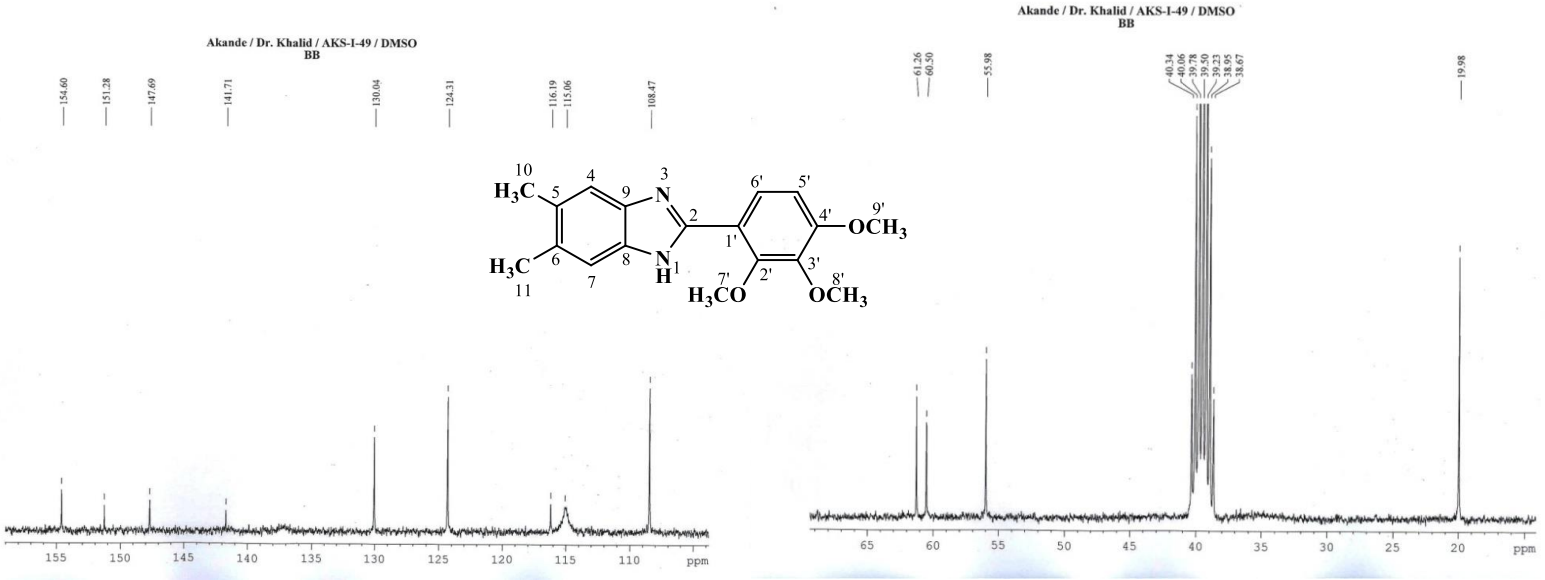

Figure 4.141. ^{13}C NMR (75 MHz, DMSO-d_6) spectra of AKS-I-49 (Expanded)

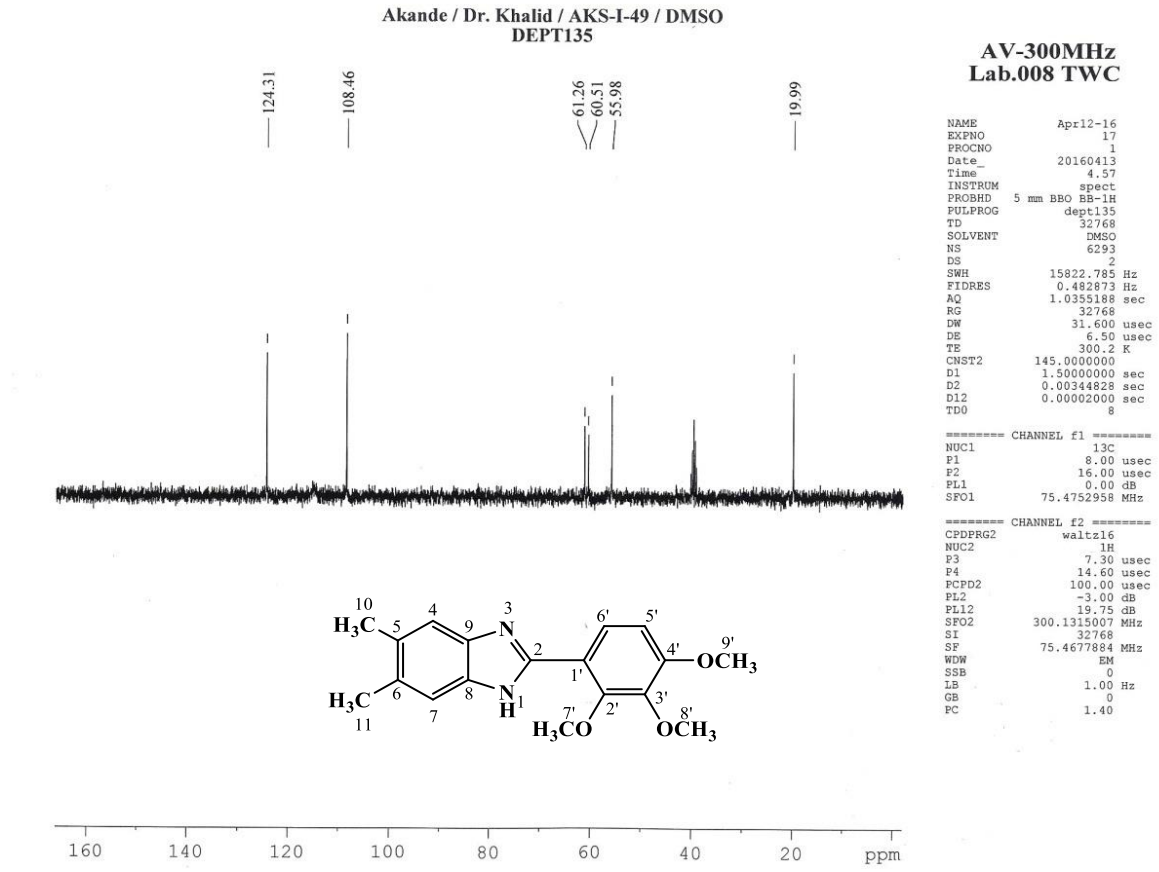

Figure 4.142. DEPTH-135 (75 MHz, DMSO-d_6) spectrum of AKS-I-49

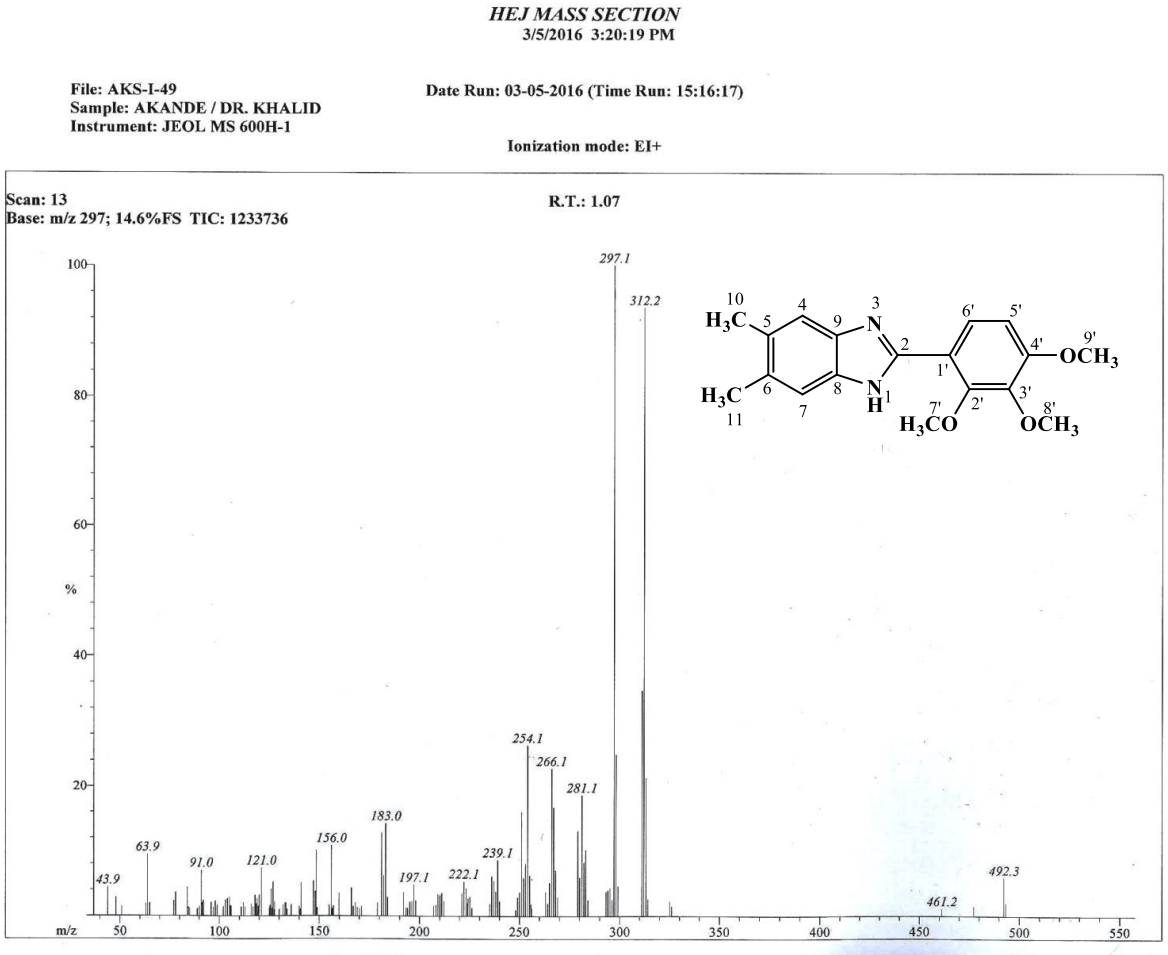

Figure 4.143. EI-MS spectrum of AKS-I-49

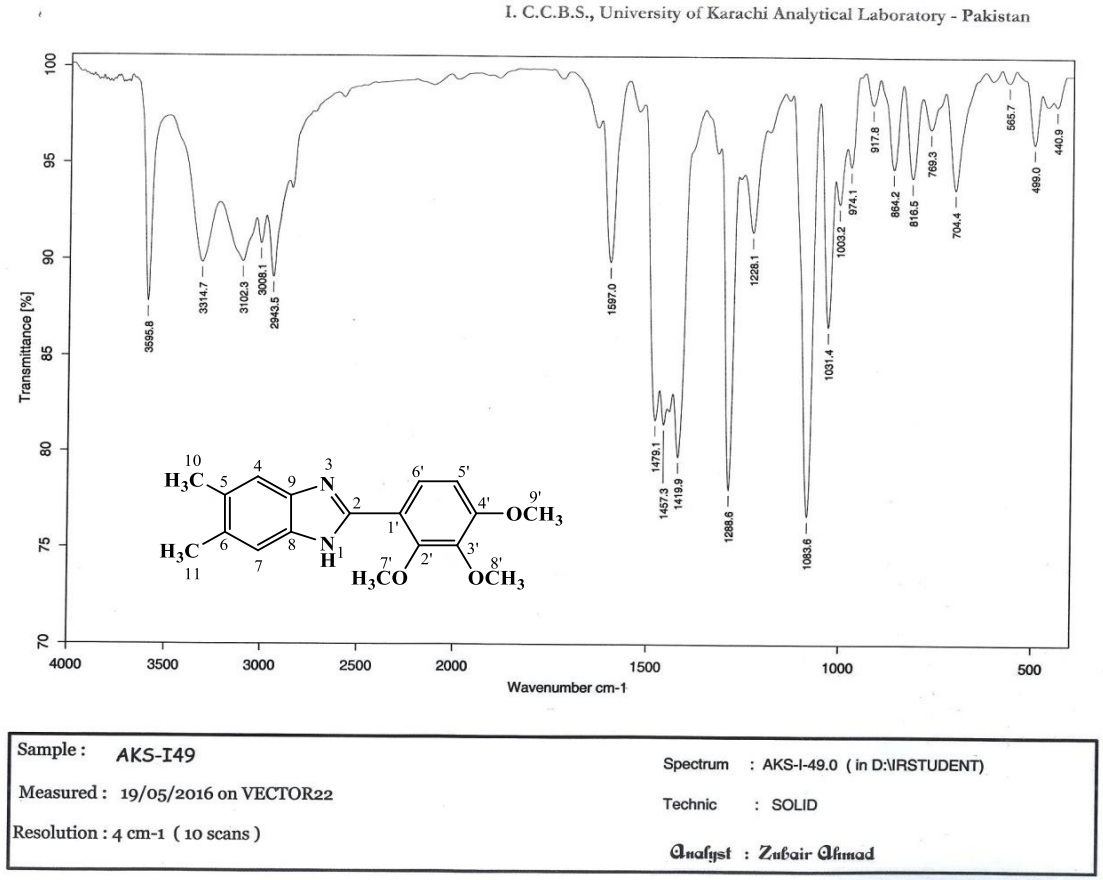

Figure 4.144. IR spectrum of AKS-I-49

THERMO ELECTRON ~ VISIONpro SOFTWARE V4.10

Operator Name	ARSHAD ALAM	Date of Report	5/20/2016
Department	Analytical laboratory#004 TWC	Time of Report	10:04:36AM
Organization	ICCBS.Karachi University.		
Information	Prof Dr. Khalid / Akande.		

Scan Graph

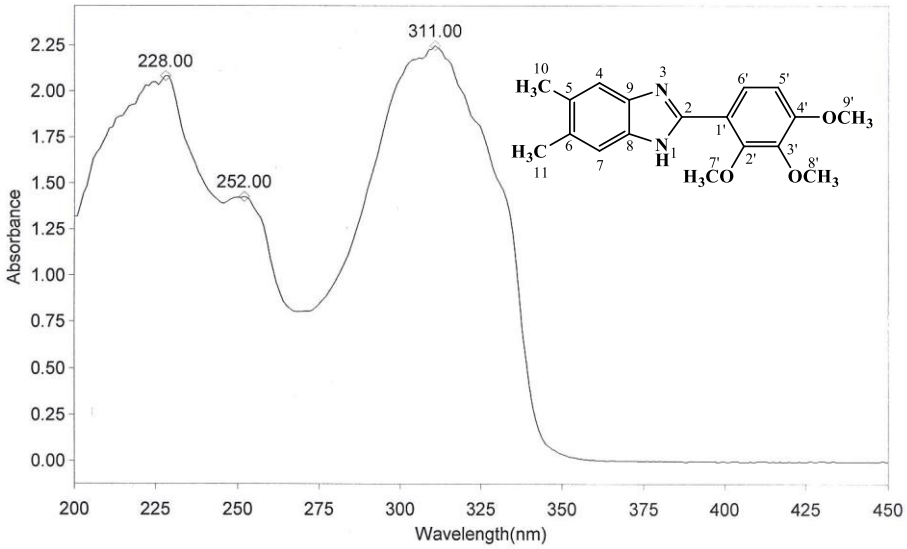

Results Table - AKS- I- 49.sre,AKS- I- 49,Cycle01

nm	A	**Peak Pick Method**
228.00	2.081	Find 8 Peaks Above -3.0000 A
252.00	1.428	Start Wavelength 200.00 nm
311.00	2.248	Stop Wavelength 450.00 nm
		Sort By Wavelength
Sensitivity	Auto	

Page 1, Scan Graph

Figure 4.145. UV spectrum of AKS-I-49

Table 4.23. Summary of the ^{1}H NMR and ^{13}C NMR spectra of AKS-I-49

Position	δ ^{1}H [mult., J_{HH} (Hz)] (ppm)	δ ^{13}C (ppm)	DEPT-135
1	11.93 [br s]	-	-
2	-	151.28	-
3	-	-	-
4	7.35 [s]	108.47	CH
5	-	130.04	-
6	-	130.04	-
7	7.35 [s]	108.47	CH
8	-	130.04	-
9	-	130.04	-
10	2.30 [s]	19.98	CH_3
11	2.30 [s]	19.98	CH_3
1′	-	115.06	-
2′	-	147.69	-
3′	-	141.71	-
4′	-	154.60	-
5′	6.98 [d, $J_{5',6'}$ = 9.2]	108.47	CH
6′	7.92 [d, $J_{6',5'}$ = 8.8]	124.31	CH
7′-OCH_3	3.88 [s]	61.26	CH_3
9′-OCH_3	3.86 [s]	55.98	CH_3
8′-OCH_3	3.82 [s]	60.50	CH_3

4.1.24 Characterisation of 2′-(1*H*-benzo[*d*]imidazol-2-yl)-3′-bromo-6′-methoxyphenol (AKS-I-50)

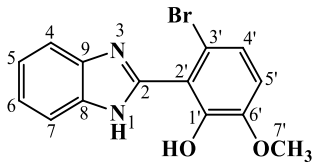

Compound 2′-(1*H*-benzo[*d*]imidazol-2-yl)-3′-bromo-6′-methoxyphenol (AKS-I-50) is a yellow solid with a yield of 41.8% (0.133 g), a m.pt. of 178-181 ^{o}C and a R_f value of 0.55 (hexane/ethyl acetate, 1:1). The six chemical shift, δ (ppm) values obtained from ^{1}H NMR spectra (400 MHz, DMSO-d_6) (figures **4.146** and **4.147)** are assigned as 11.70-11.77 (1H, br d, N-H) to amine proton, 7.60-7.62 (2H, m, H-4, H-7), 7.22-7.24 (2H, m, H-5, H-6), 7.18 (1H, d, $J_{4',5'}$ = 8.8 Hz, H-4′) and 7.07 (1H, d, $J_{5',4'}$ = 8.8 Hz, H-5′) to six methine protons, while 3.84 (3H, s, 6′-OCH_3) is to the methyl protons. The OH proton is an exchaneable one and was not seen on the spectrum. The multiplet and doublet sinals are leaning peaks, an indication that the protons involved couples to each other. The peaks for protons 4, 5, 6 and 7 were seen as multiplets from overlaps due to rapid exchange of proton between positions 1 and 3 (tautomerism).

The EI-MS spectrum (figure **4.148**) reveals a mixture of the molecular ion, M^+ and fragment ions with peak patterns spaced two mass units apart. The *m/z* of 318 and 320 are peaks corresponding to M^+ and $[M^+{+}2]$ (isotope peak due to ^{81}Br atom and the base peak). The presence of $[M^+{+}2]$-17 peak, (loss of $OH^{\bullet}$) corresponds to *m/z* of 303. The fragment ion with *m/z* of 291 is suggests a loss of C_2H_4 molecule from the isotope peak, and a further loss of $OH^{\bullet}$ is indicative of the fragment ion with *m/z* of 275, which corresponds to $[C_{12}H_8BrN_2O]^+$. The *m/z* of 209 and 167 correspond to $[C_8H_5BrNO]^+$ and $[C_{11}H_7N_2]^+$ fragments respectively. Further confirming the compound from HREI-MS analysis, the *m/z* of 318.0015 (calculated, 318.0004) was found corresponding to the molecular formula $C_{14}H_{11}BrN_2O_2$.

Figure **4.149** is the spectrum of IR active bonds with vibrational frequencies, $\bar{\upsilon}$ (cm^{-1}) assignable to some typical bonds such as N–H_{str} of amine, aromatic C–H_{str}, aliphatic C–H_{str}, aromatic C=C_{str}, C–H_b of OCH_3, C–O_{str} of ether and C–Br_{str} corresponding to 3336, ≈3100, 2925, 1585, 1450, 1245 and 989 respectively. The UV spectrum (figure **4.150**) shows maximum absorptions (λ_{max}) at 282, 229 and 214 nm indicative of n→π* and π→π* transitions. The ^{1}H NMR spectrum is summerised in table **4.24**.

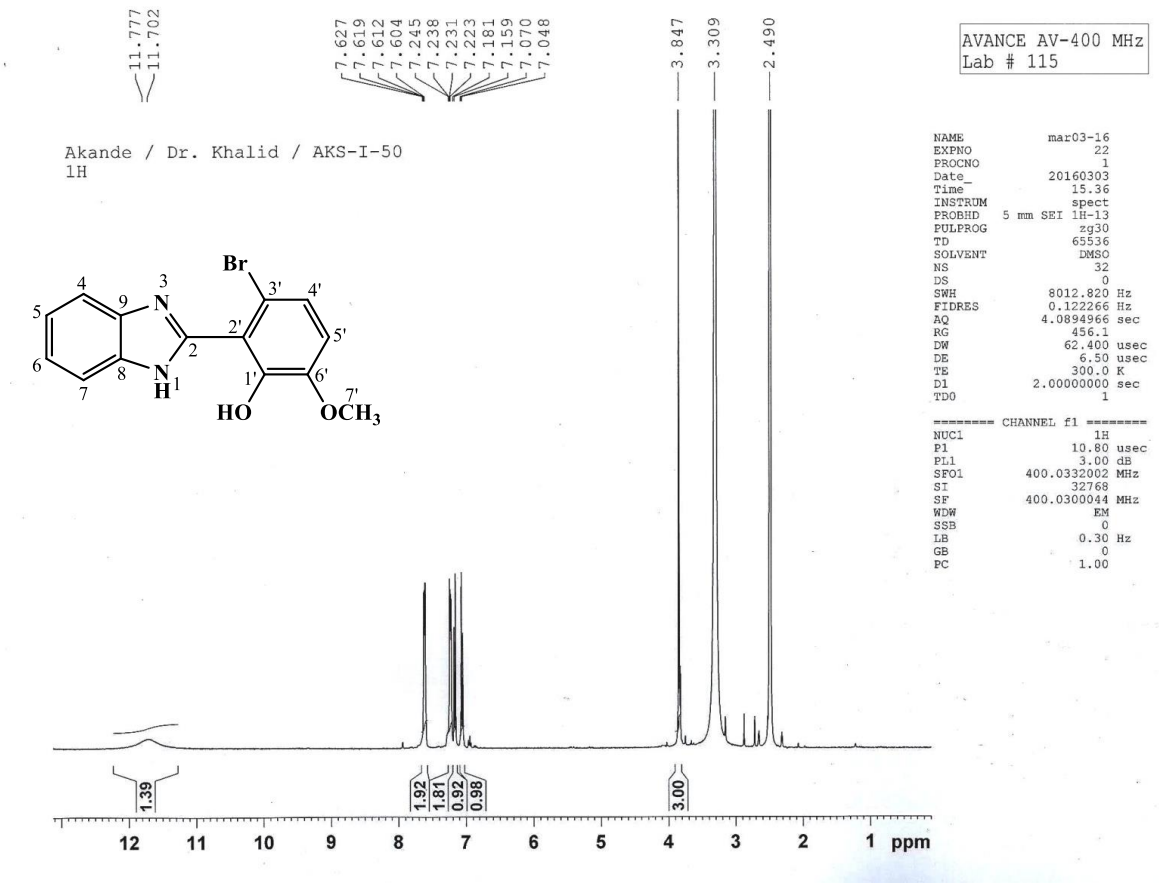

Figure 4.146. ^{1}H NMR (400 MHz, DMSO-d_6) spectrum of AKS-I-50

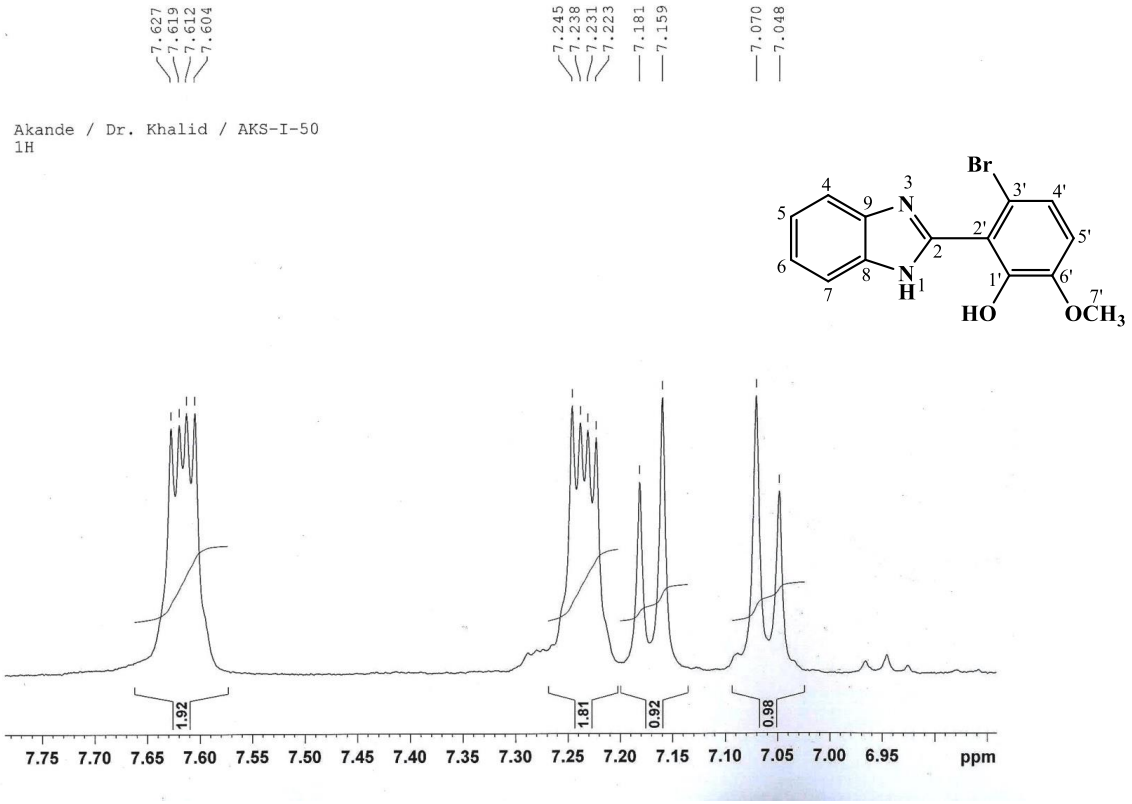

Figure 4.147. ^{1}H NMR (400 MHz, DMSO-d_6) spectrum of AKS-I-50 (Expanded)

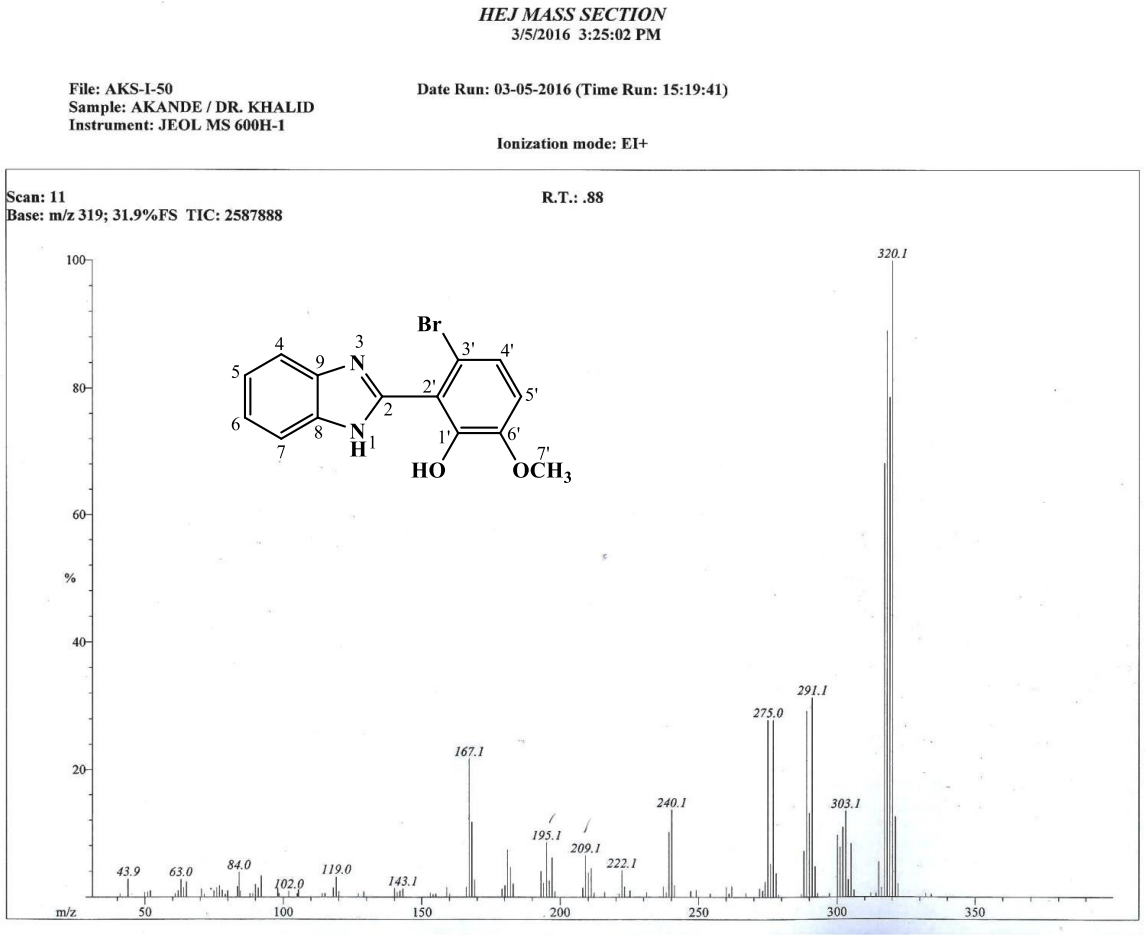

Figure 4.148. EI-MS spectrum of AKS-I-50

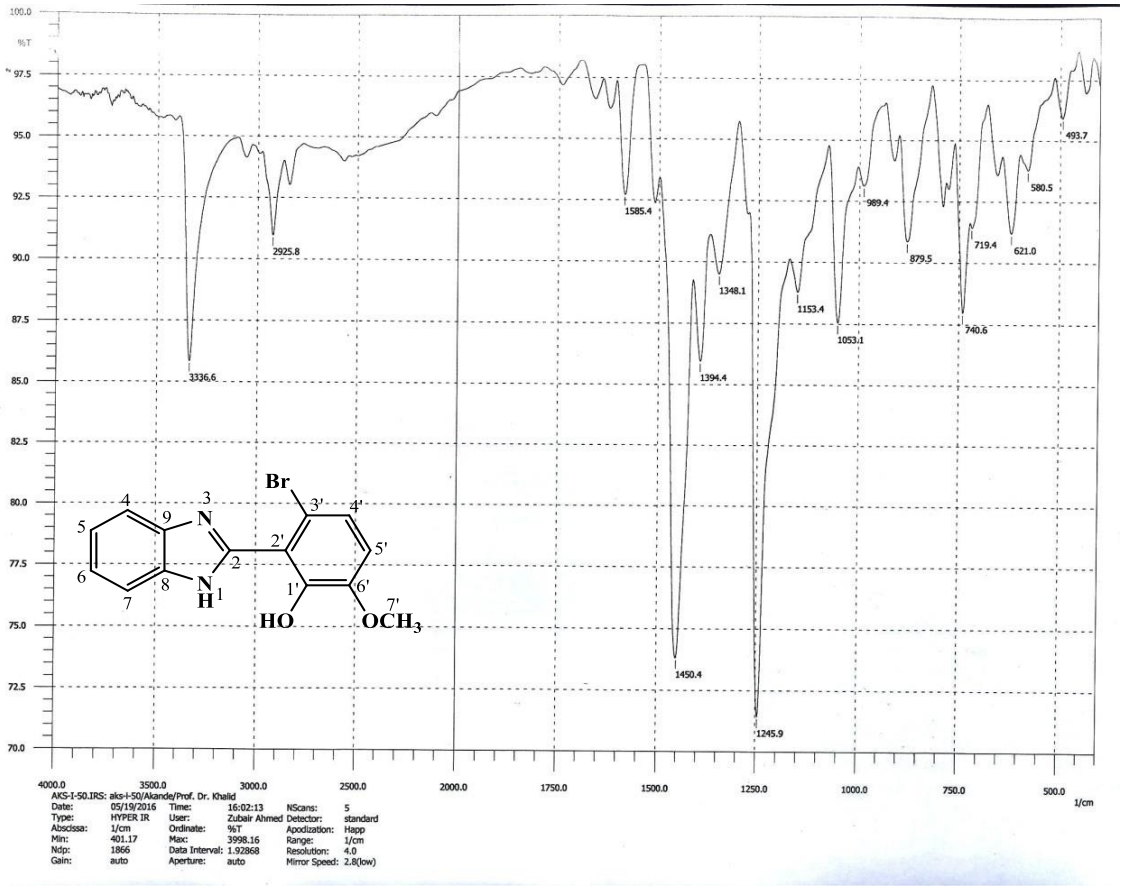

Figure 4.149. IR spectrum of AKS-I-50

THERMO ELECTRON ~ VISIONpro SOFTWARE V4.10

Operator Name	ARSHAD ALAM	Date of Report	5/20/2016
Department	Analytical laboratory#004 TWC	Time of Report	8:59:08AM
Organization	ICCBS.Karachi University.		
Information	Prof Dr. Khalid / Akande.		

Scan Graph

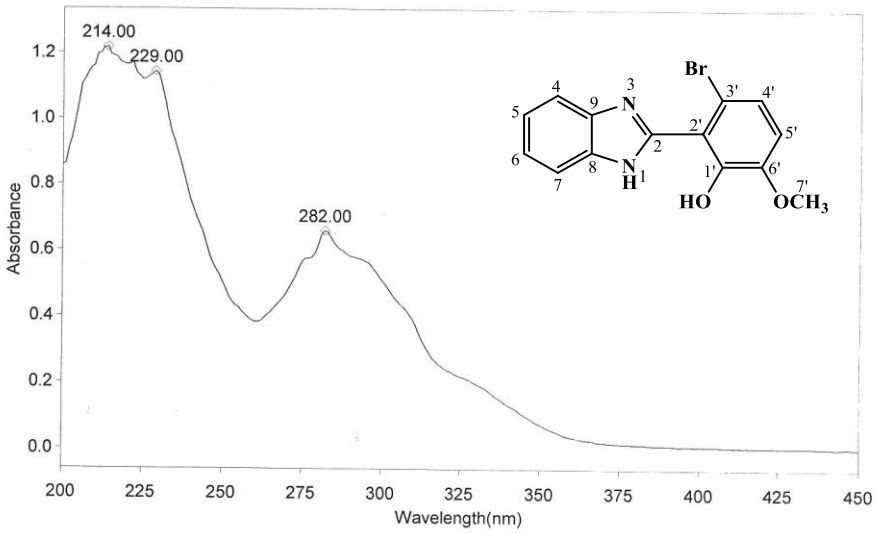

Results Table - AKS- I- 50.sre,AKS- I- 50,Cycle01

nm	A	Peak Pick Method
214.00	1.219	Find 8 Peaks Above -3.0000 A
229.00	1.144	Start Wavelength 200.00 nm
282.00	0.661	Stop Wavelength 450.00 nm
		Sort By Wavelength
Sensitivity	Medium	

Page 1, Scan Graph

Figure 4.150. UV spectrum of AKS-I-50

Table 4.24. Summary of the ^{1}H NMR and ^{13}C NMR spectra of AKS-I-50

Position	δ ^{1}H [mult., J_{HH} (Hz)] (ppm)
1	11.77 [br d]
2	-
3	-
4	7.62-7.60 [m]
5	7.24-7.22 [m]
6	7.24-7.22 [m]
7	7.62-7.60 [m]
8	-
9	-
1′-OH	Exchangeable
1′	-
2′	-
3′	-
4′	7.18 [d, $J_{4',5'}$ = 8.8]
5′	7.07 [d, $J_{5',4'}$ = 8.8]
6′	-
7′-OCH_3	3.84 [s]

4.1.25 Characterisation of 3′-bromo-2′-(5-fluoro-1*H*-benzo[*d*]imidazol-2-yl)-6′-ethoxyphenol (AKS-I-51)

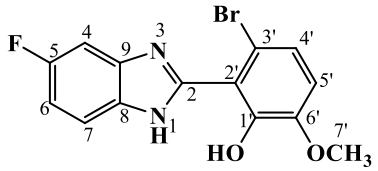

The compound, AKS-I-51 was obtained as a brown solid with a yield of 65.0% (0.219 g), a m.pt. range of 210-213 ^{o}C and a R_f of 0.50 (hexane/ethyl acetate, 1:1).

Six resonances, δ (ppm) from ^{1}H NMR spectra (400 MHz, DMSO-d_6) (figures **4.151** and **4.152**) represent nine protons at 11.56 (br s, N–H) assigned to the amine proton, 7.57-7.61 (1H, m, H-4), 7.40 (1H, dd, $J_{7,6}$ = 7.6 Hz, H-7), 7.17 (1H, d, $J_{4',5'}$ = 8.8 Hz, H-4′), 7.10 (1H, dt, $J_{6,7}$ = 9.6 Hz, H-6), 7.07 (1H, d, $J_{5',4'}$ = 8.8 Hz, H-5′) assigned to the methine protons and 3.84 (3H, s, 6′-OCH_3) assigned to the methoxy protons. The exchangeable hydroxy proton (-OH) was not seen. The influence of fluorine on the splitting pattern (multiplet) for proton on carbon 4 was observed. Furthermore, ortho coupling existed between protons at positions 5′ and 4′ with a coupling constant of 8.8 Hz.

The ^{13}C NMR spectra (75 MHz, DMSO-d_6) (figures **4.153** and **4.154**), exhibit fourteen resonances, δ (ppm) assigned as 147.85 (C-1′), 118.72 (C-2′), 112.58 (C-3′), 149.62 (C-6′), 156.95 (C-2), 160.07 (C-5), 147.56 (C-9, C-8) to eight quarternary carbons, 117.65 (C-7), 114.33, 114.07 (C-6), 110.29, 109.95 (C-4), 122.50 (C-5′, C-4′), 118.77 to five methine carbons and 56.16 (C-7′) to the methoxy carbon respectively. The DEPTH-135 (100 MHz, DMSO-d_6) spectrum shown in figure **4.155** also corroborates the respective methine, methoxy and methyl carbons.

Figure **4.156** shows the ion peaks from EI-MS analysis. The molecular ion, M^+ and the isotope ion, [M^++2] peaks have *m/z* of 336 and 338 (base peak) respectively. The dehydration of [M^++2] ion is indicative of the peak at *m/z* 320. Also, loss of CH_2=O radical suggests the peak at *m/z* 307. [M^++2]-43 cleavage is suggestive of the fragment at *m/z* 293 corresponding to $[C_{12}H_7BrFN_2O]^+$. Loss of HBr by the isotope radical ion produced the fragment at *m/z* 258 corresponding to $[C_{14}H_{10}FN_2O_2]^+$. The *m/z* of 185 corresponds to $[C_{12}H_{13}N_2]^+$ fragment. The molecular formular, $C_{14}H_{10}BrFN_2O_2$ was confirmed by HREI-MS analysis with *m/z* value of 335.9904 (calculated, 335.9910).

The IR absorption spectrum (figure **4.157**) reveals the presence of N–H_{str}, C–H_{str} of aromatic, C–H_{str} of aliphatic, C=C_{str} of aromatic, C–H_b of OCH_3, C–O_{str} of ether and C–

F_{str}, with vibrational frequencies, $\bar{\upsilon}$ (cm^{-1}) at 3336, 3100, 2931, 1591, 1450, 1247 and 1136 respectively. The UV spectrum (figure **4.158**) indicative of n→π* and π→π* transitions, shows wavelenghts of maximum absorptions (λ_{max}) at 287, 228 and 212 nm. Summary of the ^{1}H NMR and ^{13}C NMR spectra is represented in table **4.25**.

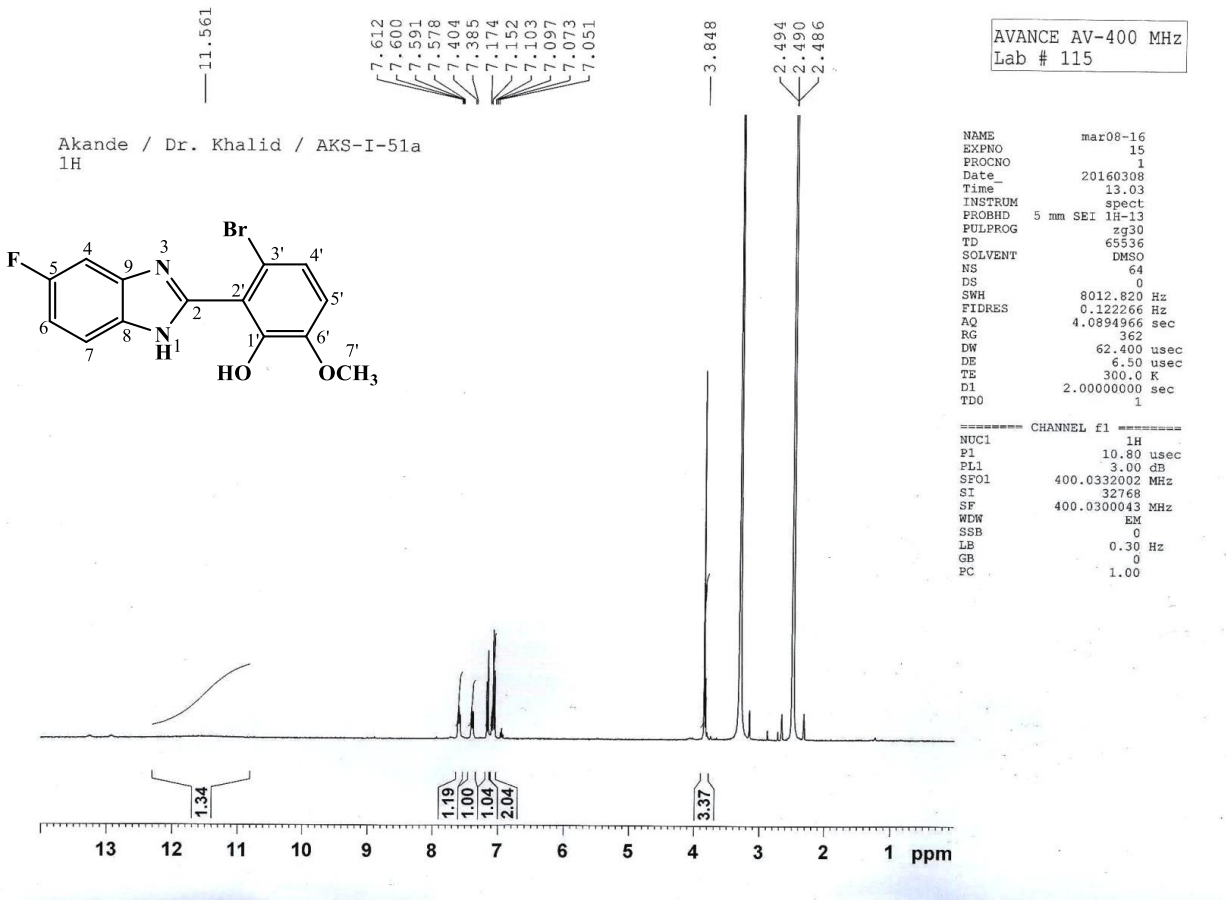

Figure 4.151. ^{1}H NMR (400 MHz, DMSO-d_6) spectrum of AKS-I-51

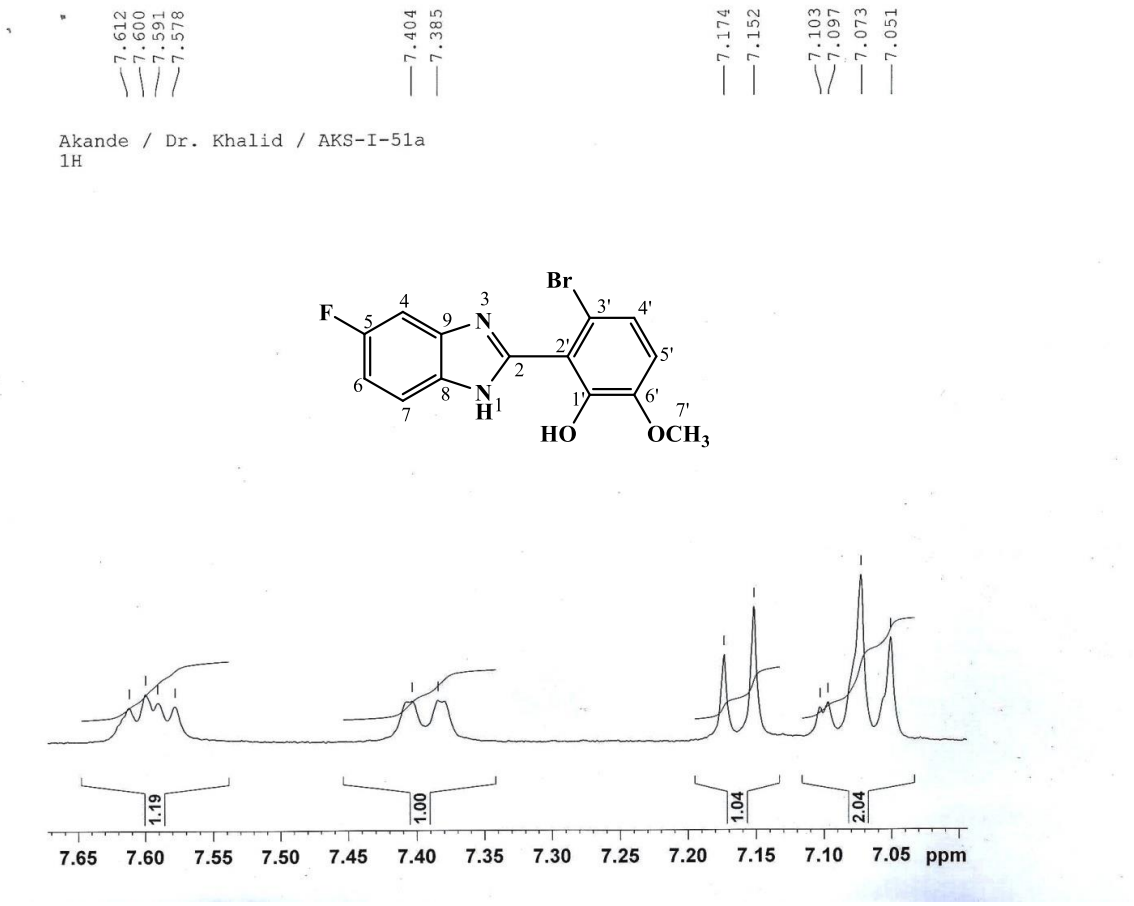

Figure 4.152. ^{1}H NMR (400 MHz, DMSO-d_6) spectrum of AKS-I-51 (Expanded)

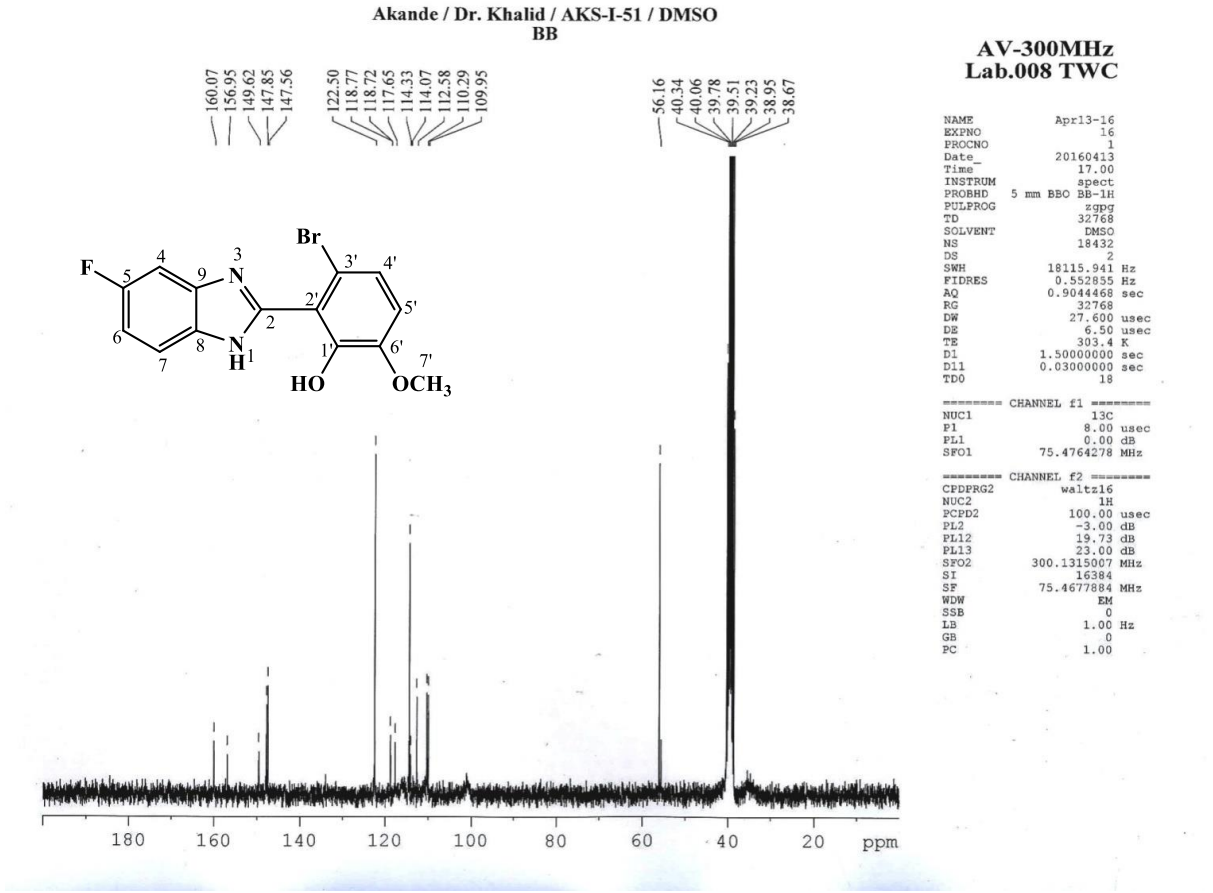

Figure 4.153. ^{13}C NMR (75 MHz, DMSO-d_6) spectrum of AKS-I-51

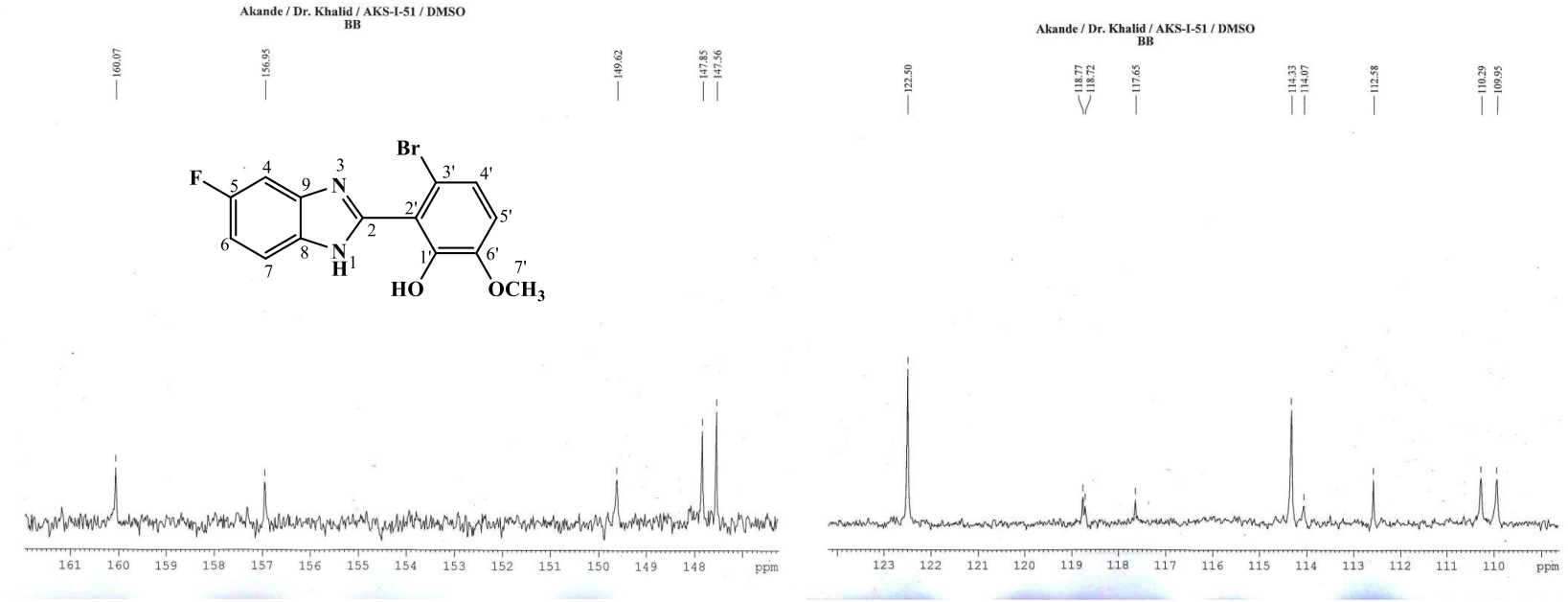

Figure 4.154. ^{13}C NMR (75 MHz, DMSO-d_6) spectra of AKS-I-51 (Expanded)

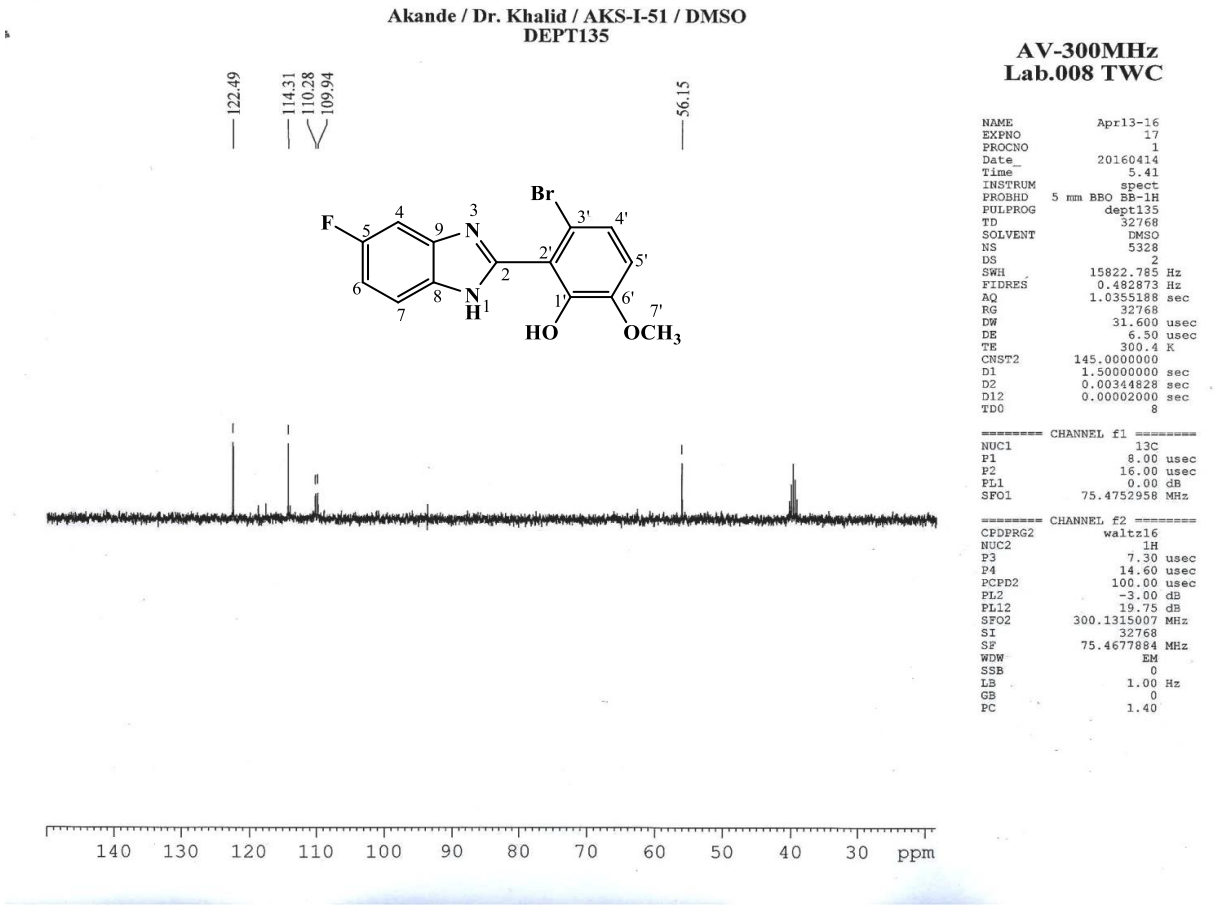

Figure 4.155. DEPTH-135 (75 MHz, DMSO-d_6) spectrum of AKS-I-51

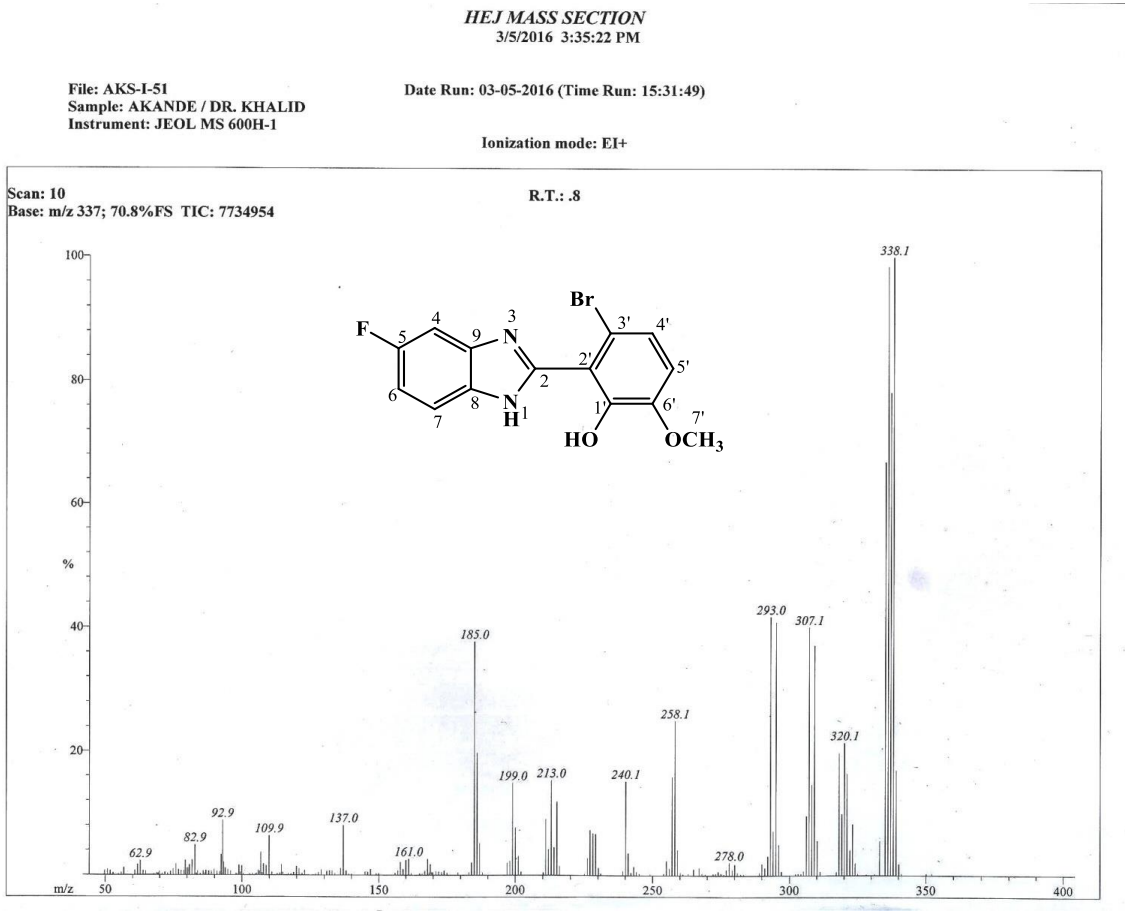

Figure 4.156. EI-MS spectrum of AKS-I-51

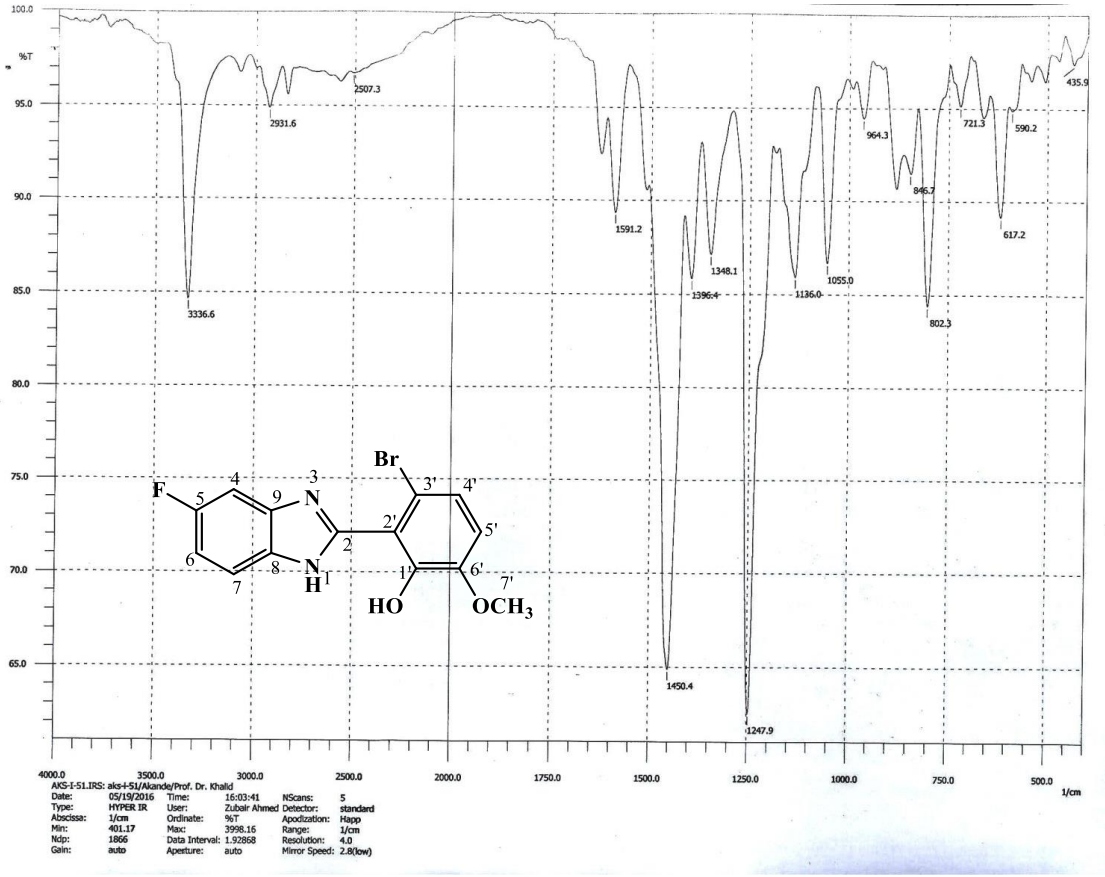

Figure 4.157. IR spectrum of AKS-I-51

THERMO ELECTRON ~ VISIONpro SOFTWARE V4.10

Operator Name	ARSHAD ALAM	Date of Report	5/20/2016
Department	Analytical laboratory#004 TWC	Time of Report	10:18:02AM
Organization	ICCBS.Karachi University.		
Information	Prof Dr. Khalid / Akande.		

Scan Graph

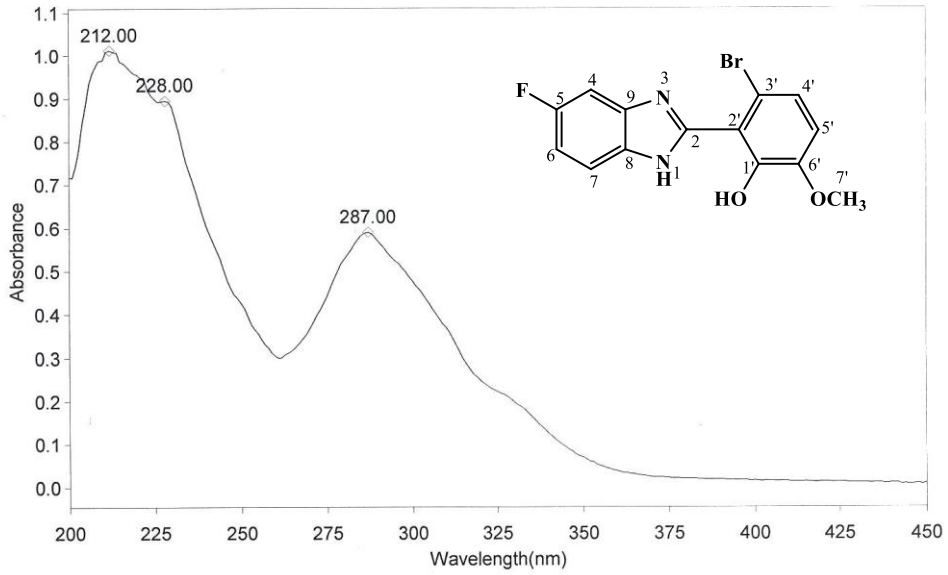

Results Table - AKS- I- 51.sre,AKS- I- 51,Cycle01

nm	A	**Peak Pick Method**
212.00	1.012	Find 8 Peaks Above -3.0000 A
228.00	0.895	Start Wavelength 200.00 nm
287.00	0.590	Stop Wavelength 450.00 nm
		Sort By Wavelength
Sensitivity	Medium	

Page 1, Scan Graph

Figure 4.158. UV spectrum of AKS-I-51

Table 4.25. Summary of the ^{1}H NMR and ^{13}C NMR spectra of AKS-I-51

Position	δ ^{1}H [mult., J_{HH} (Hz)] (ppm)	δ ^{13}C (ppm)	DEPT-135
1	11.56 [br s]	-	-
2	-	156.95	-
3	-	-	-
4	7.61-7.57 [m]	110.29, 109.95	CH
5	-	160.07	-
6	7.10-7.05 [m]	114.33, 114.07	CH
7	7.40 [dd, $J_{7,6}$ = 7.6]	118.77, 117.65	CH
8	-	147.56	-
9	-	147.56	-
1′-OH	Exchangeable	-	-
1′	-	147.85	-
2′	-	118.72	-
3′	-	112.58	-
4′	7.17 [d, $J_{4',5'}$ = 8.8]	122.50	CH
5′	7.10-7.05 [m]	122.50	CH
6′	-	149.62	-
7′-OCH_3	3.84 [s]	56.16	CH_3

4.1.26 Characterisation of 3′-bromo-2′-(5-chloro-1*H*-benzo[*d*]imidazol-2-yl)-6′-ethoxyphenol (AKS-I-52)

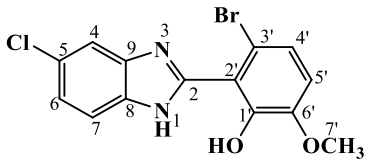

The brown compound, AKS-I-52 was obtained in solid form with a yield of 83.7% (0.296 g), a m.pt. of 214-216 ^{o}C and a R_f value of 0.52 (hexane/ethyl acetate, 1:1). Figures **4.159** and **4.160** represent the ^{1}H NMR spectra (400 MHz, DMSO-d_6) with seven resonance peaks, δ (ppm), assigned as 10.00-12.50 (2H, br s, 1′-OH, -NH) describing the amine and hydroxy protons. The methine protons resonated at 7.65 (1H, s, H-4),7.61 (1H, d, $J_{7,6}$ = 8.4 Hz, H-7), 7.25 (1H, dd, $J_{6,7}$ = 8.4 Hz, $J_{6,4}$ = 2.0 Hz, H-6), 7.17 (1H, d, $J_{4',5'}$ = 8.8 Hz, H-4′) and 7.08 (1H, d, $J_{5',4'}$ = 8.8 Hz, H-5′) while peak at 3.85 describs the methoxy protons (3H, s, 6′-OCH_3). Protons on positions 4′ and 5′ exhibit ortho coupling (coupling constant = 8.8 Hz) while protons on positions 6 and 7 also coupled with each other with proton on position 6 further displayed a meta coupling with proton on position 4.

Also shown in figures **4.161** and **4.162** are the ^{13}C NMR (75 MHz, DMSO-d_6) spectra with δ (ppm) values assigned as 147.52 (C-8, C-9), 149.69 (C-2), 126.27 (C-5), 147.76 (C-6′, C-1′), 118.85 (C-2′), 112.67 (C-3′) indicating the presence of eight quartenary carbons, 122.48 (C-5′, C-4′), 122.17 (C-6), 114.38 (C-7, C-4) representing five methine carbons and 56.16 (C-7′) representing a methoxy carbon. DEPTH-135 (100 MHz, DMSO-d_6) experiment further harmonizes the presence of the respective methine and methoxy carbons as shown in figure **4.163**.

From EI-MS spectrum (figure **4.164**), peak patterns [M^++2] and [M^++4] resulted due to isotope abundance of Br and Cl. Ion peaks at *m/z* 352, 354 and 356 coresponds to [M^+] (molecular ion peak), [M^++2] (isotope and base peak) and [M^++4] (a second isotope peak) respectively. The *m/z* of 336 [M^++2]-18, resulted from a loss in water molecule from the base peak. Cleavage on imidazole ring gave rise to fragment ion with *m/z* of 229 $[C_8H_6BrNO_2]^+$, which on further loss of HCN molecule and $H^{\bullet}$ radical produced the fragment with *m/z* of 201 $[C_7H_4BrO_2]^+$. HREI-MS analysis produced a *m/z* of 351.9602 (calculated, 351.9614) which corresponds to the formula $C_{14}H_{10}BrClN_2O_2$, and further confirming the compound.

The IR spectrum (figure **4.165**) shows absorption frequencies $\bar{\upsilon}$ (cm^{-1}) at 3336, ≈3100, 2837, 1587, 1247, 1053 and 875 indicating the presence of OH_{str} overlaping the $N–H_{str}$, aromatic $C–H_{str}$, aliphatic $C–H_{str}$, aromatic $C=C_{str}$, $C–O_{str}$, $C–Cl_{str}$ and $C–Br_{str}$ respectively. Figure **4.166** represents the UV spectrum showing maximum absorptions (λ_{max}) at 291 and 213 nm indicating $n\rightarrow\pi^*$ and $\pi\rightarrow\pi^*$ transitions. Table **4.26** gives the summary of ^{1}H NMR and ^{13}C NMR spectra.

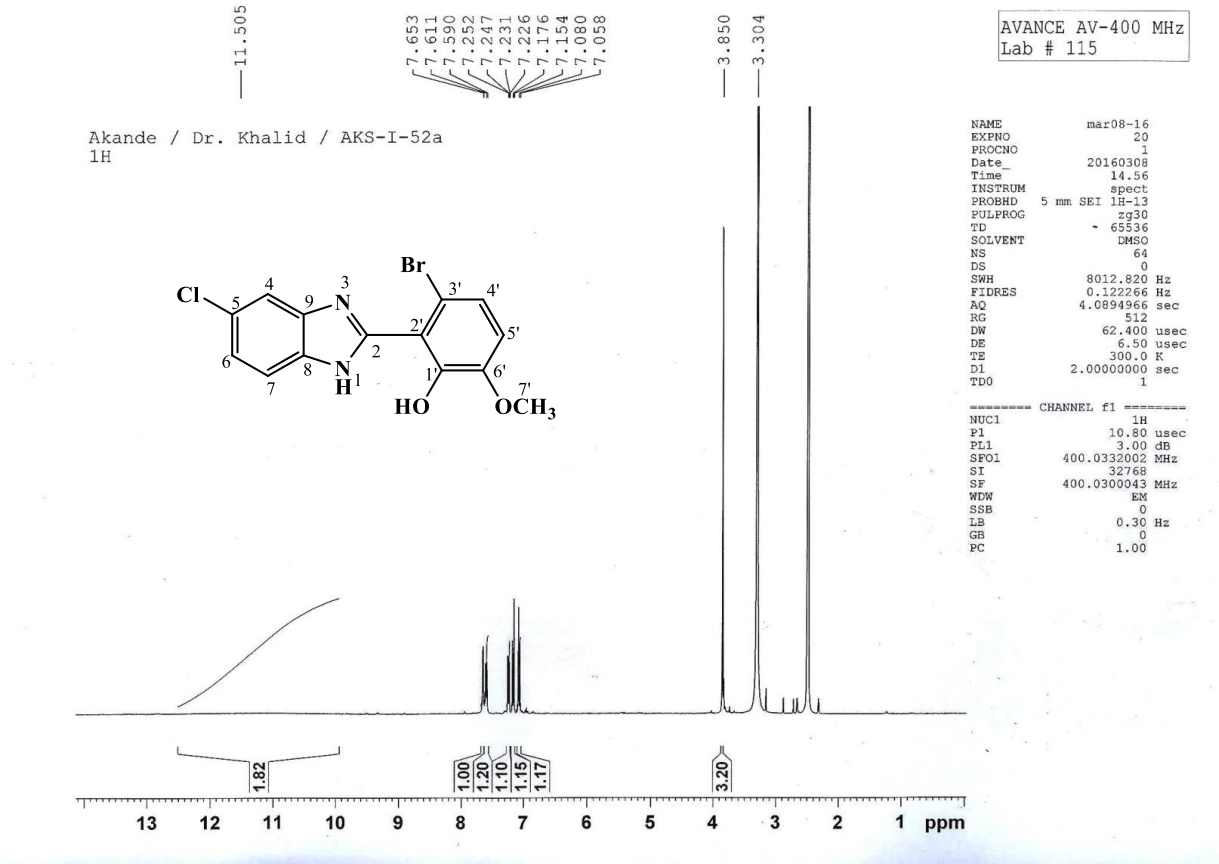

Figure 4.159. ^{1}H NMR (400 MHz, DMSO-d_6) spectrum of AKS-I-52

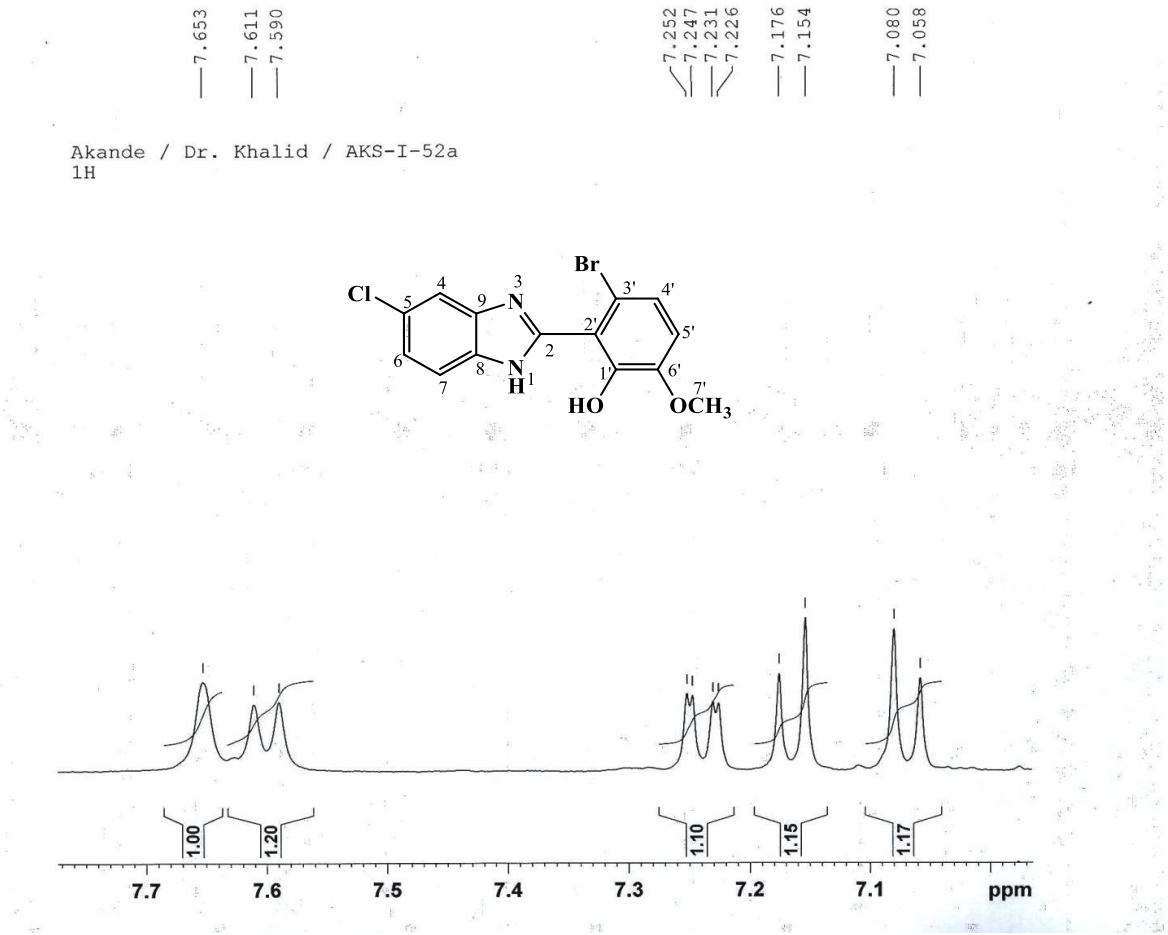

Figure 4.160. ^{1}H NMR (400 MHz, DMSO-d_6) spectrum of AKS-I-52 (Expanded)

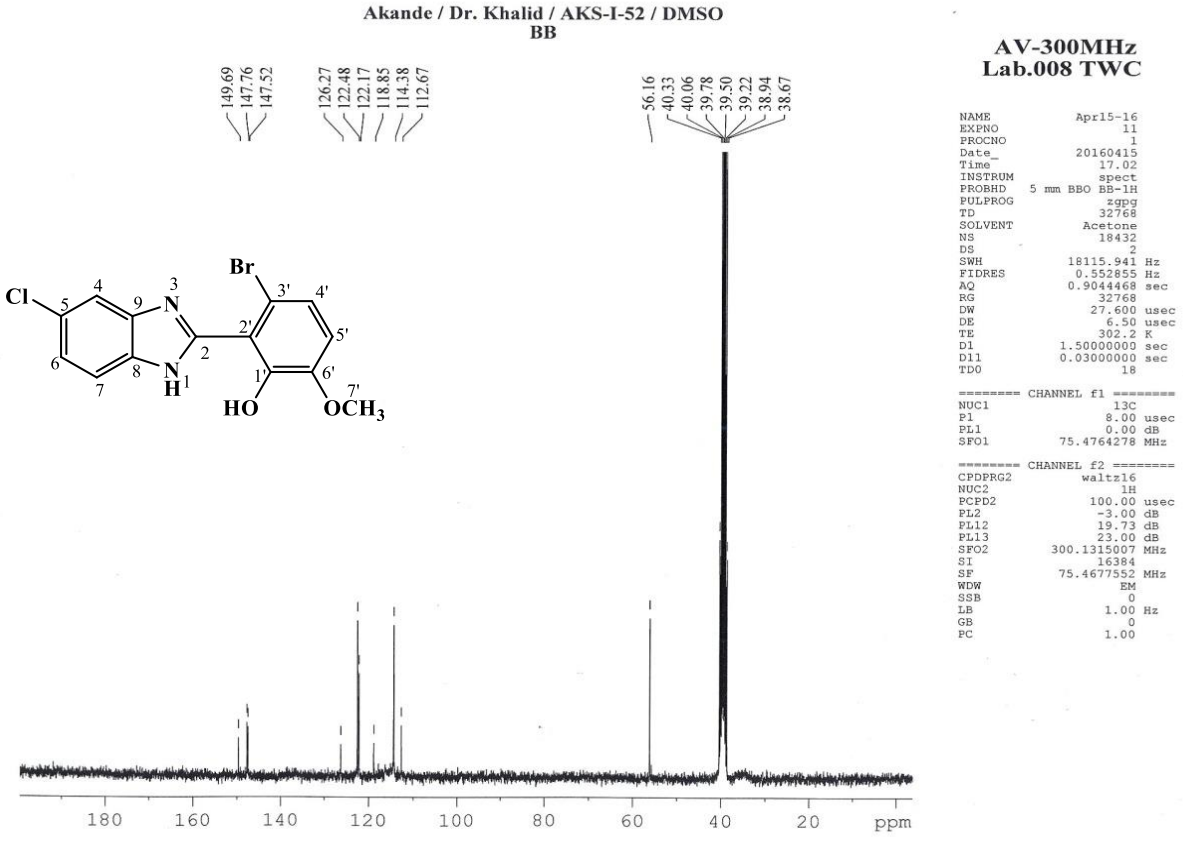

Figure 4.161. ^{13}C NMR (75 MHz, DMSO-d_6) spectrum of AKS-I-52

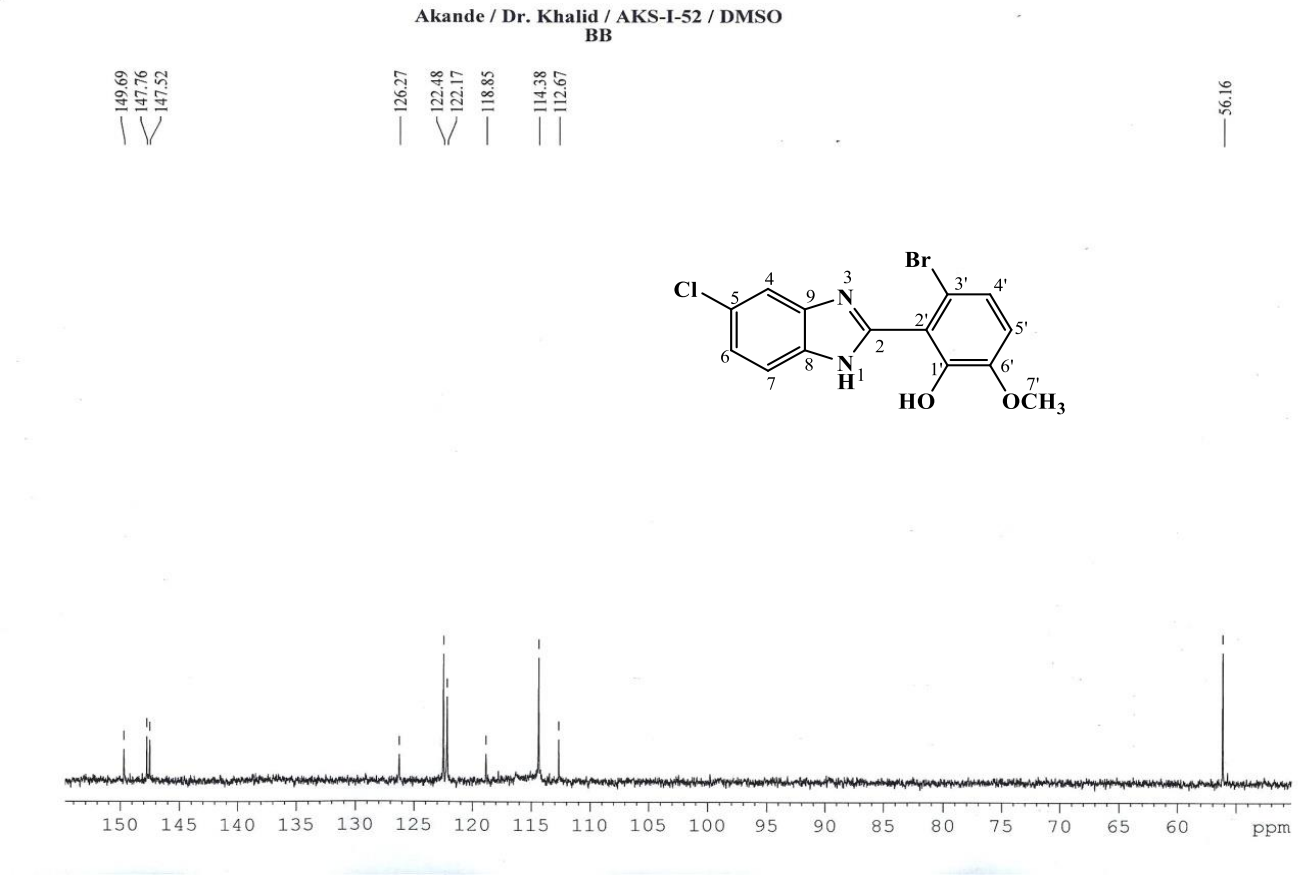

Figure 4.162. ^{13}C NMR (75 MHz, DMSO-d_6) spectrum of AKS-I-52 (Expanded)

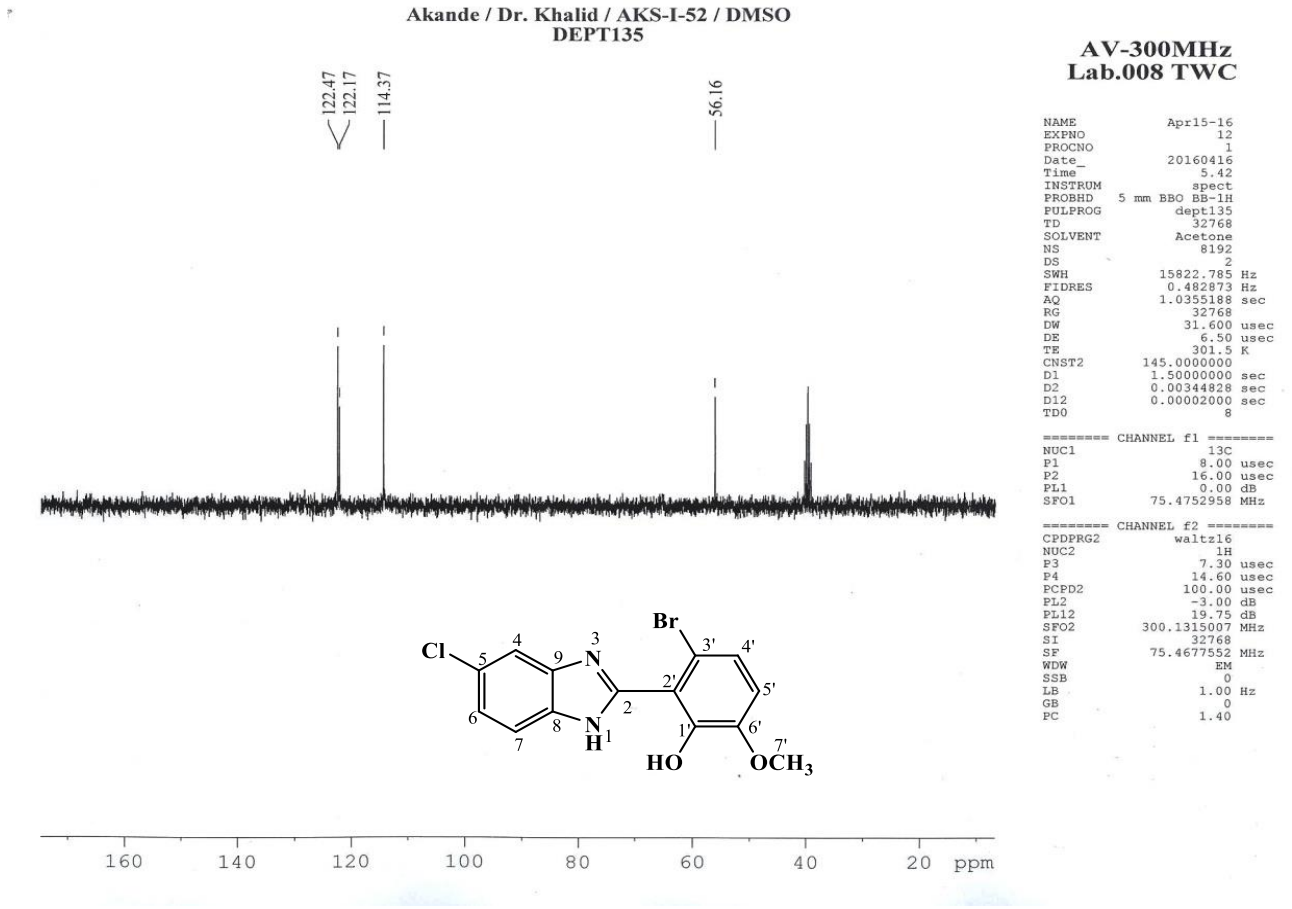

Figure 4.163. DEPTH-135 (75 MHz, DMSO-d_6) spectrum of AKS-I-52

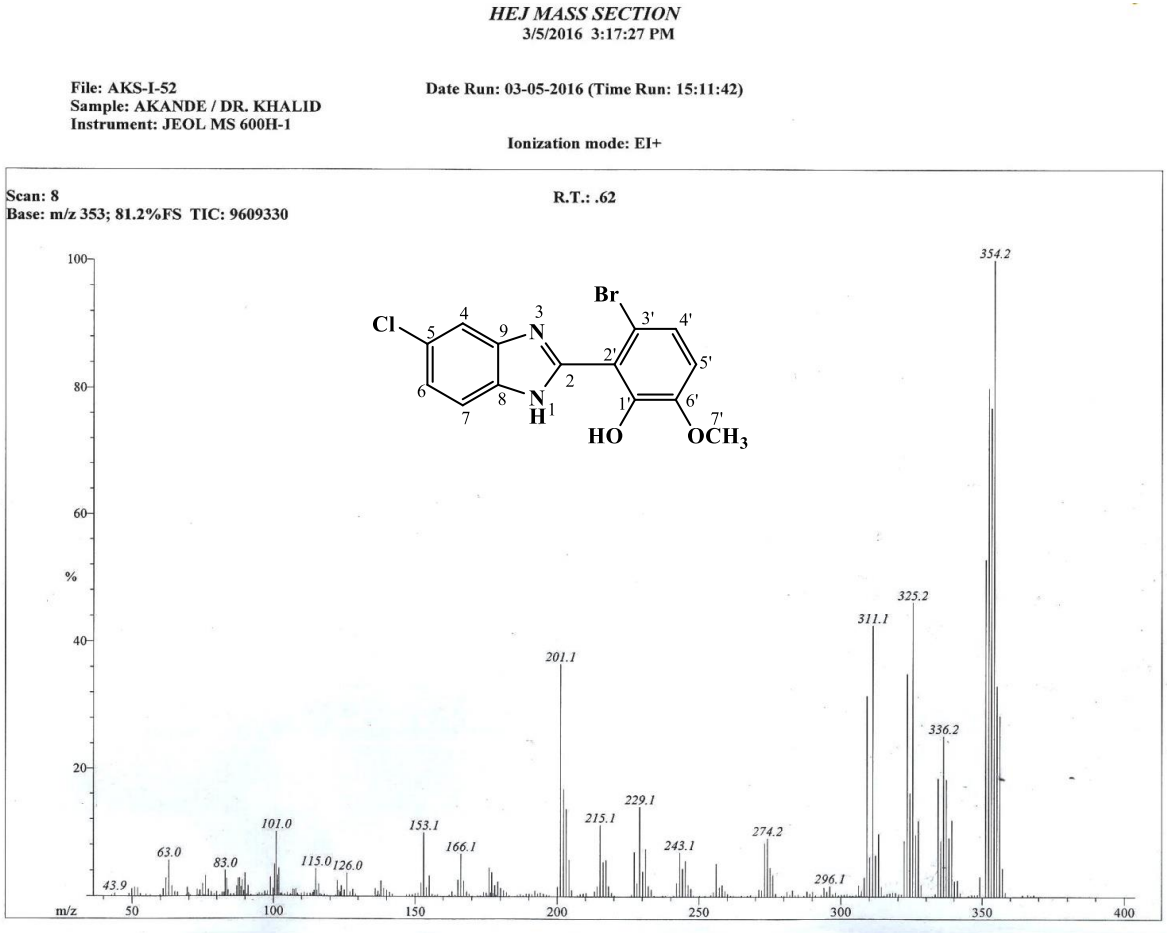

Figure 4.164. EI-MS spectrum of AKS-I-52

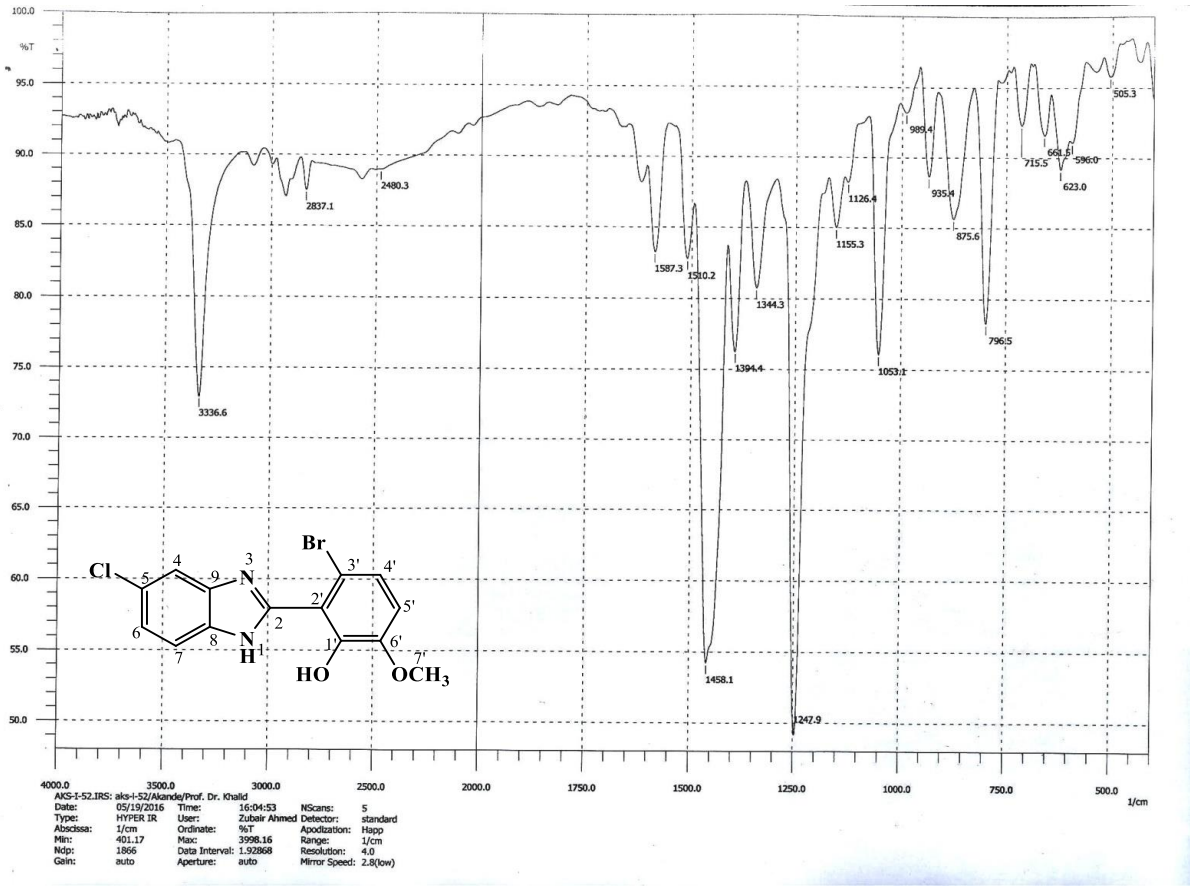

Figure 4.165. IR spectrum of AKS-I-52

THERMO ELECTRON ~ VISIONpro SOFTWARE V4.10

Operator Name	ARSHAD ALAM	Date of Report	5/20/2016
Department	Analytical laboratory#004 TWC	Time of Report	9:13:11AM
Organization	ICCBS.Karachi University.		
Information	Prof Dr. Khalid / Akande.		

Scan Graph

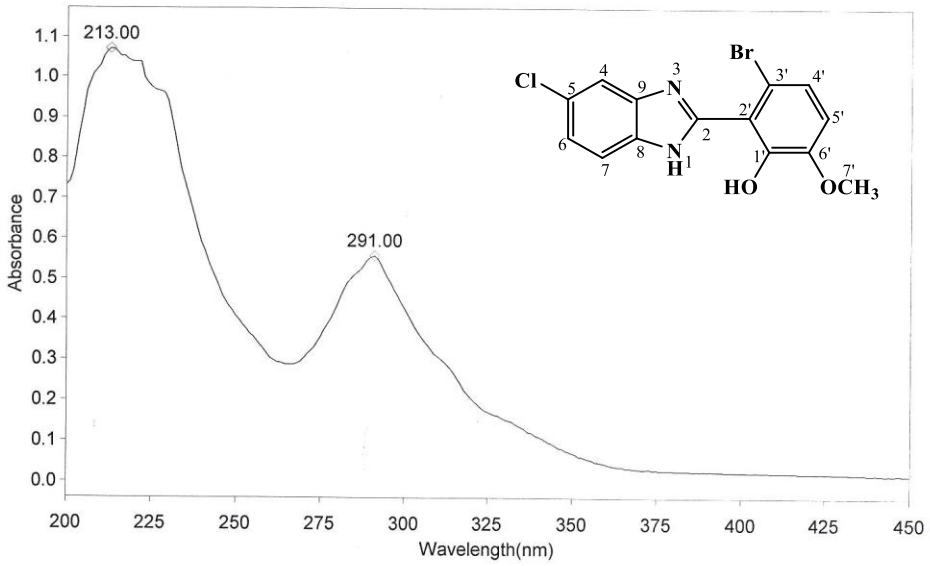

Results Table - AKS- I- 52.sre,AKS- I- 52,Cycle01

nm	A	**Peak Pick Method**
213.00	1.071	Find 8 Peaks Above -3.0000 A
291.00	0.557	Start Wavelength 200.00 nm
		Stop Wavelength 450.00 nm
		Sort By Wavelength
Sensitivity	Low	

Page 1, Scan Graph

Figure 4.166. UV spectrum of AKS-I-52

Table 4.26. Summary of the ^{1}H NMR and ^{13}C NMR spectra of AKS-I-52

Position	δ ^{1}H [mult., J_{HH} (Hz)] (ppm)	δ ^{13}C (ppm)	DEPT-135
1	12.50-10.00 [br s]	-	-
2	-	149.69	-
3	-	-	-
4	7.65 [s]	114.38	CH
5	-	126.27	-
6	7.25 [dd, $J_{6,7}$ = 8.4, $J_{6,4}$ = 2.0]	122.17	CH
7	7.61 [d, $J_{7,6}$ = 8.4]	114.38	CH
8	-	147.52	-
9	-	147.52	-
1′-OH	12.50-10.00 [br s]	-	-
1′	-	147.76	-
2′	-	118.85	-
3′	-	112.67	-
4′	7.17 [d, $J_{4',5'}$ = 8.8]	122.48	CH
5′	7.08 [d, $J_{5',4'}$ = 8.8]	122.48	CH
6′	-	147.76	-
7′-OCH_3	3.85 [s]	56.16	CH_3

4.1.27 Characterisation of 3′-bromo-2′-(5,6-dimethyl-1*H*-benzo[*d*]imidazol-2-yl)-6′-methoxyphenol (AKS-I-54)

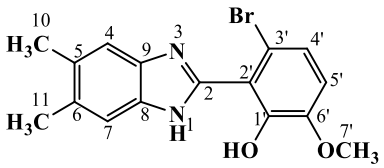

The brown compound, AKS-I-54 was obtained as a solid. It has a yield of 75.7% (0.263 g), a m.pt. of 236-239 ^{o}C and a R_f value of 0.52 in a hexane/ethyl acetate (1:1) solvent system.

The ^{1}H NMR spectra (400 MHz, DMSO-d_6) in figures **4.167** and **4.168** show six resonance peaks and the δ (ppm) values are assigned as 11.88 (br s, 1H, N-H) to the amine proton, 7.39 (2H, s, H-4, H-7), the leaning peaks at 7.16 (1H, d, $J_{4',5'}$ = 8.8 Hz, H-4′) and the doublet at 7.04 (1H, d, $J_{5',4'}$ = 8.8 Hz, H-5′) to four aromatic methine protons, 3.83 (s, 3H, 7′-OCH_3) to the methoxy protons and a 2.32 chemical shift value (6H, s, 11-CH_3, 10-CH_3) to six equivalent methyl protons. The hydroxy proton (exchangeable) was not seen on the spectrum.

The EI-MS spectrum (figure **4.169**) shows peak patterns spaced two mass units apart. The *m/z* for the molecular ion, M^+ and [M^++2] peaks are 346 (base peak) and 348 (isotope peak) respectively. M^+-18 is typical of water loss from molecular ion which corresponds to a *m/z* of 328. The peak at *m/z* 317 is indicative of M^+-CHO. Loss of radical fragments $CH_3O^{\bullet}$, $OH^{\bullet}$ and $2CH_3^{\bullet}$ suggest the peak with *m/z* of 268. The *m/z* of 225 also suggests a fragment resulting from imidazole ring cleavage while *m/z* of 195 corresponds to $[C_7H_2BrO_2]^+$ fragment. Peak at *m/z* of 90 corresponds to a tropylium ion $[C_7H_7]^+$. The *m/z* obtained from HREI-MS analysis corresponding to the formula $C_{16}H_{15}BrN_2O_2$, is 346.0295 (calculated, 346.0317), further confirming the compound.

The IR spectrum (figure **4.170**) shows absorption bands typical functional groups with vibrational frequencies, $\bar{\upsilon}$ (cm^{-1}) assigned as ≈3370, 3359, ≈3010, 2931, 2846, 1583, 1461, 1251 and 1056 to N–H_{str} of 2^{o} amine, O–H_{str}, aromatic C–H_{str}, aliphatic C–$H_{asy\ str}$ and C–$H_{sym\ str}$, aromatic C=C_{str}, C–H_b, C–O_{str} and C–Br_{str} respectively. The UV spectum in figure **4.171** shows peaks indicative of n→π* and π→π* transitions corresponding to wavelenghts of maximum absorptions (λ_{max}) at 291, 229, 222 and 213 nm. **Table 4.27** represents the summary of ^{1}H NMR spectra.

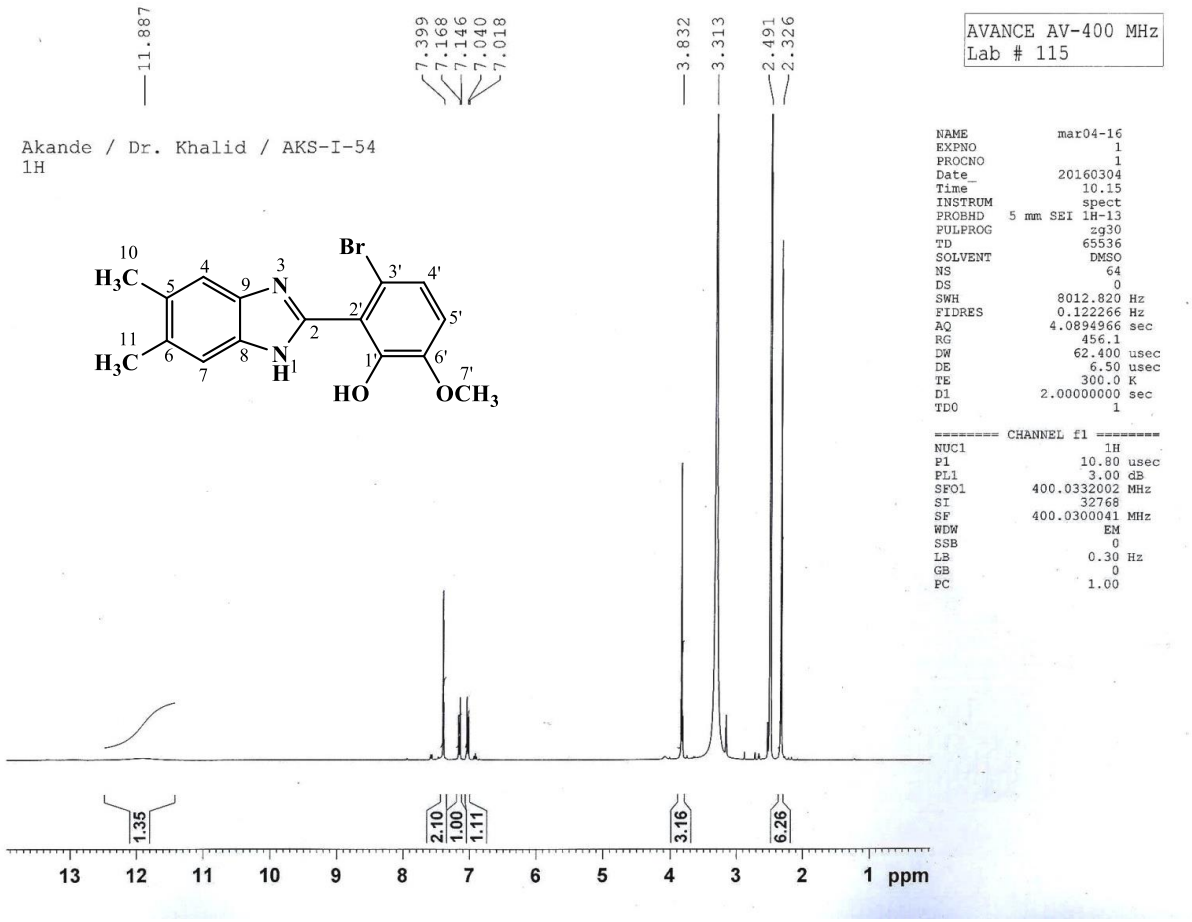

Figure 4.167. ^{1}H NMR (400 MHz, DMSO-d_6) spectrum of AKS-I-54

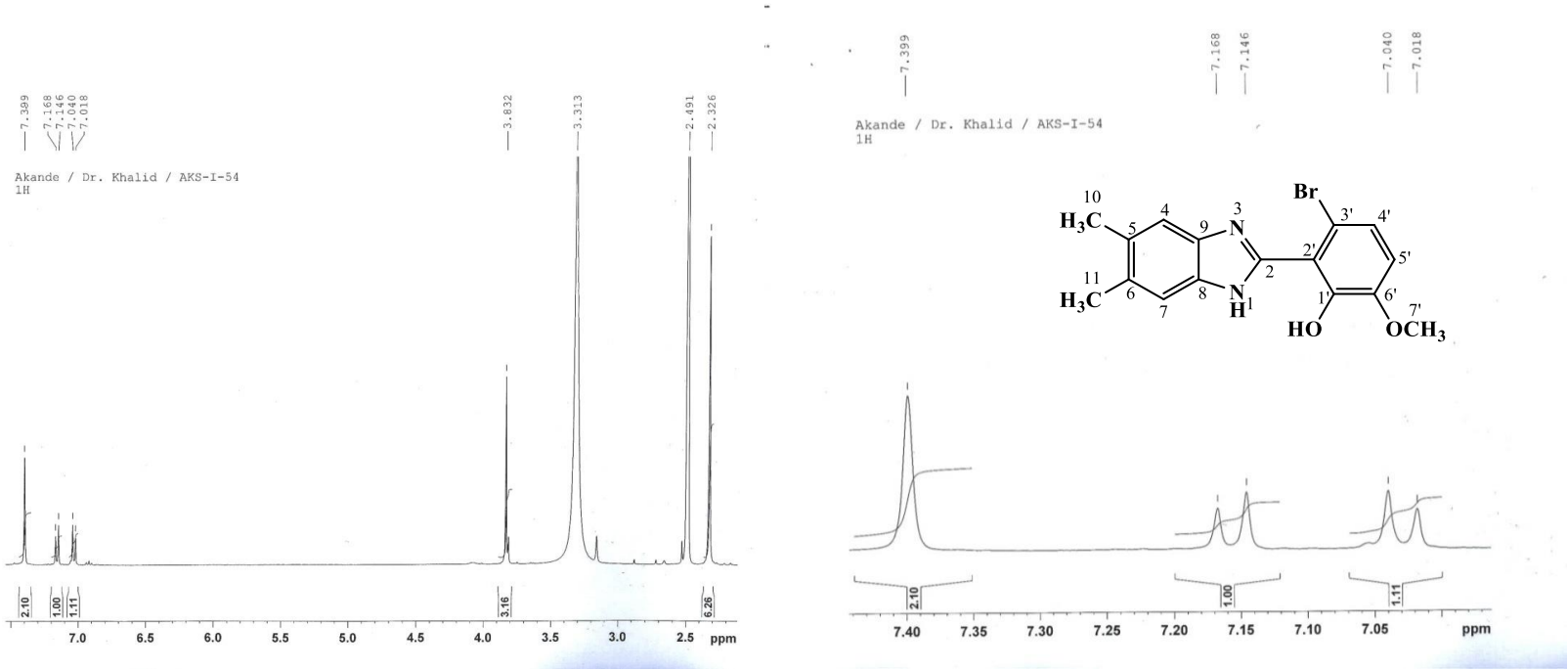

Figure 4.168. ^{1}H NMR (400 MHz, DMSO-d_6) spectra of AKS-I-54 (Expanded)

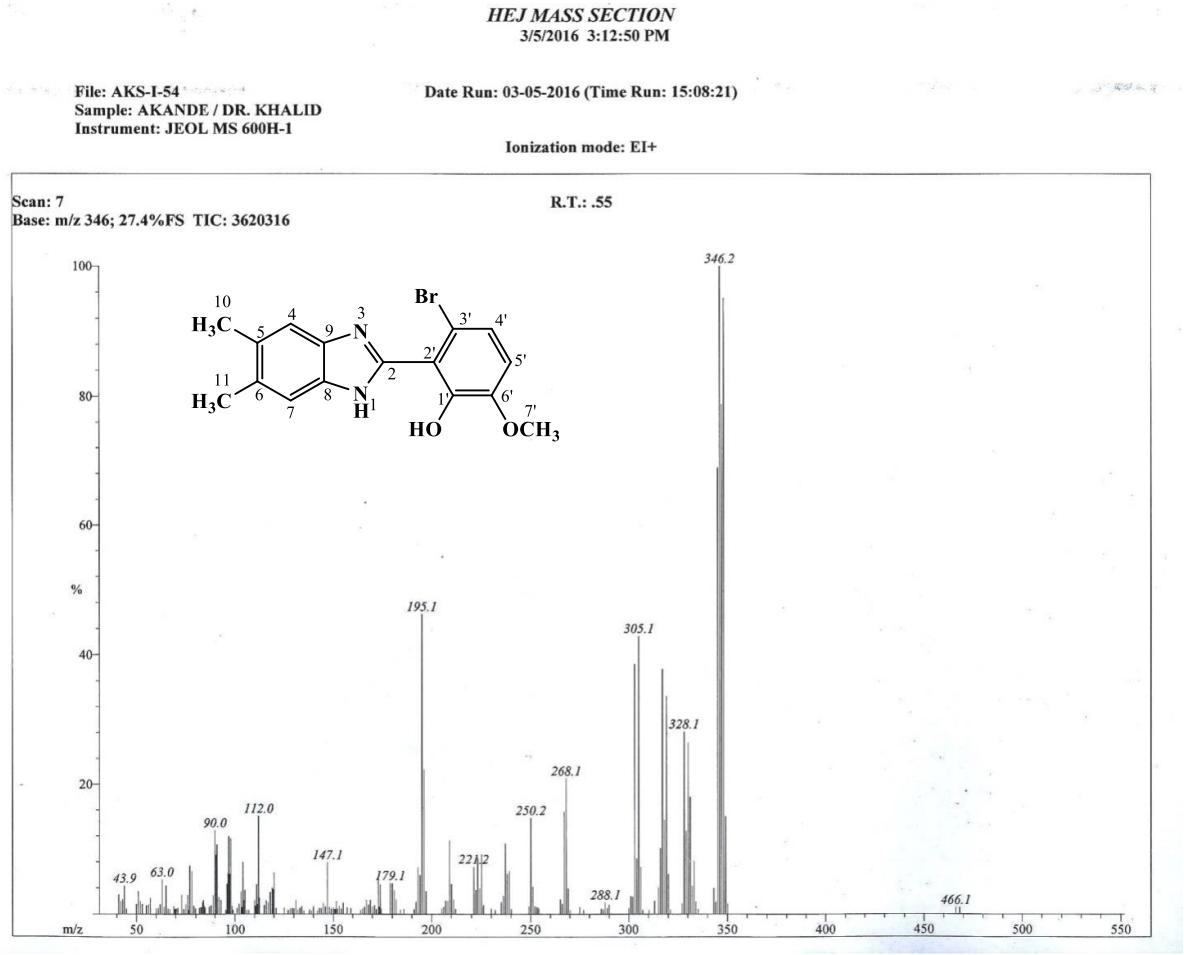

Figure 4.169. EI-MS spectrum of AKS-I-54

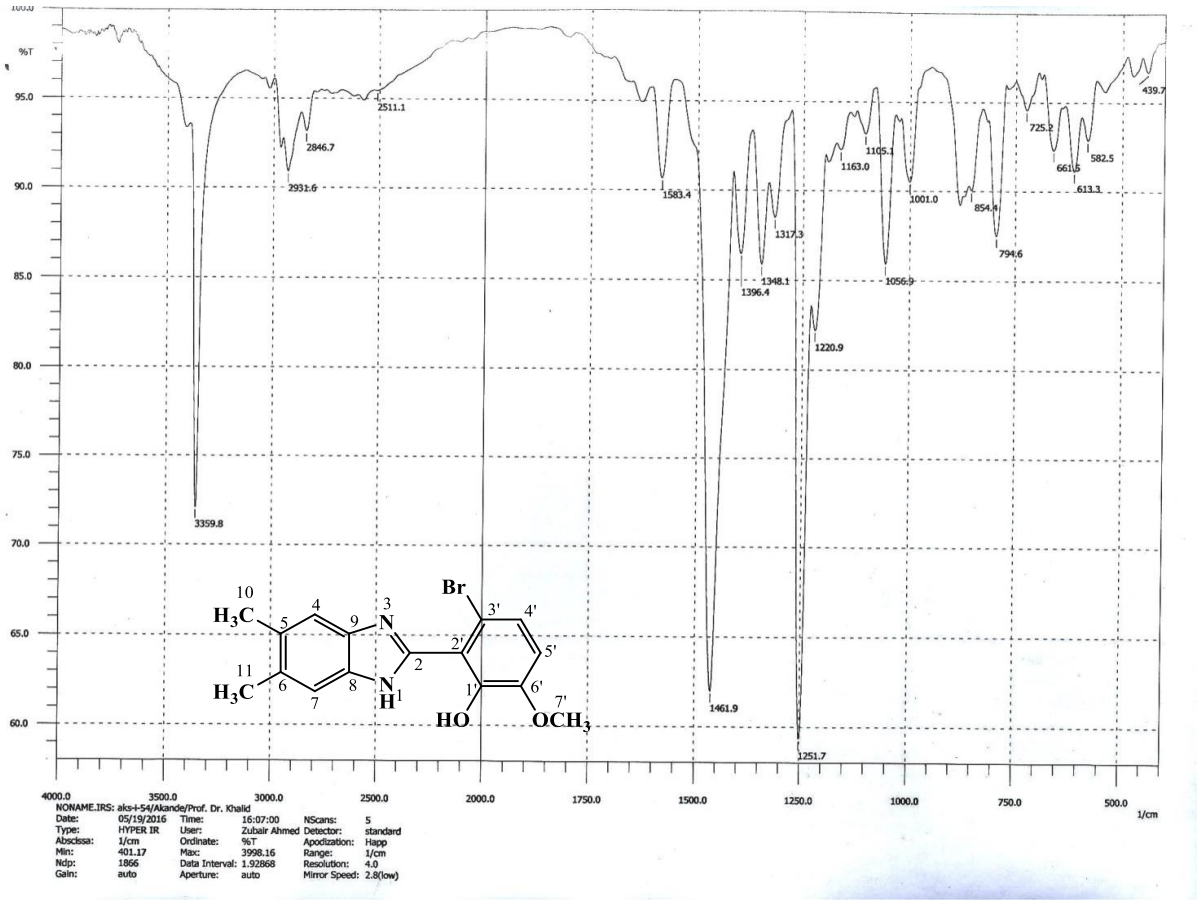

Figure 4.170. IR spectrum of AKS-I-54

THERMO ELECTRON ~ VISIONpro SOFTWARE V4.10

Operator Name	ARSHAD ALAM	Date of Report	5/20/2016
Department	Analytical laboratory#004 TWC	Time of Report	9:30:28AM
Organization	ICCBS.Karachi University.		
Information	Prof Dr. Khalid / Akande.		

Scan Graph

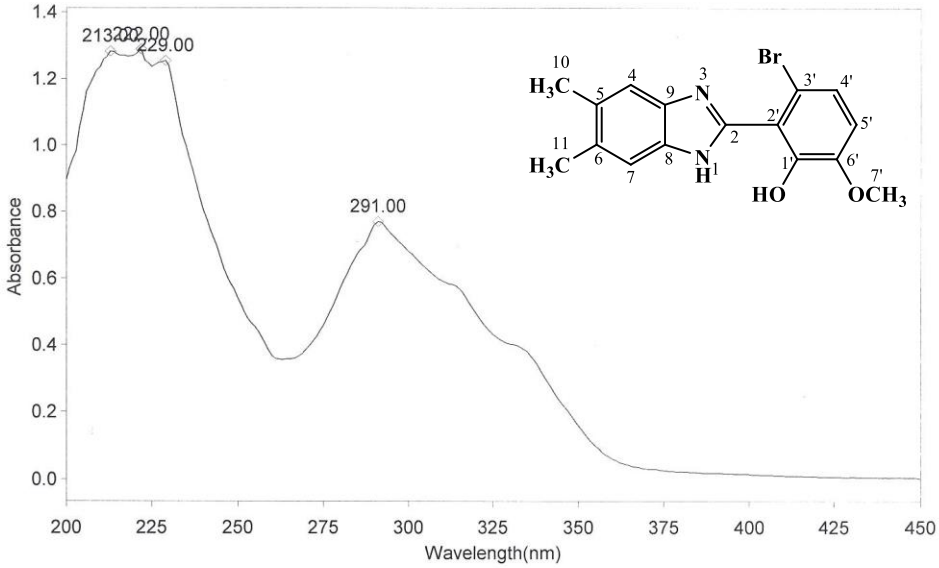

Results Table - AKS- I- 54.sre,AKS- I- 54,Cycle01

nm	A	**Peak Pick Method**
213.00	1.283	Find 8 Peaks Above -3.0000 A
222.00	1.289	Start Wavelength 200.00 nm
229.00	1.255	Stop Wavelength 450.00 nm
291.00	0.770	Sort By Wavelength
Sensitivity	Medium	

Page 1, Scan Graph

Figure 4.171. UV spectrum of AKS-I-54

Table 4.27. Summary of the ^{1}H NMR spectra of AKS-I-54

Position	δ ^{1}H [mult., J_{HH} (Hz)] (ppm)
1	11.88 [br s]
2	-
3	-
4	7.39 [s]
5	-
6	-
7	7.39 [s]
8	-
9	-
10-CH_3	2.32 [s]
11-CH_3	2.32 [s]
1′-OH	Exchangeable
1′	-
2′	-
3′	-
4′	7.16 [d, $J_{4',5'}$ = 8.8]
5′	7.04 [d, $J_{5',4'}$ = 8.8]
6′	-
7′-OCH_3	3.83 [s]

4.1.28 Characterisation of 4′-(5-fluoro-1*H*-benzo[*d*]imidazol-2-yl)-2′,6′-dimethoxy-phenol (AKS-I-55)

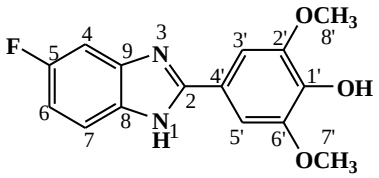

The brown compound, AKS-I-55 was obtained in solid form with a yield of 55.9% (0.161 g), m.pt. range of 311-313 ^{o}C and a R_f value of 0.36 (hexane/ethyl acetate, 7:3).

Figures **4.172** and **4.173** present the ^{1}H NMR spectra (400 MHz, DMSO-d_6). The chemical shifts, δ (ppm) obtained for five resonaces are described as follows: 9.29 was assigned to the hydroxy proton (1H, br s, 1′-OH), the multiplet peak at 7.64-7.68 due to the presence of a fluorine atom (1H, m, H-4), the other multiplet at 7.49-7.51 (3H, m, H-5′, H-3′, H-7), and a doublet of tripplet at 7.21 (1H, dt, $J_{6,7}$ = 8.8 Hz, $J_{6,4}$ = 2.4 Hz, H-6) were assigned to the methine protons while the singlet at 3.88 was assigned to the six equivalent methoxy protons (6H, s, 8′-OCH_3, 7′-OCH_3). The amine proton was not captured.

The EI-MS spectrum (figure **4.174**) reveals the molecular ion, M^+ as the base peak at *m/z* of 288 and a [M+1] peak at 289. Peaks at *m/z* of 273 and 257 correspond to [M^+-CH_3] and [M^+-OCH_3] respectively. [M^+-HF] resulted to *m/z* of 269 ion. Cleavage of the imidazole ring yielded a *m/z* of 108 $[C_6H_3FN]^+$. The *m/z* 174 and 245 corresponds to the fragments $[C_{10}H_7FN_2]^+$ and $[C_{13}H_{10}FN_2O_2]^+$ respectively. The *m/z* of 288.0908 (calculated, 288.0910), obtained from the HREI-MS analysis, corresponds to the molecular formula $C_{15}H_{13}FN_2O_3$, and further confirms the compound.

The IR absorption spectrum (figure **4.175**) shows the presence of O–H_{str}, N–H_{str}, aromatic C–H_{str}, aliphatic C–H_{str}, two aromatic C=C_{str}, C–H_b from OCH_3, symmetric and asymmetric C–O_{str} of ether and C–F_{str} corresponding to 3516, 3375, ≈3050, 2937, 1612, 1510, 1477, 1232, 1112 and 1145 cm^{-1} vibrational frequencies, $\bar{\upsilon}$ respectively. Figure **4.176** represents the UV spectrum of the compound with λ_{max} at 316 and 217 nm equivalent to n→π* and π→π* transitions respectively. Summary of the ^{1}H NMR spectra is represented in table **4.28**.

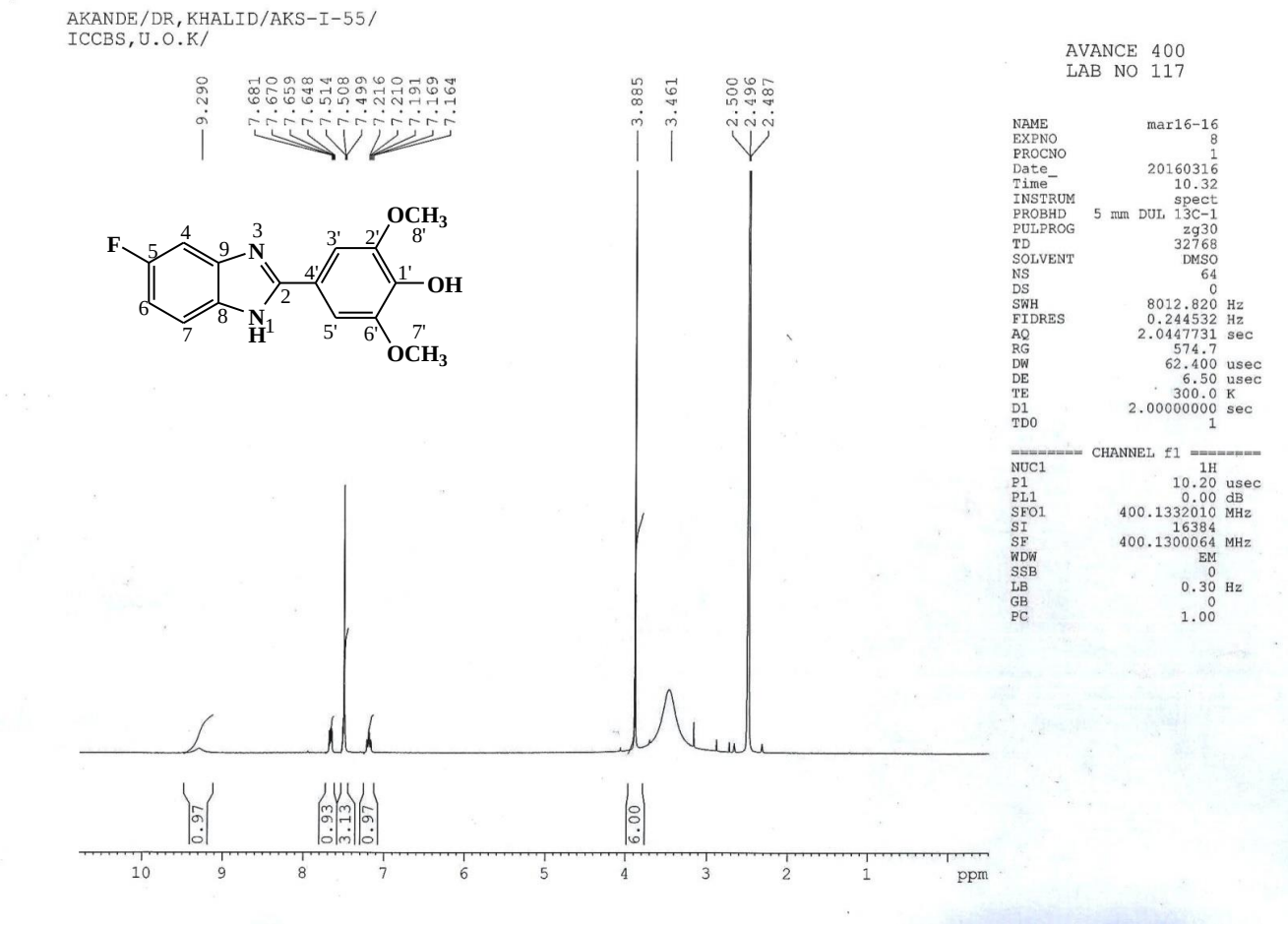

Figure 4.172. ^{1}H NMR (400 MHz, DMSO-d_6) spectrum of AKS-I-55

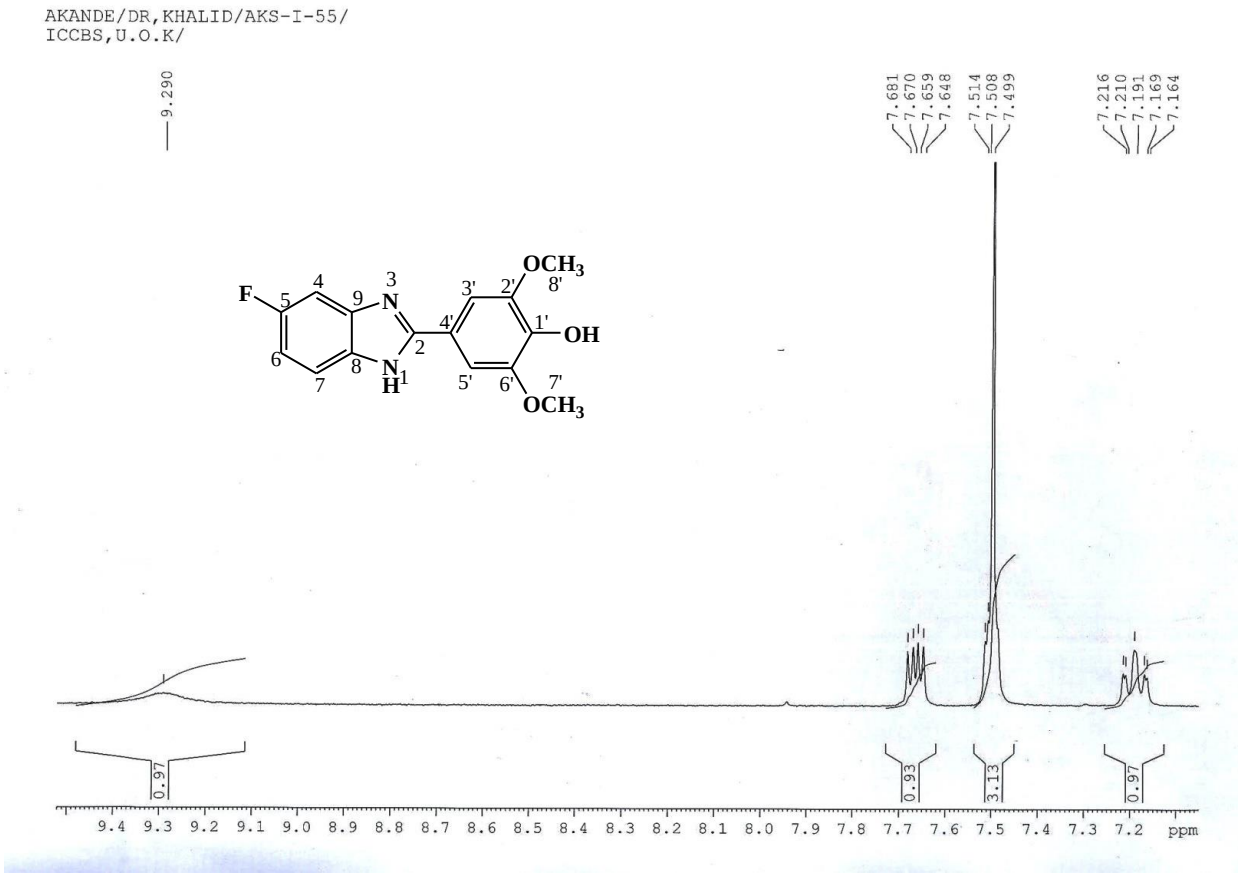

Figure 4.173. ^{1}H NMR (400 MHz, DMSO-d_6) spectrum of AKS-I-55 (Expanded)

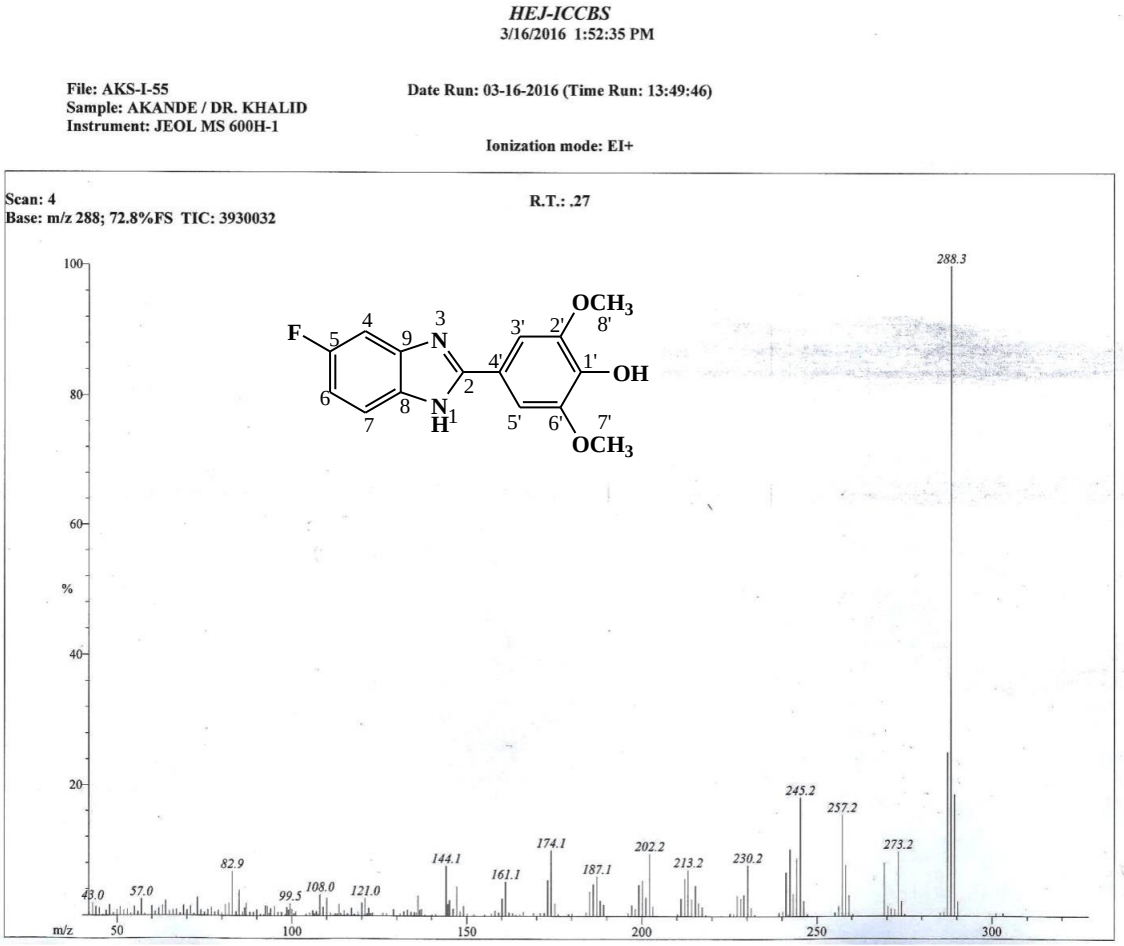

Figure 4.174. EI-MS spectrum of AKS-I-55

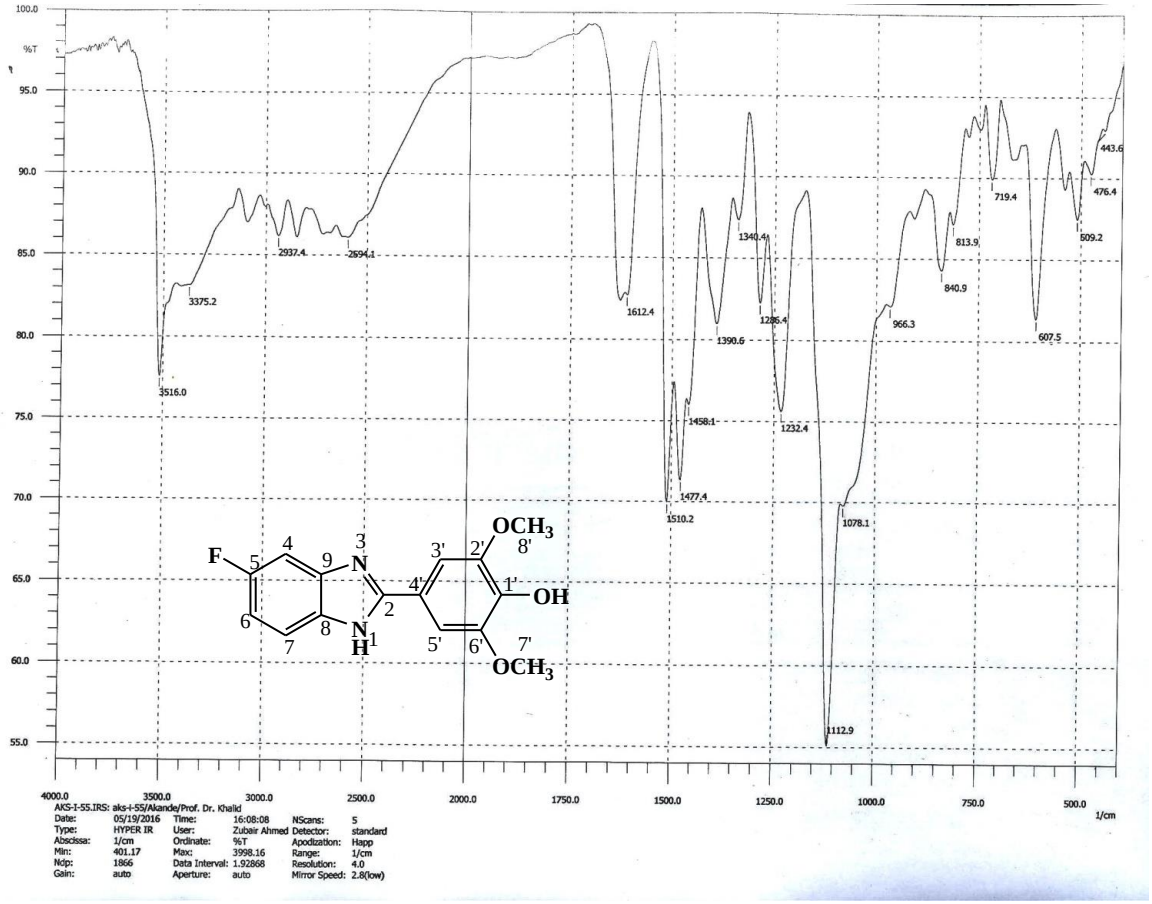

Figure 4.175. IR spectrum of AKS-I-55

THERMO ELECTRON ~ VISIONpro SOFTWARE V4.10

Operator Name	ARSHAD ALAM	Date of Report	5/20/2016
Department	Analytical laboratory#004 TWC	Time of Report	9:36:47AM
Organization	ICCBS.Karachi University.		
Information	Prof Dr. Khalid / Akande.		

Scan Graph

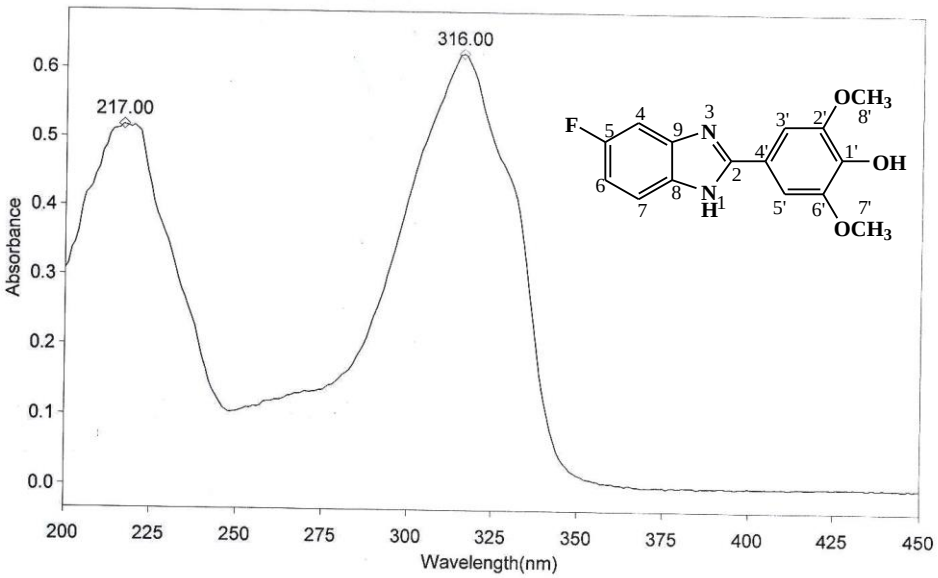

Results Table - AKS- I- 55.sre,AKS- I- 55,Cycle01

nm	A
217.00	0.518
316.00	0.624

Peak Pick Method
Find 8 Peaks Above -3.0000 A
Start Wavelength 200.00 nm
Stop Wavelength 450.00 nm
Sort By Wavelength

Sensitivity Very Low

Page 1, Scan Graph

Figure 4.176. UV spectrum of AKS-I-55

Table 4.28. Summary of the ^{1}H NMR spectra of AKS-I-55

Position	δ ^{1}H [mult., J_{HH} (Hz)] (ppm)
1	-
2	-
3	-
4	7.68-7.64 [m]
5	-
6	7.21 [dt], $J_{6,7}$ = 8.8, $J_{6,4}$ = 2.4]
7	7.51-7.49 [m]
8	-
9	-
1′-OH	9.29 [br s]
1′	-
2′	-
3′	7.51-7.49 [m]
4′	-
5′	7.51-7.49 [m]
6′	-
7′-OCH_3	3.88 [s]
8′-OCH_3	3.88 [s]

4.1.29 Characterisation of 4′-(5-chloro-1*H*-benzo[*d*]imidazol-2-yl)-2′,6′-dimethoxyphenol (AKS-I-56)

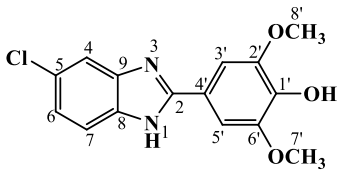

The dark-brown solid compound, AKS-I-56 has a yield of 83.0% (0.253 g), m.pt. range of 284-286 ^{o}C and a R_f value of 0.45 (hexane/ethyl acetate, 7:3).

The ^{1}H NMR spectra (400 MHz, DMSO-d_6) (figures **4.177** and **4.178**) revealed six resonance peaks. The δ (ppm) 9.24 was assigned to the hydroxyl proton at position 1′ (1H, br s, 1′-OH). The methine protons resonated at 7.68, 7.64, 7.49 and 7.32 representing (1H, s, H-4), (1H, d, $J_{7,6}$ = 8.4 Hz, H-7), (2H, s, H-3′, H-5′) and (1H, dd, $J_{6,7}$ = 8.4 Hz, $J_{6,4}$ = 2.0 Hz, H-6) respectively. Furthermore, 3.88 (s, 6H, 7′-OCH_3, 8′-OCH_3) describes the methoxy protons. However, the highly deshielded amine proton was not captured.

Fragmention patterns spaced two mass units apart due to the presence of a chlorine atom was observed in the EI-MS spectrum (figure **4.179**). The *m/z* of the molecular ion, M^+ and [M^++2] peak were seen at 304 (base peak) and 306 (isotope peak) respectively. The *m/z* of 289 and 273 resulted from fragmentations by loss of CH_3 and OCH_3 radicals respectively. M^+-CH_3-CH_2=CH_2 fragmentation corresponds to the ion with a *m/z* of 261 $[C_{12}H_6ClN_2O_3]^+$. Successive loss of OCH_3 radical, HCl and H_2O molecules suggest the peak at *m/z* of 218 corresponding to $[C_{14}H_6N_2O]^+$ fragment. Cleavage at the imidazole ring, alongside the loss of two H radicals is indicative of a fragment ion with *m/z* of 177. Also, $[C_2H_6N]^+$ fragment ion is indicative of *m/z* 44.

The IR absorption spectrum (figure **4.180**) shows vibrational frequencies, $\bar{\upsilon}$ (cm^{-1}) of bands assigned as ≈3450, ≈3200, 3114, 2941, 2844, 1504, 1467, 1234 and 1118 cm^{-1} corresponding vibrational bonds of O–H_{str}, N–H_{str}, aromatic C–H_{str}, aliphatic C–$H_{asy\ str}$ and C–$H_{sym\ str}$, aromatic C=C_{str}, C–H_b of OCH_3, symmetric and assymetric C–O-C_{str} of ether respectively. The UV spectrum (figure **4.181**) shows wavelenghts of maximum absorptions (λ_{max}) at 319 and 222 nm dipicting n→π* and π→π* transitions. Summary of ^{1}H NMR spectrum is represented in table **4.29**.

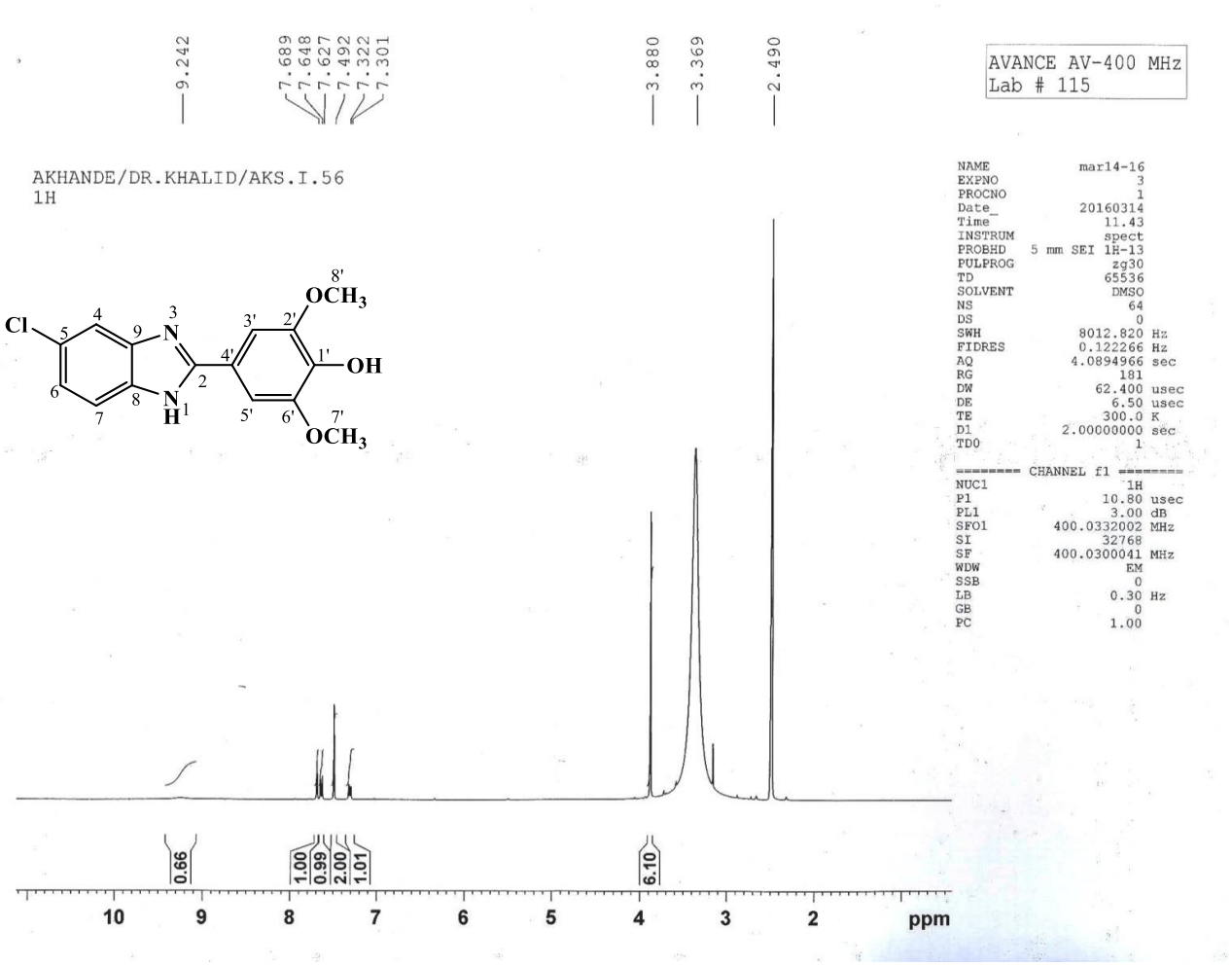

Figure 4.177. ^{1}H NMR (400 MHz, DMSO-d_6) spectrum of AKS-I-56

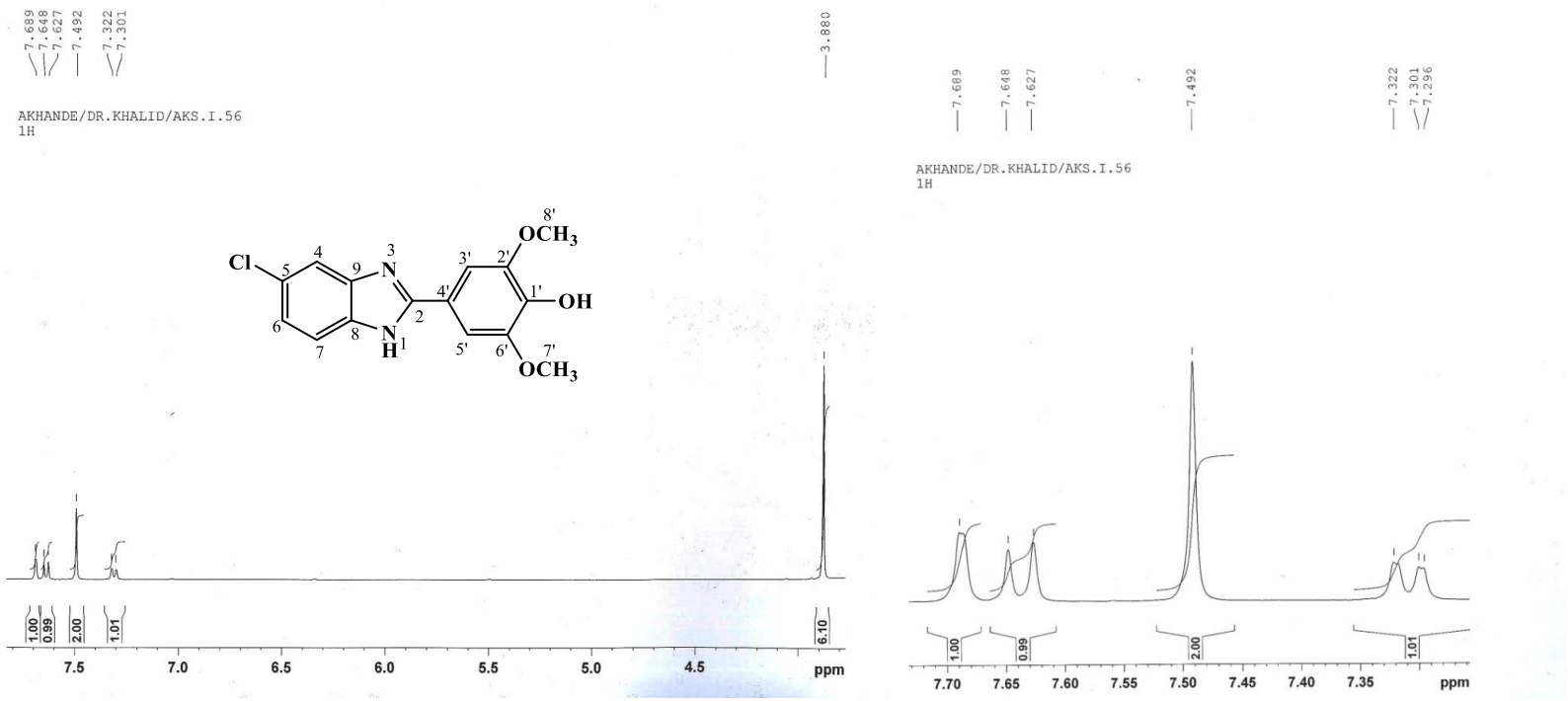

Figure 4.178. ^{1}H NMR (400 MHz, DMSO-d_6) spectra of AKS-I-56 (Expanded)

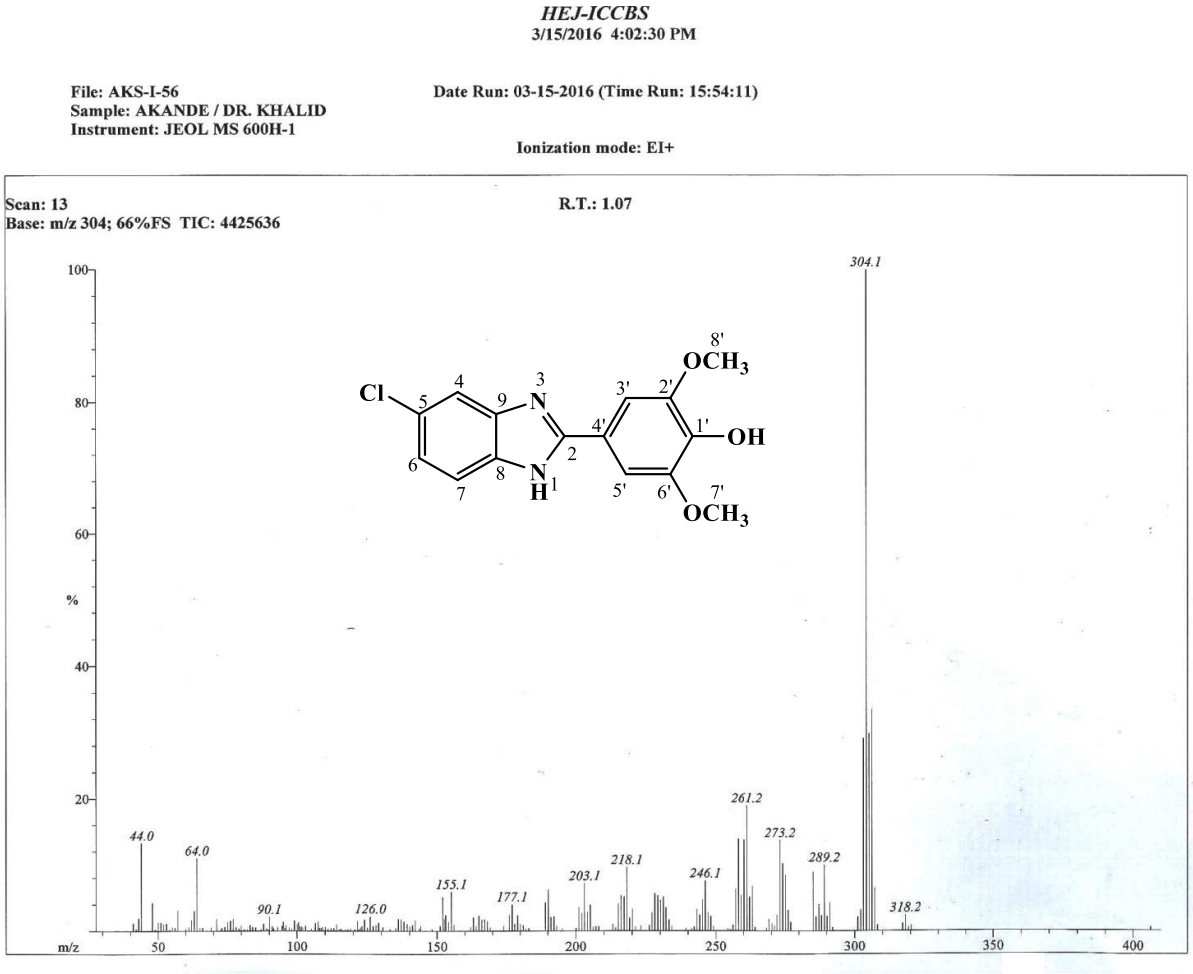

Figure 4.179. EI-MS spectrum of AKS-I-56

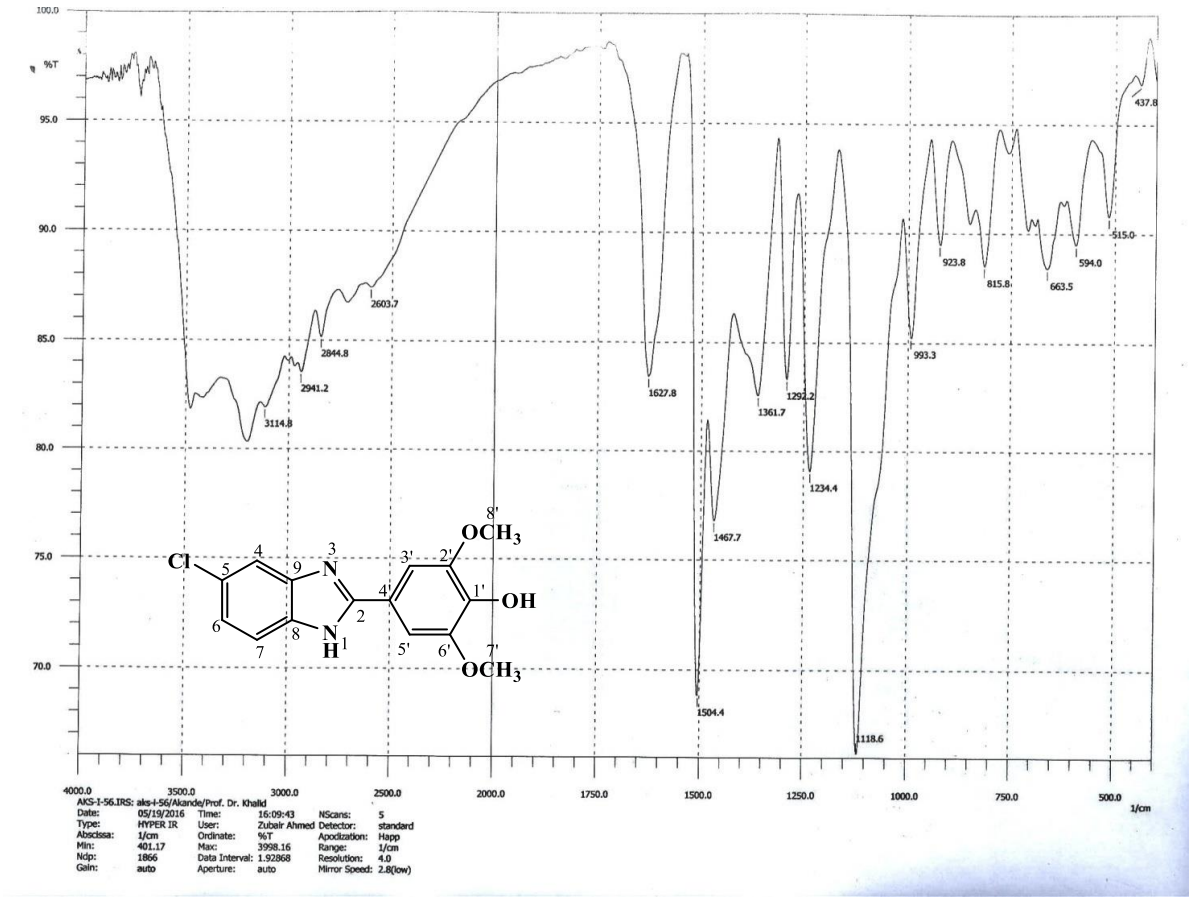

Figure 4.180. IR spectrum of AKS-I-56

THERMO ELECTRON ~ VISIONpro SOFTWARE V4.10

Operator Name	ARSHAD ALAM	Date of Report	5/20/2016
Department	Analytical laboratory#004 TWC	Time of Report	9:41:51AM
Organization	ICCBS.Karachi University.		
Information	Prof Dr. Khalid / Akande.		

Scan Graph

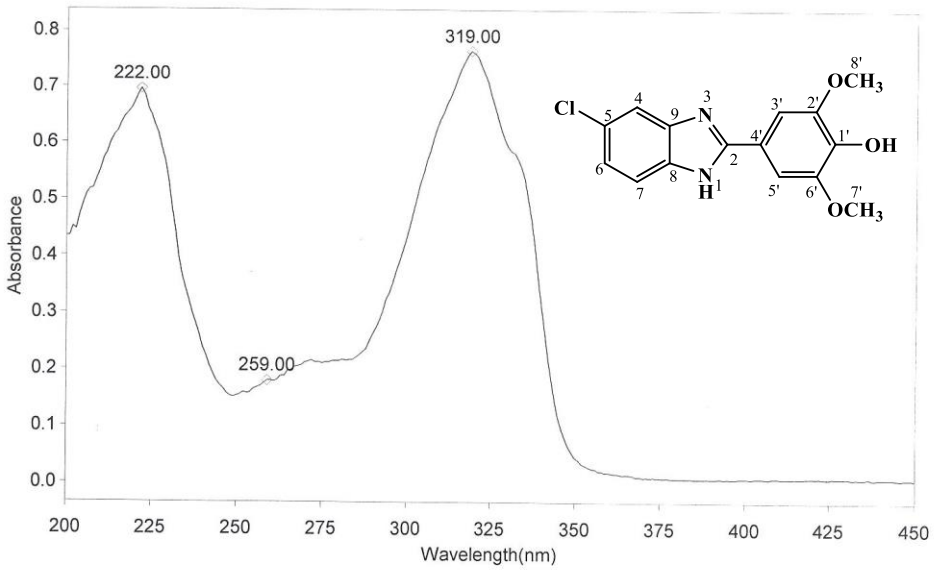

Results Table - AKS- I- 56.sre,AKS- I- 56,Cycle01

nm	A	**Peak Pick Method**
222.00	0.695	Find 8 Peaks Above -3.0000 A
259.00	0.180	Start Wavelength 200.00 nm
319.00	0.765	Stop Wavelength 350.00 nm
		Sort By Wavelength
Sensitivity	High	

Page 1, Scan Graph

Figure 4.181. UV spectrum of AKS-I-56

Table 4.29. Summary of the ^{1}H NMR spectra of AKS-I-56

Position	δ ^{1}H [mult., J_{HH} (Hz)] (ppm)
1	-
2	-
3	-
4	7.68 [s]
5	-
6	7.32 [dd, $J_{6,7}$ = 8.4, $J_{6,4}$ = 2.0]
7	7.64 [d, $J_{7,6}$ = 8.4]
8	-
9	-
1′-OH	9.24 [br s]
1′	-
2′	-
3′	7.49 [s]
4′	-
5′	7.49 [s]
6′	-
7′-OCH_3	3.88 [s]
8′-OCH_3	3.88 [s]

4.1.30 Characterisation of 4′-(5-fluoro-1*H*-benzo[*d*]imidazol-2-yl)benzene-1′,2′,3′-triol (AKS-I-57)

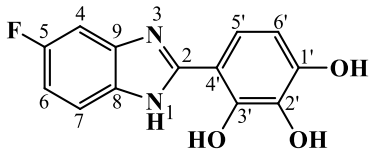

The compound, AKS-I-57 is a brown solid with a 0.237 g (91.0%) yield, m.pt. of 287-288 ^{o}C and a R_f value of 0.64 (hexane/ethyl acetate solvent system, 7:3).

Figures **4.182** and **4.183** represent the ^{1}H NMR spectra (400 MHz, DMSO-d_6), and the chemical shifts, δ (ppm) values recorded for eight resonance peaks are assigned as ≈13.90 (br s, 1H, -NH) to amine proton, 9.61 (1H, br d, 3′-OH), 8.58 (br s, 2H, 1′-OH) to two hydroxy protons (a third exchangeable hydroxy proton was not seen). The methine protons resonate at 7.56-7.62 (1H, m, H-4; most deshielded methine proton observed as a multiplet due to ortho coupling with fluorine), 7.43 (1H, d, $J_{7,6}$ = 8.0 Hz, H-7), 7.35 (1H, d, $J_{5',6'}$ = 8.8 Hz, H-5′), 7.14 (1H, dt, $J_{6,4}$ = 2.0 Hz, $J_{6,F\text{-}5}$ = 8.8 Hz, H-6; presenting further splitings as a result of ortho coupling with fluorine) and at 6.49 (1H, d, $J_{6',5'}$ = 8.4 Hz, H-6′).

Fragmentation partern from EI-MS spectrum (figure **4.184**) shows the molecular ion, M^+ peak with *m/z* of 260 as the base peak and a prominent $[M^+{+}1]$ peak at *m/z* of 261. M^+-CHO suggests an ion with *m/z* of 231. Fragment ions with *m/z* of 203 and 187 indicate the loss of $[HF{+}2H_2O]$ and $[HF{+}3H_2O]$ molecules from the molecular ion respectively. Cleavage at the imidazole ring yields an ion with *m/z* of 150 $[C_7H_4NO_3]^+$. The *m/z* of 175 and 161 correspond to $[C_9H_4FN_2O]^{\bullet+}$ and $[C_9H_6FN_2]^{\bullet+}$ fragments.

Figure **4.185** is the IR absorption spectrum indicating some vibrational frequencies, $\bar{\upsilon}$ at ≈3400, 3240, 3066, 1624, 1494, 1143 and 1110 cm^{-1}, corresponding to N–H$_{str}$, O–H$_{str}$, aromatic C–H$_{str}$, C=N$_{str}$, C=C$_{str}$, C–F$_{str}$ and C–O$_{str}$ of hydroxy respectively. The spectrum from UV analysis (figure **4.186**) shows maximum absorptions (λ_{max}) at 327, 315, and 222 nm corresponding to n→π* and π→π* transitions. Summary of the ^{1}H NMR spectrum is presented in table **4.30**.

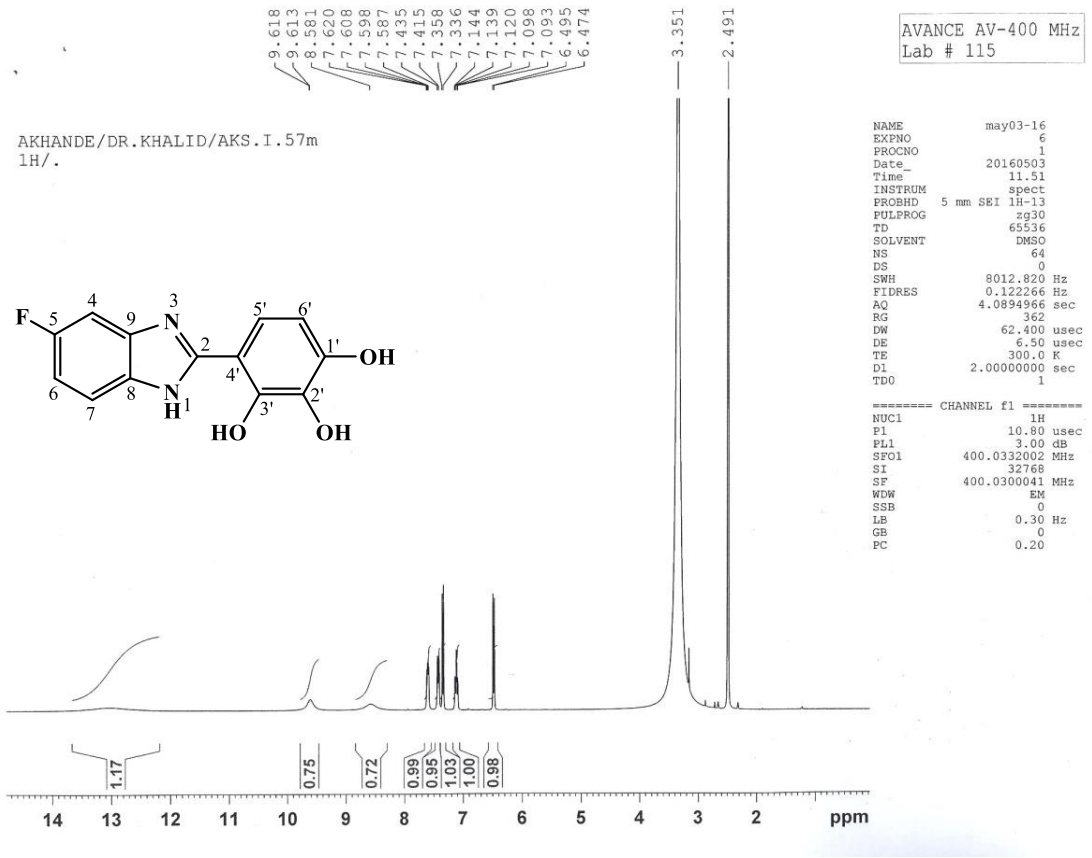

Figure 4.182. ^{1}H NMR (400 MHz, DMSO-d_6) spectrum of AKS-I-57

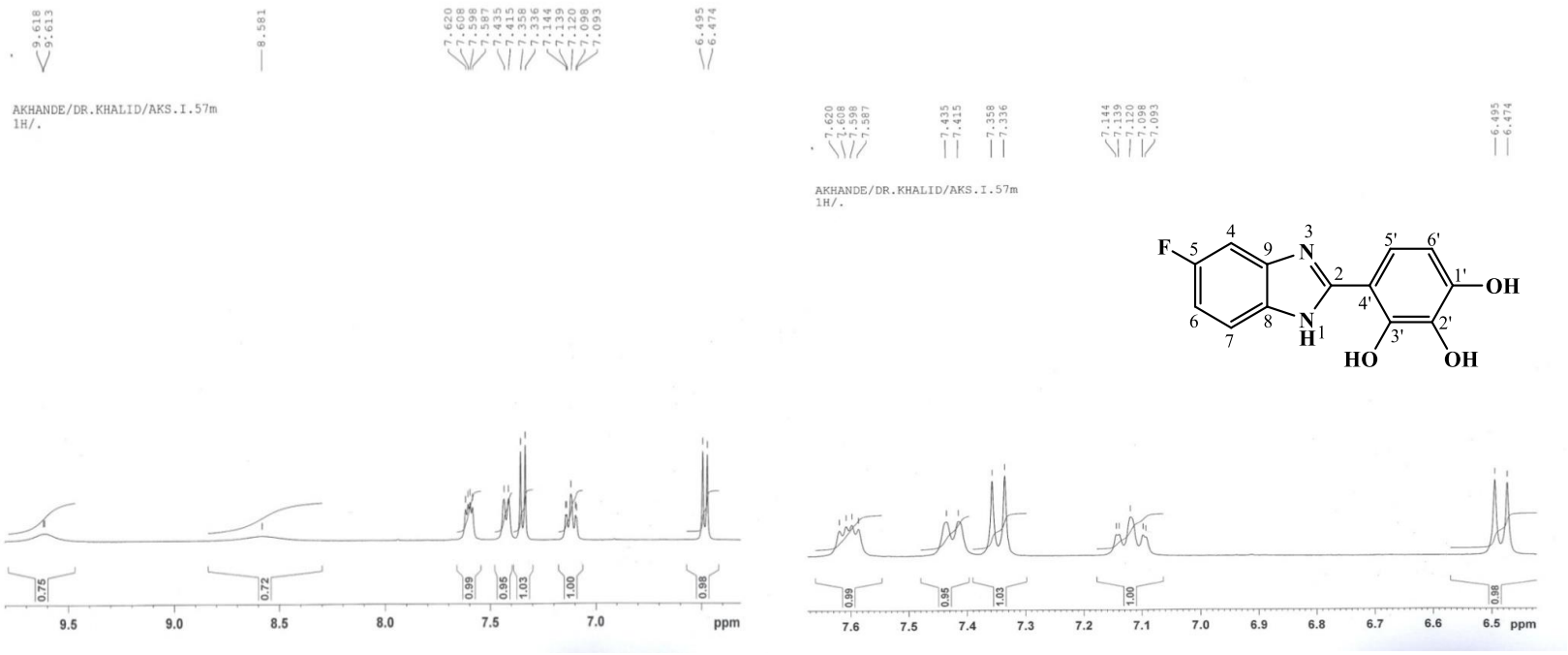

Figure 4.183. ^{1}H NMR (400 MHz, DMSO-d_6) spectra of AKS-I-57 aromatic region (Expanded)

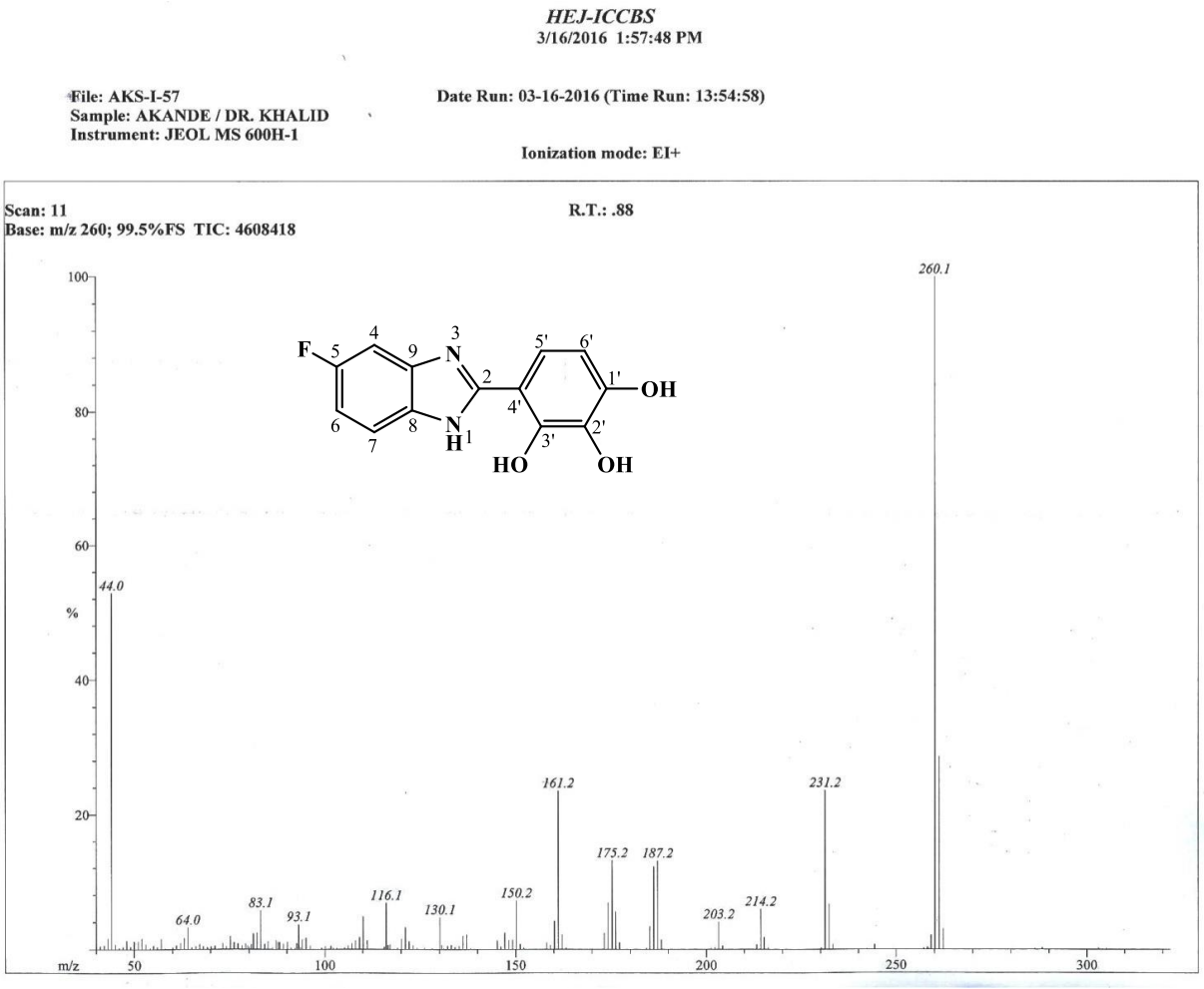

Figure 4.184. EI-MS spectrum of AKS-I-57

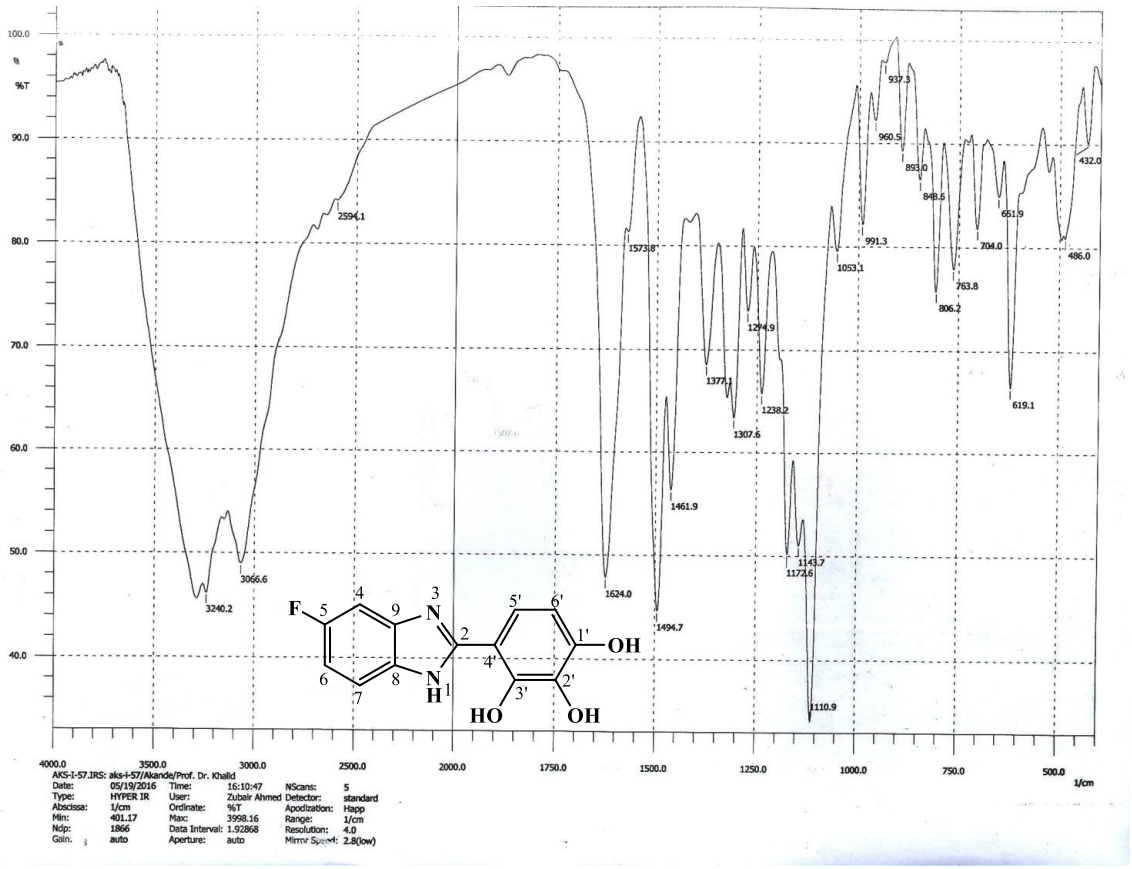

Figure 4.185. IR spectrum of AKS-I-57

THERMO ELECTRON ~ VISIONpro SOFTWARE V4.10

Operator Name	ARSHAD ALAM	Date of Report	5/20/2016
Department	Analytical laboratory#004 TWC	Time of Report	9:48:49AM
Organization	ICCBS.Karachi University.		
Information	Prof Dr. Khalid / Akande.		

Scan Graph

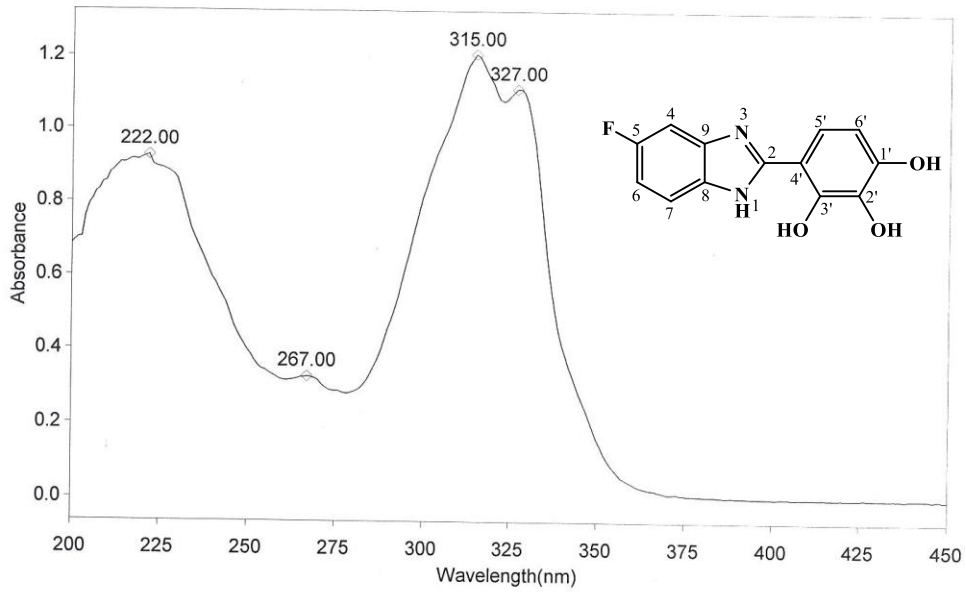

Results Table - AKS- I- 57.sre,AKS- I- 57,Cycle01

nm	A	**Peak Pick Method**
222.00	0.927	Find 8 Peaks Above -3.0000 A
267.00	0.327	Start Wavelength 200.00 nm
315.00	1.208	Stop Wavelength 450.00 nm
327.00	1.113	Sort By Wavelength
Sensitivity	Low	

Page 1, Scan Graph

Figure 4.186. UV spectrum of AKS-I-57

Table 4.30. Summary of the ^{1}H NMR spectra of AKS-I-57

Position	δ ^{1}H [mult., J_{HH} (Hz)] (ppm)
1	≈12.90 [br s]
2	-
3	-
4	7.62-7.58 [m]
5	-
6	7.14 [dt, $J_{6,F-5}$ = 8.8, $J_{6,4}$ = 2.0]
7	7.43 [d, $J_{7,6}$ = 8.0]
8	-
9	-
1′-OH	8.58 [br s]
2′-OH	Exchangeable
3′-OH	9.61 [br d]
4′	-
5′	7.35 [d, $J_{5',6'}$ = 8.8]
6′	6.49 [d, $J_{6',5'}$ = 8.4]

4.1.31 Characterisation of 4′-(5-fluoro-1*H*-benzo[*d*]imidazol-2-yl)-2′-methoxy-phenyl acetate (AKS-I-59)

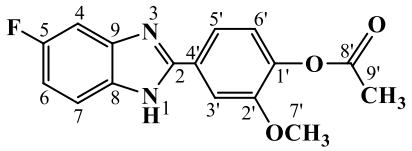

The brown solid compound, AKS-I-59 was obtained with a 55.0% (0.164 g) yield, a m.pt. range of 124-127 ^{o}C and a R_f value of 0.36 (in a hexane/ethyl acetate solvent system, 1:1).

The chemical shifts, δ (ppm) obtained from ^{1}H NMR spectra (400 MHz, DMSO-d_6) (figures **4.187** and **4.188**) are assigned to protons as 7.89 (1H, d, $J_{3',5'}$ = 1.6 Hz, H-3′), 7.75 (1H, dd, $J_{5',6'}$ = 8.4 Hz, $J_{5',3'}$ = 1.6 Hz, H-5′), 7.60-7.63 (1H, m, H-4), 7.44 (1H, dd, $J_{7,F\text{-}5}$ = 2.0 Hz, $J_{7,6}$ = 9.2 Hz, H-7), 7.29 (1H, d, $J_{6',5'}$ = 8.0 Hz, H-6′) and 7.12 (1H, dt, $J_{6,4}$ = 2.4 Hz, $J_{6,7}$ = 9.2 Hz, H-6) representing the methine protons, 3.89 (3H, s, 7′-OCH_3) representing the methoxy protons and 2.29 (3H, s, 9′-CH_3) representing the methyl protons of the acetate functional group. The amine proton was not captured. The effect of fluorine (further splittings) were also observed for H-4 and H-6 resonance peaks.

The molecular ion, M^+ and M^++1 peak from EI-MS analysis (figure **4.189**) have *m/z* of 300 and 301 respectively. The characteristic elimination of the neutral molecule CH_2=C=O (a ketene) from M^+ gave rise to the base peak at *m/z* of 258 $[C_{14}H_{11}FN_2O_2]^+$ while the peaks at *m/z* 215, 200 and 187 correspond to the fragments $[C_{14}H_{11}FN_2O_2]^+$, $[C_{12}H_9FN_2]^+$ and $[C_{11}H_8FN_2]^+$ respectively. Loss of CH_3O and CH_3C=O radicals from the molecular ion is indicative of the fragment ion with *m/z* of 228 $[C_{13}H_9FN_2O]^+$. Also, a prominent peak at 43 is suggests the cation $[CH_3C{=}O]^+$. Further confirming the compound from HREI-MS analysis, the *m/z* found corresponding to the molecular formula, $C_{11}H_7ClN_2O$ is 300.0903 (calculated 300.0910).

The IR spectrum (figure **4.190**) reveals the presence of amine N–H$_{str}$, aromatic C–H$_{str,}$ aliphatic C–H$_{asy\ str}$ and C–H$_{sym\ str,}$ C=O$_{str}$ of ester, C=N$_{str}$, C=C$_{str}$, C–H$_b$, C–O$_{str}$ of ester and C–F$_{str}$ corresponding to 3415, 3079, 2932, 2854, 1761, 1633, 1603, 1475, 1207 and 1139 cm^{-1} vibrational frequencies, $\bar{\upsilon}$ respectively. The UV spectrum (figure **4.191**) shows wavelenghts of maximum absorptions (λ_{max}) at 310 (n→π* transition) and 214 nm (π→π* transition). ^{1}H NMR spectra is summarised in table **4.31**.

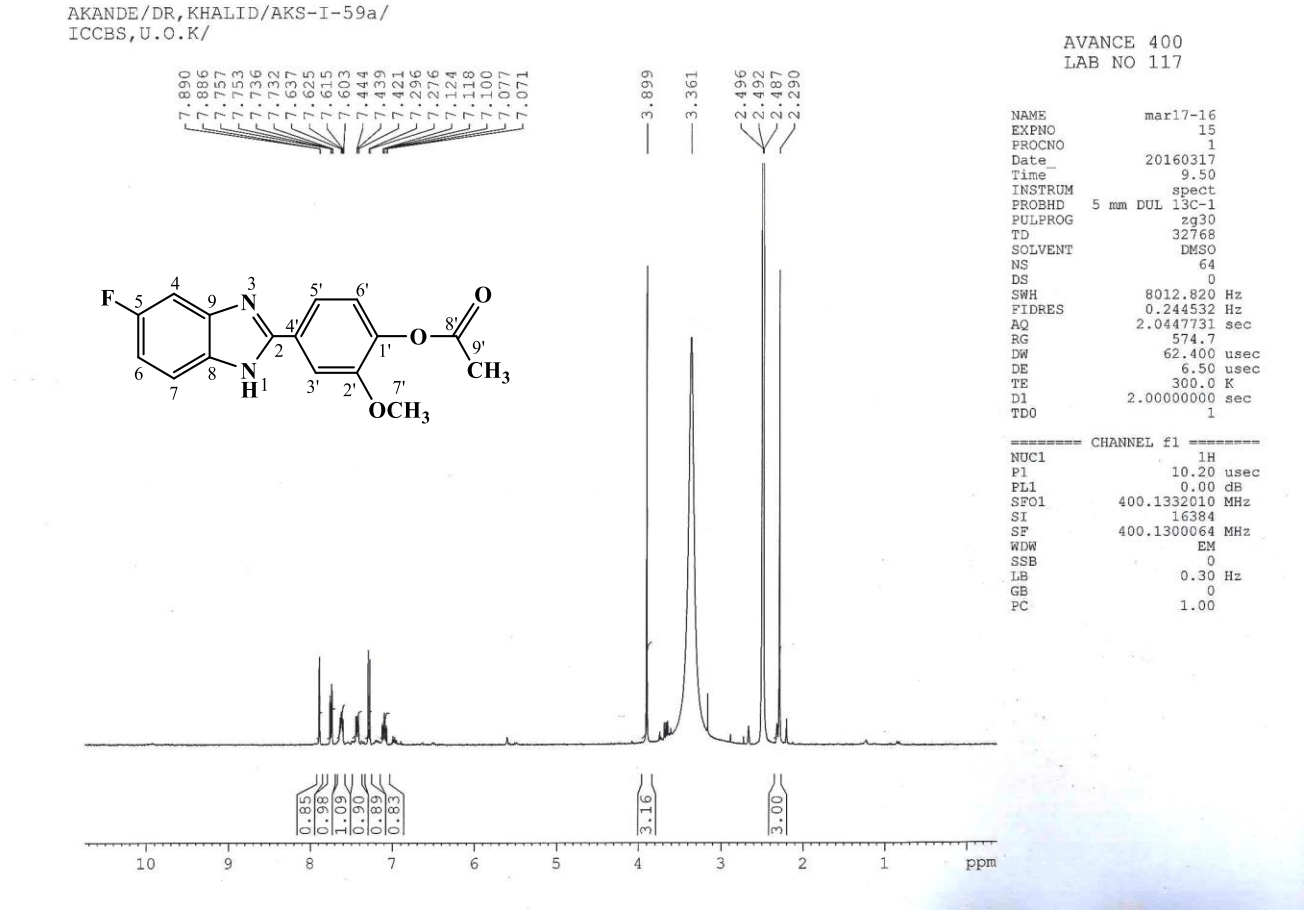

Figure 4.187. ^{1}H NMR (400 MHz, DMSO-d_6) spectrum of AKS-I-59

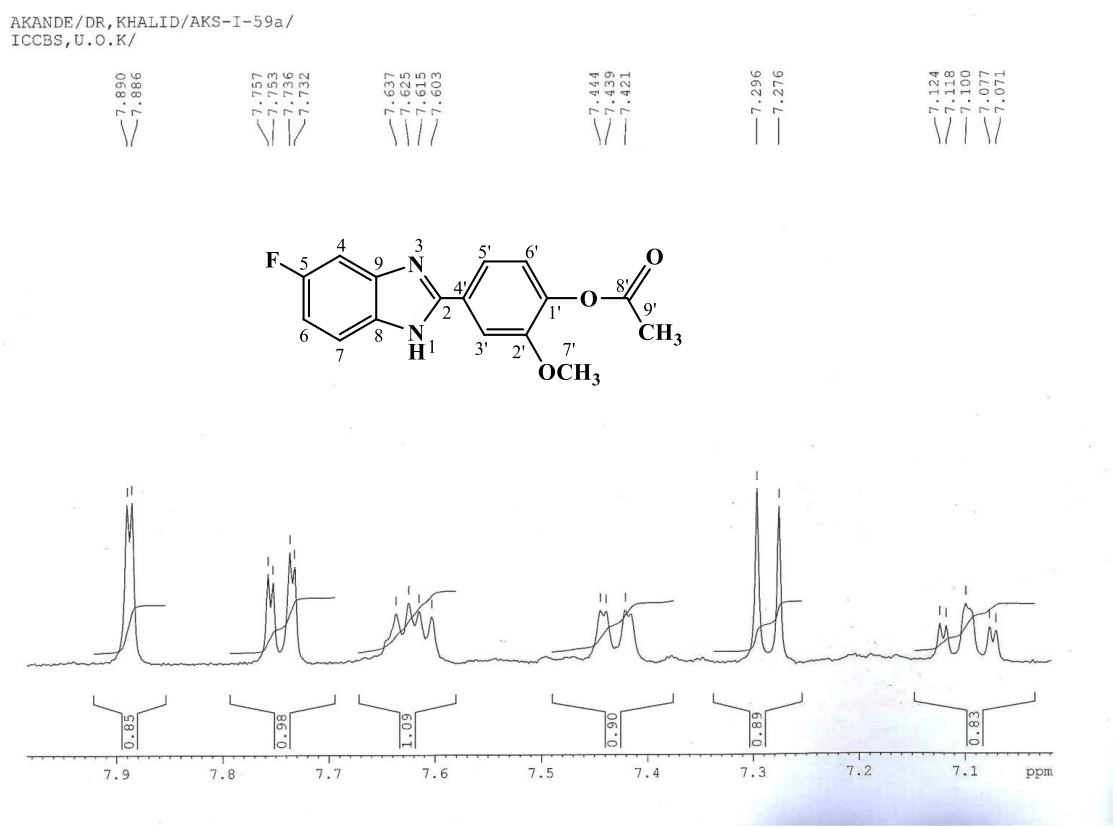

Figure 4.188. ^{1}H NMR (400 MHz, DMSO-d_6) spectrum of AKS-I-59 aromatic region (Expanded)

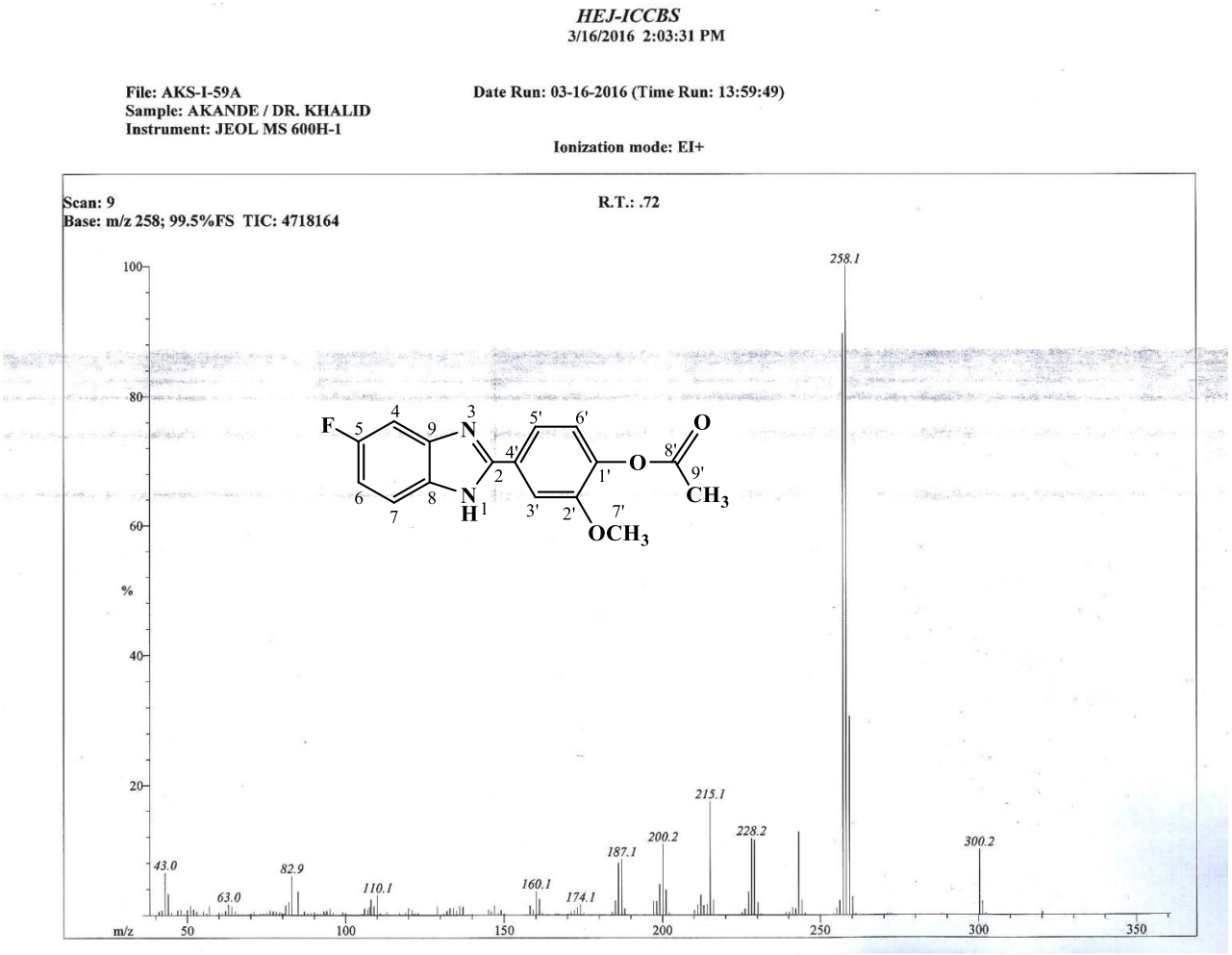

Figure 4.189. EI-MS spectrum of AKS-I-59

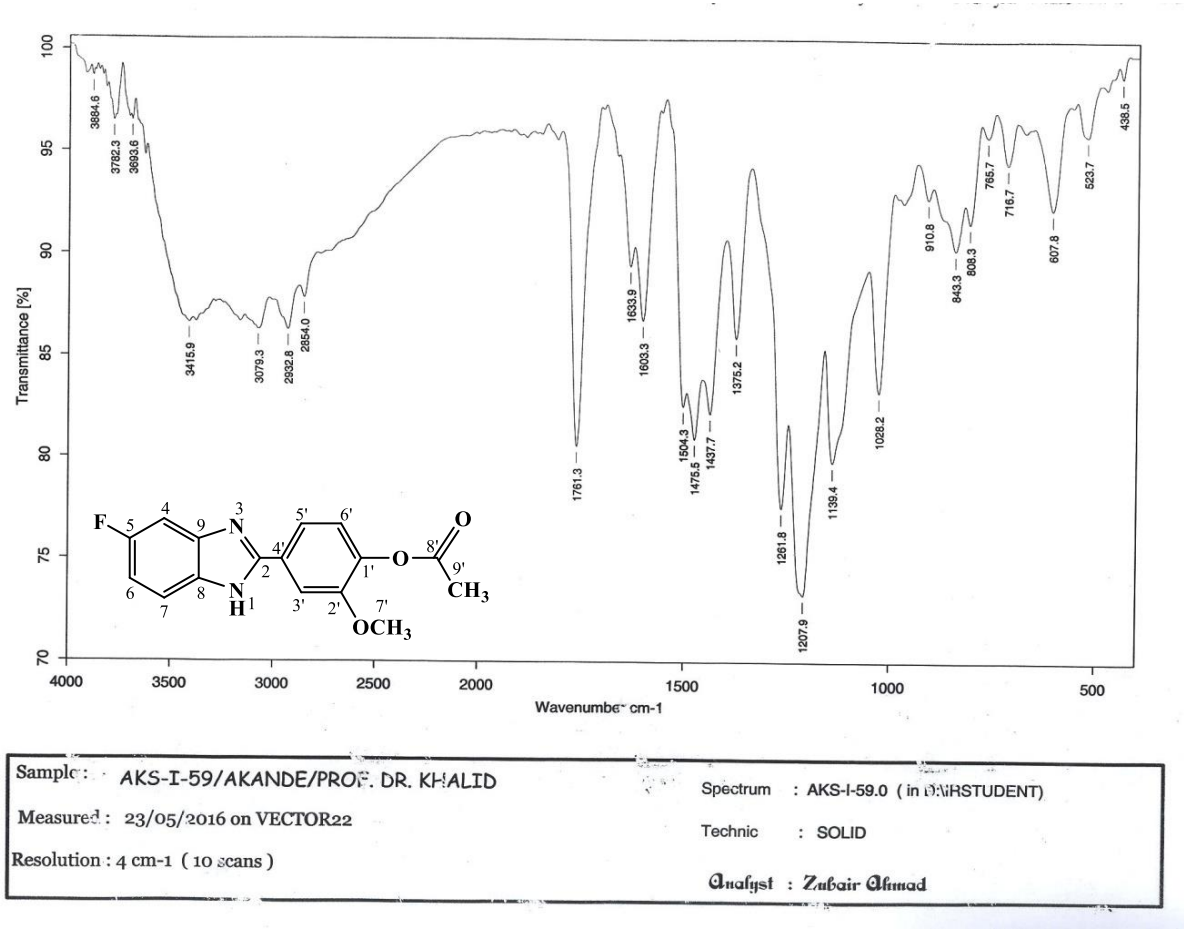

Figure 4.190. IR spectrum of AKS-I-59

THERMO ELECTRON ~ VISIONpro SOFTWARE V4.10

Operator Name	ARSHAD ALAM	Date of Report	5/24/2016
Department	Analytical laboratory#004 TWC	Time of Report	3:47:41PM
Organization	ICCBS.Karachi University.		
Information	Prof Dr.Khalid ./ Akande.		

Scan Graph

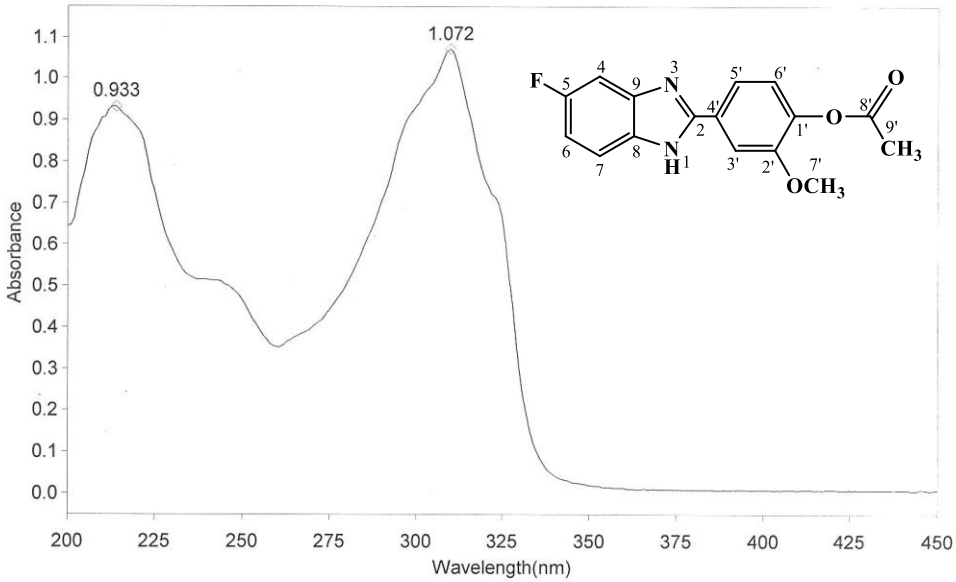

Results Table - aks-i-59.sre,aks-i-59,Cycle01

nm	A	**Peak Pick Method**
214.00	0.933	Find 8 Peaks Above -3.0000 A
310.00	1.072	Start Wavelength 200.00 nm
		Stop Wavelength 450.00 nm
		Sort By Wavelength
Sensitivity	Very Low	

Page 1, Scan Graph

Figure 4.191. UV spectrum of AKS-I-59

Table 4.31. Summary of the ^{1}H NMR spectra of AKS-I-59

Position	δ ^{1}H [mult., J_{HH} (Hz)] (ppm)
1	-
2	-
3	-
4	7.63-7.60 [m]
5	-
6	7.12 (dt, $J_{6,7}$ = 9.2, $J_{6,4}$ = 2.4]
7	7.44 [dd, $J_{7,6}$ = 9.2, $J_{7,F-5}$ = 2.0]
8	-
9	-
1′	-
2′	-
3′	7.89 [d, $J_{3',5'}$ = 1.6]
4′	-
5′	7.75 [dd, $J_{5',6'}$ = 8.4, $J_{5',3'}$ = 1.6]
6′	7.29 [d, $J_{6',5'}$ = 8.0]
7′-OCH_3	3.89 [s]
9′-CH_3	2.29 [s]

4.1.32 Characterisation of 4′-(5-chloro-1*H*-benzo[*d*]imidazol-2-yl)-2′-methoxy-phenyl acetate (AKS-I-60)

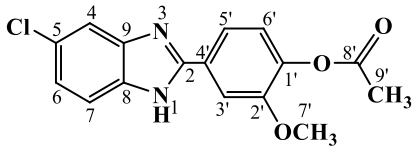

The compound, AKS-I-60 was obtained as a dark-brown soild in a 61.9% (0.196 g) yield. Its m.pt. ranges between 128-129 ^{o}C and has a R_f value of 0.38 from a hexane/ethyl acetate (1:1) solvent system.

The ^{1}H NMR spectra (400 MHz, DMSO-d_6) of the compound is represented in figures **4.192** and **4.193**. The chemical shift values, δ (ppm) obtained are assigned as 7.89 (1H, d, $J_{3',5'}$ = 1.6 Hz, H-3′), 7.76 (1H, dd, $J_{5',3'}$ = 1.6 Hz, $J_{5',6'}$ = 8.4 Hz, H-5′), 7.66 (1H, s, H-4), 7.63 (1H, d, $J_{7,6}$ = 8.8 Hz, H-7), 7.29 (1H, d, $J_{6',5'}$ = 8.4 Hz, H-6′) and 7.26 (1H, dd, $J_{6,7}$ = 8.8 Hz, $J_{6,4}$ = 2.0 Hz, H-6) to six methine protons, 3.90 (3H, s, 7′-OCH_3) to three methoxy protons, and 2.29 (3H, s, 9′-CH_3) to the methyl protons of the acetate functional group. The amine proton was not captured on the spectrum.

From EI-MS analysis (figure **4.194**), peak patterns spaced two mass units apart were observed due to the presence of a Cl atom. The *m/z* of 316 and 318 connote the molecular ion, M^+ and isotope, [M^++2] peaks. The fragmentation, M^+-H_2C=C=O produced the base peak at *m/z* 274 and a corresponding isotope peak at *m/z* 276. Loss of CH_2=O from the base peak yielded a fragment at *m/z* of 245. Loss of CH_3-CH=O from *m/z* 245 is suggestive of the peak at 203 while *m/z* of 231 indicates the fragment $[C_{12}H_8ClN_2O]^{\bullet+}$. Peak with a *m/z* of 90 corresponds to $[C_6H_4N]^+$, and on further fragmentation, losses HCN to produce an ion with *m/z* of 63 corresponding to $[C_5H_3]^+$. HREI-MS analysis further confirmed the compound whereby the *m/z* obtained at 316.0621 (calculated, 316.0615) corresponds to the molecular formula $C_{16}H_{13}ClN_2O_3$.

Vibrational frequencies, $\bar{\upsilon}$ (cm^{-1}) of some typical bonds from the IR spectrum (figure **4.195**) are 3076 (C–H_{str} aromatic), 2935 (aliphatic C–H_{str}), 1758 (C=O_{str} of ester), 1656 (C=N_{str}), 1600, 1500 (aromatic C=C_{str}), 1431 (C–H_b of CH_3/OCH_3), 1204 (C–O_{str} of ester) and 1060 (C–Cl_{str}). The UV spectrum (figure **4.196**) showed maximum absorptions (λ_{max}) corresponding to n→π* and π→π* transitions at 312, 247 and 222 nm. Represented in table **4.32** is the summary of ^{1}H NMR spectra.

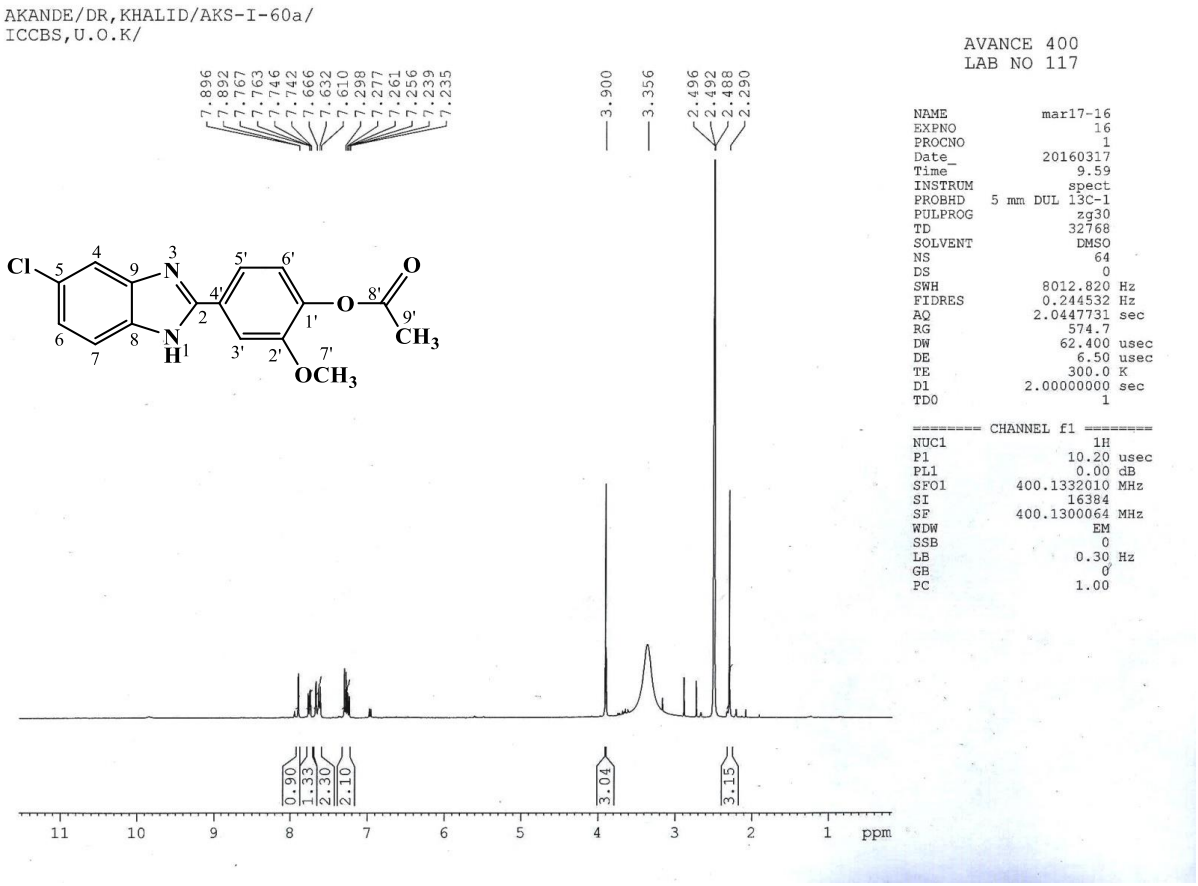

Figure 4.192. ^{1}H NMR (400 MHz, DMSO-d_6) spectrum of AKS-I-60

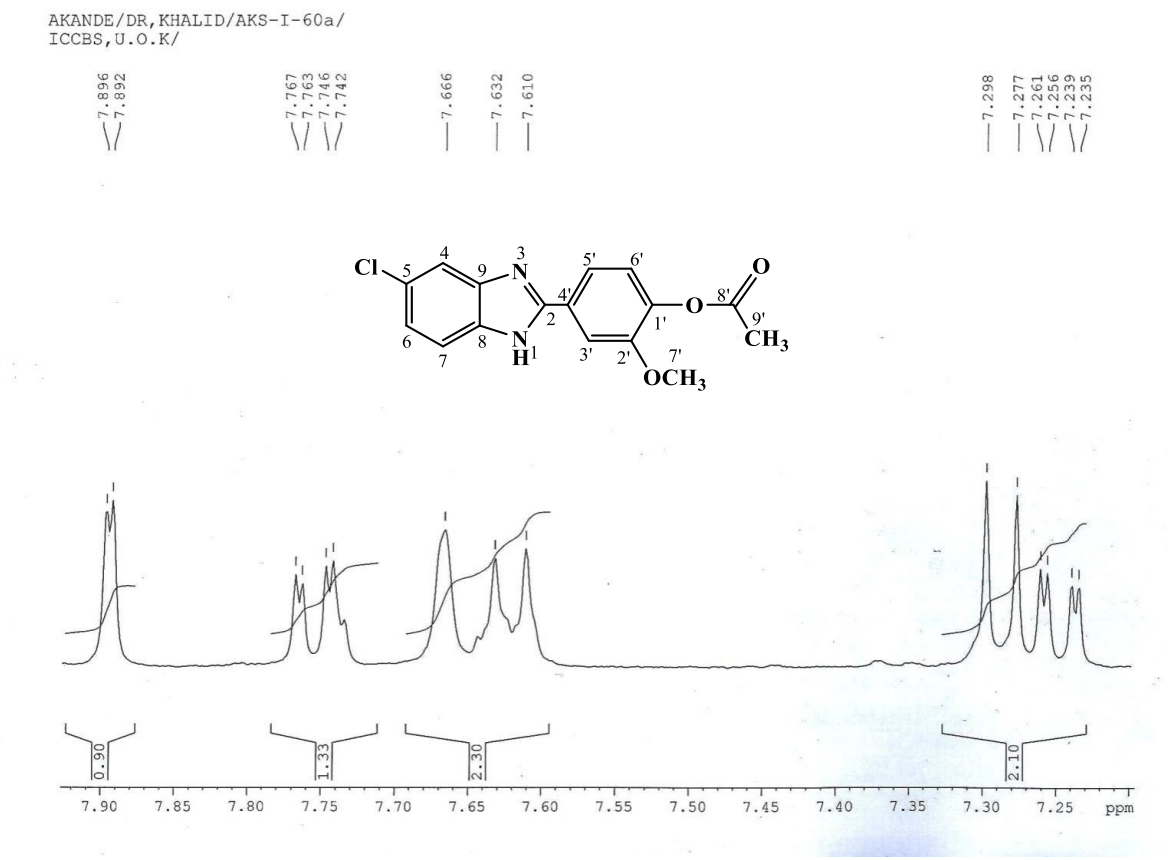

Figure 4.193. ^{1}H NMR (400 MHz, DMSO-d_6) spectrum of AKS-I-60 aromatic region (Expanded)

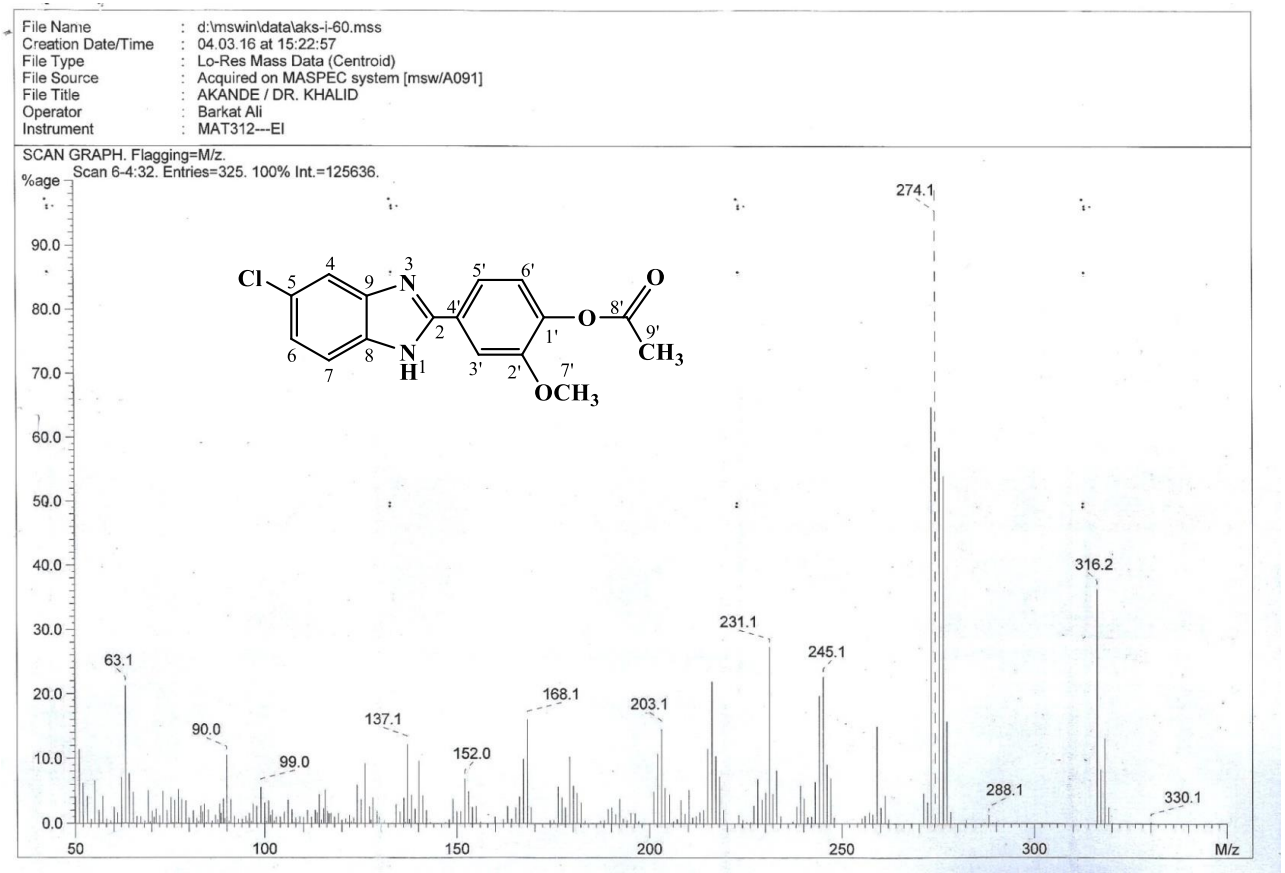

Figure 4.194. EI-MS spectrum of AKS-I-60

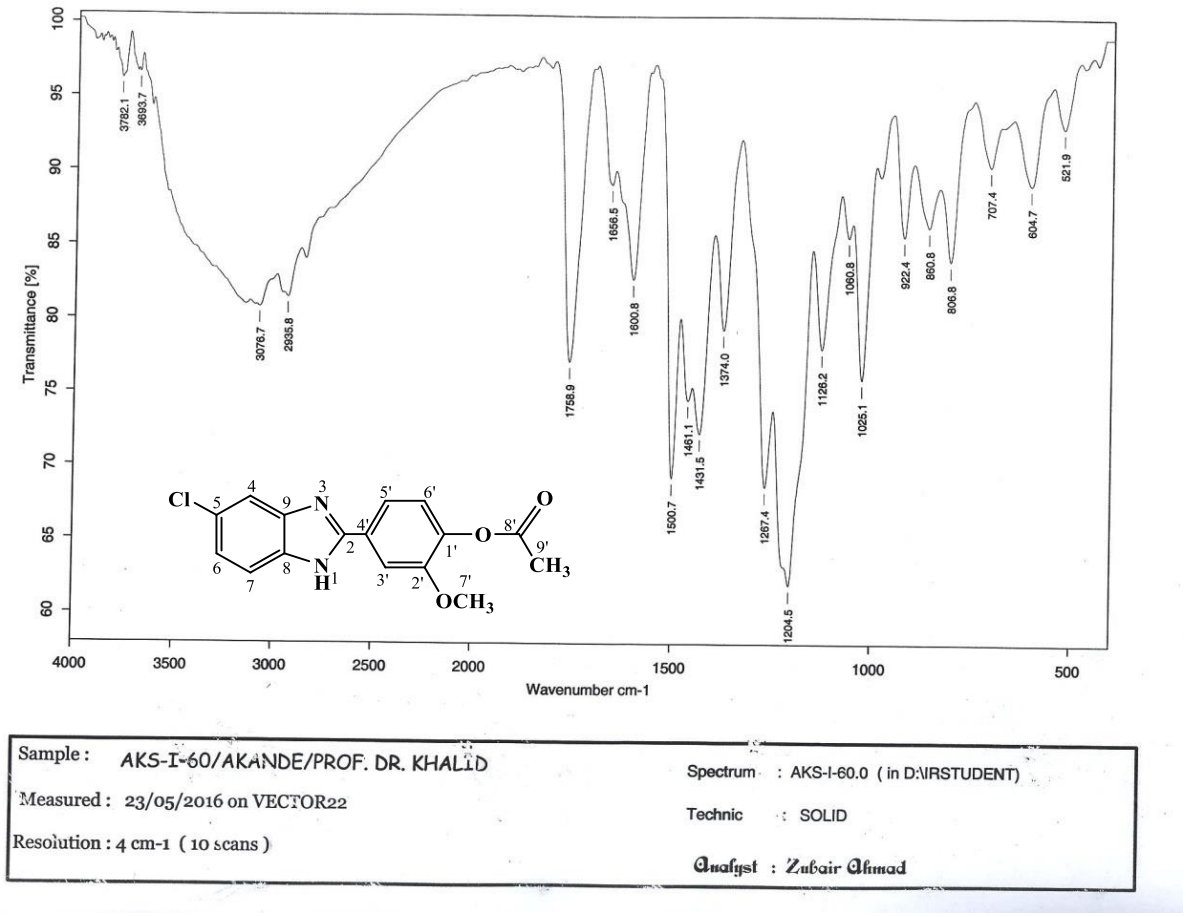

Figure 4.195. IR spectrum of AKS-I-60

THERMO ELECTRON ~ VISIONpro SOFTWARE V4.10

Operator Name	ARSHAD ALAM	Date of Report	5/24/2016
Department	Analytical laboratory#004 TWC	Time of Report	3:52:42PM
Organization	ICCBS.Karachi University.		
Information	Prof Dr.Khalid ./ Akande.		

Scan Graph

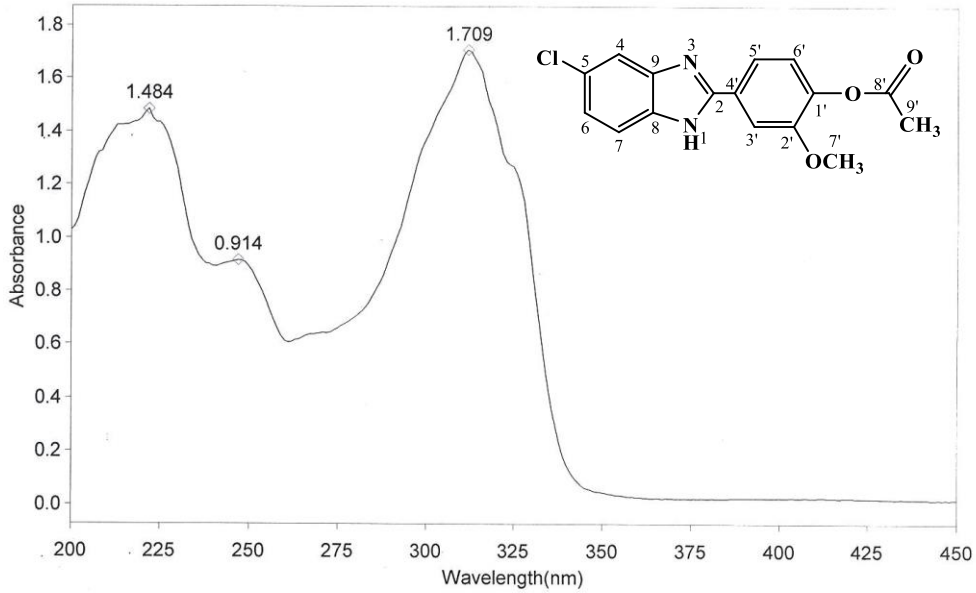

Results Table - aks-i-60.sre,aks-i-60,Cycle01

nm	A	**Peak Pick Method**
222.00	1.484	Find 8 Peaks Above -3.0000 A
247.00	0.914	Start Wavelength 200.00 nm
312.00	1.709	Stop Wavelength 450.00 nm
		Sort By Wavelength
Sensitivity	Very Low	

Page 1, Scan Graph

Figure 4.196. UV spectrum of AKS-I-60

Table 4.32. Summary of the ^{1}H NMR spectra of AKS-I-60

Position	δ ^{1}H [mult., J_{HH} (Hz)] (ppm)
1	-
2	-
3	-
4	7.66 [s]
5	-
6	7.26 [dd, $J_{6,7}$ = 8.8, $J_{6,4}$ = 2.0]
7	7.63 [d, $J_{7,6}$ = 8.8]
8	-
9	-
1′	-
2′	-
3′	7.89 [d, $J_{3',5'}$ = 1.6]
4′	-
5′	7.76 [dd, $J_{5',6'}$ = 8.4, $J_{5',3'}$ = 1.6]
6′	7.29 [d, $J_{6',5'}$ = 8.4]
7′-OCH_3	3.90 [s]
9′-CH_3	2.29 [s]

4.1.33 Characterisation of 2′-methoxy-4′-(5-nitro-1*H*-benzo[*d*]imidazol-2-yl)-phenyl acetate (AKS-I-61)

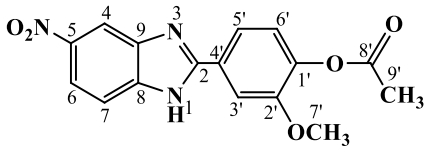

The yellow compound, AKS-I-61 was obtained as a solid substance in a yield of 70.6% (0.231 g), m.pt. of 203-207 ºC and a R_f value of 0.31 (hexane/ethyl acetate, 1:1).

Represented in figures **4.197** and **4.198** are eight signals from the ^{1}H NMR (400 MHz, DMSO-d_6) spectra. δ (ppm) values were assigned as 13.61 (1H, br s, –NH; most deshielded) to the amine proton, 8.15 (1H, d, $J_{7,6}$ = 8.4 Hz, H-7), 8.50 (1H, br s, H-4), 7.94 (1H, s, H-3′), 7.83 (2H, d, $J_{5',6'}$ = 8.4 Hz, H-5′), 7.77 (1H, br s, H-6), 7.34 (1H, d, $J_{6',5'}$ = 8.4 Hz, H-6′) to the methine protons, 3.91 (3H, s, 7′-OCH_3) to the methoxy protons and 2.29 (3H, s, 9′-CH_3) to the upfield methyl protons of the acetate functional group.

The molecular ion, M^+ peak from EI-MS spectrum (figure **4.199**) was obtained at a *m/z* of 327. Characteristic M^+-NO yielded the peak with a *m/z* of 297 and a further loss of CH_2=C=O fragment produced the peak at 255 which corresponds to $[C_{14}H_{11}N_2O_3]^+$. The base peak at *m/z* of 285 resulted from a characteristic loss of CH_2=C=O from M^+ corresponding to $[C_{14}H_{11}N_3O_4]^+$. The *m/z* of 238 is suggestive of the fragment $[C_{13}H_8N_3O_2]^+$. Peaks at *m/z* 90 and 63 correspond to $[C_6H_4N]^+$ and $[C_5H_3]^+$ fragment ions respectively. Further confirming the compound from HREI-MS analysis, the *m/z* found corresponding to the formula $C_{16}H_{13}N_3O_5$ is 327.0856 (calculated 327.0855).

The IR spectrum (figure **4.200**) shows characteristic vibrational frequencies, $\bar{\upsilon}$ for amine N–H*str*, aromatic C–H*str*, aliphatic C–H*str*, C=O*str* of ester, two aromatic C=C*str*, N=O*sym str* of nitro group, and C–O*str* of ester corresponding to 3315, 3101, 2959, 1760, 1598, 1501, 1338 and 1214 cm^{-1} respectively. The maximum absorption wavelenghts (λ_{max}) at 330, 269 and 213 nm were obtained from the UV analysis (figure **4.201**) indicating n→π* and π→π* transitions. Table **4.33** represents the summary of ^{1}H NMR spectra.

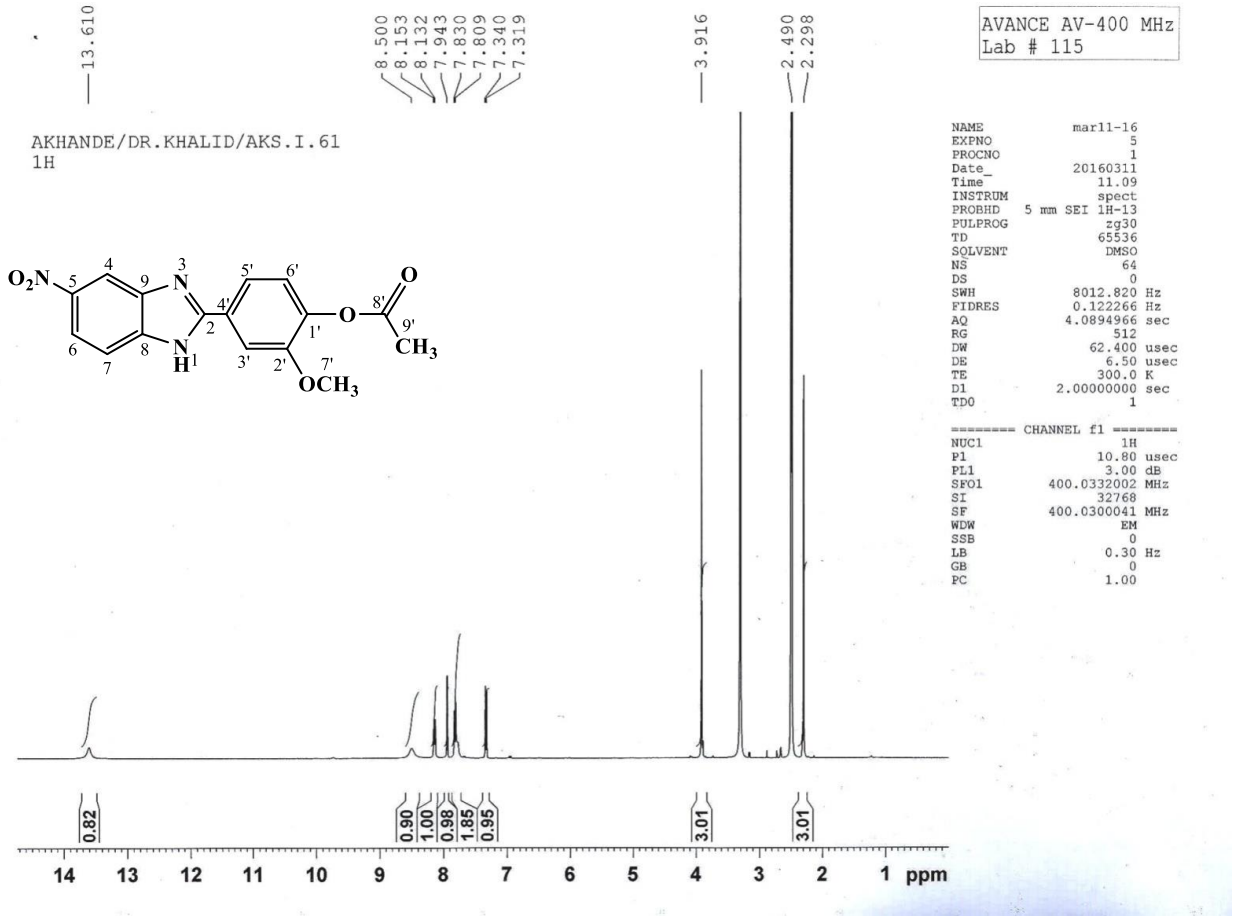

Figure 4.197. ^{1}H NMR (400 MHz, DMSO-d_6) spectrum of AKS-I-61

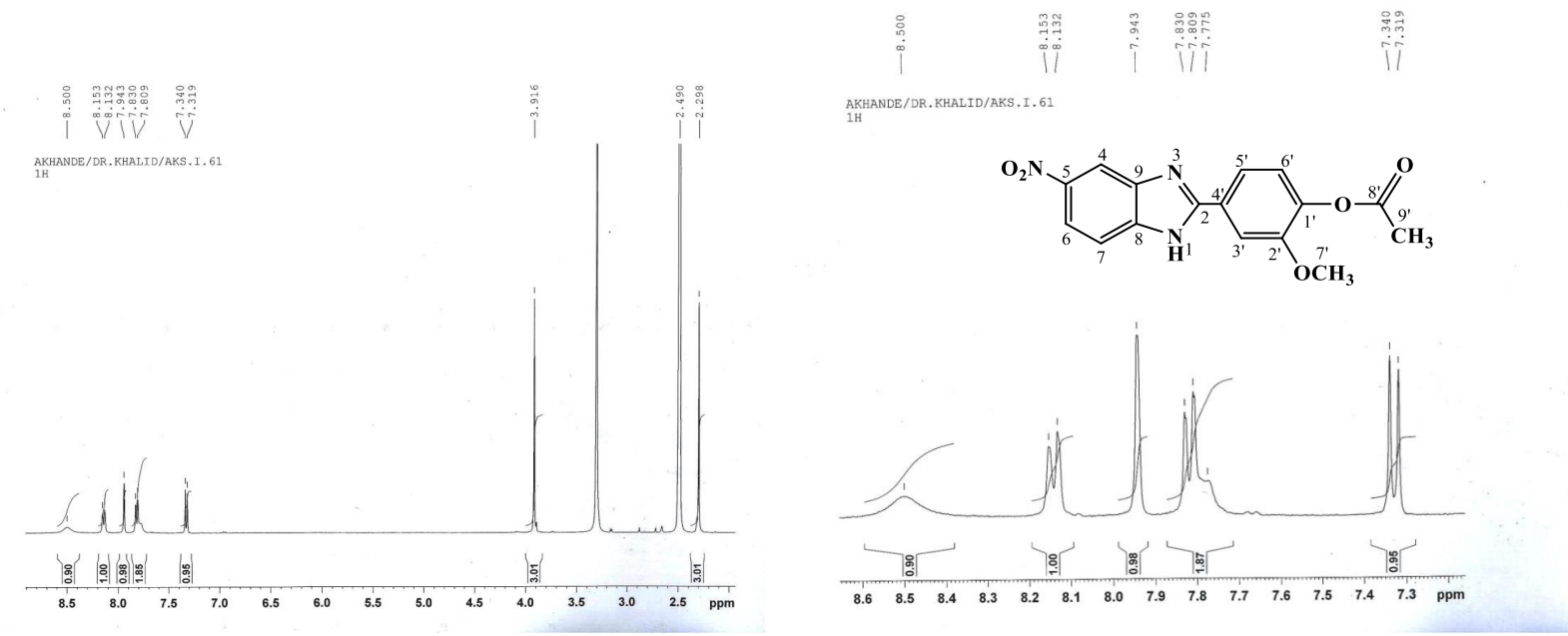

Figure 4.198. ^{1}H NMR (400 MHz, DMSO-d_6) spectra of AKS-I-61 (Expanded)

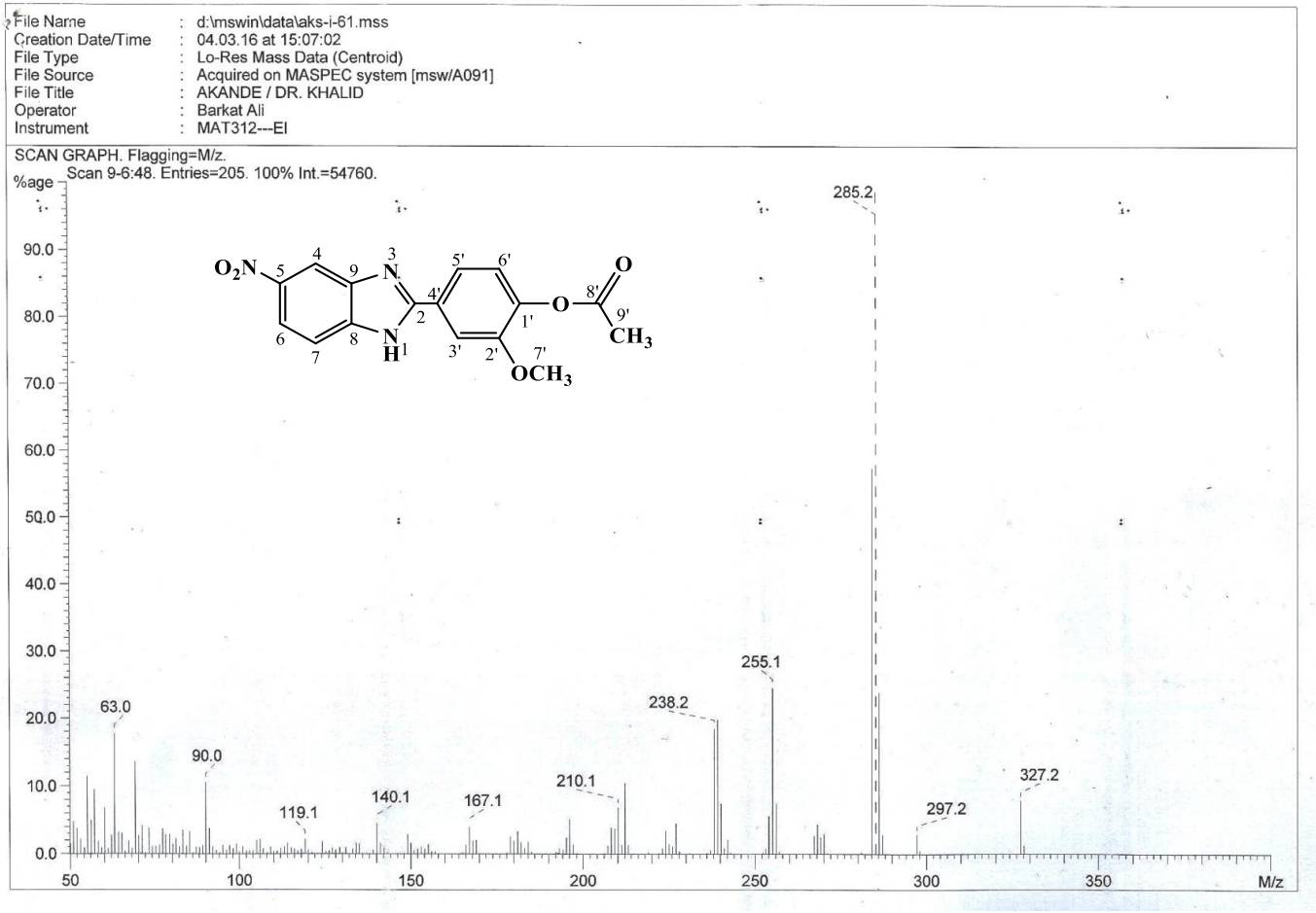

Figure 4.199. EI-MS spectrum of AKS-I-61

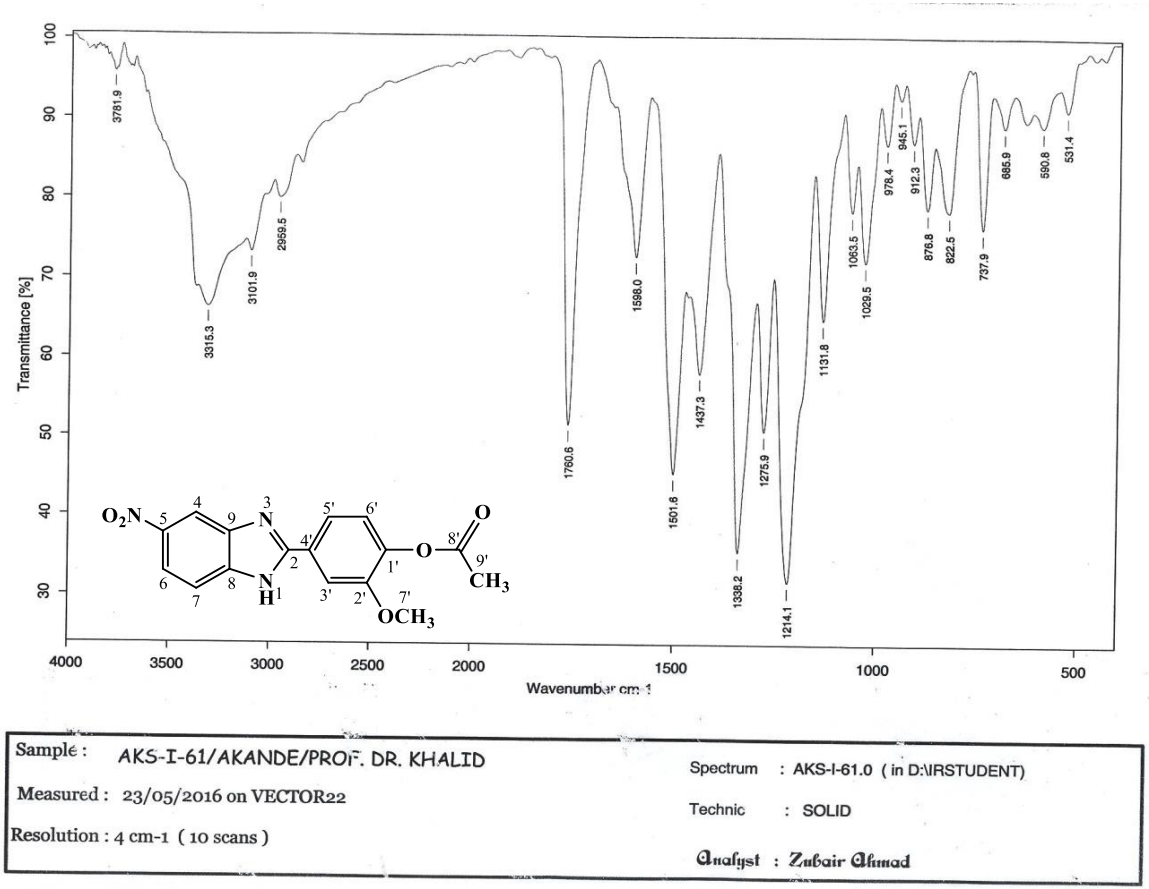

Figure 4.200. IR spectrum of AKS-I-61

THERMO ELECTRON ~ VISIONpro SOFTWARE V4.10

Operator Name	ARSHAD ALAM	Date of Report	5/24/2016
Department	Analytical laboratory#004 TWC	Time of Report	3:57:10PM
Organization	ICCBS.Karachi University.		
Information	Prof Dr.Khalid ./ Akande.		

Scan Graph

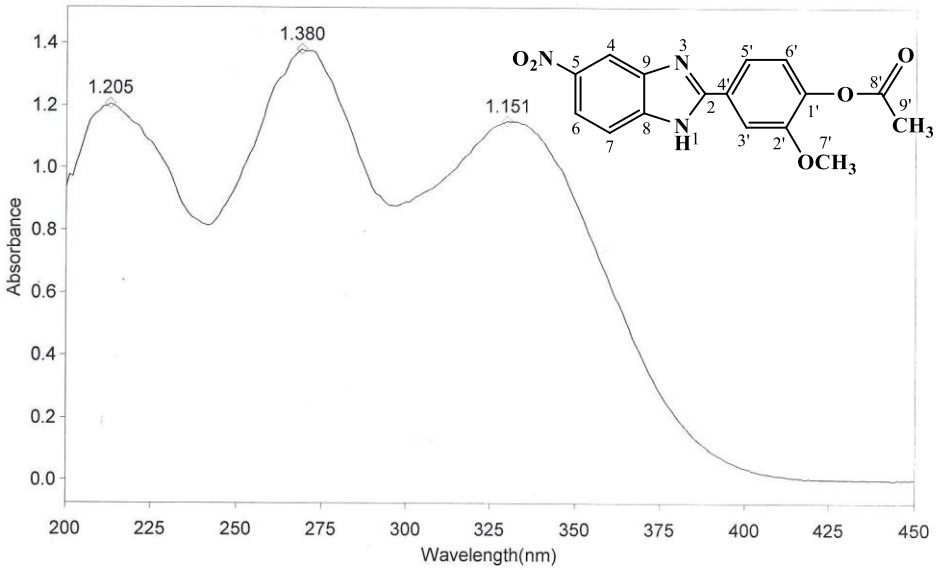

Results Table - aks-i-61.sre,aks-i-61,Cycle01

nm	A	**Peak Pick Method**
213.00	1.205	Find 8 Peaks Above -3.0000 A
269.00	1.380	Start Wavelength 200.00 nm
330.00	1.151	Stop Wavelength 450.00 nm
		Sort By Wavelength
Sensitivity	Auto	

Page 1, Scan Graph

Figure 4.201. UV spectrum of AKS-I-61

Table 4.33. Summary of the ^{1}H NMR spectra of AKS-I-61

Position	δ ^{1}H [mult., J_{HH} (Hz)] (ppm)
1	13.61 [br s]
2	-
3	-
4	8.50 [br s]
5	-
6	7.77 [br s]
7	8.15 [d, $J_{7,6}$ = 8.4]
8	-
9	-
1′	-
2′	-
3′	7.94 [s]
4′	-
5′	7.83 [d, $J_{5',6'}$ = 8.4]
6′	7.34 [d, $J_{6',5'}$ = 8.4]
7′-OCH_3	3.91 [s]
9′-CH_3	2.29 [s]

4.1.34 Characterisation of 2-(2′-bromo-4′,5′-dimethoxyphenyl)-1*H*-benzo[*d*] imidazole (AKS-I-63)

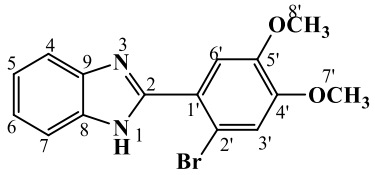

The brown solid compound, AKS-I-63 was obtained in a yield of 61.6% (0.205 g), having a m.pt. of 186-188 ^{o}C and a 0.34 R_f value obtained a hexane/ethyl acetate(1:1) solvent system.

Figures **4.202** and **4.203** show six ^{1}H NMR resonance peaks (400 MHz, DMSO-d_6) in δ (ppm) units and are assigned as 12.55 (1H, s, -NH) to the amine proton, 7.67 (1H, d, $J_{4,5}$ = 7.6 Hz, H-4), 7.20 (1H, t, $J_{5,6}$ = 7.2 Hz, H-5), 7.24 (1H, t, $J_{6,5}$ = 7.2 Hz, H-6), 7.53 (1H, d, $J_{7,6}$ = 7.2 Hz, H-7), 7.30 (1H, s, H-6′) and 7.33 (1H, d, H-3′) to the methine protons, with protons at positions 5 and 6 exhibit ortho coupling (J = 7.2 Hz). The two methoxy protons resonate at 3.85 and 3.81, both represented as (3H, s, 8′-OCH_3) and (3H, s, 7′-OCH_3) respectively.

The fragmentations obtained from EI-MS analysis (figure **4.204**) gave peak patterns spaced two mass units apart due to a bromine atom. The molecular ion, M^+ and the isotope, $[M^+ + 2]$ peaks were obtained at *m/z* of 332 (base peak) and 334 respectively. The peak with *m/z* of 319 corresponds to $[M\text{-}CH_3]^+$, while that of 303 is suggestive of a cleavage due to loss of CH_2OH from M^+. Removal of CH_3O and CH_3 radicals in succession is indicative of the fragment with *m/z* of 288 $[C_{13}H_7BrN_2O]^+$. Loss of Br radical from M^+ yielded the ion with *m/z* of 254. The *m/z* of 195 and 167 correspond to the fragment ions $[C_{13}H_{10}N_2]^+$ and $[C_6HBrO]^+$ respectively. Further confirming the compound, HREI-MS analysis yielded the *m/z* of 332.0144 (calculated, 332.0160) corresponding to the molecular formula, $C_{15}H_{13}N_2O_2Br$.

The IR spectrum (figure **4.205**) depicts vibrational frequencies, $\bar{\upsilon}$ at ≈3300, 3053, 2959, 2840, 1598, 1501, 1441, 1210 and 866 cm^{-1} corresponding to N–H_{str} of 2^{o} amine, aromatic C–H_{str}, aliphatic C–$H_{asy\ str}$ and C–$H_{sym\ str}$, two aromatic C=C_{str}, C–H_b of OCH_3, C–O_{str} of ether and C–Br_{str} respectively. The UV spectrum (figure **4.206**) gave wavelenghts of maximum absorptions (λ_{max}) at 291 and 222 nm corresponding to n→π* and π→π* transitions. The summary of ^{1}H NMR spectra is represented in table **4.34**.

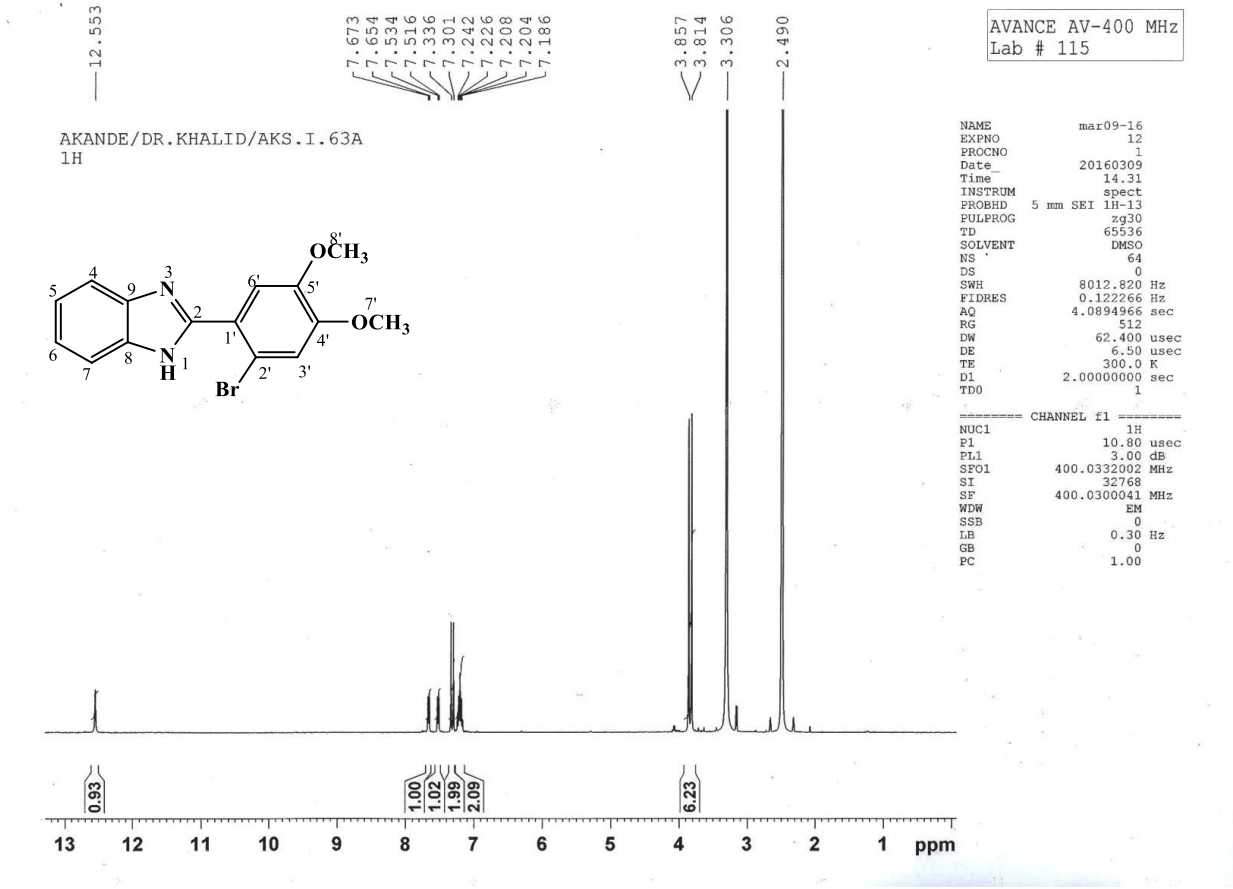

Figure 4.202. ^{1}H NMR (400 MHz, DMSO-d_6) spectrum of AKS-I-63

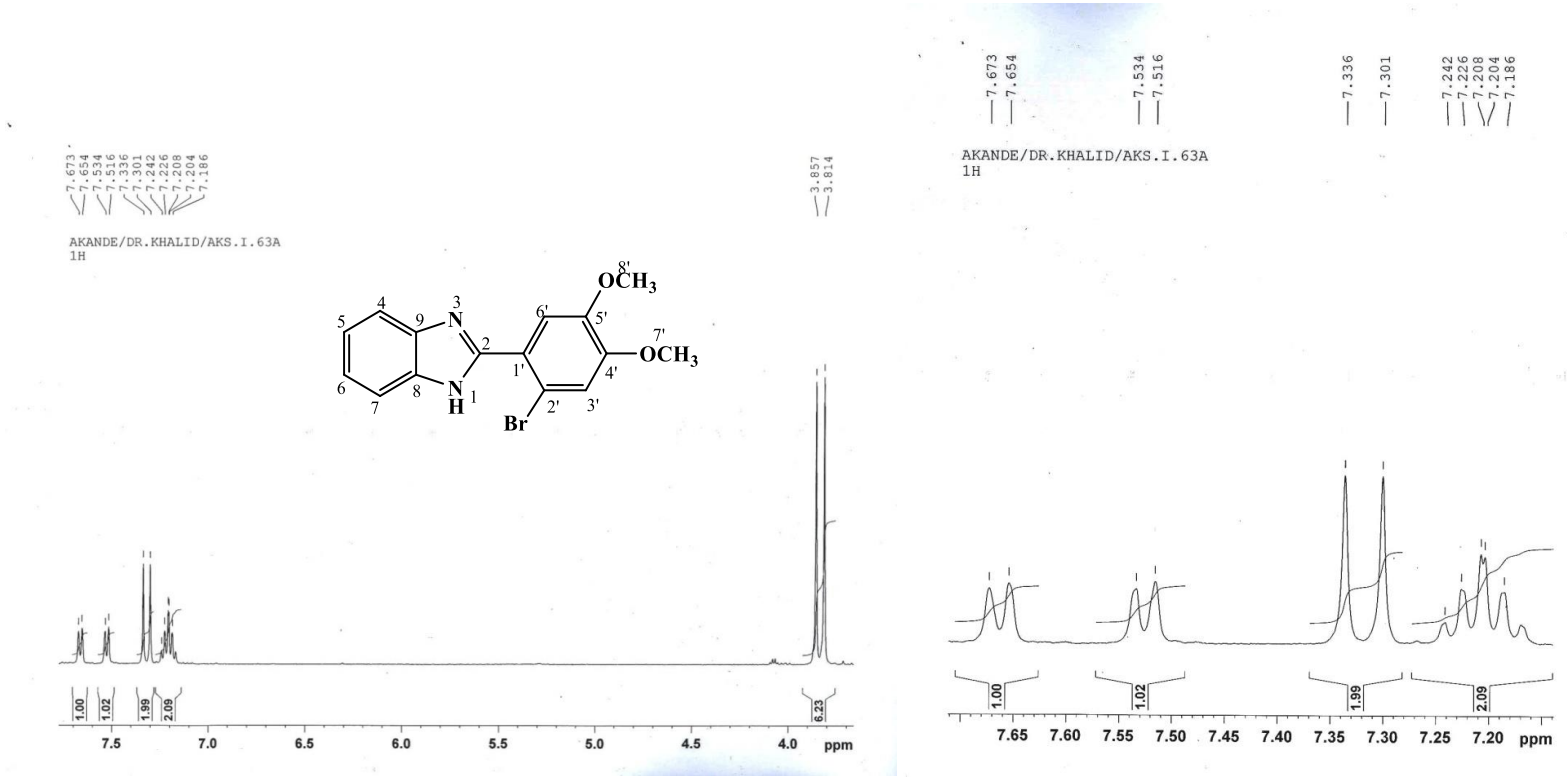

Figure 4.203. ^{1}H NMR (400 MHz, DMSO-d_6) spectra of AKS-I-63 (Expanded)

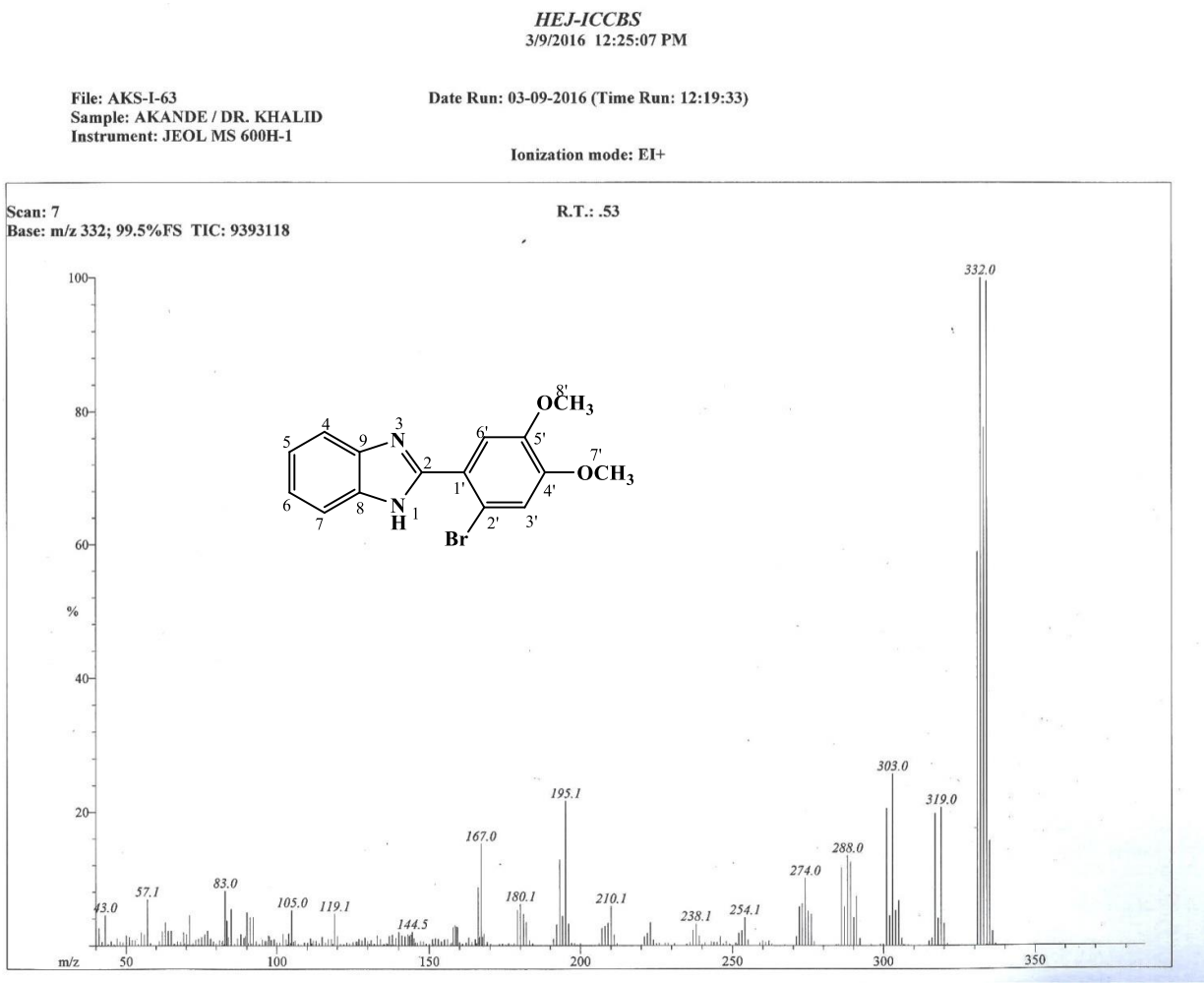

Figure 4.204. EI-MS spectrum of AKS-I-63

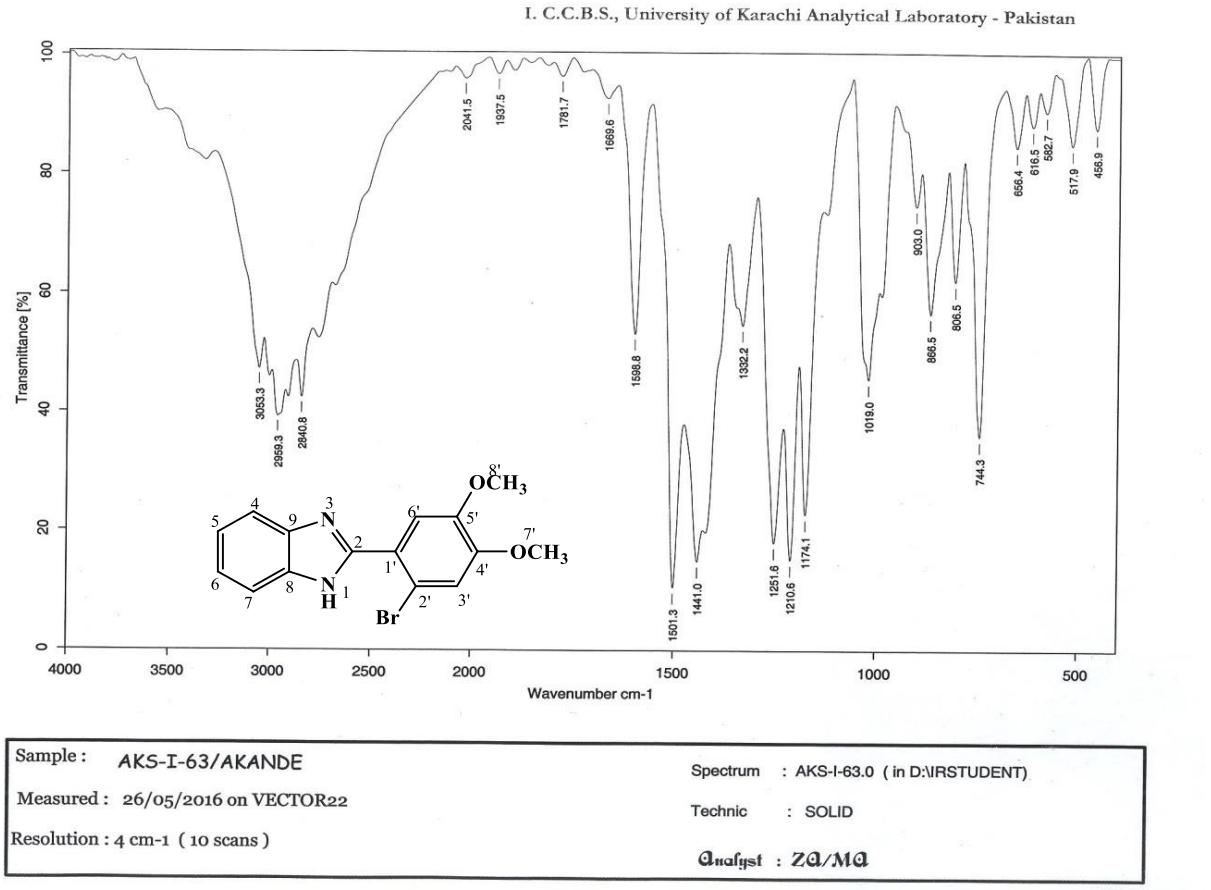

Figure 4.205. IR spectrum of AKS-I-63

THERMO ELECTRON ~ VISIONpro SOFTWARE V4.10

Operator Name	ARSHAD ALAM	Date of Report	5/26/2016
Department	Analytical laboratory#004 TWC	Time of Report	3:47:29PM
Organization	ICCBS.Karachi University.		
Information	Prof. Dr. K. M. Khan/ Akande		

Scan Graph

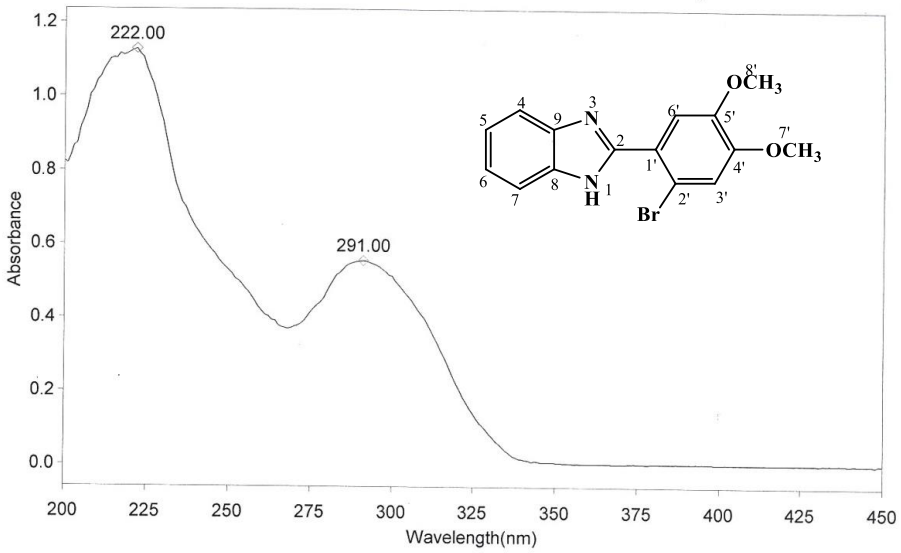

Results Table - AKS-I-63.sre,AKS-I-63,Cycle01

nm	A	**Peak Pick Method**
222.00	1.128	Find 8 Peaks Above -3.0000 A
291.00	0.555	Start Wavelength 200.00 nm
		Stop Wavelength 450.00 nm
		Sort By Wavelength
Sensitivity	Auto	

Page 1, Scan Graph

Figure 4.206. UV spectrum of AKS-I-63

Table 4.34. Summary of the ^{1}H NMR spectra of AKS-I-63

Position	δ ^{1}H [mult., J_{HH} (Hz)] (ppm)
1	12.55 [s]
2	-
3	-
4	7.67 [d, $J_{4,5}$ = 7.6]
5	7.20 [t, $J_{5,6}$ = 7.2]
6	7.24 [t, $J_{6,5}$ = 7.2]
7	7.53 [d, $J_{7,6}$ = 7.2]
8	-
9	-
1′	-
2′	-
3′	7.33 [s]
4′	-
5′	-
6′	7.30 [s]
7′-OCH_3	3.81 [s]
8′-OCH_3	3.85 [s]

4.1.35 Characterisation of 2-(2′-bromo-4′,5′-dimethoxyphenyl)-5-fluoro-1*H*-benzo[*d*] imidazole (AKS-I-64)

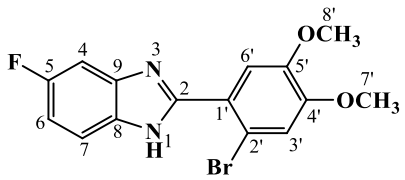

The brown solid compound, AKS-I-64 was obtained in a yield of 69.8% (0.245 g), a m.pt. range of 115-118 ^{o}C and a R_f value of 0.44 in a hexane/ethyl acetate (1:1) solvent system.

Eight resonance peaks δ (ppm) were recorded from the ^{1}H NMR spectra (500 MHz, DMSO-d_6) (figure **4.207** and **4.208**) and are assigned as 12.73 to the amine proton (1H, br d, -NH). Peaks for the methine protons were at 7.40 (1H, br d, $J_{7,6}$ = 8.5 Hz, H-7), 7.59 (1H, br s, H-4), 7.33 (1H, s, H-3′), 7.30 (1H, s, H-6′) and 7.09 (1H, dt, $J_{6,7}$ = 9.0 Hz, $J_{6,4}$ = 2.0 Hz, H-6; coupling effect of fluorine with proton at position 6 observed). The methoxy protons resonated at 3.85 and 3.81 represented as (3H, s, 8′-OCH_3) and (3H, s 7′-OCH_3) respectively.

Figure **4.209** shows peaks of fragment ions with the molecular ion, M^+ and the isotope, [M^++2] peaks at *m/z* of 350 and 352 (base peak) respectively. [M-CH_3]$^+$ is indicative of the fragment ion with *m/z* of 335, which on further cleavage at the imidazole ring produced the ion with *m/z* of 228 $[C_8H_5{}^{81}BrNO_2]^+$. The *m/z* of 321 suggests a loss of CH_3O radical from the [M^++2], which corresponds to $[C_{14}H_9{}^{81}BrFN_2O]^+$. The fragmentation, M^+-CH_2=O-CH_3 suggests the ion with *m/z* of 307 $[C_{13}H_7{}^{81}BrFN_2O]^+$. Peaks with *m/z* of 213 and 185 correspond to the fragment ions $[C_7H_2{}^{81}BrNO_2]^+$ and $[C_{11}H_6FN_2]^+$. HREI-MS analysis further confirmed the compound revealing a *m/z* of 350.0063 (calculated, 350.0066) corresponding to the formula, $C_{15}H_{12}N_2O_2BrF$.

Spectrum from IR analysis (figure **4.210**) shows vibrational frequencies, $\bar{\upsilon}$ (cm^{-1}) assignable to some functional groups such as 3568, 3004, 2953, 2836, 1633, 1602/1504, 1443, 1267/1035, 1136, and 900 corresponding to ($N–H_{str}$), (sp^2 $C–H_{str}$ aromatic), (sp^3 $C–H_{asy\ str}$ aliphatic), (sp^3 $C–H_{sym\ str}$ aliphatic), ($C=N_{str}$), ($C=C_{str}$ aromatic), ($C–H_b$), ($C–O_{str}$), ($C–F_{str}$) and ($C–Br_{str}$) respectively. Figure **4.211** represents the UV spectrum, presenting wavelenghts of maximum absorptions (λ_{max}) at 296, 222 and 214 nm indicative of n→π* and π→π* transitions. Table **4.35** shows the summary of the ^{1}H NMR spectra.

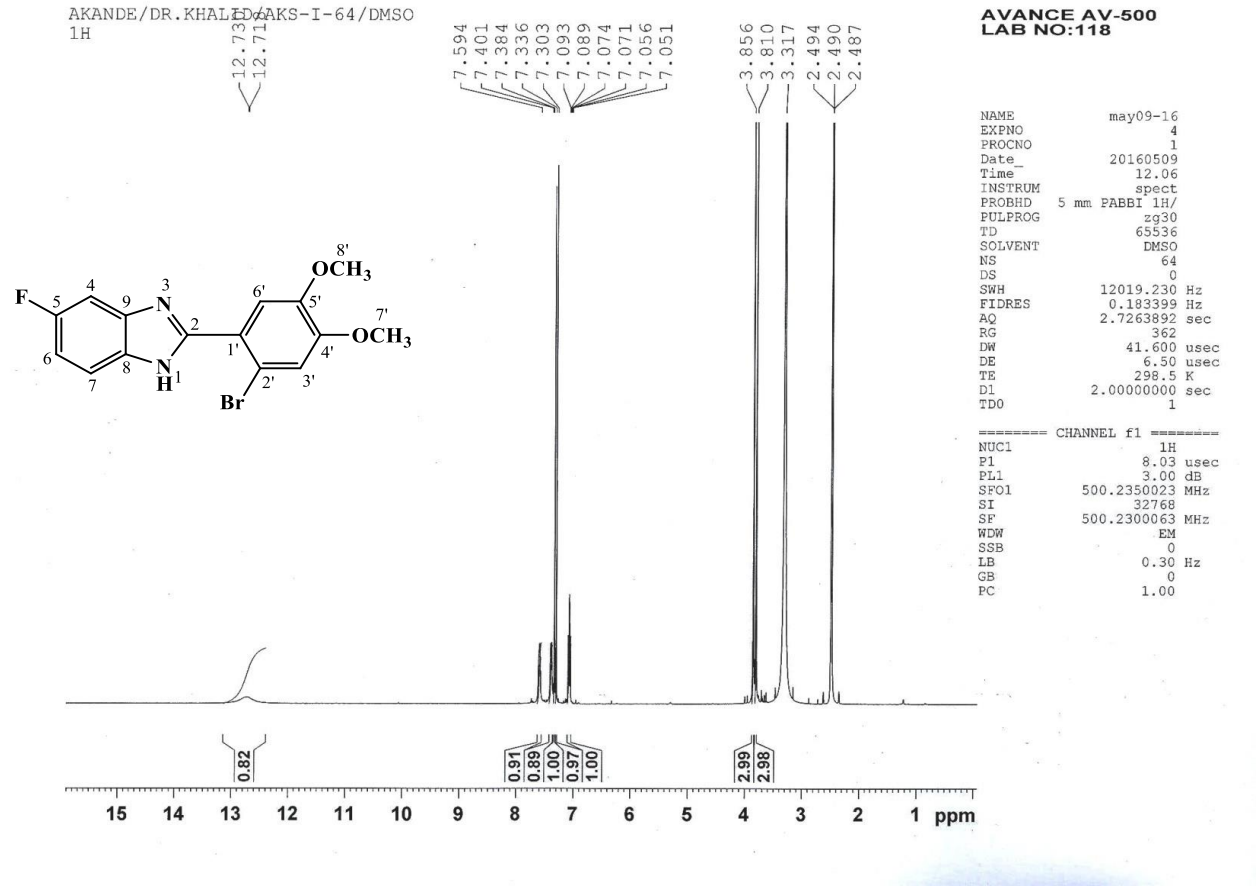

Figure 4.207. ^{1}H NMR (500 MHz, DMSO-d_6) spectrum of AKS-I-64

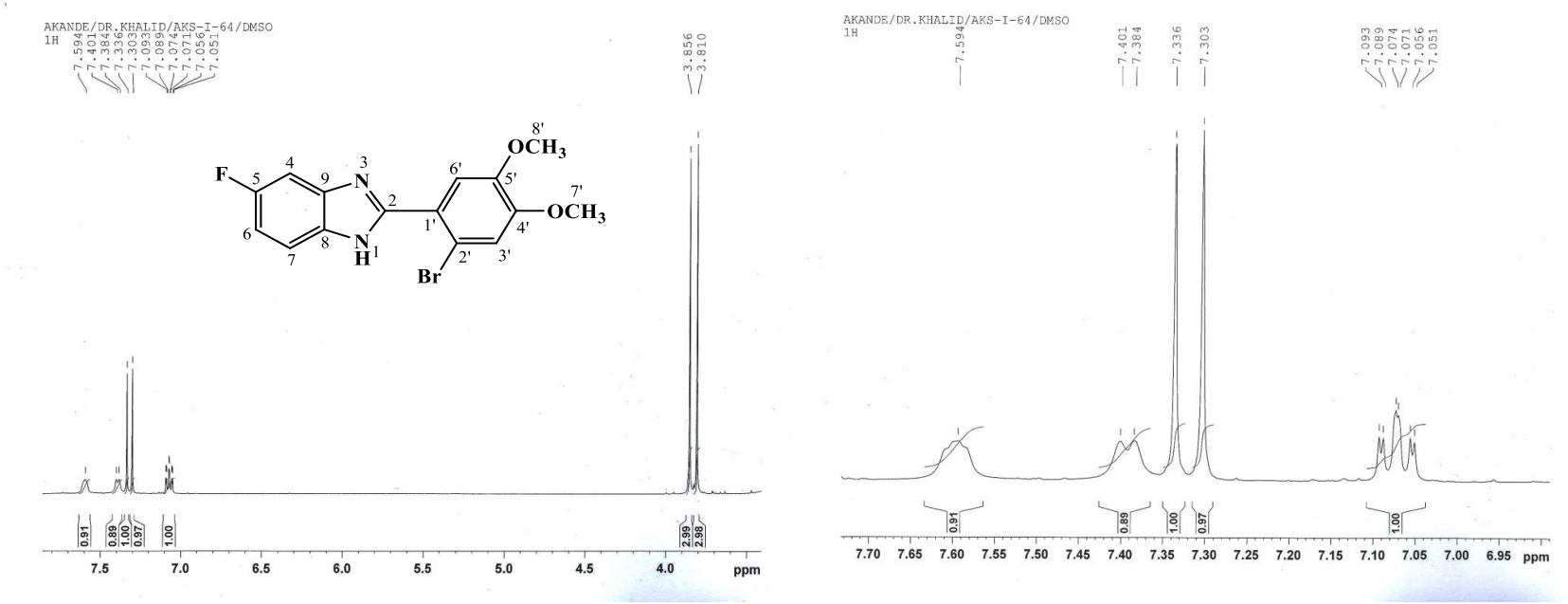

Figure 4.208. ^{1}H NMR (500 MHz, DMSO-d_6) spectra of AKS-I-64 (Expanded)

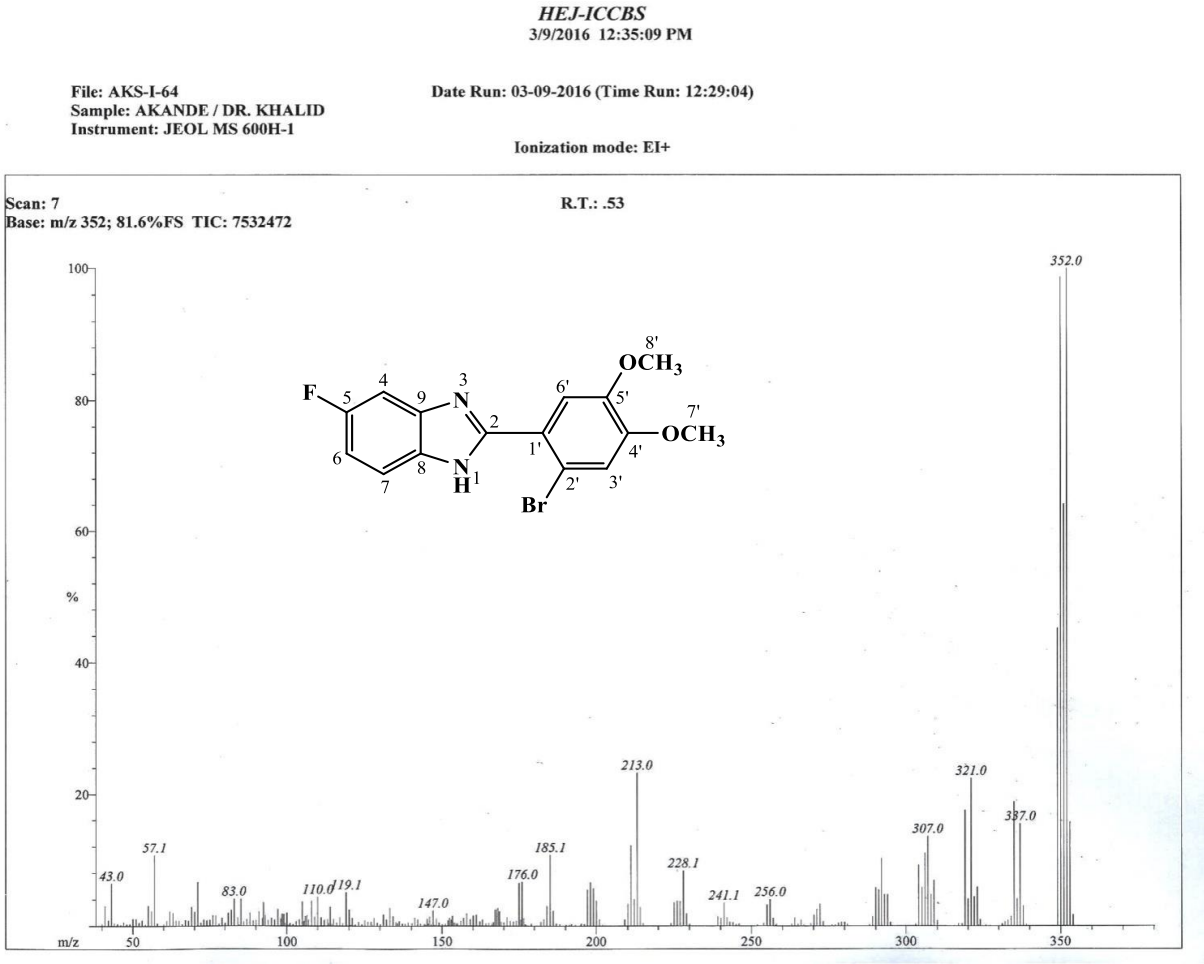

Figure 4.209. EI-MS spectrum of AKS-I-64

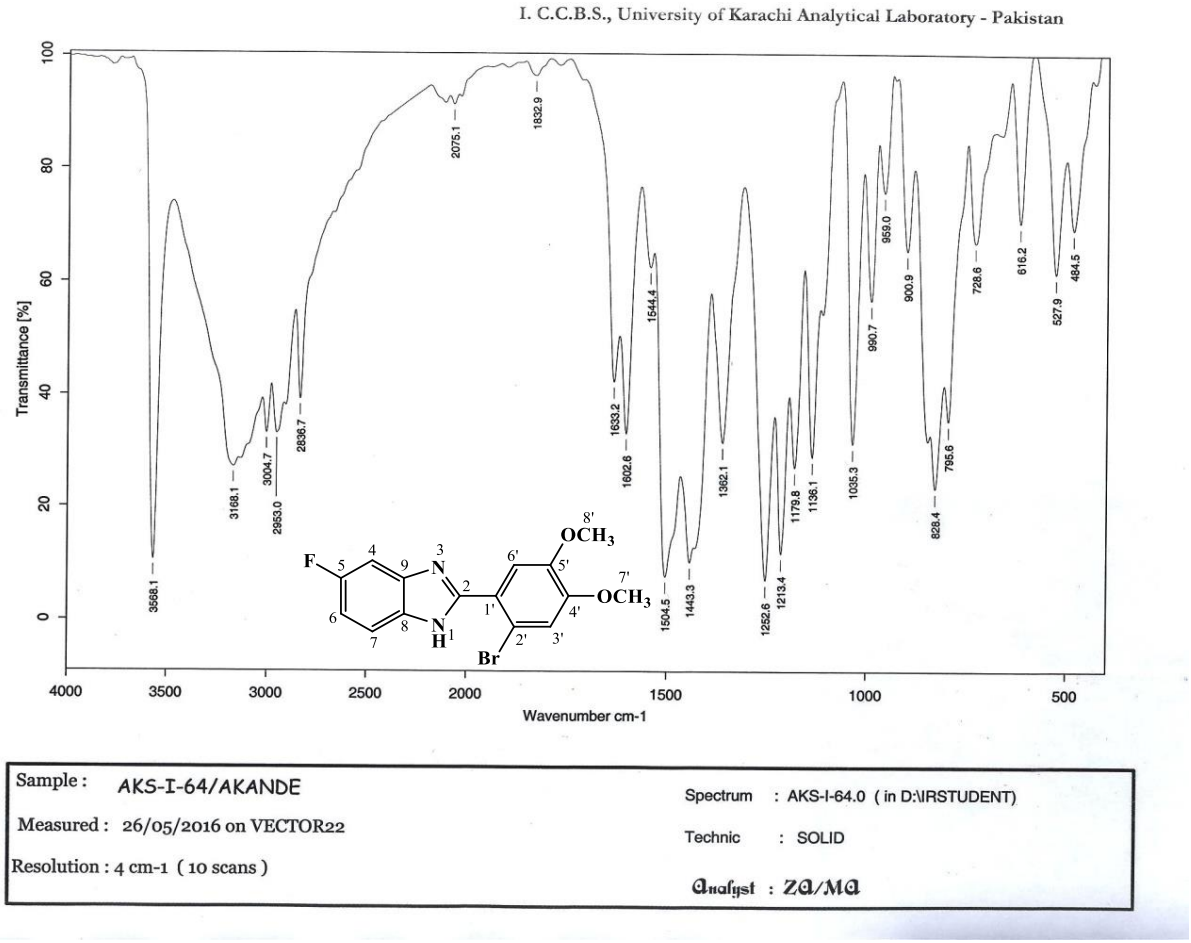

Figure 4.210. IR spectrum of AKS-I-64

THERMO ELECTRON ~ VISIONpro SOFTWARE V4.10

Operator Name	ARSHAD ALAM	Date of Report	5/26/2016
Department	Analytical laboratory#004 TWC	Time of Report	3:53:32PM
Organization	ICCBS.Karachi University.		
Information	Prof. Dr. K. M. Khan/ Akande		

Scan Graph

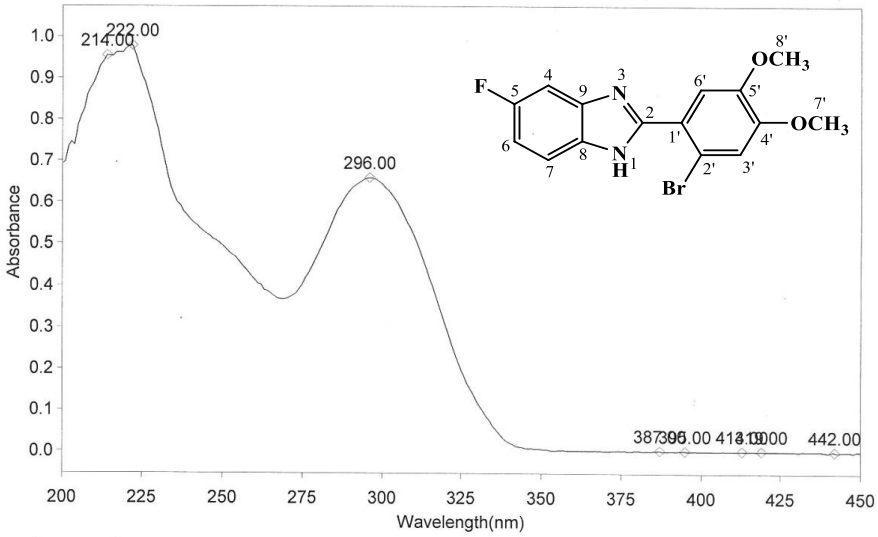

Results Table - AKS-I-64.sre,AKS-I-64,Cycle01

nm	A	**Peak Pick Method**
214.00	0.955	Find 8 Peaks Above -3.0000 A
222.00	0.978	Start Wavelength 200.00 nm
296.00	0.659	Stop Wavelength 450.00 nm
387.00	0.003	Sort By Wavelength
395.00	0.003	Sensitivity High
413.00	0.002	
419.00	0.002	
442.00	0.001	

Page 1, Scan Graph

Figure 4.211. UV spectrum of AKS-I-64

Table 4.35. Summary of the ^{1}H NMR spectra of AKS-I-64

Position	δ ^{1}H [mult., J_{HH} (Hz)] (ppm)
1	12.73 [br d]
2	-
3	-
4	7.59 [br s]
5	-
6	7.09 [dt, $J_{6,7}$ = 9.0, $J_{6,4}$ = 2.0]
7	7.40 [br d, $J_{7,6}$ = 8.5]
8	-
9	-
1′	-
2′	-
3′	7.33 [s]
4′	-
5′	-
6′	7.30 [s]
7′-OCH_3	3.81 [s]
8′-OCH_3	3.85 [s]

4.1.36 Characterisation of 2-(2′-bromo-4′,5′-dimethoxyphenyl)-5-chloro-1*H*-benzo[*d*]imidazole (AKS-I-65)

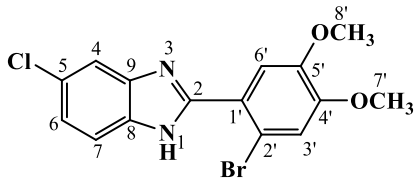

The brown solid compound, AKS-I-65 was obtained in a 58.8% (0.216 g) yield, m.pt. range of 113-115 ^{o}C and a R_f value of 0.46 (hexane/ethyl acetate solvent system, 1:1).

The following five signals in δ (ppm) units were obtained from ^{1}H NMR spectra (400 MHz, DMSO-d_6) (figures **4.212** and **4.213**): the peaks at 7.62 (1H, d, $J_{7,6}$ = 8.4 Hz, H-7; ortho coupled with proton on position 6), 7.26 (1H, dd, $J_{6,7}$ = 8.4 Hz, $J_{6,4}$ = 1.6 Hz, H-6; ortho coupled with proton on position 7), 7.66 (1H, s, H-4), 7.31 (1H, s, H-6′), 7.34 (1H, s, H-3′) all represent the methine protons while 3.86 (3H, s, 8′-OCH_3) and 3.81 (3H, s, 7′-OCH_3) represent the methoxy proton peaks. The amine proton was not captured.

From EI-MS spectrum (figure **4.214**), isotope peaks which include [M^++2] and [M^++4] peaks were obtained alongside many other fragment ion peaks, both ascribed to the presence of Cl and Br atoms. The *m/z* of 366, 368 and 370 were obtained for M^+ peak, [M^++2] (isotope and base peak) and [M^++4] (isotope peak) respectively. The peaks at *m/z* of 353 (M^+-CH_3), 337 (M^+-OCH_3) and 322 (M^+-OCH_3-CH_3) correspond to the fragment ions $[C_{14}H_9{}^{81}BrClN_2O_2]^+$, $[C_{14}H_9{}^{81}BrClN_2O]^+$ and $[C_{13}H_6{}^{81}BrClN_2O]^+$ respectively. Loss of Br radical from M^+ suggests the *m/z* of 288. Fragmentation via the imidazole ring coupled with loss of a CH_3 radical from M^+ is indicative of the fragment with *m/z* of 229, corresponding to $[C_8H_5{}^{81}BrNO_2]^+$ while a *m/z* of 201 corresponds to $[C_{11}H_6ClN_2]^+$. The *m/z* deduced from HREI-MS analysis is 365.9804 (calculated 365.9771) corresponding to the molecular formula $C_{15}H_{12}N_2O_2BrCl$.

The IR spectrum (figure **4.215**) indicated frequencies of vibration, $\bar{\upsilon}$ at ≈3350, 3092, 2939, 2840, 1602, 1497, 1435, 1257, 1213, 1028 and 989 cm^{-1}, assigned to N–H_{str}, aromatic C–H_{str}, aliphatic C–$H_{asy\ str}$ and C–$H_{sym\ str}$, aromatic C=C_{str}, C–H_b, C–O_{str} of ether, C–Cl_{str} and C–Br_{str} respectively. The maximum absorptions (λ_{max}) at 298 and 222 nm resulting from the UV analysis (figure **4.216**) were due to n→π* and π→π* transitions. Table **4.36** represents the summary of ^{1}H NMR spectra.

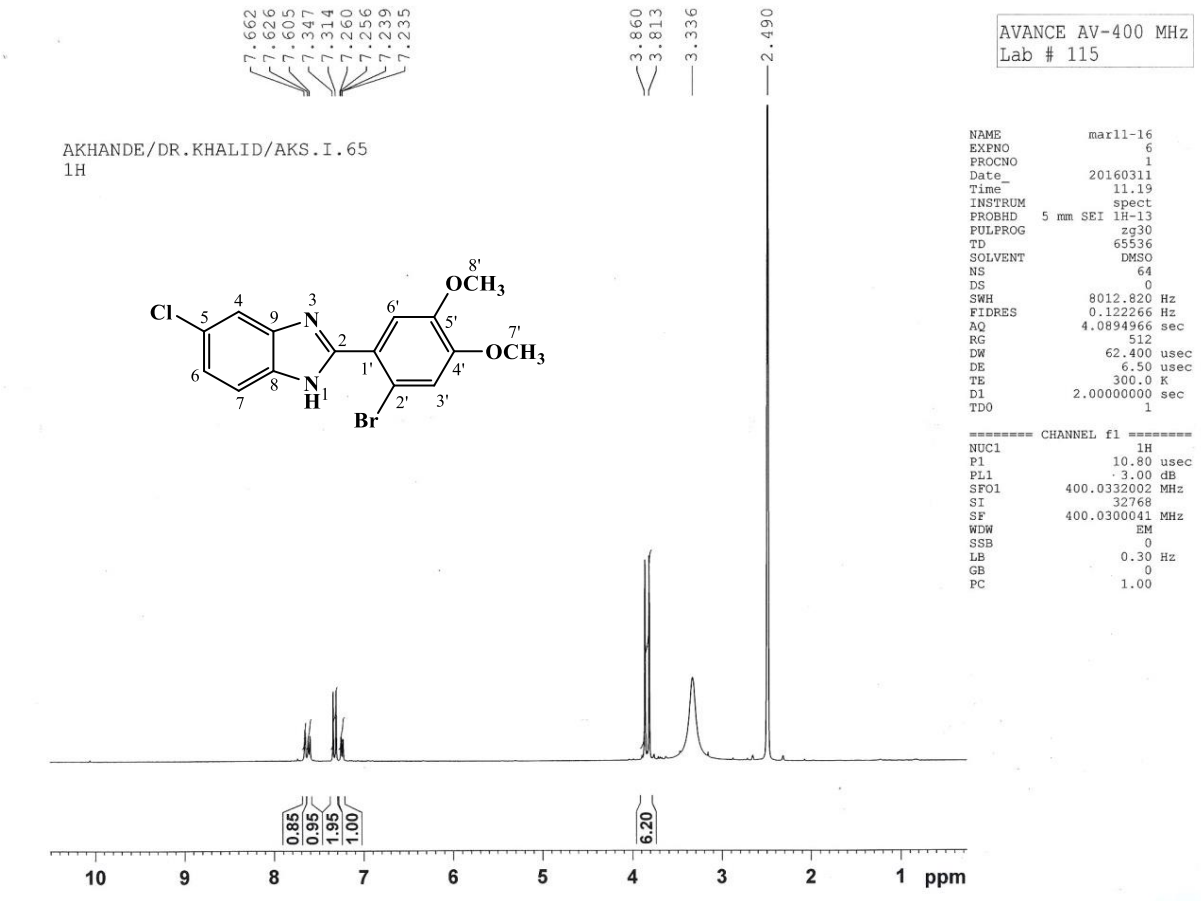

Figure 4.212. ^{1}H NMR (400 MHz, DMSO-d_6) spectrum of AKS-I-65

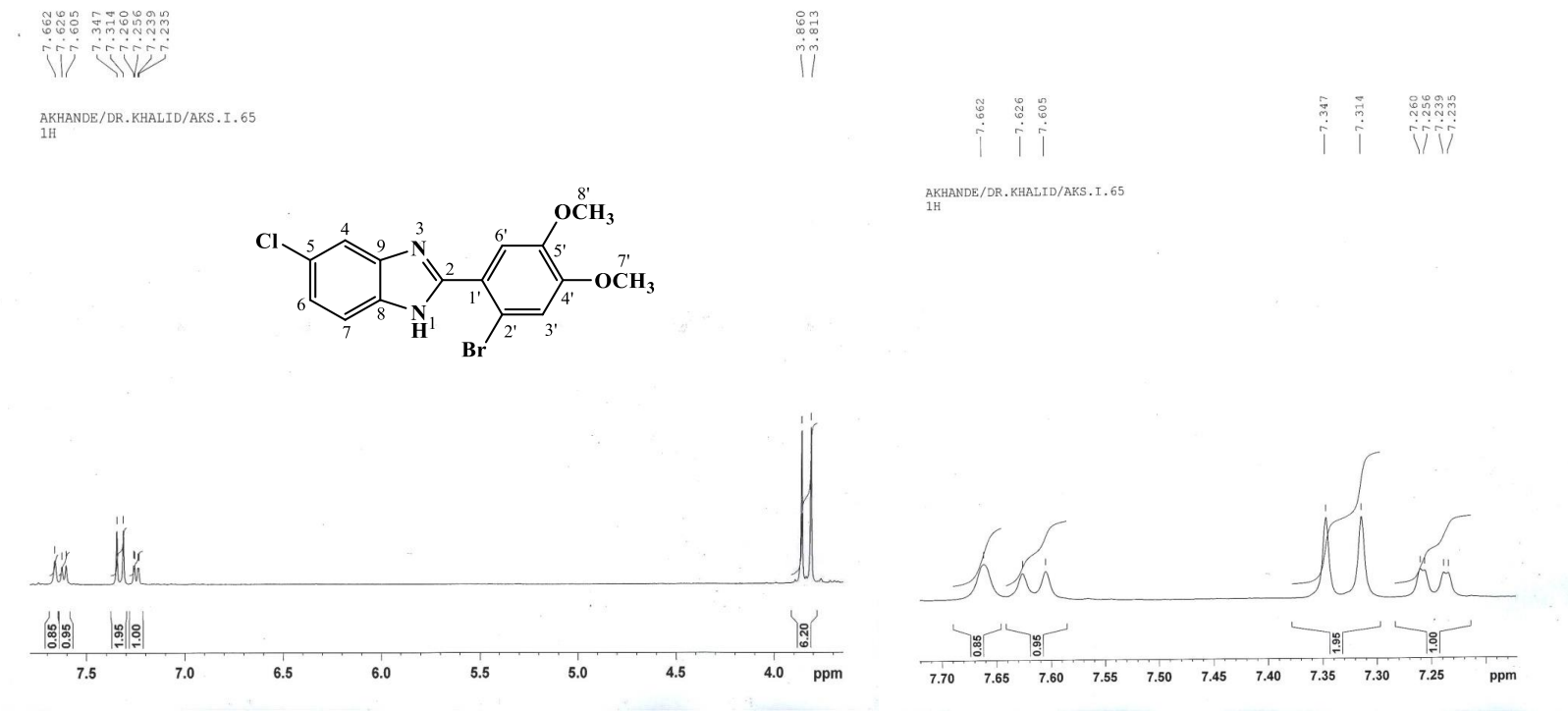

Figure 4.213. ^{1}H NMR (400 MHz, DMSO-d_6) spectra of AKS-I-65 (Expanded)

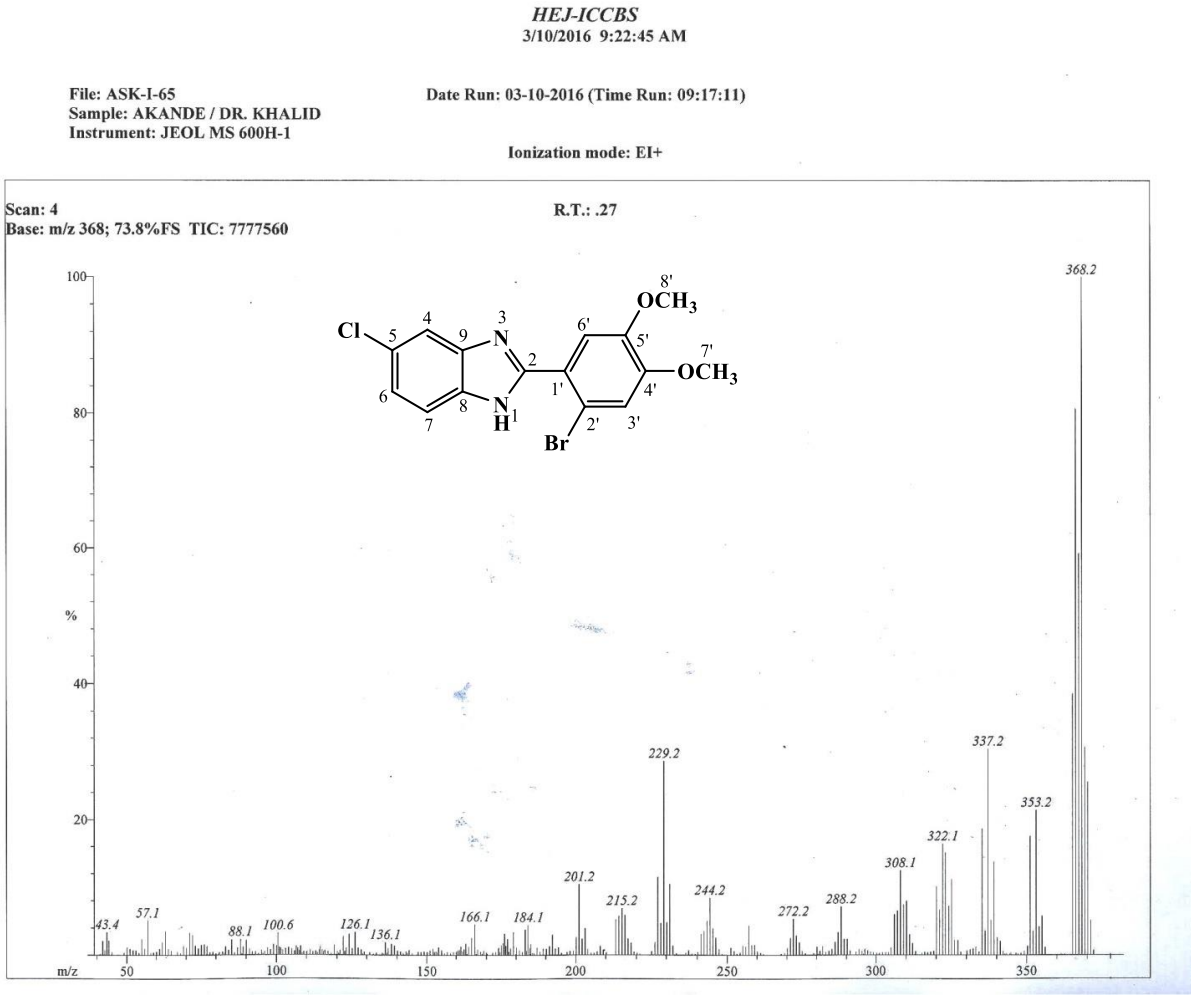

Figure 4.214. EI-MS spectrum of AKS-I-65

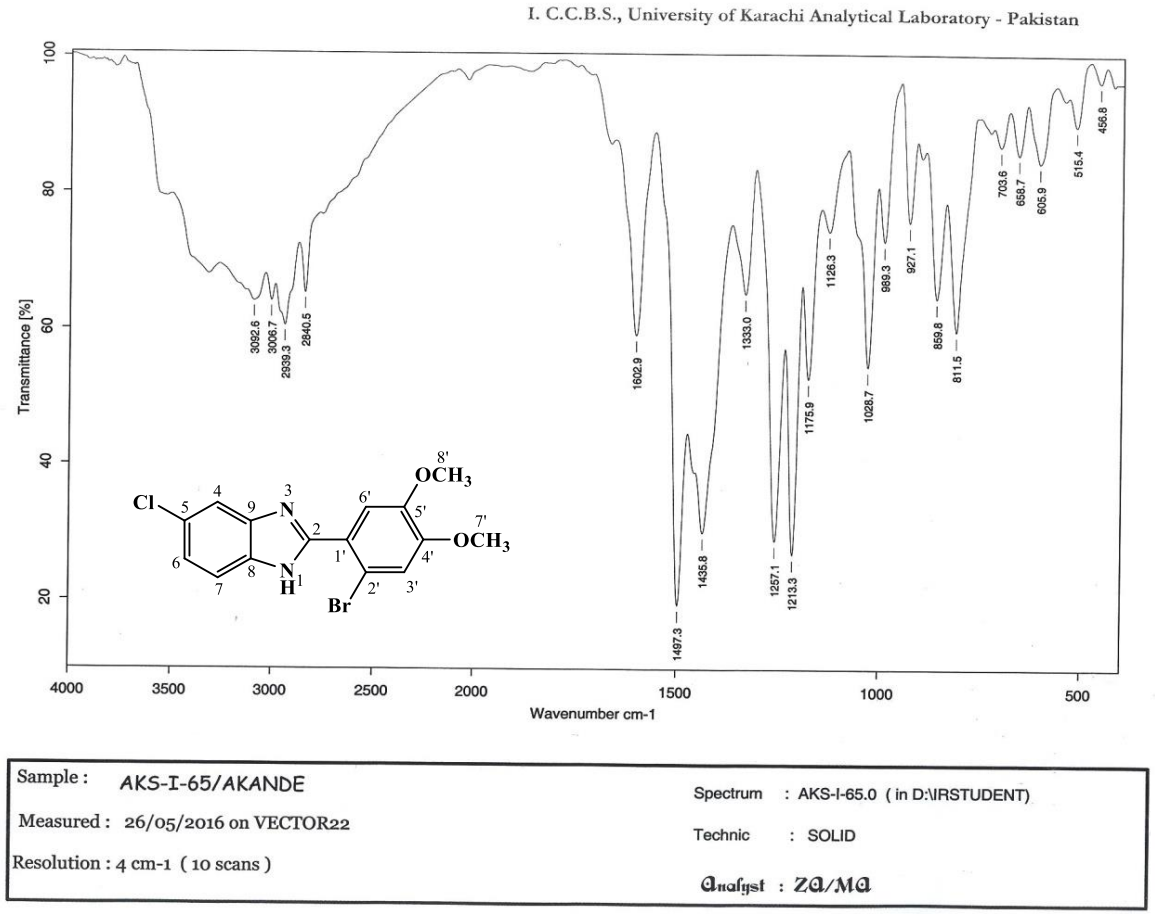

Figure 4.215. IR spectrum of AKS-I-65

THERMO ELECTRON ~ VISIONpro SOFTWARE V4.10

Operator Name	ARSHAD ALAM	Date of Report	5/26/2016
Department	Analytical laboratory#004 TWC	Time of Report	3:59:16PM
Organization	ICCBS.Karachi University.		
Information	Prof. Dr. K. M. Khan/ Akande		

Scan Graph

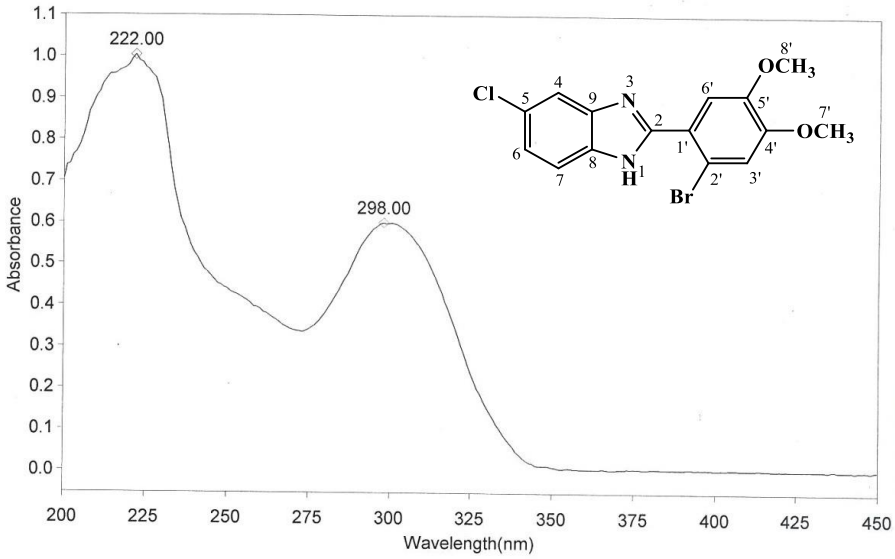

Results Table - AKS-I-65.sre,AKS-I-65,Cycle01

nm	A	**Peak Pick Method**
222.00	1.004	Find 8 Peaks Above -3.0000 A
298.00	0.600	Start Wavelength 200.00 nm
		Stop Wavelength 450.00 nm
		Sort By Wavelength
Sensitivity	Auto	

Page 1, Scan Graph

Figure 4.216. UV spectrum of AKS-I-65

Table 4.36. Summary of the ^{1}H NMR spectra of AKS-I-65

Position	δ ^{1}H [mult., J_{HH} (Hz)] (ppm)
1	-
2	-
3	-
4	7.66 [s]
5	-
6	7.26 [dd, $J_{6,7}$ = 8.4, $J_{6,4}$ = 1.6
7	7.62 [d, $J_{7,6}$ = 8.4]
8	-
9	-
1′	-
2′	-
3′	7.34 [s]
4′	-
5′	-
6′	7.31 [s]
7′-OCH_3	3.81 [s]
8′-OCH_3	3.86 [s]

4.1.37 Characterisation of 2-(2′-chloro-3′,4′-dimethoxyphenyl)-5-fluoro-1*H*-benzo[*d*]imidazole (AKS-I-73)

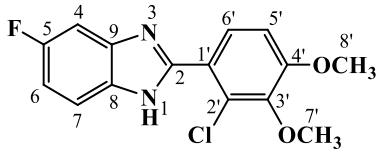

The compound, AKS-I-73 is a brown solid with a yield of 62.3% (0.191 g). It has a m.pt. range of 142-145 ^{o}C and a R_f value of 0.38 (hexane/ethyl acetate, 1:1).

Eight resonance peaks from ^{1}H NMR spectra (500 MHz, DMSO-d_6) (figures **4.217** and **4.218**) in δ (ppm) units are 12.72 (1H, br s, -NH) assigned to the amine proton, 7.57-7.60 multiplet peak (1H, m, H-4) assigned to proton on position 4, a 7.63 resonance peak (1H, d, $J_{6',5'}$ = 9.0 Hz, H-6′) represent proton on position 6′, 7.23 (1H, d, $J_{5',6'}$ = 8.5 Hz, H-5′), 7.39 (1H, d, $J_{7,6}$ = 8.5 Hz, H-7) and 7.08 (1H, dt, $J_{6,7}$ = 9.0 Hz, $J_{6,4}$ = 2.5 Hz, H-6), assigned to the remaining methine protons. The methoxy protons are at 3.91 (3H, s, 7′-OCH_3) and 3.80 (3H, s, 8′-OCH_3) chemical shifts. The broad multiplet observed for H-4, the doublets of triplet for H-6 as well as the broad doublet for H-7 are due to coupling of these protons with fluorine.

From EI-MS spectrum (figure **4.219**), the *m/z* of 306 and 308 were obtained for both the molecular ion, M^+ and the isotope, [M^++2] peaks. The fragmentation [M^+-CH_3**]** produced the radical cation with *m/z* of 291. Loss of ethene molecule and CH_3 radical from M^+ is suggestive of the fragment with *m/z* of 263 $[C_{12}H_5ClFN_2O_2]^+$, and a further loss of O radical produced the fragment with *m/z* of 248. Cleavage on the imidazole ring and a subsequent loss of CH_3 radical from M^+ yielded a *m/z* of 185 fragment. The base peak at *m/z* of 83 and peak at *m/z* of 44 correspond to $[C_5H_7O]^+$ and $[C_2H_6N]^+$ respectively. Confirming the compound from HREI-MS analysis, a *m/z* 306.0571 (calculated, 306.0566) was found corresponding to the formula $C_{15}H_{12}ClFN_2O_2$.

Absorption bands that emanated from IR analysis (figure **4.220**) show vibrational frequencies, $\bar{\upsilon}$ assignable to aromatic C–H_{str}, aliphatic C–$H_{asy\ str}$ and C–$H_{sym\ str}$, C=N_{str}, aromatic C=C_{str}, C–H_b of CH_3O, asymmetry and symmetry C–O_{str} of ether and C–F_{str} corresponding to 3151, 2945, 2845, 1630, 1596, 1460, 1284, 1041 and 1136 cm^{-1} respectively. The UV spectra (figure **4.221**) shows maximum absorption wavelenghts (λ_{max}) at 298, 248 and 213 nm corresponding to n→π* and π→π* transitions. Table **4.37** represents the summary of ^{1}H NMR spectra.

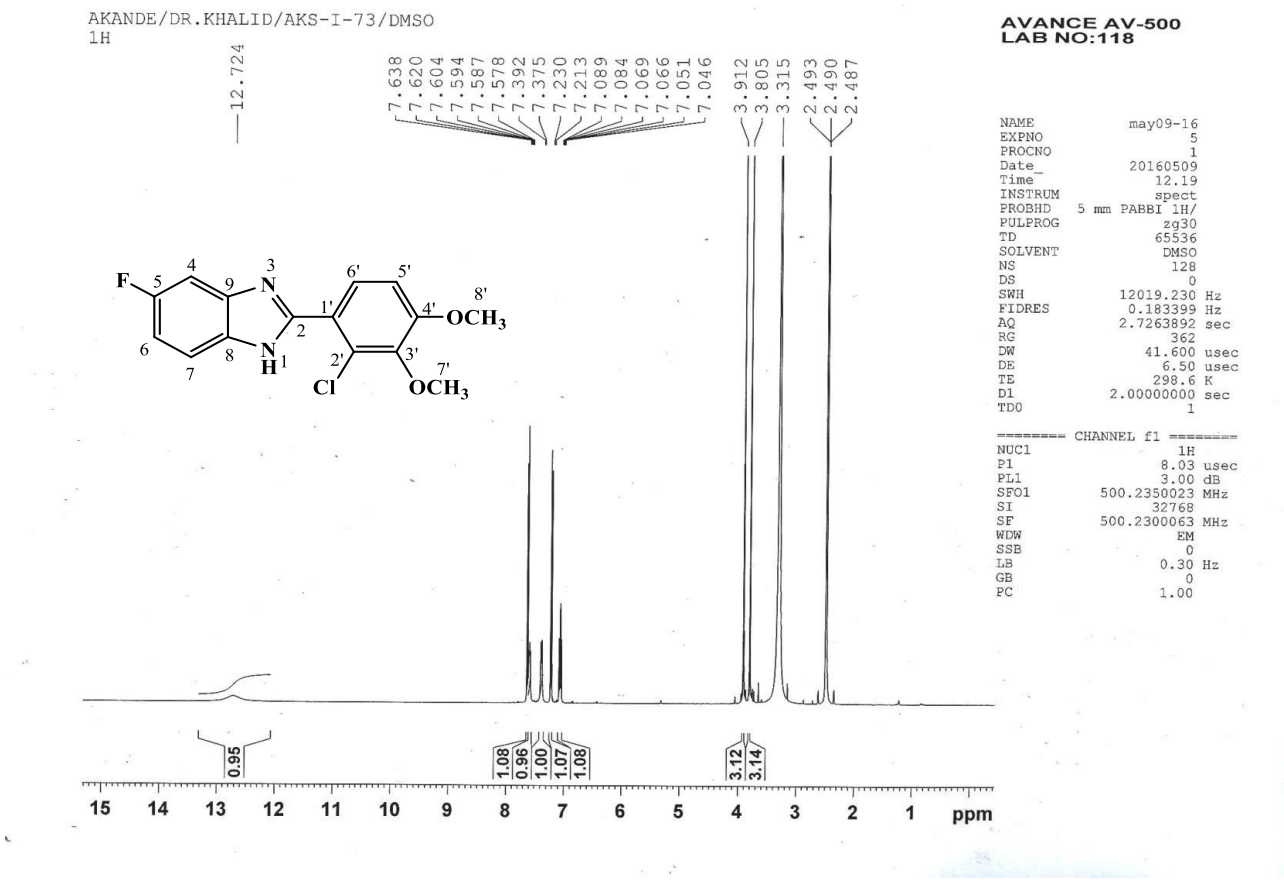

Figure 4.217. ^{1}H NMR (500 MHz, DMSO-d_6) spectrum of AKS-I-73

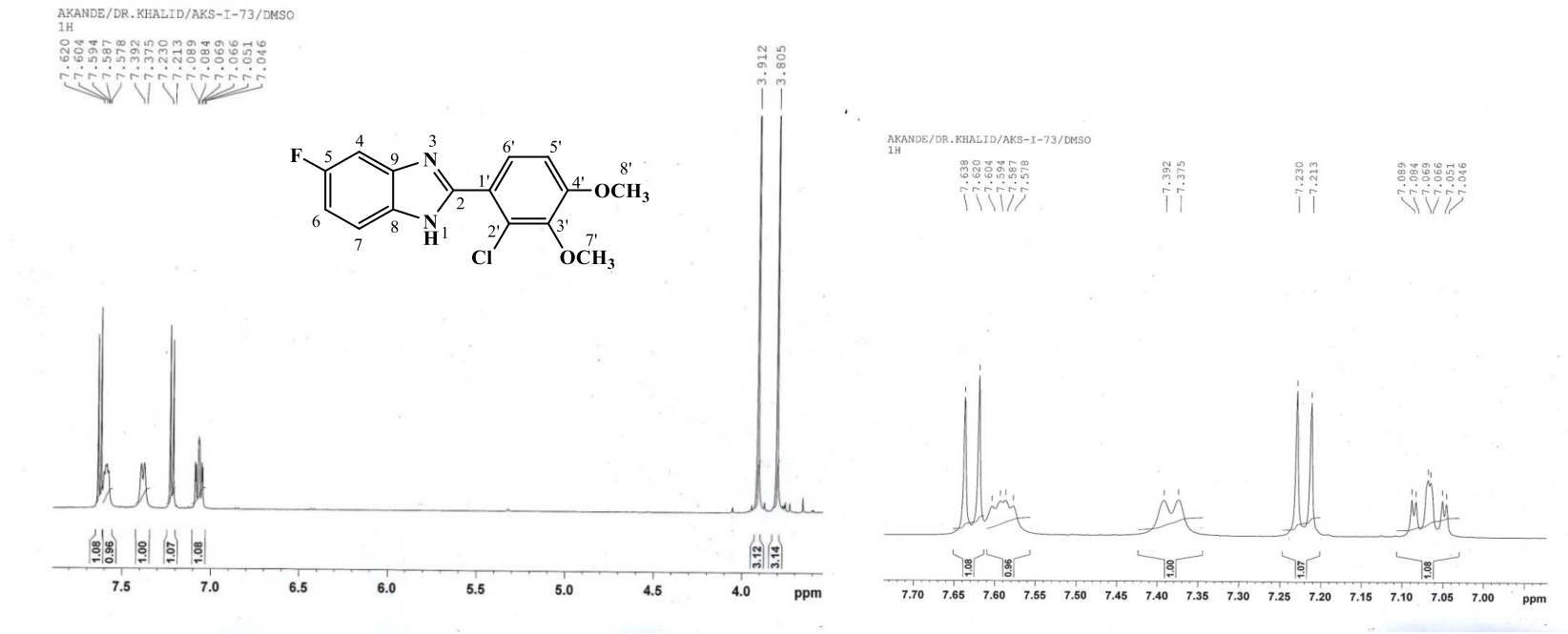

Figure 4.218. ^{1}H NMR (500 MHz, DMSO-d_6) spectra of AKS-I-73 (Expanded)

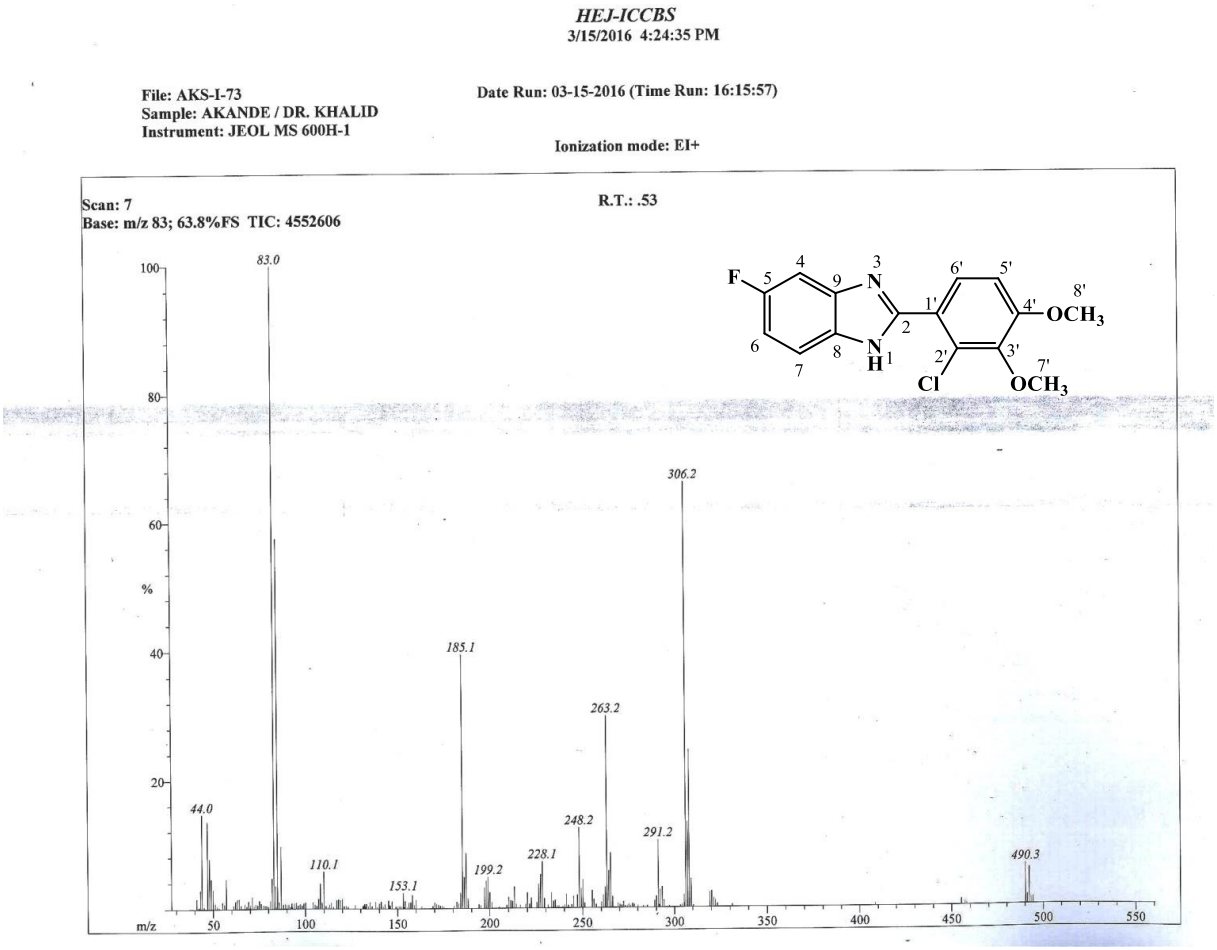

Figure 4.219. EI-MS spectrum of AKS-I-73

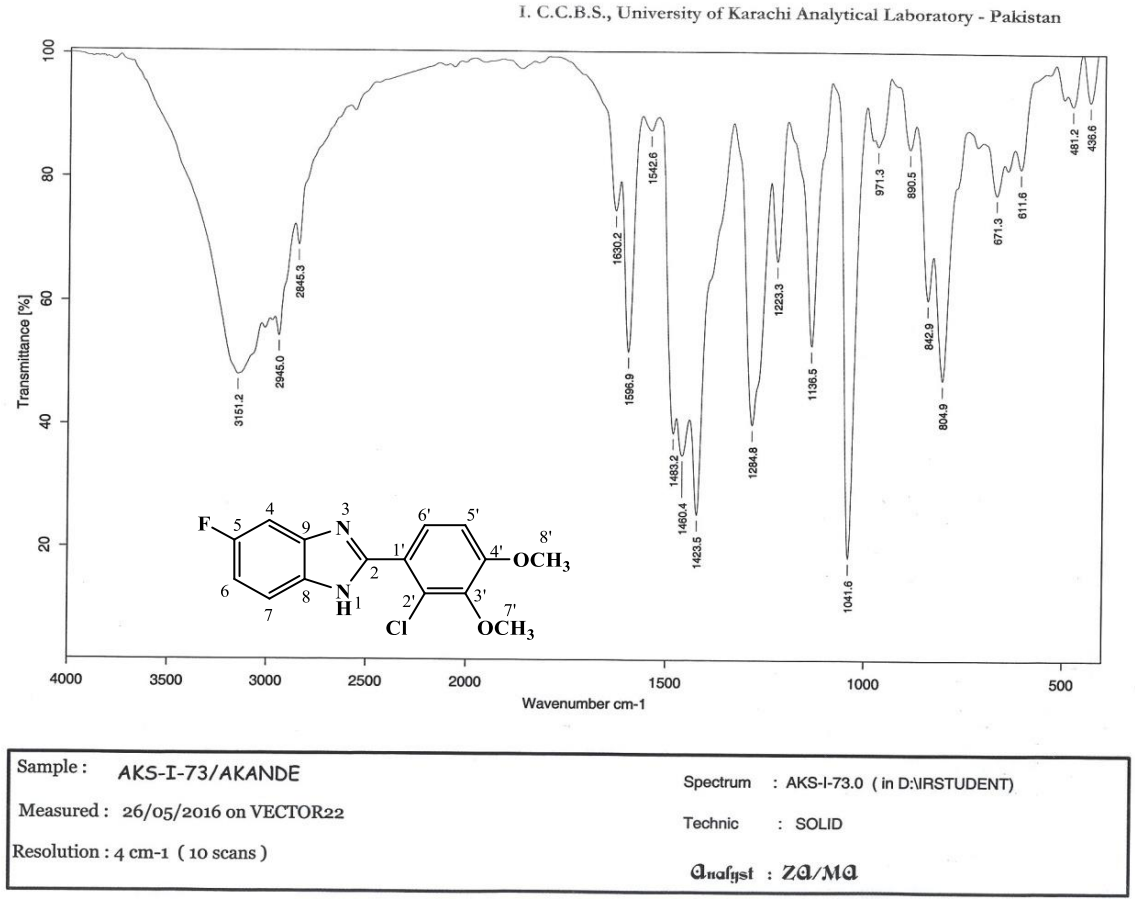

Figure 4.220. IR spectrum of AKS-I-73

THERMO ELECTRON ~ VISIONpro SOFTWARE V4.10

Operator Name	A. ALAM/ M. Asif	Date of Report	5/27/2016
Department	Analytical laboratory#004 TWC	Time of Report	3:02:43PM
Organization	ICCBS.Karachi University.		
Information	Prof.Dr.K. M. Khan/Akande		

Scan Graph

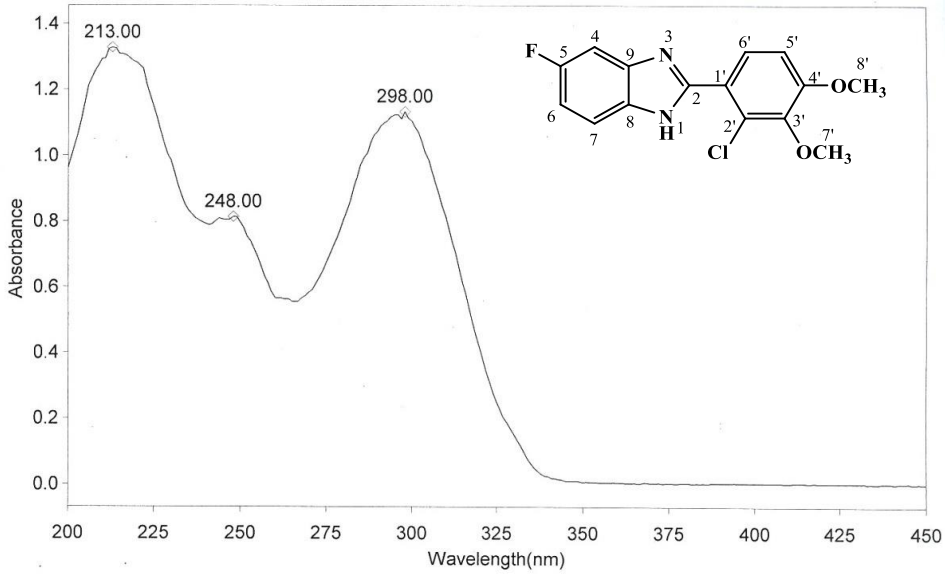

Results Table - AKS-I-73.sre,AKS-I-73,Cycle01

nm	A	**Peak Pick Method**
213.00	1.328	Find 8 Peaks Above -3.0000 A
248.00	0.814	Start Wavelength 200.00 nm
298.00	1.132	Stop Wavelength 450.00 nm
		Sort By Wavelength
Sensitivity	Low	

Page 1, Scan Graph

Figure 4.221. UV spectrum of AKS-I-73

Table 4.37. Summary of the ^{1}H NMR spectra of AKS-I-73

Position	δ ^{1}H [mult., J_{HH} (Hz)] (ppm)
1	12.72 [s]
2	-
3	-
4	7.60-7.57 [m]
5	-
6	7.08 [dt, $J_{6,7}$ = 9.0, $J_{6,4}$ = 2.5]
7	7.39 [d, $J_{7,6}$ = 8.5]
8	-
9	-
1′	-
2′	-
3′	-
4′	-
5′	7.23 [d, $J_{5',6'}$ = 8.5]
6′	7.63 [d, $J_{6',5'}$ = 9.0]
7′-OCH_3	3.91 [s]
8′-OCH_3	3.80 [s]

4.1.38 Characterisation of 2′,4′-dichloro-6′-(5,6-dimethyl-1*H*-benzo[*d*]imidazol-2-yl)phenol (AKS-I-98)

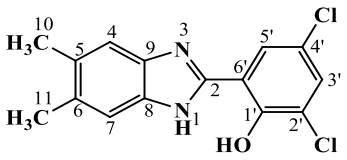

The yellow compound, AKS-I-98 is a solid obtained in a 98.0% (0.301 g) yield, with a m.pt. of 305-308 ^{o}C and a R_f value of 0.69 (hexane/ethyl acetate, 1:1).

Represented in figures **4.222** and **4.223** are the ^{1}H NMR spectra (400 MHz, DMSO-d_6) showing five resonances, δ (ppm) assigned as 13.71 to the amine proton (1H, br s, -NH), 8.11 to the most deshieded methine proton corresponding to (1H, d, $J_{5',3'}$ = 2.0 Hz, H-5′), 7.46 to the methine protons on the benzimidazole ring corresponding to (2H, s, H-4, H-7), and 7.65 (1H, d, $J_{3',5'}$ = 2.4 Hz, H-3′) to the methine proton at position 3′. The singlet at 2.34 which corresponds to (6H, s, 11-, 10-CH_3) was assigned to the six chemically equivalent dimethyl protons. However, the resonance peak expected for the exchangeable hydroxyl proton was not seen.

The fragmentation pattern from EI-MS analysis is characteristic of a molecular ion, M^+ peak and two isotope [M^++2] and [M^++4] peaks, as shown in figure **4.224**. The M^+, [M^++2] and [M^++4] peaks have *m/z* of 306 (isotope peak), 308 and 310 respectively. M^+-CH_3 and M^+-Cl fragmentations correspond to *m/z* of 291 and 271 respectively. Loss of two CH_3 radical together with a Cl radical is suggestive of a *m/z* of 243 $[C_{13}H_6ClN_2O]^+$. Cleavage on the imidazole ring followed by loss of Cl radical from M^+ yielded the ion with *m/z* of 153, and the *m/z* of 91 fragment is typical of tropylium ion $[C_7H_7]^+$. From HREI-MS analysis, the *m/z* found corresponding to the molecular formula, $C_{15}H_{12}N_2OCl_2$ is 306.0334 (calculated, 306.0327), and it further confirms the compound.

The IR spectrum in figure **4.225** shows the absorption bands of IR active bonds. Some vibrational frequencies, $\bar{\upsilon}$ assigned as 3071, 2970, 1618, 1485, 1416 and 1260 cm^{-1} correspond to aromatic C–H_{str}, aliphatic C–H_{str}, two aromatic C=C_{str}, C-H_b of CH_3 and hydroxy C–O_{str} respectively. Figure **4.226** represents the UV spectrum showing maximum absorptions (λ_{max}) at 346, 334, 307 and 230 nm corresponding to n→π* and n→π* transitions. The summary of ^{1}H NMR spectra is represented in table **4.38**.

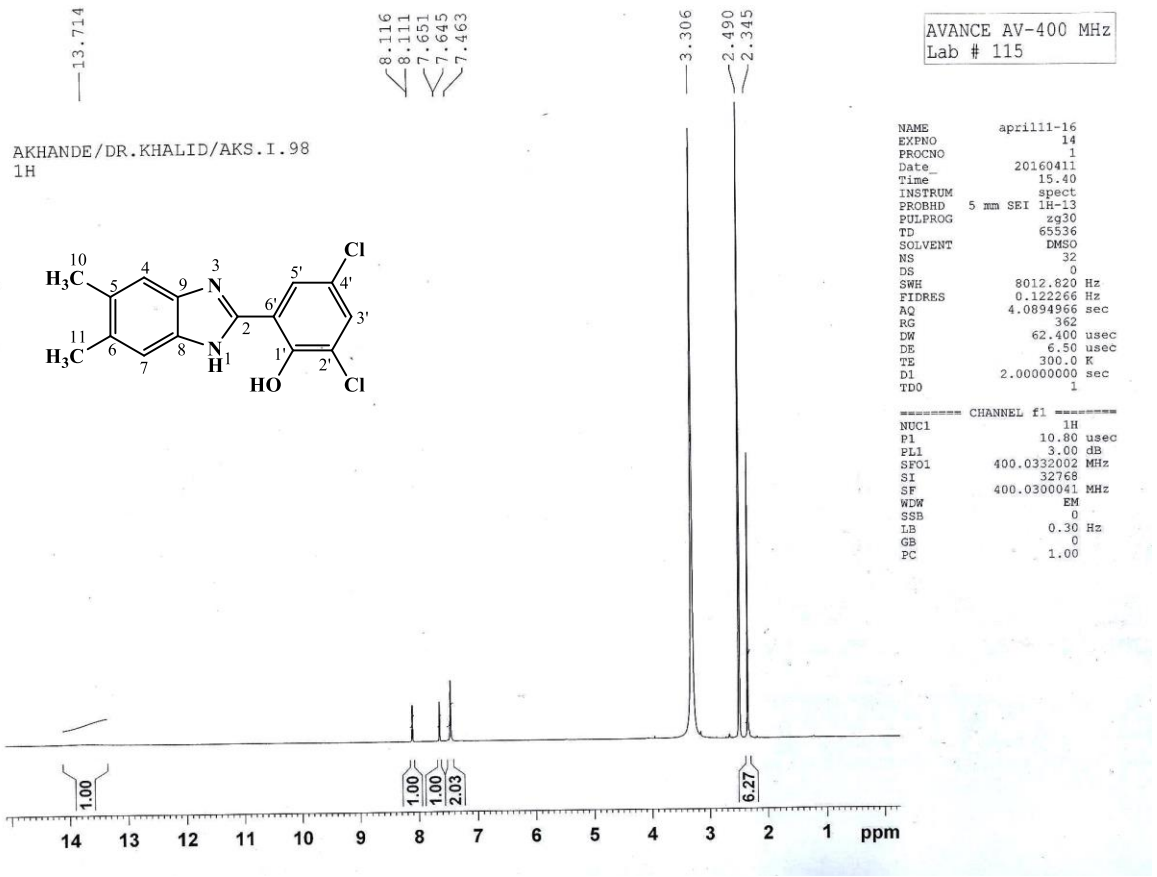

Figure 4.222. ^{1}H NMR (400 MHz, DMSO-d_6) spectrum of AKS-I-98

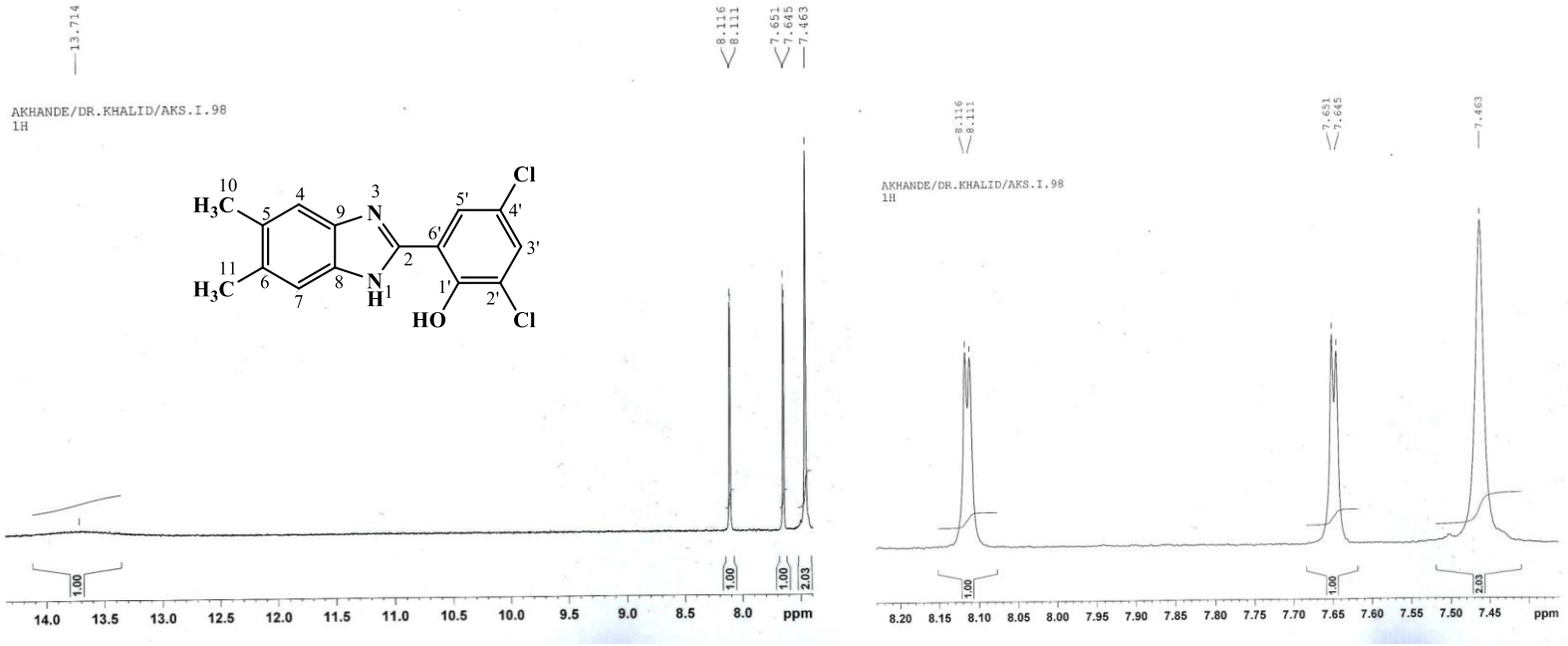

Figure 4.223. ^{1}H NMR (400 MHz, DMSO-d_6) spectra of AKS-I-98 (Expanded)

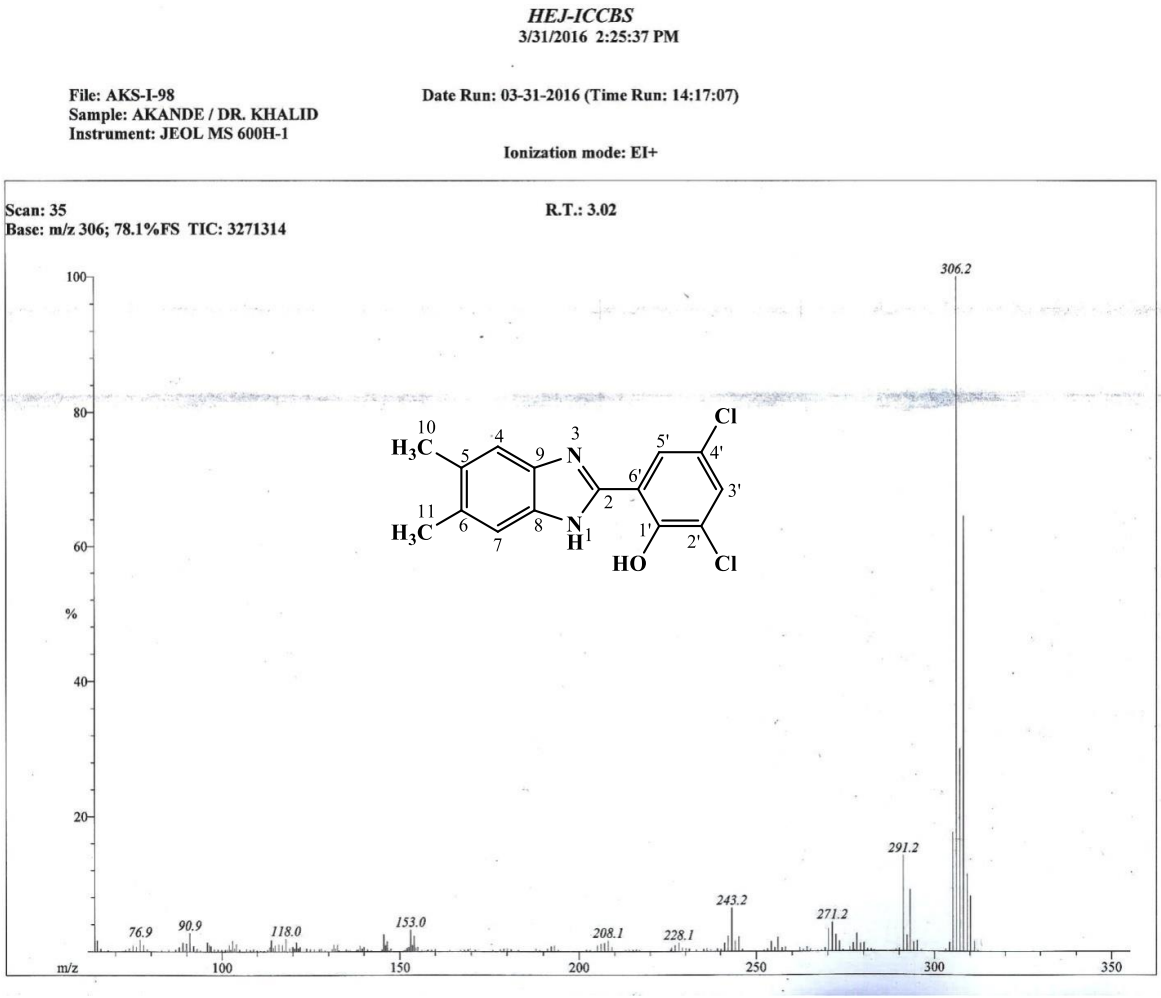

Figure 4.224. EI-MS spectrum of AKS-I-98

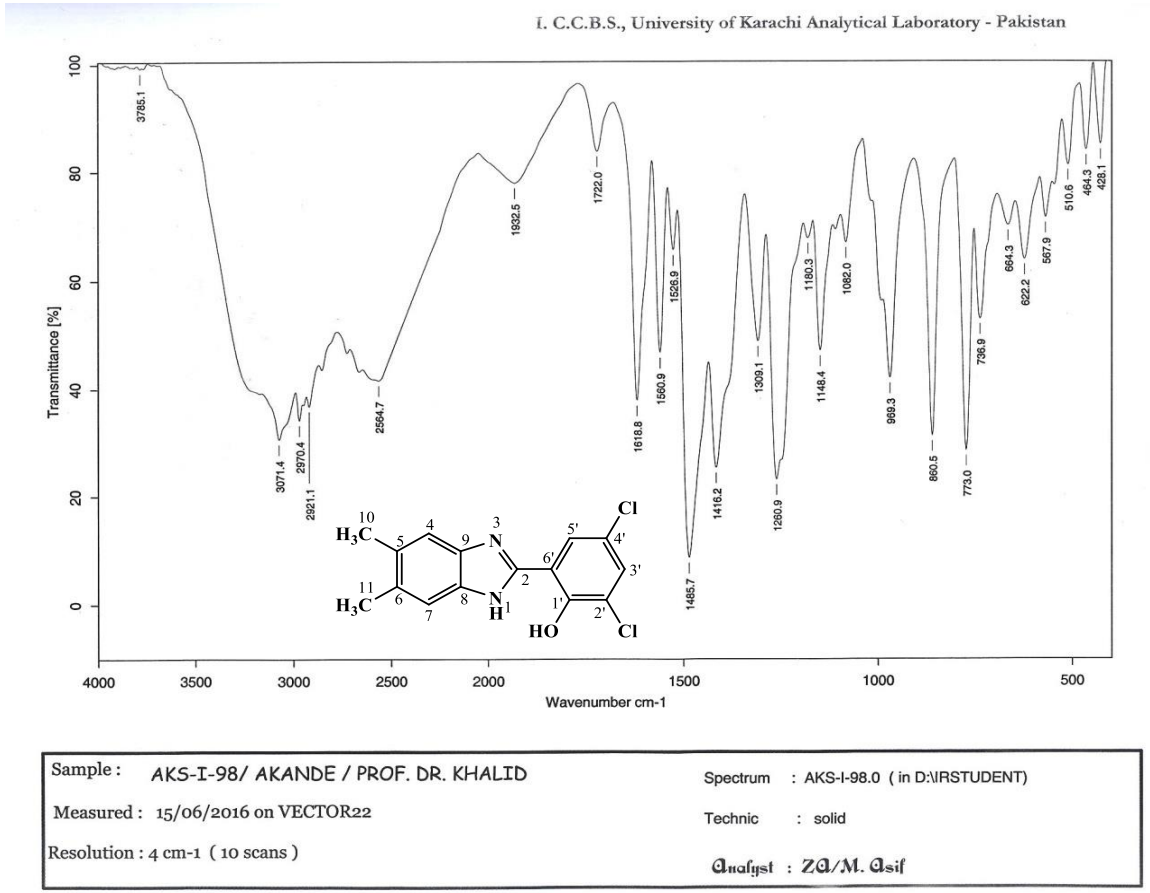

Figure 4.225. IR spectrum of AKS-I-98

THERMO ELECTRON ~ VISIONpro SOFTWARE V4.10

Operator Name	A. ALAM/ M. Asif	Date of Report	6/15/2016
Department	Analytical laboratory#004 TWC	Time of Report	12:56:33PM
Organization	ICCBS.Karachi University.		
Information	Akande/Prof. Dr. Khalid M. Khan		

Scan Graph

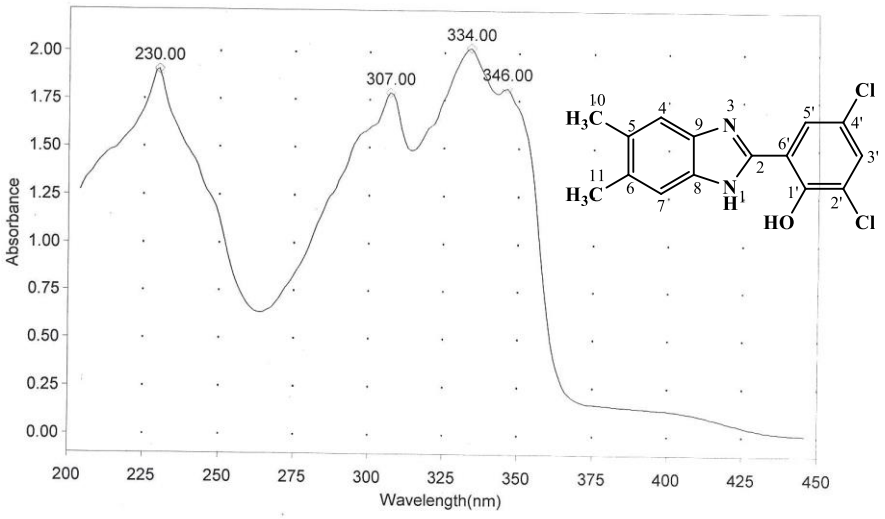

Results Table - AKS-I-98.sre,AKS-I-98,Cycle01

nm	A	**Peak Pick Method**
230.00	1.905	Find 8 Peaks Above -3.0000 A
307.00	1.789	Start Wavelength 200.00 nm
334.00	2.024	Stop Wavelength 450.00 nm
346.00	1.816	Sort By Wavelength
Sensitivity	High	

Page 1, Scan Graph

Figure 4.226. UV spectrum of AKS-I-98

Table 4.38. Summary of the ^{1}H NMR spectra of AKS-I-98

Position	δ ^{1}H [mult., J_{HH} (Hz)] (ppm)
1	13.71 [s]
2	-
3	-
4	7.46 [s]
5	-
6	-
7	7.46 [s]
8	-
9	-
1′-OH	-
1′	-
2′	-
3′	7.65 [d, $J_{3',5'}$ = 2.4]
4′	-
5′	8.11 [d, $J_{5',3'}$ = 2.0]
6′	-
10-CH_3	2.34 [s]
11-CH_3	2.34 [s]

4.1.39 Characterisation of 4′-(5-fluoro-1*H*-benzo[*d*]imidazol-2-yl)benzene-1′,3′-diol (AKS-I-99)

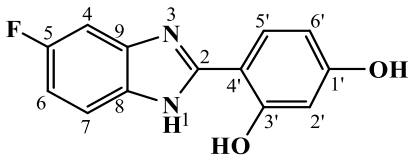

The compound, AKS-I-99 is a brown solid. It was obtained in a yield of 65.6% (0.160 g) with a m.pt. range of 260-263 ^{o}C and a R_f value of 0.70 in a hexane/ethyl acetate (1:1) solvent system.

The ^{1}H NMR spectra (400 MHz, DMSO-d_6) in figures **4.227** and **4.228** show eight resonances assigned as δ (ppm) 13.06 to the highly deshielded amine proton (1H, br s, -NH) and 10.14 to hydroxy proton on carbon-3′ (1H, s, 3′-OH; the other exchageable hydroxyl proton has its resonance peak missing). Also, the peaks at 7.84 (1H, d, $J_{5',6'}$ = 8.4 Hz, H-5′), 7.44 (1H, dd, $J_{7,F\text{-}5}$ = 1.2 Hz, $J_{7,6}$ = 8.8 Hz, H-7), 7.59-7.62 (1H, m, H-4), 7.15 (1H, dt, $J_{6,4}$ = 2.0 Hz, $J_{6,7}$ = 8.8 Hz, H-6), 6.47 (1H, dd, $J_{6',2'}$ = 1.6 Hz, $J_{6',5'}$ = 8.8 Hz, H-6′) and 6.43 (1H, s, H-2′) were deduced for the six methine protons. Further splitting of peaks was observed for protons at positions 7, 6 and 4 due to the presence of fluorine in ortho or meta position these protons.

The EI-MS spectrum (figure **4.229**) shows mass-to-charge ratios, *m/z* peaks for the molecular ion, M^+ and M^++1 at 244 (base peak) and 245. The *m/z* of 215 corresponds to M^+-CHO while a further loss of an ethene molecule yielded the fragment with *m/z* of 187 $[C_{10}H_6FN_2O]^+$. Cleavage on the imidazole ring of M^+ produced the fragment with *m/z* of 108. The peak at *m/z* 174 is suggestive of the fragment ion $[C_9H_6N_2O_2]^+$. Further confirming the compound from HREI-MS analysis, the *m/z* of 244.0651 (calculated, 244.0648) was found corresponding to the formula, $C_{13}H_9N_2O_2F$.

The IR absorption spectrum (figure **4.230)** shows vibrational frequencies, $\bar{\upsilon}$ assignable as 3347, 1617, 1492, 1145 and 1110 cm^{-1} to N–H$_{str}$ of amine, two aromatic C=C$_{str}$, phenolic C–O$_{str}$ and C–F$_{str}$ respectively. The broad-band in the region of 3400-29000 cm^{-1} is due OH-hydrogen bonded stretching vibration. The wavelenghts of maximum absorptions (λ_{max}) from the UV analysis (figure **4.231**) were obtained at 316, 293, 245 and 215 nm indicative of n→π* and n→π* transitions. Table **4.39** represents the summary of ^{1}H NMR spectra.

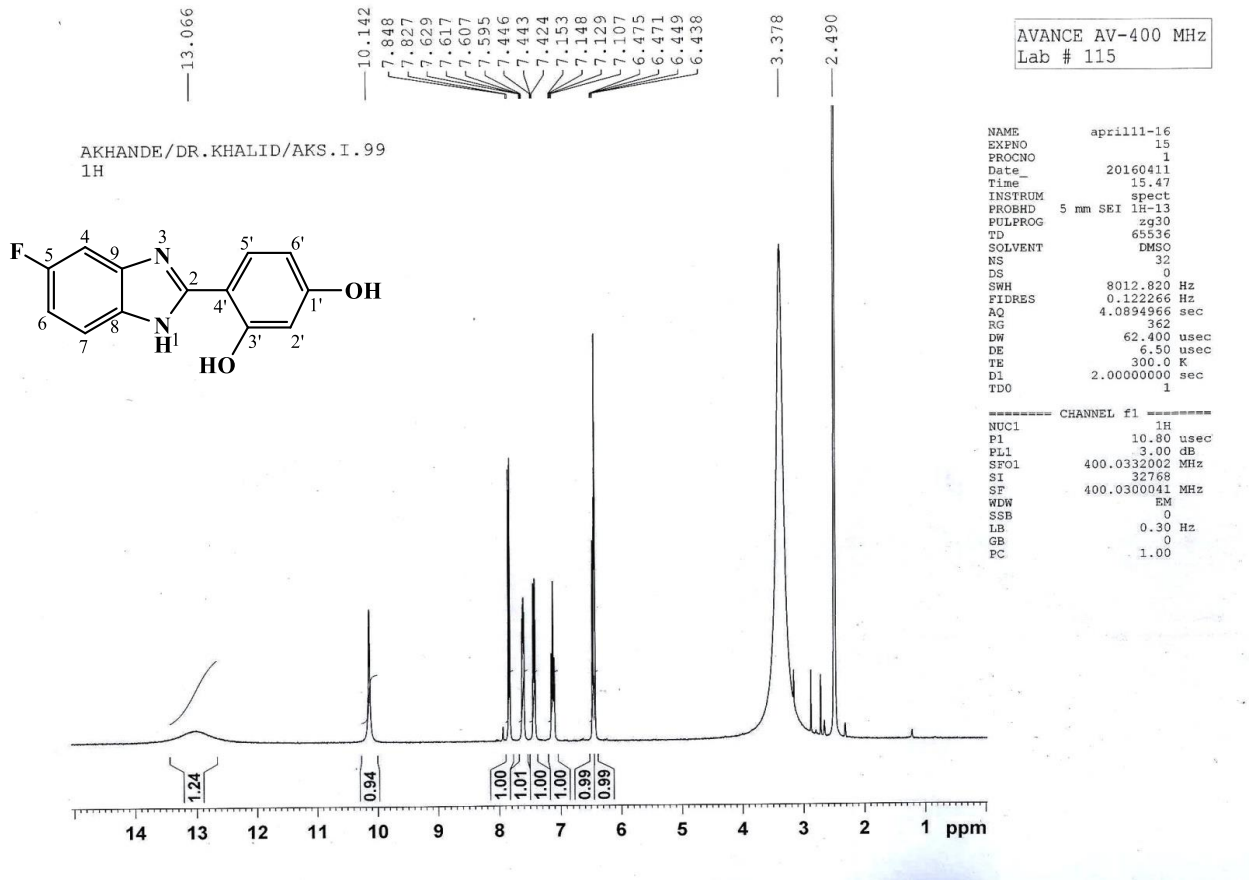

Figure 4.227. ^{1}H NMR (400 MHz, DMSO-d_6) spectrum of AKS-I-99

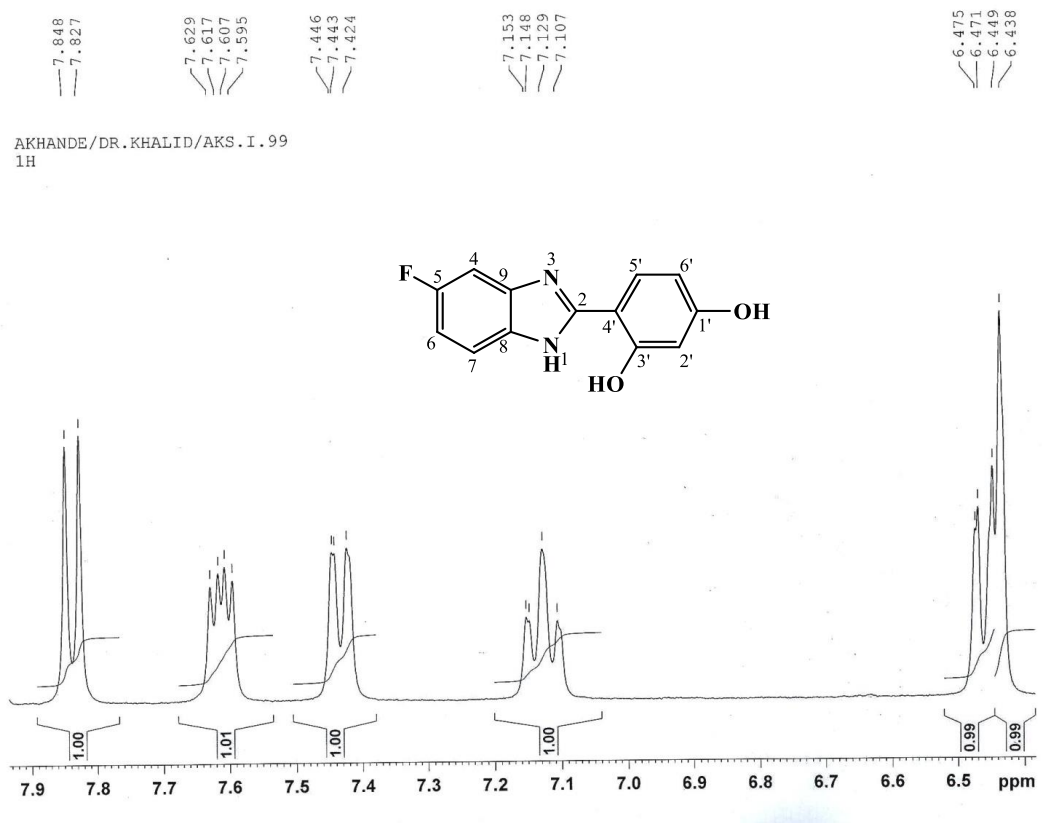

Figure 4.228. ^{1}H NMR (400 MHz, DMSO-d_6) spectrum of AKS-I-99 aromatic region (Expanded)

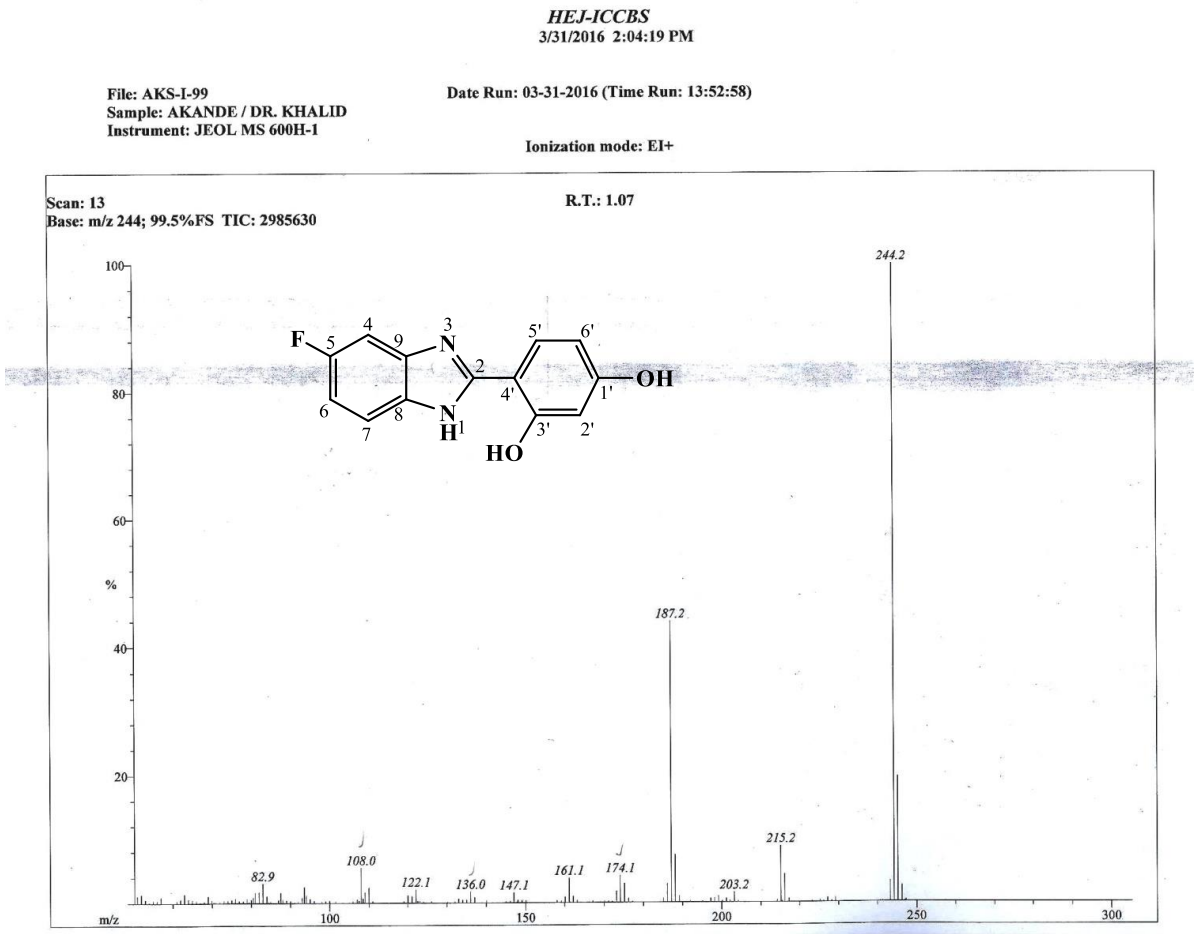

Figure 4.229. EI-MS spectrum of AKS-I-99

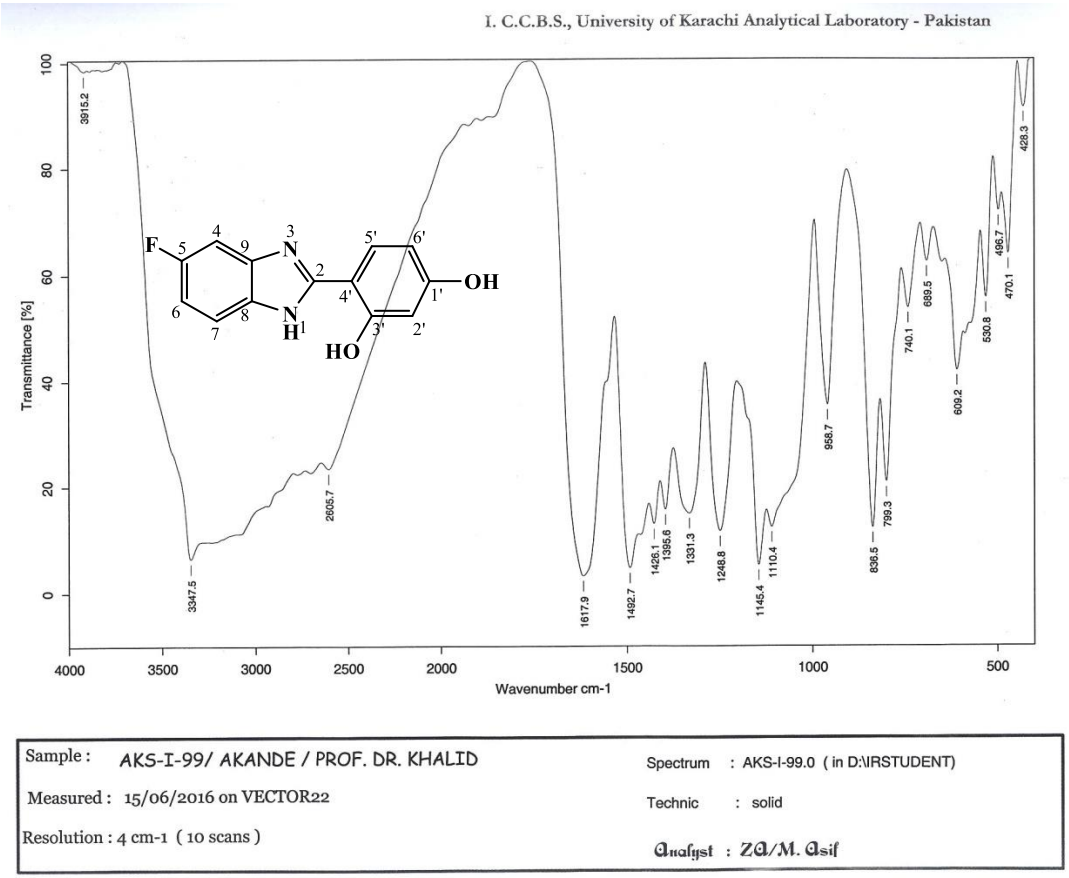

Figure 4.230. IR spectrum of AKS-I-99

THERMO ELECTRON ~ VISIONpro SOFTWARE V4.10

Operator Name	A. ALAM/ M. Asif	Date of Report	6/15/2016
Department	Analytical laboratory#004 TWC	Time of Report	1:04:08PM
Organization	ICCBS.Karachi University.		
Information	Akande/Prof. Dr. Khalid M. Khan		

Scan Graph

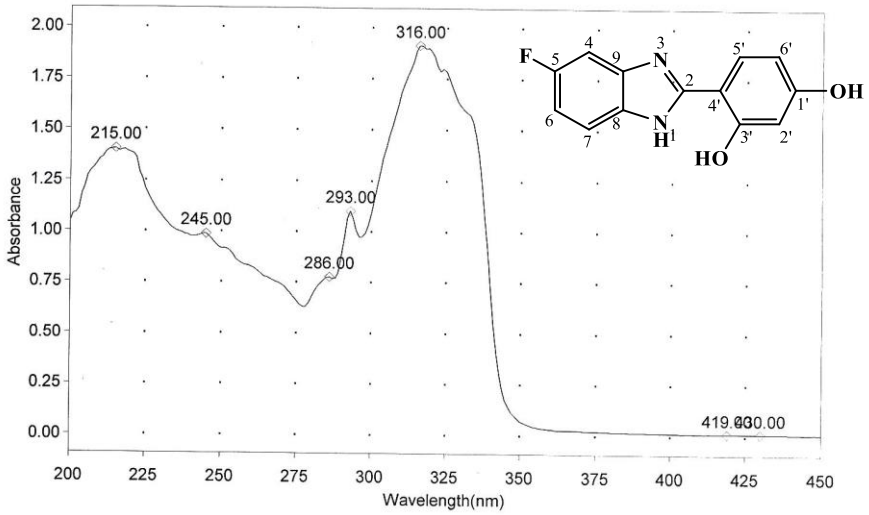

Results Table - AKS-I-99.sre,AKS-I-99,Cycle01

nm	A
215.00	1.404
245.00	0.987
286.00	0.776
293.00	1.100
316.00	1.913
419.00	0.013
430.00	0.012

Peak Pick Method
Find 8 Peaks Above -3.0000 A
Start Wavelength 200.00 nm
Stop Wavelength 450.00 nm
Sort By Wavelength
Sensitivity High

Page 1, Scan Graph

Figure 4.231. UV spectrum of AKS-I-99

Table 4.39. Summary of the ^{1}H NMR spectra of AKS-I-99

Position	δ ^{1}H [mult., J_{HH} (Hz)] (ppm)
1	13.06 [br s]
2	-
3	-
4	7.62-7.59 [m]
5	-
6	7.15 [dt, $J_{6,7}$ = 8.8, $J_{6,4}$ = 2.0]
7	7.44 [dd, $J_{7,6}$ = 8.8, $J_{7,F\text{-}5}$ = 1.2]
8	-
9	-
1′-OH	Exchangable
3′-OH	10.14 [s]
1′	-
2′	6.43 [s]
3′	-
4′	-
5′	7.84 [d, $J_{5',6'}$ = 8.4]
6′	6.47 [dd, $J_{6',5'}$ = 8.8, $J_{6',2'}$ = 1.6]

4.1.40 Characterisation of 2′-(5,6-dimethyl-1*H*-benzo[*d*]imidazol-2-yl)benzene-1′,4′-diol (AKS-I-100)

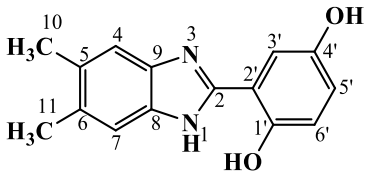

The compound, AKS-I-100 is a brown soid obtained with a yield of 84.2% (0.214 g). It has a m.pt. range of 315-317 ^{o}C and a R_f value of 0.67 (hexane/ethyl acetate, 1:1).

Figures **4.232** and **4.233** show signals obtained from ^{1}H NMR analysis (400 MHz, DMSO-d_6) and six resonance peaks, δ (ppm) were obtained. The peak at ≈12.80 was assigned to the amine proton (1H, br s, -NH) while the hydroxyl proton on carbon 1′ resonated at 9.11 (1H, s, 1′-OH; the other hydroxy proton has its resonance peak missing due to an exchange effect). The resonances at 7.42, 7.38 and 6.85 were assigned to the methine protons corresponding to (2H, s H-4, H-7), (1H, s, H-3′), (2H, s, H-5′, H-6′) respectively. The peak at 2.33 represents the six chemically equivalent dimethyl protons which corresponds to (6H, s, 5-CH_3, 6-CH_3).

Electron impact-mass spectrometry (EI-MS) analysis resulted in a spectrum (figure **4.234**) with many fragmentation patterns. The *m/z* at 254 (base peak) and 255 both represent peaks for the molecular ion, M^+ and a [M^++1] radical cations respectively. The fragmentation, M^+-CH_3 refers to a *m/z* of 239, and further loss of CH_2=C=O is indicative of a *m/z* 197. The *m/z* of 225 is suggests a loss of CHO radical from the molecular ion. Typical of a tropylium ion is the peak at *m/z* of 91. Further confirming the compound from HREI-MS analysis, the *m/z* of 254.1065 (calculated, 254.1055) was found corresponding to the molecular formular, $C_{15}H_{14}N_2O_2$.

The IR spectrum (figure **4.235**) indicated vibrational absorption frequencies, $\bar{\upsilon}$ at 3481, 3260, 2920, 2856, 1626, 1561, 1503 and 1098 cm^{-1} corresponding to N–H_{str}, OH_{str}, aliphatic C–$H_{asy\ str}$ and C–$H_{sym\ str}$, C–N_{str}, two aromatic C=C_{str} and phenolic C–O_{str} respectively. The UV spectrum in figure **4.236** shows absorption wavelenght maxima (λ_{max}) at 339, 307, 298, 228 and 222 nm corresponding to n→π* and n→π* transitions. Table **4.40** is the summary of ^{1}H NMR spectra of the compound.

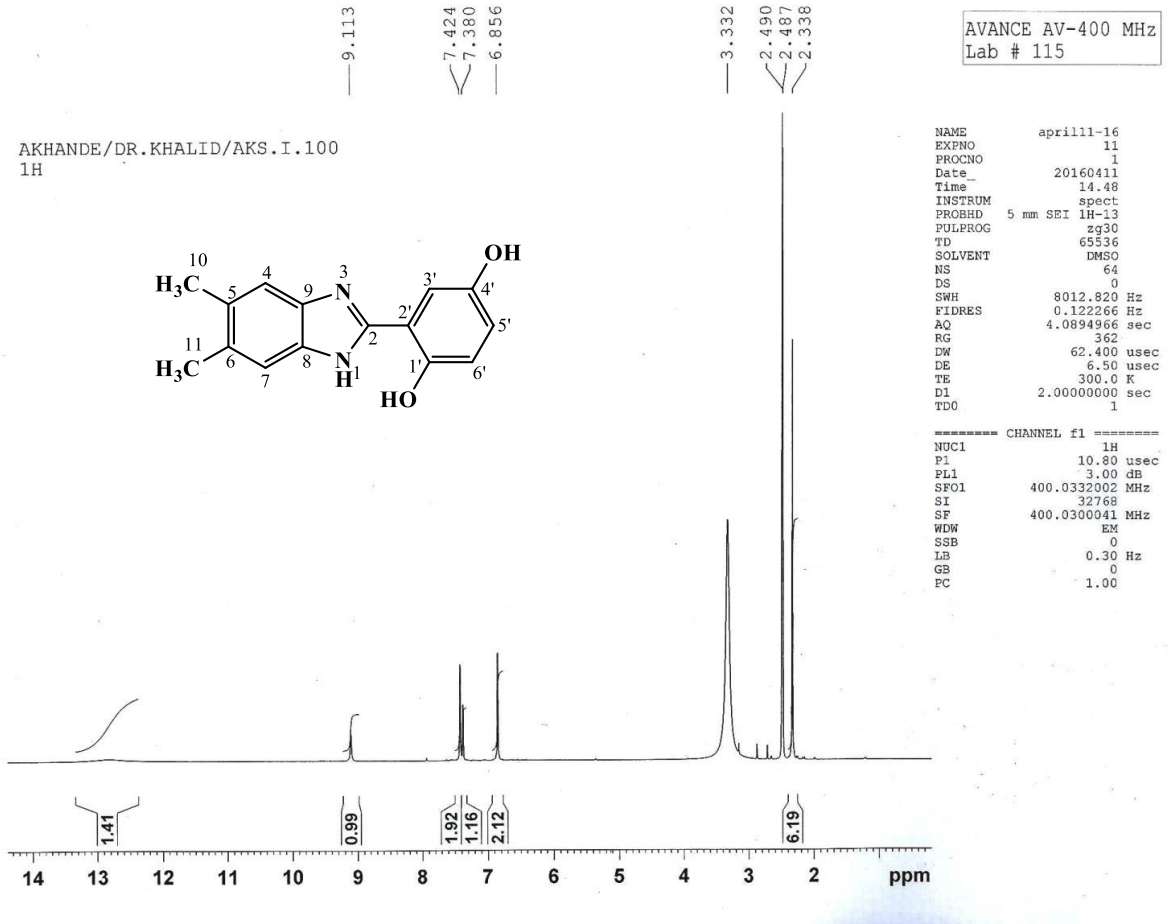

Figure 4.232. ^{1}H NMR (400 MHz, DMSO-d_6) spectrum of AKS-I-100

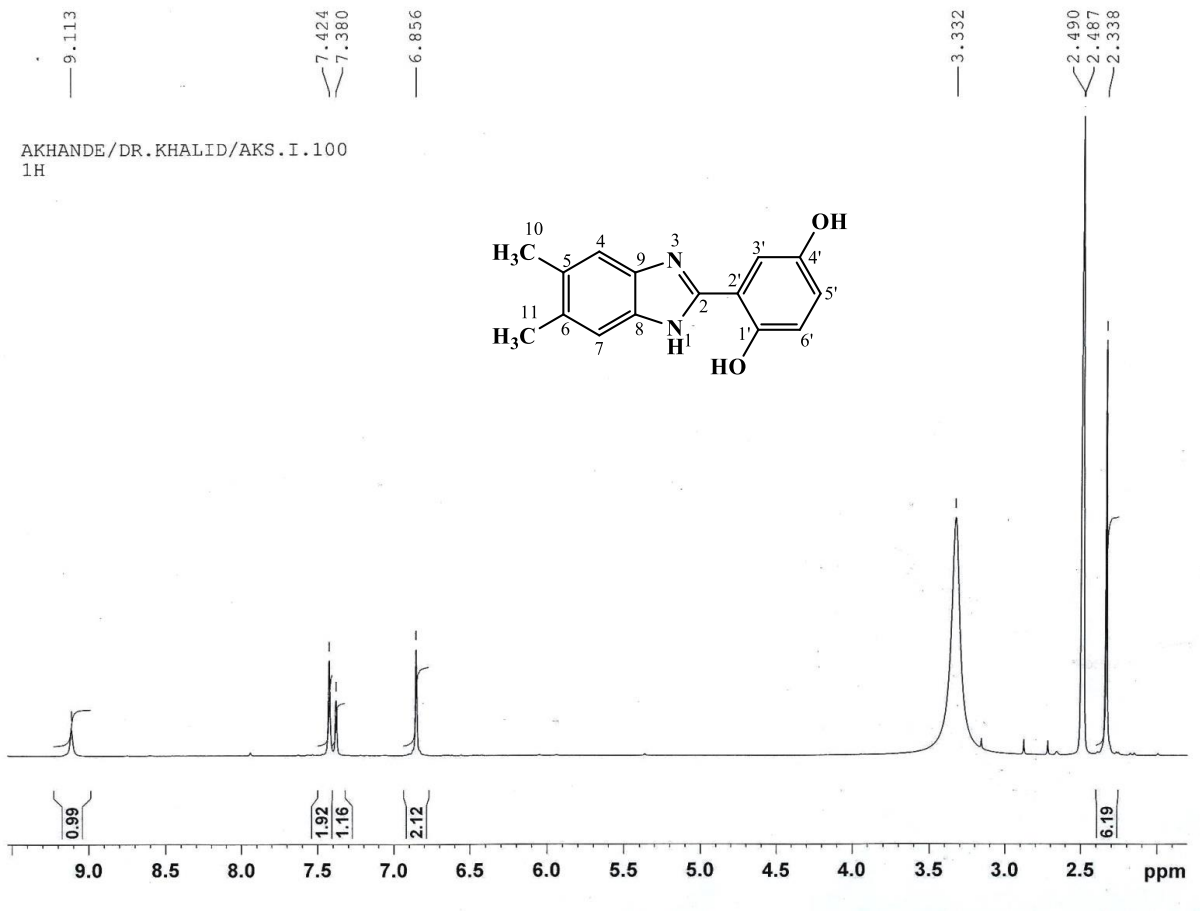

Figure 4.233. ^{1}H NMR (400 MHz, DMSO-d_6) spectrum of AKS-I-100 (Expanded)

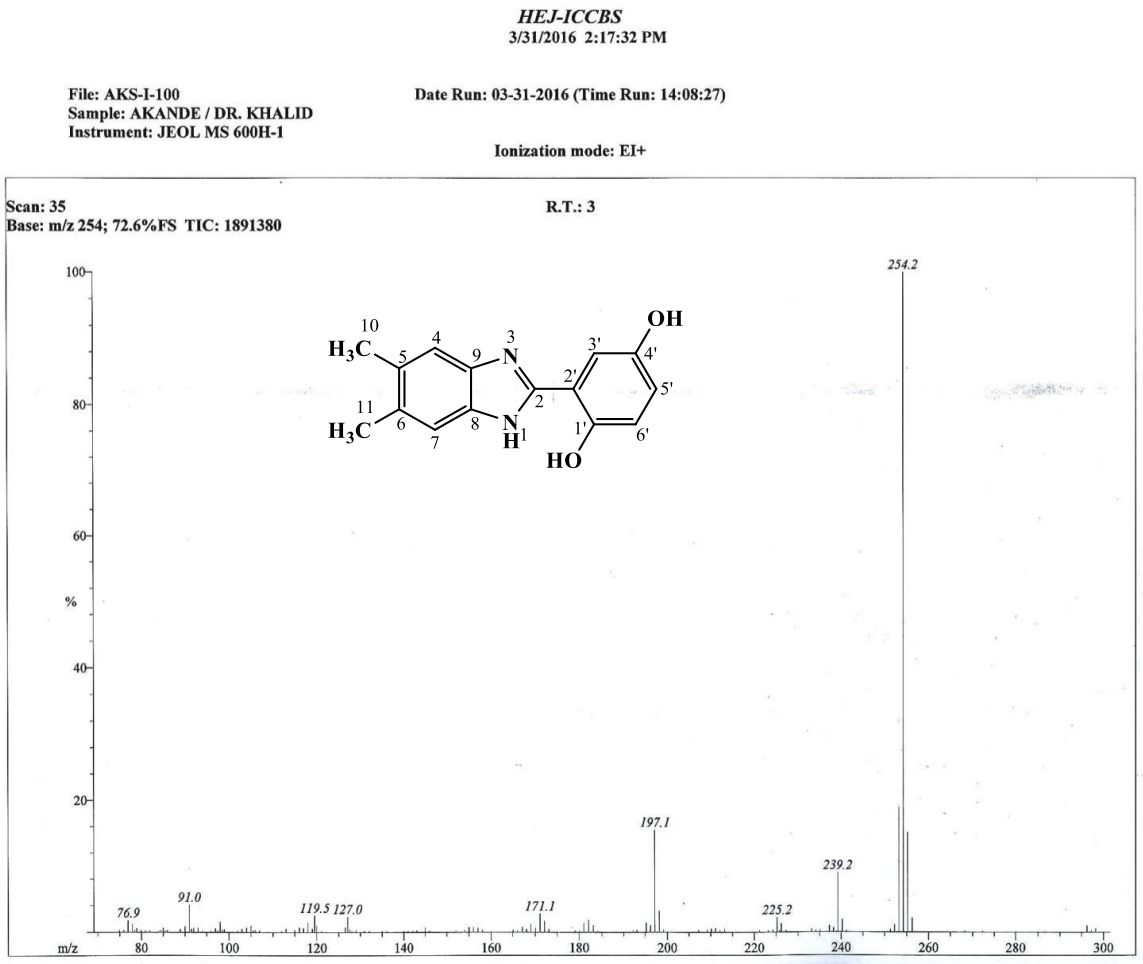

Figure 4.234. EI-MS spectrum of AKS-I-100

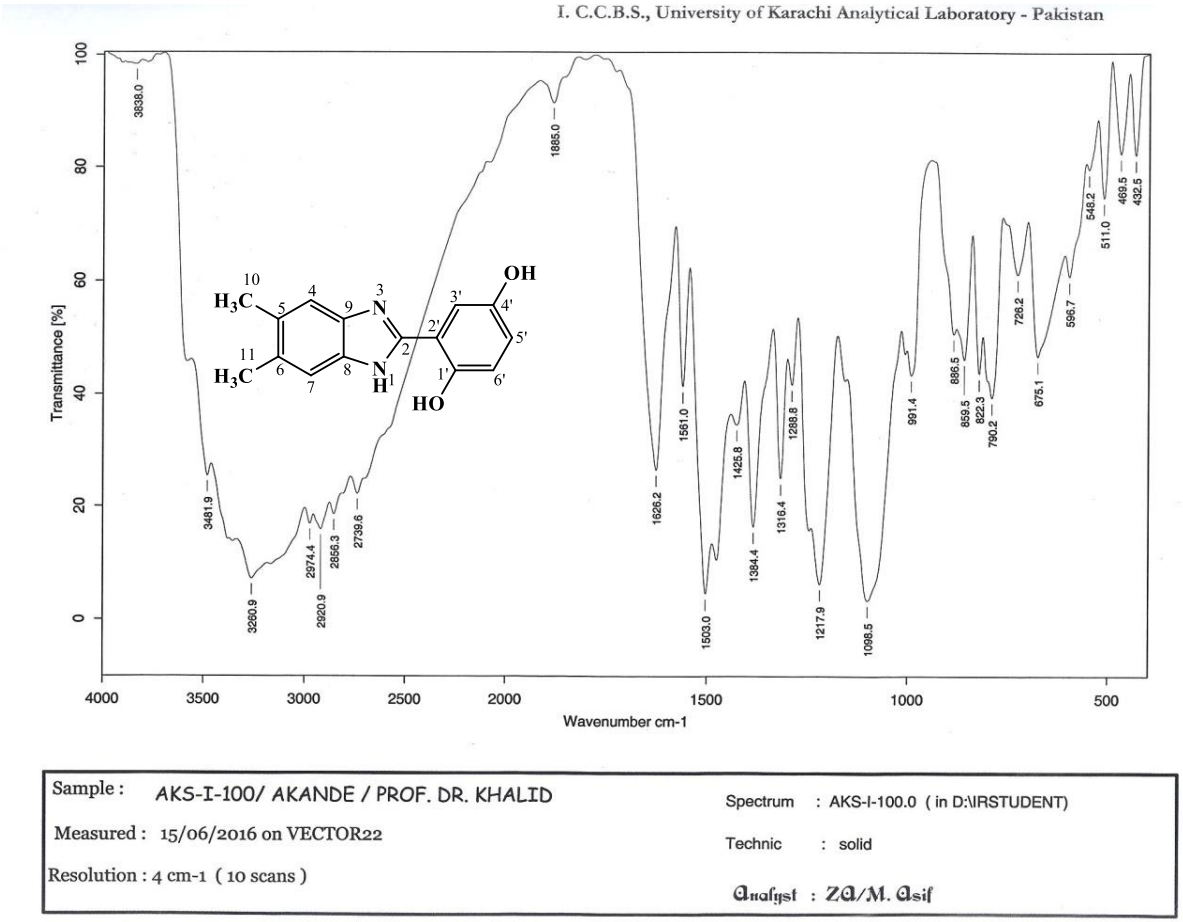

Figure 4.235. IR spectrum of AKS-I-100

THERMO ELECTRON ~ VISIONpro SOFTWARE V4.10

Operator Name	A. ALAM/ M. Asif	Date of Report	6/15/2016
Department	Analytical laboratory#004 TWC	Time of Report	1:07:53PM
Organization	ICCBS.Karachi University.		
Information	Akande/Prof. Dr. Khalid M. Khan		

Scan Graph

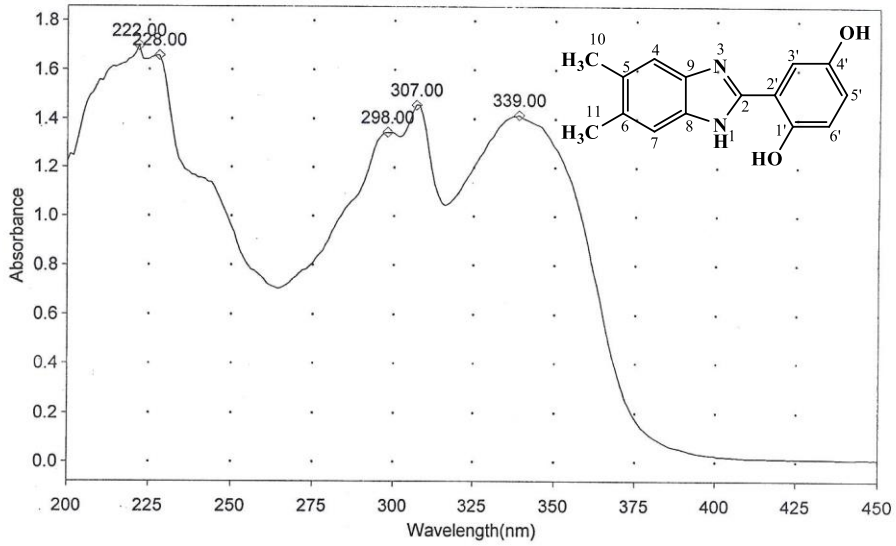

Results Table - AKS-I-100.sre,AKS-I-100,Cycle01

nm	A	**Peak Pick Method**
222.00	1.697	Find 8 Peaks Above -3.0000 A
228.00	1.658	Start Wavelength 200.00 nm
298.00	1.346	Stop Wavelength 450.00 nm
307.00	1.458	Sort By Wavelength
339.00	1.417	Sensitivity Medium

Page 1, Scan Graph

Figure 4.236. UV spectrum of AKS-I-100

Table 4.40. Summary of the ^{1}H NMR spectra of AKS-I-100

Position	δ ^{1}H [mult., J_{HH} (Hz)] (ppm)
1	12.80 [br s]
2	-
3	-
4	7.42 [s]
5	-
6	-
7	7.42 [s]
8	-
9	-
1′-OH	9.11 [s]
1′	-
2′	-
3′	7.38 [s]
4′-OH	Exchangeable
4′	-
5′	6.85 [s]
6′	6.85 [s]
10-CH_3	2.33 [s]
11-CH_3	2.33 [s]

4.2 Anthelmintic activity

The *in-vitro* egg hatch inhibitory assay was employed, using gastro-intestinal nematode eggs of cattle, to determine the anthelmintic efficacy of five representative, synthesised benzimidazoles namely 2-(3′-(benzyloxy)-4′-methoxyphenyl)-5-fluoro-1*H*-benzo[*d*] imidazole (AKS-I-35), 2-(3′-(benzyloxy)-4′-methoxyphenyl)-5-nitro-1*H*-benzo[*d*] imidazole (AKS-I-37), 3′-bromo-2′-(5-chloro-1*H*-benzo[*d*]imidazol-2-yl)-6′-methoxy phenol (AKS-I-52), 4′-(5-fluoro-1*H*-benzo[*d*]imidazol-2-yl)benzene-1′,2′,3′-triol (AKS-I-57) and 2-(2′-bromo-4′,5′-dimethoxyphenyl)-1*H*-benzo[*d*]imidazole (AKS-I-63). These compounds were utilised based on the type of substituents attached to the benzimidazole pharmacophore at 2- and 5-positions.

Table **4.41** shows the mean percentage egg hatch inhibition (%EHI) and IC_{50} values obtained for these compounds. The mean percent egg hatch inhibition increased with increasing concentrations. All the compounds subjected to egg hatch inhibition test showed potent inhibitory effect, except AKS-I-52 and AKS-I-35 which exhibited low and no inhibitions, respectively. The highest mean percent egg hatch inhibition was observed for AKS-I-63 at 100 μg/μL (80.47±5.42) while at 50, 25 and 12.5 μg/μL, the percent inhibitions were at 75.36±5.92, 62.50±7.22 and 40.99±2.84, respectively. A high percent inhibition was also recorded at 100 μg/μL for AKS-I-37, however, inhibition dropped drastically at lower concentrations. The mechanism involved in inhibiting eggs from hatching and larvae from developing in the developmental phases of many parasites could be linked to the disruption of cell division, while the formation and development of important structures will be hindered as well (Ferreira *et al.*, 2013). Thus, from this study at higher doses of 100 and 50 μg/mL, most of the tested compounds presented high to moderate level of egg hatch inhibition (i.e. most eggs did not hatch), and at these concentrations as observed for AKS-I-57 and Albendazole (the standard drug used), eggs either contain inactive/dead larvae within the shells or seen to have completely disintegrated (egg cell division altered and none of the eggs hatched) when viewed under an inverted light microscope.

Table 4.41. Mean percent inhibition and IC_{50} values

Sample Code	Concentration	Mean %EHI±SEM	IC_{50} (μg/mL)	UCL	LCL
AKS-I-35	100 μg/μL	No Inhibition	--	--	--
	50 μg/μL	No Inhibition			
	25 μg/μL	No Inhibition			
	12.5 μg/μL	No Inhibition			
AKS-I-37	100 μg/μL	74.23±7.26	70.25	81.76	61.28
	50 μg/μL	14.97±3.99			
	25 μg/μL	3.50±0.00			
	12.5 μg/μL	1.85±0.00			
AKS-I-52	100 μg/μL	14.56±1.51	1594.63	251890.00	398.73
	50 μg/μL	13.20±1.08			
	25 μg/μL	6.84±1.52			
	12.5 μg/μL	4.86±1.50			
AKS-I-57	100 μg/μL	Disintegration of egg cells	34.11	44.63	18.71
	50 μg/μL	Disintegration of egg cells			
	25 μg/μL	46.19±4.37			
	12.5 μg/μL	37.00±3.12			
AKS-I-63	100 μg/μL	80.47±5.42	17.49	24.01	11.51
	50 μg/μL	75.36±5.92			
	25 μg/μL	62.50±7.22			
	12.5 μg/μL	40.99±2.84			
Albendazole (positive control)	100 μg/μL	Disintegration of egg cells	11.38	13.84	6.72
	50 μg/μL	Disintegration of egg cells			
	25 μg/μL	87.27±6.39			
	12.5 μg/μL	62.74±13.20			

Key: EHI = egg hatch inhibition SEM = Standard error of mean
UCL = Upper confidence limit LCL = Lower confidence limit
IC_{50} = concentration required to inhibit 50% of eggs from hatching

According to the guidelines adopted by the World Association for the Advancement of Veterinary Parasitology (WAAVP) for evaluating anthelmintic drug efficacy *in vitro*, an egg hatching inhibition >90% is considered effective while between 80–90% is termed to be moderately effective (Ferreira *et al.*, 2013). Thus, from the results obtained, two of the five tested compounds can be classified as effective and moderately effective compounds.

Moreover, the compound AKS-I-63 presented a 50% hatching inhibition of eggs (IC_{50}) at 17.49 μg/μL, a close value when compared with the standard drug, Albendazole (IC_{50} = 11.38 μg/μL). This is the lowest IC_{50} value among the tested compounds, thus indicating that AKS-I-63 exhibits the highest inhibitory effect on nematode eggs. The IC_{50} for AKS-I-37, AKS-I-52 and AKS-I-57 however, are 70.25, 1594.63 and 34.11 μg/μL respectively. According to Le Jambre (1995), an IC_{50} of more than 0.12 μg/mL (120 μg/μL) was reported for resistant nematode strains. Thus, from the IC_{50} values obtained in this study, it can further be inferred that AKS-I-63, AKS-I-57 and AKS-I-37 exhibited high inhibitory activities and potent efficacy. Also, high susceptibility of nematode eggs to these three compounds has been established, by relating their IC_{50} values to what was reported according to the WAAVP's guideline of susceptibility range whereby IC_{50}<0.100 μg/mL (100 μg/μL) means high inhibitory potentials (Belew *et al.*, 2012).

The change in the effect of a stressor (usually a chemical/compound) on an organism caused by varying the levels of exposure (i.e. dose or concentration level), after a certain exposure time and route, can be described as a dose-response relationship (Crump *et al.*, 1976). This relationship, often expressed by a sigmoidal dose-response curve on a simple X-Y graph, describes the connection between the response to drug treatment (stressor) and drug dose (expressed as logarithm of concentration). The dose-response curves are usually interpreted by parameters such as the baseline response that is commonly referred to as the threshold dose (bottom), the maximum response (top), the slope, and the drug concentration that provokes a response halfway between baseline and maximum (IC_{50} or EC_{50}) (Motulsky and Christopoulos, 2002).

The shape of slope from the dose-response curve obtained from this study (figure **4.237**) describes the change in the percent inhibition as concentration increases. The dose-response curve for AKS-I-37 suggests that the initial wide increase in concentration at

the threshold point (bottom) implies a relatively minimal inhibition/response effect, until a point when the slope began to steepen indicating a significant impact on egg inhibition even with small increase in dose/concentration. However, the dose-response curve for AKS-I-52 and AKS-I-63 exhibited a gradual response relationship with an increase in concentration.

Many synthesised benzimidazole analogs from literature have been reported to demonstrate anthelminthic activities (Rajamanickam *et al.*, 2015; Alam *et al.*, 2014; Babu and Selvakumar, 2013; Sawant and Kawade, 2011; Lingala *et al.*, 2011). Ouattara *et al.*, 2011 synthesised a series of benzimidazolyl-chalcone derivatives from 2-acetylbenzimidazole. The preliminary structure-activity relationship studies carried out established an increased nematicidal activity against *Haemonchus contortus*, several times more than the standard chalcone (1,3-diphenylprop-2-en-1-one) utilised when the phenyl group of the standard chalcone was replaced by 2-benzimidazolyl group as well as an activity of about five times higher than ivermectin. They further concluded that the 2-(arylpropenone) benzimidazoles synthesised could be a new pharmacophore for nematicidal activity against eggs and larvae of *H. contortus*.

Munguia *et al.*, 2013 evaluated the *in vitro* and *in vivo* anthelmintic potentials, as well as an *ex vivo* intraparasitary diffusion studies of Valerolactam-benzimidazole hybrids against the rat parasitic nematode, *Nippostrongylus brasiliensis*. From the *in vitro* studies, three of the synthesisd benzimidazole hybrids demonstrated better activity than the reference drugs Albendazole, Febendazole, and Levamizole. However, among the treated groups of rats, the *in vivo* studies exhibited very low efficacy at the assayed doses, coupled with a non dose-dependent effect on efficacy. Also, some benzimidazoles with 1,2,4-triazole moity at 2-position were evaluated for their *in vitro* anthelmintic activity against the earth worm, *Pheretima posthumous*, from which most of the synthesised compounds indicated potent activity compared to Albendazole and Piperazine (Kumar and Sahoo, 2014).

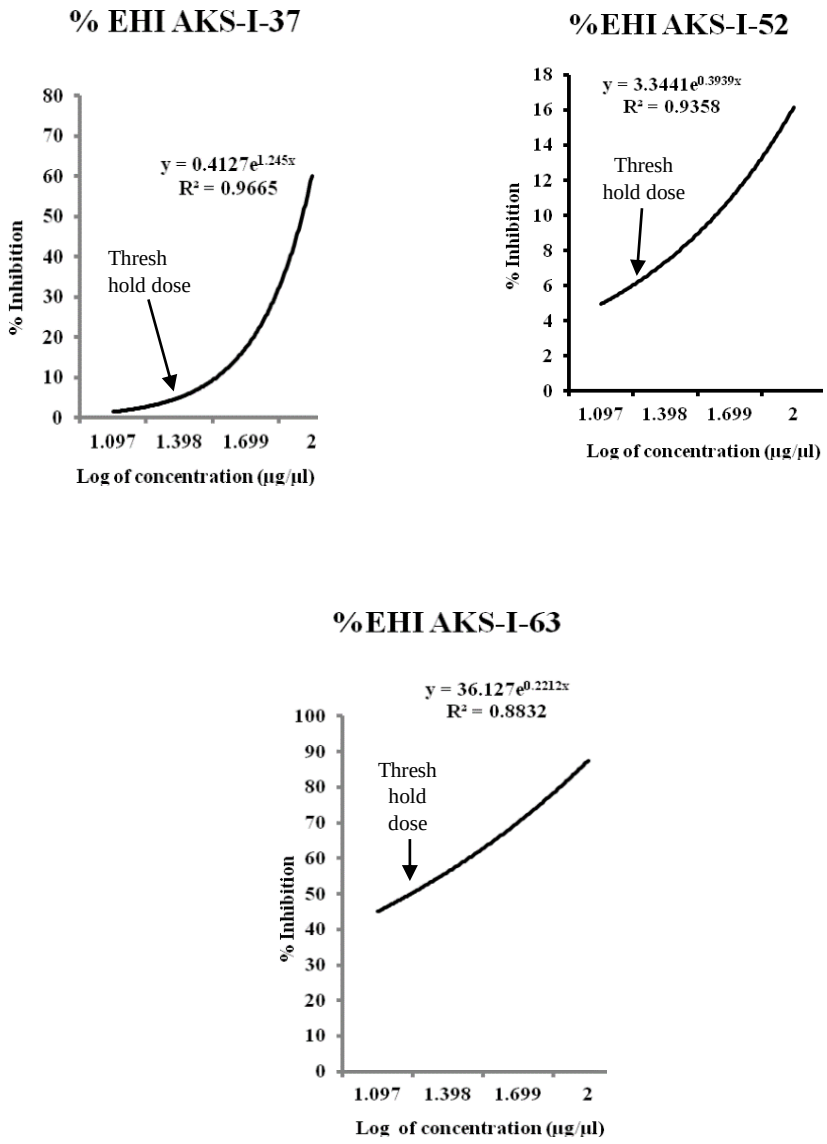

Figure 4.237. Dose response curves

CHAPTER FIVE

5.0 CONCLUSION AND RECOMMENDATION

A number of public health issues of humans and problems of livestock production are often caused by helminthiasis, majorly in places where adequate sanitary facilities and practises are lacking. A number of helminth infections are gradually becoming resistant to many drugs frequently employed to eradicate or ease the burden of these infections.

A library of synthesised benzimidazoles, which include new derivatives, of high purity and moderate to high yields were reported. This was achieved by reacting *o*-phenylenediamines and substituted *o*-phenylenediamines with various aldehydes under oxidative condition through a one-pot cyclocondensation reaction pathway. The pathway was presumed to include the formation of metasulfite adducts and a further cyclodehydrogenation of the subsequently generated aniline Schiff's bases, *in situ*. Two classes of benzimidazoles – 2-furanyl- and 2-phenylbenzimidazoles – with derivatives bearing substituent(s) such as chloro-, fluoro-, nitro-, and methyl moieties at 5 and/or 6 positions were synthesised and are additions to the library of synthesised organic compounds. Most of the compounds tested for their inhibitory activity showed dose-dependent egg hatch inhibition against gastrointestinal nematodes of cattle, with the highest mean percent egg hatch inhibitory potential exhibited by 2-(2′-bromo-4′,5′-dimethoxyphenyl)-1*H*-benzo[*d*]imidazole. Three new 2-phenylbenzimidazoles exhibited the most promising anthelmintic activity at varying concentrations when compared with Albendazole and their biological efficacy established. Thus, they could serve as leads to developing drugs essential for managing helminthiasis both in human and veterinary medicine.

However, there is a need to further determine the efficacy of these compounds *in vivo* since *in vitro* study may not be able to estimate the value of *in vivo* activity in a biological system, due to factors such as differentials in bioavailability (i.e. absorption and metabolism), biotransformation and drug interaction. Also, the pharmacokinetic, structure activity relationship (SAR) and toxicological profile of these compounds could further be carried out in order to explore their possibility in clinical use.

REFERENCES

Ajani, O.O., Ezeoke, E.K., Edobor-Osoh, A. and Ajani, A.O. 2013. Facile synthesis and characterisation of new 2,3-disubstituted benzimidazole derivatives. *International Research Journal of Pure & Applied Chemistry* 3.1: 10-21.

Alam, F., Dey, B.K., Sharma, K., Chakraborty, A. and Kalita, P. 2014. Synthesis, antimicrobial and anthelmintic activity of some novel benzimidazole derivatives. *Int. J. Drug Res. Tech*. 4.3: 31-38.

Alasmary, F.A.S., Snelling, A.M., Zain, M.E., Alafeefy, A.M., Awaad, A.S. and Karodia, N. 2015. Synthesis and evaluation of selected benzimidazole derivatives as potential antimicrobial agents. *Molecules* 20: 15206-15223.

Albonico, M., Allen, H., Chitsulo, L., Engels, D., Gabrielli, A.F., Savioli, L. and Brooker, S. 2008. "Controlling soil transmitted helminthiasis in pre-school age children through preventive chemotherapy". *PLoS Neglected Tropical Diseases* 2.3: e126.

Albonico, M., Bickle, Q., Ramsan, M., Montresor, A., Savioli, L. and Taylor, M. 2003. Efficacy of mebendazole and levamisole alone or in combination against intestinal nematode infections after repeated targeted mebendazole treatment in Zanzibar. *Bulletin of the World Health Organization* 81: 343-352.

Alemayehu, M., Birhan, W., Belyhun, Y., Sahle, M. and Tessema, B. 2014. Prevalence of smear positive tuberculosis, intestinal Parasites and their co-infection among tuberculosis suspects in Gondar University Hospital and Gondar Poly Clinic, North West Ethiopia. *J. Microb. Biochem. Technol*. 6.4: 179-184.

Almeida, F.A., Garcia, K.C.O.D., Torgerson, P.R. and Amarante, A.F.T., 2010. Multiple resistance to anthelmintics by *Haemonchus contortus* and *Trichostrongylus colubriformis* in sheep in Brazil. *Parasitology International* 59: 622-625.

Al-Rashood, K.A. and Abdel-Aziz, H.A. 2010. Thiazolo[3,2-*a*]benzimidazoles: Synthetic strategies, chemical transformations and biological activities. *Molecules* 15: 3775-3815.

Álvarez-Sánchez, M.A., Mainar-Jaime, R.C., Pérez García, J. and Rojo-Vázquez, F.A. 2002. A review of the methods for the detection of anthelmintic resistance. *Revista Ibérica de Parasitología* 62.1-2: 51-59.

Ayhan-Kilcigil, G. and Altanlar, N. 2003. Synthesis and antimicrobial activities of some new benzimidazole derivatives. *Il Farmaco* 58: 1345-1350.

Babu, I.S. and Selvakumar, S. 2013. An antibacterial, antifungal and anthelmintic evaluations of some synthesisd chalcone derived benzimidazoles. *Biosciences Biotechnology Research Asia* 10.2: 891-896.

Bansal, Y, and Silakari, O. 2012. The therapeutic journey of benzimidazoles: A review. *Bioorganic & Medicinal Chemistry* 20: 6208-6236.

Belew, S., Hussien, J., Regassa, F., Belay, K. and Tolosa, T. 2012. Susceptibility assay of *Haemonchus contortus* to commonly used anthelmintics in Jimma, southwest Ethiopia. *Trop. Anim. Health Prod.*, 5 pages.

Bethony, J., Brooker, S., Albonico, M., Geiger, S.M., Loukas, A., Diemert, D. and Hotez, P.J. 2006. Soil-transmitted helminth infections: ascariasis, trichuriasis, and hookworm. *Lancet* 367: 1521-32.

Brahmachari, G. 2009. Bioactive Natural Products: Chemistry and Biology. Alpha science international limited, Oxford, United Kingdom. p 734.

Brooke, E.M., Meagan, A., Greg, B., Michael, B., Yamilette, M.C.A., James, D.E., Mallory, F., Cody, H., Edward, E.H., Olivia, H., George, J.K., Aspen, M.M., José T.M., Paul, P., Lucy, F.R. and Bernhard, J. 2014. *The Atlas of Infectious Diseases*. Oregon State University. Carto group.

Brooker, S., Clements, A.C., Hotez, P.J., Hay, S.I., Tatem, A.J., Bundy, D.A. and Snow, R.W. 2006. The co-distribution of *Plasmodium falciparum* and hookworm among African schoolchildren. *Malaria Journal* 5: 99.

Bruch, M. D. (Ed.) 1996. NMR spectroscopy technique (practical spectroscopy series volume 21). 2nd edition, revised and expanded. Marcel Dekker Inc. NY. USA.

Cala, A.C., Chagas, A.C.S., Oliveira, M.C.S., Matos, A.P., Borges, L.M.F., Sousa, L.A.D., Souza, F.A. and Oliveira, G.P. 2012. *In vitro* anthelmintic effect of *Melia azedarach* L. and *Trichilia classenii* C. against sheep gastrointestinal nematodes. *Exp. Parasitol.* 130: 98-102.

Camurça-Vasconcelos, A.L.F., Bevilaqua, C.M.L., Morais, S.M., Maciel, M.V., Costa, C.T.C., Macedo, I.T.F., Oliveira, L.M.B., Braga, R.R., Silva, R.A., Vieira, L.S.

and Navarro, A.M.C. 2008. Anthelmintic activity of *Lippia sidoides* essential oil on sheep gastrointestinal nematodes. *Veterinary Parasitology* 154: 167-170.

Camurça-Vasconcelos, A.L.F., Bevilaqua, C.M.L., Morais, S.M., Maciel, M.V., Costa, C.T.C., Macedo, I.T.F., Oliveira, L.M.B., Braga, R.R. Silva, R.A. and Vieira, L.S. 2007. Anthelmintic activity of *Croton zehntneri* and *Lippia sidoides* essential oils. *Veterinary Parasitology* 148: 288-294.

Castro, G.A. 1996. Helminths: Structure, Classification, Growth, and Development (Chapter 86). Baron, S. (Ed.), Medical Microbiology, 4th edition. Galveston (TX): University of Texas Medical Branch, Galveston.

Caytan, E., Remauld, G.S., Tenailleau, E., and Akoka, S. 2007. 'Precise and accurate quantitative ^{13}C NMR with reduced experimental time'. *Telanta* 71.3: 1016-1021.

Chari, M.A., Zaied-A-Mosaa, Shobha, D. and Malayalama, S. 2013. Synthesis of multifunctionalised 2-substituted benzimidazoles using copper(II)hydroxide as efficient solid catalyst. *International Journal of Organic Chemistry* 3: 243-250.

Charlier, J., van der Voort, M., Kenyon, F., Skuce, P., Vercruysse, J. 2014. Chasing helminths and their economic impact on farmed ruminants. *Trends Parasitol.* 30.7: 361-367.

Chawla, A., Kaur, R. and Goyal, A. 2011. Importance of microwave reactions in the synthesis of novel benzimidazole derivatives: A review. *J. Chem. Pharm. Res.* 3.6: 925-944.

Cheson, B.D. and Leoni, L. 2011. Bendamustine: Mechanism of action and clinical data. *Clin. Adv. Hematol. Oncol.* 9.8 Suppl. 19: 1-11.

Chou, C-T., Yellol, G.S., Chang, W-J., Sun, M-L. and Sun, C.M. 2011. Microwave assisted straightforward synthetic method for benzimidazole linked quinoxalinones on soluble polymer support. *Tetrahedron* 67: 2110-2117.

Crump, K.S., Hoel, D.G., Langley, C.H. and Peto, R. 1976. "Fundamental carcinogenic processes and their implications for low dose risk assessment". *Cancer Research* 36.9 (Part1): 2973-9.

Dada-Adegbola, H.O., Oluwatoba, O.A. and Falade, C.O. 2013. Asymptomatic malaria and intestinal helminth co-infection among children in a rural community in Southwest Nigeria. *Malaria World Journal* 4.18: 1-6.

Diao, X., Wang, Y., Jiang, Y. and Dawei, M. 2009. Assembly of substituted 1H-benzimidazoles and 1,3-dihydrobenzimidazol-2-ones via CuI/L-Proline catalyzed coupling of aqueous ammonia with 2-iodoacetanilides and 2-iodophenylcarbamates. *J. Org. Chem.* 74: 7974-7977.

Eicher, T. and Hauptmann, S. 2003. The Chemistry of Heterocycles: Structure, Reactions, Syntheses, and Applications. 2nd Ed., Wiley-VCH.

Engels, D. and Savioli, L. 2006. Reconsidering the underestimated burden caused by Neglected Tropical Diseases. *Trends in Parasitology* 22.8: 363-366.

Ezeamama, A.E., Friedman, J.F., Olveda, R.M., Acosta, L.P., Kurtis, J.D., Mor, V. and Mcgarvey, S.T. 2005. Functional significance of low-intensity polyparasite helminth infections in anemia. *Journal of Infectious Disease* 192: 2160-2170.

Ferreira, L.E., Castro, P.M.N., Chagas, A.C.S., França, S.C. and Beleboni, R.O. 2013. *In vitro* anthelmintic activity of aqueous leaf extract of *Annona muricata* L. (Annonaceae) against *Haemonchus contortus* from sheep. *Experimental Parasitology* 134: 327-332.

Getachew, M., Tafess, K., Zeynudin, A. and Yewhalaw, D. 2013. Prevalence soil transmitted helminthiasis and malaria co-infection among pregnant women and risk factors in Gilgel Gibe dam Area, Southwest Ethiopia. *BMC Research Notes* 6: 263.

Gilleard, J.S. and Beech, R.N. 2007. Population genetics of anthelmintic resistance in parasitic nematodes. *Parasitol.* 134.8: 1133-47.

Grant, W., Bisset, S., Prichard, R.K., Hotez, P., Bethony, J., Gilleard, J., Sternberg, P., Gasser, R., Mardis, E.R., Wilson, R.K. and Mitreva, M. 2010. Anthelmintic resistance in parasitic nematodes. A consortium. 6 pages.

Gurvinda, S., Maninderjit, K. and Mohan, C. 2013. Benzimidazole: the latest information on biological activities. *International Research Journal of Pharmacy* 4.1: 82-87.

Hall, A., Hewitt, G., Tuffrey, V. and de Silva, N. 2008. A review and meta-analysis of the impact of intestinal worms on child growth and nutrition. *Matern. Child Nutr.* 4.1: 118-236.

Hegedus, A., Hell, Z. and Potor, A. 2006. Zeolite-catalyzed environmentally friendly synthesis of benzimidazole derivatives. *Synthetic Communications* 36: 3625-3630.

Heinz, B.A. and Vance, L.M. 1995. The antiviral compound Enviroxime targets the 3A coding region of rhinovirus and poliovirus. *J. Virol.* 69.7: 4189-4197.

Holden-Dye, L. and Walker, R.J., 2007. Anthelmintic drugs, *WormBook*, Maricq, V. and McIntire, S.L. Ed. The *C. elegans* Research Community, WormBook, doi/10.1895/wormbook.1.143.1. http://www.wormbook.org.

Hotez, P.J.,Molyneux,D.H., Fenwick,A., Ottesen,E.,Sachs, S.E.andSachs, J.D. 2007. Incorporating a rapid-impact package for neglected tropical diseases with programs for HIV/AIDS, tuberculosis and malaria. *PLoS Med.* 4.9: e277.

Hotez, P.J., Ottesen, E., Fenwick, A. and Molyneux, D. 2006. The neglected tropical diseases: the ancient afflictions of stigma and poverty, and the prospects for their control elimination. In: Pollard, A.J. and Finn, A. (Eds.), *Hot Tropics Infection and Immunity in Children III*. New York: Springer, US.

Hotez, P.J., Brindley, P.J., Bethony, J.M., King, C.H., Pearce, E.J. and Jacobson, J. 2008. Helminth infections: the great neglected tropical diseases. *J. Clin. Invest.* 118.4: 1311-1321.

Hotez, P.J., de Silva, N., Brooker, S. and Bethony. J. 2003. Soil transmitted helminth infections: the nature causes and burden of the condition. Working paper No. 3, disease control priorities project, Bethesda, Maryland. Fogarty International Center, National Institutes of Health.

Jaeger, L.H. and Carvalho-Costa, F.A. 2017. Status of benzimidazole resistance in intestinal nematode populations of livestock in Brazil: a systematic review *BMC Veterinary Research* 13:358.

Jaya, P.P., Karthikeyan, E., Lohita, M., Goutham, T.P., Subhash, M., Shaheena, P., Prashanth, Y. and Sai, N.K. 2015. Benzimidazole: an important scaffold in drug discovery. *Asian J. Pharm. Tech.* 5.3: 138-152.

Jia, T-W., Melville, S., Utzinger, J., King, C.H. and Zhou, X-N. 2012. Soil-transmitted helminth reinfection after drug treatment: A systematic review and meta-analysis. *PLoS Negl. Trop. Dis.* 6(5): e1621. doi:10.1371/journal.pntd.0001621.

Jimenez-Cisneros, B.E. and Maya-Rendon, C. 2007. "Helminths and Sanitation". *Communicating Current Research and Educational Topics and Trends in Applied Microbiology*, Méndez-Vilas, A. (Ed.). ©FORMATEX. Pp 60-71.

Kalidhar, U. and Kaur, A., 2011. An overview on some benzimidazole and sulfonamide derivatives with anti-microbial activity. *Research Journal of Pharmaceutical, Biological and Chemical Sciences* 2.4: 1116-1135.

Kalsi, P. S. 2004. Spectroscopy of organic compounds, 6th edition. New Delhi: New Age International Ltd.

Katiki, L.M., Chagas, A.C.S., Bizzo, H.R., Ferreirad, J.F.S. and Amarante, A.F.T. 2011. Anthelmintic activity of *Cymbopogon martinii*, *Cymbopogon schoenanthus* and *Mentha piperita* essential oils evaluated in four different *in vitro* tests. *Veterinary Parasitology* 183: 103-108.

Kealey, A. and Smith, R. 2010. Neglected tropical diseases: nfection, modeling and control. *Journal of Health Care for the Poor and Underserved* 21: 53-69.

Keiser, J., Tritten, L., Adelfio, R. and Vargas, M. 2012. Effect of combinations of marketed human anthelmintic drugs against Trichuris muris *in vitro* and *in vivo*. *Parasites and Vectors* 5: 292-299.

Khan, K.M., Shah, Z., Ahmad, V.U., Ambreen, N., Khan, M., Taha, M., Rahim, F., Noreen, S., Perveen, S., Choudhary, M.I. and Voelter, W. 2012. 6-Nitrobenzimidazole derivatives: Potential phosphodiesterase inhibitors: Synthesis and structure-activity relationship. *Bioorganic and Medicinal Chemistry* 20: 1521-1526.

Khokra, S.L. and Choudhary, D. 2011. Benzimidazole, an important scaffold in drug discovery. *Asian Journal of Biochemical and Pharmaceutical Research* 3.1: 476-486.

Kumar, P. S. and Sahoo, J. 2014. Anthelmintic evaluation of some novel synthesisd 1,2,4-triazole moiety clubbed with benzimidazole ring. *Oriental Journal of Chemistry* 30.1: 211-217.

Kumar, V., Khandare, D.G., Chatterjee, A. and Banerjee, M. 2013. DBSA mediated chemoselective synthesis of 2-substituted benzimidazoles in aqueous media. *Tetrahedron Letters* 54: 5505-5509.

Lam, T., Hilgers, M.T., Cunningham, M.L., Kwan, B.P, Nelson, K.J., Brown-Driver, V., Ong, V., Trzoss, M., Hough, G., Shaw, K.J. and Finn, J. 2014. Structure-based design of new dihydrofolate reductase antibacterial agents: 7-(Benzimidazol-1-yl)-2,4-diaminoquinazolines. *Journal of Medicinal Chemistry* 57: 651-668.

Le Jambre, L. F. 1995. Relationship of blood loss to worm numbers, biomass and egg production in *Haemonchus* infected Sheep. *International Journal of Parasitology* 25: 269-273.

Lingala, S., Nerella, R. and Rao, K.R.S.S. 2011. Synthesis, antimicrobial and anthelmintic activity of some novel benzimidazole derivatives. *International Journal of Pharmaceutical Sciences Review and Research* 10.2: 100-105.

López, S.E., Restrepo, J., Pérez, B., Ortiz, S. and Salazar, J. 2009. One pot microwave promoted synthesis of 2-aryl-1*H*bBenzimidazoles using sodium hydrogen sulfite. *Bull. Korean Chem. Soc.* 30.7: 1628-1630.

Luong, T.V. 2003. De-worming school children and hygiene intervention. *Int. J. Environ. Health Res.* 1: 153-159.

Mahato, S.B., Nandy, A.K. and Roy, G. 1992. Triterpenoids. *Phytochemistry* 31: 2199-2249.

Maruthamuthu, S.R., Christina, R., Stella P., Bharathi D.A. G. and Ranjith, R. 2016. The chemistry and biological significance of imidazole, benzimidazole, benzoxazole, tetrazole and quinazolinone nucleus. *J. Chem. Pharm. Res.* 8.5: 505-526.

Mhimbira, F., Hella, J., Said, K., Kamwela, L., Sasamalo, M., Maroa, T., Chiryamkubi, M., Mhalu, G., Schindler, C., Reither, K., Knopp, S., Utzinger, J., Gagneux, S. and Fenner, L. 2017. Prevalence and clinical relevance of helminth co-infections among tuberculosis patients in urban Tanzania. *PLoS Negl. Trop. Dis.* 11.2: e0005342. doi:10.1371/journal.pntd.0005342.

Mkhize, B.T., Mabaso, M., Mamba, T., Napier, C.E. and Mkhize-Kwitshana, Z.L. 2017. The interaction between HIV and intestinal helminth parasites co-infection with nutrition among adults in KwaZulu-Natal, South Africa. *BioMed Research International,* Volume 2017, Article ID 9059523, 12 pages.

Mkhize-Kwitshana, Z.L. and Mabaso, M.H. 2012. "Status of medical parasitology in South Africa: new challenges and missed opportunities" *Trends in Parasitology* 28.6: 217-219.

Mohan, L.P.R.A., Sridhar, R.A., Saratchandra, B.M. and Mutyala, K.R. 2015. Simple and efficient one-pot synthesis of 2-Substituted benzimidazoles from θ-Diaminoarene and aryl aldehydes. *Synthetic Communications* 45.21: 24362443.

Molefe, N.I., Tsotetsi, A.M., Ashafa, A.O.T. and Thekisoe, O.M.M. 2012. *In vitro* anthelmintic activity of *Artemisia afra* and *Mentha longifolia* against parasitic gastro-intestinal nematodes of livestock. *Bangladesh J. Pharm.* 7: 157-163.

Molefe, N.I., Tsotetsi, A.M., Ashafa, A.O.T. and Thekisoe, O.M.M. 2013. *In vitro* anthelmintic activity of *Cotyledon orbiculata, Hermannia depressa* and *Nicotiana glauca* extracts against parasitic gastrointestinal nematodes of livestock. *Journal of Medicinal Plants Research* 7.9: 536-542.

Motulsky, H. and Christopoulos, A., 2002. Fitting dose response curves: An excerpt from a forthcoming book: Fitting models to biological data using linear and nonlinear regression. A practical guide to curve fitting. 53 pages. GraphPad Software, Inc. www.graphpad.com.

Mulu, A, Kassu, A., Legesse, M., Erko, B., Nigussie, D., Shimelis, T., Belyhun, Y., Moges, B., Ota, F. and Elias, D. 2014. Helminths and malaria co-infections are associated with elevated serum IgE. *Parasites & Vectors* 7:240.

Mulu, A., Maier, M. and Liebert, U.G. 2013. Deworming of intestinal helminths reduces HIV-1 subtype C viremia in chronically co-infected individuals. *International Journal of Infectious Diseases* 17: e897-e901.

Munguia, B., Mendina, P., Espinosa, R., Lanz, A., Saldana, J., Andina, M. J., Ures, X., Lopez, A., Manta, E. and Dominguez, L. 2013. Synthesis and anthelmintic evaluation of novel valerolactam-benzimidazole hybrids. *Letters in Drug Design & Discovery* 10: 1007-1014.

Norris, J., Adelman, C., Spantchak, Y. and Marano, K. 2012. Social and economic impact review on Neglected Tropical Diseases. Economic policy/briefing paper, Hudson Institute (Washinton DC) and Global Network for Neglected Tropical Diseases, 36 pages.

Omitola, O.O., Mogaji, H.O., Oluwole, A.S., Adeniran, A.A., Alabi, O.M. and Ekpo, U.F. 2016. Geohelminth infections and nutritional status of preschool aged children in a Periurban settlement of Ogun State. *Scientifica*, Volume 2016, Article ID 7897351, 9 pages.

Ouattara, M., Sissouma, D., Koné, M. W., Menan, H. E., Touré, S. A. and Ouattara, L. 2011. Synthesis and anthelmintic activity of some hybrid benzimidazolyl-chalcone derivatives. *Tropical Journal of Pharmaceutical Research* 10.6: 767-775.

Panda, S.S. and Jain, S.C. 2011. Synthesis of 2-arylbenzimidazoles in water. *Synthetic Communications* 41: 729-735.

Panda, S.S., Malik, R. and Jain, S.C. 2012. Synthetic approaches to 2-arylbenzimidazoles: A review. *Current Organic Chemistry* 16: 1905-1919.

Panic, G., Duthaler, U., Speich, B. and Keiser, J. 2014. Repurposing drugs for the treatment and control of helminth infections. *International Journal for Parasitology: Drugs and Drug Resistance* 4: 185-200.

Pantziarka, P., Bouche, G., Meheus, L., Sukhatme, V. and Sukhatme, V.P. 2014. "Repurposing drugs in Oncology (ReDO) – mebendazole as an anti-cancer agent." *ecancermedicalscience* 8.1: 443.

Patel, K.V., and Singh, A. 2009. Synthesis, characterisation and chelating properties of benzimidazole-salicylic acid combined molecule. *E-Journal of Chemistry* 6.1: 281-288.

Pavia, D. L., Lampman, G. M., Kriz, G. S. 2001. Introduction to Spectroscopy, 3rd edition. USA: Thompson Learning Inc.

Radatz, C.S., Silva, R.B., Perin, G., Lenardão, E.J., Jacob, R.G. and Alves, D. 2011. Catalyst-free synthesis of benzodiazepines and benzimidazoles using glycerol as recyclable solvent. *Tetrahedron Letters* 52: 4132-4136.

Rajamanickam, G., Selvaraj, J., Selvaraj, S., Rajendran, T. and Sarker, Md. M.R. 2015. *In vitro* anthelmintic and antimicrobial activity of novel series of quinoxaline-2,3-dione-6-sulphonyl benzimidazole(s). *Journal of Chemical and Pharmaceutical Sciences* 8.4: 656-660.

Ramanpreet, W., Hedaitullah, M., Naaz, S.F., Iqbal, K. and Lamba, H.S. 2011. Benzimidazole derivatives – an overview. *International Journal of Research in Pharmacy and Chemistry* 1.3: 565-574.

Roepstorff, A. and Nansen, P. 1998. Epidemiology, diagnosis and control of helminth pearasite of swine. FAO Animal Health Manual, Rome.

Rosso, D., Miller, J. and Marek, T. 1996. *Class action: improving school performance in the developing world through better health and nutrition*. The World Bank, directions in development.

Sanchez, A.L., Gabrie, J.A., Usuanlele, M-T., Rueda, M.M., Canales, M. and Gyorkos, T.W. 2013. Soil-transmitted helminth infections and nutritional status in school-age children from fural communities in Honduras. *PLoS Neglected Tropical Diseases* 7.8: e2378.

Santosh, P.C., Pandeya, S.N. and Pathak, A.K. 2011. Benzimidazole: a versatile chemical entity. *IJRAP* 2.6: 1726-1737.

Sawant, R. and Kawade, D. 2011. Synthesis and biological evaluation of some novel 2-phenyl benzimidazole-1-acetamide derivatives as potential anthelmintic agents. *Acta Pharm.* 61: 353-361.

Schwob, T. and Kempe, R. 2016. A reusable Co catalyst for the selective hydrogenation of functionalized nitroarenes and the direct synthesis of imines and benzimidazoles from nitroarenes and aldehydes. *Angew. Chem. Int. Ed.*, Wiley-VCH Verlag GmbH & Co. KGaA, Weinheim, 55: 15175-15179.

Secci, D., Bolasco, A., D'Ascenzio, M., Sala, Fd., Yáñez, M. and Carradoria, S. 2012. Conventional and microwave-assisted synthesis of benzimidazole derivatives and their *in vitro* inhibition of human cyclooxygenase. *J. Heterocyclic Chem.* 49: 1187-1195.

Silverstein, R.M., Webster, F.X. and Kiemle, D.J. 2005. Spectrometric identification of organic compounds, 7th edition. United States of America: John Wiley & Sons, Inc.

Simon, G.G. 2016. Impacts of neglected tropical disease on incidence and progression of HIV/AIDS, tuberculosis, and malaria: scientific links. *International Journal of Infectious Diseases* 42: 54-57.

Skolnik, R. and Ahmed, A. 2010. Ending the neglect of Neglected Tropical Diseases. Policy Brief (PRB). www.prb.org, 6 pages.

Speich, B., Moser, W., Ali, S.M., Ame, S.M., Albonico, M., Hattendorf, J. and Keiser, J. 2016. Efficacy and re-infection with soil-transmitted helminths 18-weeks post-treatment with albendazole-ivermectin, albendazolemebendazole, albendazole-oxantel pamoate and mebendazole. *Parasites & Vectors* 9:123.

Surpur, M.P., Singh, P.R., Patil, S.B. and Samant, S.D. 2007. One-pot synthesis of benzimidazoles from *o*-nitroanilines under microwaves via a reductive cyclization. *Synthetic Communications* 37: 1375-1379.

Sutherland, I.A. and Leathwick, D.M., 2011. Anthelmintic resistance in nematode parasites of cattle: a global issue? *Trends Parasitol.* 27: 176-181.

Tagawa, Y., Yamagata, K. and Sumoto, K. 2008. Improved, convenient and environmentally benign synthesis of biological active benzimidazoles using activated carbon and molecular oxygen. *Heterocycles* 75: 415-418.

Taylor-Robinson, D.C., Maayan, N., SoaresWeiser, K., Donegan, S. and Garner, P. 2015. "Deworming drugs for soil transmitted intestinal worms in children: effects on

nutritional indicators, haemoglobin, and school performance.". *The Cochrane Database of Systematic Reviews* 7: CD000371. PMID 26202783.

Tchinda, V.H.M., Ponka, R., Ndzi, E.S., Madocgne, A.K., Amédée, M., Tchinda, M.G. and Moyou, R.S. 2012. Prevalence of malaria and soil-transmitted helminth infections and their association with under-nutrition in schoolchildren residing in Mfou health district in Cameroon. *Journal of Public Health and Epidemiology* 4.9: 253-260.

Temirak, A., Shaker, Y.M., Ragab, F.A.F., Ali, M.M., Soliman, S.M., Mortier, J., Wolber, G., Ali, H.I. and El Diwani, H.I. 2014a. Synthesis, biological evaluation, and docking studies of new 2-furylbenzimidazoles as anti-angiogenic agents: Part II. *Arch. Pharm. Chem. Life Sci.* 347: 291-304.

Temirak, A., Shaker, Y.M., Ragab, F.A.F., Ali, M.M., Ali, H.I. and El Diwani, H.I. 2014b. Part I. Synthesis, biological evaluation and docking studies of new 2-furylbenzimidazoles as antiangiogenic agents. *European Journal of Medicinal Chemistry* 87: 868-880.

Tian, L-G., Chen, J-X., Wang, T-P., Cheng, G-J., Steinmann, P., Wang, F-F., Cai, Y-C., Yin, X-M., Guo, J., Zhou, L. and Zhou, X-N. 2012. Co-infection of HIV and intestinal parasites in rural area of China. *Parasites & Vectors* 5: 36.

Townsend, L.B. and Wise, D.S. 1990. The synthesis and chemistry of certain anthelmintic benzimidazoles. *Parasitology Today* 6.4: 107-112.

ur Rehman, M., Imran, M., Arif, M., Farooq, M. 2013. Mannich base derivatives of Benzimidazole: Synthesis and antimicrobial properties – a short review. *World Applied Programming* 3.12: 558-564.

van Riet, E., Hartgers, F.C. and Yazdanbakhsh, M. 2007. Chronic helminth infections induce immunomodulaion consequences and mechanism. *Immunobiology* 212.6: 475-479.

Vercruysse, J., Albonico, M., Behnke, J.M., Kotze, A.C., Prichard, R.K., McCarthy, J.S., Montresor, A. and Levecke, B. 2011. Is anthelmintic resistance a concern for the control of human soil-transmitted helminths? *International Journal for Parasitology: Drugs and Drug Resistance* 1: 14-27.

Verdecchia, P., Angeli, F., Gentile, G., Mazzotta, G. and Reboldi, G. 2011. Telmisartan for the reduction of cardiovascular morbidity and mortality. *Expert Rev. Clin. Pharmacol.* 4.2: 151-161.

Weires, N.A., Boster, J. and Magolan, J. 2012. Combined Pd/C and montmorillonite catalysis for one-pot synthesis of benzimidazoles. *Eur. J. Org. Chem.* 6508-6512.

Williams, A.R., Ropiak, H.M., Fryganas, C., Desrues, O., Mueller-Harvey, I. and Thamsborg, S.M. 2014. Assessment of the anthelmintic activity of medicinal plant extracts and purified condensed tannins against free-living and parasitic stages of *Oesophagostomum dentatum. Parasites & Vectors* 7: 518.

Williams, D. H. And Fleming, I. 1987. Spectroscopic methods in organic chemistry, 4th edition. UK: McGraw-Hill limited.

Williams, K.R. and King, R.W. 1990. Showcasing 2D NMR spectroscopy in an undergraduate setting. *Journal of Chemical Education* 67.5: A125.

World Health Organisation (WHO) 2004. *Water, sanitation and hygiene links to health*: Retrieved May 31, 2016, from (http://www.who.int/water_sanitation_ health/facts 2004/en/print.html).

World Health Organisation (WHO) 2006. *Preventive chemotherapy in human helminthiasis: coordinated use of anthelminthic drugs in control interventions.* A manual for health professionals and programme managers (PDF). WHO Press, Geneva, Switzerland. 61 pages.

World Health Organisation (WHO) 2012a. *Soil-transmitted helminthiases: eliminating soil-transmitted helminthiases as a public health problem in children*. Geneva: In progress report 2001-2010 and strategic plan 2011-2020. WHO Library Cataloguing-In-Publication Data, 20 pp. WHO/HTM/NTD/PCT/2012.4. (http:// www.who.int/about/licensing/copyright_for*m*/zn/index.html).

World Health Organisation (WHO) 2012b. *Research priorities for helminth infections: Technical report of the TDR disease reference group on helminth infections*. Geneva: In WHO technical report series 972. (http://www.who.int/about/ licensing/copyright_for*m*/zn/index.html).

World Health Organization (WHO) 2002. *Prevention and Control of Schistosomiasis and Soil-Transmitted Helminthiasis.* Geneva: In: WHO technical report series 912.

Yang, D., Fokas, D., Li, J., Yu, L. and Baldino, C. M. 2005. A versatile method for the synthesis of benzimidazoles from *o*-nitroanilines and aldehydes in one step *via* a reductive cyclisation. *Synthesis* pp 47-56.

Yap, P., Utzinger, J., Hattendorf, J. and Steinmann, P. 2014. Influence of nutrition on infection and re-infection with soil-transmitted helminths: a systematic review. *Parasites & Vectors* 7:229.

Yar, M. S., Abdullah, M.M. and Majeed, J. 2009. *In vitro* anti-tubercular screening of newly synthesisd benzimidazole derivatives. *World Acad. Sci. Engr. Tech.* 55: 593-99.

Zerdo, Z., Yohanes, T. and Tariku, B. 2016. Soil-transmitted helminth re-infection and associated risk factors among school-age children in Chencha district, Southern Ethiopia: A cross-sectional study. *Journal of Parasitology Research,* Volume 2016, Article ID 4737891, 7 pages.

Zhou, M., Eun, Y-J., Guzei, I.A. and Weibel, D.B. 2013. Structure-activity studies of Divin: An inhibitor of bacterial cell division. *ACS Med. Chem. Lett.* pp. A-F. dx.doi.org/10.1021/ml400234x.